University of Wisconsin Milwaukee
UWM Digital Commons

Theses and Dissertations

May 2019

Multi-Segment Pile-Supported Bridge Approach Slabs for Control of Differential Settlement

Ahmed Bahumdain
University of Wisconsin-Milwaukee

Follow this and additional works at: https://dc.uwm.edu/etd

 Part of the Civil Engineering Commons

Recommended Citation
Bahumdain, Ahmed, "Multi-Segment Pile-Supported Bridge Approach Slabs for Control of Differential Settlement" (2019). *Theses and Dissertations*. 2042.
https://dc.uwm.edu/etd/2042

This Dissertation is brought to you for free and open access by UWM Digital Commons. It has been accepted for inclusion in Theses and Dissertations by an authorized administrator of UWM Digital Commons. For more information, please contact open-access@uwm.edu.

MULTI-SEGMENT PILE-SUPPORTED BRIDGE APPROACH SLABS FOR CONTROL OF DIFFERENTIAL SETTLEMENT

by

Ahmed Zohuir Bahumdain

A Dissertation Submitted in

Partial Fulfillment of the

Requirements for the Degree of

Doctor of Philosophy

in Engineering

at

The University of Wisconsin-Milwaukee

May 2019

ABSTRACT

MULTI-SEGMENT PILE-SUPPORTED BRIDGE APPROACH SLABS FOR CONTROL OF DIFFERENTIAL SETTLEMENT

by

Ahmed Zohuir Bahumdain

The University of Wisconsin-Milwaukee, 2019

Under the Supervision of Professor Habib Tabatabai

The roughness of the transition between the bridge and the roadway is a well-known issue that affects roughly 25% of the bridges in the United States. As soil underneath the approach slab settles, deferential settlement develops between the bridge and the approaching roadway. This may negatively affect the ride quality for travelers and result in substantial long-term maintenance costs. Because of the differential settlement, bumps could develop at the ends of the bridge when abrupt changes in slope (exceeding 1/125) occurs.

This study was aimed at mitigating the formation of bumps at the ends of the bridge through a new design concept for the approach area. The proposed design takes advantage of settlement-reducing piles that would support various approach slab segments and control their settlement. These pile elements are intended to control the roughness of the transition such that acceptable slope changes develop between various segments of the approach slab and thus improve the performance of the approach slab system.

In this study, a comprehensive review of literature as well as a review of various state practices regarding the approach area was performed. A set of finite element models were developed, and parametric studies were performed to evaluate the soil/approach slab settlement

behind bridge abutments for various soil conditions, and to quantify the pile head settlement and load distribution along piles as a function of pile-soil parameters. It has been determined that the degree of compressibility the embankment and natural soils, length of the approach slab, height of the abutment, and height and side slope of the embankment influence the potential development of bumps at approaches to bridges.

Empirical relationships are developed that relate various soil parameters to the longitudinal soil deformation profile behind bridge abutments. Empirical relationships and design charts are also developed to estimate pile head settlement for piles that are used to control soil settlement under the approach slab. Ultimately, a set of recommendations and design procedures are provided regarding the use and design of multi-segment pile-supported approach slabs for control of differential settlement.

Dedicated to my beloved wife Saliha and my darling kids Savannah and Adam.

TABLE OF CONTENTS

ABSTRACT ..... **ii**

TABLE OF CONTENTS ..... **v**

LIST OF FIGURES ..... **xi**

LIST OF TABLES ..... **xxv**

ACKNOWLEDGMENTS ..... **xxxii**

CHAPTER 1 - INTRODUCTION **1**

1.1 Background 1

1.2 Problem statement 2

1.3 Objectives and Scope of work 3

1.4 Outline of Dissertation 5

CHAPTER 2 - LITERATURE REVIEW **7**

2.1 Definition of the bump 7

2.2 Maintenance considerations 8

2.3 Factors affecting the formation of the bump 11

2.3.1 Settlement of soil underneath approach area 13

2.3.2 Embankment fill 15

2.3.3 Abutment 17

2.3.3.1 Abutment type 17

2.3.3.2 Abutment foundation type 19

2.3.3.3 Movement of the abutment 19

2.3.4 Approach slab 20

2.3.5 Drainage 21

2.3.6 Construction method 22

2.3.7 Traffic volume 23

2.3.8 Bridge skew 23

2.4 Mitigation techniques 24

2.5 Optimum approach slab configuration 27

CHAPTER 3 - STATES PRACTICES RELATED TO APPROACH SLABS 35

3.1 Approach slab preference 35

3.2 Approach slab/pavement end support 38

3.3 Approach slab configuration with skewed bridges 41

3.4 Approach slab connection mechanism to the superstructure 43

3.5 Approach slab dimensions 45

3.6 Embankment and backfill considerations 49

CHAPTER 4 - DEVELOPMENT OF FINITE ELEMENT SOIL-STRUCTURE INTERACTION MODEL 51

4.1 Introduction 51

4.2 Geometry and boundary conditions 53

4.3 Contact behavior at soil-structure interfaces 53

4.4 Analysis procedures 55

4.5 Simulating non-linear behavior of soil 55

4.5.1 Modified Drucker-Prager/Cap constitutive model (MDPCM) 56

4.5.2 Modified Cam-Clay model (MCCM) 60

4.6 Material properties 63

CHAPTER 5 - SIMULATION OF SOIL SETTLEMENT BEHIND BRIDGE ABUTMENTS 68

5.1 Chapter background 68

5.2 Chapter problem statement 69

5.3 Chapter objectives 71

5.4 Development and verification of transverse soil finite element model 71

5.4.1 Introduction 71

5.4.2 Geometry and boundary conditions 72

5.4.3 Analysis procedures for transverse soil model 73

5.4.4 Material properties 74

5.4.5 Verification analysis 74

5.4.5.1 One-dimensional analysis 75

5.4.5.2 Two-dimensional analysis 80

5.4.6 Initial model 86

5.4.7 Element type and size 89

5.5 Parametric study on transverse two-dimensional FEM 91

5.6 Development and verification of longitudinal soil-structure FEM 97

5.6.1 Introduction 97

5.6.2 Geometry and boundary conditions 98

5.6.3 Contact behavior at structure-soil interfaces 101

5.6.4 Analysis procedures for longitudinal soil-structure model 102

5.6.5 Material properties 102

5.6.6 Verification analysis 103

5.6.7 Initial model 108

5.6.8 Element type and size 112

5.7 Parametric study on longitudinal two-dimensional FEM 115

5.7.1 Differential settlement of approach slab 118

5.7.2 Soil settlement profile 123

5.8 Evaluating soil's longitudinal settlement profile behind bridge abutment 128

5.9 Evaluating logistic function parameters 134

5.9.1 Logistic function parameter (*a*) 136

5.9.1.1 Adjustment of (*a*) 143

5.9.2 Logistic function parameter (*b*) 147

5.9.3 Logistic function parameter (*c*) 150

5.10 Case study 153

5.11 Chapter summary and conclusion 156

CHAPTER 6 - PILE-SUPPORTED APPROACH SLABS 158

6.1 Chapter background 158

6.2 Chapter problem statement 159

6.3 Chapter objectives 163

6.4 Settlement-reducing piles 163

6.4.1 Introduction 163

6.4.2 Load transfer mechanism in piles 164

6.4.3 Load capacity of piles 165

6.5 Pile cap design 167

6.6 Development and verification of finite element soil-structure interaction models 168

6.6.1 Introduction 168

6.6.2 Geometry and boundary conditions 170

6.6.3 Contact behavior at structure-soil interfaces 172

6.6.4 Analysis procedures for single pile-soil model 172

6.6.5 Material properties 173

6.6.6 Initial model 173

6.6.7 Element type and size 174

6.6.8 Comparison with analytical solution 175

6.7 Parametric study 177

6.7.1 Load capacity of the pile 181

6.7.2 Pile head settlement 182

6.7.3 Load distribution along the pile shaft 186

6.7.4 Proximity to the abutment wall 202

6.8 Evaluating pile head settlement using analytical method 203

6.9 Evaluating load distribution along the pile using analytical method 207

6.10 Chapter summary and conclusion 235

CHAPTER 7 - FULL-SCALE SIMULATION OF MULTI-SEGMENT PILE-SUPPORTED APPROACH SLAB SYSTEM 237

CHAPTER 8 - SUMMARY, CONCLUSIONS AND RECOMMENDATIONS 253

8.1 Recommendation for future research 260

REFERENCES 261

APPENDICES 267

Appendix A - Settlement-induced slope of the approach slab 268

Appendix B - Longitudinal soil settlement profile 273

Appendix C - Pile-soil model results 291

CURRICULUM VITAE 299

LIST OF FIGURES

Figure 1.1 Typical longitudinal cross section of a bridge. 2

Figure 1.2 Bump formation at the end of the bridge 3

Figure 2.1 Slope of approach slab 8

Figure 2.2 Factors influence the formation of the bump at the end of the bridge (Briaud, James and Hoffman 1997) 13

Figure 2.3 Vertical stress imposed on natural soil by embankment fill and abutment (Wahls 1990) 15

Figure 2.4 Typical wall abutment 18

Figure 2.5 Typical stub abutment 18

Figure 2.6 Mechanism of void formation due to abutment movement (Puppala, et al. 2008) 20

Figure 2.7 Typical subsurface drainage system (Hoppe 1999, White, et al. 2005) 22

Figure 2.8 Distribution of tensile stress in skewed approach slab (Cai, Voyiadjis and Shi 2005) 24

Figure 2.9 Proposed approach slab configuration (Hoppe 1999) 26

Figure 2.10 proposed approach slab (Wong and Small 1994) 28

Figure 2.11 Surface deformation of angled slabs (Wong and Small 1994) 28

Figure 2.12 Current Taxis DOT approach slab (Seo, Ha and Briaud 2002) 29

Figure 2.13 Single span approach slab (Seo, Ha and Briaud 2002) 30

Figure 2.14 Layout of the finite element analysis (Cai, Voyiadjis and Shi 2005) 31

Figure 2.15 Stress distribution in flat slab (Cai, Voyiadjis and Shi 2005) 32

Figure 2.16 Stress distribution in ribbed slab (Cai, Voyiadjis and Shi 2005) 32

Figure 2.17 Standard (top) versus proposed (bottom) approach slab (Abu-Farsakh and Chen 2014) 33

Figure 2.18 Pile-supported approach slab (Bakeer, Shutt, et al. 2005) 34

Figure 3.1 DOTs preference regarding use of approach slab 38

Figure 3.2 Typical approach slab supported on sleeper slab 39

Figure 3.3 Typical approach slab with thickened edge..... 39

Figure 3.4 Approach slab/pavement end support type..... 41

Figure 3.5 Approach slab/Pavement end configuration with skewed bridges..... 43

Figure 3.6 Approach slab connection mechanism to the superstructure 45

Figure 3.7 Approach slab length (*ft*)..... 47

Figure 3.8 Approach slab thickness (*in*) 47

Figure 4.1 Two-Dimensional transverse model..... 52

Figure 4.2 Two-Dimensional longitudinal model..... 52

Figure 4.3 Three-Dimensional pile-soil system model..... 53

Figure 4.4 Pressure-overclosure relationship (ABAQUS 2015)..... 54

Figure 4.5 Slipping behavior of the coulomb friction model (ABAQUS 2015) 55

Figure 4.6 Drucker-Prager/Cap failure surface (ABAQUS 2015)..... 56

Figure 4.7 Yield/flow surface in the deviatoric plane (ABAQUS 2015) 57

Figure 4.8 Potential plastic flow of MDPCM (ABAQUS 2015)..... 59

Figure 4.9 Typical consolidation curves (Coduto 2001) 60

Figure 4.10 Yield surface of Modified Cam-Clay model (Helwany 2007)..... 61

Figure 4.11 Hardening behavior of the MCCM (Zaman, Gioda and Booker 2000) 62

Figure 4.12 Softening behavior of the MCCM (Zaman, Gioda and Booker 2000)..... 62

Figure 5.1 Typical longitudinal cross section of a bridge..... 68

Figure 5.2 Simulated example of longitudinal soil deformation behind bridge abutment 70

Figure 5.3 Layout of the two-dimensional transverse model 72
Figure 5.4 Boundary condition of the Two-Dimensional transverse model..... 73
Figure 5.5 Geometry of the settlement problem 76
Figure 5.6 Boundary condition of the settlement problem 77
Figure 5.7 Finite element mesh of the comparison model..... 78
Figure 5.8 Vertical deformation contour at the end of the analysis (MCCM) (*ft*)..... 79
Figure 5.9 Deformed mesh at the end of the analysis (MDPCM) (*ft*) 79
Figure 5.10 Simulated vs. Analytical settlement history of the clay layer 80
Figure 5.11 Soil profile at Clinton bridge site (Laguros et al. 1991)..... 81
Figure 5.12 Finite element discretization of the simulated soil at Clinton bridge site 83
Figure 5.13 Vertical deformation contour at the end of the analysis (*ft*)..... 83
Figure 5.14 Excess pore pressure contour at the end of the analysis (*psf*) 83
Figure 5.15 Simulated surface settlement profile of the natural soil 84
Figure 5.16 Simulated surface settlement profile of the embankment fill..... 85
Figure 5.17 Simulated excess pore pressure history..... 86
Figure 5.18 Vertical deformation contour of analysis No.1 (*ft*) 87
Figure 5.19 Vertical deformation contour of analysis No.2 (*ft*) 87
Figure 5.20 Vertical deformation contour of analysis No.3 (*ft*) 88
Figure 5.21 Vertical deformation contour of analysis No.4 (*ft*) 88
Figure 5.22 Vertical deformation contour of analysis No.5 (*ft*) 88
Figure 5.23 Vertical deformation contour of analysis No.6 (*ft*) 88
Figure 5.24 Simulated surface settlement at the center of the embankment fill..... 89
Figure 5.25 Element used to simulate the soil 90

Figure 5.26 Simulated surface settlement at the center of the embankment fill with respect to element size 91
Figure 5.27 Finite element discretization of the two-dimensional transverse model 94
Figure 5.28 Surface settlement at the center of the embankment fill of the Two-Dimensional transverse model 94
Figure 5.29 Simulated excess pore pressure history with H_e = 10 *ft* (3.0 *m*) 96
Figure 5.30 Simulated excess pore pressure history with H_e = 20 *ft* (6.1 *m*) 96
Figure 5.31 Simulated excess pore pressure history with H_e = 30 *ft* (9.1 *m*) 97
Figure 5.32 Two-dimensional longitudinal model layout 98
Figure 5.33 Layout of the two-dimensional longitudinal model with wall abutment 99
Figure 5.34 Layout of the two-dimensional longitudinal model with stub abutment 100
Figure 5.35 Abutment wall and approach slab boundary conditions 100
Figure 5.36 Boundary condition used for the longitudinal verification FEM 104
Figure 5.37 Finite element discretization of the longitudinal direction at Clinton bridge site ... 105
Figure 5.38 Vertical deformation contour at the end of the analysis (*ft*) 105
Figure 5.39 Excess pore pressure contour at the end of the analysis (*psf*) 105
Figure 5.40 Simulated longitudinal settlement profiles at Clinton bridge-site 106
Figure 5.41 Simulated excess pore pressure history 107
Figure 5.42 Layout of the initial model (wall abutment) 108
Figure 5.43 Vertical deformation contour of analysis No.1 (*ft*) (H_a=H_e) 109
Figure 5.44 Vertical deformation contour of analysis No.2 (*ft*) (H_a=H_e) 109
Figure 5.45 Vertical deformation contour of analysis No.1 (*ft*) (H_a=10 *ft*) 110
Figure 5.46 Vertical deformation contour of analysis No.2 (*ft*) (H_a=10 *ft*) 110

Figure 5.47 Vertical deformation contour of analysis No.1 (*ft*) (H_a=5 *ft*) 110

Figure 5.48 Vertical deformation contour of analysis No.2 (*ft*) (H_a=5 *ft*) 110

Figure 5.49 Simulated slope of the approach slab (H_a=H_e=30 *ft*) 111

Figure 5.50 Simulated slope of the approach slab (H_a=10 *ft*) 111

Figure 5.51 Simulated slope of the approach slab (H_a=5 *ft*) 112

Figure 5.52 Element type used for (a) soil (b) concrete 113

Figure 5.53 Simulated differential settlement of approach slab with respect to element size 115

Figure 5.54 Finite element discretization of the two-dimensional longitudinal model 118

Figure 5.55 Simulated slope of the approach slab for soil profile No.1 119

Figure 5.56 Simulated slope of the approach slab for soil profile No.2 119

Figure 5.57 Simulated slope of the approach slab for soil profile No.3 120

Figure 5.58 Simulated slope of the approach slab for soil profile No.4 120

Figure 5.59 Simulated slope of the approach slab for soil profile No.5 121

Figure 5.60 Simulated slope of the approach slab for soil profile No.6 121

Figure 5.61 Simulated slope of the approach slab for soil profile No.7 122

Figure 5.62 Simulated slope of the approach slab for soil profile No.8 122

Figure 5.63 Simulated slope of the approach slab for soil profile No.9 123

Figure 5.64 Simulated longitudinal soil settlement profile for soil profile No.1 124

Figure 5.65 Simulated longitudinal soil settlement profile for soil profile No.2 124

Figure 5.66 Simulated longitudinal soil settlement profile for soil profile No.3 125

Figure 5.67 Simulated longitudinal soil settlement profile for soil profile No.4 125

Figure 5.68 Simulated longitudinal soil settlement profile for soil profile No.5 126

Figure 5.69 Simulated longitudinal soil settlement profile for soil profile No.6 126

Figure 5.70 Simulated longitudinal soil settlement profile for soil profile No.7 127

Figure 5.71 Simulated longitudinal soil settlement profile for soil profile No.8 127

Figure 5.72 Simulated longitudinal soil settlement profile for soil profile No.9 128

Figure 5.73 Various functions fitted to the soil deflection profile behind bridge abutment 129

Figure 5.74 Standard logistic sigmoid function 130

Figure 5.75 Calculation of (a) using a vertical strip (longitudinal-direction) 137

Figure 5.76 Calculation of (a) a_e and (b) a_n 138

Figure 5.77 Scatter plot between total volumetric strain and settlement component (a_e) 140

Figure 5.78 Scatter plot between total volumetric strain and settlement component (a_n) 141

Figure 5.79 Simulated versus predicted a 143

Figure 5.80 Layout of the transverse simulation (additional fill) 144

Figure 5.81 Vertical deformation contour (transverse direction) of soil profile No.1 (*ft*) 145

Figure 5.82 Vertical deformation contour (transverse direction) of soil profile No.1 with additional fill (*ft*) 145

Figure 5.83 Vertical deformation contour (longitudinal direction) of soil profile No.1 (analysis#3) (*ft*) 145

Figure 5.84 Simulated versus predicted (a) 147

Figure 5.85 Scatter Plot between parameter (b) and ($C_c \times H_a / H_e$) 148

Figure 5.86 Simulated versus predicted b 150

Figure 5.87 Scatter plot between parameter a and c 151

Figure 5.88 Simulated versus predicted c 153

Figure 5.89 Finite element discretization of the case study model 154

Figure 5.90 Deformed mesh at the end of the analysis (*ft*) 154

Figure 5.91 Distribution of excess pore pressure at the end of the analysis (*psf*)..... 155

Figure 5.92 Simulated versus predicted soil settlement profile for the case study..... 155

Figure 6.1 Managing approach slab differential settlement..... 158

Figure 6.2 Schematic of the proposed pile supported approach slab segments..... 160

Figure 6.3 Distribution of pile axial load (a) skin friction and end-bearing without downdrag (b) skin friction without end-bearing and downdrag (c) skin friction, end-bearing and downdrag (d) end-bearing and downdrag..... 165

Figure 6.4 Top view of pile-soil model 169

Figure 6.5 Cross section of the single pile-soil model (a) without granular backfill (b) with granular backfill..... 169

Figure 6.6 Boundary condition of the pile-soil model (top view) 171

Figure 6.7 Boundary condition of the single pile-soil model with or without the backfill layer (vertical section)..... 171

Figure 6.8 Vertical deformation contour at the end of the analysis (*ft*)..... 176

Figure 6.9 Excess pore pressure contour at the end of the analysis (*psf*) 176

Figure 6.10 Simulated pile load-settlement curve 177

Figure 6.11 Finite element discretization of the single pile-soil model (No backfill)..... 180

Figure 6.12 Finite element discretization of the single pile-soil model (with backfill)..... 180

Figure 6.13 Pile head settlement for D_p=18 in (460 *mm*) 183

Figure 6.14 Pile head settlement for D_p=12 in (305 *mm*) 183

Figure 6.15 Pile head settlement for D_p=6 in (152 *mm*) 184

Figure 6.16 Pile settlement design chart for $H_b/H_f = 0.0$ 185

Figure 6.17 Pile settlement design chart for $H_b/H_f = 0.40$ 185

Figure 6.18 Pile settlement design chart for $H_b/H_f = 0.80$ 186

Figure 6.19 Axial force distribution in pile with D_p=18 in (460 *mm*), L_p=35 *ft* (10.7 *m*), and H_b/H_f=0 187

Figure 6.20 Axial force distribution in pile with D_p=18 in (460 *mm*), L_p=45 *ft* (13.7 *m*), and H_b/H_f=0 187

Figure 6.21 Axial force distribution in pile with D_p=18 in (460 *mm*), L_p=55 *ft* (16.8 *m*), and H_b/H_f=0 188

Figure 6.22 Axial force distribution in pile with D_p=18 in (460 *mm*), L_p=35 *ft* (10.7 *m*), and H_b/H_f=0.40 188

Figure 6.23 Axial force distribution in pile with D_p=18 in (460 *mm*), L_p=45 *ft* (13.7 *m*), and H_b/H_f=0.40 189

Figure 6.24 Axial force distribution in pile with D_p=18 in (460 *mm*), L_p=55 *ft* (16.8 *m*), and H_b/H_f=0.40 189

Figure 6.25 Axial force distribution in pile with D_p=18 in (460 *mm*), L_p=35 *ft* (10.7 *m*), and H_b/H_f=0.80 190

Figure 6.26 Axial force distribution in pile with D_p=18 in (460 *mm*), L_p=45 *ft* (13.7 *m*), and H_b/H_f=0.80 190

Figure 6.27 Axial force distribution in pile with D_p=18 in (460 *mm*), L_p=55 *ft* (16.8 *m*), and H_b/H_f=0.80 191

Figure 6.28 Axial force distribution in pile with D_p=12 in (305 *mm*), L_p=35 *ft* (10.7 *m*), and H_b/H_f=0.0 191

Figure 6.29 Axial force distribution in pile with D_p=12 in (305 *mm*), L_p=45 *ft* (13.7 *m*), and H_b/H_f=0.0 192

Figure 6.30 Axial force distribution in pile with D_p=12 in (305 *mm*), L_p=55 *ft* (16.8 *m*), and H_b/H_f=0.0 192

Figure 6.31 Axial force distribution in pile with D_p=12 in (305 *mm*), L_p=35 *ft* (10.7 *m*), and H_b/H_f=0.40 193

Figure 6.32 Axial force distribution in pile with D_p=12 in (305 *mm*), L_p=45 *ft* (13.7 *m*), and H_b/H_f=0.40 193

Figure 6.33 Axial force distribution in pile with D_p=12 in (305 *mm*), L_p=35 *ft* (16.8 *m*), and H_b/H_f=0.40 194

Figure 6.34 Axial force distribution in pile with D_p=12 in (305 *mm*), L_p=35 *ft* (10.7 *m*), and H_b/H_f=0.80 194

Figure 6.35 Axial force distribution in pile with D_p=12 in (305 *mm*), L_p=45 *ft* (13.7 *m*), and H_b/H_f=0.80 195

Figure 6.36 Axial force distribution in pile with D_p=12 in (305 *mm*), L_p=55 *ft* (16.8 *m*), and H_b/H_f=0.80 195

Figure 6.37 Axial force distribution in pile with D_p=6 in (152 *mm*), L_p=35 *ft* (10.7 *m*), and H_b/H_f=0.0 196

Figure 6.38 Axial force distribution in pile with D_p=6 in (152 *mm*), L_p=45 *ft* (13.7 *m*), and H_b/H_f=0.0 196

Figure 6.39 Axial force distribution in pile with D_p=6 in (152 *mm*), L_p=55 *ft* (16.8 *m*), and H_b/H_f=0.0 197

Figure 6.40 Axial force distribution in pile with D_p=6 in (152 *mm*), L_p=35 *ft* (10.7 *m*), and H_b/H_f=0.40 197

Figure 6.41 Axial force distribution in pile with D_p=6 in (152 *mm*), L_p=45 *ft* (13.7 *m*), and H_b/H_f=0.40 198

Figure 6.42 Axial force distribution in pile with D_p=6 in (152 *mm*), L_p=45 *ft* (13.7 *m*), and H_b/H_f=0.40 198

Figure 6.43 Axial force distribution in pile with D_p=6 in (152 *mm*), L_p=35 *ft* (10.7 *m*), and H_b/H_f=0.80 199

Figure 6.44 Axial force distribution in pile with D_p=6 in (152 *mm*), L_p=45 *ft* (13.7 *m*), and H_b/H_f=0.80 199

Figure 6.45 Axial force distribution in pile with D_p=6 in (152 *mm*), L_p=55 *ft* (16.8 *m*), and H_b/H_f=0.80 200

Figure 6.46 Location of L_{dd} with respect to Q 201

Figure 6.47 Location of L_{dd} with respect to L_p 201

Figure 6.48 Axial force distribution with respect to (H_b/H_f) 202

Figure 6.49 Vertical soil deformation contour with respect to pile-soil influence zone (a) D_p = 18 *in* (b) D_p = 6 *in* 203

Figure 6.50 Simulated versus predicted pile head settlement 207

Figure 6.51 Simulated versus predicted Q_{dd} 208

Figure 6.52 Simulated versus predicted (Q_{ps}) 209

Figure 6.53 Simulated versus predicted L_{dd} 210

Figure 6.54 Normalized/Idealized pile load with D_p=18 in (460 *mm*), L_p=35 *ft* (10.7 *m*), and H_b/H_f=0 211

Figure 6.55 Normalized/Idealized pile load with D_p=18 in (460 *mm*), L_p=45 *ft* (13.7 *m*), and H_b/H_f=0 211

Figure 6.56 Normalized/Idealized pile load with D_p=18 in (460 *mm*), L_p=55 *ft* (16.8 *m*), and H_b/H_f=0 212

Figure 6.57 Normalized/Idealized pile load with D_p=18 in (460 *mm*), L_p=35 *ft* (10.7 *m*), and H_b/H_f=0.40 212

Figure 6.58 Normalized/Idealized pile load with D_p=18 in (460 *mm*), L_p=45 *ft* (13.7 *m*), and H_b/H_f=0.40 213

Figure 6.59 Normalized/Idealized pile load with D_p=18 in (460 *mm*), L_p=55 *ft* (16.8 *m*), and H_b/H_f=0.40 213

Figure 6.60 Normalized/Idealized pile load with D_p=18 in (460 *mm*), L_p=35 *ft* (10.7 *m*), and H_b/H_f=0.80 214

Figure 6.61 Normalized/Idealized pile load with D_p=18 in (460 *mm*), L_p=45 *ft* (13.7 *m*), and H_b/H_f=0.80 214

Figure 6.62 Normalized/Idealized pile load with D_p=18 in (460 *mm*), L_p=55 *ft* (16.8 *m*), and H_b/H_f=0.80 215

Figure 6.63 Normalized/Idealized pile load with D_p=12 in (305 *mm*), L_p=35 *ft* (10.7 *m*), and H_b/H_f=0.0 215

Figure 6.64 Normalized/Idealized pile load with D_p=12 in (305 *mm*), L_p=45 *ft* (13.7 *m*), and H_b/H_f=0.0 216

Figure 6.65 Normalized/Idealized pile load with D_p=12 in (305 *mm*), L_p=55 *ft* (16.8 *m*), and H_b/H_f=0.0 216

Figure 6.66 Normalized/Idealized pile load with D_p=12 in (305 *mm*), L_p=35 *ft* (10.7 *m*), and H_b/H_f=0.40 217

Figure 6.67 Normalized/Idealized pile load with D_p=12 in (305 *mm*), L_p=45 *ft* (13.7 *m*), and H_b/H_f=0.40 217

Figure 6.68 Normalized/Idealized pile load with D_p=12 in (305 *mm*), L_p=55 *ft* (16.8 *m*), and H_b/H_f=0.40 218

Figure 6.69 Normalized/Idealized pile load with D_p=12 in (305 *mm*), L_p=35 *ft* (10.7 *m*), and H_b/H_f=0.80 218

Figure 6.70 Normalized/Idealized pile load with D_p=12 in (305 *mm*), L_p=45 *ft* (13.7 *m*), and H_b/H_f=0.80 219

Figure 6.71 Normalized/Idealized pile load with D_p=12 in (305 *mm*), L_p=55 *ft* (16.8 *m*), and H_b/H_f=0.80 219

Figure 6.72 Normalized/Idealized pile load with D_p=6 in (152 *mm*), L_p=35 *ft* (10.7 *m*), and H_b/H_f=0.0 220

Figure 6.73 Normalized/Idealized pile load with D_p=6 in (152 *mm*), L_p=45 *ft* (13.7 *m*), and H_b/H_f=0.0 220

Figure 6.74 Normalized/Idealized pile load with D_p=6 in (152 *mm*), L_p=55 *ft* (16.8 *m*), and H_b/H_f=0.0 221

Figure 6.75 Normalized/Idealized pile load with D_p=6 in (152 *mm*), L_p=35 *ft* (10.7 *m*), and H_b/H_f=0.40 221

Figure 6.76 Normalized/Idealized pile load with D_p=6 in (152 *mm*), L_p=45 *ft* (13.7 *m*), and H_b/H_f=0.40 222

Figure 6.77 Normalized/Idealized pile load with D_p=6 in (152 *mm*), L_p=55 *ft* (16.8 *m*), and H_b/H_f=0.40 222

Figure 6.78 Normalized/Idealized pile load with D_p=6 in (152 *mm*), L_p=35 *ft* (10.7 *m*), and H_b/H_f=0.80 223

Figure 6.79 Normalized/Idealized pile load with D_p=6 in (152 *mm*), L_p=45 *ft* (13.7 *m*), and H_b/H_f=0.80 223

Figure 6.80 Normalized/Idealized pile load with D_p=6 in (152 *mm*), L_p=55 *ft* (16.8 *m*), and H_b/H_f=0.80 224

Figure 6.81 Development of axial load distribution in pile 226

Figure 6.82 Simulated versus predicted Q_{dd} 230

Figure 6.83 Simulated versus predicted L_{dd} 230

Figure 6.84 Simulated versus predicted Q_b 234

Figure 6.85 Simulated versus predicted Q_{ps} 234

Figure 7.1 Longitudinal cross section of the full-scale model 238

Figure 7.2 Transverse cross section of the full-scale model 239

Figure 7.3 Finite element discretization of the full-scale model 239

Figure 7.4 Vertical deformation contour of the full-scale simulation (*ft*) 240

Figure 7.5 Excess pore pressure contour of the full-scale simulation (*psf*) 240

Figure 7.6 Simulated longitudinal soil settlement profile of the full-scale model 241

Figure 7.7 Simulated transition profile of the full-scale model 242

Figure 7.8 Determination of pile size and length 243

Figure 7.9 Longitudinal cross section of the proposed two-segment pile-supported approach slabs 244

Figure 7.10 Transverse cross section of the proposed two-segment pile-supported approach slabs 245

Figure 7.11 Finite element discretization of the full-scale with two-segment pile-supported approach slabs 245
Figure 7.12 Finite element discretization of piles and cap (a) $S_{e\text{-}p} = 8\ ft$ (b) $S_{e\text{-}p} = 4.5\ ft$ (c) No edge-pile 246
Figure 7.13 Vertical deformation contour of the full-scale model with two-segment pile-supported approach slabs (*ft*) 247
Figure 7.14 Excess pore pressure contour of the full-scale model with two-segment pile-supported approach slabs (*psf*) 247
Figure 7.15 Simulated transition profile of the full-scale model with two-segment pile-supported approach slabs 248
Figure 7.16 Axial load distribution in piles with $S_{e\text{-}p} = 8\ ft$ 249
Figure 7.17 Axial load distribution in piles with $S_{e\text{-}p} = 4.5\ ft$ 249
Figure 7.18 Axial load distribution in piles with no edge-pile 250
Figure 7.19 Pile heads settlement in the transverse direction 250
Figure 7.20 Detailed connection between various approach slab segments 252
Figure 8.1 Bump formation mechanism at the end of the bridge 253
Figure 8.2 Schematic of the proposed multi-segment pile-supported approach slab system 258
Figure 8.3 Detailed connection between various approach slab segments 260

LIST OF TABLES

Table 2.1 Proposed IRIS rating for approach slab (Bakeer, Shutt, et al. 2005) 8

Table 2.2 The significance of the bump at the end of the bridge (Hoppe 1999) 10

Table 2.3 Recommended practices to maintain low maintenance cost (Dupont and Allen 2002) 11

Table 3.1 DOTs preference of approach slab 37

Table 3.2 Approach slab/pavement end support type 40

Table 3.3 Approach slab/Pavement end configuration with skewed bridges 42

Table 3.4 Approach slab connection mechanism to the superstructure 44

Table 3.5 Length of the approach slab using equation-based criterion 46

Table 3.6 Approach slab dimensions 48

Table 3.7 Embankment and backfill consideration 50

Table 4.1 Description of the simulation used in this study 51

Table 4.2 Material parameters used for the structural components 63

Table 4.3 Typical coefficients of permeability (k) for various types of soil (Carter and Bentley 2016) 65

Table 4.4 Soil properties used for the natural soil layer 65

Table 4.5 Soil properties used for the embankment fill layer 66

Table 4.6 Soil properties used for the backfill soil layer 66

Table 4.7 Input parameters used to simulate the soils 67

Table 5.1 Input parameters used to simulate the soils 78

Table 5.2 Input parameters used to simulate the soil at Clinton bridge site 82

Table 5.3 Parameters range used in the initial model simulation 87

Table 5.4 Size and number of the elements used in the analysis 91

Table 5.5 Two-Dimensional transverse model parametric study matrix 92

Table 5.6 Range of parameters used in the simulation 93

Table 5.7 Parameters range used in the initial model 109

Table 5.8 Size and number of the elements used in the analysis 114

Table 5.9 Two-Dimensional longitudinal model parametric study matrix 116

Table 5.10 Soil profiles considered in the longitudinal model parametric study 117

Table 5.11 Range of parameters used in accordance with each soil profile (refer to Table 5.10) 117

Table 5.12 Logistic function parameters that best fit simulated soil deflection profile (soil profile No.1) 131

Table 5.13 Logistic function parameters that best fit simulated soil deflection profile (soil profile No.2) 132

Table 5.14 Logistic function parameters that best fit simulated soil deflection profile (soil profile No.3) 132

Table 5.15 Logistic function parameters that best fit simulated soil deflection profile (soil profile No.4) 132

Table 5.16 Logistic function parameters that best fit simulated soil deflection profile (soil profile No.5) 133

Table 5.17 Logistic function parameters that best fit simulated soil deflection profile (soil profile No.6) 133

Table 5.18 Logistic function parameters that best fit simulated soil deflection profile (soil profile No.7) 133

Table 5.19 Logistic function parameters that best fit simulated soil deflection profile (soil profile No.8) 134
Table 5.20 Logistic function parameters that best fit simulated soil deflection profile (soil profile No.9) 134
Table 5.21 Pearson's correlation coefficient among logistic function parameters 135
Table 5.22 Decomposition of the simulated ultimate settlement a 135
Table 5.23 Pearson's correlation coefficient between logistic function parameters and backfill soil properties 136
Table 5.24 Pearson's correlation coefficient between logistic function parameters and embankment soil properties 136
Table 5.25 Pearson's correlation coefficient between logistic function parameters and natural soil properties 136
Table 5.26 Correlation coefficient between logistic function parameters and geometric parameters 136
Table 5.27 Pearson's correlation coefficient between a_n and a_e with volumetric elastic and plastic deformation 139
Table 5.28 Regression parameters of the ultimate settlement components (a_n) and (a_e). 142
Table 5.29 Regression parameters of the logarithmic function 149
Table 5.30 Regression parameters for the exponential relationship 152
Table 5.31 Level of strain at the middle of each layer 156
Table 5.32 Summary of the developed equation 157
Table 6.1 Element size versus simulated Δ_{PH} 175
Table 6.2 Parametric study matrix for the single pile-soil model 177

Table 6.3 Range of parameters tested in accordance with D_p 179

Table 6.4 Pile load carrying capacity 181

Table 6.5 Pearson's correlation coefficient between Δ_{PH} and various pile geometry, loading and soil parameters 204

Table 6.6 Regression parameters values for equation 6-8 206

Table 6.7 Estimated $Ldd@Qdd = 0$ versus predicted L_{dd} 231

Table 6.8 Summary of the developed pile head settlement/load distribution equations 236

Table 8.1 Summary of the developed equation of longitudinal settlement profile parameters .. 255

Table 8.2 Summary of the developed pile head settlement/load distribution equations 256

Table A.1 Summary of the resulting slope of the approach slab for soil profile No.1 268

Table A.2 Summary of the resulting slope of the approach slab for soil profile No.2 269

Table A.3 Summary of the resulting slope of the approach slab for soil profile No.3 269

Table A.4 Summary of the resulting slope of the approach slab for soil profile No.4 270

Table A.5 Summary of the resulting slope of the approach slab for soil profile No.5 270

Table A.6 Summary of the resulting slope of the approach slab for soil profile No.6 271

Table A.7 Summary of the resulting slope of the approach slab for soil profile No.7 271

Table A.8 Summary of the resulting slope of the approach slab for soil profile No.8 272

Table A.9 Summary of the resulting slope of the approach slab for soil profile No.9 272

Table B.1 Longitudinal soil settlement profile behind bridge abutment (Soil profile No.1, Analysis No.1) 273

Table B.2 Longitudinal soil settlement profile behind bridge abutment (Soil profile No.1, Analysis No.12) 274

Table B.3 Longitudinal soil settlement profile behind bridge abutment (Soil profile No.2, Analysis No.1) 275
Table B.4 Longitudinal soil settlement profile behind bridge abutment (Soil profile No.2, Analysis No.12) 276
Table B.5 Longitudinal soil settlement profile behind bridge abutment (Soil profile No.3, Analysis No.1) 277
Table B.6 Longitudinal soil settlement profile behind bridge abutment (Soil profile No.3, Analysis No.12) 278
Table B.7 Longitudinal soil settlement profile behind bridge abutment (Soil profile No.4, Analysis No.1) 279
Table B.8 Longitudinal soil settlement profile behind bridge abutment (Soil profile No.4, Analysis No.12) 280
Table B.9 Longitudinal soil settlement profile behind bridge abutment (Soil profile No.5, Analysis No.1) 281
Table B.10 Longitudinal soil settlement profile behind bridge abutment (Soil profile No.5, Analysis No.12) 282
Table B.11 Longitudinal soil settlement profile behind bridge abutment (Soil profile No.6, Analysis No.1) 283
Table B.12 Longitudinal soil settlement profile behind bridge abutment (Soil profile No.6, Analysis No.12) 284
Table B.13 Longitudinal soil settlement profile behind bridge abutment (Soil profile No.7, Analysis No.1) 285

Table B.14 Longitudinal soil settlement profile behind bridge abutment (Soil profile No.7, Analysis No.12) 286

Table B.15 Longitudinal soil settlement profile behind bridge abutment (Soil profile No.8, Analysis No.1) 287

Table B.16 Longitudinal soil settlement profile behind bridge abutment (Soil profile No.8, Analysis No.12) 288

Table B.17 Longitudinal soil settlement profile behind bridge abutment (Soil profile No.9, Analysis No.1) 289

Table B.18 Longitudinal soil settlement profile behind bridge abutment (Soil profile No.9, Analysis No.12) 290

Table C.1 Pile head settlement and load distribution along the pile [D_p = 18 *in* (458 *mm*), L_p = 35 *ft* (10.7 *m*)] 291

Table C.2 Pile head settlement and load distribution along the pile [D_p = 18 *in* (458 *mm*), L_p = 45 *ft* (13.7 *m*)] 292

Table C.3 Pile head settlement and load distribution along the pile [D_p = 18 *in* (458 *mm*), L_p = 55 *ft* (16.8 *m*)] 293

Table C.4 Pile head settlement and load distribution along the pile [D_p = 12 *in* (305 *mm*), L_p = 35 *ft* (10.7 *m*)] 294

Table C.5 Pile head settlement and load distribution along the pile [D_p = 12 *in* (305 *mm*), L_p = 45 *ft* (13.7 *m*)] 295

Table C.6 Pile head settlement and load distribution along the pile [D_p = 12 *in* (305 *mm*), L_p = 55 *ft* (16.8 *m*)] 296

Table C.7 Pile head settlement and load distribution along the pile [D_p = 6 *in* (152 *mm*), L_p = 35 *ft* (10.7 *m*)] 297

Table C.8 Pile head settlement and load distribution along the pile [D_p = 6 *in* (152 *mm*), L_p = 45 *ft* (13.7 *m*)] 297

Table C.9 Pile head settlement and load distribution along the pile [D_p = 6 *in* (152 *mm*), L_p = 55 *ft* (16.8 *m*)] 298

ACKNOWLEDGMENTS

It is a great pleasure to acknowledge my deepest appreciation to the persons who helped me throughout my Ph.D. I would like to express my sincere gratitude to my advisor Professor Habib Tabatabai for the valuable guidance and continuous support during the course of my Ph.D. study. It was a great honor to work under his supervision.

I would also like to thank Jazan University for the financial support throughout my graduate studies.

I am extremely grateful to my parents Zohair Bahumdain and Khadijah Henawi for their endless support and motivation. I am also very much thankful to my father-in-law Yahya Babair for the continuous support and constant encouragement. My completion of Ph.D. could not have been accomplished without their support.

Finally, I would especially like to thank my beloved wife Saliha Babair, to whom I am very much indebted, for her sacrifices, understanding, encouragement and invaluable support during my Ph.D. journey.

CHAPTER 1 - INTRODUCTION

1.1 Background

Reliability and long-term durability of bridge structures is of utmost importance (Nabizadeh, Tabatabai and Tabatabai 2018, Tabatabai, Nabizadeh and Tabatabai 2018, Tabatabai and Nabizadeh 2018). The bridge approach slab is part of a transition system in which the end of the bridge is connected to the roadway pavement (Figure 1.1). Its function is to carry traffic loads and provide drivers with a smooth ride as their vehicle travels from the roadway to the bridge and vice versa (Abu-Farsakh and Chen 2014).

Due to settlement of embankment fill and natural soil, a bump (or bumps) can develop at the ends of the bridge. These bumps are a well-known problem occurring nationwide. They affect about 25% of the bridges in the United States, resulting in an estimated $100 million per year in maintenance expenditures (Briaud, James and Hoffman 1997). The bump at the end of the bridge can lead to unsafe driving conditions, vehicle damage, and additional maintenance cost. Furthermore, distress, fatigue, and deterioration of the bridge deck and expansion joints are possible consequences of such a problem (Briaud, James and Hoffman 1997, Hu, et al. 1979, Nicks 2015).

Besides soil settlement, several other factors have been reported to influence the formation of the bump at the ends of the bridge. These include improper design of the approach slab (length and thickness), abutment type, skewness of the bridge, traffic volume, construction method, and loss of the backfill material due to erosion.

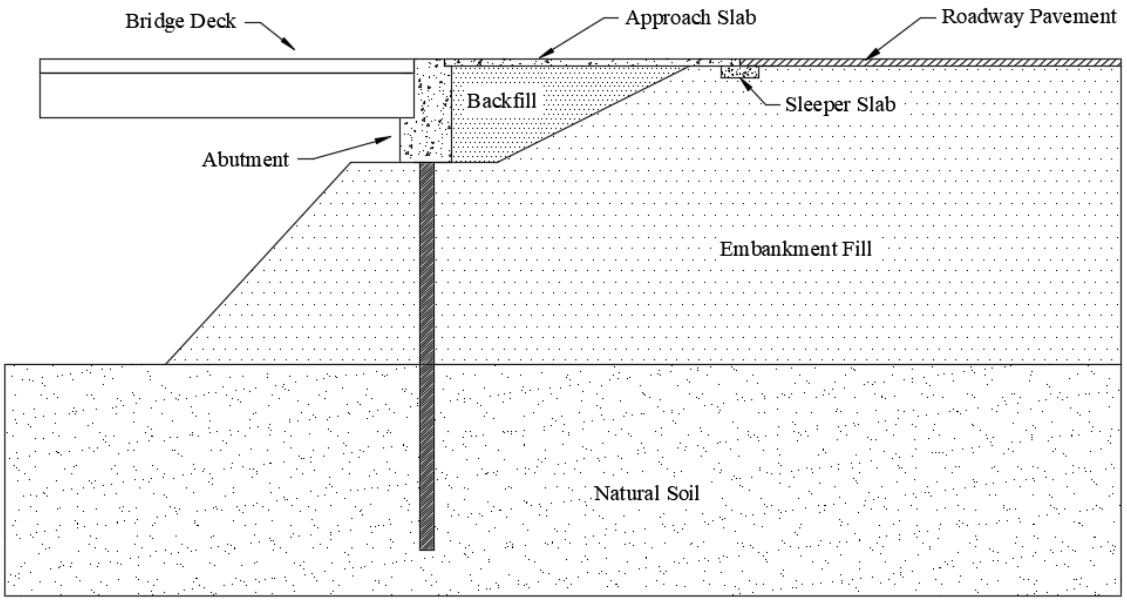

Figure 1.1 Typical longitudinal cross section of a bridge.

1.2 Problem statement

The common bump at the ends of bridges is considered an important bridge management issue, because it could lead to costly and frequent maintenance operations to bring the problem under control. Examples of needed maintenance operations include leveling, mudjacking, building an approach slab (if not used originally), repair or replacement of the approach slab, drainage repairs, and implementation of soil improvement techniques. Repetitive maintenance operation could negatively impact the travelling public, especially when lane closures are required. The average cost of such maintenance operations has been estimated to be $2,000 per year per bridge (Briaud, James and Hoffman 1997, Dupont and Allen 2002).

As soil underneath the approach slab settles, deferential settlement develops and affects the riding quality as well as the structural integrity of the bridge system. As a result, two bumps could develop at the end of the bridge; at the approach slab/ bridge joint, and at the approach slab/ pavement interface, (Figure 1.2). The development of the bumps is attributed to the change

in slope between the bridge and approach slab (φ_1) and between approach slab and pavement (φ_2) (Abu-Farsakh and Chen 2014).

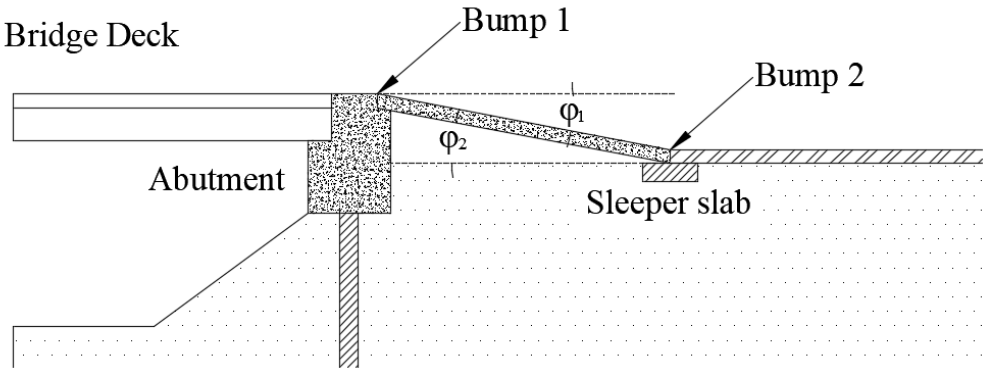

Figure 1.2 Bump formation at the end of the bridge

Historically, the use of approach slab has been a way to significantly reduce, but not eliminate, the bump at the end of the bridge. The approach slab covers the problematic area of approximately 20-40 *ft* (6.1-12.2 *m*) from the bridge abutment. In addition, it provides a smooth grade transition for drivers, reduces vehicle impact on the bridge, and prevents direct water infiltration behind the abutment wall (Briaud, James and Hoffman 1997). Therefore, many researchers believe that proper design of the approach slab could permanently solve the bump problem.

1.3 Objectives and Scope of work

This study is aimed at mitigating the formation of bumps at the ends of the bridge by introducing a new design concept for the approach slab. The proposed design takes advantage of settlement-reducing piles to control settlement in multi-segment approach slabs. These pile elements are intended to control the roughness of the transition such that acceptable slope changes develop between various segments of the approach slab and thus improve the performance of the approach slab system. It is hoped that the new design would lessen the need

for repetitive maintenance operations and thus lessen maintenance costs. Ultimately, the new design may offer an effective design approach to limit the impact of any bump formations to acceptable levels.

The proposed work plan to achieve to the objectives of this research includes the following tasks:

1- Conduct comprehensive literature review of previous work to collect information regarding the causes and mitigation techniques regarding bump formation at the ends of the bridge.
2- Examine state practices related to the design and construction of the approach slabs and approach areas. These include the preferred methods and configuration of the approach slab, backfill and embankment fill.
3- Develop soil-structure finite element models that could predict soil settlement behind bridge abutments. This includes:
    a. Conducting verification analyses to compare field-measured soil settlements with the developed finite element model.
    b. Developing two baseline finite element models to examine several aspects related to the construction of the bridge approach areas, and to assess the severity of the bump at the end of the bridge under various soil conditions. These aspects include the natural soil type and height, embankment soil type and height, side slope of embankment fill, backfill soil compaction level, slope of backfill area, erosion of backfill material, abutment type, and length of approach slab.

c. Developing relationships to evaluate the long-term soil settlement profile along a longitudinal line behind the bridge abutment.

4- Develop a soil-structure finite element model that could predict pile head settlement for various pile-soil conditions. These include the length and size of pile, type and height of backfill layer, type and height of embankment soil, and type and height of natural soil. Only cast-in-place concrete piles were considered. Additionally:

   a. Develop relationships to evaluate pile head settlement and pile load distribution under various pile-soil conditions.

   b. Develop criteria to select size, spacing, and length of piles to achieve acceptable transition between the bridge and the roadway.

   c. Develop procedures to achieve the desired transition profile using multi-segment pile-supported approach slabs.

5- Verify the developed procedures and relationships using a full-scale finite element model. This include the prediction of the longitudinal soil settlement profile, pile head settlement, and differential settlement of the approach slab.

6- Propose design recommendations to control the settlement-induced bumps at the ends of bridges by limiting slope changes to acceptable levels under varying soil conditions.

1.4 Outline of Dissertation

Chapter 1 presents background of the problems associated with bridge approach slabs, problem statement, research objectives, and scope of work.

Chapter 2 presents a review of previous works related to the definition, causes and mitigation techniques for bump formation at the ends of the bridge. This chapter also reviews previous work related to the optimum approach slab configuration.

Chapter 3 examines state practices regarding the approach slabs and approach areas. These include the preferred methods and configurations of the approach slab, backfill and embankment fill.

Chapter 4 discusses the general aspects of the development of finite element models used in this research. These include geometry and boundary conditions, contact behavior at soil-structure interfaces, analysis procedures, and material properties.

Chapter 5 presents simulation results for the soil settlement profiles behind bridge abutments in longitudinal and transverse directions. Empirical relationships for predicting settlements are also provided in this chapter.

Chapter 6 presents simulation results for the pile head settlement and axial load distribution along the piles. Empirical relationships and design charts for predicting pile head settlements are provided in this chapter. In addition, proposed procedures and recommendations for the design multi-segment pile-supported bridge approach slabs are provided in this chapter.

Chapter 7 presents an overall assessment of the developed procedures and design charts using a full-scale simulation of a multi-segment pile-supported bridge approach slab system.

Chapter 8 provides summary and conclusions of the work conducted in this study, and provides recommendations for future research.

CHAPTER 2 - LITERATURE REVIEW

2.1 Definition of the bump

Two bumps could develop at the end of the bridge: one at the approach slab/bridge joint, and the other at the approach slab/pavement interface, (Figure 1.2). These bumps can be attributed to changes in slope between the bridge and approach slab (φ_1) and between approach slab and pavement (φ_2) (Abu-Farsakh and Chen 2014).

The severity of the bump is mainly controlled by the amount of the differential settlement of the approach slab. The differential settlement could be assessed using several methods. These include the relative elevation, slope change, and the International Roughness Index (IRI) (Puppala, et al. 2008).

The relative elevation is defined as the absolute vertical difference between the two ends of the approach slab. In a survey of bridge movements, Walkinshaw (1978) noted that bridge approaches with differential settlement of greater than or equal to 2.5 *in* (64 *mm*) were considered annoyance to drivers. Long et al. (1999) conducted a survey of 1,181 bridges in Illinois to assess the severity of the bump. The survey revealed that bridges with differential settlement of 2-3 *in* (50-75 *mm*) were considered a significant issue from a rideability standpoint.

The slope change is typically referred to the rate of settlement between the bridge and the roadway pavement. This rate can be expressed in terms of differential settlement between the two ends of the approach slab divided by the length of the approach slab (slope of the approach slab) (Figure 2.1). Long et al. (1999) concluded that a slope of 1/125 to 1/100 is tolerable.

Greater slopes would be a riding discomfort to drivers and maintenance operations are required in such cases (Long, et al. 1999).

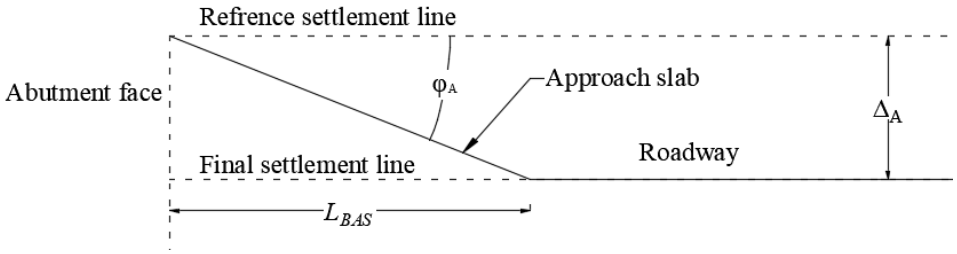

Figure 2.1 Slope of approach slab

The International Roughness Index (IRI) is a laser-profile-based pavement rating system that is often used to assess the riding quality over a given road section. The IRI was modified later to accommodate the approach slab (IRIS) with the ability to evaluate the ride quality along the approach slab (Bakeer, Shutt, et al. 2005). Table 2.1 shows typical IRIS rating values.

Table 2.1 Proposed IRIS rating for approach slab (Bakeer, Shutt, et al. 2005)

IRIS range *in/mile* (*mm/km*)	Approach slab rating
0.00 - 247 (0.00 – 3900)	Very good
254 - 500 (4000 – 7900)	Good
507 - 628 (8000 – 9900)	Fair
634 - 755 (10000 – 11900)	Poor
760 (12000) and greater	Very poor

Therefore, a differential settlement of up to 2.5 *in* (64 *mm*), slope change of 1/125, or an IRIS value of 500 *in/mile* (7900 *mm/km*) may be considered acceptable from a ride quality standpoint. These represent the maximum values allowed for the approach slab.

2.2 Maintenance considerations

The bump at the end of the bridge is considered a maintenance issue, since it may lead to maintenance operations to keep it within a tolerable limit. It is inevitable that settlement would take place underneath the approach slab over time. Therefore, bumps could develop and complications (such as rough driving conditions and deterioration of the bridge deck and/or

approach slab) may arise that require maintenance operations. Repair or replacement of the approach slab may be required in case of significant damage. Repetitive maintenance operations negatively impact the travelling public, especially when lane closures are required.

In recent years, several studies conducted surveys that aim to assess the significance of this problem as perceived by transportation agencies. The following is a review these studies.

In a survey of 758 bridge approach areas in Oklahoma, Laguros et al. (1990) reported that the bump at the end of the bridge affected about 83% of the bridges in Oklahoma. Another survey by Hoppe (1999), which included responses from 38 State Departments of Transportation (DOTs), concluded that 55% of the DOTs considered the bump as major maintenance problem. Table 2.2 shows the result of this survey. Dupont et al. (2002) conducted a survey of DOTs. In that survey, one question asked whether the bump at the end of the bridge was a major maintenance problem. The survey revealed that 48% of the DOTs considered it a major maintenance problem, 28% indicated that the bump was not an issue, and the remaining 24% indicated that it was an issue in some cases.

Table 2.2 The significance of the bump at the end of the bridge (Hoppe 1999)

State	Significance	State	Significance
AZ	Not significant	MO	Significant
CA	Significant	MT	Significant
CT	Moderate	ND	Significant
DE	Significant	NE	Significant
FL	Moderate	NH	Not Significant
GA	Significant	NJ	Moderate
ID	Significant	NM	Significant
IN	Moderate	NY	Moderate
IA	Moderate	OH	Moderate
IL	Significant	OK	Significant
KS	Significant	OR	Significant
KY	Significant	SC	Significant
LA	Significant	SD	Significant
MA	Moderate	TX	Not Significant
MD	Moderate	VT	Not Significant
ME	Not significant	VA	Moderate
MI	Moderate	WA	Significant
MN	Significant	WI	Significant
MS	Significant	WY	Not Significant

Typically, DOTs require biannual inspections of all bridges through which maintenance operations are recommended based on the findings. Examples of needed maintenance operations for the approach area include leveling, mudjacking, building an approach slab (if not used originally), improving drainage, and implementation of soil improvement techniques. The type of maintenance, frequency of repairs, and the type of materials and equipment needed are critical factors in the total maintenance cost during the lifetime of the bridge. The average maintenance cost for repairing the bump at the end of the bridge in the United States is on the order of $667 per year per bridge (1997 dollars) (Briaud, James and Hoffman 1997). Dupont and Allen (2002) conducted an evaluation of maintenance operations in the state of Kentucky. It was reported that repairing the bump at the end of bridge cost approximately $2000 per year per bridge. Furthermore, Dupont and Allen (2002) recommended several practices that aim to reduce the maintenance cost and formation of the bump. Table 2.3 summarizes those recommendations.

Table 2.3 Recommended practices to maintain low maintenance cost (Dupont and Allen 2002)

Recommended practice	How the bump is reduced?	Additional cost
Lowering of the approach slab	When settlement is not dominant, lowering the approach slab would help toward the periodic maintenance of applying asphalt cement overlaying.	Insignificant, a design consideration.
Surcharging prior construction	Applying surcharge allows the natural soil to undergo some of its total settlement before construction the approach fill.	Difficult to evaluate, need a good project plan.
Designing of a sufficient maintenance plan	Developing a good maintenance plan and keeping up with it has proven to minimize the occurrence of the bump.	Insignificant, need a well-designed plan.
Implement specifications for select embankment fill.	Utilizing a specific material for the approach fill will enhance the performance of the approach area.	May add some cost based upon the selected material.
Enhancing the drainage system	Improving the drainage will decrease erosion of the backfill soil.	Insignificant.
Require warranties on the bridge approach area	Contractors will provide better design alternatives and techniques to ensure better results.	Might be costly.
Leveling of the embankment slope	Reducing the side slope adds more resistance to the settlement and lateral movement in the embankment and natural soil.	Minimal, needs more filling material.
Improving the approach slab design	Improving the approach slab design/configuration would help in reducing the differential settlement between its two ends.	Insignificant, needs more concrete and steel.

It could be concluded from these studies that the bump at the end of the bridge is a significant maintenance issue in the United States, which requires substantial maintenance expenditures during the lifetime of the bridge. Therefore, any new approach slab concepts designed to overcome this problem could potentially reduce long-term maintenance costs for bridges.

2.3 Factors affecting the formation of the bump

Irick and Copas (1969), McLaren (1970), Wick and Stoelhorst (1982), Adrani (1987), and Karemer and Sajer (1991) identified the factors that contribute to the bump formation at the ends of the bridge. These include the consolidation of the natural soil and embankment fill, inadequate construction practices, poor drainage control systems, erosion of the backfill soil, traffic loading, and abutment type.

Laguros, Zaman, and Mahmood (1986) surveyed all state DOTs. The survey concluded that the types of the natural soil and embankment fill along with the construction method were the most significant factors affecting the formation of the bump at the ends of the bridge. Furthermore, it was noted that factors such as frost heave and freeze thaw cycles, lateral movement of the abutment, and abutment type influenced the bump formation. In a second phase of the same study, Laguros, Zaman, and Mahmood (1990) reported that the age of the approach area, type of the abutment, height of the embankment, drainage behind the abutment wall, traffic volume, and skewness of the bridge were among the factors that influenced the bump formation.

A synthesis study of 48 states, conducted by Briaud, James and Hoffman (1997), discussed various aspects related to the bump at the ends of the bridge. This study identified the most common factors that contribute to the formation of the bump. These factors include the height of the embankment, type of abutment foundation, natural soil profile, traffic volume, thermal expansion and contraction of the bridge, precipitation, and the side slope of the approach area. These factors and others are illustrated in Figure 2.2.

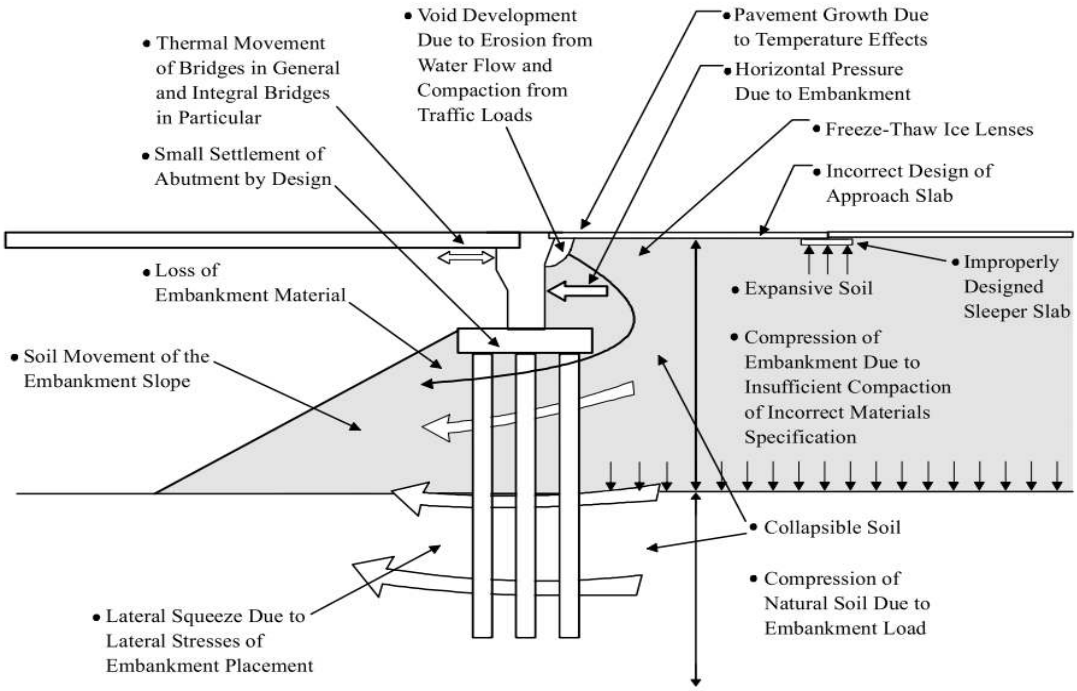

Figure 2.2 Factors influence the formation of the bump at the end of the bridge (Briaud, James and Hoffman 1997)

It could be concluded from the latter discussion that several factors are involved in the formation of the bump at the end of the bridge. The consolidation of the natural soil and embankment fill and loss of backfill material are among the significant factors that affect the differential settlement of the approach slab. Nevertheless, several other factors such as the height of the embankment, type of the abutment, approach slab design, traffic volume, drainage issues, and construction methods also influence the bump formation. Such factors should be considered when anticipating the total settlement underneath the approach slab.

2.3.1 Settlement of soil underneath approach area

In general, the weight of any soil layer or structure will impose stresses on the underlying soil layers. These stresses will eventually cause dimensional changes in the soil volume (decrease in volume) through which settlement of soil occurs.

Typically, settlement of soil consists of three different stages: initial settlement (immediate), primary compression settlement (consolidation), and secondary compression (creep). The total settlement can be evaluated as a summation of these components as follows:

$$S_t = S_I + S_P + S_S \quad \text{2-1}$$

Where

S_t = Total settlement at time (t).

S_i = Initial settlement.

S_p = Settlement due to primary compression (consolidation).

S_s = Settlement due to secondary compression (creep).

The initial settlement (S_i) takes place immediately after the load is applied on the soil mass. This is caused by shear strain and the decrease of void ratio between soil particles. In bridge construction, the initial settlement typically develops before the construction of the approach slab. This stage is influenced by the degree of saturation of the soil, where partially saturated soils tend to produce greater initial settlement than fully saturated soils (Puppala, et al. 2008, McCarthy 2007).

The primary settlement (S_p) is typically referred to as time-dependent settlement (consolidation). It takes place when stress gradually transfers from water to soil particles (dissipation of water). In granular soils, such as sands and gravels, this stage occurs rapidly, due to the high permeability of such soils. However, in fine soils, such as clays and silts, this stage could take several years due to the low permeability of such soils (Puppala, et al. 2008, McCarthy 2007).

The secondary settlement (S_s) is also time-depended in which the volume of the soil is decreased due to creep. In this stage, the void ratio of the soil mass decreases further under constant application of the load. The secondary settlement is usually neglected in granular soils. However, in highly plastic fine soils, the secondary compression settlement could be as significant as the primary settlement (Puppala, et al. 2008, McCarthy 2007).

Wahls (1990) noted that a significant portion of the stress imposed on the natural soil develops from the self-weight of the embankment fill. Figure 2.3 compares the vertical stress imposed on the natural soil by embankment fill and bridge abutment.

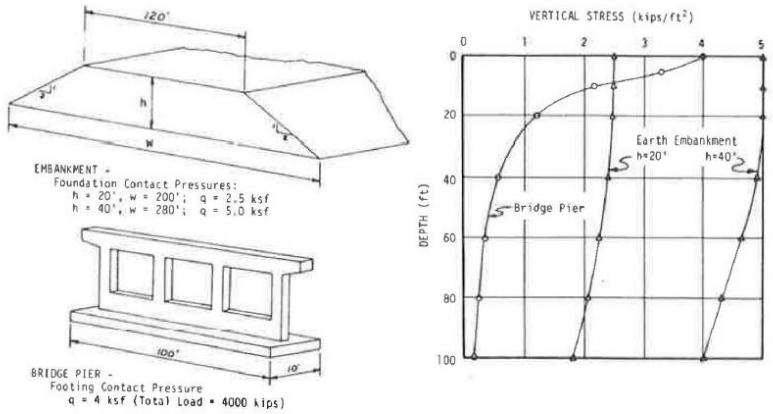

Figure 2.3 Vertical stress imposed on natural soil by embankment fill and abutment (Wahls 1990)

It is well known that post-construction settlement issues are more dominate in cohesive soils. Accordingly, it is very important to investigate cohesive natural soils before constructing the embankment fill. Doing so would help anticipate the total settlement underneath the approach slab (Wahls 1990).

2.3.2 Embankment fill

The embankment fill plays a significant role when it comes to the bump formation at the ends of the bridge as it is the source of the stress imposed on the natural soil. The embankment fill area could be defined as the area extending from the back of the abutment wall to an average

distance of about 100 *ft* (31 *m*). This area includes the backfill material, approach slab, and a portion of the roadway pavement (Puppala, et al. 2008, White, et al. 2005). Within the approach slab, greater differential settlement is expected when tall embankment fills are employed. Long et al. (1999) classified the height of the embankment fill into: low $H_e \leq 10$ *ft* (3.0 *m*), medium 10 *ft* (3.0 *m*) $\leq H_e \leq 26$ *ft* (8.0 *m*), and high $H_e > 26$ *ft* (8.0 *m*), where H_e is the height of the embankment fill.

The embankment fill undergoes global as well as local settlement over time. Global settlement takes place in deeper natural soil layers due to consolidation. On the other hand, erosion, movement of the abutment wall, and compression of the embankment fill are the main contributors to the local settlement (Washington State Department of Transportation 2015). Typically, an embankment fill, such as non-cohesive granular soil that is compacted well results in little or negligible settlement. However, low cost fill materials that are readily and locally available are widely used, especially when high embankment fills are needed. Frequently, the readily-available fill contains significant clay materials, which could result in significant time-dependent consolidation, even with good compaction (Briaud, James and Hoffman 1997, McLaren 1970, Dupont and Allen 2002). According to Hoppe (1999), 49% of the DOTs require embankment fills that are highly permeable and non-plastic, while the remaining DOTs may permit the use of readily available highway embankment fill that might not perform satisfactorily.

The side slope of the embankment fill, oriented in the transverse direction (see Figure 5.4), is another factor that influences the settlement. Typically, the embankment fill is built with a slope of 1:2 (1 vertical to 2 horizontal) (see Chapter 3). Allen and Meade (1988), Kramer and

Sajer (1991), and Dupont and Allen (2002) reported that leveling the slope of the embankment (by constructing wing walls) adds more resistance to settlement and lateral movement of the soil.

2.3.3 Abutment

The abutment is a vital part of the bridge system that carries a large portion of the bridge load and provides vertical and lateral support at the end of the bridge. The type of the abutment (wall or stub), abutment foundation type, and movement of the abutment influence the formation of the bump at the end of the bridge. An overview of these elements will be presented in the following sections.

2.3.3.1 Abutment type

There are several types of abutment that are commonly used on bridges. For the purposes of this study, the wall and stub abutments will be examined.

The wall abutment consists of a wall that extends the full height of the embankment fill (Figure 2.4). The wall abutment typically experiences higher lateral earth pressure (induced by the full height of the embankment fill) when compared with other abutment types (Briaud, James and Hoffman 1997, Wahls 1990).

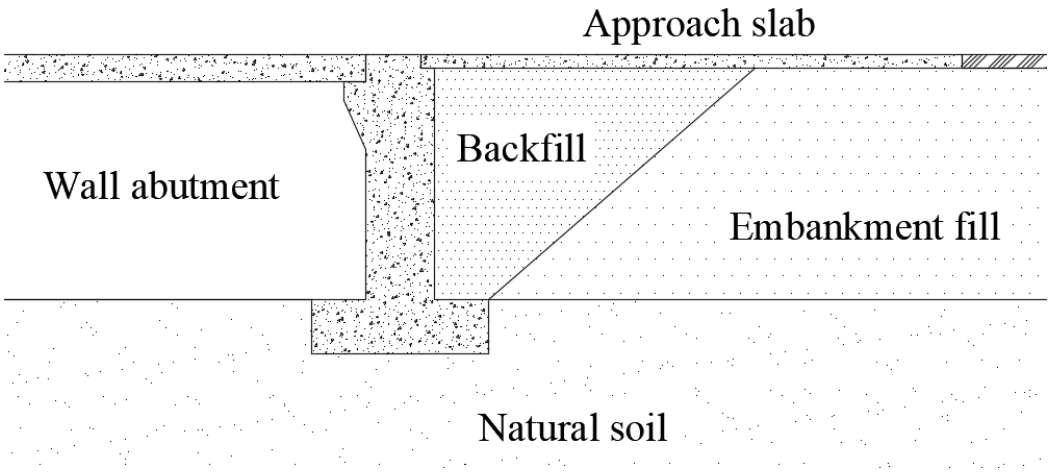

Figure 2.4 Typical wall abutment

The stub abutment has a shorter wall and is typically founded near the top of the embankment fill (Figure 2.5). Due to the relatively short height of the wall, the lateral earth pressure on the stub abutment is lower than in other abutment types (Briaud, James and Hoffman 1997, Wahls 1990).

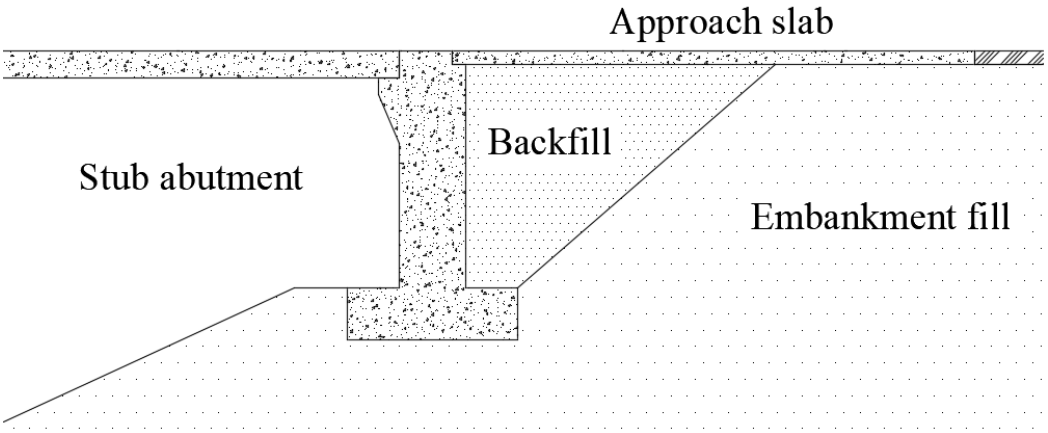

Figure 2.5 Typical stub abutment

A wing wall is usually attached to the abutment at each side to retain the embankment fill. It could be attached at different angles with respect to the abutment. Typically, the wing wall extends along the longitudinal with the height decreasing as the distance from the abutment increases (Briaud, James and Hoffman 1997, Wahls 1990).

Proper compaction of soil near the abutment backwall is difficult to achieve due to the confined space in that area. Hoppe (1999) reported that 50% of the DOTs have had difficulty in obtaining the specified degree of backfill compaction near the abutment wall. Consequently, as this area becomes larger, the soil would become more vulnerable to settlement and/or washout. This could lead to the formation of a void underneath the approach slab.

2.3.3.2 Abutment foundation type

The abutment wall is either supported on piles or on spread footing. The type of the foundation influences the differential settlement of the approach slab, since one end of the approach slab is supported on the bridge abutment. Typically, pile-supported abutments induce negligible settlement. This in turn leads to great differential settlement of the approach slab, thus, increasing the chance for forming bumps. On the other hand, abutments that are supported on spread footings tend to generate higher settlement. This in turn could lead to low differential settlement in the approach slab and lessen the chances of the bump formation (Laguros, Zaman and Mahomood 1990).

2.3.3.3 Movement of the abutment

The movement of the abutment affects both the bridge and the embankment fill and can influence the formation of the bump. In integral bridges, thermal expansion and/or contraction of the bridge causes the abutment wall to move laterally towards or away from the adjacent soil. These cyclic movements induce large horizontal displacement in the backfill soil, resulting in a formation of a void underneath the approach slab. Figure 2.6 shows the mechanism of the void formation due to the abutment movement (Puppala, et al. 2008).

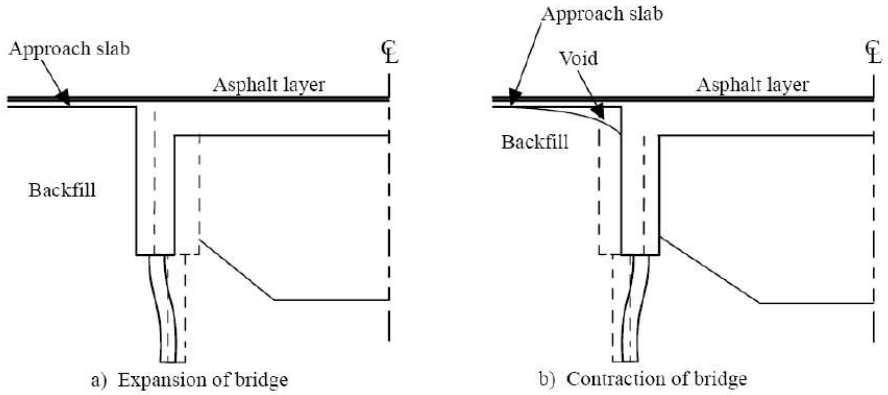

Figure 2.6 Mechanism of void formation due to abutment movement (Puppala, et al. 2008)

2.3.4 Approach slab

The approach slab offers several advantages and some disadvantages when employed at the end of the bridge. Some of the advantages include facilitating a smooth transition between the bridge and the roadway, reducing truck impact on the abutment, and preventing water infiltration behind abutment wall. Some of the disadvantages include higher construction cost, and maintenance issues that are related to the differential settlement.

Typically, the approach slab is a reinforced concrete member that is supported on the abutment at one end and on a sleeper slab at the other end. The approach slab is usually extended to a certain distance to cover the problematic area where a void could develop. It is designed to carry dead load and traffic live load. The approach slab typically has two steel reinforcement layers at the top and bottom.

Connecting the approach slab to the abutment helps in directing the surface water away from the abutment back wall through which erosion of the backfill material could occur (Phares and Dahlberg 2015). There are two ways to connect the approach slab to the bridge abutment in which the approach slab would rest on a corbel or lip built onto the abutment. One way is to

extend reinforcing steel dowels from the bridge deck into the approach slab. Another way involves placing inclined bars to form an integrated connection between the approach slab and the abutment. In both ways, the bars are meant to restrict the relative horizontal movement between the approach slab and the bridge abutment while allowing the slab to rotate. The approach slab could also have no positive connection (no steel bars across the interface) with the superstructure (Greimann, et al. 2008). In such cases, the approach slab could gradually separate from the bridge.

The design parameters for the approach slab can significantly influence the bump at the end of the bridge. The length and thickness of the approach slab, type of support at the approach slab/pavement connection, and type of connection to the bridge are important factors that should be taken into consideration in any approach slab design. The design of the approach slab must assure that the slab can withstand the anticipated differential settlement and that the resulting slope is within tolerable limits (see Section 2.1).

2.3.5 Drainage

Utilizing proper drainage systems can help control the erosion of the backfill material and reduce hydrostatic pressure behind the abutment wall. Adequate drainage system should keep the water away from behind the abutment. Poor drainage can lead to slope instability, slope subsidence, and significant damage to the bridge abutment and approach slab; all of which are factors contributing to the formation of the bump at the end of the bridge. In that manner, both surface and subsurface drainage should be counted for in the bridge approach system. One approach to keep the runoff water away from the backfill involves using gutters and paved ditches along both sides of the pavement (Briaud, James and Hoffman 1997, Lenke 2006).

Examples of subsurface drainage enhancement include utilizing plastic drainpipes, abutment weep holes, joints sealing, and free-draining granular fills. White et al. (2005) reported three different drainage systems that are commonly used. These include employing porous backfill around a perforated drainpipe, wrapping a geotextile around the porous fill, and utilizing a vertical geo-composite drainage system. Figure 2.7 shows the three subsurface drainage systems.

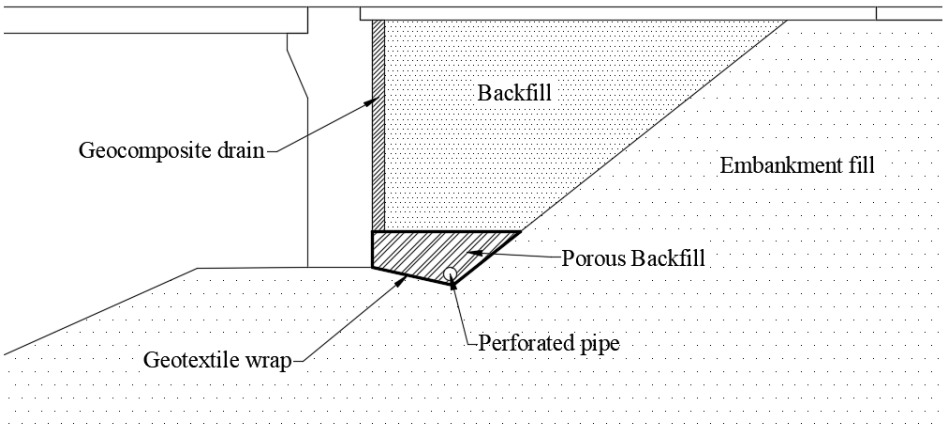

Figure 2.7 Typical subsurface drainage system (Hoppe 1999, White, et al. 2005)

2.3.6 Construction method

Factors that can influence the formation of the bump include compaction level, lift thickness, and sequence of construction. The required compaction level of the backfill/embankment fill varies among DOTs. Nevertheless, most DOTs require the fill to be compacted to over 90% of the standard proctor value. The lift thickness ranges from a minimum of 4 *in* (101 *mm*) (Washington DOT) to a maximum of 12 *in* (305 *mm*) (Taxes DOT) (Hoppe 1999).

According to Hoppe (1999), most DOTs construct the embankment fill before constructing the bridge abutment. This allows the embankment to undergo some of its total

settlement before opening the bridge to the public. Typically, the type of abutment influences the order of construction. When a stub abutment is employed, the embankment is typically construed first, and the abutment is placed near the top of the embankment. However, when a wall abutment is employed, the abutment is constructed first (Hoppe 1999).

2.3.7 Traffic volume

The average daily traffic (ADT), vehicle speed and weight, and number of cycles of loading can influence the formation of the bump at the end of the bridge when no approach slab is employed. Based on the compressibility and/or level of compaction of the soil, the approach fill could be further compressed due to heavy traffic loading. When an approach slab is employed, it significantly decreases the severity of the bump caused by this void. The approach slab is usually designed to sustain full traffic loading in a free span, even if it has lost contact with the underlying soil. In such cases, the traffic volume, and vehicle velocity would not have any effect on the formation of the bump at the end of the bridge (Dupont and Allen 2002, Puppala, et al. 2008, Lenke 2006).

2.3.8 Bridge skew

Laguros, Zaman, and Mahmood (1990) reported that skewed approach fills were associated with higher settlement than non-skewed approach fills. However, a relationship between the settlement and the degree of skewness could not be established.

Nassif et al. (2002), conducted finite element analyses to evaluate the performance of skewed approach slabs under differential settlement. It is reported that skewed approach slabs developed higher tensile stresses than straight approach slabs.

Cai, Voyiadjis and Shi (2005) agreed with the findings of Nassif et al. (2002), and showed that, in skewed approach slabs, the tensile stress distribution along the long side of the approach slab increases as the differential settlement increases (Figure 2.8).

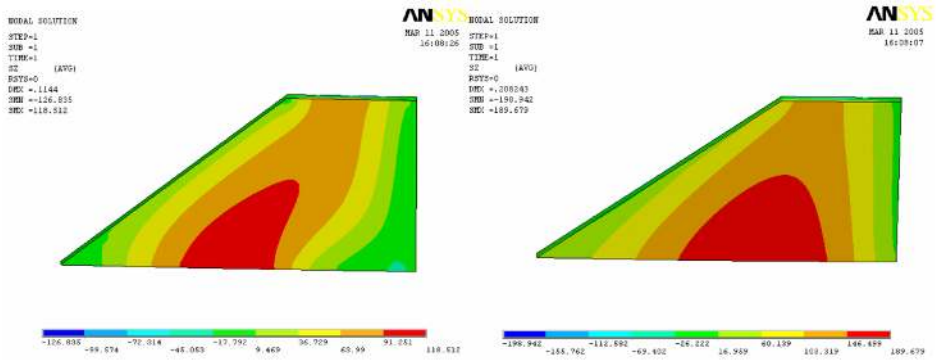

(a) Settlement = 0.5 in. (b) Settlement = 6 in.

Figure 2.8 Distribution of tensile stress in skewed approach slab (Cai, Voyiadjis and Shi 2005)

2.4 Mitigation techniques

The mitigation techniques that are typically used after formation of the bump are classified into four groups:

- Improvement of the natural soil;
- Improvement of the embankment fill;
- Enhancement of the drainage and erosion control system; and
- Improvement of the approach slab design.

Wick and Stoelhorst (1982) recommended several practices to control the differential settlement of the approach slab. These include supporting the approach slab/pavement end with a sleeper slab, cement stabilization of the embankment fill, and implementation of drainage control systems.

Karemer and Sajer (1991), made several recommendations to minimize the differential settlement of the approach slab. One recommendation was to level out the slope of the embankment with wing walls. This was intended to reduce creep settlement of the natural soil, especially of highly plastic and/or organic soils. They also recommended that good quality control of embankment materials and compaction specifications would help reduce the settlement of the embankment fill. Another recommendation was to straighten the backwall face of the abutment. This was intended to simplify the compaction process near the abutment wall.

Briaud, James and Hoffman (1997) made several recommendations regarding the design, construction and maintenance of the bridge approach area to minimize or eliminate the bump. These recommendations are summarized as follows:

- Utilizing an approach slab particularly when excessive settlement is anticipated.
- Implementation of an adequate drainage and erosion control system.
- Performing routine inspection and maintenance to enhance performance of the approach area and improve the overall rideability.

Hoppe (1999) conducted a survey of various states regarding issues related to the approach slab. The objective of this study was to compare various state practices including those adopted by Virginia DOT. Ultimately, design recommendations were made for mitigating the differential settlement of the approach slab. The recommendations are listed below and illustrated in Figure 2.9:

- Utilizing a full-width, curb-to-curb, approach slab. This was intended to lessen the void formation due to water seepage.

- Appropriate design of the approach slab. The length of the approach slab is typically designed to ensure gradual transition between the bridge and the roadway.
- Lowering the approach slab below the base course level. This was aimed at ease of placement of future asphalt overlays. The Virginia DOT design required the approach slab to be lowered 28 *in* (700 *mm*) below the road surface (Figure 2.9).
- Pre-cambering of the embankment fill for a distance equal to the length of the approach slab (Figure 2.9). This was intended to account the post-construction settlement.

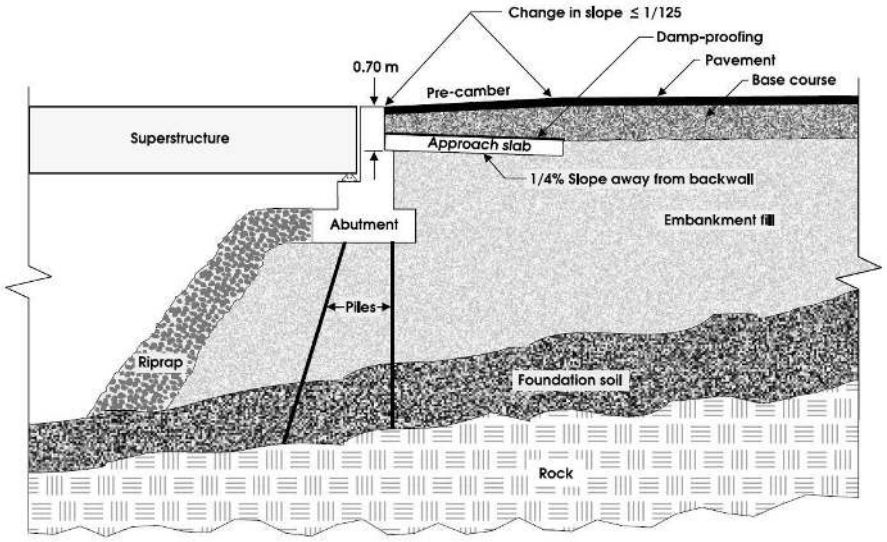

Figure 2.9 Proposed approach slab configuration (Hoppe 1999)

A later study by Dupont and Allen (2002) agreed with the Hoppe (1999) recommendations and made recommendations for reducing differential settlement. These recommendations were discussed in section 2.2 (see Table 2.3).

Mistry (2005) recommended several practices regarding the design of the approach slab. Some of the recommendations are summarized below.

- Cooperation between structural and geotechnical engineers, especially in the decision to use an approach slab. The decision should be based on long-term performance and life cycle cost, instead of the initial cost of the project.
- Standardized use of a sleeper slab. This was meant to prevent excessive settlement and cracking at the approach slab/pavement connection.
- Using a well-drained granular backfill material to accommodate expansion and contraction of the bridge abutment, especially in integral abutment bridges.
- Connecting the approach slab to the superstructure with a hinge connection.
- Providing two layers of polyethylene sheets or fabric underneath the approach slab to reduce friction caused by the horizontal movement of integral abutments.
- Limiting skew angle to 30 degrees to minimize the magnitude and lateral eccentricity of the longitudinal forces.

2.5 Optimum approach slab configuration

This section is a review of previous studies that proposed various approach slab configurations to mitigate the formation of the bump and to improve the overall ride quality of the bridge approach area.

Wong and Small (1994) proposed utilizing an angled approach slab that is sloping down beneath the pavement (Figure 2.10). According to their findings, the formation of the bump was attributed to the abrupt change in the material stiffness between the approach slab and the pavement. Consequently, it was anticipated that this slab configuration would result in a smoother and more gradual change in the material stiffness.

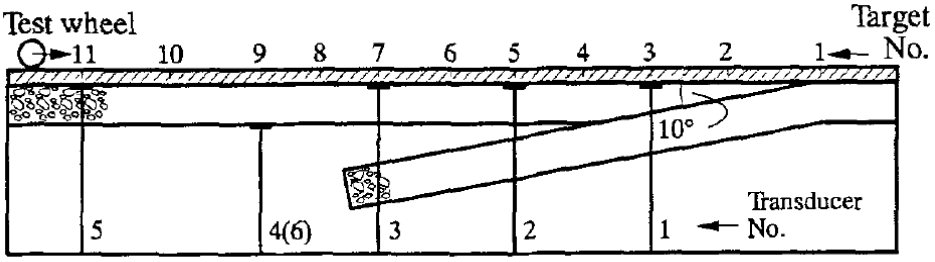

Figure 2.10 proposed approach slab (Wong and Small 1994)

Physical models of pavements and approach slabs have been examined in a laboratory-scale test track. Three different approach slab orientations of 0, 5, and 10 degrees have been evaluated. As a result, it was concluded that the severity of bump decreases as the oriented angle of the approach slab increases. Figure 2.11 shows the surface deformation of the three orientations used in the study.

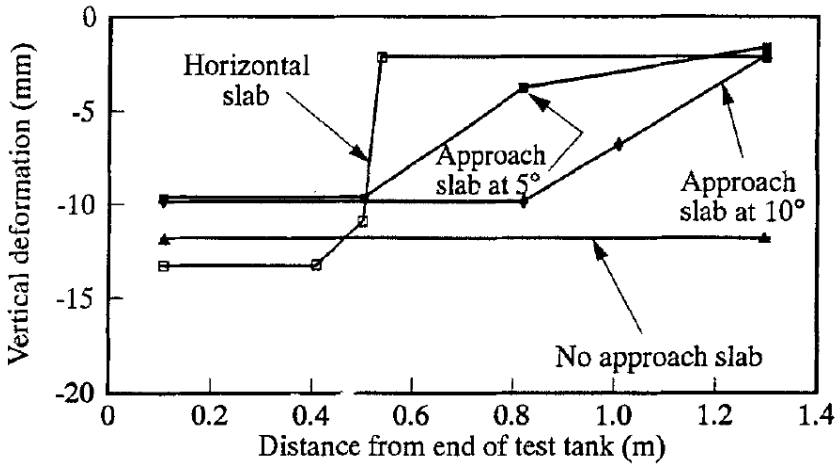

Figure 2.11 Surface deformation of angled slabs (Wong and Small 1994)

Seo, Ha and Briaud (2002) examined the performance of the approach slabs for the Texas DOT. The typical approach slab had a thickness of 12 *in* (305 *mm*) and consisted of two 20 *ft* (6.1 *m*) spans. The slab was designed to be supported on the abutment wall, embankment fill, support slab and sleeper slab (Figure 2.12). In addition, a wide flange steel beam was employed at the end of approach slab to accommodate the thermal movements of the pavement.

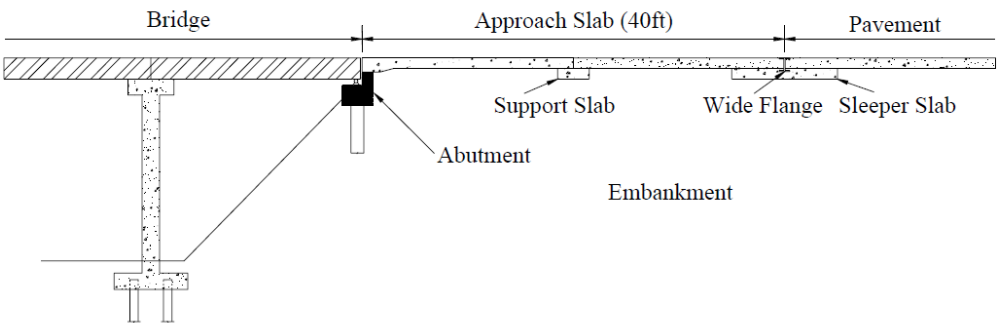

Figure 2.12 Current Taxis DOT approach slab (Seo, Ha and Briaud 2002)

Finite element analyses were carried out in this study. As a result, the following conclusion were drawn:

- The differential settlement between the bridge and the embankment fill is unavoidable when the abutment is supported on piles.
- The abutment wall has a significant influence on the differential settlement. The friction between the abutment wall and the adjacent backfill soil restricts some of the soil in the vicinity of the abutment wall, while the soil away remains unsupported and settles more.
- The transition zone, where most of the settlement occurs, is approximately 40 *ft* (12.2 *m*) away from the back of the abutment wall.
- The width of the support slab, sleeper slab, and the height of the embankment were found to influence the differential settlement of the approach slab. The optimum width of the support slab and sleeper slab was found to be 5 *ft* (1.5 *m*).

Seo, Ha and Briaud (2002) proposed a new approach slab concept to simplify the construction, reduce cost, and lessen the need for good compaction in the backfill area. The proposed approach slab was a single 20 *ft* (6.1 *m*) slab supported on the abutment wall at one end and a sleeper slab at the other end (Figure 2.13). The slab was designed to carry the loads

without the support of the soil. The wide flange steel beam was kept in this design to accommodate thermal movement of the pavement.

After examining the proposed approach slab, the following conclusion were drawn;

- The single-span approach slab has performed better and resulted in a smaller bump than the current two-span approach slab.
- Highly compacted embankment soils result in a smaller bump at the approach slab/pavement end.

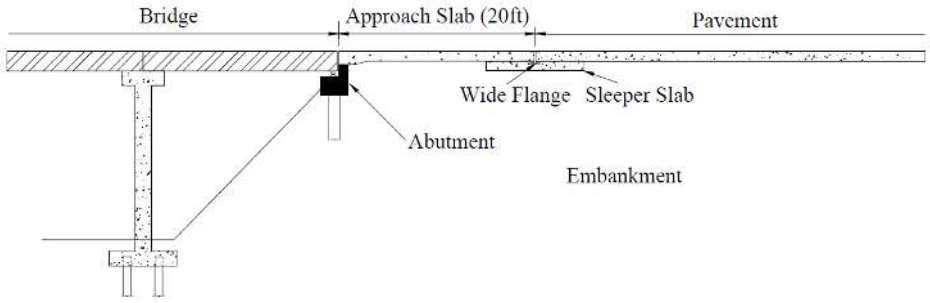

Figure 2.13 Single span approach slab (Seo, Ha and Briaud 2002)

Cai, Voyiadjis and Shi (2005) performed a numerical study of the performance of two different approach slab types (flat versus ribbed) under a given differential settlement. The presumed settlement profiles employed in the analysis were based on a partial embankment contact with the approach slab. This study was aimed at establishing a relationship between the internal forces and deformation in the slab with some of the design parameters including length and thickness. Figure 2.14 shows the layout used in their study.

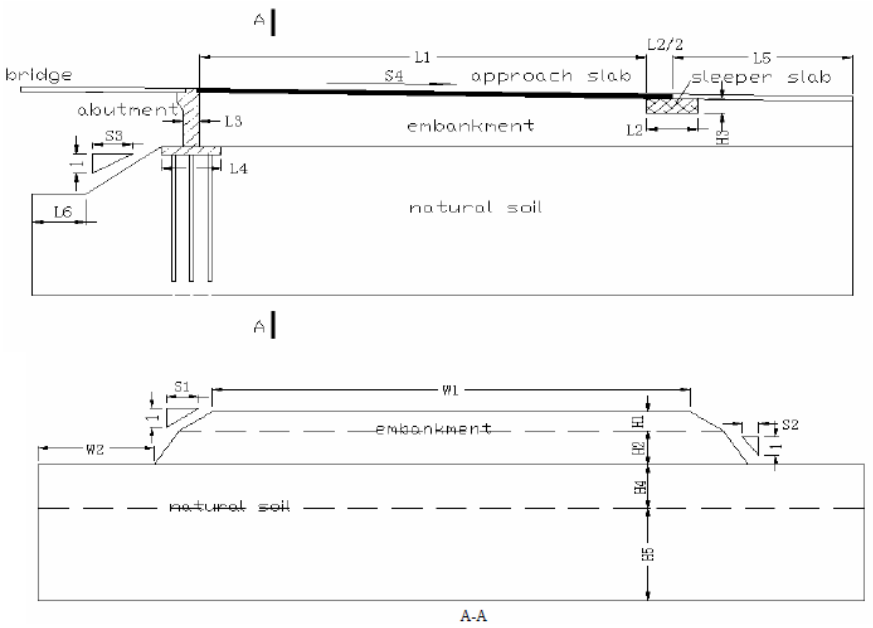

Figure 2.14 Layout of the finite element analysis (Cai, Voyiadjis and Shi 2005)

As a result of the study, it was concluded that the flat approach slab was more applicable for short spans, i.e. 20 to 40 *ft* (6.1 to 12.2 *m*) because the longer spans required greater thickness. In such cases, ribbed approach slab was preferred. The slab on beam behavior in ribbed slabs would significantly reduce the internal stresses and deformation, thus reducing the amount of reinforcement. Figures 2.15 and 2.16 show the stress distribution in a flat and ribbed approach slab with a 6 *in* (152 *mm*) embankment settlement.

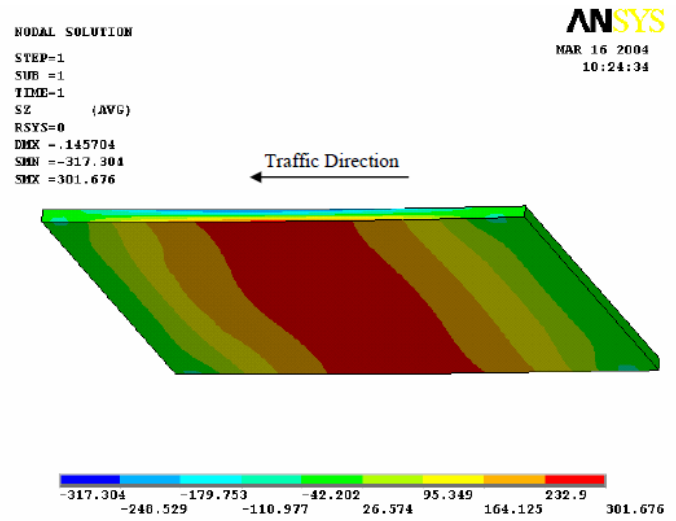

Figure 2.15 Stress distribution in flat slab (Cai, Voyiadjis and Shi 2005)

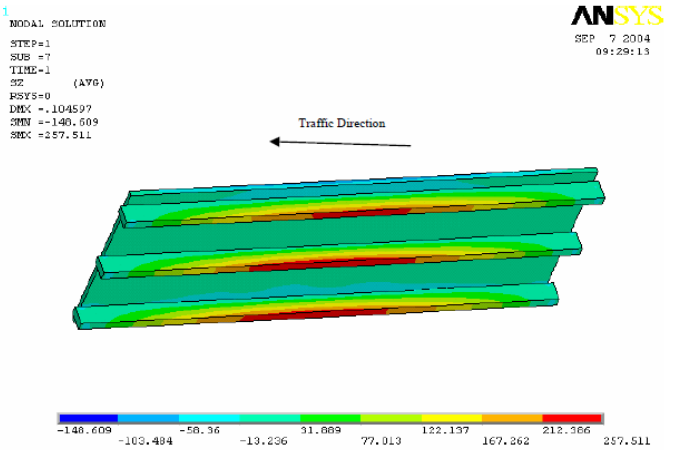

Figure 2.16 Stress distribution in ribbed slab (Cai, Voyiadjis and Shi 2005)

The connection between the approach slab and the bridge abutment was also investigated in their study. As a result, it was recommended that an inclined bar be used to connect the approach slab with the abutment. This connection would allow free rotation between the approach slab and abutment while restricting the relative horizontal movement between them.

Abu-Farsakh and Chen (2014) examined the performance of a proposed approach slab that relied upon increasing its rigidity as well as reinforcing the embankment soil underneath the sleeper slab. The rigidity of the proposed approach slab was increased by increasing its thickness to 16 *in* (406 *mm*) and utilizing more steel reinforcement. The reinforcing of the embankment

soil was made by adding six layers of geogrid spaced at 12 *in* (305 *mm*). The soil reinforcement was designed to mitigate the embankment settlement and increase its bearing capacity. Figure 2.17 shows the standard and the proposed approach slab layout.

Both approach slabs were monitored for one and a half year. The proposed approach slab performed better than the standard slab. Furthermore, the proposed approach slab underwent most of its total settlement during the test period, while the standard approach slab continued settling after the test.

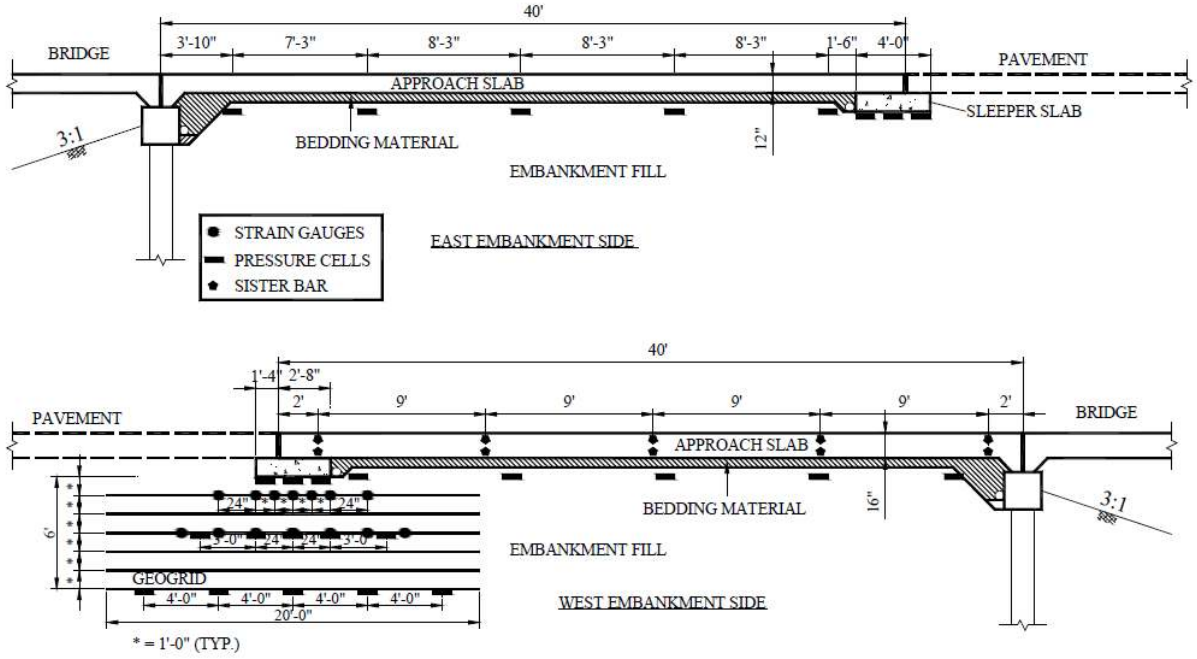

Figure 2.17 Standard (top) versus proposed (bottom) approach slab (Abu-Farsakh and Chen 2014)

Das et al. (1999) evaluated the performance of the pile-supported approach slabs in Louisiana. The pile-supported approach slabs were frequently used in the southeastern part of Louisiana, due to the existence of weak soils in that area.

The typical pile-supported approach slab had an 80-120 *ft* (24-37 *m*) long span. Timber piles with variable lengths were used, with the longer piles located near the approach slab/bridge end and the shorter piles located near the approach slab/pavement end (Figure 2.18).

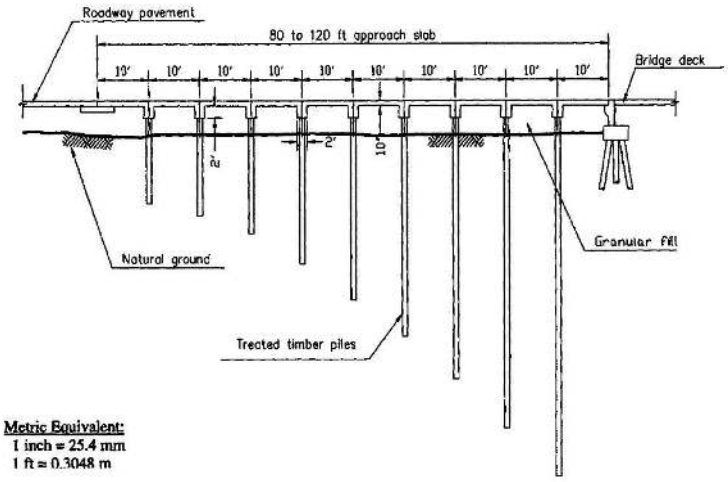

Figure 2.18 Pile-supported approach slab (Bakeer, Shutt, et al. 2005)

The performance of the pile-supported approach slab was evaluated by visual inspection, surveys and assessment of road surface condition. It was noted that while many pile-supported approach slabs performed well, many others settled enough to develop a bump at the approach slab/pavement end. The reason for such settlement was attributed mainly to the unanticipated negative skin friction (downdrag force) imposed on the piles. Accordingly, it was pointed out that soil should undergo most of its consolidation before installing the piles to overcome the negative skin friction.

CHAPTER 3 - STATES PRACTICES RELATED TO APPROACH SLABS

As discussed in Chapter 2, the design parameters of the approach slab and approach area have a significant effect on the bump formation at the ends of the bridge. This include the configuration of the approach slab, connection of the approach slab to superstructure, support type at the approach slab/pavement end, backfill material, and side slope of the embankment fill. In this phase of the study, an extensive examination of bridge manuals/guidelines published by all DOTs was conducted. The objective was to understand and compare the current practices (as of 2017) related to the design of the approach slab and the approach area.

An examination of the bridge manuals (including standard drawings) was carried out and practices relevant to the design criteria and parameters of the approach slab and approach area were retrieved. These include the state's preference for utilizing an approach slab at the end of the bridge, support type at the approach slab/pavement connection, approach slab configuration with skewed bridges, details of connection to the superstructure, approach slab dimensions (length and thickness), and other information related to the approach area.

3.1 Approach slab preference

Approach slabs are typically utilized for new bridges under all conditions. Nevertheless, some of the DOTs require certain conditions before requiring the use of an approach slab. Some of these conditions include the superstructure length, height of the embankment, adjacent roadway pavement type, abutments type, average daily traffic (ADT), and average annual daily traffic (AADT). For instance, Colorado DOT provides the following conditions:

- The superstructure length is over 250 *ft* (76 *m*).
- The adjacent roadway pavement is concrete.
- When high embankment fills are used.
- When the district requests it.
- All post-tensioned structures.

Data from bridge manuals (Table 3.1 and Figure 3.1) show that approximately 41% of the DOTs prefer the use of the approach slab for all bridges, while 22% specify certain conditions before employing the approach slab. Roughly 2% do not prefer the use of the approach slab; however, their practice is to design the bridge abutment for future possibility of adding an approach slab. The remaining 35% did not mention any preference in utilizing an approach slab at the ends of the bridge.

Table 3.1 DOTs preference of approach slab

DOT	Preference	DOT	Preference
Arizona	Preferred	Montana	Not preferred
Alaska	—	Nebraska	Preferred
Alabama	—	Nevada	Preferred
Arkansas	—	New Hampshire	Preferred
California	Preferred	New Jersey	Preferred
Colorado	Preferred under certain conditions	New Mexico	Preferred
Connecticut	Preferred	North Carolina	Preferred
District of Columbia	Preferred	North Dakota	—
Delaware	Preferred under certain conditions	New York	Preferred under certain conditions
Florida	Preferred	Ohio	Preferred
Georgia	—	Oklahoma	—
Hawaii	—	Oregon	—
Idaho	Preferred under certain conditions	Pennsylvania	Preferred
Illinois	—	Rhode Island	—
Indiana	—	South Carolina	Preferred under certain conditions
Iowa	—	South Dakota	Preferred
Kansas	Preferred	Tennessee	—
Kentucky	Preferred under certain conditions	Texas	—
Louisiana	—	Utah	Preferred
Maine	Preferred under certain conditions	Vermont	Preferred under certain conditions
Maryland	Preferred under certain conditions	Virginia	Preferred
Massachusetts	—	Washington	Preferred
Michigan	Preferred	West Virginia	Preferred under certain conditions
Minnesota	—	Wisconsin	Preferred under certain conditions
Mississippi	—	Wyoming	Preferred
Missouri	Preferred		

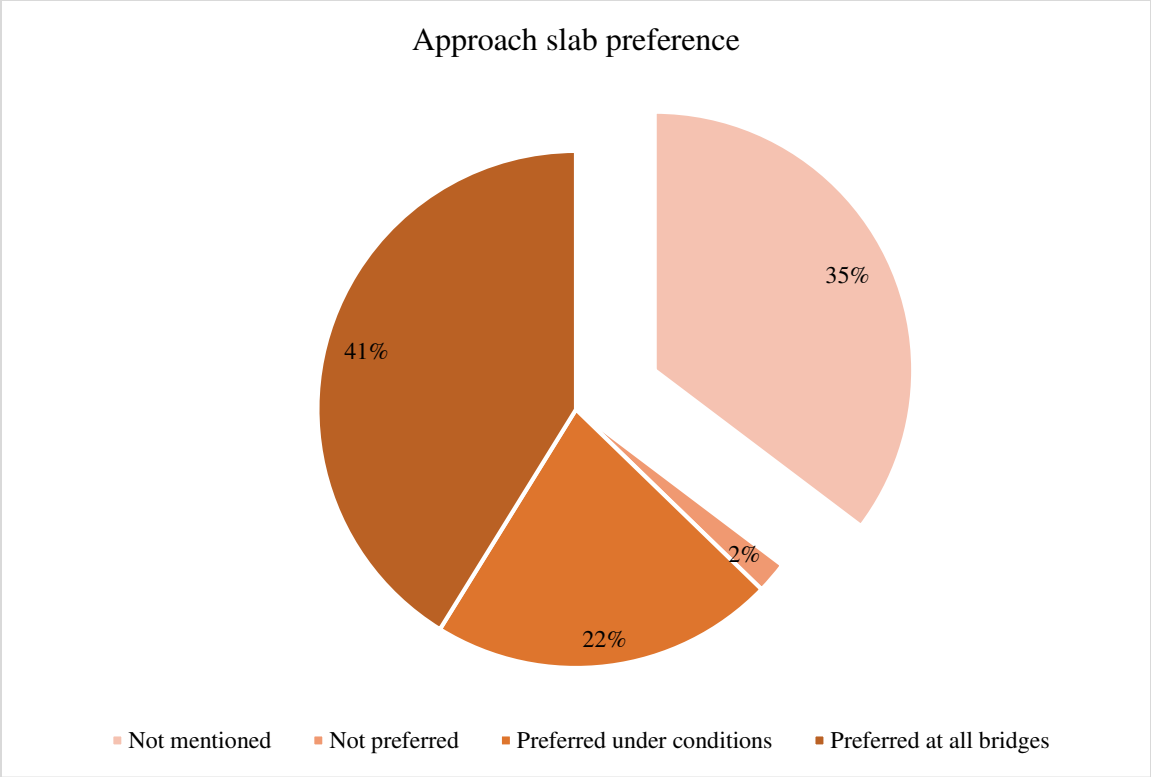

Figure 3.1 DOTs preference regarding use of approach slab

3.2 Approach slab/pavement end support

The approach slab/pavement end is usually supported on the embankment soil (soil support), sleeper slab (Figure 3.2), or a thickened slab edge at the end of the approach slab (Figure 3.3). Typically, a sleeper slab or a thickened edge is utilized when the adjacent roadway pavement is rigid (concrete roadway). This aims to mitigate the abrupt change between the approach slab and the roadway pavement. The South Carolina DOT defines the sleeper slab as "*a foundation slab, inverted tee-beam or L-beam placed transversely supporting the end of the approach slab away from the bridge. Sleeper slabs should be used to provide an off-bridge joint at the end of the approach slab*"

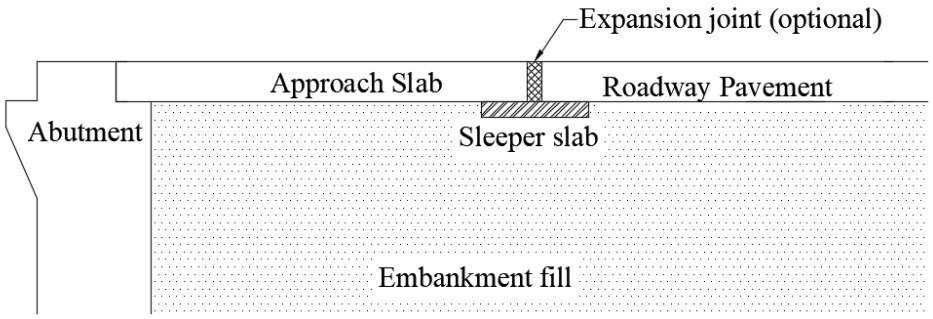

Figure 3.2 Typical approach slab supported on sleeper slab

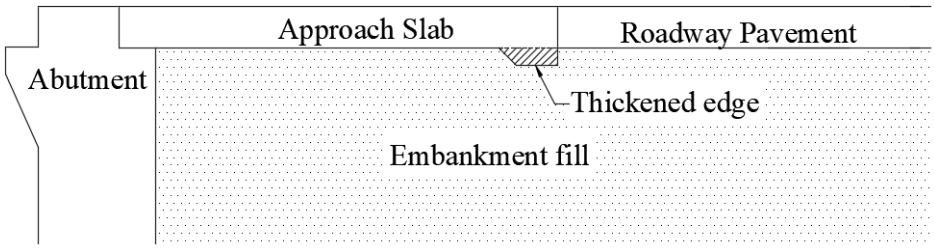

Figure 3.3 Typical approach slab with thickened edge

Data from bridge manuals (Table 3.2 and Figure 3.4) show that approximately 51% of the DOTs use only sleeper slab, 4% use only thickened edge, and 6% use either sleeper slab or thickened edge (design decision) to support the end of the approach slab at the roadway pavement. Roughly, 20% of the DOTs rely on the embankment fill to provide the support for the approach slab. The remaining 19% did not mention the support type at the approach slab/pavement end.

Table 3.2 Approach slab/pavement end support type

DOT	Support type at end of BAS	DOT	Support type at end of BAS
Arizona	Sleeper slab	Montana	—
Alaska	—	Nebraska	Sleeper slab
Alabama	Sleeper slab/Thickened edge	Nevada	Sleeper slab
Arkansas	Sleeper slab	New Hampshire	Sleeper slab
California	Fill support	New Jersey	Sleeper slab
Colorado	Sleeper slab	New Mexico	Sleeper slab
Connecticut	Fill support	North Carolina	Sleeper slab
District of Columbia	Sleeper slab	North Dakota	—
Delaware	Sleeper slab/Thickened edge	New York	Sleeper slab
Florida	—	Ohio	Fill support
Georgia	Fill support	Oklahoma	Fill support
Hawaii	—	Oregon	Fill support
Idaho	Sleeper slab	Pennsylvania	Sleeper slab
Illinois	Sleeper slab	Rhode Island	Sleeper slab
Indiana	Sleeper slab/Thickened edge	South Carolina	Sleeper slab
Iowa	Thickened edge	South Dakota	Sleeper slab
Kansas	Sleeper slab	Tennessee	Sleeper slab
Kentucky	Fill support	Texas	Sleeper slab
Louisiana	Fill support	Utah	Sleeper slab
Maine	—	Vermont	—
Maryland	—	Virginia	Fill support
Massachusetts	Thickened edge	Washington	Fill support
Michigan	Sleeper slab	West Virginia	—
Minnesota	Sleeper slab	Wisconsin	Sleeper slab
Mississippi	—	Wyoming	Sleeper slab
Missouri	Sleeper slab		

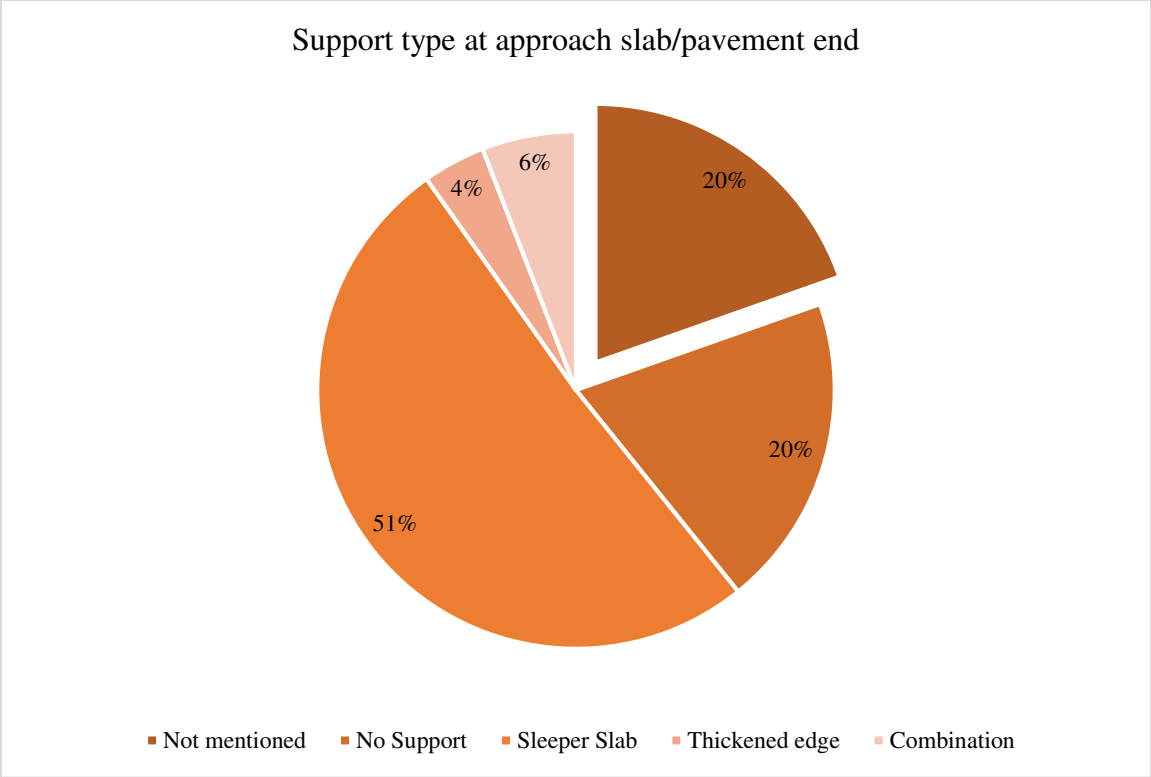

Figure 3.4 Approach slab/pavement end support type

3.3 Approach slab configuration with skewed bridges

Two approach slab configurations could be used along with skewed bridges. The approach slab/pavement end could be made parallel to the skewed bridge or squared off. Typically, the decision for employing one configuration over the other would be based on the adjacent pavement type along with the skew angle. Frequently, the parallel approach slab/pavement end is employed when the adjacent pavement is flexible (asphalt pavement), and when the skew angle of the bridge is less than 30 degrees. The squared off approach slab/pavement end is employed when the adjacent pavement is rigid (concrete pavement), and when the skew angle of the bridge is greater than 30 degrees. Nevertheless, some DOTs would use either configuration regardless of the pavement material.

Data from bridge manuals (Table 3.3 and Figure 3.5) show that approximately 33% of the DOTs employ the parallel approach slab/pavement end when the bridge is skewed, 18% employ the squared off approach slab/pavement end, and 20% use one configuration over the other based on the adjacent pavement type and/or the skew angle. The remaining 29% did not mention the approach slab configuration with skewed bridges.

Table 3.3 Approach slab/Pavement end configuration with skewed bridges

DOT	Approach slab end configuration	DOT	Approach slab configuration
Arizona	Pavement type/Skew degree	Montana	—
Alaska	—	Nebraska	Follows skew angle
Alabama	Pavement type/Skew degree	Nevada	Follows skew angle
Arkansas	Squared off	New Hampshire	—
California	Pavement type/Skew degree	New Jersey	Follows skew angle
Colorado	Follows skew angle	New Mexico	—
Connecticut	Pavement type/Skew degree	North Carolina	Pavement type/Skew degree
District of Columbia	Follows skew angle	North Dakota	Squared off
Delaware	—	New York	Pavement type/Skew degree
Florida	Pavement type/Skew degree	Ohio	Follows skew angle
Georgia	Follows skew angle	Oklahoma	—
Hawaii	—	Oregon	Follows skew angle
Idaho	Pavement type/Skew degree	Pennsylvania	Follows skew angle
Illinois	Follows skew angle	Rhode Island	—
Indiana	Squared off	South Carolina	—
Iowa	Squared off	South Dakota	—
Kansas	Squared off	Tennessee	Follows skew angle
Kentucky	Follows skew angle	Texas	Squared off
Louisiana	Squared off	Utah	—
Maine	Follows skew angle	Vermont	Follows skew angle
Maryland	—	Virginia	Follows skew angle
Massachusetts	Follows skew angle	Washington	Squared off
Michigan	Squared off	West Virginia	—
Minnesota	Pavement type/Skew degree	Wisconsin	Follows skew angle
Mississippi	—	Wyoming	Pavement type/Skew degree
Missouri	—		

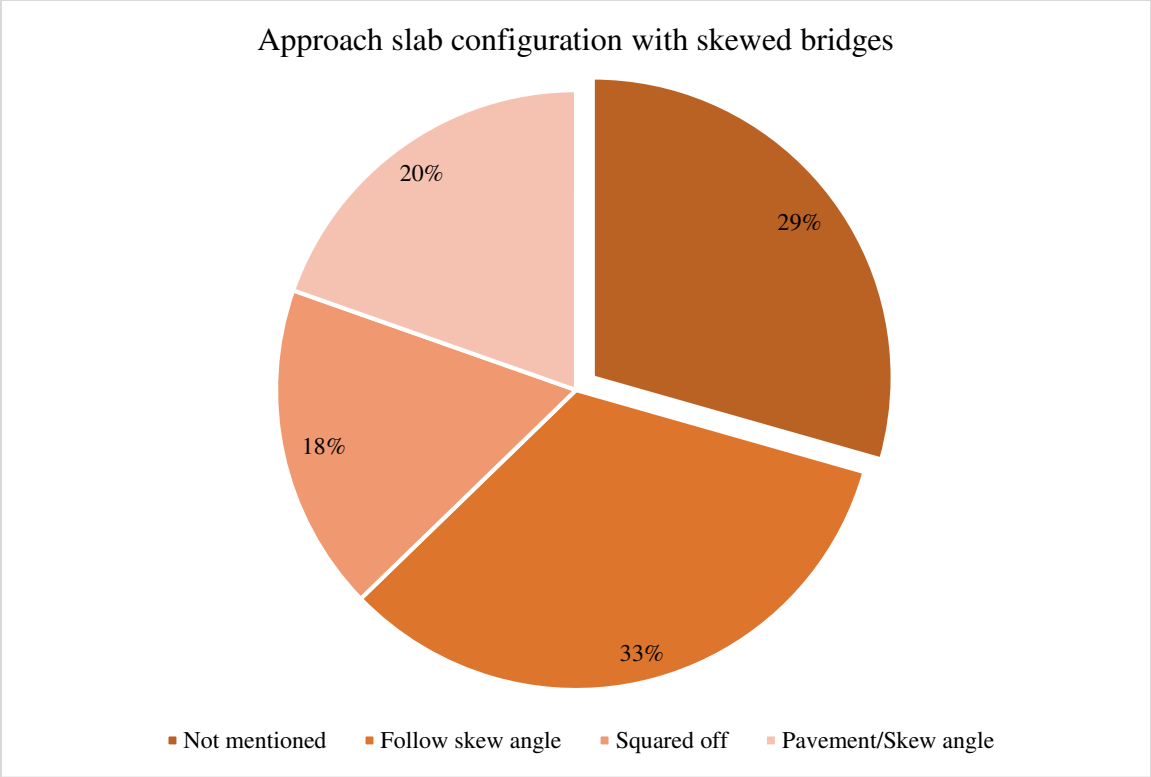

Figure 3.5 Approach slab/Pavement end configuration with skewed bridges

3.4 Approach slab connection mechanism to the superstructure

Connecting the approach slab to the superstructure (through reinforcement) restricts the relative movements between the approach slab and the abutment and allows a free rotation of the approach slab at the approach slab/bridge interface. In addition, it allows the expansion joint to be moved away from the wall abutment (that could reduce erosion of the backfill material).

Data from bridge manuals (Table 3.4 and Figure 3.6) show that approximately 61% of the DOTs connect the approach slab to the superstructure and 4% use no connection mechanism (reinforcement). Roughly 16% of the DOTs make connect or not connect based on the type of approach slab. The remaining 19% did not mention the connection type used between the approach slab and the superstructure.

Table 3.4 Approach slab connection mechanism to the superstructure

DOT	Connection mechanism	DOT	Connection mechanism
Arizona	Connection to superstructure	Montana	—
Alaska	—	Nebraska	Connection to superstructure
Alabama	Based on BAS type	Nevada	Connection to superstructure
Arkansas	No connection	New Hampshire	—
California	Connection to superstructure	New Jersey	Connection to superstructure
Colorado	Connection to superstructure	New Mexico	—
Connecticut	Connection to superstructure	North Carolina	Based on BAS type
District of Columbia	Connection to superstructure	North Dakota	Connection to superstructure
Delaware	Based on BAS type	New York	Based on BAS type
Florida	Connection to superstructure	Ohio	Connection to superstructure
Georgia	No connection	Oklahoma	Connection to superstructure
Hawaii	—	Oregon	Connection to superstructure
Idaho	Connection to superstructure	Pennsylvania	Based on BAS type
Illinois	Connection to superstructure	Rhode Island	Connection to superstructure
Indiana	Connection to superstructure	South Carolina	Connection to superstructure
Iowa	Connection to superstructure	South Dakota	—
Kansas	Connection to superstructure	Tennessee	Connection to superstructure
Kentucky	Connection to superstructure	Texas	Connection to superstructure
Louisiana	—	Utah	Connection to superstructure
Maine	No connection	Vermont	Based on BAS type
Maryland	—	Virginia	Based on BAS type
Massachusetts	Based on BAS type	Washington	Connection to superstructure
Michigan	—	West Virginia	—
Minnesota	Connection to superstructure	Wisconsin	Connection to superstructure
Mississippi	—	Wyoming	Connection to superstructure
Missouri	Connection to superstructure		

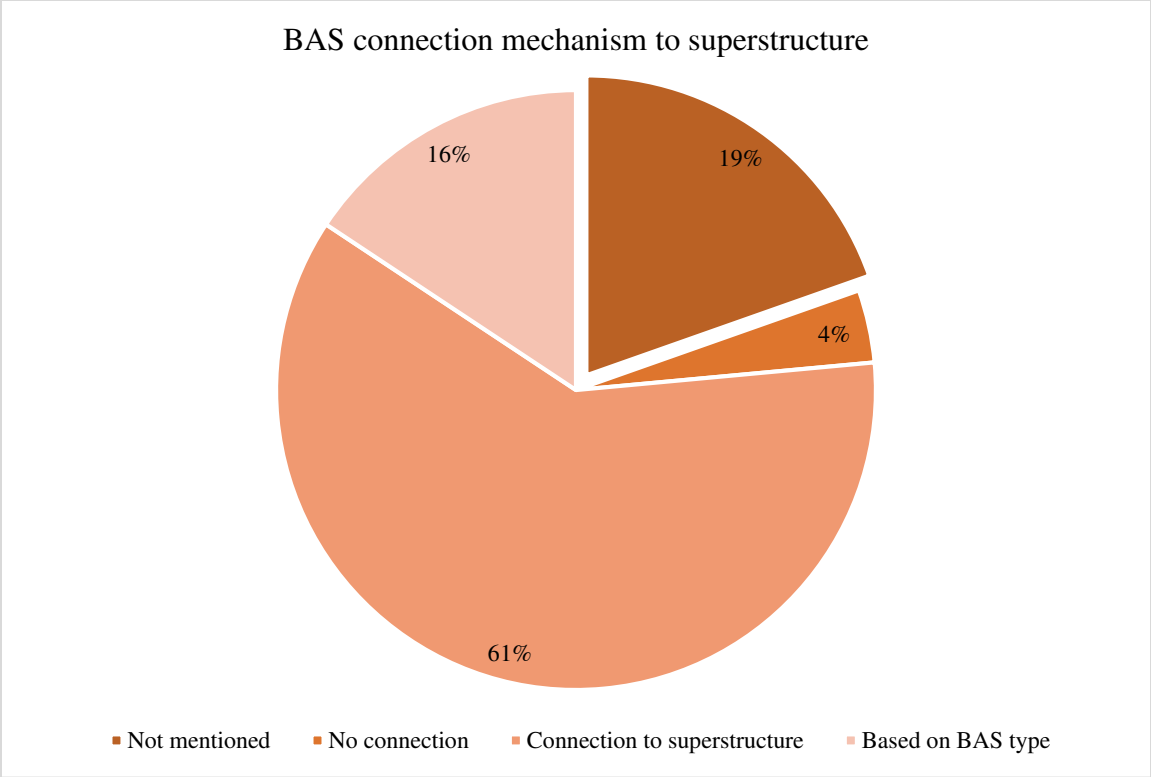

Figure 3.6 Approach slab connection mechanism to the superstructure

3.5 Approach slab dimensions

The length and thickness of the approach slabs are typically designed to ensure that the approach slab sustains the imposed internal stresses and deformations. Usually, the approach slab is designed to carry its own dead weight, future wearing surface as dead load, and traffic live load. The length and thickness must be determined such that the approach slab maintains a smooth transition between the bridge and the roadway pavement.

Figures 3.7, 3.8, and Table 3.6 show the length and thickness of the approach slab as indicated by various DOTs in their bridge manuals. The data show that most DOTs use an approach slab length of 15-30 *ft* (4.6-9.1 *m*) with an average length of 20 *ft* (6.1 *m*). In addition, some DOTs utilize an equation-based criterion to determine the length of the approach slab.

These are shown in Table 3.5. The data also show that most DOTs use an approach slab thickness of 9-15 *in* (229-381 *mm*) with an average thickness of 12 *in* (305 *mm*).

Table 3.5 Length of the approach slab using equation-based criterion

DOT	Approach slab length	Parameters
Colorado	$20 \sin \theta$	θ = skew angle of the bridge
Nevada	$2D$	D = structure depth
New York	$1.5H_a$	H_a = abutment height
Ohio	$1.5(H + w + 1.5)/\cos \theta$	H = height of the embankment w = width of the footing heel θ = skew angle of the bridge

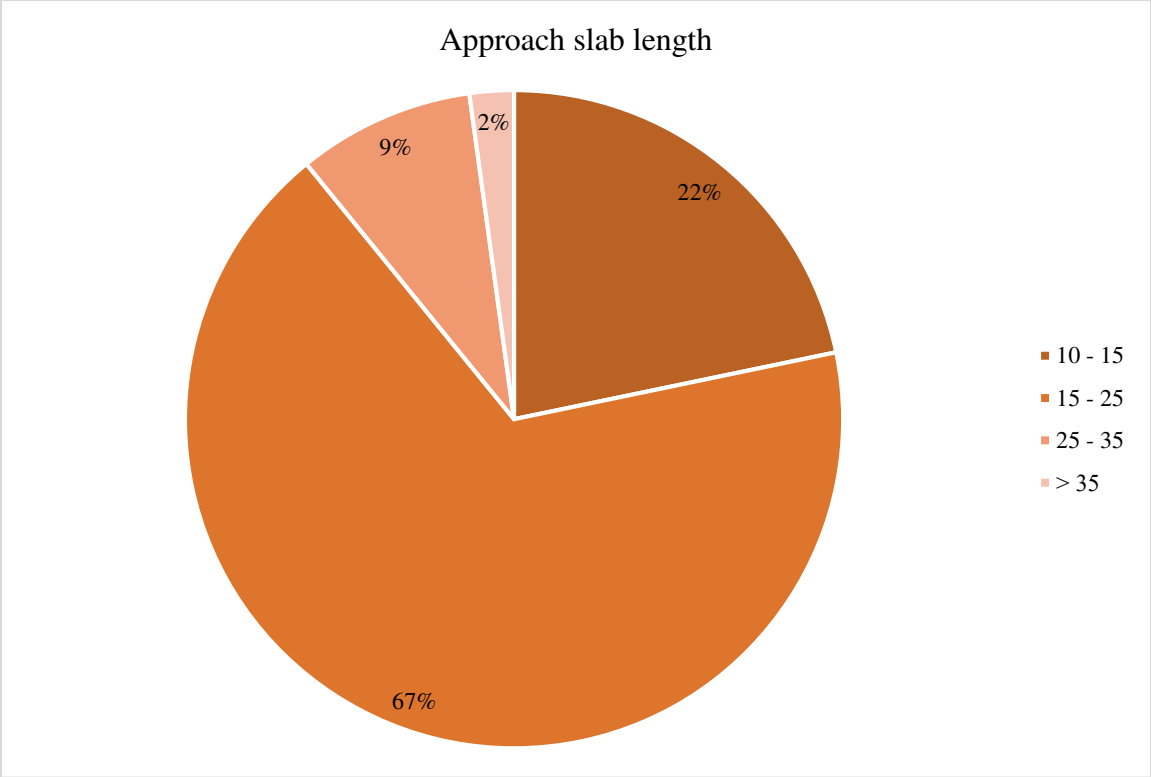

Figure 3.7 Approach slab length (*ft*)

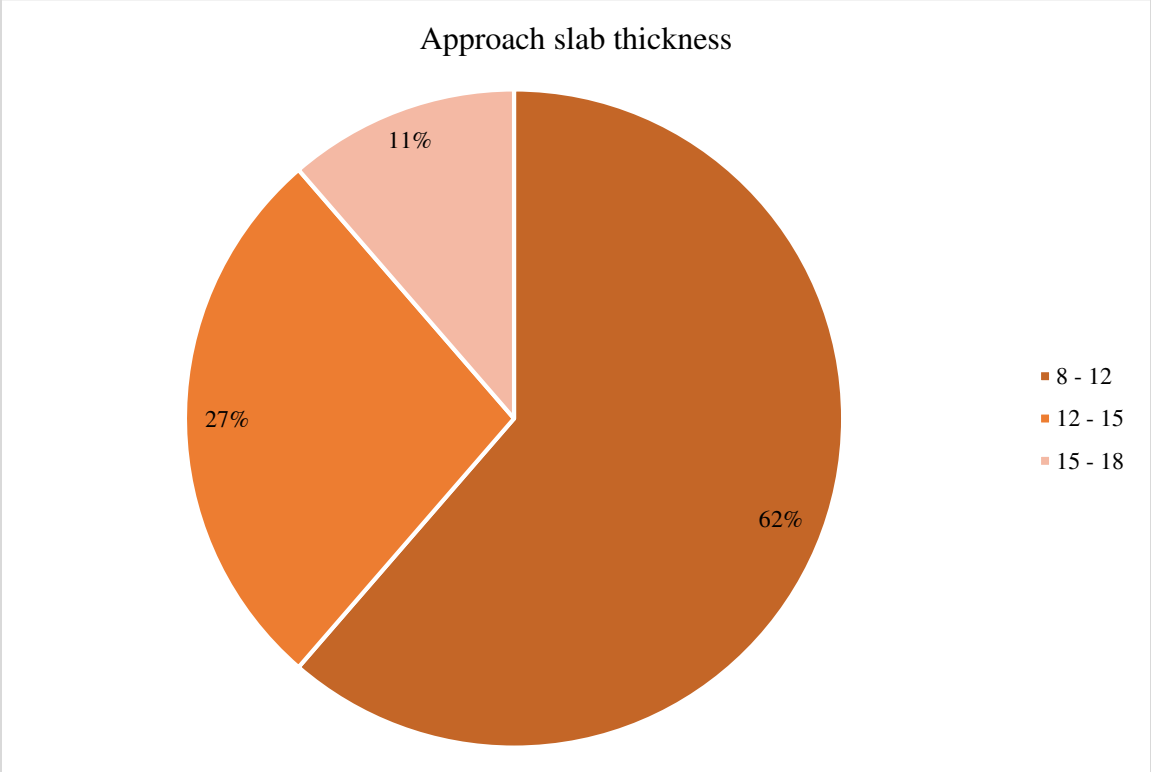

Figure 3.8 Approach slab thickness (*in*)

Table 3.6 Approach slab dimensions

DOT	Length (*L*) *ft* (*m*) Thickness (*T*) *in* (*mm*)	DOT	Length (*L*) *ft* (*m*) Thickness (*T*) *in* (*mm*)
Arizona	$L \geq 15$ (4.6) $T = 12$ (305)	Montana	—
Alaska	—	Nebraska	$L = 20$ (6.1) $T = 14$ (356)
Alabama	$L = 20$ (6.1) $T \geq 10$ (254)	Nevada[1]	$L \geq 24$ (7.3) $T = 12$ (305)
Arkansas	$L \geq 16$ (4.9) $T \geq 9$ (229)	New Hampshire	$L \geq 10$ (3) $T = 15$ (381)
California	$L = 30$ (9.1) $T = 12$ (305)	New Jersey	$L \geq 10$ (3) $T = 18$ (457)
Colorado[1]	$L \geq 20$ (6.1) $T = 12$ (305)	New Mexico	$L \geq 14$ (4.3) —
Connecticut	$L = 16$ (4.9) $T = 15$ (381)	North Carolina	$L \geq 15$ (4.6) $T \geq 12$ (305)
District of Columbia	$L \geq 20$ (6.1) $T = 15$ (381)	North Dakota	$L = 20$ (6.1) $T = 14$ (356)
Delaware	18 (5.5) $\leq L \leq$ 30 (9.1) $T = 16$ (406)	New York[1]	10 (3) $\geq L \geq$ 25 (7.6) $T = 12$ (305)
Florida	$L \geq 30$ (9.1) $T = 12$ (305)	Ohio[1]	$L \geq 15$ (4.6) 12 (305) $\leq T \leq$ 17 (432)
Georgia	$L \geq 20$ (6.1) $T = 10$ (254)	Oklahoma	$L \geq 20$ (6.1) $T = 13$ (330)
Hawaii	—	Oregon	$L \geq 20$ (6.1) $T \geq 12$ (305)
Idaho	$L = 20$ (6.1) $T = 12$ (305)	Pennsylvania	$L \geq 25$ (7.6) $T \geq 16$ (406)
Illinois	$L = 30$ (9.1) $T = 15$ (381)	Rhode Island	$L = 14$ (4.3) $T = 14$ (356)
Indiana	$L = 20$ (6.1) $T \geq 10$ (254)	South Carolina	$L = 20$ (6.1) $T = 12$ (305)
Iowa	$L = 60$ (18.3) $T = 10$ (254)	South Dakota	$L = 20$ (6.1) $T = 9$ (229)
Kansas	$L = 33$ (10.1) $T \geq 10$ (254)	Tennessee	$L = 24$ (7.3) $T = 12$ (305)
Kentucky	$L \geq 20$ (6.1) $T = 17$ (432)	Texas	$L = 20$ (6.1) $T = 13$ (330)
Louisiana	$L \geq 20$ (6.1) $T \geq 10$ (254)	Utah	$L \geq 25$ (7.6) —
Maine	$L = 15.5$ (4.7) $T = 8$ (203)	Vermont	$L \geq 15$ (4.6) $T \geq 14$ (356)
Maryland	—	Virginia	$L \geq 20$ (6.1) $T = 15$ (381)
Massachusetts	$L \geq 10$ (3) $T = 10$ (254)	Washington	$L \geq 25$ (7.6) $T = 13$ (330)
Michigan	$L = 20$ (6.1) $T = 12$ (305)	West Virginia	$L \geq 20$ (6.1) $T = 12$ (305)
Minnesota	$L = 20$ (6.1) $T = 12$ (305)	Wisconsin	$L = 20$ (6.1) $T = 16$ (406)
Mississippi	—	Wyoming	$L = 25$ (7.6) $T = 10$ (254)
Missouri	$L = 20$ (6.1) $T = 12$ (305)		

[1] Utilizes equation-based criterion to determine the length of the approach slab (refer to Table 3.5)

3.6 Embankment and backfill considerations

Information regarding the type of the backfill material, slope of the backfill area, compaction level of the backfill area, and the side slope of the embankment fill were retrieved from the bridge manuals. The data (Table 3.7) show that the customary practice in the backfill area is to utilize a free draining granular material backfill material with a slope of 1:1 (1 vertical to 1 horizontal) and compacted to 95% of the standard proctor. The data also show that a slope of 1:2 (1 vertical to 2 horizontal) is commonly used on the sides of the embankment fills.

Table 3.7 Embankment and backfill consideration

DOT	Backfill type	Slope of backfill area (V to H)	Compaction level (%)	Side slope of embankment (V to H)
Arizona	Free draining, non-expansive	—	95	—
Colorado	Flow-fill	1 to 2	90	1 to 2
Connecticut	Granular	1 to 1.5	—	1 to 2
D. Columbia	Granular	—	95	—
Delaware	Granular	—	—	1 to 2
Georgia	—	—	—	1 to 2
Illinois	Granular	—	—	1 to 2
Kansas	Granular	—	—	1 to 2
Kentucky	Granular	1 to 1	—	1 to 2
Louisiana	Granular	1 to 1	—	1 to 2
Maine	Granular	—	—	—
Maryland	—	—	95	—
Massachusetts	Gravel	—	—	1 to 2
Michigan	Granular	1 to 1	95	1 to 1
Minnesota	—	—	—	1 to 2
Montana	Selected	—	95	1 to 2
Nebraska	Granular	—	—	—
Nevada	Granular	—	95	1 to 2
N.Hampshire	Granular	—	—	—
New Jersey	Porous	1 to 1	—	—
N.Carolina	Selected	—	—	1 to 2
New York	—	1 to 2	95	—
Ohio	Porous	—	—	1 to 2
Oklahoma	Granular	1 to 1	—	—
Oregon	Granular	1 to 1	—	—
Pennsylvania	Granular	—	—	—
S.Carolina	Coarse aggregate	2 to 1	—	1 to 2
South Dakota	Granular	—	95	1 to 3
Tennessee	Granular, aggregate	—	95	—
Utah	Selected, porous	—	—	—
Vermont	Granular	—	—	—
Virginia	Granular, free draining	—	—	1 to 2
Washington	Gravel	—	95	1 to 2
West Virginia	—	—	—	1 to 2
Wisconsin	Granular	1 to 1.5	—	1 to 2
Wyoming	Granular	—	—	—

CHAPTER 4 - DEVELOPMENT OF FINITE ELEMENT SOIL-STRUCTURE INTERACTION MODEL

4.1 Introduction

The analytical modeling of any structure can be represented through a finite number of elements that are computationally assembled and analyzed to obtain a solution for the structure. For the purpose of this study, the commercial finite element software ABAQUS was used to run the developed model that was constructed to analyze the soil-structure interaction effects.

In this study, three finite element models were developed, and parametric studies were performed to evaluate the soil/approach slab settlement behind bridge abutments for various soil conditions (Chapter 5), and to quantify the pile head settlement and load distribution along piles as a function of pile-soil parameters (Chapter 6). Table 4.1 shows general description of the employed models.

Table 4.1 Description of the simulation used in this study

Finite element model type	Objective	Examined parameter
Two-Dimensional Transverse (Figure 4.1)	Simulate the soil settlement behind bridge abutments.	Height of embankment fill
		Embankment soil type
		Side slope of embankment fill
		Height of natural soil
		Natural soil type
Two-Dimensional Longitudinal (Figure 4.2)	Simulate the formation of the bump at the end of the bridge.	Erosion of backfill material
		Slope of backfill area
		Backfill soil compaction level
		Abutment type
Three-Dimensional Pile-Soil System (Figure 4.3)	Simulate the behavior of piles founded on various pile-soil conditions.	Length of approach slab segment
		Number of approach slab segments
		Pile size (diameter)
		Pile length

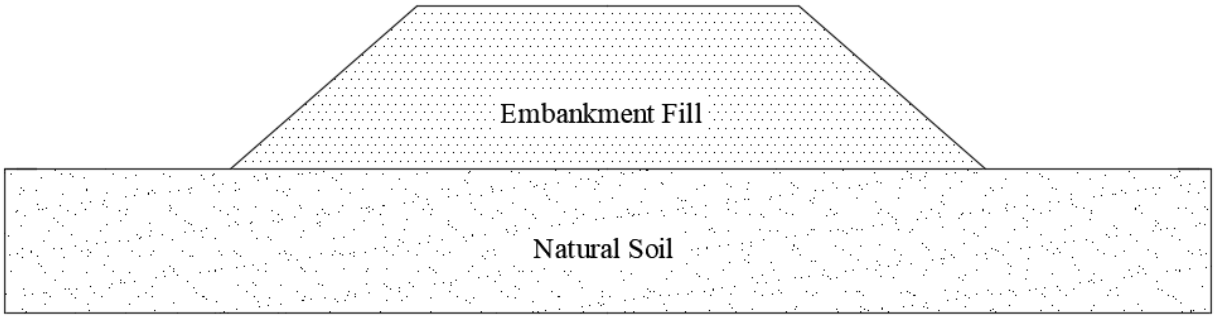

Figure 4.1 Two-Dimensional transverse model

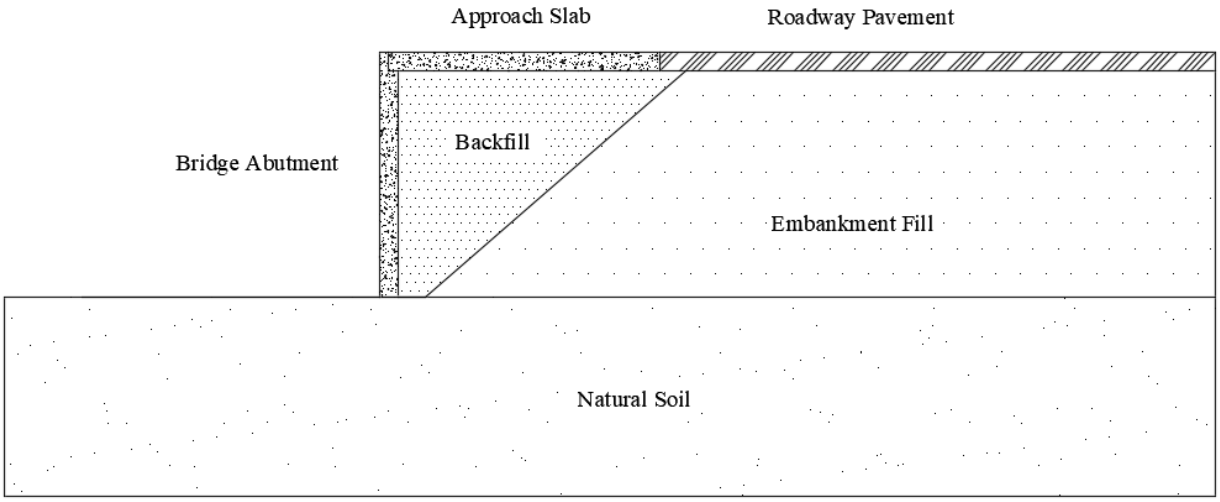

Figure 4.2 Two-Dimensional longitudinal model

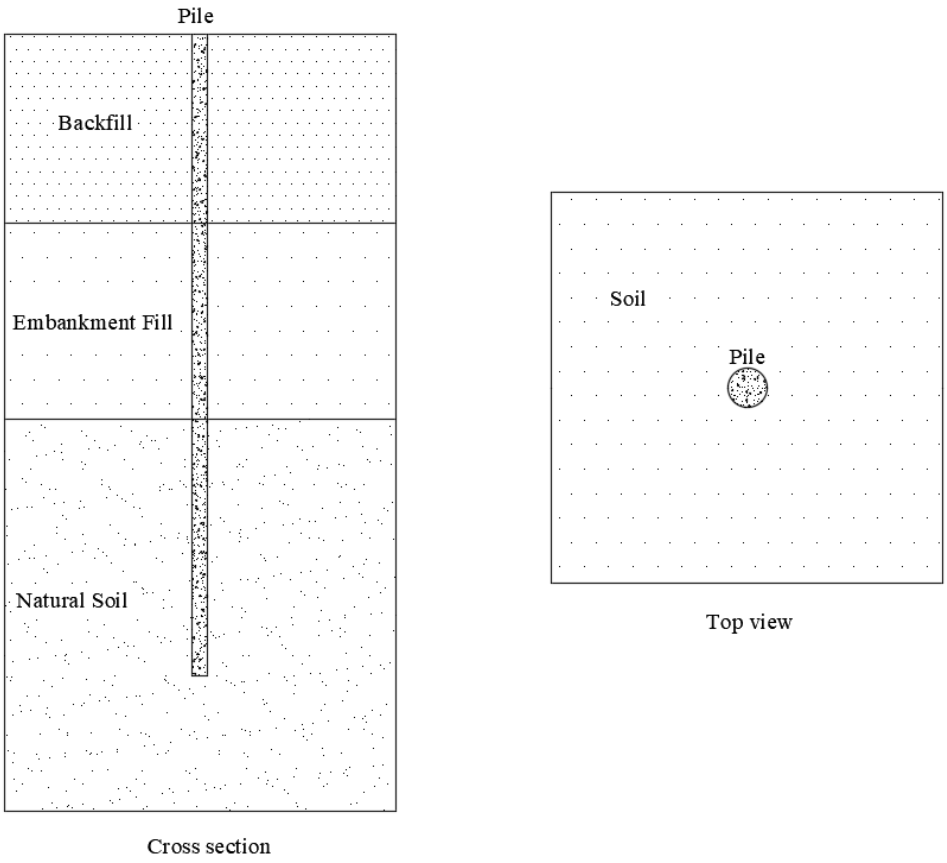

Figure 4.3 Three-Dimensional pile-soil system model

4.2 Geometry and boundary conditions

The geometry and boundary conditions of each finite model was discussed separately (see Sections 5.4.2, 5.6.2, and 6.6.2).

4.3 Contact behavior at soil-structure interfaces

A typical soil-structure system involves the interactions between several structural elements with the soil. The contact behavior at these interfaces must include interface elements that can transfer the load in the normal as well as tangential directions.

In the finite element software ABAQUS, the load transfer mechanism in the direction normal to the contact surface can be represented by a contact pressure-overclosure relationship. This type of relationship minimizes the penetration across the interfaces and does not allow the

transfer of tensile stress between the two elements in contact (master and slave elements). According to ABAQUS (2015), the pressure-overclosure relationship can be described as follows: *"when two surfaces are in contact, any contact pressure can be transmitted between them. The surfaces separate if the contact pressure reduces to zero. Separated surfaces come into contact when the clearance between them reduces to zero*" (ABAQUS 2015, 37.1.2 Contact pressure-overclosure relationships). Figure 4.4 illustrates the default pressure-overclosure relationship.

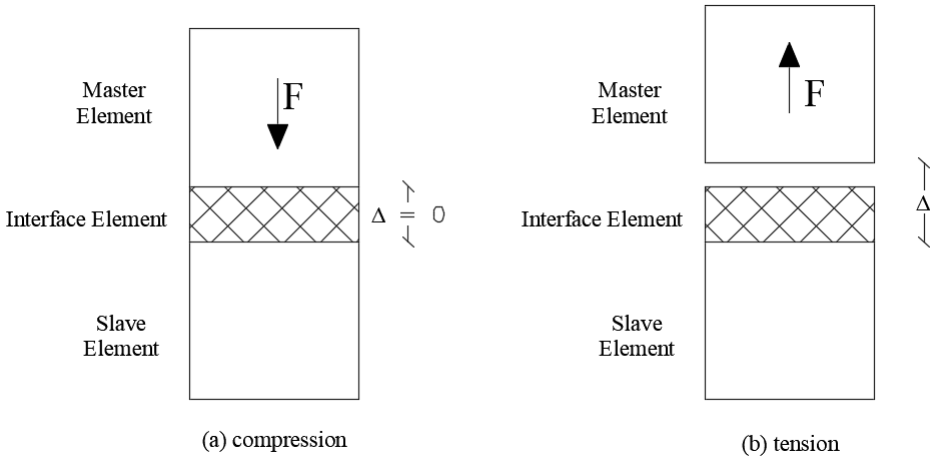

Figure 4.4 Pressure-overclosure relationship (ABAQUS 2015)

On the other hand, the load transfer mechanism in the tangential direction can be represented by the coulomb friction model defined within ABAQUS. The coulomb friction model relates the maximum allowable frictional shear stress, τ, across an interface to the contact pressure, p. According to ABAQUS (2015), the coulomb friction model can be described as follows: "*two contacting surfaces can carry shear stresses up to a certain magnitude across their interface before they start sliding relative to one another; this state is known as sticking*" (ABAQUS 2015, 37.1.5 Frictional behavior). Specifically, the coulomb friction model defines a critical shear stress, τ_{crit}, at which sliding of the surfaces begins. The magnitude of τ_{crit} is proportional to p, represented by $\tau_{crit} = \mu p$, where μ is the coefficient of friction. The stick/slip

calculations within ABAQUS determine when a point transitions from sticking to slipping or from slipping to sticking based upon the value of τ (ABAQUS 2015). Figure 4.5 illustrates the slipping behavior of the coulomb friction model.

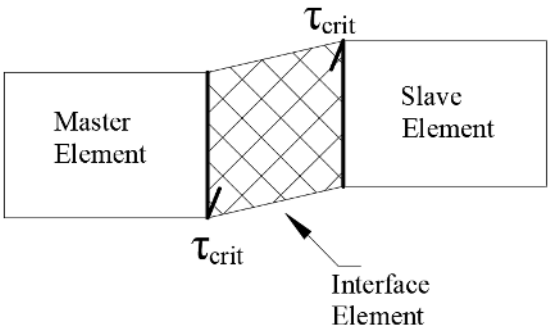

Figure 4.5 Slipping behavior of the coulomb friction model (ABAQUS 2015)

ABAQUS (2015) provides general rules to assign the master and slave elements to the modeled component. Accordingly, master elements should be assigned to those parts that are larger, stiffer and have coarser mesh.

4.4 Analysis procedures

The analysis procedures of each finite model was discussed separately (see Sections 5.4.3, 5.6.4, and 6.6.4).

4.5 Simulating non-linear behavior of soil

When soil is subjected to load, it undergoes elastic and plastic strain. Elastic strain is reversible while plastic strain is irreversible and causes permanent deformation in the material. Elasticity theory, namely Hooke's law, is typically used to describe the reversible deformation of the material, while plasticity theory is used to describe the irreversible behavior of the material.

Ultimately, the total strain (ε) is decomposed into an elastic strain component (ε_e) and plastic strain component (ε_p).

Soil constitutive models, such as the Modified Drucker-Prager/Cap model and Modified Cam-Clay model, are typically designed to include both elastic and plastic behavior of the soil under various types of loading. These constitutive models are developed based on experimental results, typically triaxial shear and isotropic consolidation tests.

4.5.1 Modified Drucker-Prager/Cap constitutive model (MDPCM)

The MDPCM is widely used in finite element analyses to model the behavior of soils and rocks. It is designed such that it can fit the Mohr-Coulomb shear failure surface with an additional cap surface. The cap provides a plastic hardening mechanism and helps control volume dilatancy of the material (ABAQUS 2015). The yield surface of the MDPCM consists of three segments: shear failure surface segment, F_s, compression cap segment, F_c, and transition segment in which connects F_s with F_c (Figures 4.6 and 4.7).

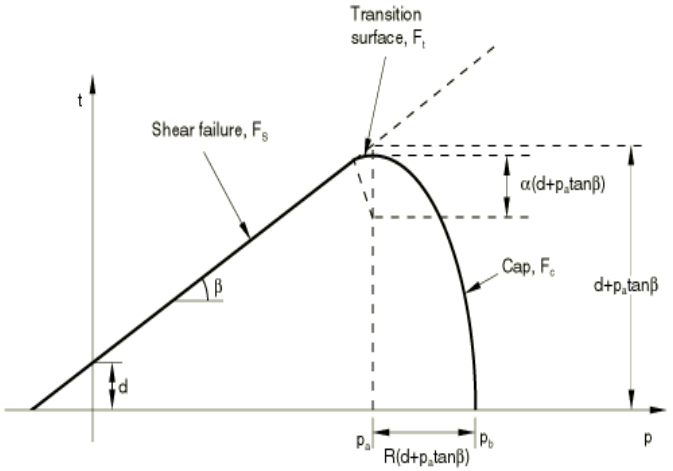

Figure 4.6 Drucker-Prager/Cap failure surface (ABAQUS 2015)

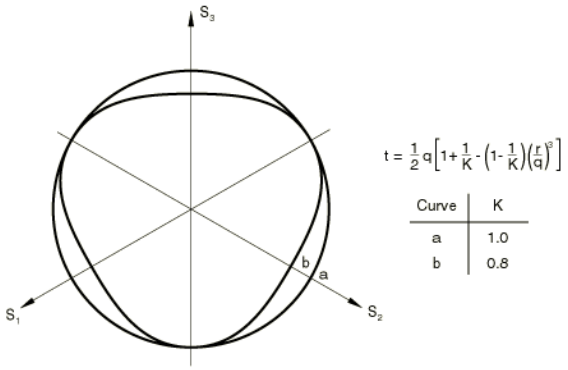

Figure 4.7 Yield/flow surface in the deviatoric plane (ABAQUS 2015)

The shear failure surface, F_s, is defined in terms of the modified cohesion, d, and modified angle of internal friction, β, and is given by

$$F_s = t - p\tan\beta - d = 0 \qquad 4\text{-}1$$

Where

p = Equivalent pressure stress = $-\frac{1}{3}trace(\sigma) = -\frac{1}{3}(\sigma_1 + \sigma_2 + \sigma_3)$

t = Deviatoric stress measure = $\frac{q}{2}\left[1 + \frac{1}{K} - \left(1 - \frac{1}{K}\right)\left(\frac{r}{q}\right)^3\right]$

q = Mises equivalent stress = Shear stress = $\sqrt{\frac{1}{2}[(\sigma_1 - \sigma_2)^2 + (\sigma_2 - \sigma_3)^2 + (\sigma_1 - \sigma_3)^2]}$

K = Parameter that controls the shape of the yield surface on the deviatoric plane, typically $0.778 \leq K \leq 1.0$ (see Figure 4.7).

r = Third stress invariant.

The cap failure surface, F_c, and transition surface, F_t, are given as

$$F_c = \sqrt{(p - p_a)^2 + \left(\frac{Rt}{1 + \alpha - \frac{\alpha}{\cos\beta}}\right)^2} - R(d + p_a \tan\beta) = 0 \qquad 4\text{-}2$$

$$F_t = \sqrt{(p - p_a)^2 + \left[t - \left(1 - \frac{\alpha}{\cos\beta}\right)(d + p_a \tan\beta)\right]^2} - \alpha(d + p_a \tan\beta) = 0 \qquad 4\text{-}3$$

Where

R = Eccentricity parameter that controls the shape of the cap surface.

α = Parameter that shape of define the transition yield surface, typically $0.01 \leq \alpha \leq 0.05$.

p_a = Parameter that controls the hardening/softening behavior as a function of volumetric plastic strain = $\frac{p_b + Rd}{1 + R\tan\beta}$

p_b = Hydrostatic yield stress (user-defined).

The plastic flow (Figure 4.8) is defined by a non-associated segment on the shear failure and transition region, G_s, and an associated segment on the cap region, G_c, given as

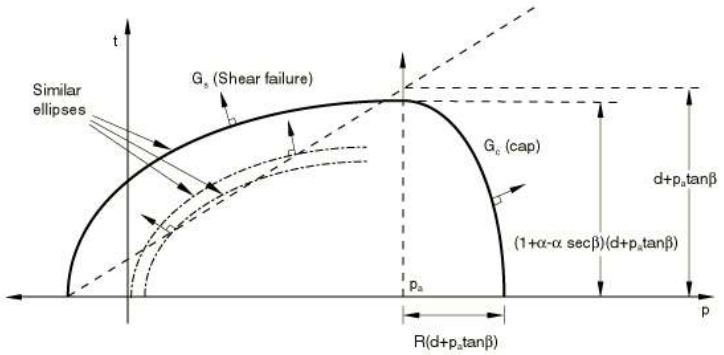

Figure 4.8 Potential plastic flow of MDPCM (ABAQUS 2015)

$$G_s = \sqrt{[(p_a - p)\tan\beta]^2 + \left(\frac{t}{1+\alpha-\frac{\alpha}{\cos\beta}}\right)^2} \quad 4\text{-}4$$

$$G_c = \sqrt{(p - p_a)^2 + \left(\frac{Rt}{1+\alpha-\frac{\alpha}{\cos\beta}}\right)^2} \quad 4\text{-}5$$

The hardening/softening behavior is described by a piecewise linear function that relates p_b and volumetric plastic strain, ε_v^p. This can be typically described as a function of the soil's void ratio, e, along with the effective normal stress, σ_v'. This relationship is ideally represented in a semilogarithmic plot (Figure 4.9) that can be also expressed in terms of volumetric strain, ε_v.

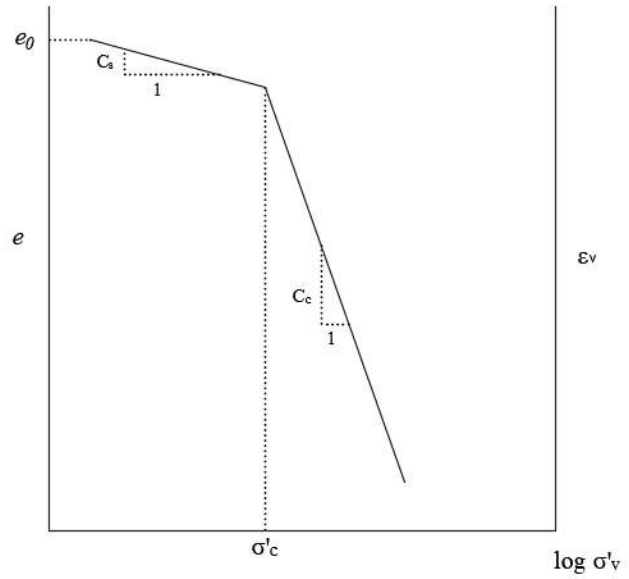

Figure 4.9 Typical consolidation curves (Coduto 2001)

The above figure shows that e and ε_v are indirectly related to σ_v' during the loading and unloading curves represented by the compression and swelling indexes, C_c and C_s, respectively. From this relationship, the volumetric plastic strain can be derived as (Helwany 2007)

$$\varepsilon_{vol}^{pl} = \frac{C_c - C_s}{(\ln 10)(1 + e_0)} \ln \frac{\sigma'}{\sigma_c'} \qquad 4\text{-}6$$

4.5.2 Modified Cam-Clay model (MCCM)

The MCCM is critical state criterion that is used to describe the behavior of fully saturated clay soils. The soil reaches the critical state after passing through series states of yielding resulting in strain hardening or softening. At that stage, change in soil volume occurs with no additional shear stress (Zaman, Gioda and Booker 2000).

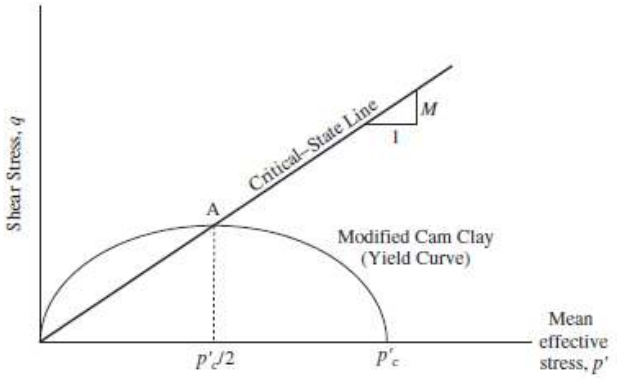

Figure 4.10 Yield surface of Modified Cam-Clay model (Helwany 2007)

The critical state envelope of the MCCM is given as follows:

$$f(p, q, p_c) = \left[\frac{q}{M}\right]^2 + p(p - p_c) = 0 \qquad 4\text{-}7$$

Where

p = Mean effective stress = $\frac{1}{3}(\sigma_1 + \sigma_2 + \sigma_3)$

p_c = Preconsoldation pressure.

M = Slope of critical state envelope = $\frac{6 \sin \varphi'}{3 - \sin \varphi'}$

q = Shear stress = $\sigma_1 - \sigma_3$

The size of the initial yield surface (Figure 4.10) is mainly controlled by p_c. The soil behaves in a plastic manner when the state of the stress touches the yield envelope. The hardening or softening behavior of the soil is described by the over consolidation ratio (OCR). Ultimately, when the soil is normally consolidated or lightly overconsolidated, hardening behavior occurs. On the other hand, when the soil is heavily overconsolidated, softening behavior occurs. Figures 4.11 and 4.12 show the hardening and softening behavior, respectively.

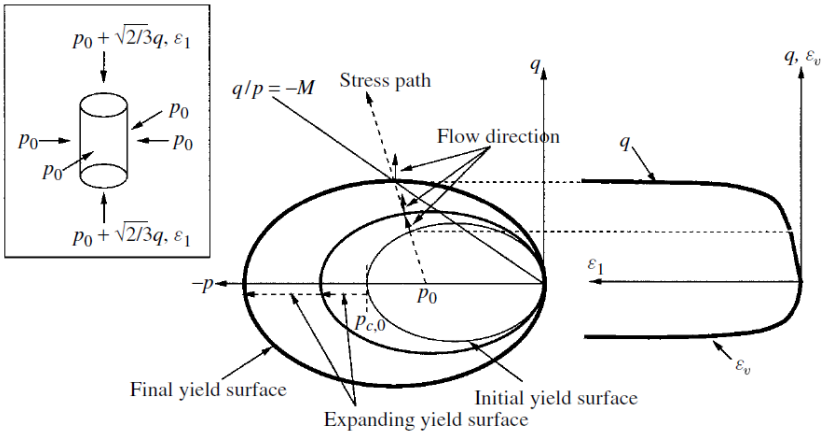

Figure 4.11 Hardening behavior of the MCCM (Zaman, Gioda and Booker 2000)

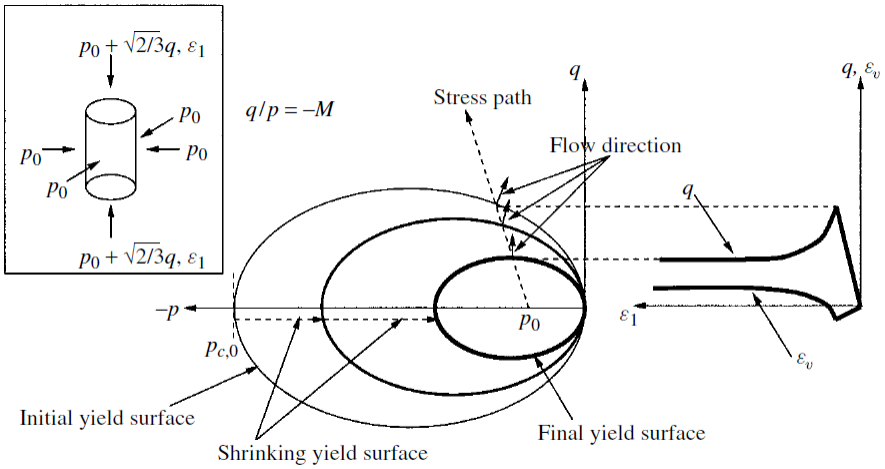

Figure 4.12 Softening behavior of the MCCM (Zaman, Gioda and Booker 2000)

The elastic behavior can be described by bulk modulus, K. The change in the bulk stiffness for loading and unloading is represented by

Loading $$\dot{p} = -\frac{p}{\lambda}\dot{\varepsilon}_v = K\dot{\varepsilon}_v \qquad 4\text{-}8$$

Unloading $$\dot{p} = -\frac{p}{\kappa}\dot{\varepsilon}_v = K\dot{\varepsilon}_v \qquad 4\text{-}9$$

Where κ and λ are modified compression index and modified swelling index, respectively.

4.6 Material properties

The concrete in the structural components, i.e. abutment wall, approach slab, pile and roadway pavement, was assumed to be behave in a linearly elastic manner with a modulus of elasticity that is consistent with a design compressive strength of 4000 *psi* (28 *MPa*). Table 4.2 shows the concrete material parameters assumed for the abutment wall, approach slab, pile and roadway pavement.

Table 4.2 Material parameters used for the structural components

Parameter	Concrete
Density (γ) pcf (kN/m^3)	150 (24)
Modulus of elasticity (E) ksi (MPa)	3,605 (24,856)
Poisson's ratio (ν)	0.21

The soil properties play a significant role in the settlement analysis. These properties are typically collected from fundamental soil tests such as the triaxial and consolidation tests. In this study, a wide range of soil properties were adopted from test results reported by other researchers representing a variety of soil conditions from across the United States.

Three different zones were considered in the analysis; the natural soil, the embankment fill, and the backfill soil. For the purpose of this study, the backfill soil was selected to be sand, which was classified based on the degree of the compaction (i.e. 95% or 90%). The natural and embankment soils were considered to be clay and were classified based on the degree of compressibility (i.e. highly compressible, moderately compressible, or low compressible). According to Coduto (2001), the degree of compressibility of soils can be determined based on a parameter that is related to the compression index, C_c, and the initial void ratio, e_0. The soil is considered low compressible (LC) when $\left(\frac{C_c}{1+e_0}\right)$ falls between 0.0 to 0.10, moderately

compressible (MC) when $\left(\frac{C_c}{1+e_0}\right)$ falls between 0.10 to 0.20, and highly compressible (HC) when $\frac{C_c}{1+e_0}$ is greater than 0.20.

Additionally, empirical relationships and typical values were used to obtain the soil parameters needed for the settlement analysis when actual test results for these parameters were not reported. Some of the empirical relationships used are listed below (B. M. Das 2011)

- Initial void ratio (e_0):

$$e_0 = \frac{C_c}{1.15} + 0.35 \quad \text{4-10}$$

- Swelling index (C_s):

$$C_s = 0.1C_c \quad \text{4-11}$$

- Specific gravity of clay soil (G_s):

$$G_s = 2.70 \rightarrow 2.90 \quad \text{4-12}$$

- Water content (w):

$$\gamma = \frac{(1+w)G_s\gamma_w}{1+e_0} \quad \text{4-13}$$

- Coefficient of permeability (k):

$$k = m_v \times \gamma_w \times C_v \quad \text{4-14}$$

Where:

C_v = Coefficient of consolidation = $10^{-1.2697\ln(LL)+2.1515}$

LL =Liquid limit.

m_v = Volume coefficient of compressibility = $\Delta e/[\Delta\sigma'(1+e_{av})]$

e_{av} = Average void ratio during consolidation.

Δe = Total change of void ratio caused by an effective stress increase of ($\Delta\sigma'$).

Carter and Bentley (2016) provide typical values of coefficient of permeability (k) for various types of soil based on the Unified Soil Classification System (USCS). Table 4.3 shows typical ranges of coefficient of permeability.

Table 4.3 Typical coefficients of permeability (k) for various types of soil (Carter and Bentley 2016)

Soil type	Coefficient of permeability (k) *ft/s* (*m/s*)
well-graded gravel	$\geq 3.3\times10^{-3}$ ($\geq 1.0\times10^{-3}$)
well-graded sand	$\geq 3.3\times10^{-5}$ ($\geq 1.0\times10^{-5}$)
Low to moderate plastic clay	$\geq 1.6\times10^{-7}$ ($\geq 5.0\times10^{-8}$)
Highly plastic clay	$\geq 6.6\times10^{-9}$ ($\geq 2.0\times10^{-9}$)

Three types of clay soils (low compressible, moderately compressible, and highly compressible) were assumed for the natural and embankment soils. In addition, two types of granular sand backfill soils (90% and 95% compaction levels) were assumed. Tables 4.4, 4.5, and 4.6 shows the soil properties used for the natural soil, embankment soil, and the backfill soil, respectively.

Table 4.4 Soil properties used for the natural soil layer

Soil region	Natural soil		
Soil type / parameter	Clay – LC (Monley and Wu 1993)	Clay – MC (Allen and Meade 1988)	Clay – HC (Das, et al. 1999)
Cohesion (C') psi (kPa)	3.47 (23.9)	2.10 (14.5)	1.74 (12.0)
Angle of internal friction (φ') (^{0})	30	28	24
Unit weight (γ) pcf (kN/m3)	114.7 (18.0)	120.0 (18.9)	112.5 (17.7)
Modulus of Elasticity (E) ksi (MPa)	2.43 (16.75)	2.08 (14.36)	1.74 (11.97)
Poisson's ratio (ν)	0.30	0.40	0.40
Compression index (C_c)	0.152	0.240	0.5
Swelling index (C_s)	0.0152	0.024	0.05
Initial void ratio (e_0)	0.48	0.56	0.79
Moisture content (w) (%)	7.6	10.0	20.4
Specific gravity (G_s)	2.70	2.80	2.90
Permeability (k) *ft/s* (*m/s*)	7.9×10^{-8} (2.4×10^{-8})	1.4×10^{-8} (4.3×10^{-9})	2.0×10^{-9} (6.1×10^{-10})

Table 4.5 Soil properties used for the embankment fill layer

Soil region	Embankment fill		
Soil type / parameter	Clay – LC (Laguros, et al. 1991)	Clay – MC (Laguros, et al. 1991)	Clay – HC (Allen and Meade 1988)
Cohesion (C') psi (kPa)	3.50 (24.1)	1.20 (8.3)	0.5 (3.4)
Angle of internal friction (φ') (^{0})	34	30	29
Unit weight (γ) pcf (kN/m3)	122.0 (19.2)	127 (20.0)	130 (20.4)
Modulus of Elasticity (E) ksi (MPa)	1.56 (10.77)	1.39 (9.58)	1.22 (8.38)
Poisson's ratio (ν)	0.30	0.40	0.40
Compression index (C_c)	0.087	0.30	0.42
Swelling index (C_s)	0.014	0.03	0.042
Initial void ratio (e_0)	0.43	0.61	0.72
Moisture content (w) (%)	3.5	12.8	19.4
Specific gravity (G_s)	2.70	2.80	2.90
Permeability (k) *ft/s* (*m/s*)	2.8×10^{-7} (8.53×10^{-8})	7.3×10^{-8} (2.2×10^{-8})	8.9×10^{-9} (2.7×10^{-9})

Table 4.6 Soil properties used for the backfill soil layer

Soil Region	Backfill soil	
Soil type / parameter	Sand - 95% (McGrath, et al. 2002)	Sand - 90% (McGrath, et al. 2002)
Cohesion (C') psi (kPa)	0.0	0.0
Angle of internal friction (φ') (^{0})	43	38
Unit weight (γ) pcf (kN/m3)	128.0 (20.1)	126 (19.8)
Modulus of Elasticity (E) ksi (MPa)	2.90 (20.0)	1.90 (13.1)
Poisson's ratio (ν)	0.30	0.30
Initial void ratio (e_0)	0.50	0.68
Permeability (k) *ft/s* (*m/s*)	1.0×10^{-3} (3.0×10^{-4})	2.2×10^{-3} (6.7×10^{-4})

The modified Drucker-Prager/Cap material model was used to describe the soil behavior in the computer models. The input parameters needed in the finite element analysis to model the soil were obtained such that they would match the properties provided in the above tables. Table 4.7 shows the input parameters used to model the soil.

Table 4.7 Input parameters used to simulate the soils

-	Soil layer							
	Natural			Embankment			Backfill	
	LC[1]	MC[2]	HC[3]	LC[1]	MC[2]	HC[3]	90%[4]	95%[5]
γ pcf (kN/m^3)	114.7 (18.0)	120.0 (18.9)	112.5 (17.7)	122.0 (19.2)	127 (20.0)	130 (20.4)	128.0 (20.1)	126 (19.8)
k ft/s (m/s)	7.9×10^{-8} (2.4×10^{-8})	1.4×10^{-8} (4.3×10^{-9})	2×10^{-9} (6.1×10^{-10})	2.8×10^{-7} (8.5×10^{-8})	7.3×10^{-8} (2.2×10^{-8})	8.9×10^{-9} (2.7×10^{-9})	1×10^{-3} (3×10^{-4})	2.2×10^{-3} (7×10^{-4})
e_0	0.48	0.56	0.79	0.43	0.61	0.72	0.50	0.68
μ[6]	0.38	0.35	0.30	0.45	0.38	0.37	0.47	0.55
E ksi (MPa)	2.43 (16.75)	2.08 (14.36)	1.74 (11.97)	1.56 (10.77)	1.39 (9.58)	1.22 (8.38)	2.90 (20.0)	1.90 (13.1)
ν	0.30	0.40	0.40	0.30	0.40	0.40	0.30	0.30
d psi (kPa)	3,116 (21,484)	1,899 (13,093)	1,589 (10,956)	3,081 (21,243)	1,077 (7,426)	451 (3,110)	≈ 0.0	≈ 0.0
β (^{0})	50	48	43	54	50	49	57	60
K	1.0							
α	0.1							
R	0.2							

[1] low compressible clay. [2] moderate compressible clay. [3] high compressible clay.

[4] 90% standard proctor compacted granular soil. [5] 95% standard proctor compacted granular soil.

[6] concrete to soil coefficient of friction, assumed = 2/3 tan(φ').

CHAPTER 5 - SIMULATION OF SOIL SETTLEMENT BEHIND BRIDGE ABUTMENTS

5.1 Chapter background

The bridge approach slab is part of a transition system in which the end of the bridge is connected to the roadway pavement (Figure 5.1). Its function is to carry traffic loads and provide drivers with a smooth ride as their vehicle travels from the roadway to the bridge and vice versa (Abu-Farsakh and Chen 2014).

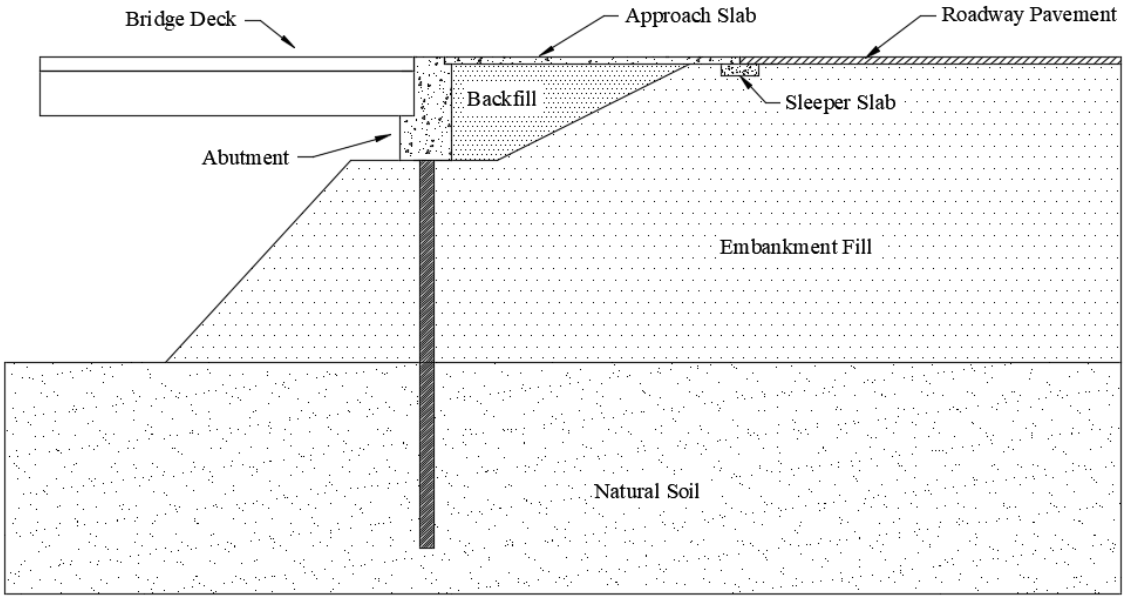

Figure 5.1 Typical longitudinal cross section of a bridge

Due to excessive long-term settlement of soil under the bridge approach slab, a bump can typically develop at the end of the bridge. The bump at the end of the bridge is a well-known problem that affects about 25% of the bridges in the United States, resulting in an estimated $100 million per year in maintenance expenditures (Briaud, James and Hoffman 1997). The bump at the end of the bridge can lead to unsafe driving conditions, vehicle damage, and additional

maintenance cost. Furthermore, distress, fatigue, and deterioration of the bridge deck and expansion joint are possible consequences of such a problem (Briaud, James and Hoffman 1997, Hu, et al. 1979, Nicks 2015).

Thus, an accurate prediction of the ultimate soil deflection profile behind the bridge abutment is an important parameter in the proper design of the approach slab, and for the mitigation of the bump at the end of the bridge. Terzaghi's theories of consolidation are widely used in many geotechnical engineering applications including estimations of settlement of fine-grained soils. The one-dimensional consolidation theory is not always effective in predicting the settlement profile behind bridge abutments (Helwany 2007).

5.2 Chapter problem statement

The longitudinal soil deflection profile behind bridge abutment is rather difficult to predict using a closed-form solution. The difficulty arises due to the nature of the problem (i.e. two- or three-dimensional problem) as well as the number of factors involved. Some of these factors include the variation in the soil profile, the interaction between the abutment wall and the adjacent backfill soil, the size of the backfill area, and the sequential construction of the embankment fill, approach slab and the roadway pavement.

Typically, the soil profile would consist of several soil layers, with some layers deforming in a time-dependent manner, due to primary and secondary settlements. Additionally, the friction developed between the abutment wall and the adjacent soil (backfill soil) restricts some of the soil movement in the vicinity of the abutment wall, while the soil away from the wall would not be similarly affected and would therefore have larger settlement. This type of behavior would typically result in a curved soil settlement profile behind the bridge abutment.

Figure 5.2 shows this pattern of settlement for a soft clay soil based on a finite element model (discussed later).

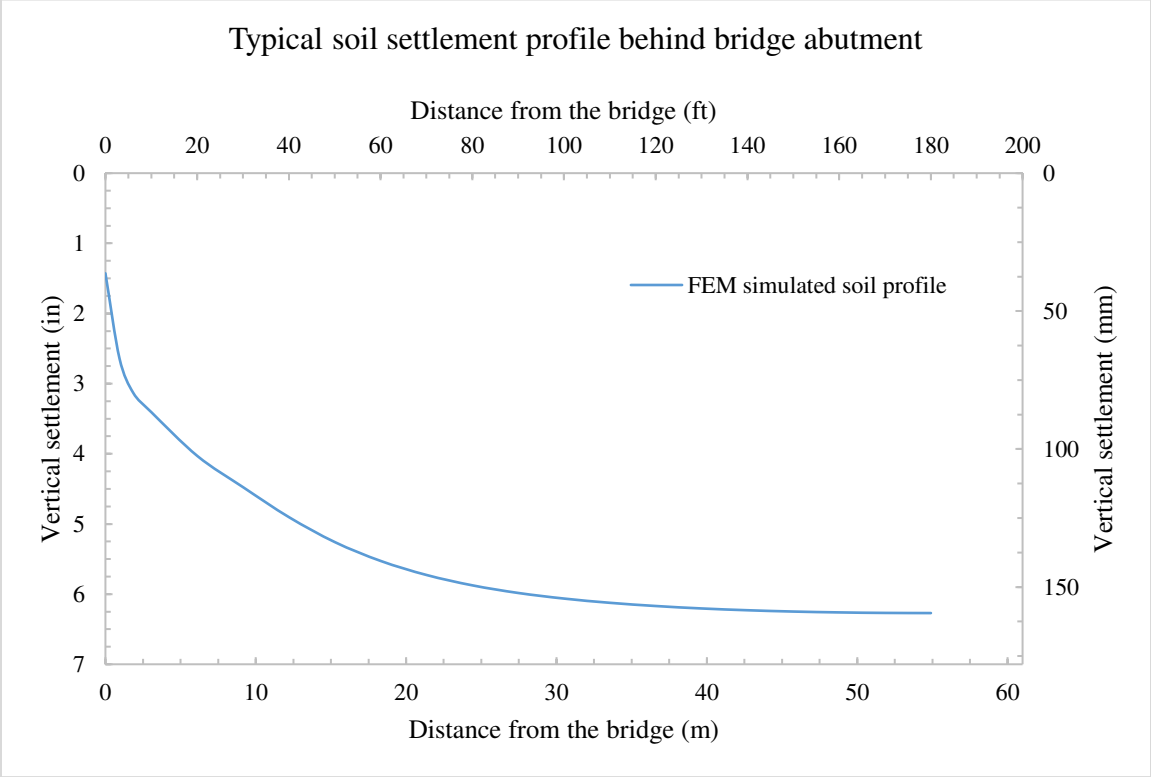

Figure 5.2 Simulated example of longitudinal soil deformation behind bridge abutment

The size of the backfill area is another factor to consider in such a problem, as the backfill would be in direct contact with the abutment wall as well as the embankment fill. As will be discussed in this chapter, the impact of the backfill soil on the deflected profile would primarily depend on the embankment's height, compressibility of the soil, and the abutment type. Additionally, the sequence of construction of the embankment fill would have a significant impact on the overall deformation of the soil as it would directly affect the development of excess pore water pressure within the underlying soils, and thus influence their ultimate settlement. Overall, the longitudinal soil deformation behind bridge abutment is considered one of the main concerns for engineers because of the uncertainties associated with such factors.

Finite element methods are widely used to solve engineering problems, including estimating long-term soil settlement. The advantage of this analytical approach can simulate full-scale conditions with a various range of parameters. Therefore, it can serve as a practical tool in predicting the longitudinal soil settlement profile behind bridge abutment.

5.3 Chapter objectives

The objective of this phase of the study is to develop empirical relationships that can be used to evaluate the ultimate soil settlement profile along a longitudinal line behind the bridge abutment. Such equations would be beneficial in making reliable predictions of the long-term differential settlement of the approach slab, and to plan its design. The empirical equations are derived by conducting a parametric study using a finite element model that includes the effects of various parameters on the soil deflection profile.

5.4 Development and verification of transverse soil finite element model

5.4.1 Introduction

In this phase of the study, a two-dimensional transverse model was generated to perform long-term soil settlement analysis. In this simulation, the embankment fill is to be constructed on top of the natural soil layer. The objective of this analysis was to quantify the surface deformation of the soil in a location that is away from the bridge abutment. The outcome of this simulation can be used to roughly estimate the resulting differential settlement the approach slab founded on similar soil conditions. Figure 5.3 shows the general layout of the two-dimensional transverse model.

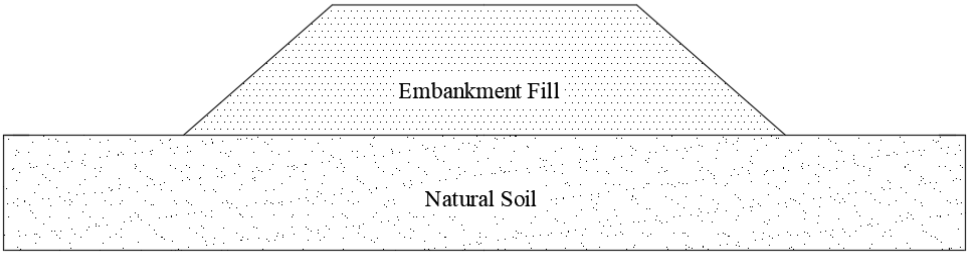

Figure 5.3 Layout of the two-dimensional transverse model

5.4.2 Geometry and boundary conditions

An important aspect of the soil finite element model is selecting the location and types of boundary conditions (i.e. displacement and/or pore pressure boundary conditions) in an efficient and effective manner.

The bottom of the model would represent a location where no soil movement occurs. This location can be determined using the standard penetration test (typically provided in the borehole log profile) whereas a high value indicates a hard layer, such as bedrock. At this location, both vertical and horizontal movements are restricted (assumed to be zero). In addition, no water seepage would be expected to occur at this location, thus, impervious boundary was assumed. The top surfaces of the soil were free to move in all directions. Furthermore, water would be expected to flow through the top surfaces, thus, pervious boundary was assumed.

The soil mass must be sufficiently extended in the transverse direction to capture the behavior of the soil. Laguros et al. (1991) recommend extending the natural soil mass a distance of at least 2 ($D_e + D_{se}$), where D_e is the base width of the embankment fill and D_{se} is the base width of the sloped part of the embankment fill. Figure 5.4 shows the geometry and boundary conditions used in this analysis.

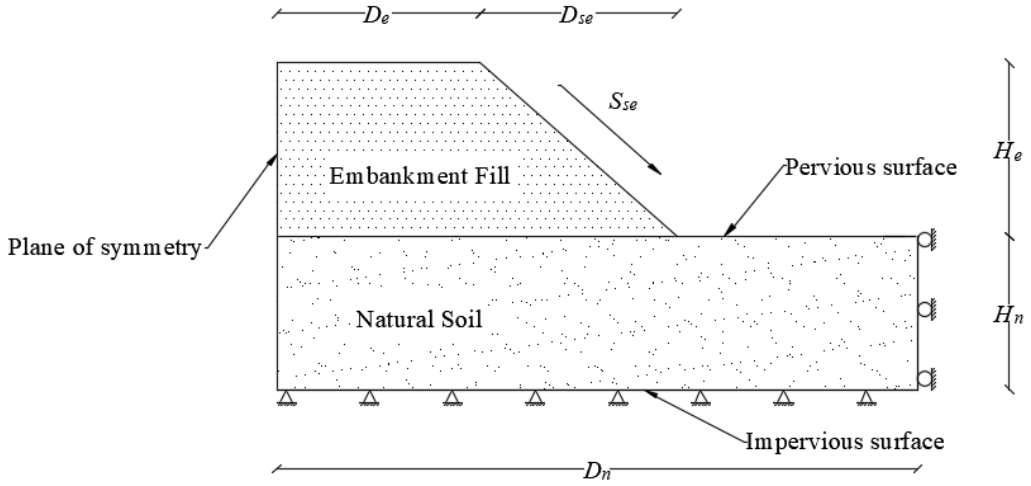

Figure 5.4 Boundary condition of the Two-Dimensional transverse model

In the above figure,

H_e = height of the embankment fill.

S_{se} = side slope of the embankment fill.

H_n = height of the natural soil layer.

D_n = base width of the natural soil.

In this study, H_e, D_e, S_{se}, H_n and D_n were varied according to the parametric study matrix found in Table 5.5.

5.4.3 Analysis procedures for transverse soil model

In soil settlement analysis, timing is a very important factor that influences the soil behavior. This was taken into consideration during the simulation in which the construction of the embankment fill was implemented in a sequential manner. Hopkins (1985) provides an empirical equation to estimate the rate of the loading of embankment fill, T_c, in days, based on its height, H_e, in feet, as follows:

$$T_c = 10^{(1.2376 \log H_e + 0.1122)} \quad 5\text{-}1$$

Accordingly, the analysis procedures used to run the transverse soil model included the following steps:

1- Applying a geostatic load on the natural soil layer. In this step, the effective self-weight of the natural soil was applied. The geostatic step assures that equilibrium is satisfied within the natural soil layer, and that the initial stress condition in all elements falls within the initial yield surface.
2- Constructing the embankment fill over a period of time. In this step, the effective self-weight of the embankment soil was applied. This was done in a coupled (consolidation) step where the load of the embankment is applied in a timely manner using equation 5-1.
3- Consolidation step/steps. In this step/steps, the calculations of the primary settlement (consolidation process) and secondary settlement (creep) were made.

5.4.4 Material properties

The Modified Drucker-Prager/Cap material model was used to simulate the behavior of the soils. Table 4.7 shows the input parameters used to model the soil.

5.4.5 Verification analysis

In this part of the study, a finite element model was generated to simulate the long-term soil behavior. The objective was to compare the simulated ultimate soil settlement with analytical solution (one-dimensional Terzaghi's theory) as well as an actual bridge-site (two-dimensional analysis).

5.4.5.1 One-dimensional analysis

In this part of the analysis, the simulation of the soil behavior using the Modified Cam-Clay model and Modified Drucker-Prager/Cap model were compared against the Terzaghi's one-dimensional consolidation solution. This comparison was helpful in selecting the material model that fits the provided data in which allows for an accurate calibration of the material parameters.

Terzaghi's one-dimensional consolidation theory assumes that water flow and deformation of the soil occurs in one direction only, i.e. the vertical direction, and ignores any lateral deformation of the soil. It gives an estimated solution for the settlement of a fully saturated clay layer having a thickness, H_c, and subjected to a uniform pressure, $\Delta\sigma$. The ultimate settlement, S_c, for a normally consolidated clay is given as follows: (B. M. Das 2011)

$$S_c = \frac{H_c C_c}{1 + e_0} \log \frac{\sigma_0' + \Delta\sigma'}{\sigma_0'} \qquad 5\text{-}2$$

Where

C_c = Compression index.

C_s = Swelling index.

e_0 = Initial void ratio.

σ_0' = Average effective vertical stress.

In order to simulate similar behavior of Terzaghi's one-dimensional solution, a normally consolidated fully saturated clay layer was considered in this analysis. The clay layer was assumed to be located between two sand layers (Figure 5.5). A uniform pressure of $\Delta\sigma$ = 2100 *psf* (100 *kPa*) was to be applied on the top of the sand layer.

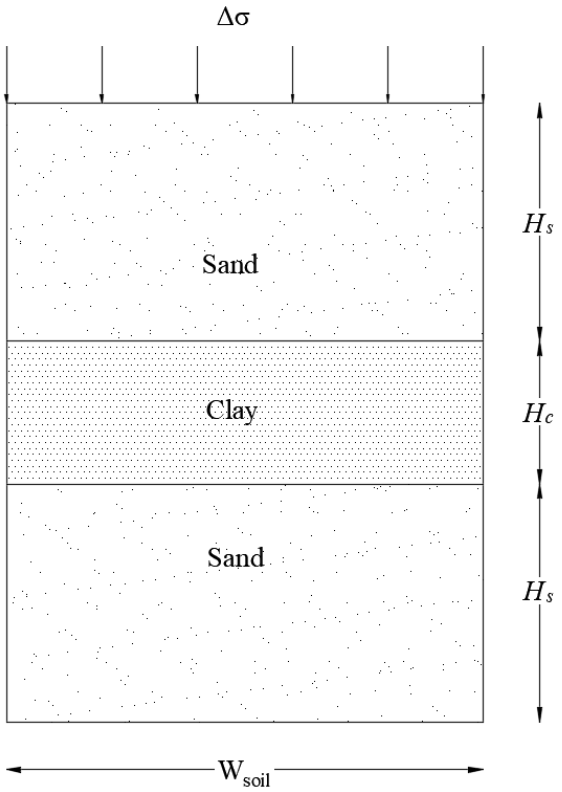

Figure 5.5 Geometry of the settlement problem

For this analysis, a one-dimensional finite element model was generated. A strip along the vertical direction was modeled, $W_{soil} = 1\ ft$ (0.3 m). In addition, one-half of the geometry, across the horizontal axis, was modeled. Along the vertical sides, the soil was assumed to move in the vertical direction only. Figure 5.6 shows the boundary conditions used in the analysis.

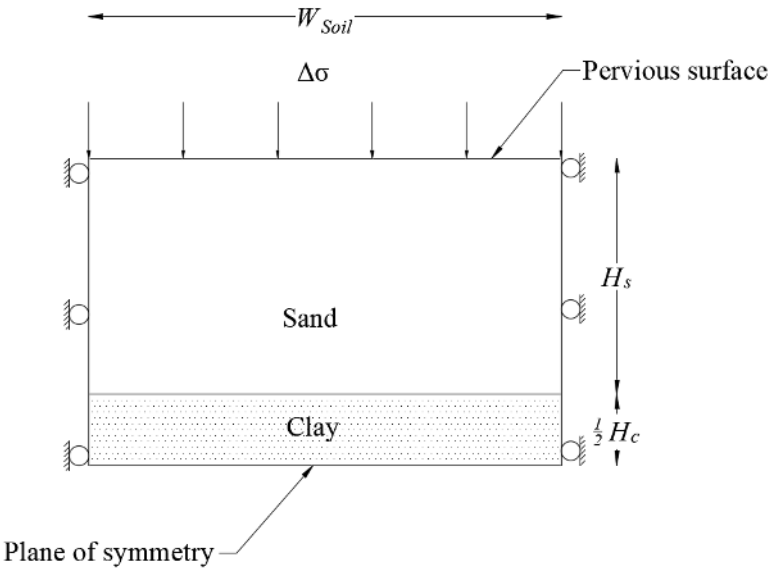

Figure 5.6 Boundary condition of the settlement problem

In the above figures,

H_s = height of the sand layer.

H_c = height of the clay layer.

In this analysis, H_s and H_c were taken as 20 *ft* (6.1 *m*), and 3 *ft* (1.0 *m*), respectively. The input parameters used to simulate the soils are shown in Table 5.1. Figure 5.7 shows the finite element discretization.

Table 5.1 Input parameters used to simulate the soils

Soil layer			
-	Clay		Sand
Material model / parameter	MCCM (Helwany 2007)	MDPCM	Elastic (McGrath, et al. 2002)
Unit weight (γ) pcf (kN/m^3)	122.0 (19.0)		128.0 (20.1)
Permeability (k) ft/s (m/s)	1.97×10^{-3} (6.0×10^{-8})		1×10^{-3} (3×10^{-4})
Initial void ratio (e_0)	0.80		0.50
Modulus of Elasticity (E) ksi (MPa)	-		2.90 (20.0)
Poisson's ratio (ν)	0.28		0.30
Modified swelling index (κ)	0.01957	-	-
Modified compression index (λ)	0.1174	-	-
Slope of the critical line (M)	1.0	-	-
Over consolidation ratio (OCR)	1.0		-
Size of the yield surface (β)	1.0	-	-
Swelling index (C_s)	-	0.045	-
Compression index (C_c)	-	0.27	-
Modified Cohesion (d') psi (kPa)	-	0	-
Modified Angle of internal friction (β') (^{0})	-	45	-
Yield surface shape (K)	1.0	1.0	-
Transition surface radius (α)	-	0.1	-
Cap eccentricity (R)	-	0.2	-

Figure 5.7 Finite element mesh of the comparison model

Figures 5.8 and 5.9 show the deformed mesh of the soil at the end of the analysis when modeled using the Modified Cam-Clay model and Modified Drucker-Prager/Cap model, respectively.

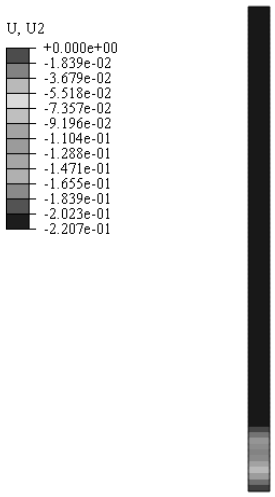

Figure 5.8 Vertical deformation contour at the end of the analysis (MCCM) (*ft*)

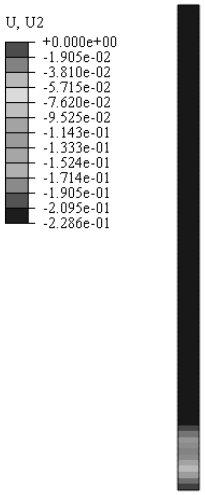

Figure 5.9 Deformed mesh at the end of the analysis (MDPCM) (*ft*)

Figure 5.22 shows the simulated settlement history of the clay layer. The figure shows that the Modified Cam-Clay model and Modified Drucker-Prager/Cap model simulated the soil settlement behavior reasonably well when compared with Terzaghi's one-dimensional solution. Hence, both material models can be used to describe the soil behavior using parameters values shown in Table 5.1 (i.e. size of the yield surface, β, yield surface shape, K, transition surface radius, α, and cap eccentricity, R).

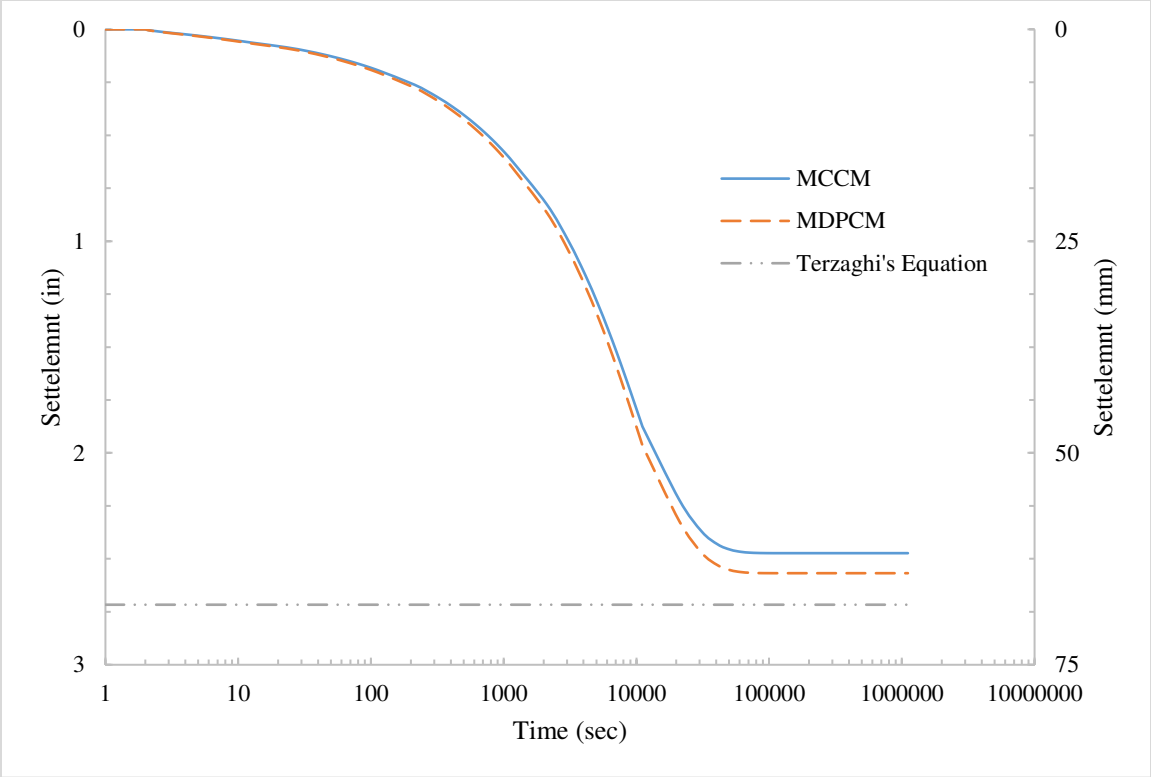

Figure 5.10 Simulated vs. Analytical settlement history of the clay layer

5.4.5.2 Two-dimensional analysis

In this part of the study, an attempt was made to evaluate the surface settlement profile at an existent bridge-site. Laguros et al. (1991) conducted detailed field measurements and laboratory tests on several bridge sites in Oklahoma through which soil settlement history were recorded. Simulation analyses of the settlement history were also conducted, using finite element method, in order to compare with the recorded soil settlement.

In this analysis, the soil settlement at the Clinton bridge-site was simulated. The objective of this simulation was to verify the settlement of the soil in using a two-dimensional model. At this site, an approximate 8 *in* (203 *mm*) of surface settlement was recorded. The height of the embankment fill was H_e = 25 *ft* (7.5 *m*). The natural soil consisted of two soil layers. The top layer was a silty clay with a height of $H_{n\text{-}Top}$ =14 *ft* (4.3 *m*). The bottom layer was a sandy silt with a height of $H_{n\text{-}Bottom}$ =8 *ft* (2.4 *m*). Laguros et al. (1991) reported that the natural soil layers

were highly saturated (filled with water). It has been also reported that maintenance to the bridge approach area was performed several times in the past (overlaid with asphalt). Figure 5.11 shows the transverse layout of the soil profile at bridge Clinton site.

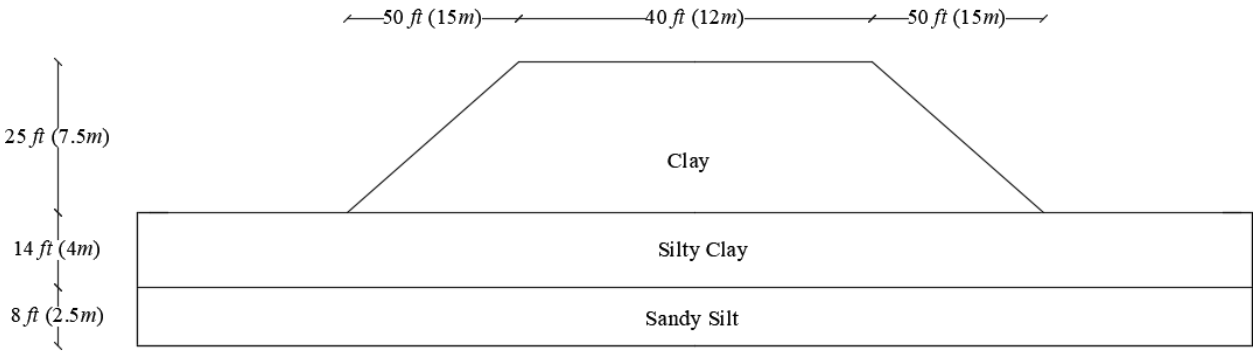

Figure 5.11 Soil profile at Clinton bridge site (Laguros et al. 1991)

An attempt was made by Laguros et al. (1991) to simulate the surface soil settlement at this site using finite element method. In their analysis, the simulation was performed merely on the natural soil layers. The embankment fill was replaced with an equivalent surcharge of 2750 *psf* (132 *kPa*). This was to address the problems associated with the consolidation behavior of the natural soil layers. The bottom layer of the natural soil (sandy silt) was simulated using linear elastic material model. On the other hand, the top layer of the natural soil (silty clay) was simulated using the Modified Cam-Clay material model. Figure 5.15 shows the result of Laguros et al. (1991) simulation. The analysis indicated that the natural soil layers had contributed to approximately 65% of the recorded settlement, 5.2 *in* (132 *mm*). The remaining 35% was attributed to the consolidation of the embankment fill.

The finite element analysis software, ABAQUS, was used in this part of the study to simulate the surface settlement of the natural soil at Clinton bridge site. The embankment fill was modeled in this simulation. This was to address the simulation of the longitudinal soil settlement, which was conducted at a later phase of the study (see Section 5.7). The properties of the natural

soil and embankment fill were obtained from the borehole soil profile reported by Laguros et al. (1991). Similar to their analysis, the top layer of the natural soil was simulated using the Modified Cam-Clay material model. However, the Modified Drucker-Prager/Cap material model was used to simulate the behavior of the bottom natural soil layer as well as the embankment fill. Table 5.2 shows the input properties of the soil at the Clinton bridge site.

Table 5.2 Input parameters used to simulate the soil at Clinton bridge site

-	Soil layer		
	Natural Soil		Embankment fill
	Top (silty clay)	Bottom (sandy silt)	Clay
Material model / parameter	MCCM	MDPCM	MDPCM
Unit weight (γ) pcf (kN/m^3)	106 (16.7)	127 (20)	110 (17.3)
Permeability (k) ft/s (m/s)	1.5×10^{-9} (4.6×10^{-10})	3.3×10^{-6} (1×10^{-6})	2.3×10^{-6} (7×10^{-7})
Initial void ratio (e_0)	0.725	0.53	0.50
Modulus of Elasticity (E) ksi (MPa)	-	2.38 (16.4)	1.35 (9.3)
Poisson's ratio (ν)	0.40	0.40	0.30
Modified swelling index (κ)	0.012	-	-
Modified compression index (λ)	0.20	-	-
Slope of the critical line (M)	1.33	-	-
Over consolidation ratio (OCR)	1.70	-	-
Size of the yield surface (β)	1.0	-	-
Swelling index (C_s)	-	-	0.0171
Compression index (C_c)	-	-	0.171
Modified Cohesion [d'] psi (kPa)	-	0	8180
Modified Angle of internal friction [β'] (^{0})	-	52.5	50.2
Yield surface shape [K]	1.0	1.0	1.0
Transition surface radius [α]	-	0.1	0.1
Cap eccentricity [R]	-	0.2	0.2

The finite element model was generated with boundary condition as described in section 5.4.2. The simulation was run for a simulated total time that allows initial, primary (dissipation of water) and secondary (creep) settlements of the modeled soil to be completed. The load on the embankment fill layer was applied over 69 days (Laguros et al. 1991). Figure 5.12 shows the finite element discretization of the simulated soil.

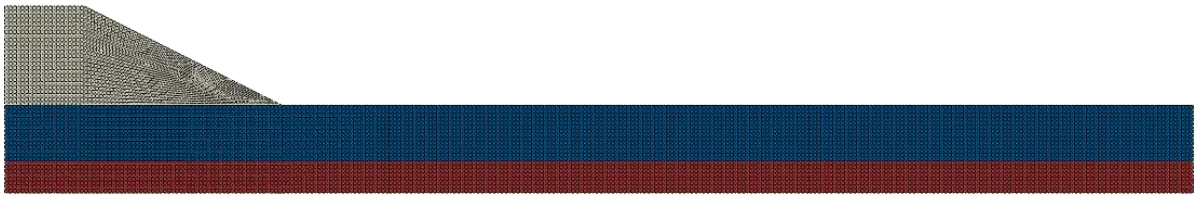

Figure 5.12 Finite element discretization of the simulated soil at Clinton bridge site

The results from the finite element analysis are presented in Figures 5.13 through 5.17. Figure 5.13 shows the vertical deformation contour of the simulated soils at the end of the analysis. Figure 5.14 shows the distribution of pore pressure at the end of the analysis.

Figure 5.13 Vertical deformation contour at the end of the analysis (*ft*)

Figure 5.14 Excess pore pressure contour at the end of the analysis (*psf*)

Figure 5.15 shows the surface settlement profile of the natural soil. The figure indicates that the ultimate surface settlement under the center of the embankment was 5.7 *in* (142 *mm*), which compared with the simulation result of Laguros et al. (1991) with a relatively good agreement. The slight difference in the deflection shape could be attributed to the loading procedure and element size used in the presented simulation. Figure 5.16 shows the surface settlement profile at the surface of the embankment layer. A surface settlement of 7.3 *in* (185 *mm*) was encountered at the center of the embankment fill. This was in good agreement with the

reported settlement of 8 *in* (203 *mm*). The difference between the reported and simulated settlement can be attributed to the maintenance performed on this bridge-site in which resurfaced several times, which was not considered in the analysis.

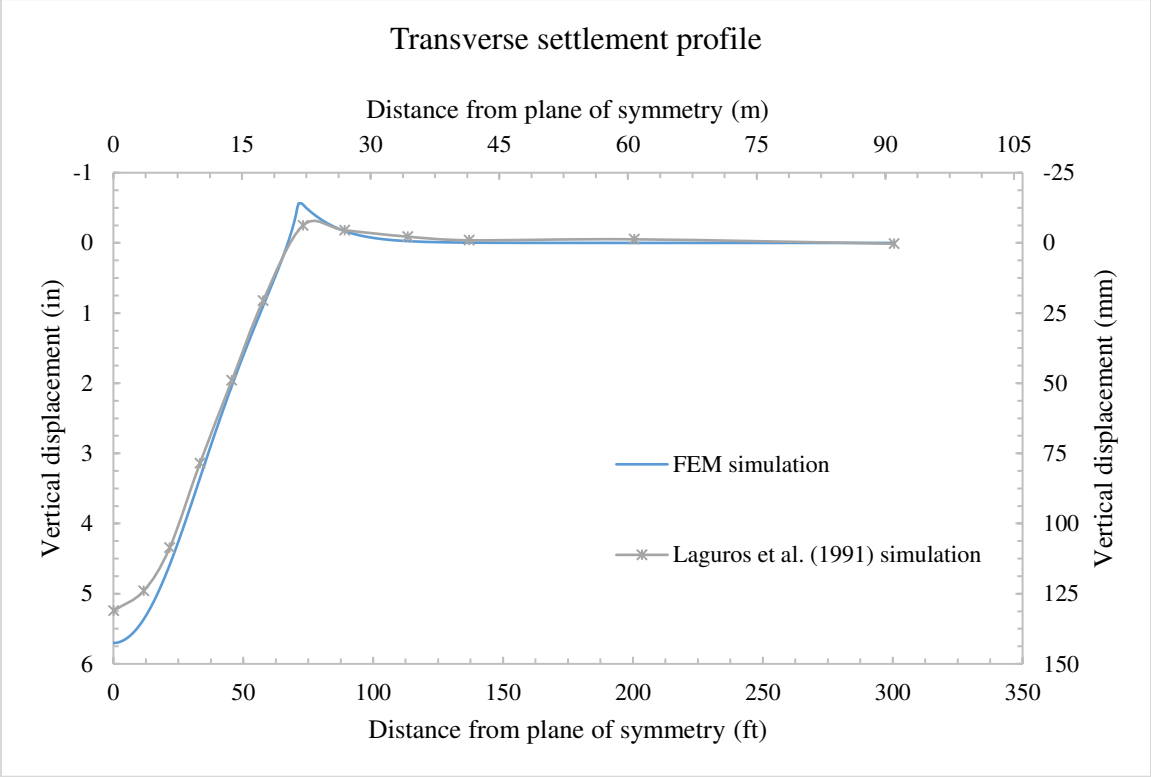

Figure 5.15 Simulated surface settlement profile of the natural soil

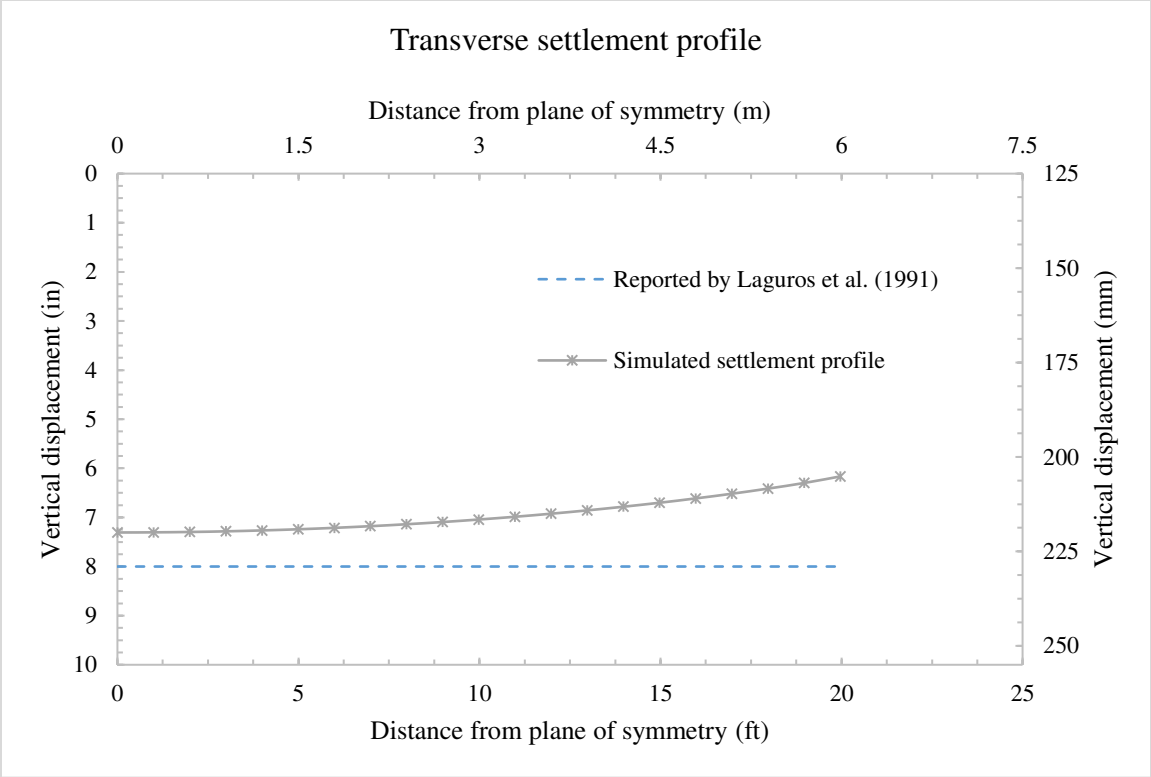

Figure 5.16 Simulated surface settlement profile of the embankment fill

Figure 5.17 shows excess pore pressure history at the center of the silty clay layer. The figure shows how excess pore pressure increases as the embankment is constructed. The pore pressure peaked at time right after the end of the embankment's construction. A maximum pore pressure of 1020 *psf* (49 *kPa*) was encountered. This was higher than what obtained by Laguros et al. (1991) simulation of 500 *psf* (24 *kPa*). The difference could be attributed to the use of the modeled embankment fill in which allowed the buildup of the pore pressure. The figure also indicates that it took the natural soil layer (silty clay) about 7 years to reach a degree of consolidation of 95%.

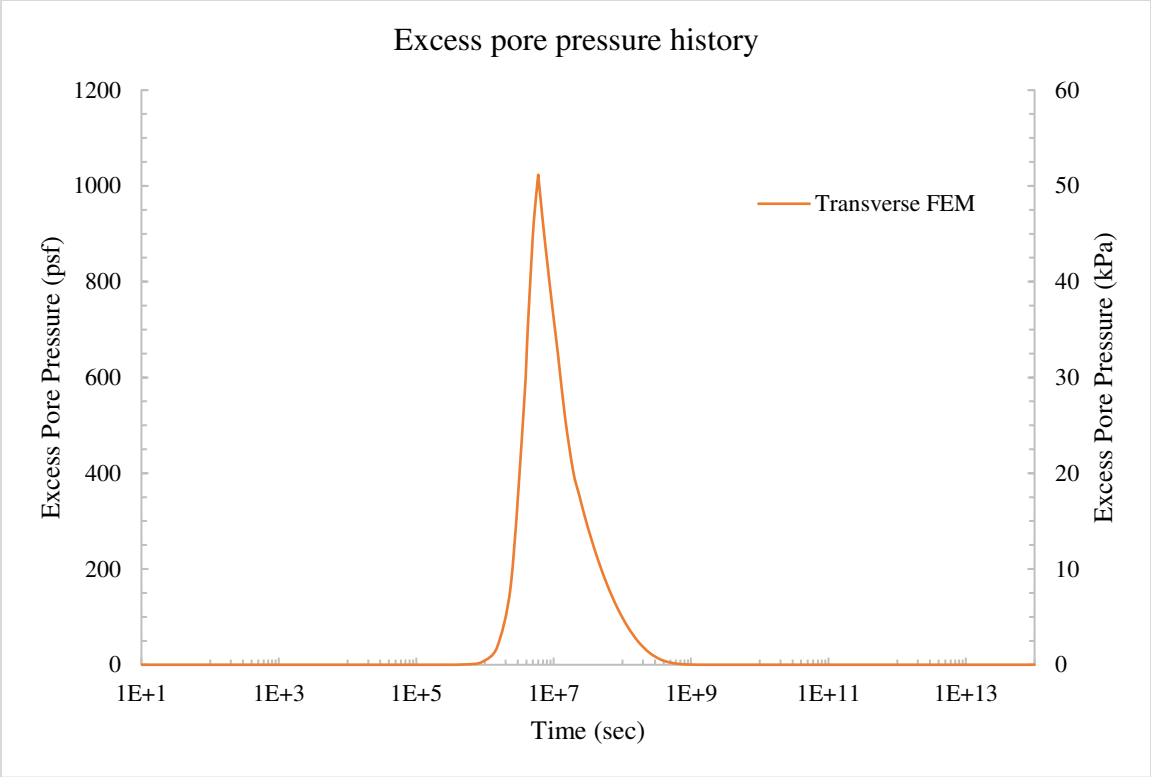

Figure 5.17 Simulated excess pore pressure history

5.4.6 Initial model

An initial model was used in this phase of the study to test the effect of varying the side slope of the embankment, S_{se}. The slopes were selected based upon the common practices of bridge construction in the United States (see Chapter 3). The layout used in the initial model was similar to that shown in Figure 5.4. The soil profile consisted of a highly compressible embankment fill and highly compressible natural soil. In this simulation, the base width of the embankment soil, D_e, was set as 40 *ft* (12 *m*) (see Section 5.5). H_e, H_n, and S_{se} were varied according to Table 5.3. The material used to simulate the soil was described in section 5.4.4.

Table 5.3 Parameters range used in the initial model simulation

Analysis No.	Side slope of the embankment fill (S_{se}) (vertical to horizontal)	Height of embankment fill (H_e) *ft* (*m*)	Height of natural soil (H_n) *ft* (*m*)
1	1 to 2	30 (9.1)	30 (9.1)
2		20 (6.1)	
3		10 (3.0)	
4	1 to 1.5	30 (9.1)	
5		20 (6.1)	
6		10 (3.0)	

The surface settlement at the center of the embankment fill was retrieved at the end of each analysis. Figures 5.18 through 5.23 show the deformed contour of the simulated soils. Figure 5.24 shows the simulated surface settlement at the center of the embankment fill.

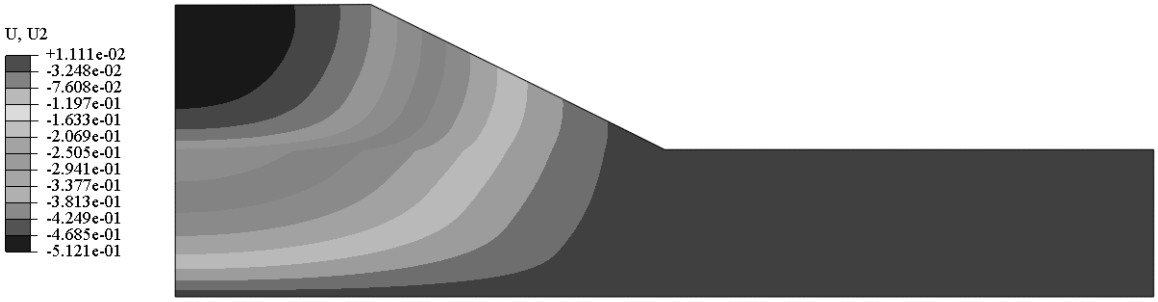

Figure 5.18 Vertical deformation contour of analysis No.1 (*ft*)

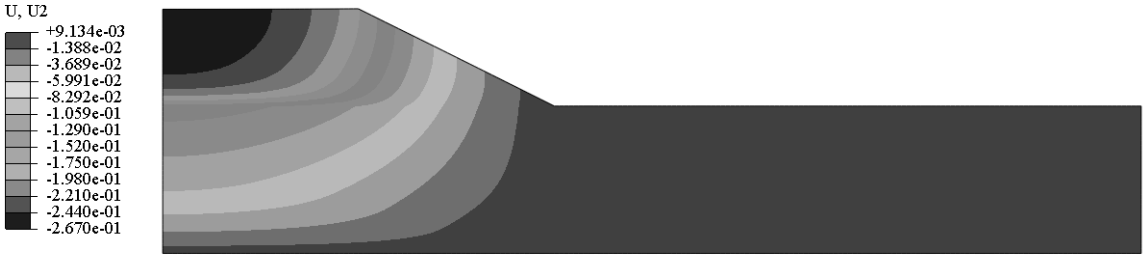

Figure 5.19 Vertical deformation contour of analysis No.2 (*ft*)

Figure 5.20 Vertical deformation contour of analysis No.3 (*ft*)

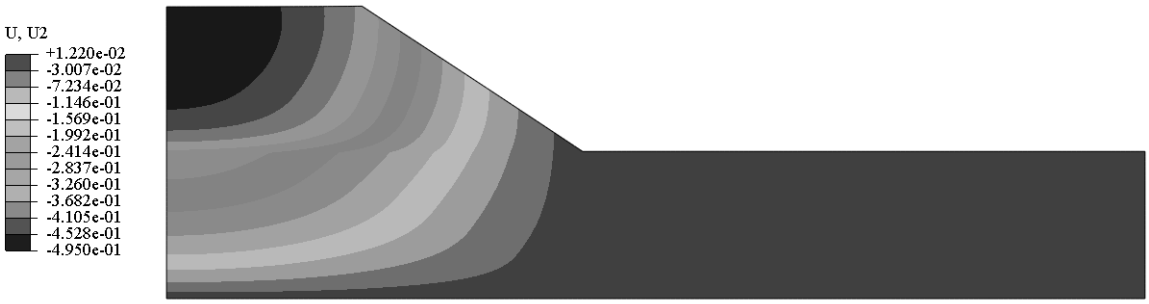

Figure 5.21 Vertical deformation contour of analysis No.4 (*ft*)

Figure 5.22 Vertical deformation contour of analysis No.5 (*ft*)

Figure 5.23 Vertical deformation contour of analysis No.6 (*ft*)

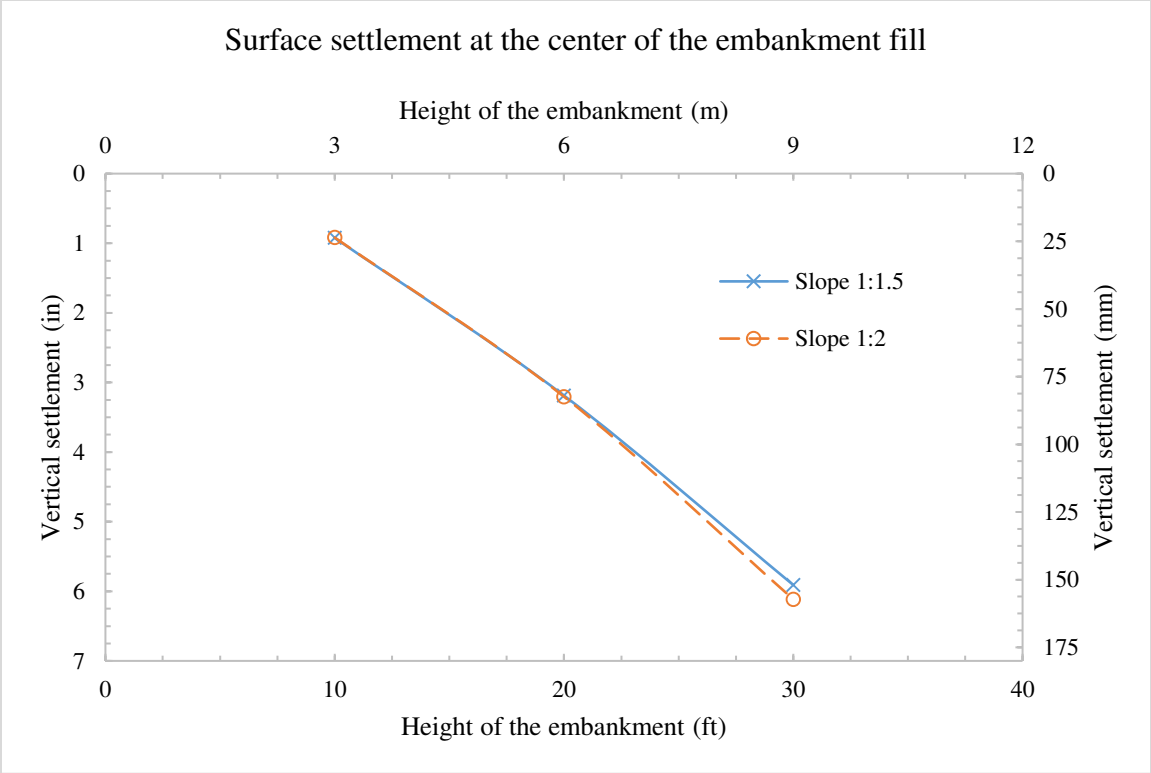

Figure 5.24 Simulated surface settlement at the center of the embankment fill

The above figures show that varying the side slope of the embankment would generally affect the surface settlement. This could be attributed to the increase of the filling material associated with the side slope of 1:2 (1 vertical to 2 horizontal) compared with 1:1.5 (1 vertical to 1.5 horizontal). Nevertheless, the overall effect of varying the side slope did not exceed 2%. Consequently, it has been concluded that varying the side slope of the embankment fill from 1:1.5 to 1:2 (vertical to horizontal) have no significant effect on the overall surface settlement of the embankment fill.

5.4.7 Element type and size

As a porous material, soil contains voids that can be filled with air and/or water. Thus, the element used to discretize the soil was a four-node, plane strain quadrilateral element with bilinear displacement and pore pressure (element code: CPE4P). This type of element has the capability to capture deformation as well as excess pore pressure history. In this element, each

node consists of two displacement degrees of freedom (U_x and U_y) and one pore pressure degree of freedom (*Por*) (ABAQUS 2015). Figure 5.25 shows the element type and degrees of freedom used in the simulation.

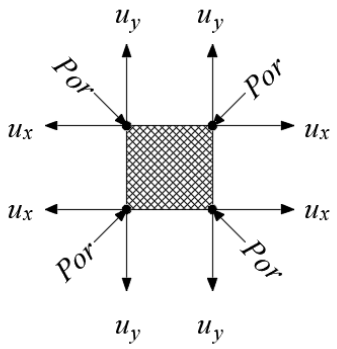

Figure 5.25 Element used to simulate the soil

The initial model (Section 5.4.6) was used to determine the proper element sizes that would maintain the accuracy of results while reducing the computational time. This was done by monitoring the surface settlement at the center of the embankment fill as a function of different element sizes.

The soil profile used in this simulation had a layout similar to what shown in Figure 5.4. It consisted of highly compressible embankment fill with height H_e = 30 *ft* (9.1 *m*), highly compressible natural soil with height H_n = 30 *ft* (9.1 *m*), base width of the embankment fill D_e = 40 *ft* (12*m*), base width of the sloped part of the embankment fill D_{se} = 60 *ft* (18 *m*), side slope of the embankment fill S_{se} = 1:2 (1 vertical to 2 horizontal), and base width of the natural soil D_n = 200 *ft* (61 *m*).

The element size was reduced in each subsequent simulation and surface settlement at the center of the embankment fill was obtained accordingly. Table 5.4 shows the size and number of the elements used in the analysis. Figure 5.27 shows the result of this analysis.

Table 5.4 Size and number of the elements used in the analysis

Element size (length × width) *ft* × *ft* (*m* × *m*)	Total number of elements
5.0 × 5.0 (1.5 × 1.5)	351
2.5 × 2.5 (0.8 × 0.8)	2,214
1.0 × 1.0 (0.3 × 0.3)	8,856
0.5 × 0.5 (0.2 × 0.2)	35,471
0.25 × 0.25 (0.1 × 0.1)	141,884

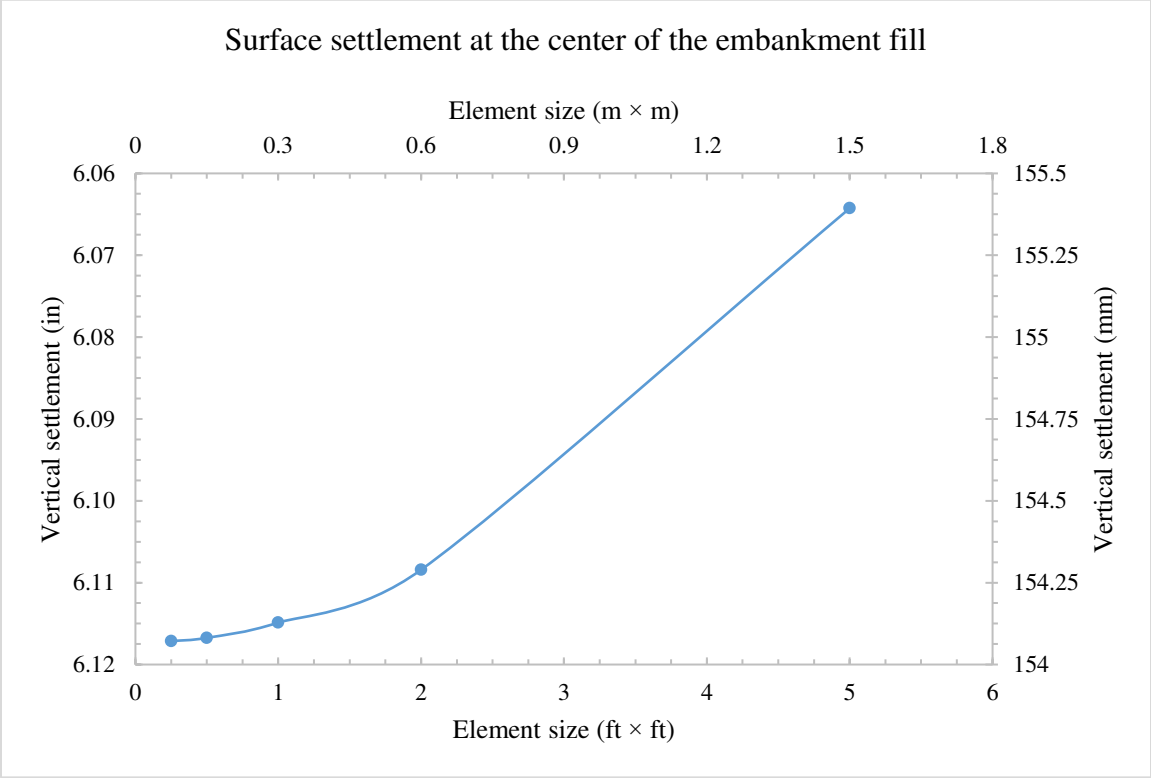

Figure 5.26 Simulated surface settlement at the center of the embankment fill with respect to element size

The above figure shows that the surface settlement at the center of the embankment fill becomes nearly steady (maximum 0.04% error) when the element size is at or less than 1.0 *ft* × 1.0 *ft* (0.30 *m* × 0.30 *m*), and therefore, this element size was used in this study.

5.5 Parametric study on transverse two-dimensional FEM

A parametric study was conducted using finite element analysis to quantify the effects of various parameters on the surface settlement profile of the embankment fill. The parameters considered were the height of embankment fill, H_e, embankment soil type, side slope of the

embankment fill, S_{se}, natural soil height, H_n, and natural soil type. The heights of the embankment fill were selected upon the height category. Long et al. (1999) classified the heights of the embankment fill into: low $H_e \leq 10\ ft$ ($3.0\ m$), medium $10\ ft$ ($3.0\ m$) $\leq H_e \leq 26\ ft$ ($8.0\ m$), and high $H_e > 26\ ft$ ($8.0\ m$). The height of the natural soil was fixed at $H_n = 30\ ft$ ($9.1\ m$). This was to address the effect of the bridge construction practices on the performance of the embankment fill. In this simulation, the base width of the embankment soil, D_e, was set at $40\ ft$ ($12\ m$), one-half of a typical two-directions two-lanes highway bridge (AASHTO 2001). Table 5.5 shows the parameters used in this analysis along with their ranges. Table 5.6 shows the variation of each parameter used in the simulation.

Table 5.5 Two-Dimensional transverse model parametric study matrix

Parameter	Range
Height of embankment fill (H_e)	10, 20, and 30 *ft* (3.0, 6.1 and 9.1 *m*)
Embankment soil type (Compressibility Degree)	High, moderate and low
Side slope of embankment fill (S_{se}) (Vertical to Horizontal)	1 to 2
Height of natural soil (H_n)	30 *ft* (9.1 *m*)
Natural soil type (Compressibility Degree)	High, moderate and low

Table 5.6 Range of parameters used in the simulation

Analysis No.	Side slope of embankment fill (S_{se}) (Vertical to Horizontal)	Height of embankment fill (H_e) *ft* (*m*)	Embankment soil type (compressibility degree)	Natural soil type (compressibility degree)	Height of natural soil (H_n) *ft* (*m*)
1	1 to 2	10 (3)	High	High	30 (9.1)
2		20 (6.1)			
3		30 (9.1)			
4		10 (3)	Moderate		
5		20 (6.1)			
6		30 (9.1)			
7		10 (3)	Low		
8		20 (6.1)			
9		30 (9.1)			
10		10 (3)	High	Moderate	
11		20 (6.1)			
12		30 (9.1)			
13		10 (3)	Moderate		
14		20 (6.1)			
15		30 (9.1)			
16		10 (3)	Low		
17		20 (6.1)			
18		30 (9.1)			
19		10 (3)	High	Low	
20		20 (6.1)			
21		30 (9.1)			
22		10 (3)	Moderate		
23		20 (6.1)			
24		30 (9.1)			
25		10 (3)	Low		
26		20 (6.1)			
27		30 (9.1)			

The finite element model was generated as described in section 5.4. The models were run for a simulated total time that allowed the completion of initial, primary (dissipation of water), and secondary (creep) settlements of the modeled soil. The load on the embankment fill was applied according to equation 5-1. Additional surcharge pressure was applied on the top surface of the embankment. The pressure was equivalent to the load induced by the approach slab/pavement of 150 *pcf* (24 kN/m^3). A typical finite element discretization of the two-dimensional transverse model is shown in Figure 5.27. Figure 5.28 shows the simulated surface settlement at the center of the embankment.

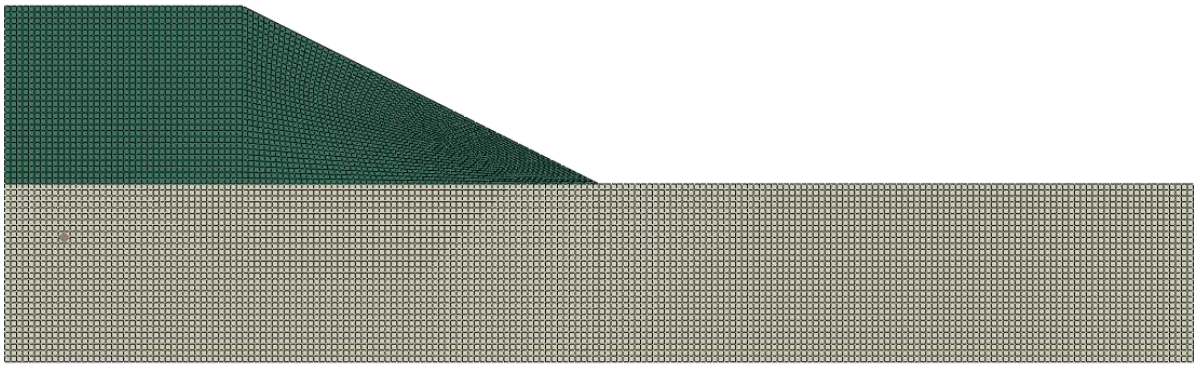

Figure 5.27 Finite element discretization of the two-dimensional transverse model

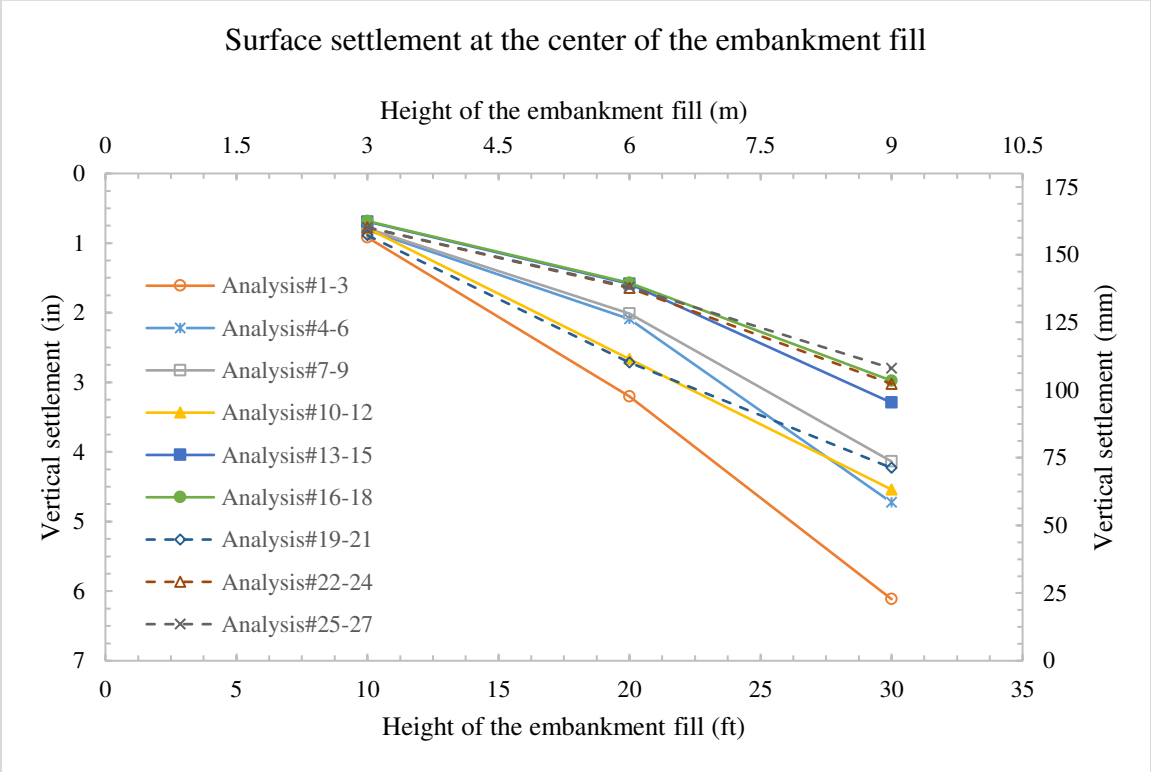

Figure 5.28 Surface settlement at the center of the embankment fill of the Two-Dimensional transverse model

The above figure shows that the height of the embankment fill has a significant effect on the overall surface settlement. In order to put the results into perspective, one end of a 20 *ft* (6.1 *m*) approach slab was assumed to be rested on the surface of the embankment fill, and the resulting differential settlement was evaluated accordingly (see Section 2.1). As a result, employing a low embankment fill height of 10 *ft* (3.0 *m*) would yield a slope of (0.3/125 – 0.5/125), which in this case, would always result in a smooth slope change between the bridge

and the roadway pavement. Employing a medium embankment fill height of 20 *ft* (6.1 *m*) would yield a slope of (0.8/125 – 1.7/125), which in this case, would fluctuate between smooth to rough transition based upon the soil conditions. On the other hand, employing a high embankment fill height of 30 *ft* (9.1 *m*) would yield a slope of (> 1.5/125), which in this case, would always result in a rough transition between the bridge and the roadway pavement. Ultimately, it can be concluded that embankment fill height of H_e > 20 *ft* (6.1 *m*) would be problematic in terms of the transition performance. The slope of the approach slab must be checked against soil conditions in such cases.

Figures 5.29 to 5.31 show the excess pore pressure history at the middle of the natural soil layer. The figures indicate that it would take between 2 months (analysis#27) to 14 years (analysis#1) for the natural soil layer to reach 95% consolidation. This variation would depend mainly upon the soil conditions, i.e. height and type of the soils.

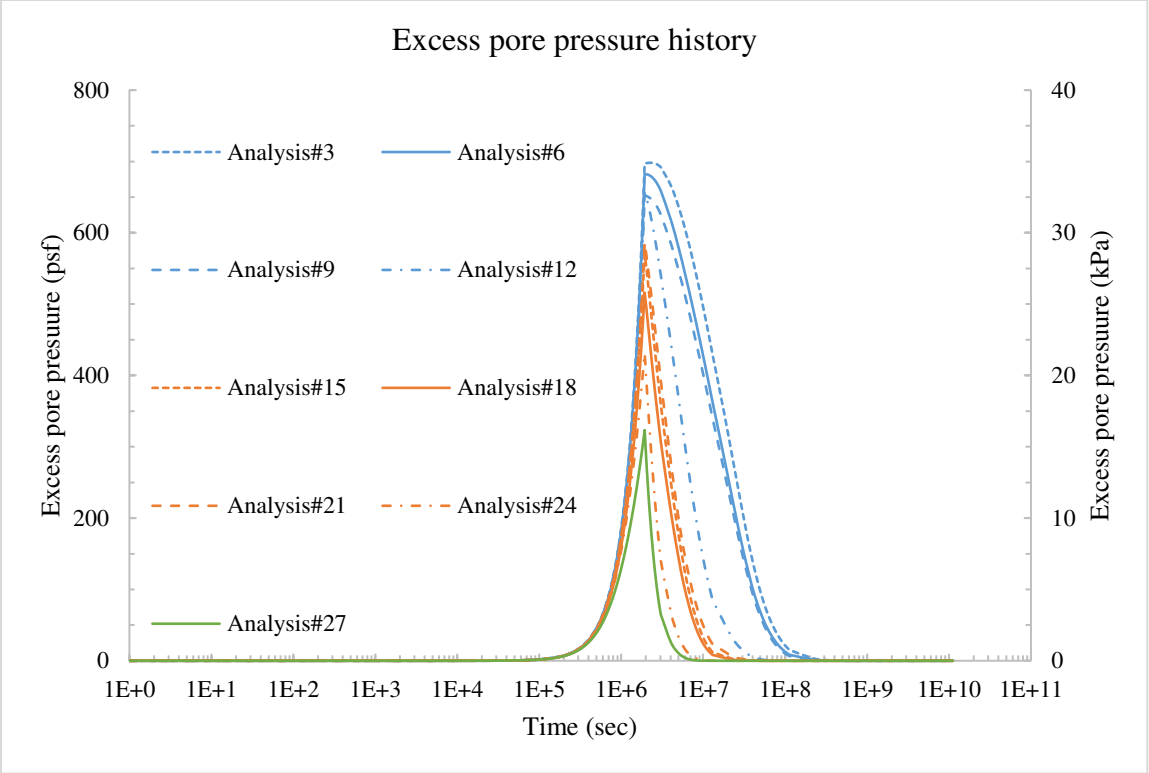

Figure 5.29 Simulated excess pore pressure history with H_e = 10 *ft* (3.0 *m*)

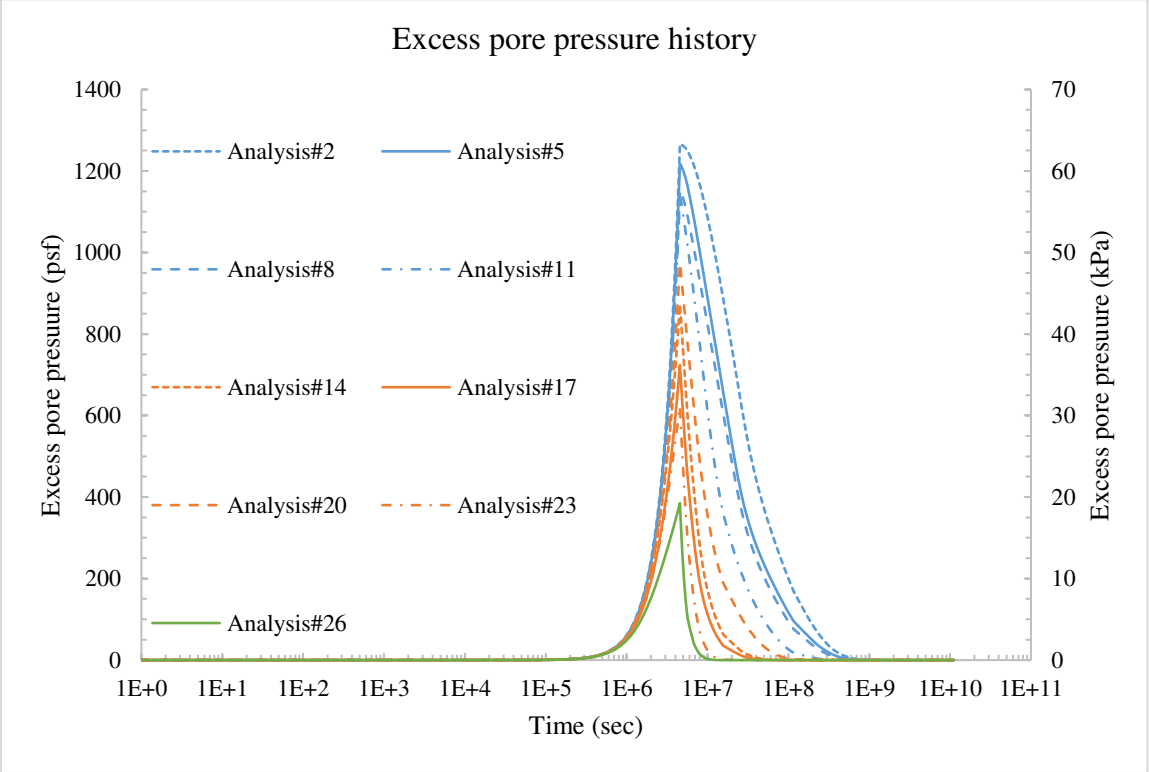

Figure 5.30 Simulated excess pore pressure history with H_e = 20 *ft* (6.1 *m*)

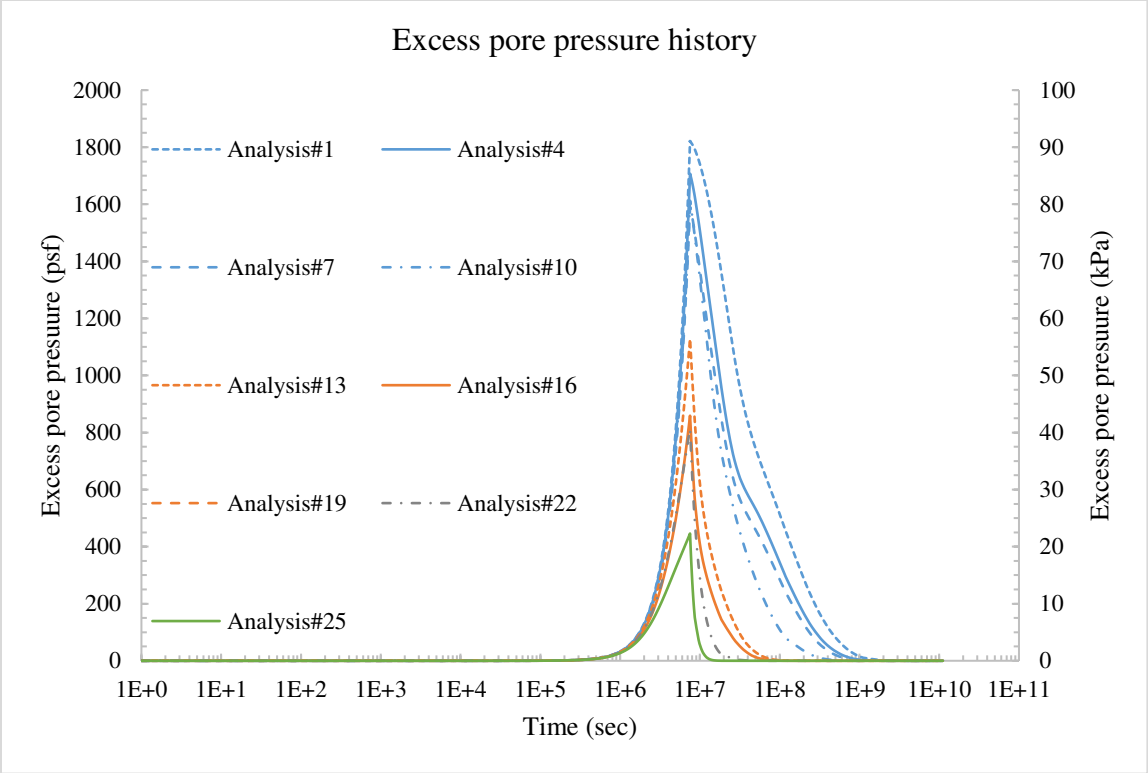

Figure 5.31 Simulated excess pore pressure history with H_e = 30 *ft* (9.1 *m*)

5.6 Development and verification of longitudinal soil-structure FEM

5.6.1 Introduction

The longitudinal-direction finite element model can be generally used to estimate the roadway and soil surface deflection profiles. The effect of the abutment wall on the adjacent soil is counted for in this type of model, where it retains the soil movement due to friction. The outcome of the two-dimensional longitudinal model can be used to evaluate the severity of the bump at the end of the bridge.

In this study, a two-dimensional finite element model was generated to performed long-term soil-structure analysis. The developed finite element model consisted of the following components; approach slab, abutment wall, roadway pavement, granular backfill soil, embankment fill, and natural soil, as shown in Figure 5.32.

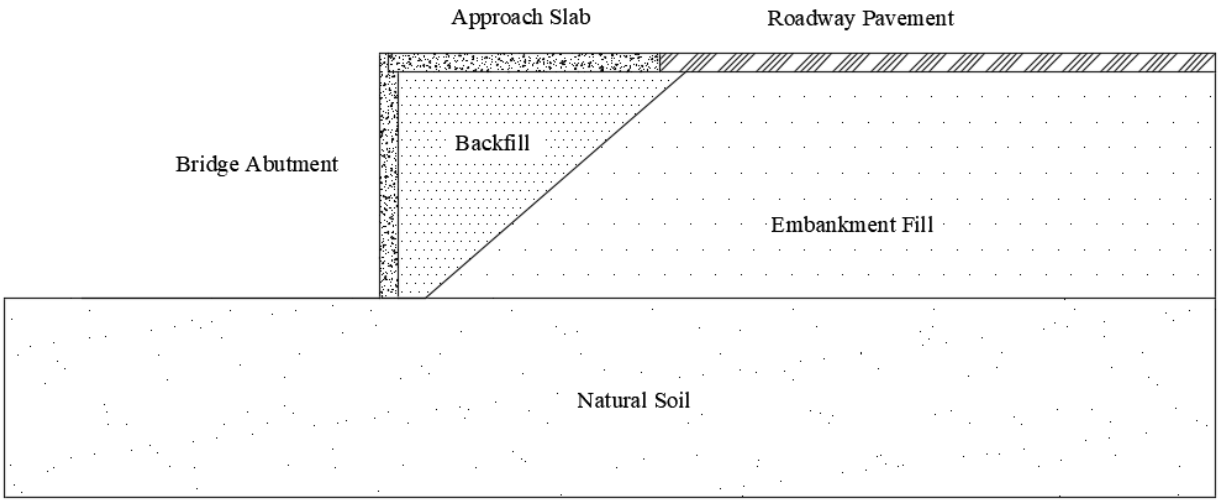

Figure 5.32 Two-dimensional longitudinal model layout

5.6.2 Geometry and boundary conditions

An important aspect of the soil-structure finite element model is selecting the location and types of boundary conditions (i.e. displacement and/or pore pressure boundary conditions) in an efficient and effective manner. Typically, the bottom of the model would represent a location where no soil movement occurs (vertical and horizontal). This location can be determined using the standard penetration test (typically provided in the borehole log profile) whereas a high value indicates a hard layer, such as bedrock. At this location, both vertical and horizontal movements are restricted (assumed to be zero). In addition, no water seepage would be expected to occur at this location, thus, impervious boundary was assumed. The top surfaces of the soil were free to move in all directions. Furthermore, water would be expected to flow through the top surfaces, thus, pervious boundary was assumed.

The soil mass must be sufficiently extended in the longitudinal direction to capture the behavior of the soil. Briaud and Lim (1997) recommend extending the soil mass to a distance of $3(H_e + H_n)$ from the back of the abutment wall to one end of the embankment model, L_e, and a distance of $3H_n$ to the opposite end of the model, L_e. The H_e and H_n parameters are the heights of

the embankment fill and natural soil, respectively (Figure 5.33). Along these vertical boundaries, the soil was assumed to move in the vertical direction only.

The nodes at the bottom of the abutment were fixed against horizontal and vertical movements, representing foundation support. The approach slab was connected to the abutment with a pin connection at the middle of the approach slab. This connection restricts the relative horizontal and vertical movements between the approach slab and the abutment while allowing free rotation. Figures 5.33 and 5.34 show the geometric and boundary condition parameters used in the finite element model for bridges with wall and stub abutments, respectively. Figure 5.35 shows the connections between the approach slab and the abutment and between the abutment wall and its foundation.

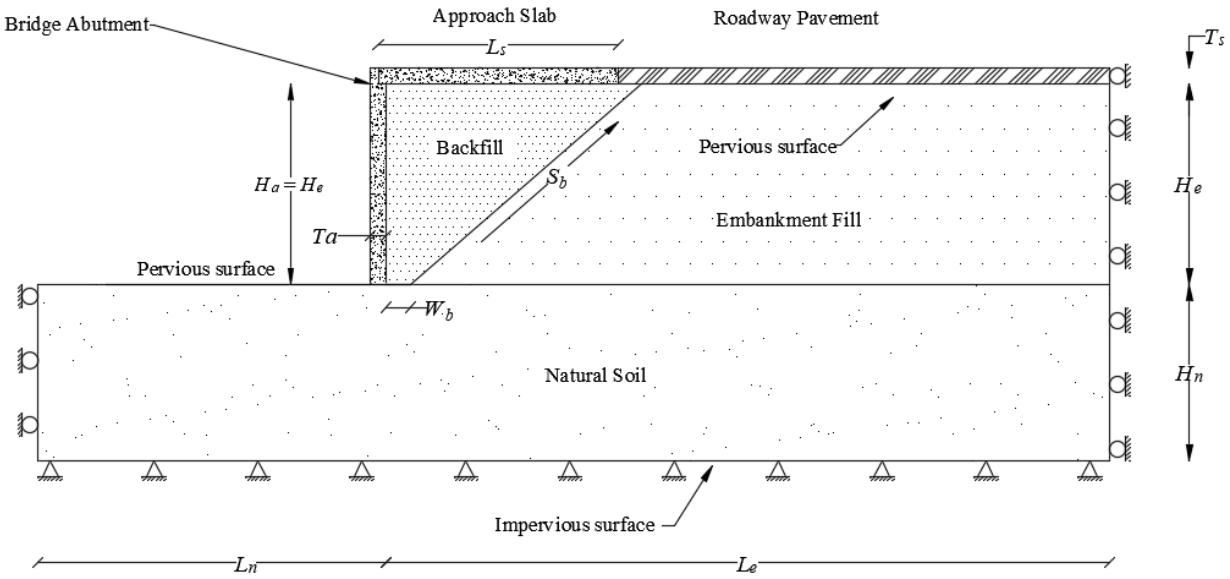

Figure 5.33 Layout of the two-dimensional longitudinal model with wall abutment

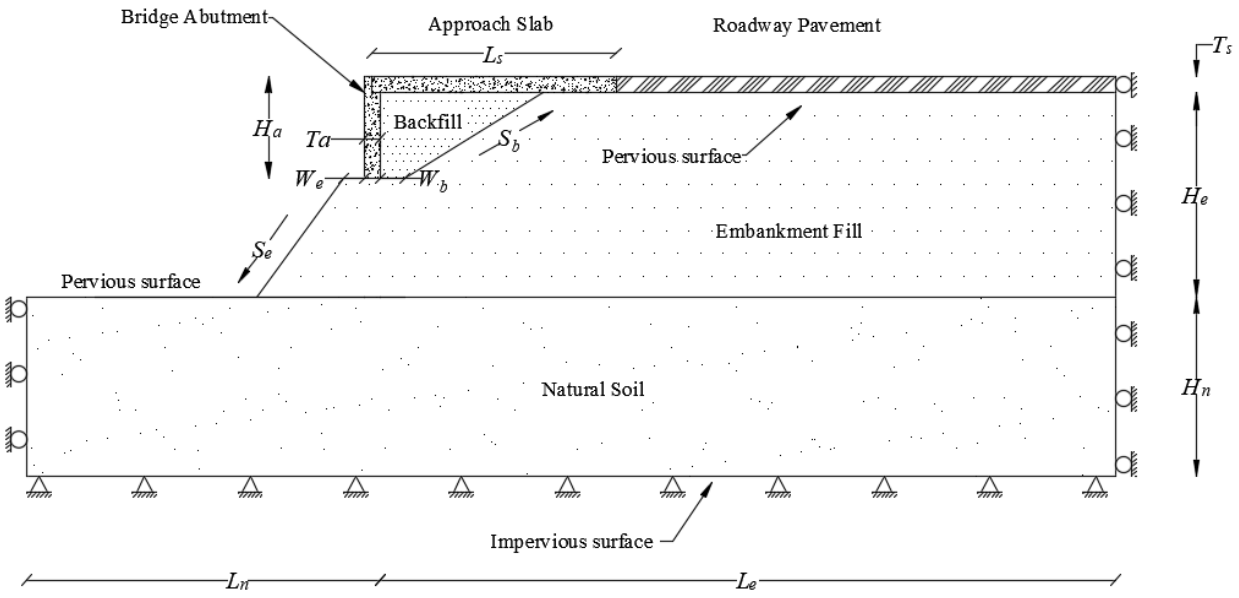

Figure 5.34 Layout of the two-dimensional longitudinal model with stub abutment

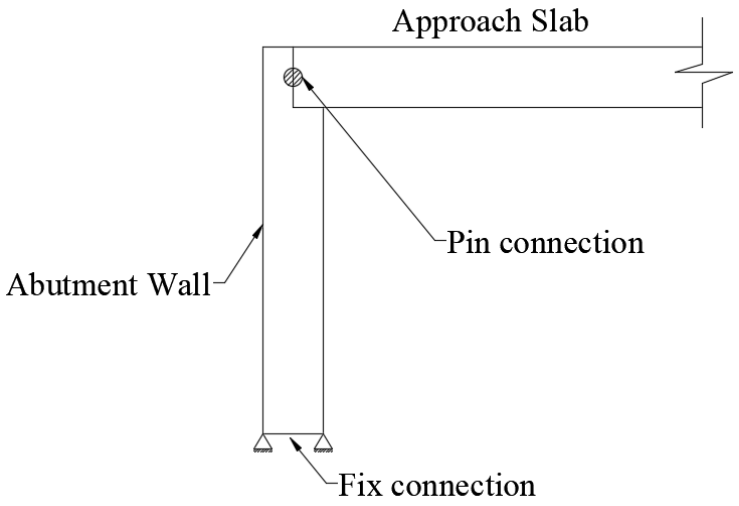

Figure 5.35 Abutment wall and approach slab boundary conditions

In the above figures,

S_e = Slope of the embankment fill.

S_b = Slope of the backfill soil.

W_b = Width of the base of the backfill soil.

W_e = Width of the base of the embankment fill in front of the bridge abutment.

H_a = Height of the abutment wall.

T_a = Thickness of the abutment wall.

L_s = Length of the approach slab.

T_s = Thickness of the approach slab.

In this study, H_e, H_n, H_a, and S_b were varied according to the study matrix found in Table 5.9. L_e and L_n were fixed at 180 *ft* (55 *m*), and 90 *ft* (27 *m*), respectively. They were determined as a function of the embankment fill and natural soil heights. L_s, T_s, T_a, W_b, W_e, were fixed at 20 *ft* (6.1 *m*), 12 *in* (305 *mm*), 2 *ft* (0.6 *m*), and 3 *ft* (0.9 *m*), respectively. In addition, S_e was fixed at 1:1.5 (1 vertical to 1.5 horizontal). These geometries were chosen to reflect the most common bridge-construction practices across the United States (see Chapter 3).

5.6.3 Contact behavior at structure-soil interfaces

The developed two-dimensional finite element model involves the interaction between the several structural components and the soil (i.e. abutment wall with soil, approach slab with soil, and roadway pavement with soil). Interface elements were introduced across these interfaces in order to transfer the load in the normal as well as tangential directions using the pressure-overclosure relationship as well as coulomb friction model defined within ABAQUS (see Section 4.2). In this analysis, the concrete surfaces (i.e. abutment wall, approach slab, and roadway pavement) were assigned to behave as master elements while soil surfaces were assigned to behave as slave elements.

5.6.4 Analysis procedures for longitudinal soil-structure model

The analysis procedures used to run the longitudinal soil-structure model included the following steps:

1- Applying a geostatic load on the natural soil layer. In this step, the effective self-weight of the natural soil was applied. The geostatic step assures that equilibrium is satisfied within the natural soil layer, and that the initial stress condition in all elements falls within the initial yield surface.

2- Constructing the embankment fill and bridge abutment over a period of time. In this step, the effective self-weight of the embankment soil and abutment was applied. This is done in a coupled (consolidation) step where the load of the embankment is applied in a timely manner using equation 5-1.

3- Adding the approach slab, and roadway pavement. This is also done in a coupled (consolidation) step where the load of the approach slab and roadway pavement was applied in a timely manner. The construction of the approach slab and roadway pavement was assumed to occur after the completion of the embankment fill and assumed to be constructed over a ten-day period.

4- Consolidation step/steps. In this step/steps, the calculations of the primary settlement (consolidation process) and secondary settlement (creep) were made.

5.6.5 Material properties

The concrete in the abutment wall, approach slab, and roadway pavement was assumed to behave in a linearly elastic manner with a modulus of elasticity that was consistent with a design compressive strength of 4000 *psi*. Table 4.2 shows the input parameters used to simulate the

concrete. On the other hand, the modified Drucker-Prager/Cap material model was used to simulate the behavior of the soils. Table 4.7 shows the input parameters used to model the soil.

5.6.6 Verification analysis

In this part of the study, an attempt was made to evaluate the longitudinal surface settlement profile at the Clinton bridge-site (see Section 5.4.5.2 for detailed description of the Clinton bridge-site). The soil profile consisted of clay embankment layer with height H_e = 25 *ft* (7.5 *m*) and two natural soil layers; top silty clay with height $H_{n\text{-}Top}$ =14 *ft* (4.3 *m*) and bottom sandy silt layer with height $H_{n\text{-}Bottom}$ = 8 *ft* (2.4 *m*). No information was provided regarding the approach slab length, backfill material, and abutment type/height. An assumed approach slab length L_s = 20 *ft* (6.1 *m*), and thickness T_s = 13 *in* (330 *mm*) were used in this simulation. The backfill material was assumed to be compacted to 90% of the standard proctor value with side slope S_b = 1:1 (1 vertical to 1 horizontal). These assumptions were based upon the information found in Oklahoma's bridge manual (see Section 3.5). The abutment wall was assumed as wall abutment with height $H_a = H_e$ and thickness T_a = 2 *ft* (0.6 *m*). Accordingly, L_n and L_e were set as 66 *ft* (20 *m*) and 141 *ft* (43 *m*), respectively. They were determined based on Briaud and Lim (1997) recommendation (see Section 5.6.2). The layout of the FEM used in this simulation is shown in Figure 5.36.

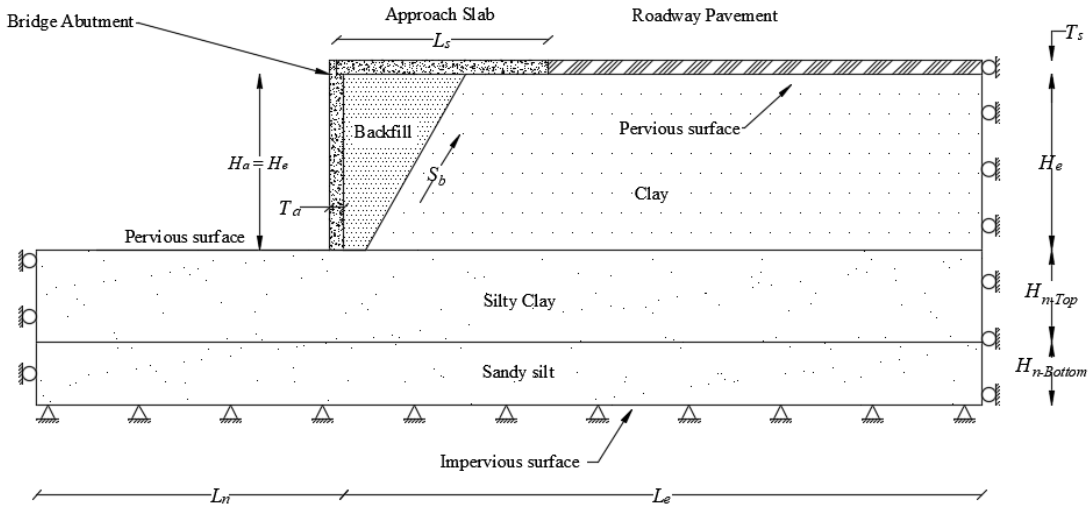

Figure 5.36 Boundary condition used for the longitudinal verification FEM

The finite element model was generated as described in sections 5.6.1 through 5.6.5. Table 5.2 shows the input parameters used to simulate the natural and embankment layers. Table 4.7 shows the input parameters used to simulate the backfill material. The FEM was run for a simulated total time that allows initial, primary (dissipation of water) and secondary (creep) settlements of the modeled soil to be completed. The load on the embankment/backfill fill layers was applied according to equation 5-1. An additional approach slab and roadway pavement self-weight of 150 *pcf* (24 kN/m^3) was applied on the top surface of the embankment fill. The finite element discretization of the verification model is shown in Figure 5.37. Figures 5.38 and 5.39 show the deformed contour of the vertical deformation and excess pore pressure at the end of the analysis, respectively.

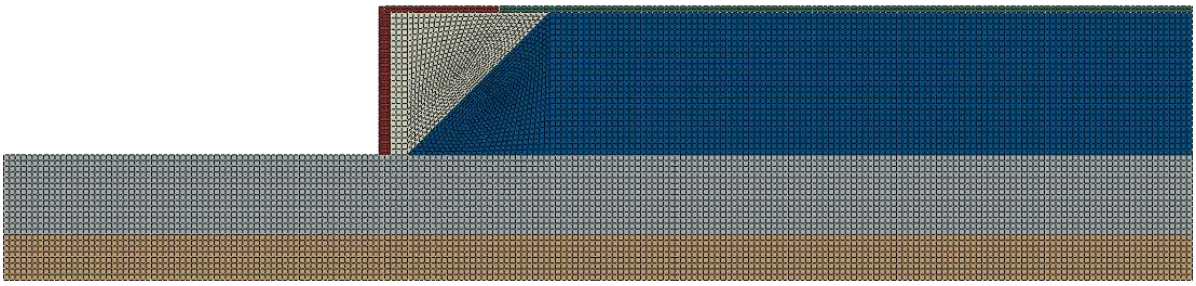

Figure 5.37 Finite element discretization of the longitudinal direction at Clinton bridge site

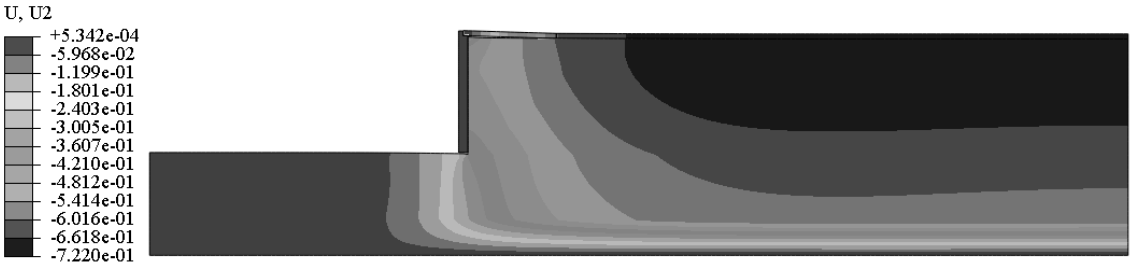

Figure 5.38 Vertical deformation contour at the end of the analysis (*ft*)

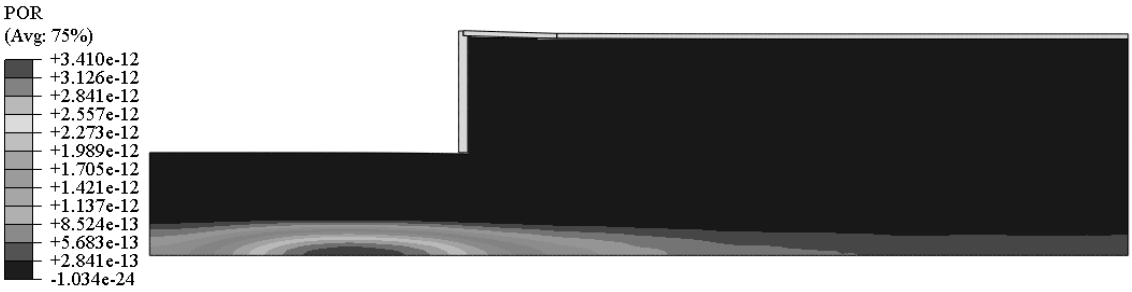

Figure 5.39 Excess pore pressure contour at the end of the analysis (*psf*)

Figure 5.40 shows the simulated longitudinal settlement profile for the roadway surface as well as the underneath soil. The FEM analysis shows a settlement of 8.5 *in* (216 *mm*) at a distance of 71 *ft* (21.6 *m*) from the bridge abutment. Within the approach slab, a differential settlement of 7.4 *in* (188 *mm*) was observed. This was compared with the history settlement reported by Laguros et al. (1991) of 8 *in* (203 *mm*) with a relatively good agreement. The difference between the reported and FEM analysis could be attributed to the type of model used in this simulation (see Section 5.9.1.1).

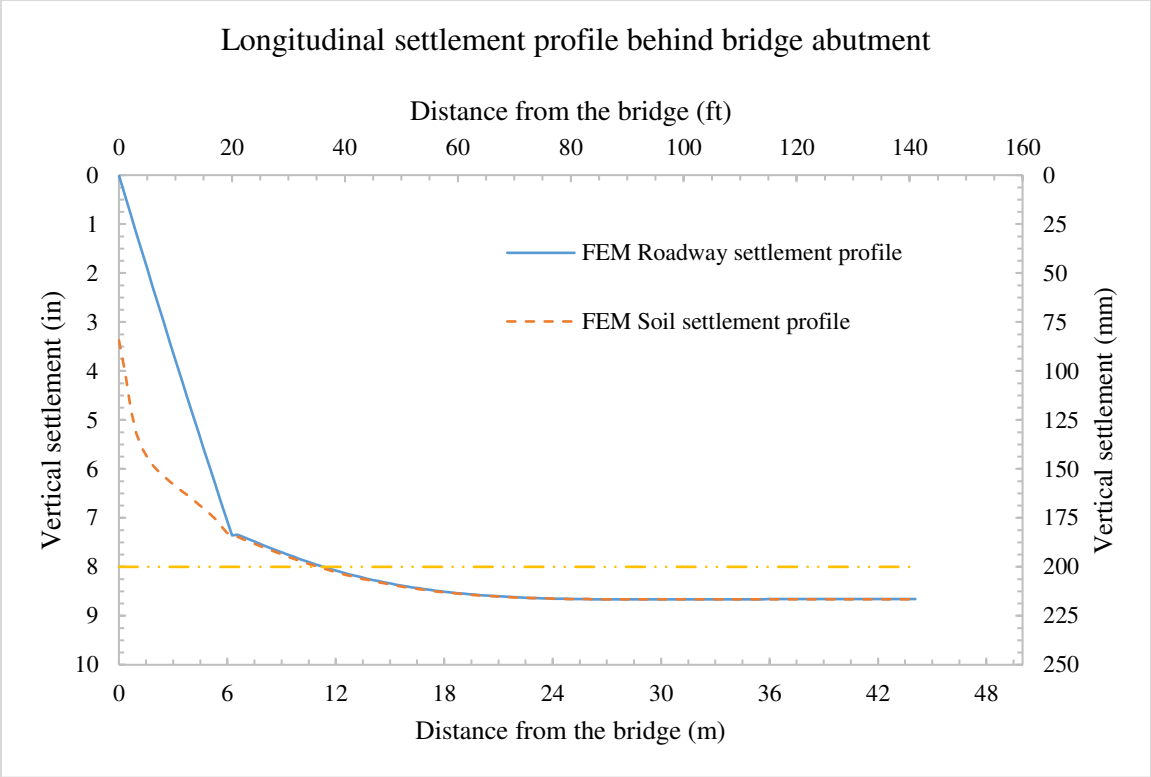

Figure 5.40 Simulated longitudinal settlement profiles at Clinton bridge-site

Figure 5.41 shows the simulated history of the excess pore pressure of the silty clay layer (first layer of the natural soil) at a distance away from the bridge. The pore pressure history was compared with the history obtained from the transverse settlement (see Section5.4.5.2) with a good agreement.

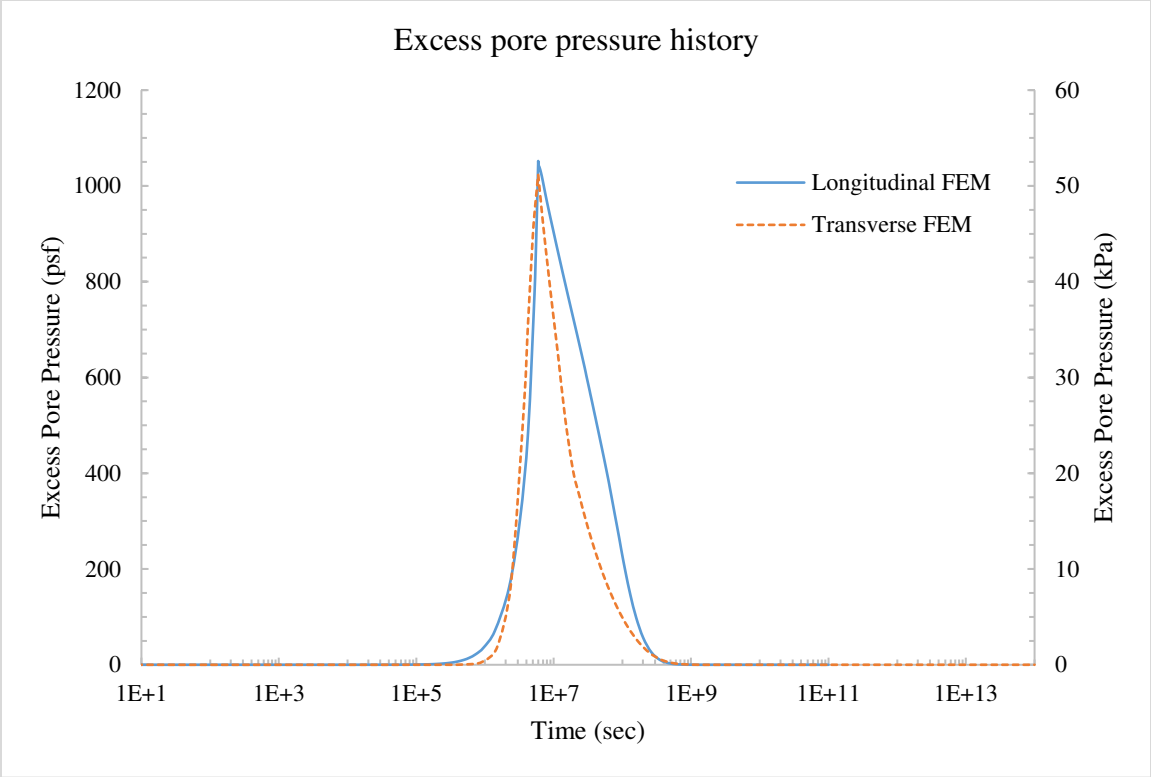

Figure 5.41 Simulated excess pore pressure history

Ultimately, the following conclusions were drawn:

- As the distance from the back of the abutment wall increases, the effect of the abutment wall on the soil settlement profile would gradually diminishes. Approximately, 80% of the maximum longitudinal settlement occurs within the first 20 *ft* (6.1 *m*). This was coincided with the finding of Seo et al. (2002).
- The approach slab settled enough to develop a noticeable bump. The differential settlement of the approach slab was 7.4 *in* (188 *mm*). This resulted in a slope of 3.9/125 which indicates a very rough transition.
- The consolidation of the natural soil and embankment fill was the main reason for the bump formation at this site.
- The type of FEM model would generally influence the result of the soil settlement. Comparing the results with the transverse model (see Section5.4.5.2),

the far away soil settlement of 8.6 *in* (218 *mm*) resulted from the longitudinal model was greater than 7.3 *in* (185 *mm*) resulted from the transverse model. This could be attributed to the effect side slope of the embankment S_{se}, which was not considered. A later study confirmed this finding (see Section 5.9.1.1)

5.6.7 Initial model

An initial model was used in this phase of the study to test the effect of the erosion of the backfill material. A hypothesis trench size of 3:6 (3 vertical to 6 horizontal) was simulated to examine its effect on the approach slab performance (resulting slope). The erosion was assumed to fully developed eight months after the end of the bridge construction, i.e. eight months after the bridge is open to the public. Figure 5.42 shows the layout of the trench simulation.

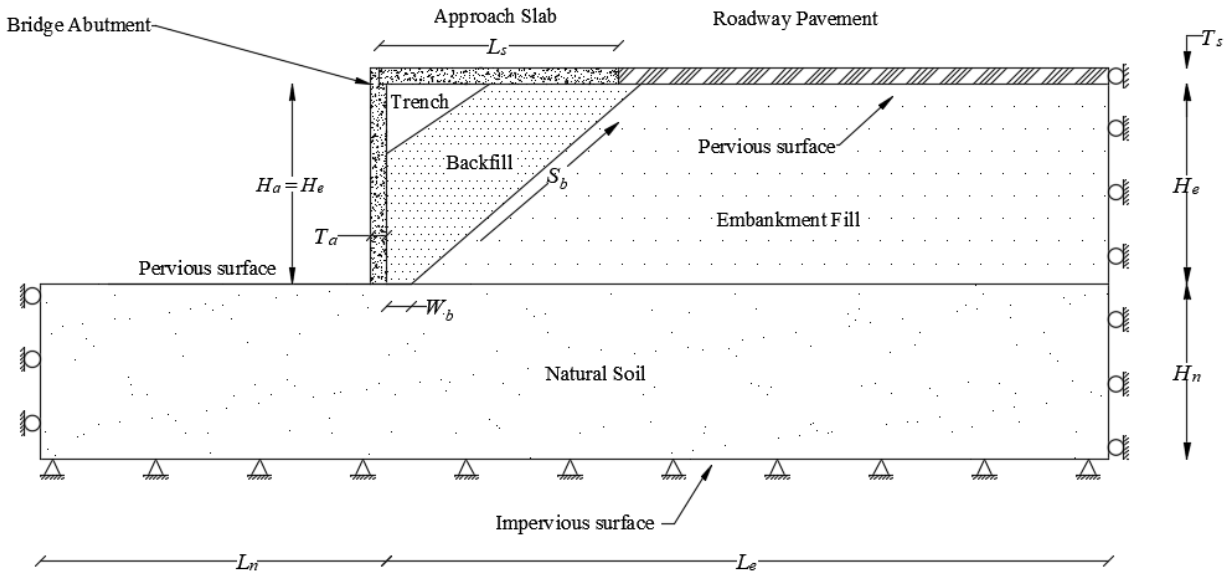

Figure 5.42 Layout of the initial model (wall abutment)

The soil profile used in this simulation consisted of a granular backfill, highly compressible embankment fill and high compressible natural soil. In this analysis, S_b = 1:2 (1 vertical to 2 horizontal), H_e = 30 *ft* (9.1 *m*) and H_n = 30 *ft* (9.1 *m*). Three abutment wall heights,

30 *ft* (9.1 *m*), 10 *ft* (3.0 *m*) and 5 *ft* (1.5 *m*), were tested. The backfill soil compaction level, and S_b were varied according to Table 5.7.

Table 5.7 Parameters range used in the initial model

Analysis No.	Erosion condition	S_b (Vertical to Horizontal)	Backfill level of compaction
1	No	1 to 2	95 %
2	Yes		
3	No	1 to 1	
4	Yes		
5	No	1 to 2	90 %
6	Yes		
7	No	1 to 1	
8	Yes		

Figures 5.43 to 5.48 show the FEM deformed contour of analyses No. 1 and 2. Figures 5.49 to 5.51 show the simulated slope of the approach slab.

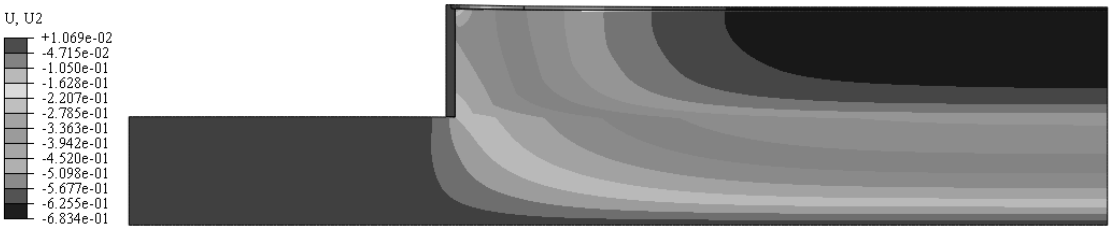

Figure 5.43 Vertical deformation contour of analysis No.1 (*ft*) (H_a=H_e)

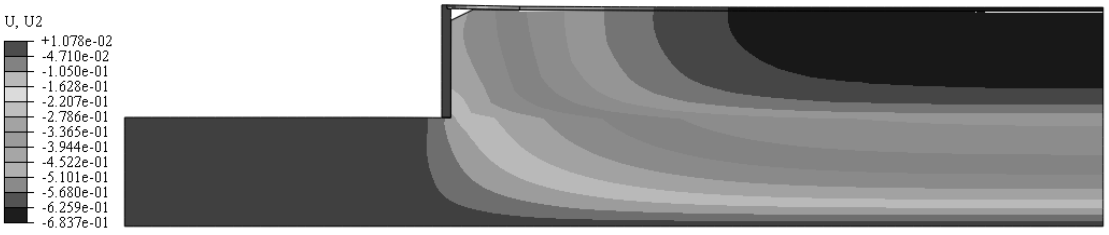

Figure 5.44 Vertical deformation contour of analysis No.2 (*ft*) (H_a=H_e)

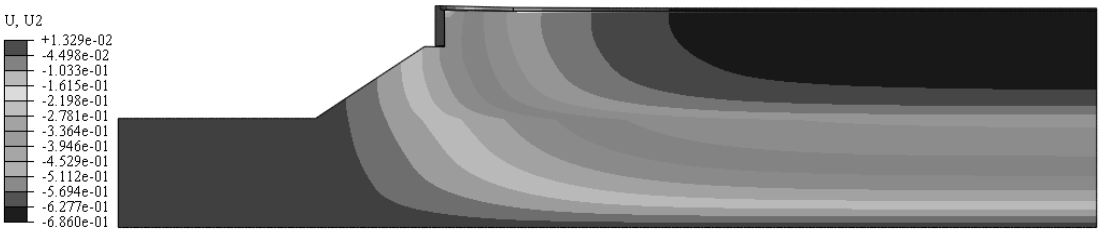

Figure 5.45 Vertical deformation contour of analysis No.1 (*ft*) (H_a=10 *ft*)

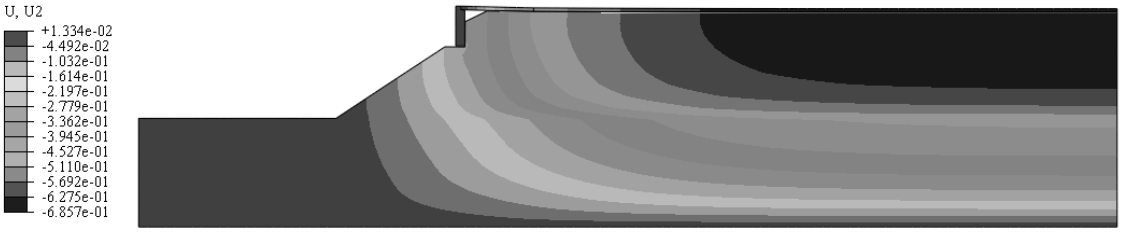

Figure 5.46 Vertical deformation contour of analysis No.2 (*ft*) (H_a=10 *ft*)

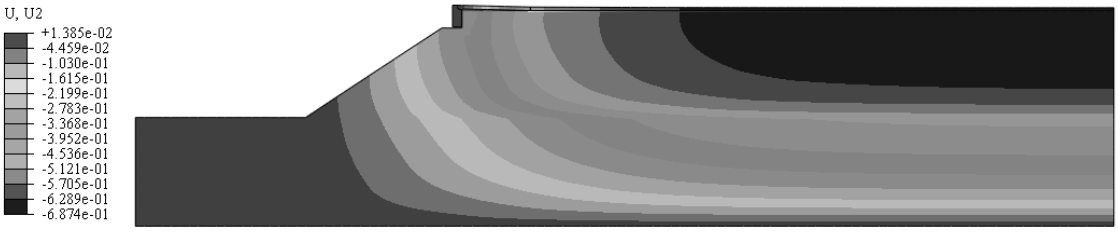

Figure 5.47 Vertical deformation contour of analysis No.1 (*ft*) (H_a=5 *ft*)

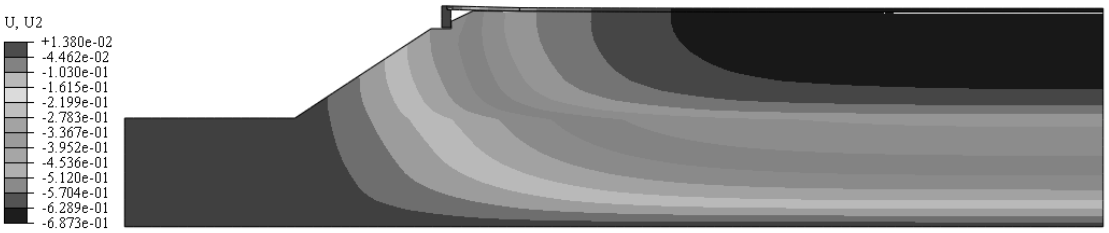

Figure 5.48 Vertical deformation contour of analysis No.2 (*ft*) (H_a=5 *ft*)

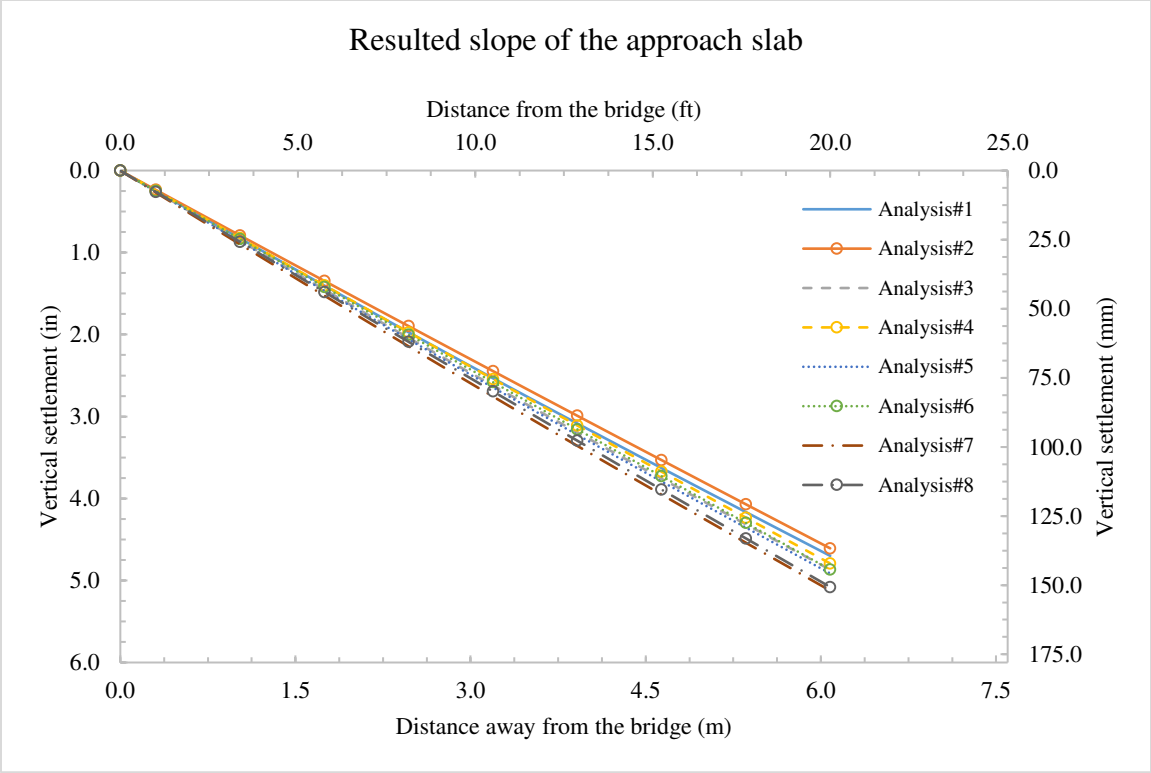

Figure 5.49 Simulated slope of the approach slab (H_a=H_e=30 *ft*)

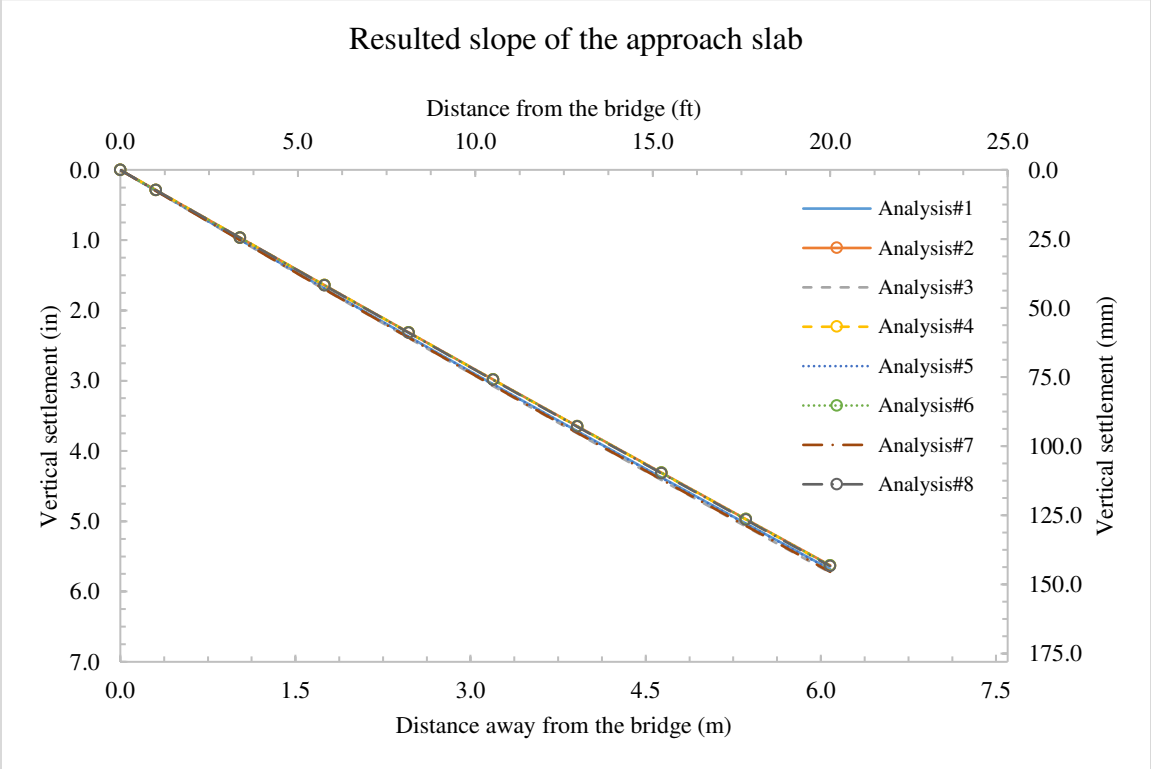

Figure 5.50 Simulated slope of the approach slab (H_a=10 *ft*)

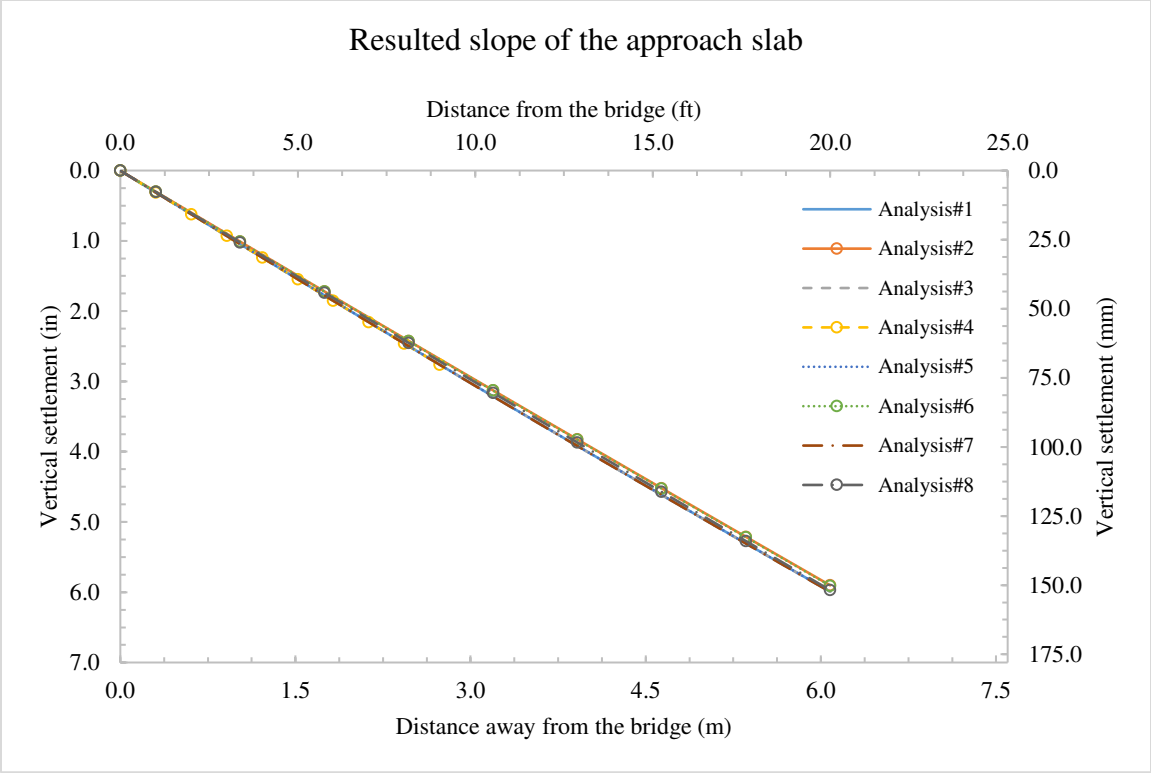

Figure 5.51 Simulated slope of the approach slab (H_a=5 *ft*)

It can be concluded from the above figures that the effect of introducing trench (erosion in the backfill) on the performance of the approach slab is not significant. In fact, the resulting slope of the approach slab with eroded backfill was, in general, less than the intact backfill. This can be attributed to the loss of some of the backfill weight that was removed during the simulation. Nevertheless, the overall effect on the resulting slope of the approach slab did not exceed 2%. Consequently, it has been concluded that the erosion has no significant effect on the overall performance of the approach slab.

5.6.8 Element type and size

As a porous material, soil contains voids that can be filled with air and/or water. Thus, the element used to discretize the soil was a four-node, plane strain quadrilateral element with bilinear displacement and pore pressure (element code: CPE4P). This type of element has the capability to capture deformation as well as excess pore pressure history. In this element, each

node consists of two displacement degrees of freedom (U_x and U_y) and one pore pressure degree of freedom (*Por*). On the other hand, a four-node, plane strain quadrilateral element with bilinear displacement was used to discretize the bridge abutment, approach slab, and roadway pavement (element code: CPE4). In this element, each node consists of two displacement degrees of freedom (U_x and U_y) (ABAQUS 2015). Figure 5.52 shows the element type and degrees of freedom for these elements.

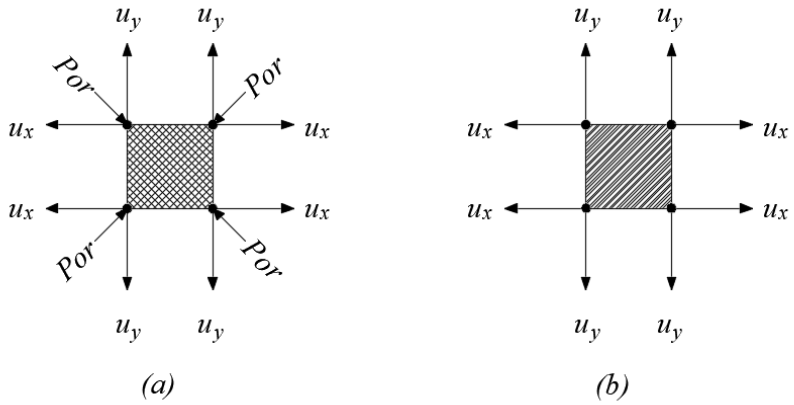

Figure 5.52 Element type used for (a) soil (b) concrete

The initial model (see Section 5.6.7) was used to determine the proper element sizes that would maintain the accuracy of results while reducing the computational time. This was done by monitoring the differential settlement of the modeled approach slab as a function of element size. The element size was applied uniformly to all components of the model (i.e. approach slab, abutment, roadway pavement and soil).

The soil profile used in the initial model has similar layout shown in Figure 5.33. It consisted of wall abutment ($H_a = H_e$) constructed against a 95% compacted granular backfill with S_b = 1:2 (1 vertical to 2 horizontal), highly compressible embankment fill with height H_e = 30 *ft* (9.1 *m*) and highly compressible natural soil with height H_n = 30 *ft* (9.1 *m*). The materials

used to model the concrete in the abutment wall, approach slab, and roadway pavement as well as soil are described in section 5.6.5.

The element size was reduced in each subsequent run and settlement at the end of the approach slab was obtained accordingly. Table 5.8 shows the size and number of the elements used in the analysis. Figure 5.53 shows the result of this analysis.

Table 5.8 Size and number of the elements used in the analysis

Element size (length × width) *ft* × *ft* (*m* × *m*)	Total number of elements
5.0 × 5.0 (1.5 × 1.5)	683
2.5 × 2.5 (0.8 × 0.8)	2,467
1.0 × 1.0 (0.3 × 0.3)	15,216
0.5 × 0.5 (0.2 × 0.2)	60,143
0.25 × 0.25 (0.1 × 0.1)	241,094

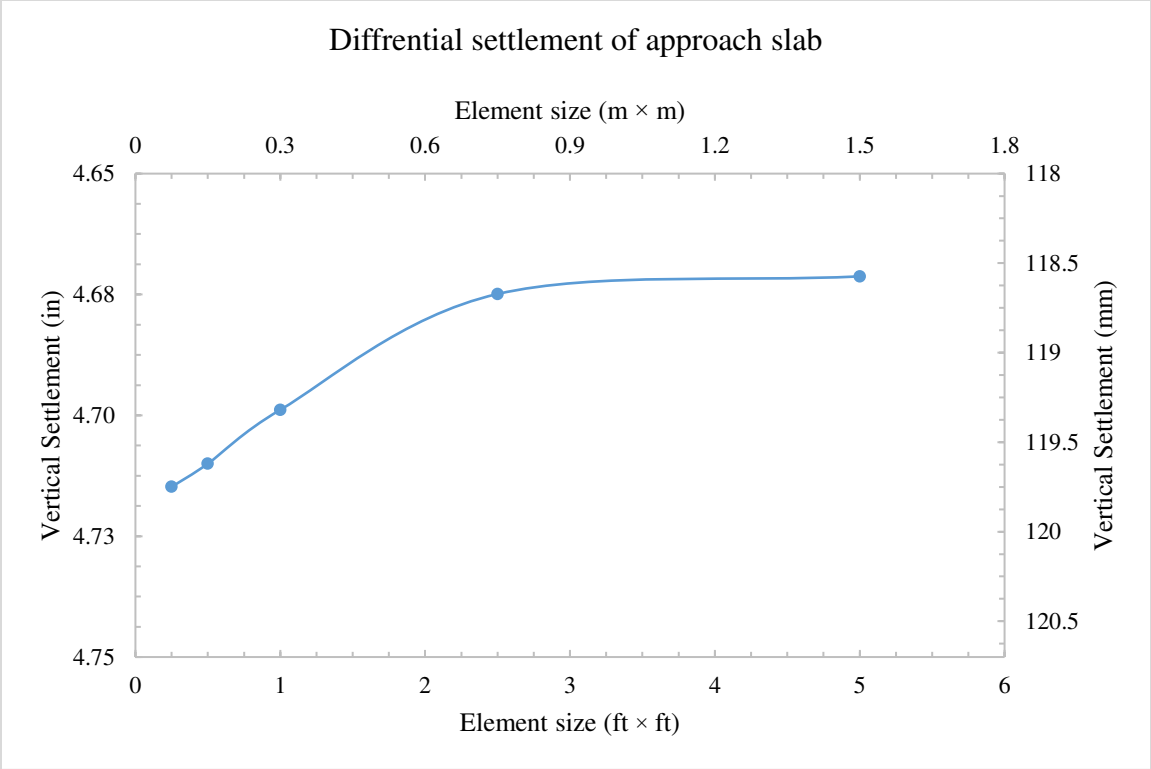

Figure 5.53 Simulated differential settlement of approach slab with respect to element size

Figure 5.53 shows that the differential settlement of the approach slab becomes nearly steady (maximum 0.2% error) when the element size is at or less than $1.0\,ft \times 1.0\,ft$ ($0.30\,m \times 0.30\,m$), and therefore, this element size was used in this study.

5.7 Parametric study on longitudinal two-dimensional FEM

A parametric study was conducted using finite element analysis to quantify the effects of various parameters on the soil's longitudinal settlement profile behind the bridge abutment. The parameters considered were the length of the approach slab, L_s, height of embankment fill, H_e, embankment soil type, height of natural soil, H_n, natural soil type, backfill soil type, slope of backfill area, S_b, and abutment type/height, H_a. Table 5.9 shows these parameters along with their ranges.

To efficiently minimize the number of analyses performed in this parametric study, the following assumptions were made. First, each soil profile was idealized into three distinct homogenous soil layers; backfill soil, embankment fill, and natural soil. Second, only soil profiles that were expected to cause settlements resulting in an approach slab slope of 1/125 (or greater) were considered. This was done to exclude situations where soil settlement would not pose a ride quality issue. Third, it was assumed that the embankment fill would never be any worse (more prone to settlement) than the natural soil. In other words, the embankment fill would not be more compressible than the natural soil. This is particularly the case in bridge constructions, since the embankment fill can be either a selected (better) fill brought to the site, or a readily available local fill from the nearby natural soil (Briaud, James and Hoffman 1997, McLaren 1970, Dupont and Allen 2002). Table 5.10 shows the soil profiles considered in this study.

Table 5.9 Two-Dimensional longitudinal model parametric study matrix

Parameter	Value
Length of approach slab segment L_s	20 *ft* (6.1 *m*)
Height of embankment fill H_e	20 and 30 *ft* (6.1 and 9.1 *m*)
Embankment soil type (Compressibility Degree)	High, moderate and low
Height of natural soil H_n	30 *ft* (9.1 *m*)
Natural soil type (Compressibility Degree)	High, moderate and low
Backfill soil compaction level	90% and 95%
Backfill slope S_b (vertical to horizonal)	1 to 1 and 1 to 2
Abutment type/height H_a	Wall abutment/$H_a = H_e$ Stub abutment/H_a = 10 *ft* (3.0 *m*) Stub abutment/H_a = 5 *ft* (1.5 *m*)

Table 5.10 Soil profiles considered in the longitudinal model parametric study

Soil profile No.	H_n *ft (m)*	H_e *ft (m)*	Natural soil type (compressibility degree)	Embankment soil type (compressibility degree)
1	30 (9.1)	30 (9.1)	High	High
2				Moderate
3				Low
4			Moderate	Moderate
5				Low
6			Low	Low
7		20 (6.1)	High	High
8				Moderate
9				Low

Accordingly, each soil profile was examined using various choices of parameters to quantify their effect on the ultimate longitudinal soil settlement profile behind the bridge abutment. Table 5.11 shows the variations of all parameter associated with each examined soil profile.

Table 5.11 Range of parameters used in accordance with each soil profile (refer to Table 5.10)

Analysis No.	Abutment type/height *ft (m)*	Backfill level of compaction	Backfill slope S_b (vertical to horizontal)
1	Wall abutment/$H_a = H_e$	95%	1 to 2
2			1 to 1
3		90%	1 to 2
4			1 to 1
5	Stub abutment/H_a = 10 (3.0)	95%	1 to 2
6			1 to 1
7		90%	1 to 2
8			1 to 1
9	Stub abutment/H_a = 5 (1.5)	95%	1 to 2
10			1 to 1
11		90%	1 to 2
12			1 to 1

The finite element model was generated using material properties shown in Tables 4.2 and 4.6. The boundary conditions, analysis steps, elements types, and contact behavior were used as described in section 5.6. The models were run for a simulated total time that allowed the completion of initial, primary (dissipation of water), and secondary (creep) settlements of the modeled soil. The load on the embankment fill layer was applied according to equation 5-1. An additional approach slab and roadway pavement surcharge of 150 *pcf* (24 kN/m^3) was applied on

the top surface of the embankment fill. A typical finite element discretization of the two-dimensional longitudinal model is shown in Figure 5.54.

Figure 5.54 Finite element discretization of the two-dimensional longitudinal model

5.7.1 Differential settlement of approach slab

The differential settlement of the approach slab was the interest of this phase of the study. The objective was to quantify the resulted approach slab slope against different abutment wall-soil conditions (see Tables 5.10 and 5.11). The result of the finite element analysis is shown in Figures 5.55 to 5.63.

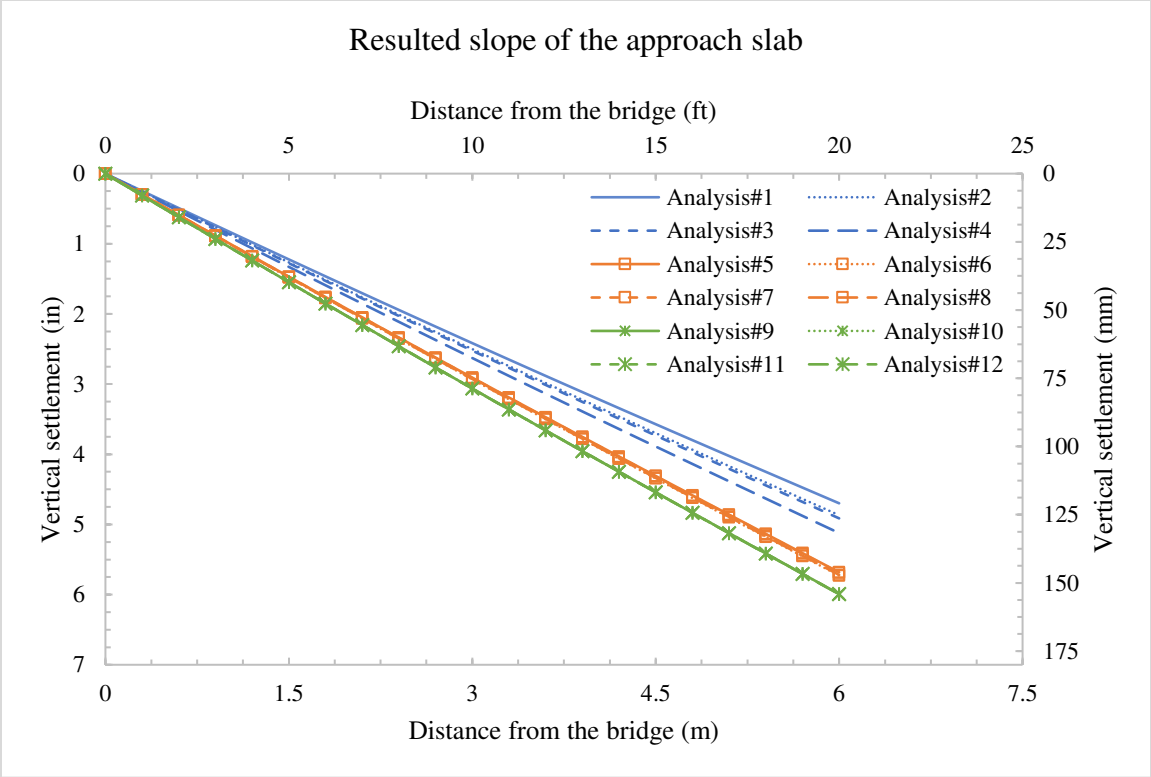

Figure 5.55 Simulated slope of the approach slab for soil profile No.1

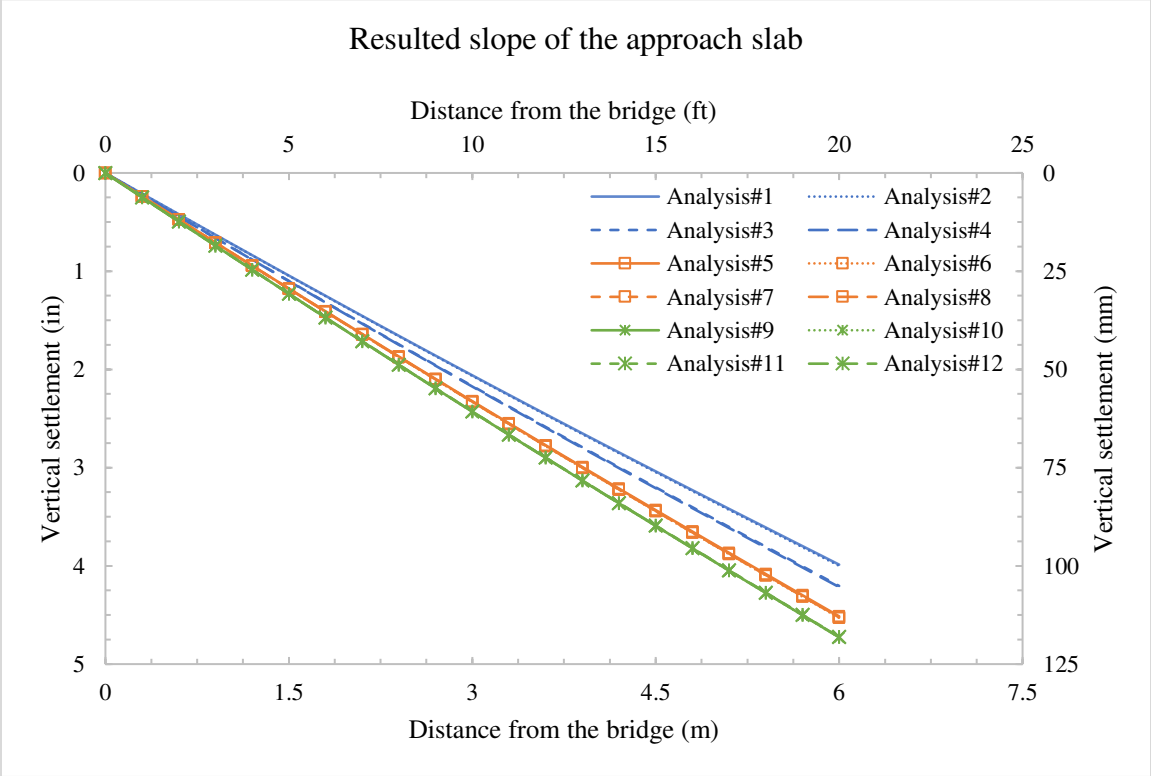

Figure 5.56 Simulated slope of the approach slab for soil profile No.2

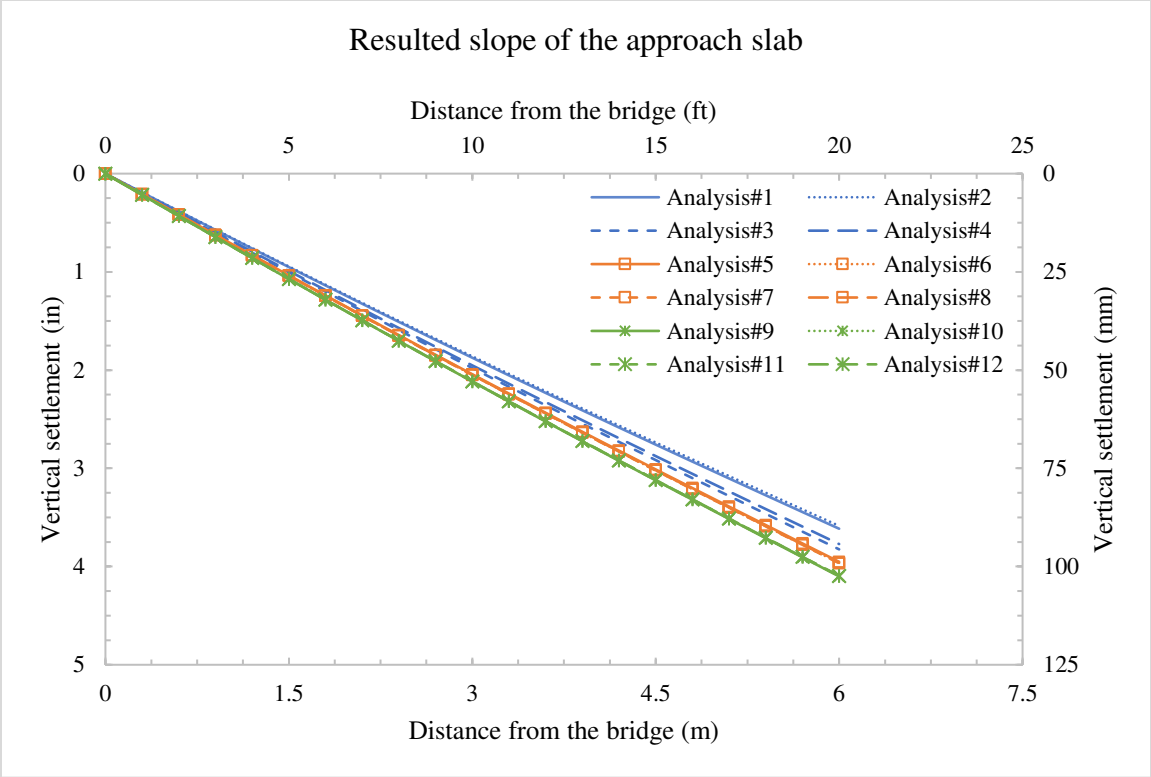

Figure 5.57 Simulated slope of the approach slab for soil profile No.3

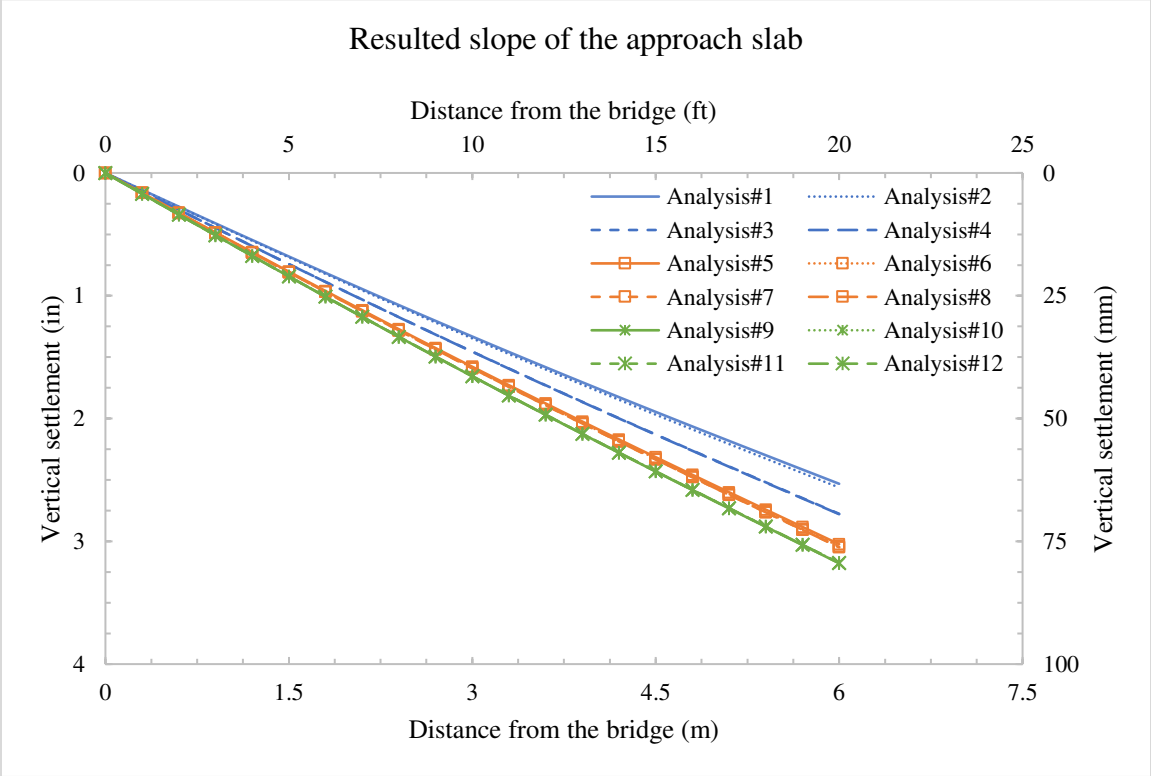

Figure 5.58 Simulated slope of the approach slab for soil profile No.4

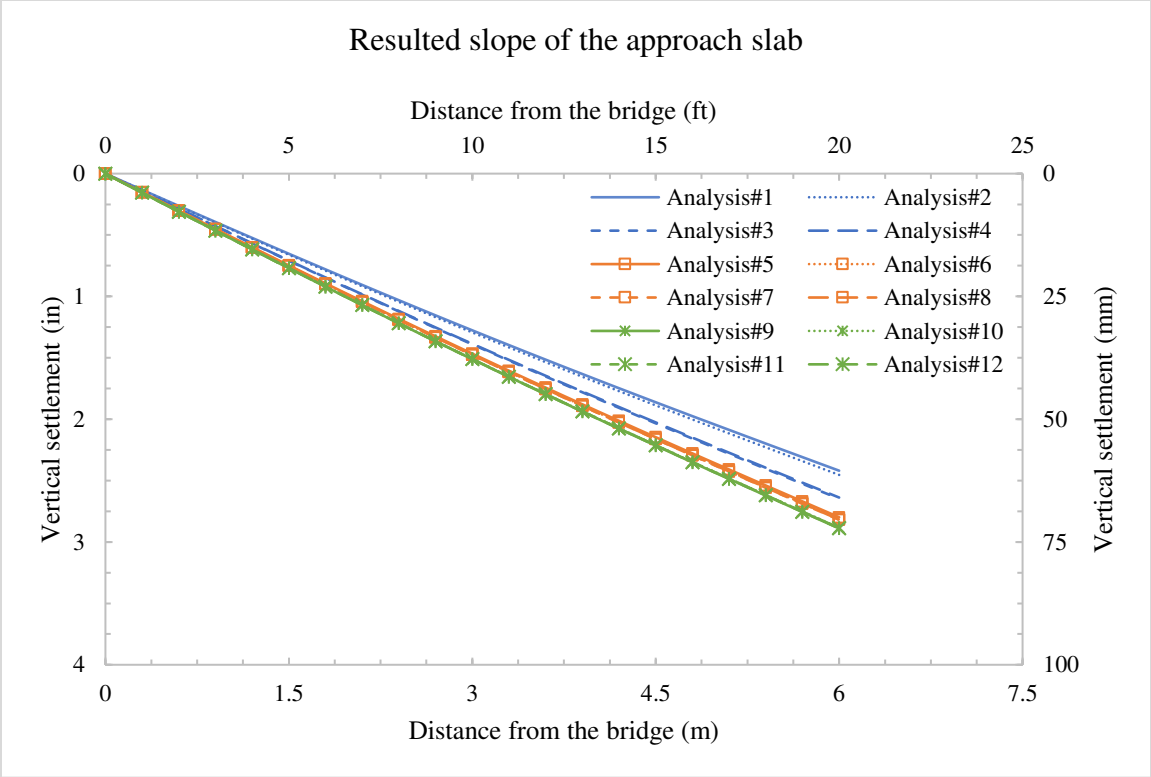

Figure 5.59 Simulated slope of the approach slab for soil profile No.5

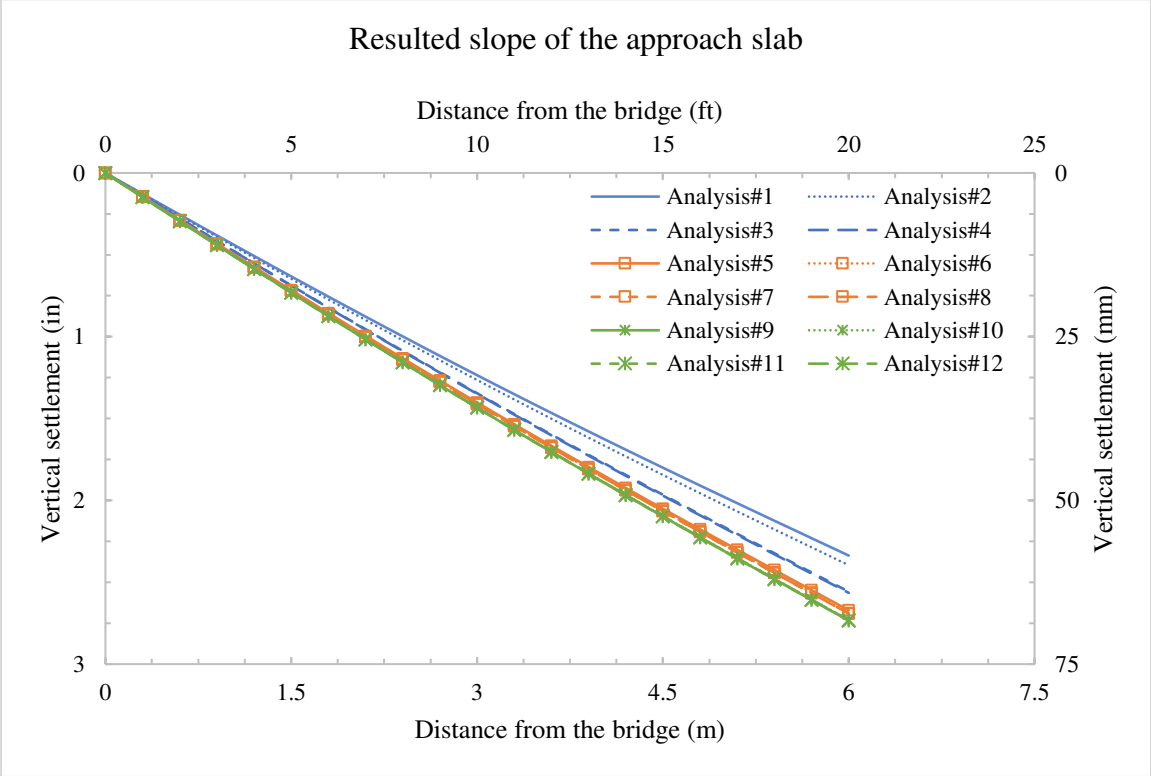

Figure 5.60 Simulated slope of the approach slab for soil profile No.6

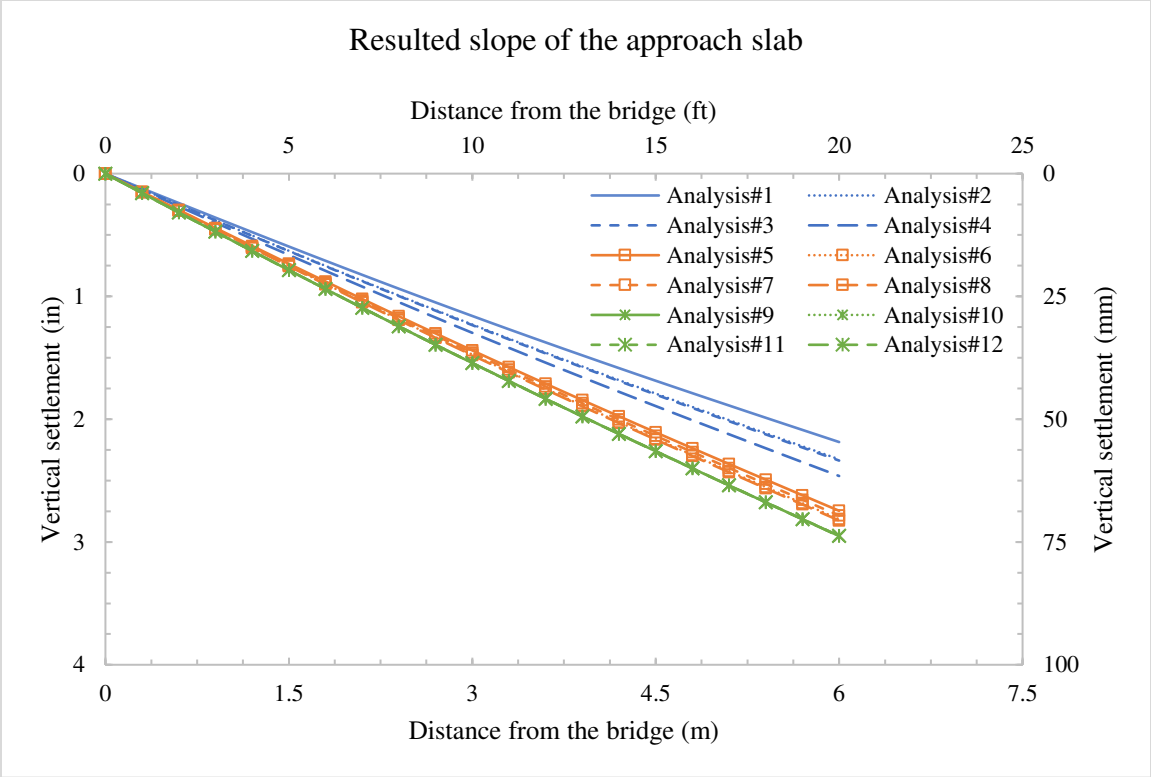

Figure 5.61 Simulated slope of the approach slab for soil profile No.7

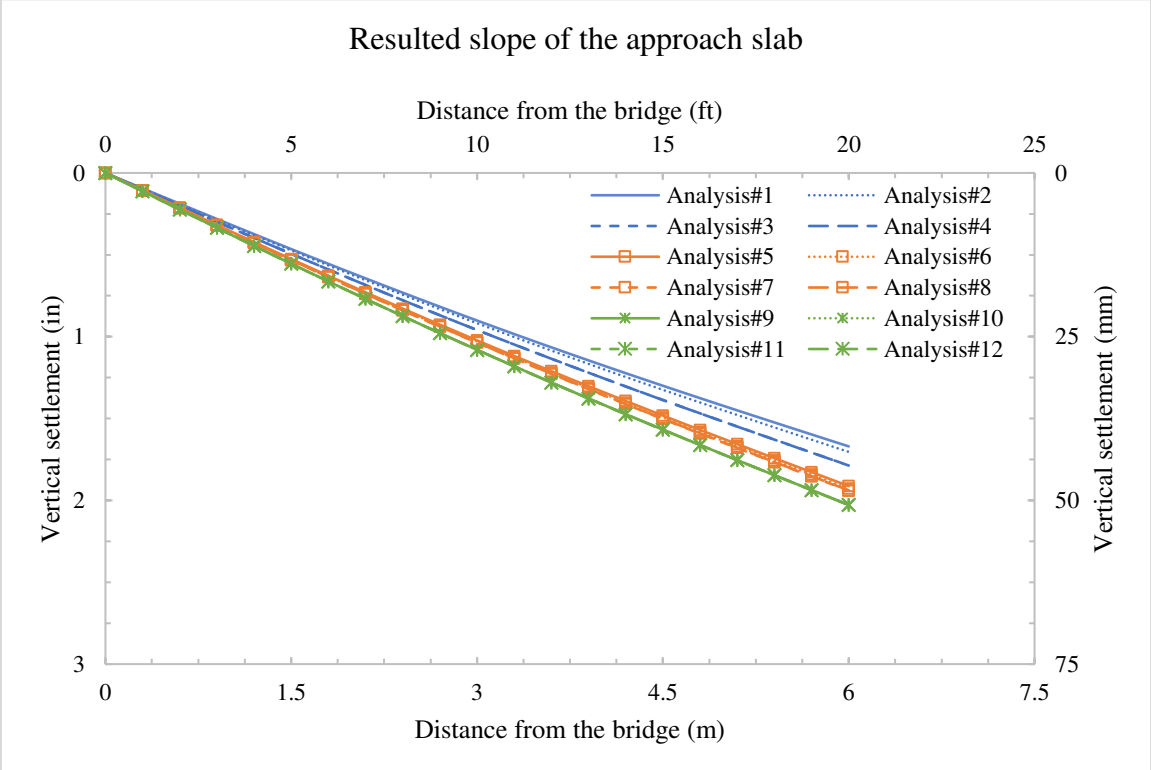

Figure 5.62 Simulated slope of the approach slab for soil profile No.8

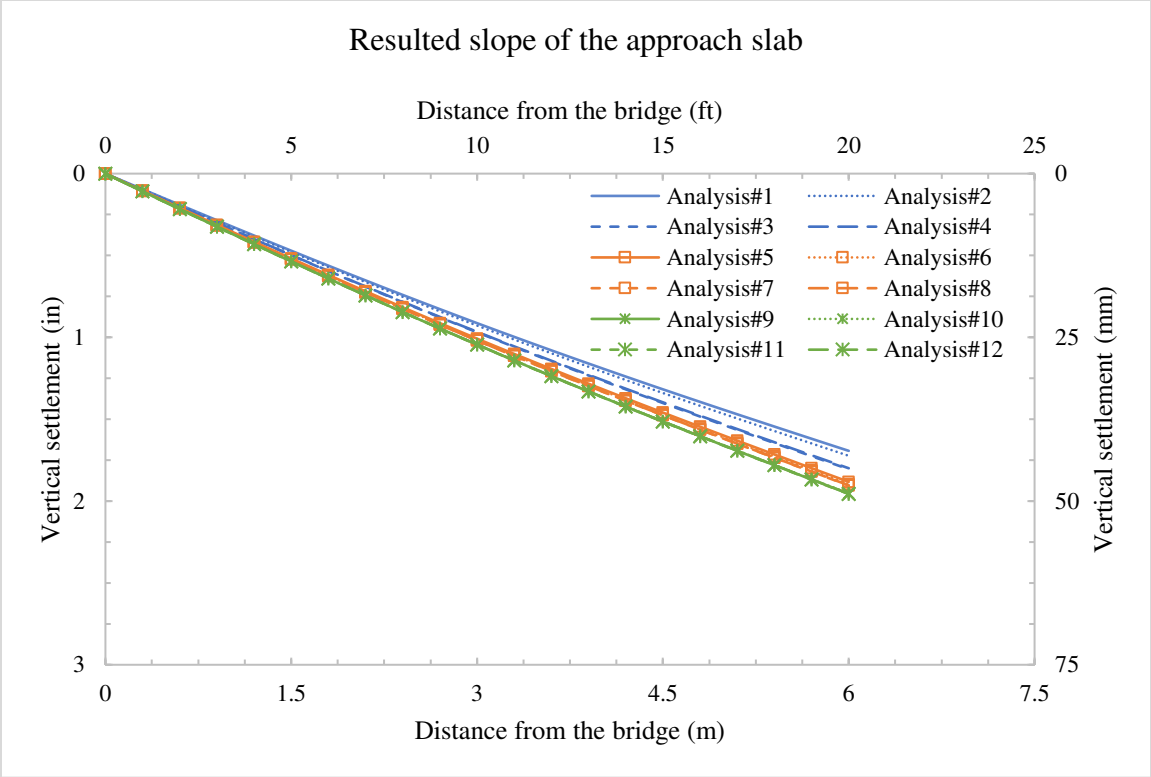

Figure 5.63 Simulated slope of the approach slab for soil profile No.9

The above figures show that the abutment wall type/height had a significant effect on the resulting slope of the approach slab. The finite element results indicated that the abutment wall type/height can influence the slope by up to 26%. On the other hand, compaction level and backfill side slope can affect the approach slab slope by up to 10% in wall abutments. In stub abutments, this effect is negligible. Overall, it can be concluded that utilizing 95% backfill with slope of 1:2 (1 vertical to 2 horizontal), and wall abutment would yield the smallest approach slab slope.

5.7.2 Soil settlement profile

The settlement at the surface of the embankment fill was the interest of this phase of the study. The objective was to quantify the soil longitudinal settlement profile behind bridge abutment against different abutment wall-soil conditions (see Tables 5.10 and 5.11). The result of the finite element analysis is shown in Figures 5.64 to 5.72.

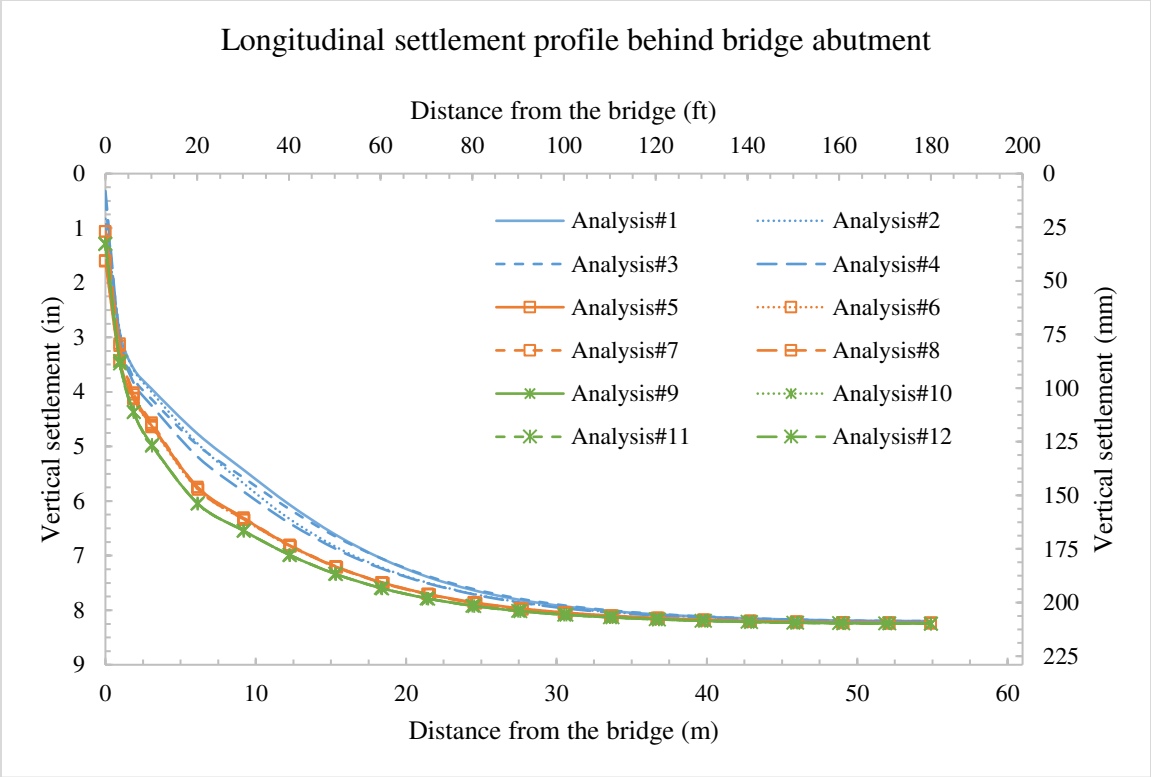

Figure 5.64 Simulated longitudinal soil settlement profile for soil profile No.1

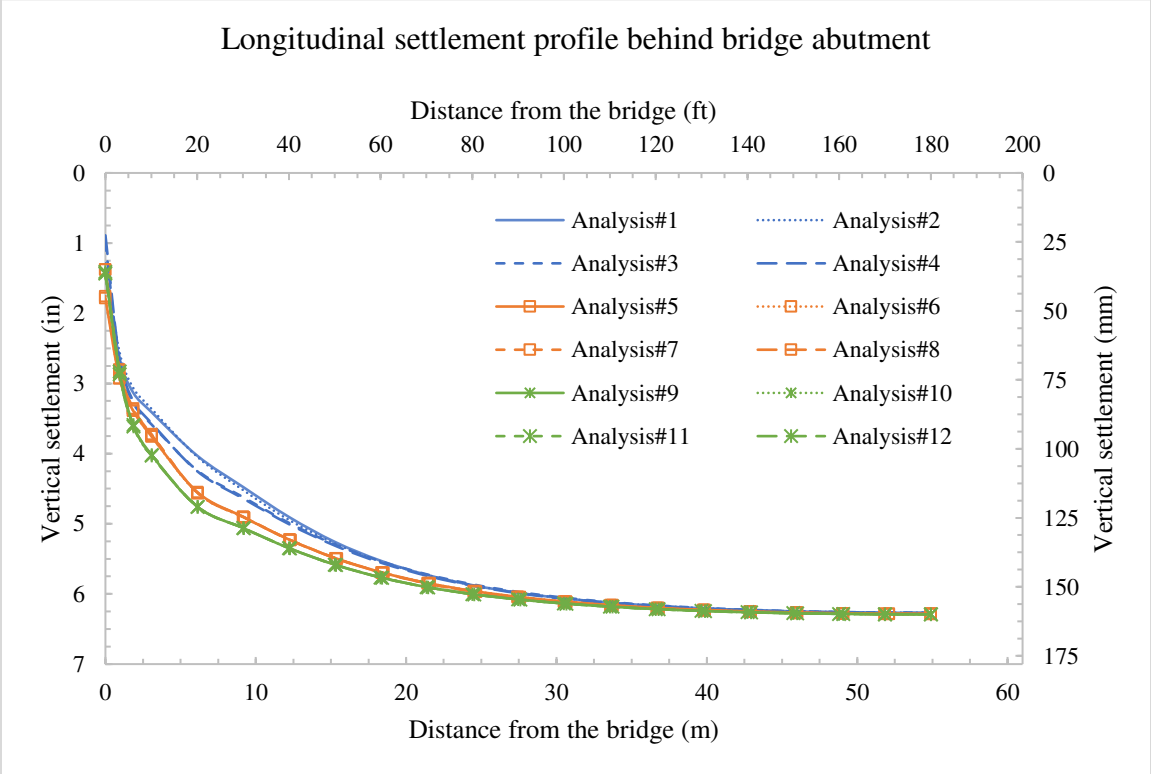

Figure 5.65 Simulated longitudinal soil settlement profile for soil profile No.2

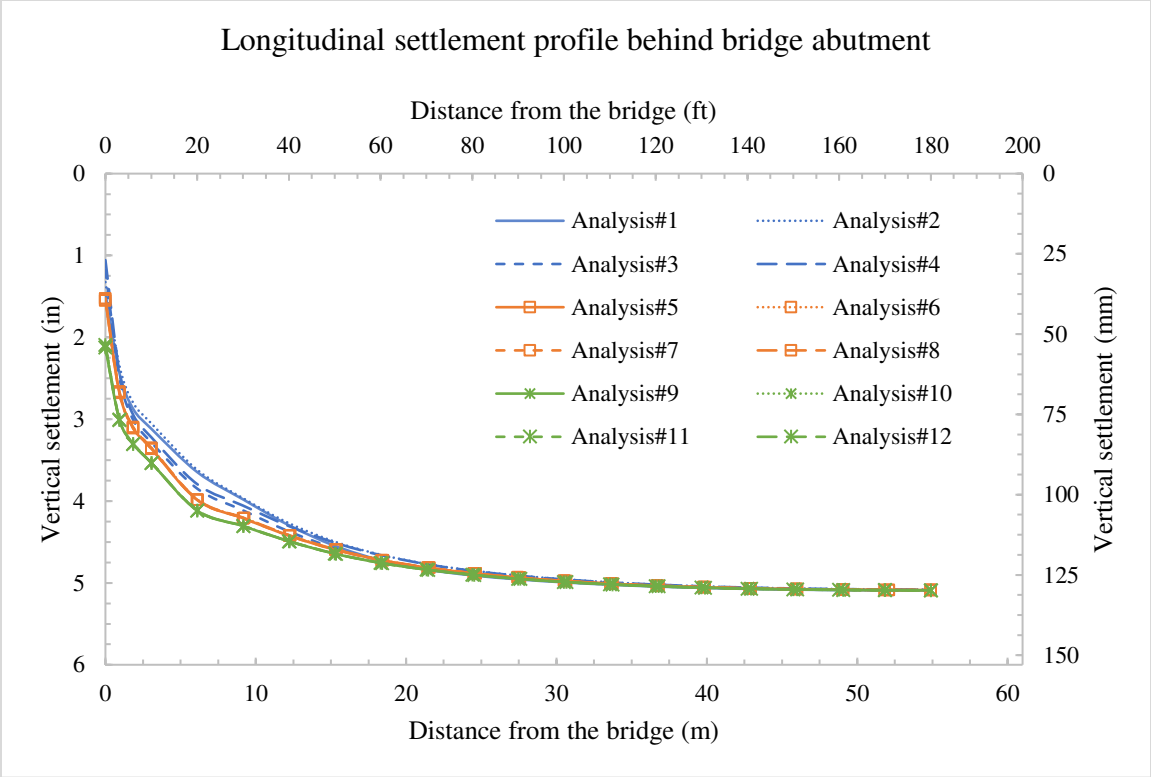

Figure 5.66 Simulated longitudinal soil settlement profile for soil profile No.3

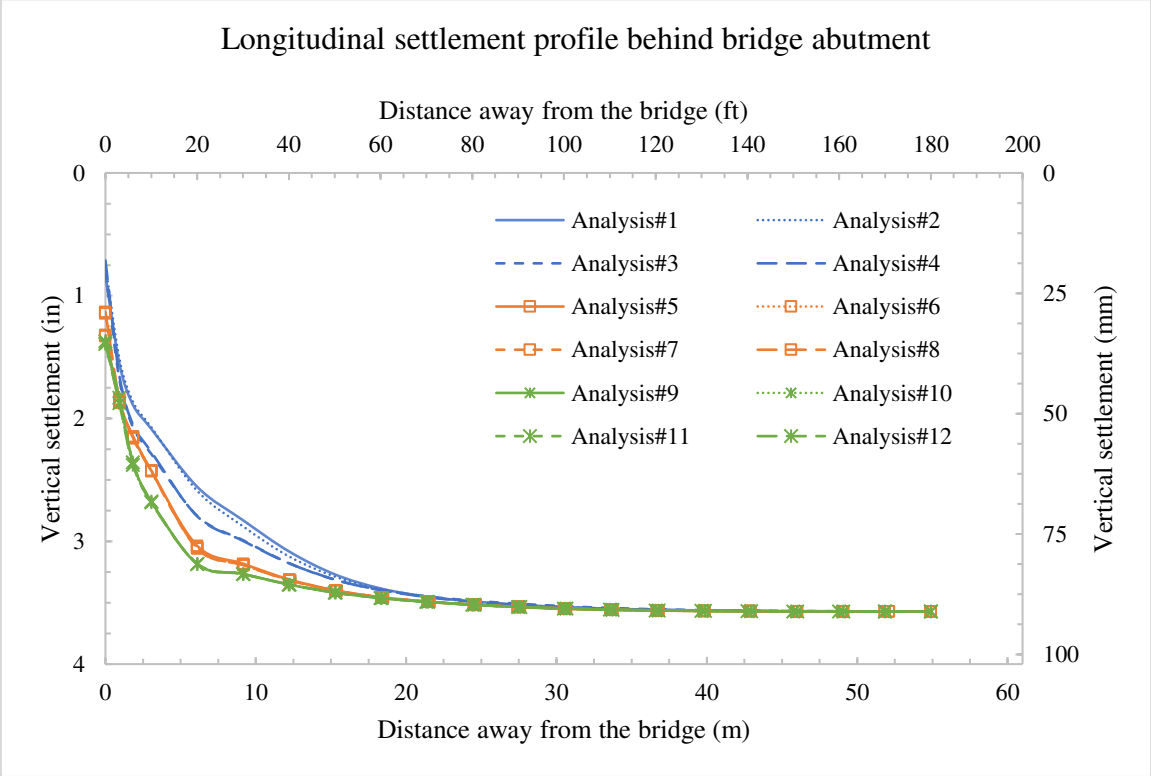

Figure 5.67 Simulated longitudinal soil settlement profile for soil profile No.4

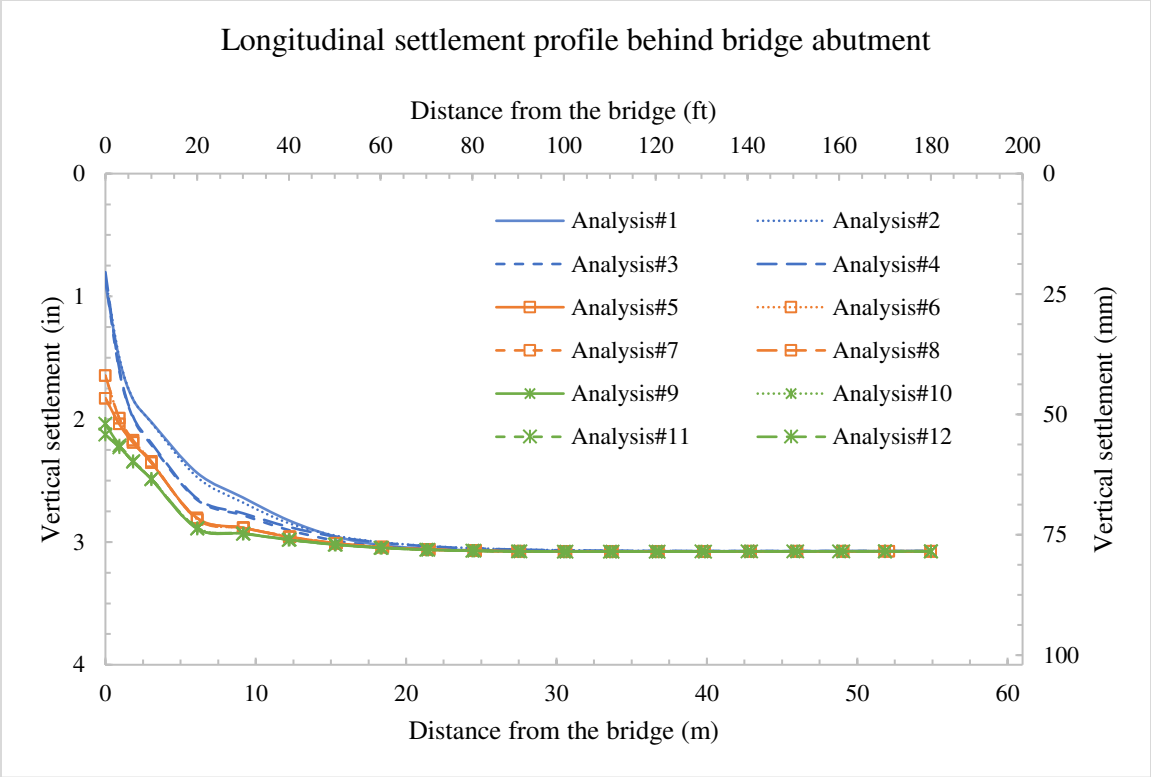

Figure 5.68 Simulated longitudinal soil settlement profile for soil profile No.5

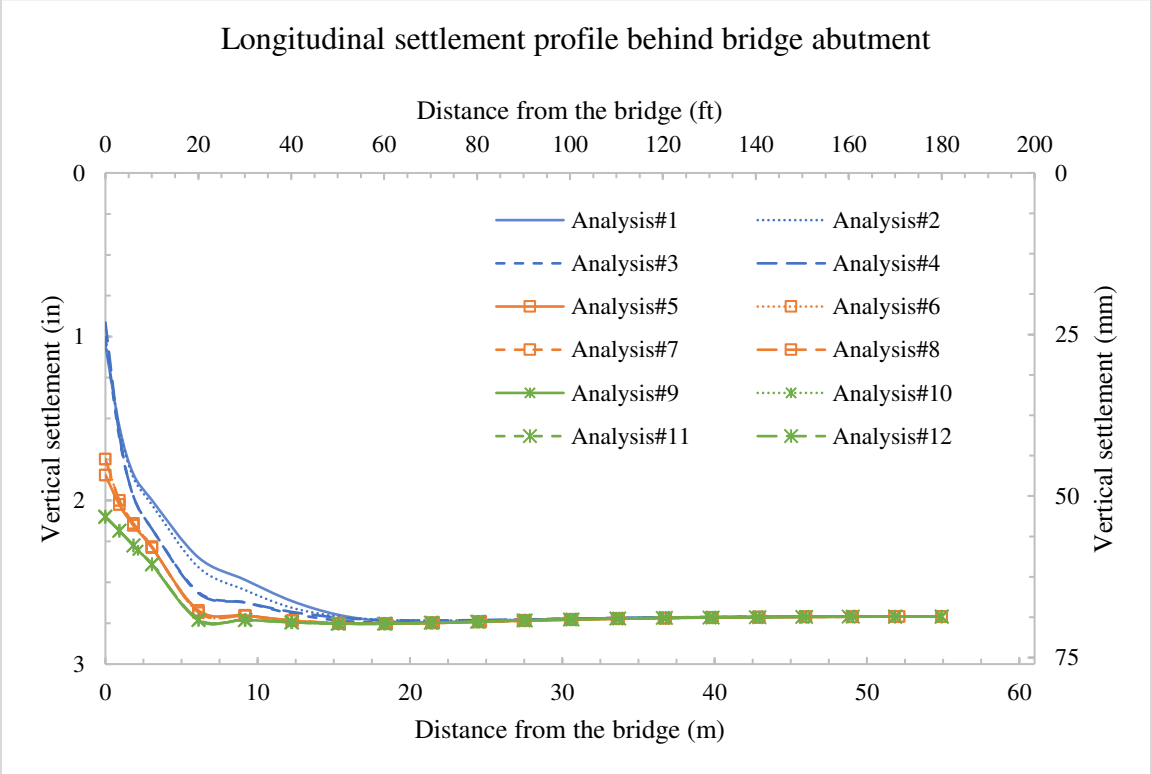

Figure 5.69 Simulated longitudinal soil settlement profile for soil profile No.6

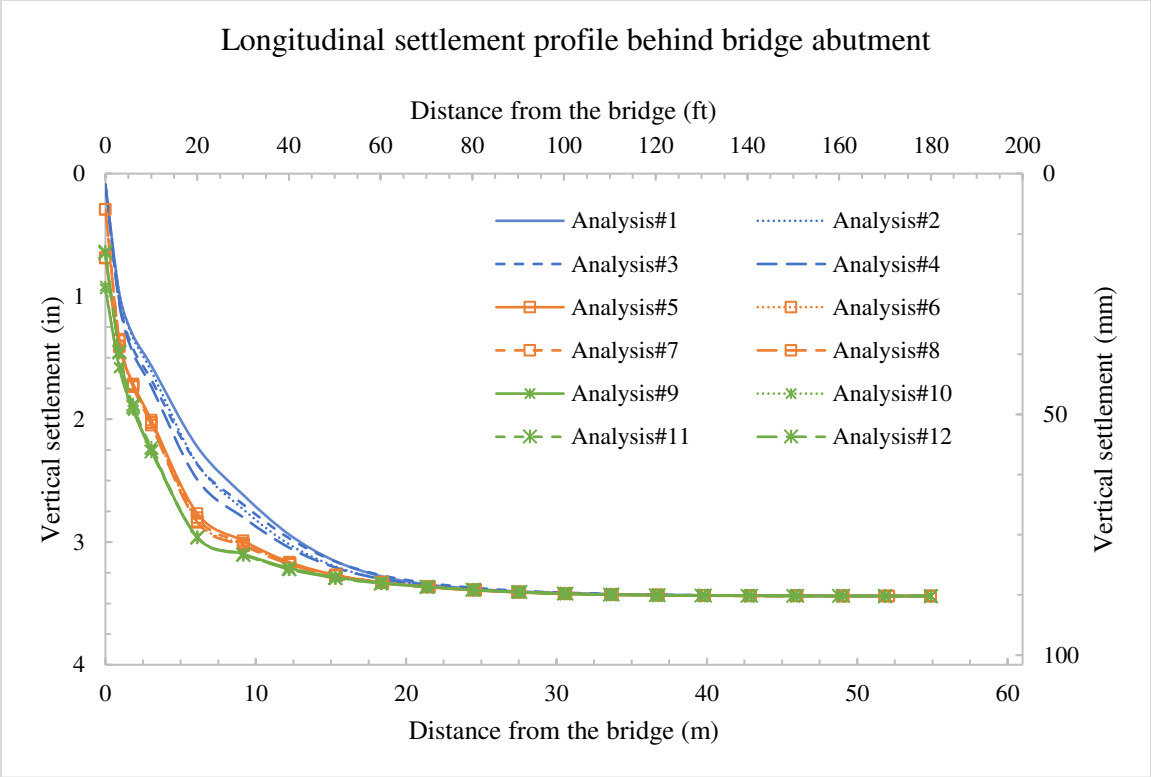

Figure 5.70 Simulated longitudinal soil settlement profile for soil profile No.7

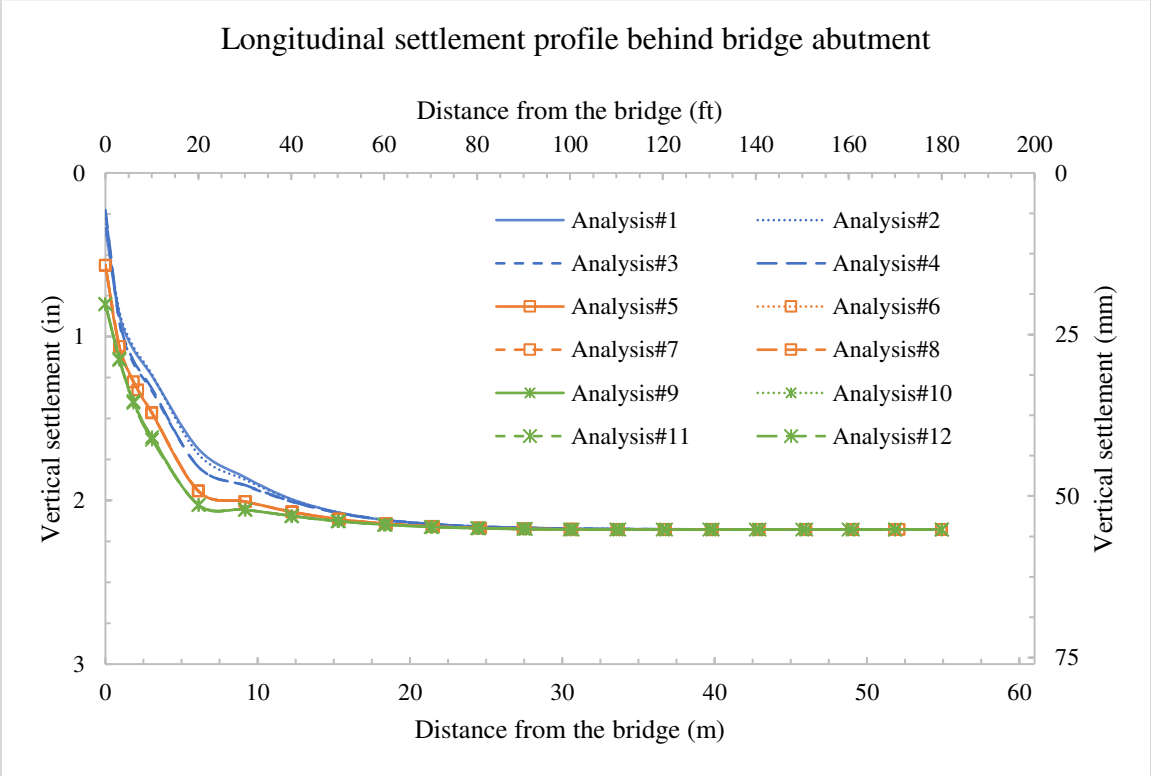

Figure 5.71 Simulated longitudinal soil settlement profile for soil profile No.8

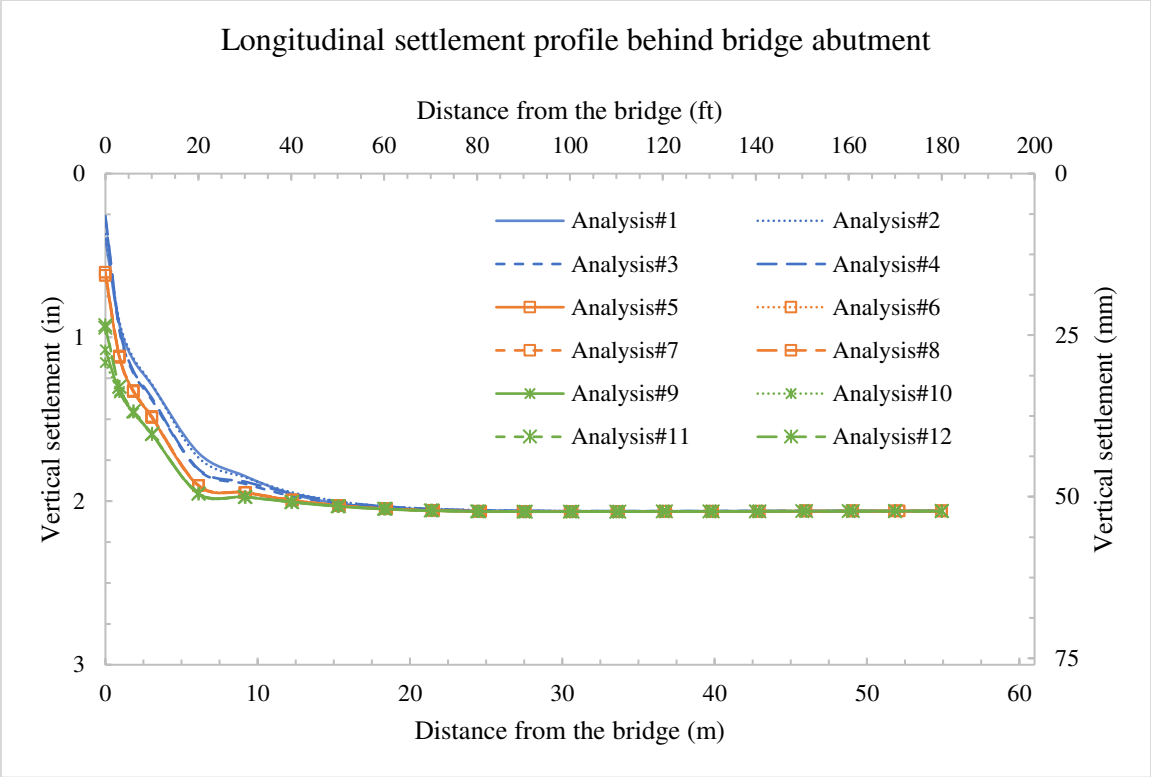

Figure 5.72 Simulated longitudinal soil settlement profile for soil profile No.9

5.8 Evaluating soil's longitudinal settlement profile behind bridge abutment

Various trials were made, using curve fitting software (curve expert), to find the best fit curve representing the deflected soil profile (see Section 5.7.2) as a function of distance from the bridge abutment. The software runs various built-in equation models that are matched with a given curve (soil deflection profile in this case) to determine the best fit equation using linear and nonlinear regression analyses. The best fitted functions matching the soil profile obtained from finite element results are shown in Figure 5.73. Accordingly, it was noted that the logistic function represented the best overall model for the ultimate soil deformation (settlement) profile along the longitudinal direction.

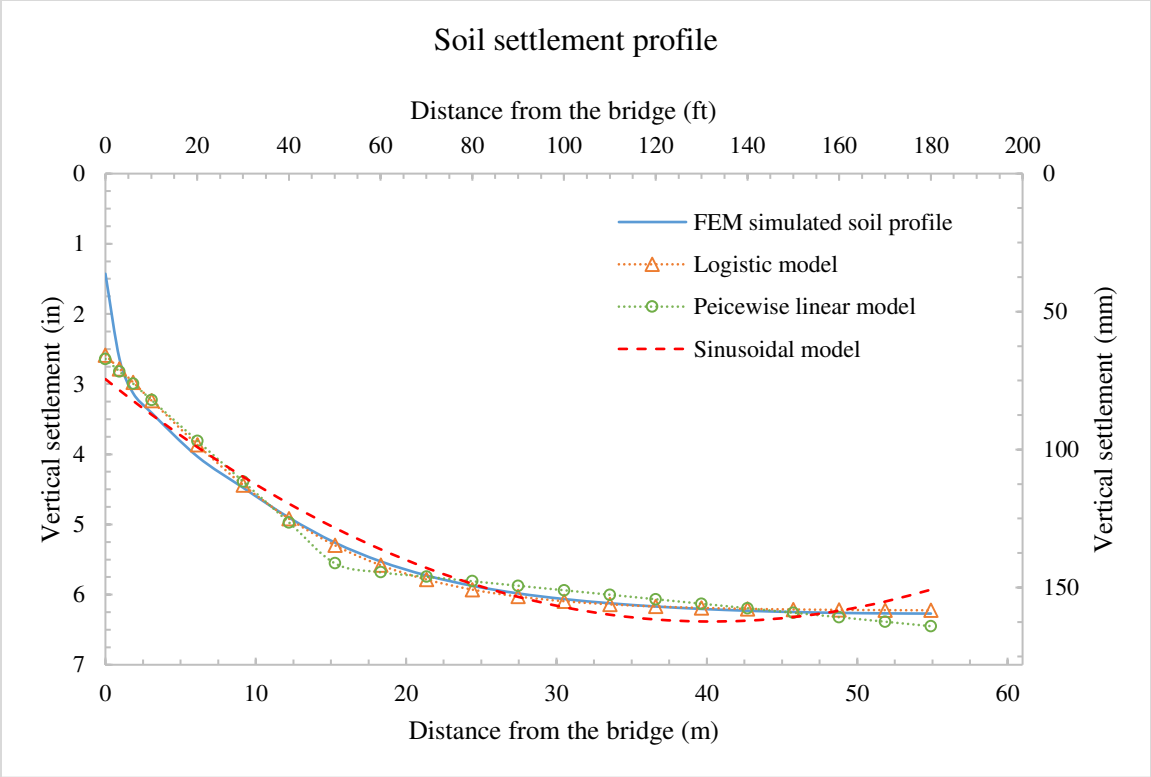

Figure 5.73 Various functions fitted to the soil deflection profile behind bridge abutment

The logistic function has a wide range of applications in several fields including engineering, statistics, and geoscience. It is frequently used to model a population with semi exponential growth. The logistic function, also called logistic curve, is a sigmoid curve (*S*-shaped curve) that is defined by the following equation

$$y = \frac{a}{1 + be^{-cx}} \qquad 5\text{-}3$$

Where

y = Vertical settlement at (x) distance away from the bridge abutment

a = Maximum displacement.

b = Parameter that affects the y-intercept.

c = Parameter that affects steepness of the curve.

A standard logistic sigmoid function is shown in Figure 5.74 (with a = -1, b = 1, and c = 1).

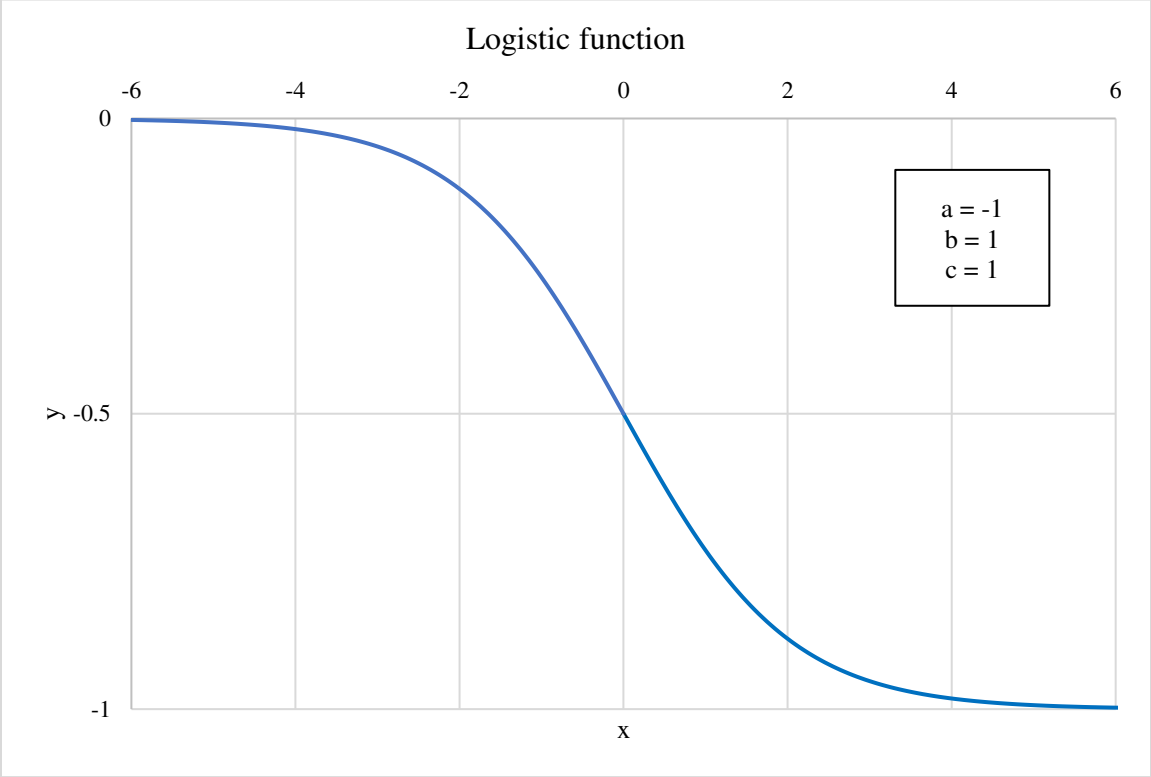

Figure 5.74 Standard logistic sigmoid function

Figure 5.74 shows that as x approaches $+\infty$, y approaches a, and as x approaches $-\infty$, y approaches zero. The derivative of the logistic function can be written as

$$\frac{d_y}{d_x} = cy\left[1 - \frac{y}{a}\right] \qquad 5\text{-}4$$

In the above equation, when y approaches zero, $\frac{d_y}{d_x} \to ky$. This indicates that when y is small, the logistic curve behaves exponentially (with a slope similar to an exponential curve). On the other hand, when y approaches a, $\frac{d_y}{d_x} \to 0$. This indicates that when y is large, the logistic curve becomes a horizontal line with a slope of zero. Accordingly, the intercept of a tangent to the horizontal line is represented by the maximum displacement a.

The logistic function consists of three parameters; *a*, *b*, and *c*. Referring to Figure 5.73, parameter *a* would represent the maximum soil deformation along the longitudinal direction. In other words, *a* represents magnitude of the soil settlement at a location away from the bridge abutment. Parameter *b* represents the settlement of the soil right at the interface between the abutment wall and the backfill soil, and parameter *c* represents the steepness of the curve behind abutment.

Accordingly, a nonlinear statistical analysis (nonlinear regression) was conducted in order to evaluate each of the logistic function parameters *a*, *b*, and *c* that would best fit the simulated soil deflection profiles. The least-square method, which minimize the sum of squared residuals, was used in this analysis. The coefficient of determination (R^2), and the standard error of estimate (S_{est}) were utilized to assess the goodness of fit. Tables 5.12 through 5.20 show the logistic function parameters that fit each of the simulated soil deflection profile.

Table 5.12 Logistic function parameters that best fit simulated soil deflection profile (soil profile No.1)

Soil profile No. (refer to Table 5.10)	Analysis No. (refer to Table 5.11)	Logistic function parameters			Statistical result	
		a *in* (*mm*)	*b*	*c*	R^2	S_{est} *in* (*mm*)
1	1	8.20 (208)	1.87	0.038	0.983	0.19 (4.90)
	2		1.88	0.043	0.980	0.20 (5.20)
	3		1.75	0.038	0.970	0.25 (6.40)
	4		1.73	0.043	0.964	0.26 (6.70)
	5		1.40	0.052	0.956	0.25 (6.40)
	6		1.39	0.052	0.956	0.26 (6.70)
	7		1.69	0.058	0.930	0.34 (8.50)
	8		1.66	0.061	0.930	0.36 (9.10)
	9		1.45	0.048	0.973	0.20 (5.20)
	10		1.44	0.048	0.971	0.22 (5.50)
	11		1.61	0.05	0.962	0.25 (6.40)
	12		1.58	0.05	0.961	0.26 (6.70)

Table 5.13 Logistic function parameters that best fit simulated soil deflection profile (soil profile No.2)

Soil profile No. (refer to Table 5.10)	Analysis No. (refer to Table 5.11)	Logistic function parameters			Statistical result	
		a in (*mm*)	*b*	*c*	R^2	S_{est} in (*mm*)
2	1	6.30 (159)	1.41	0.042	0.984	0.12 (3.00)
	2		1.46	0.043	0.982	0.13 (3.40)
	3		1.31	0.043	0.965	0.18 (4.60)
	4		1.34	0.044	0.963	0.18 (4.60)
	5		1.15	0.053	0.951	0.19 (4.90)
	6		1.13	0.053	0.951	0.19 (4.90)
	7		1.35	0.061	0.930	0.25 (6.40)
	8		1.33	0.061	0.930	0.25 (6.40)
	9		1.15	0.047	0.974	0.14 (3.70)
	10		1.16	0.047	0.973	0.14 (3.70)
	11		1.24	0.049	0.965	0.17 (4.30)
	12		1.24	0.049	0.964	0.17 (4.30)

Table 5.14 Logistic function parameters that best fit simulated soil deflection profile (soil profile No.3)

Soil profile No. (refer to Table 5.10)	Analysis No. (refer to Table 5.11)	Logistic function parameters			Statistical result	
		a in (*mm*)	*b*	*c*	R^2	S_{est} in (*mm*)
3	1	5.10 (129)	1.17	0.057	0.981	0.10 (2.40)
	2		1.2	0.054	0.976	0.11 (2.70)
	3		1.1	0.06	0.957	0.13 (3.40)
	4		1.11	0.055	0.953	0.14 (3.70)
	5		0.76	0.054	0.970	0.10 (2.40)
	6		0.76	0.054	0.969	0.10 (2.40)
	7		0.95	0.065	0.943	0.14 (3.70)
	8		0.88	0.061	0.949	0.13 (3.40)
	9		0.82	0.051	0.983	0.07 (1.80)
	10		0.87	0.053	0.976	0.08 (2.10)
	11		0.96	0.058	0.959	0.12 (3.00)
	12		0.97	0.058	0.959	0.12 (3.00)

Table 5.15 Logistic function parameters that best fit simulated soil deflection profile (soil profile No.4)

Soil profile No. (refer to Table 5.10)	Analysis No. (refer to Table 5.11)	Logistic function parameters			Statistical result	
		a in (*mm*)	*b*	*c*	R^2	S_{est} in (*mm*)
4	1	3.60 (91)	1.46	0.061	0.983	0.07 (1.80)
	2		1.54	0.065	0.981	0.07 (1.80)
	3		1.29	0.07	0.964	0.08 (2.10)
	4		1.33	0.07	0.961	0.08 (2.10)
	5		1.15	0.108	0.966	0.07 (1.80)
	6		1.1	0.105	0.965	0.07 (1.80)
	7		1.45	0.124	0.963	0.07 (1.80)
	8		1.42	0.125	0.959	0.08 (2.10)
	9		1.15	0.085	0.981	0.06 (1.50)
	10		1.15	0.086	0.982	0.06 (1.50)
	11		1.23	0.091	0.975	0.06 (1.50)
	12		1.24	0.092	0.975	0.06 (1.50)

Table 5.16 Logistic function parameters that best fit simulated soil deflection profile (soil profile No.5)

Soil profile No. (refer to Table 5.10)	Analysis No. (refer to Table 5.11)	Logistic function parameters			Statistical result	
		a *in* (*mm*)	*b*	*c*	R^2	S_{est} *in* (*mm*)
5	1	3.10 (78)	1.27	0.074	0.980	0.05 (1.20)
	2		1.31	0.079	0.978	0.05 (1.20)
	3		1.25	0.099	0.966	0.06 (1.50)
	4		1.26	0.097	0.959	0.06 (1.50)
	5		0.51	0.082	0.992	0.01 (0.30)
	6		0.48	0.077	0.991	0.01 (0.30)
	7		0.69	0.104	0.983	0.02 (0.60)
	8		0.62	0.097	0.985	0.02 (0.60)
	9		0.66	0.081	0.994	0.01 (0.30)
	10		0.75	0.089	0.991	0.02 (0.60)
	11		0.96	0.109	0.979	0.04 (0.90)
	12		0.97	0.11	0.979	0.04 (0.90)

Table 5.17 Logistic function parameters that best fit simulated soil deflection profile (soil profile No.6)

Soil profile No. (refer to Table 5.10)	Analysis No. (refer to Table 5.11)	Logistic function parameters			Statistical result	
		a *in* (*mm*)	*b*	*c*	R^2	S_{est} *in* (*mm*)
6	1	2.70 (69)	1.02	0.09	0.979	0.04 (0.90)
	2		1.09	0.105	0.982	0.04 (0.90)
	3		1.17	0.138	0.977	0.04 (0.90)
	4		1.27	0.131	0.974	0.04 (0.90)
	5		0.36	0.115	0.950	0.02 (0.60)
	6		0.36	0.114	0.952	0.02 (0.60)
	7		0.5	0.142	0.973	0.02 (0.60)
	8		0.51	0.133	0.974	0.02 (0.60)
	9		0.52	0.116	0.980	0.02 (0.60)
	10		0.58	0.123	0.982	0.02 (0.60)
	11		0.83	0.131	0.982	0.02 (0.60)
	12		0.92	0.133	0.983	0.02 (0.60)

Table 5.18 Logistic function parameters that best fit simulated soil deflection profile (soil profile No.7)

Soil profile No. (refer to Table 5.10)	Analysis No. (refer to Table 5.11)	Logistic function parameters			Statistical result	
		a *in* (*mm*)	*b*	*c*	R^2	S_{est} *in* (*mm*)
7	1	3.45 (87)	2.89	0.076	0.982	0.08 (2.10)
	2		2.94	0.085	0.981	0.08 (2.10)
	3		2.59	0.078	0.975	0.10 (2.40)
	4		2.64	0.087	0.973	0.10 (2.40)
	5		1.60	0.105	0.980	0.06 (1.50)
	6		1.61	0.106	0.979	0.07 (1.80)
	7		1.97	0.12	0.973	0.07 (1.80)
	8		1.95	0.121	0.971	0.06 (1.50)
	9		1.93	0.094	0.983	0.06 (1.50)
	10		1.96	0.1	0.980	0.06 (1.50)
	11		2.24	0.107	0.970	0.08 (2.10)
	12		2.27	0.111	0.968	0.08 (2.10)

Table 5.19 Logistic function parameters that best fit simulated soil deflection profile (soil profile No.8)

Soil profile No. (refer to Table 5.10)	Analysis No. (refer to Table 5.11)	Logistic function parameters			Statistical result	
		a in (*mm*)	*b*	*c*	R^2	S_{est} in (*mm*)
8	1	2.20 (55)	2.01	0.089	0.981	0.04 (0.90)
	2		2.1	0.093	0.980	0.04 (0.90)
	3		1.98	0.103	0.966	0.05 (1.20)
	4		2.02	0.102	0.966	0.05 (1.20)
	5		1.19	0.122	0.988	0.02 (0.60)
	6		1.17	0.122	0.988	0.02 (0.60)
	7		1.37	0.133	0.986	0.02 (0.60)
	8		1.35	0.133	0.985	0.02 (0.60)
	9		1.19	0.092	0.992	0.01 (0.30)
	10		1.21	0.094	0.991	0.01 (0.30)
	11		1.64	0.119	0.981	0.04 (0.90)
	12		1.65	0.119	0.981	0.04 (0.90)

Table 5.20 Logistic function parameters that best fit simulated soil deflection profile (soil profile No.9)

Soil profile No. (refer to Table 5.10)	Analysis No. (refer to Table 5.11)	Logistic function parameters			Statistical result	
		a in (*mm*)	*b*	*c*	R^2	S_{est} in (*mm*)
9	1	2.10 (52)	1.82	0.103	0.982	0.04 (0.90)
	2		1.91	0.108	0.979	0.04 (0.90)
	3		1.94	0.128	0.967	0.05 (1.20)
	4		1.94	0.125	0.963	0.05 (1.20)
	5		0.82	0.108	0.990	0.01 (0.30)
	6		0.77	0.103	0.991	0.01 (0.30)
	7		0.94	0.119	0.986	0.01 (0.30)
	8		0.93	0.118	0.987	0.01 (0.30)
	9		1.1	0.106	0.993	0.01 (0.30)
	10		0.94	0.095	0.991	0.01 (0.30)
	11		1.42	0.131	0.981	0.02 (0.60)
	12		1.45	0.131	0.980	0.02 (0.60)

5.9 Evaluating logistic function parameters

The next step would be to evaluate each of the logistic function parameters (*a*, *b*, and *c*) individually to see if they can be determined using geometric and soil parameters. For this purpose, correlation and regression analysis were carried out.

First, a correlation analysis was conducted to examine the relationship among the logistic function parameters. Table 5.21 shows the result of this study. Accordingly, the result indicate that the three parameters are not correlated with each other, except for parameters (*a*) and (*c*) for which a strong negative correlation exists.

Table 5.21 Pearson's correlation coefficient among logistic function parameters

Parameter	*a*	*b*	*c*
a	1.00	0.170	-0.830
b	0.170	1.00	-0.083
c	-0.830	-0.083	1.00

Subsequently, another analysis was carried out to examine the correlation between parameters a, b, and c with fundamental soil properties (backfill soil, embankment soil, and natural soil), as well as geometric parameters. In this analysis, a was decomposed into two components; ultimate settlement resulting from the natural soil a_n, and ultimate settlement resulting from the embankment fill a_e, in which ($a = a_n + a_e$). This was to examine the contribution of each soil layer to the total surface settlement a. Table 5.22 shows the decomposition of the simulated ultimate settlement a.

Table 5.22 Decomposition of the simulated ultimate settlement a

Soil profile No. (refer to Table 5.10)	a *in* (*mm*)	a_n *in* (*mm*)	a_e *in* (*mm*)
1	8.20 (208)	5.50 (141)	2.70 (67)
2	6.30 (159)	4.90 (124)	1.40 (35)
3	5.10 (129)	3.90 (98)	1.20 (31)
4	3.60 (91)	2.20 (55)	1.40 (36)
5	3.10 (78)	1.80 (47)	1.30 (31)
6	2.70 (69)	1.50 (37)	1.20 (32)
7	3.45 (87)	1.90 (48)	1.55 (39)
8	2.20 (55)	1.70 (44)	0.50 (11)
9	2.10 (52)	1.50 (37)	0.60 (15)

Table 5.23 shows the result of the correlation study between the logistic function parameters and backfill soil properties. Table 5.24 shows the result of the correlation study between the logistic function parameters and embankment soil properties. Table 5.25 shows the result of the correlation study between the logistic function parameters and natural soil properties. Table 5.26 shows the result of the correlation study between the logistic function parameters and geometric parameters.

Table 5.23 Pearson's correlation coefficient between logistic function parameters and backfill soil properties

Soil properties	a	a_n	a_e	b	c
φ'	0.000	0.000	0.000	-0.133	-0.211
γ	0.000	0.000	0.000	-0.125	-0.233
e_0	0.000	0.000	0.000	-0.125	-0.233
E	0.000	0.000	0.000	0.125	0.233

Table 5.24 Pearson's correlation coefficient between logistic function parameters and embankment soil properties

Soil properties	a	a_n	a_e	b	c
C'	-0.443	-0.393	-0.471	-0.651	0.309
φ'	-0.435	-0.389	-0.453	-0.643	0.307
γ	0.475	0.406	0.545	0.682	-0.312
ν	0.384	0.362	0.355	0.588	-0.294
C_c	0.472	0.405	0.537	0.720	-0.312
C_s	0.486	0.409	0.572	0.691	-0.312
e_0	0.476	0.406	0.547	0.683	-0.312
E	-0.497	-0.410	-0.606	-0.699	0.309

Table 5.25 Pearson's correlation coefficient between logistic function parameters and natural soil properties

Soil properties	a	a_n	a_e	b	c
C'	-0.307	-0.388	-0.039	-0.461	0.492
φ'	-0.355	-0.455	-0.026	-0.500	0.430
γ	-0.276	-0.361	0.000	-0.352	0.184
ν	0.247	0.307	0.041	0.388	-0.471
C_c	0.354	0.455	0.024	0.495	-0.413
C_s	0.354	0.455	0.024	0.495	-0.413
e_0	0.354	0.455	0.024	0.495	-0.414
E	-0.350	-0.447	-0.031	-0.503	0.464

Table 5.26 Correlation coefficient between logistic function parameters and geometric parameters

Geometric parameters	a	a_n	a_e	b	c
H_e	0.548	0.509	0.525	-0.526	-0.458
H_a	0.000	0.000	0.000	0.460	-0.211
S_b	0.000	0.000	0.000	0.011	0.016
H_a / H_e	0.145	-0.135	-0.139	0.622	-0.082

5.9.1 Logistic function parameter (a)

As shown in Tables 5.23, 5.24 and 5.25, parameter a does not have a strong correlation with the backfill soil properties. Nevertheless, stronger correlation exists between a and the embankment fill as well as natural soil fundamental properties. Therefore, the problem can be further simplified to include only the embankment fill and natural soil layers. This was done by considering a vertical soil strip (along the longitudinal-direction) with a unit longitudinal length

that includes the pavement roadway (as a pressure), embankment fill layer, and natural soil layer, as shown in Figure 5.75.

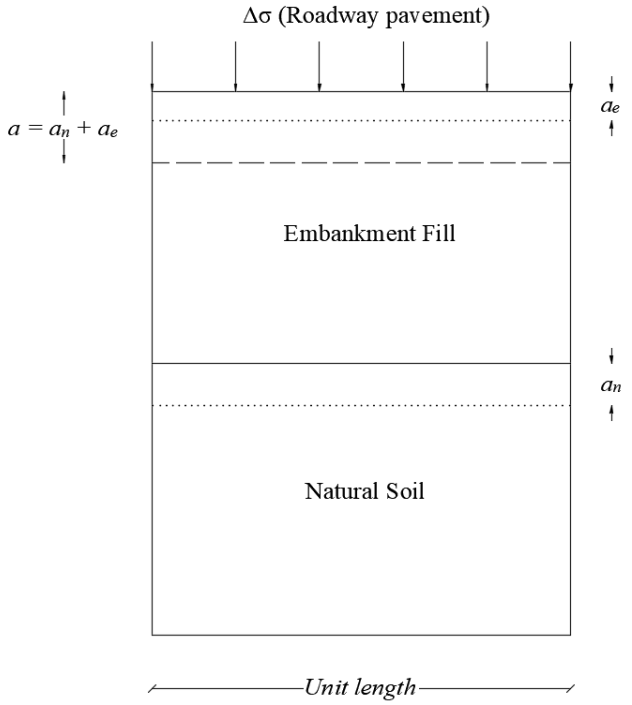

Figure 5.75 Calculation of (a) using a vertical strip (longitudinal-direction)

In general, the weight of any soil layer or structure will impose stresses on the underlying soil layers. These stresses will eventually cause dimensional changes in the soil volume (decrease in the volume) through which settlement of soil occurs. This settlement can be expressed by the summation of three separate components; the initial settlement (reduction of void ratio), primary settlement (dissipation of water), and secondary settlement (creep). According to the MDPCM model, this settlement can be expressed in terms of total strain. Therefore, the ultimate settlement can be represented by the volumetric elastic and plastic strains developed within the soil layer. Accordingly, it was assumed that the deformation of the soil away from the abutment takes place only in the vertical direction. Such an assumption would allow explaining the settlement of each soil layer by its elastic and plastic volumetric deformation. Ultimately, the total volumetric strain can be expressed as:

$$d\varepsilon_v = d\varepsilon_v^e + d\varepsilon_v^p \quad 5\text{-}5$$

The total volumetric strain can be evaluated individually for each soil layer. This was done by further simplifying the problem into two separate parts (presented in Figure 5.75): settlement of the embankment fill due to the weight of the roadway pressure a_e and settlement of the natural soil due to the weight of the embankment fill a_n, as shown in Figure 5.76.

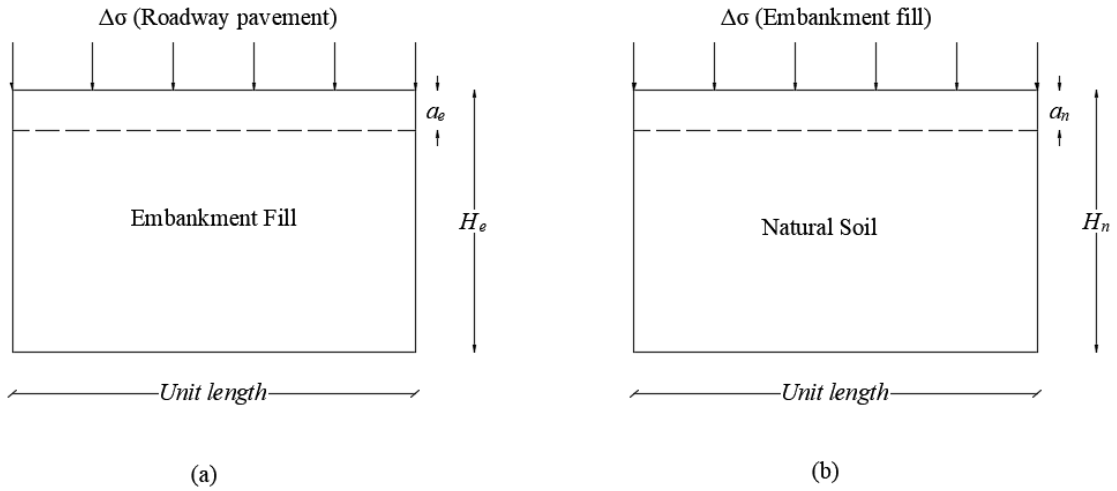

Figure 5.76 Calculation of (a) a_e and (b) a_n

The volumetric elastic deformation of soil can be conveniently represented by a linear elastic deformation using Hooke's law as follows:

$$\varepsilon_v^e = \frac{\sigma_0 + \Delta\sigma}{E} \quad 5\text{-}6$$

Where, σ_0, $\Delta\sigma$, E are the in-situ pressure, surcharge pressure, and modulus of elasticity of soil, respectively. The volumetric elastic strain can be adjusted to accommodate for the nonlinear behavior of the soil (within the elastic region). This is particularly the case with the over-consolidated soils, where a nonlinear deformation based on over-consolidation ratio (OCR) is expected. Therefore, an overburden stress ratio term (increase of the stress ratio) $\left(\frac{\sigma_0+\Delta\sigma}{\sigma_0}\right)$ can be

introduced in the above equation in order to account for the nonlinear behavior. Accordingly, equation 5-6 becomes:

$$\varepsilon_v^{e.adj} = \frac{\sigma_0 + \Delta\sigma}{E}\left[\frac{\sigma_0 + \Delta\sigma}{\sigma_0}\right] \quad 5\text{-}7$$

The soil behavior will remain in the elastic region until the state of the stress reaches the yield stress, defined as the pre-consolidation pressure, σ_c, or the modified long-term cohesion of the soil, *d*, whichever is greater. Subsequently, plastic deformation occurs. Within the plastic region, σ_c, along with C_s and C_c are used to define the hardening behavior of the soil. Ultimately, the volumetric plastic strain can be evaluated using the following equation (Helwany 2007)

$$\varepsilon_v^p = \frac{C_c - C_s}{(\ln 10)(1 + e_0)} \ln\frac{\sigma_0 + \Delta\sigma}{\sigma_c} \quad 5\text{-}8$$

The volumetric elastic and plastic deformation defined by equations 5-6, 5-7 and 5-8 were used to evaluate the maximum longitudinal ultimate surface settlement, *a*. Accordingly, statistical analysis was carried out to determine the relationship between the maximum longitudinal settlement components a_n and a_e with volumetric elastic and plastic deformation. Table 5.27 shows the result of this analysis.

Table 5.27 Pearson's correlation coefficient between a_n and a_e with volumetric elastic and plastic deformation

Equation	Natural soil settlement (a_n)	Embankment soil settlement (a_e)
ε_v^e	0.954	0.903
ε_v^p	0.967	0.418
$(\sigma_0 + \Delta\sigma)/\sigma_0$	0.808	-0.669
$\varepsilon_v^{e.adj}$	0.955	0.911
$\varepsilon_v^{e.adj} + \varepsilon_v^p$	0.963	0.726
$\varepsilon_v^{e.adj} * H$	0.953	0.807
$\varepsilon_v^p * H$	0.967	0.693
$\left[\varepsilon_v^{e.adj} * H\right] + \left[\varepsilon_v^p * H\right]$	0.963	0.901

As shown in the above table, a very strong correlation exists between the total strain $\left(\varepsilon_v^{e.adj} + \varepsilon_v^p\right)$ and the simulated settlement components a_e and a_n. Accordingly, scatter plots, shown in Figures 5.77 and 5.78, were constructed to examine the relationship between them.

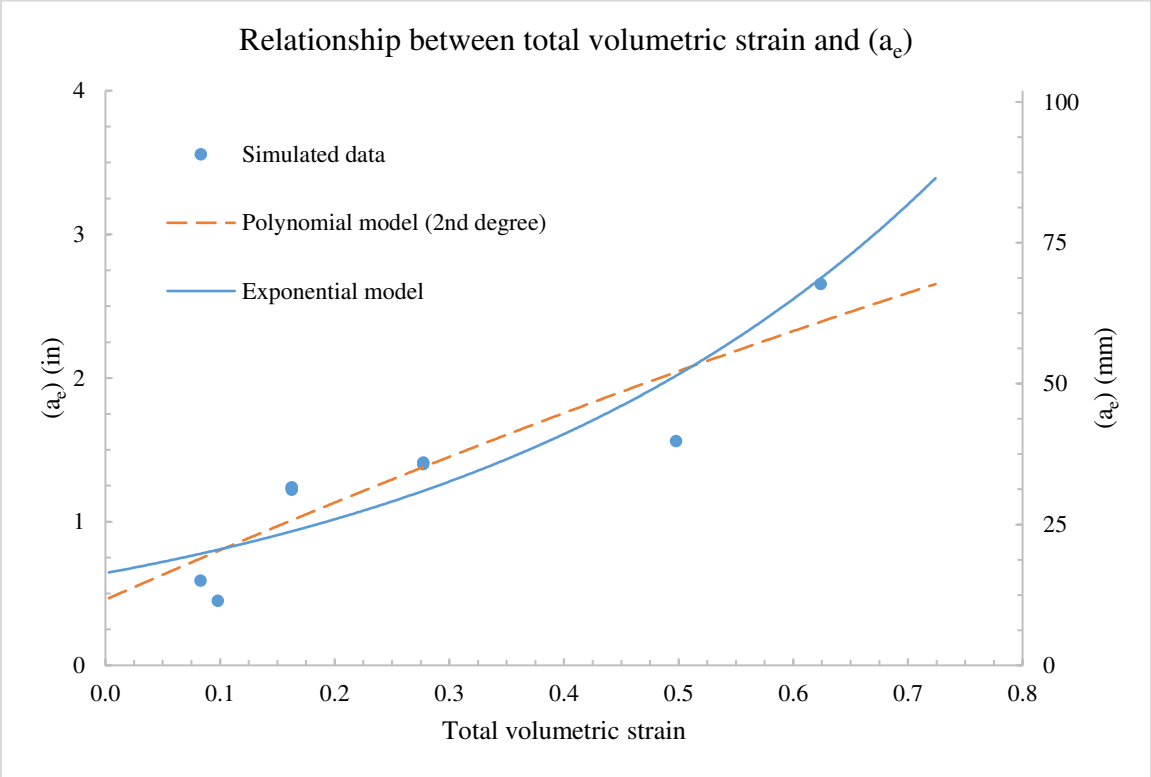

Figure 5.77 Scatter plot between total volumetric strain and settlement component (a_e)

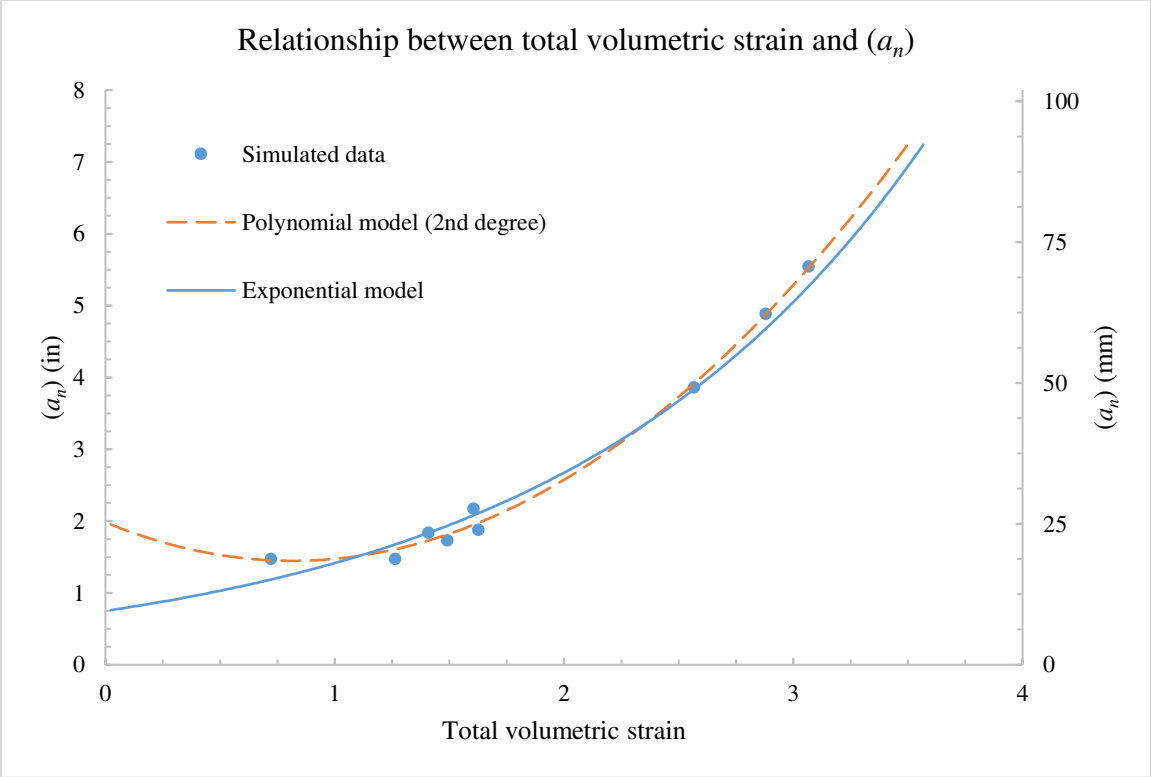

Figure 5.78 Scatter plot between total volumetric strain and settlement component (a_n)

Various trials were made, using curve fitting software (curve expert), to find the best fit curve between the simulated ultimate soil components and the total volumetric strain. The best fit curves are shown in the above figures. It is concluded that the relationship between $\left(\varepsilon_v^{e.adj} + \varepsilon_v^p\right)$ and a_e may be represented by an exponential function. Similar observation was made for the relationship between $\left(\varepsilon_v^{e.adj} + \varepsilon_v^p\right)$ and a_n. Therefore, an exponential relationship could be proposed as follows:

$$a_n = C_n H_n e^{\left(\beta_n \varepsilon_v^{e.adj} + \alpha_n \varepsilon_v^p\right)} \qquad 5\text{-}9$$

$$a_e = C_e H_e e^{\left(\beta_e \varepsilon_v^{e.adj} + \alpha_e \varepsilon_v^p\right)} \qquad 5\text{-}10$$

In which,

$$a = a_n + a_e \quad (5\text{-}11)$$

and

a = Ultimate settlement at the top surface of the embankment fill.

a_n = Settlement component at the top surface of the natural soil.

a_e = Settlement component at the top surface of the embankment fill.

H_n = Height of the natural soil layer.

H_e = Height of the embankment fill.

C_e, C_n, β_n, β_e, α_n and α_e = Regression parameters.

Accordingly, a regression analysis was conducted using the method of least squares in order to determine the best fit for the exponential relationships proposed above. Table 5.28 shows the results for the regression parameters C_e, C_n, β_n, α_n, β_e and α_e.

Table 5.28 Regression parameters of the ultimate settlement components (a_n) and (a_e).

Parameter	Value
C_n	383×10^{-6}
β_n	27.00
α_n	38.60
C_e	4980×10^{-6}
β_e	61.00
α_e	23.00

The final equation was evaluated by substituting the value of various parameters (found in Table 5.28) into equations 5-9, 5-10. Thus, the maximum longitudinal surface settlement, a, can be evaluated using the following equation

$$a = 383 \times 10^{-6} H_n e^{\left(27\,\varepsilon_v^{e.adj} + 38.6\,\varepsilon_v^{p}\right)} + 4980 \times 10^{-6} H_e e^{\left(61\,\varepsilon_v^{e.adj} + 23\,\varepsilon_v^{p}\right)} \quad (5\text{-}12)$$

Equations 5-12 provides an empirical estimation of the ultimate soil settlement away from bridge abutment. This empirical equation has resulted in a coefficient of determination R^2 = 0.999, and standard error of estimate S_{est} = 0.07 *in* (1.80 *mm*). This indicates that the value of *a* can be accurately predicted from the proposed equation 5-12. Figure 5.79 shows the simulated versus predicted *a*.

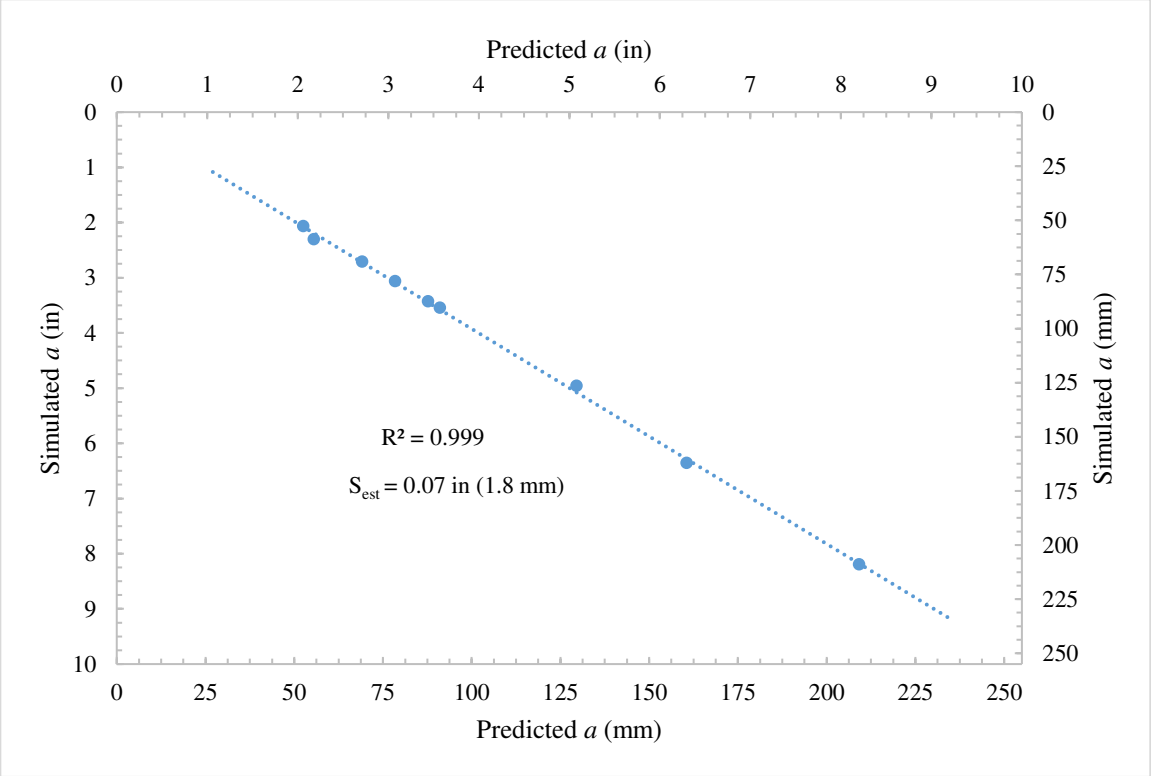

Figure 5.79 Simulated versus predicted *a*

5.9.1.1 Adjustment of (*a*)

In general, the type of FEM influences the result of the analysis. As in this study, two-dimensional longitudinal model was used to perform the analysis. This type of model does not consider the effect of the side slope of the embankment fill (in the transverse direction). This eventually results in an overestimation of the maximum settlement, *a*. In order to include the effect of the side slope in the calculation of *a*, maximum surface settlements from the transverse and longitudinal models were compared.

In this analysis, all soil profiles (shown in Table 5.10) were tested. The analysis was carried out such that the side slope of the embankment fill, oriented in the transverse direction, was straightened up, by adding more filling material (A_3 in Figure 5.80). The maximum surface settlements of the sloped and straightened embankment fills were compared with the maximum longitudinal surface settlement, *a*.

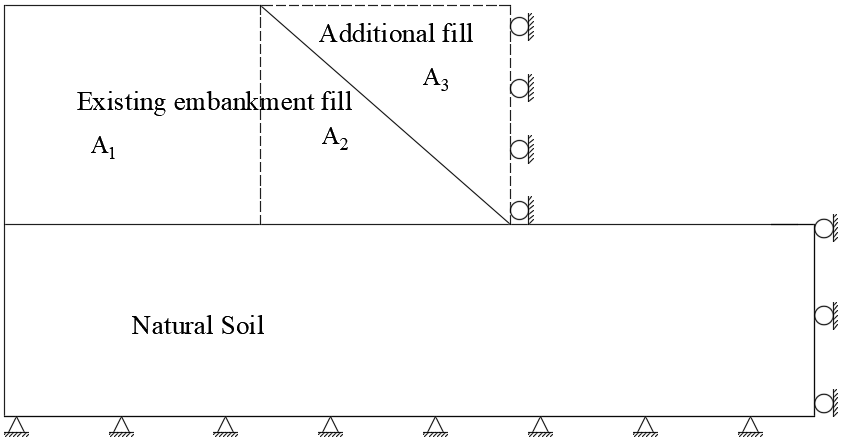

Figure 5.80 Layout of the transverse simulation (additional fill)

Figures 5.81 through 5.83 show the result of the analysis using soil profile No.1 (see Table 5.10).

Figure 5.81 Vertical deformation contour (transverse direction) of soil profile No.1 (*ft*)

Figure 5.82 Vertical deformation contour (transverse direction) of soil profile No.1 with additional fill (*ft*)

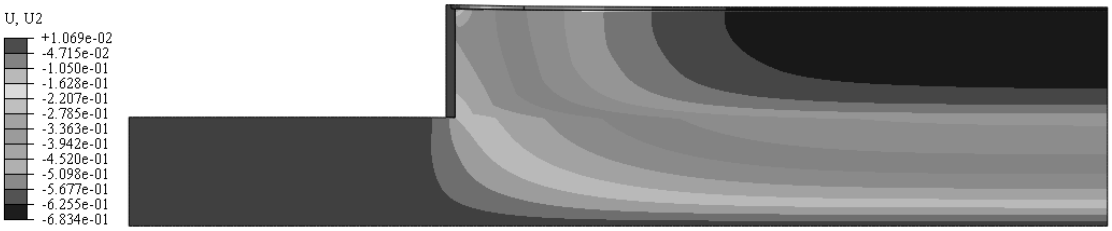

Figure 5.83 Vertical deformation contour (longitudinal direction) of soil profile No.1 (analysis#3) (*ft*)

The above figures show that the anticipated maximum surface settlement from the transverse model (Figure 5.81) was less than the longitudinal model (Figure 5.83). Figure 5.82 shows that after adding more fill, the surface settlement at the center of the embankment has increased to relatively match the maximum longitudinal settlement, *a*. Similar observation was found with all tested soil profiles. Accordingly, a relationship was sought by relating the area ratio of embankment fill to the maximum longitudinal settlement, *a*. Ultimately, the difference in the filling area was assumed to be proportional with *a* as follows:

$$a_{adj} = a\left(1 - \frac{A_3}{A_1 + A_2}\right) \quad \text{5-13}$$

Where

$A_1 + A_2$ = Total transverse area of the embankment fill (see Figure 5.80)

A_3 = Transverse area of the additional fill (see Figure 5.80).

Accordingly, regression analysis was conducted using the method of least squares to determine the best fit for the latter relationship. Consequently, the final equation was evaluated as follows:

$$a_{adj} = 0.92a\left(1 - \frac{A_3}{A_1 + A_2}\right) + 0.82 \quad \text{5-14}$$

Equation 5-14 provides an empirical relationship that relates the maximum longitudinal settlement, *a*, with the maximum transverse surface settlement. Figure 5.84 shows the simulated versus predicted *a* using equation 5-14.

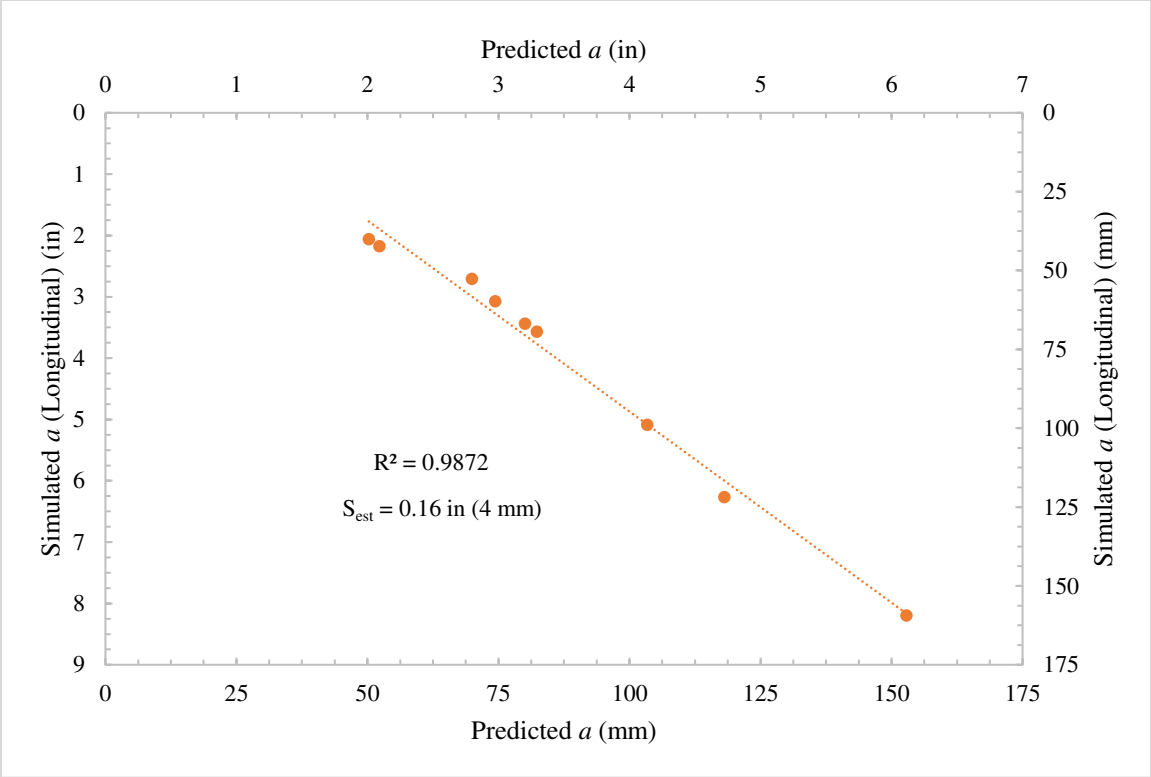

Figure 5.84 Simulated versus predicted (a)

5.9.2 Logistic function parameter (b)

As shown in Tables 5.24 and 5.26, parameter (b) has a strong correlation with the embankment soil properties as well as the geometric parameters. They include embankment compression index (C_c) ($r = 0.720$) and the abutment to embankment height ratio (H_e / H_a) ($r = 0.622$). Accordingly, it was observed that the correlation coefficient increases to ($r = 0.808$) as a result of multiplying the embankment compression index with the abutment to embankment height ratio (i.e. $C_c \times H_a / H_e$). Thus, a scatter plot, shown in Figure 5.85, was constructed between parameter (b) and ($C_c \times H_a / H_e$).

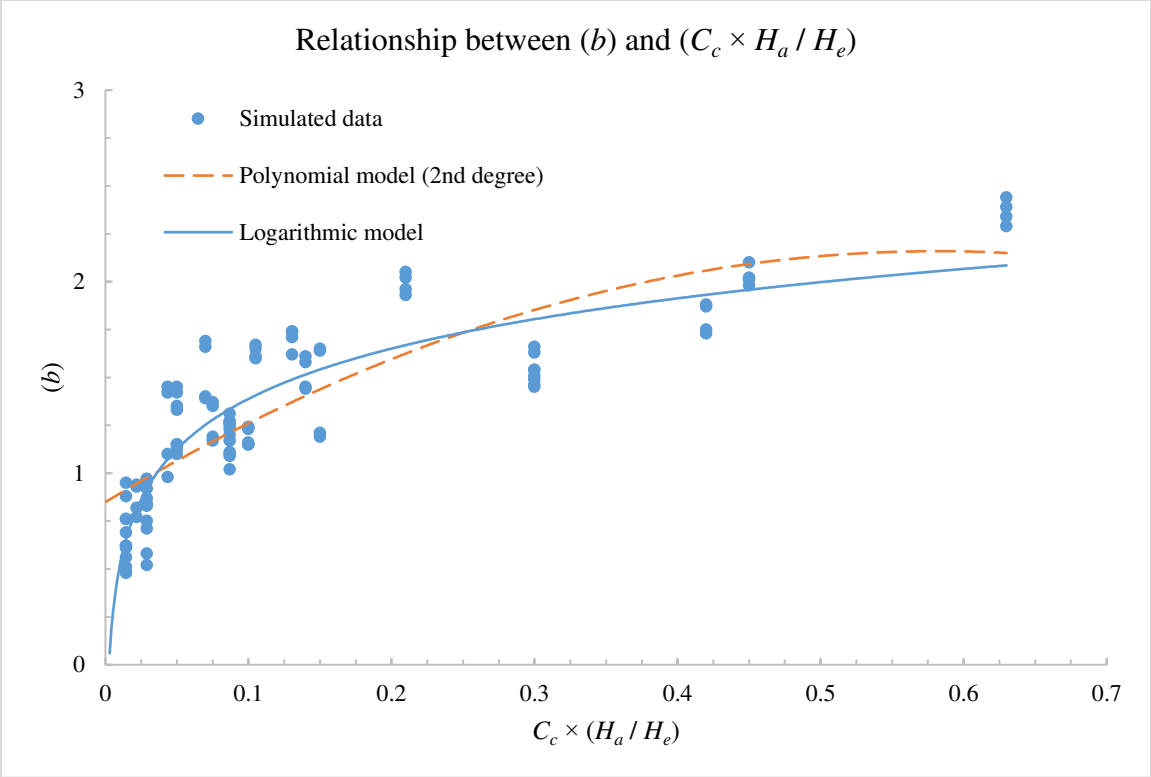

Figure 5.85 Scatter Plot between parameter (b) and ($C_c \times H_a / H_e$)

Various trials were made, using curve fitting software (curve expert), to find the best fit curve between the logistic function parameter, b, with ($C_c \times H_a / H_e$). The best fit curves are shown in the above figures. It is concluded that the relationship between parameter b and ($C_c \times H_a / H_e$) may be best represented by a logarithmic function as shown below:

$$b = \vartheta \, ln\left(C_c \times \frac{H_a}{H_e}\right) + \Psi \qquad 5\text{-}15$$

Where

C_c = Compression index of the embankment fill.

H_e = Height of the embankment fill.

H_a = Height of the abutment wall.

ϑ and Ψ = Regression parameters.

Consequently, a regression analysis was conducted using the method of least squares in order to determine the best fit parameters for the logarithmic relationship. Table 5.29 shows the results for the regression parameters ϑ and Ψ.

Table 5.29 Regression parameters of the logarithmic function

Parameter	Value
ϑ	0.38
Ψ	2.26

The final equation was evaluated by substituting the parameters value (found in Table 5.29) into equation 5-15 as follows:

$$b = 0.38\, ln\left(C_c \times \frac{H_a}{H_e}\right) + 2.26 \qquad 5\text{-}16$$

Equation 5-16 provides an empirical estimation for the parameter *b*, which controls the magnitude of the settlement at the interface between the abutment wall and adjacent soil. This empirical equation resulted in a coefficient of determination $R^2 = 0.794$, and standard error of estimate $S_{est} = 0.15$. This indicates that the value of *b* can be predicted reasonably well using equation 5-16. Figure 5.86 shows the simulated versus predicted *b*.

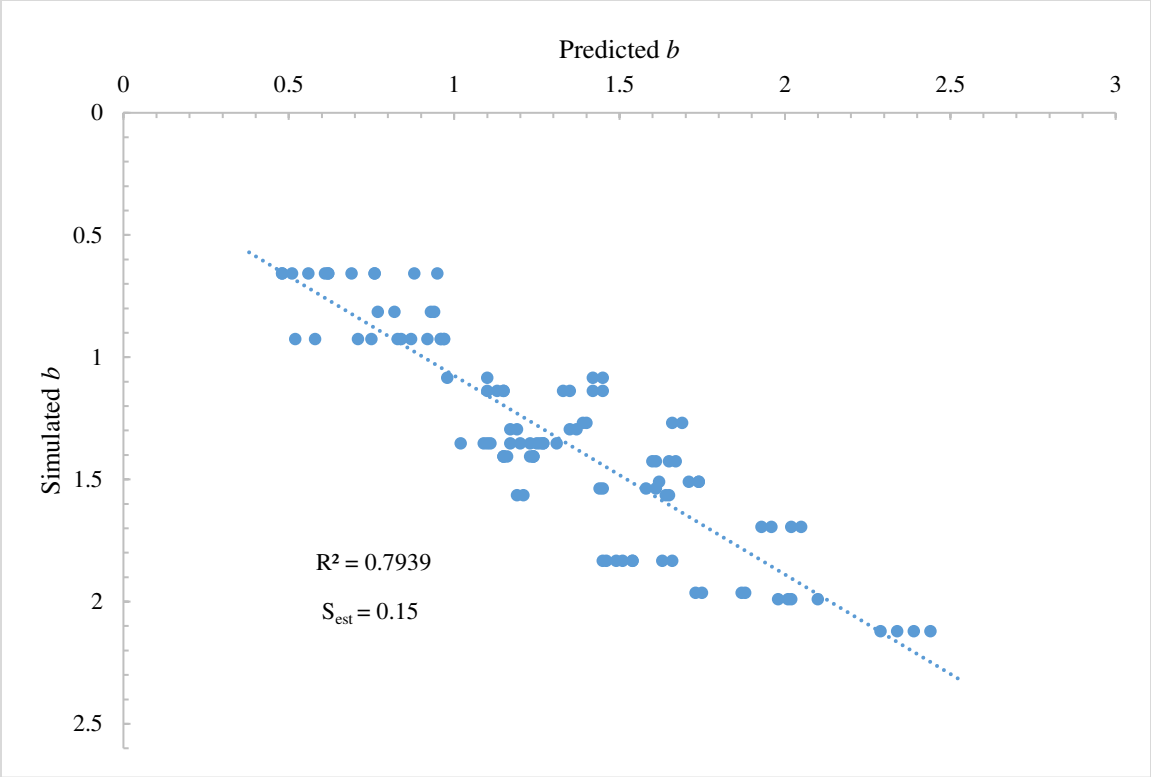

Figure 5.86 Simulated versus predicted *b*

5.9.3 Logistic function parameter (*c*)

As shown in Table 5.21, a very strong negative correlation exists between parameters *a* and *c*, with a value of (r = -0.830). Figure 5.87 shows a scatter plot between parameter *a* and *c*.

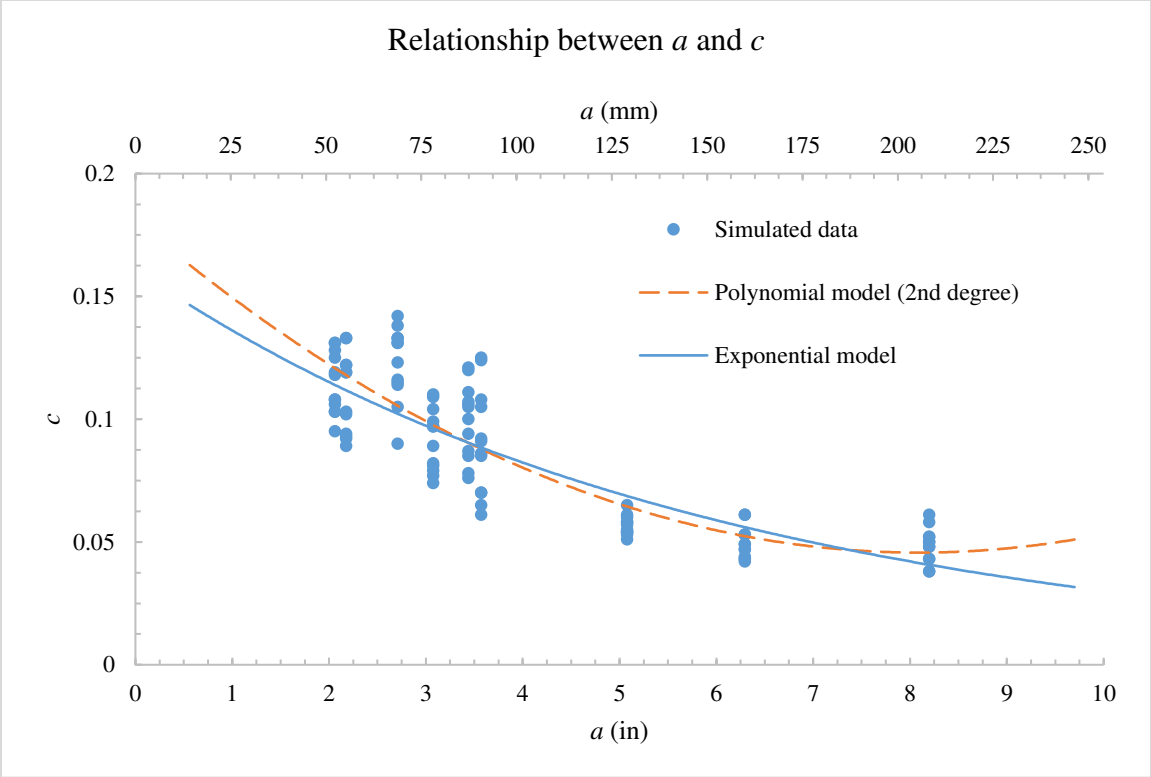

Figure 5.87 Scatter plot between parameter a and c

Various trials were made, using curve fitting software (curve expert), to find the best fit curve of the logistic function parameter, c. The best fit curves are shown in the above figures. It is concluded that the relationship between c and a may follow an exponential function. Therefore, an exponential function could be proposed as follows:

$$c = \eta e^{\omega a} \qquad 5\text{-}17$$

Where

η and ω = Regression parameters.

Accordingly, a regression analysis was conducted using the method of least squares in order to determine the best fit for the exponential relationship. Table 5.30 shows the results for the parameters η and ω.

Table 5.30 Regression parameters for the exponential relationship

Parameter	Value
η	0.172188
ω	-0.18195 when (a) is in inches -0.00716 when (a) is in millimeters

The final equation was evaluated by substituting the parameters value (found in Table 5.30) into equation 5-17 as follows:

When a is in inches

$$c = 0.172\mathrm{e}^{-0.182a} \tag{5-18}$$

When a is in millimeters

$$c = 0.172\mathrm{e}^{-0.007a} \tag{5-19}$$

Equations 5-18 and 5-19 provide an empirical relationship between the logistic function parameters a and c. This empirical equation has resulted in a coefficient of determination R^2 = 0.730, and standard error of estimate S_{est} = 0.015. This indicates that the value of c can be predicted reasonably well using Equations 5-18 and 5-19. Figure 5.88 shows the simulated versus predicted c.

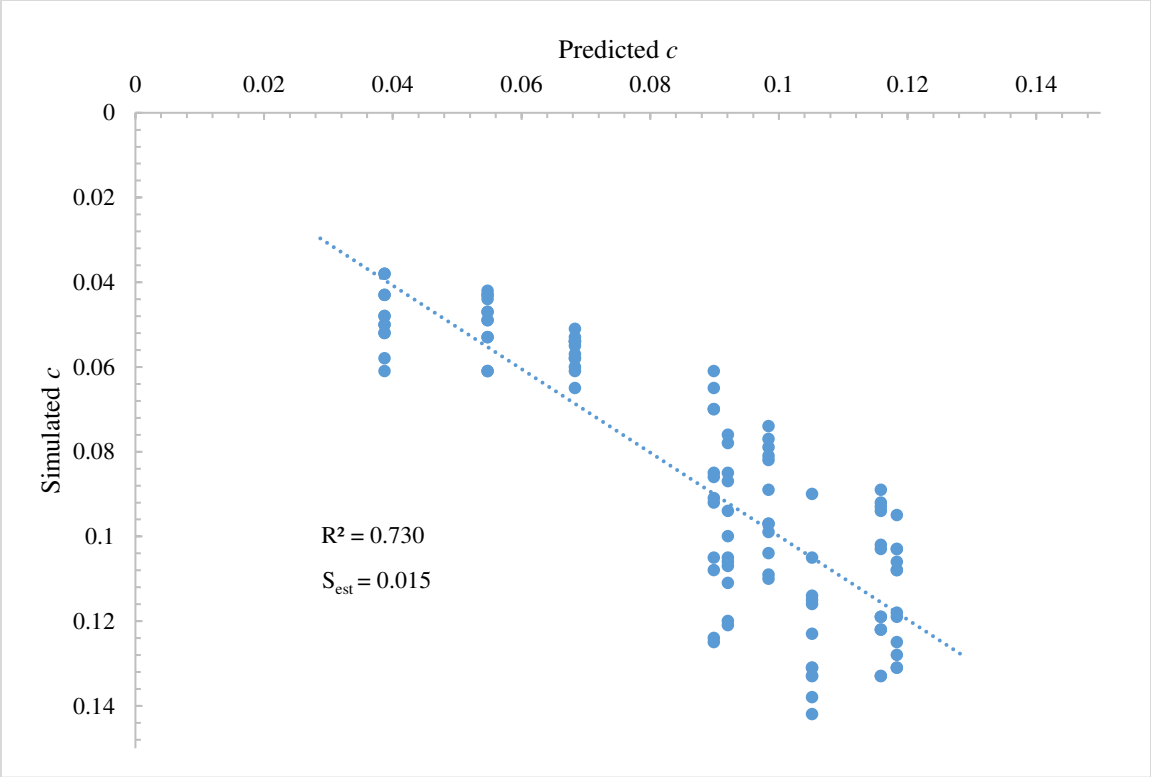

Figure 5.88 Simulated versus predicted c

5.10 Case study

A case study was considered and examined, using the finite element method, to investigate the accuracy of the developed empirical equations with respect to estimating the longitudinal soil deflection profile behind bridge abutment.

The soil profile used in the case study is similar to that shown in Figure 5.33. It consisted of a wall abutment with height $H_a = H_e$ constructed against a 95% compacted granular backfill with S_b = 1:2 (1 vertical to 2 horizontal), low compressible embankment fill with height H_e = 25 *ft* (7.6 *m*) and moderate compressible natural soil with height H_n = 35 *ft* (10.7 *m*). The material properties associated with the concrete in the abutment wall, approach slab, and roadway pavement as well as soil properties are shown in Tables 4.2 and 4.7, respectively.

The boundary conditions, analysis steps, elements type, and contact behavior were described in section 5.6. Figure 5.89 shows the finite element discretization of the case study model.

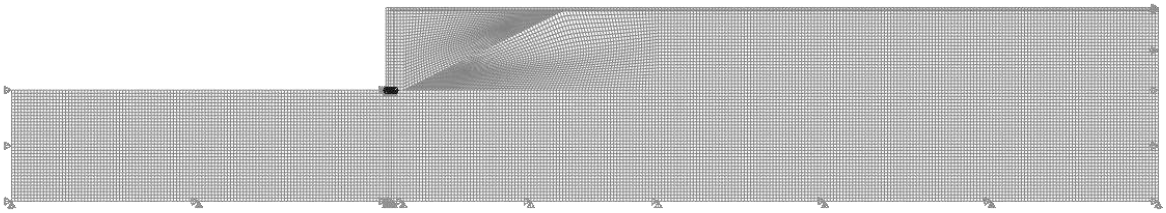

Figure 5.89 Finite element discretization of the case study model

Results from the finite element analysis of are presented in Figures 5.90, 5.91 and 5.92. Figure 5.90 shows the vertical deformation of the abutment, approach slab, roadway, embankment fill, and natural soil at the end of the analysis. Figure 5.91 shows the distribution of excess pore pressure at the end of the analysis. Figure 5.92 shows the simulated soil deformation profile along the longitudinal direction.

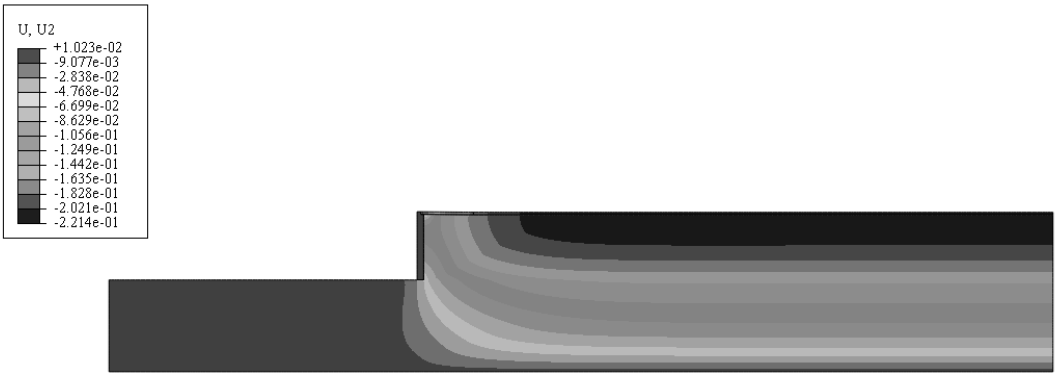

Figure 5.90 Deformed mesh at the end of the analysis (*ft*)

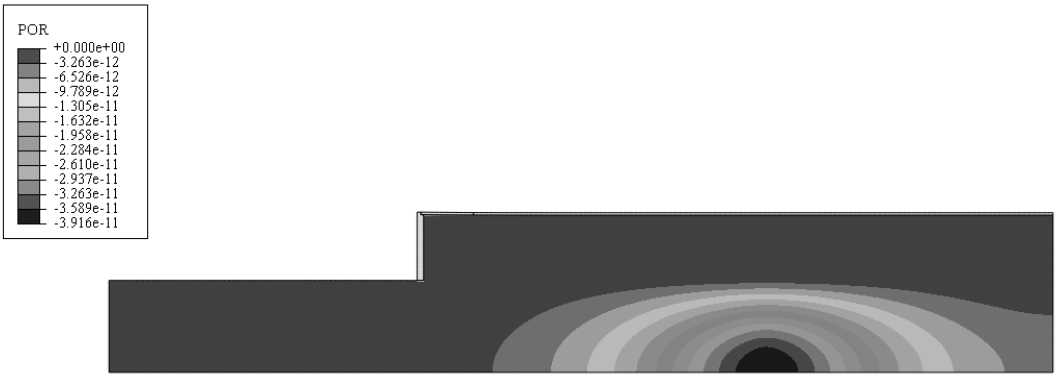

Figure 5.91 Distribution of excess pore pressure at the end of the analysis (*psf*)

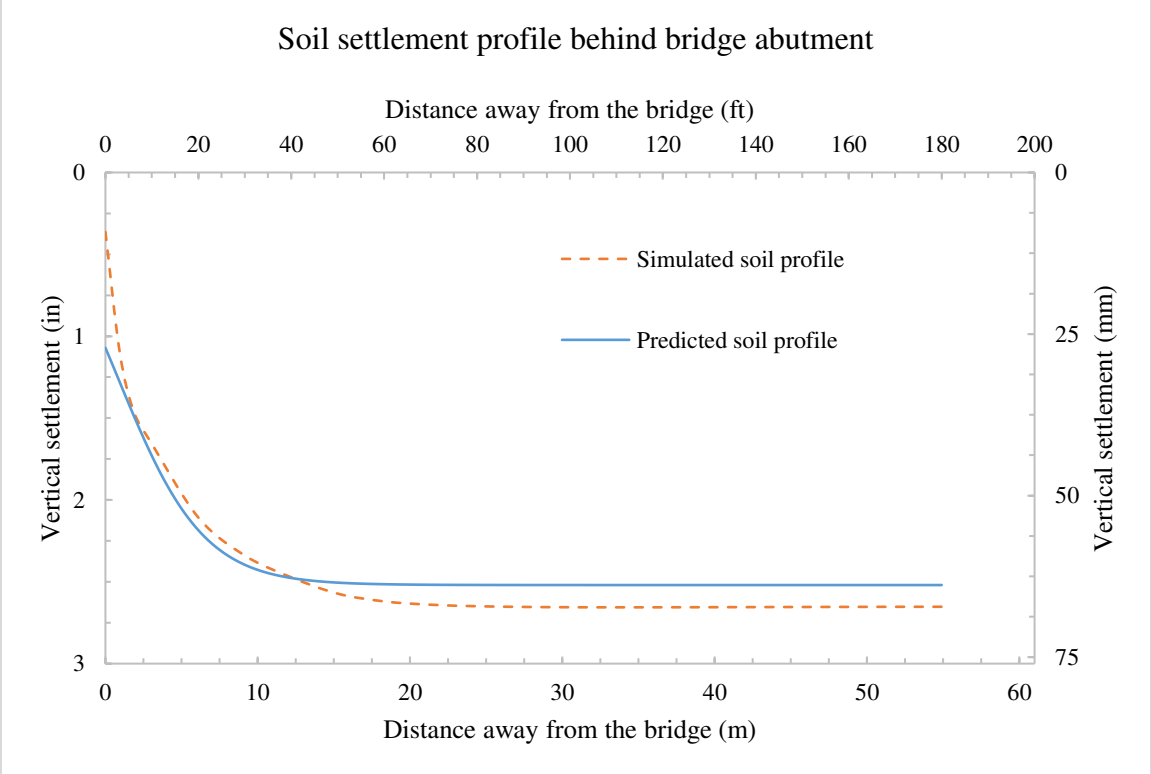

Figure 5.92 Simulated versus predicted soil settlement profile for the case study

Figure 5.92 indicates that the far away settlement, *a*, and settlement adjacent to abutment wall were 2.6 *in* (66 *mm*) and 0.4 *in* (10 *mm*), respectively. The developed logistic empirical function (equation 5-3) was used to predict the longitudinal soil deformation profile. First, equation 5-12 was used to determine the value of the ultimate settlement far away from bridge

abutment, a. The developed level of strain was individually evaluated for embankment fill and natural soil layers. Table 5.31 shows the level of strain at the middle of each layer.

Table 5.31 Level of strain at the middle of each layer

Strain	Embankment Fill	Natural Soil
$\varepsilon_v^{e.adj}$	0.0048	0.0225
ε_v^{p}	0	0.016

Substituting the values of $\varepsilon_v^{e.adj}$ and ε_v^{p} into equation 5-12, a yields to 2.5 *in* (64 *mm*). Subsequently, substituting C_c = 0.087, H_e = 25 *ft* (7.6 *m*), and H_n = 35 *ft* (10.7 *m*) into equation 5-16, b yields to 1.53. Lastly, substituting a = 2.5 *in* into equation 5-18 yields to c = 0.11. Figure 5.92 shows the simulated versus predicted soil profiles. The figure shows that the developed logistic function predicted the soil deformation along the longitudinal direction reasonably well when compared with the finite element results.

5.11 Chapter summary and conclusion

The objective of this study was to provide engineers with a reasonably accurate, yet simple, empirical equations that could be used to predict the longitudinal soil deformation behind bridge abutments. Such equations would be beneficial in making reliable predictions of the long-term differential settlement of the approach slab and could facilitate more accurate design recommendations to address bridge approach settlements.

Parametric studies were conducted, using finite element model, to quantify the effects of various parameters on the transverse as well as longitudinal soil deflection profile behind bridge abutments. These include the length of the approach slab, height of embankment fill, embankment soil type, height of natural soil, natural soil type, backfill soil type, slope of backfill area, and abutment type.

As a result, it can be concluded that embankment fill height of $H_e > 20\,ft$ ($6.1\,m$) would be problematic in terms of the transition performance. The slope of the approach slab must be checked against soil conditions in such cases. In addition, it was observed that the soil longitudinal deflection profile could be represented by a logistic function curve. Therefore, a set of empirical equations were developed that define the various parameters of the logistic function. Table 5.32 shows a summary of the developed equations.

Table 5.32 Summary of the developed equation

General form/parameters	Developed equations
General form of the logistic function y = vertical settlement at a distance of x from the bridge abutment.	$\mathrm{y} = \dfrac{a}{1 + be^{-cx}}$
Logistic function parameter (a) Maximum displacement.	$a = 383 \times 10^{-6} H_n e^{\left(27\,\varepsilon_v^{e.adj} + 38.6\,\varepsilon_v^{p}\right)} + 4980 \times 10^{-6} H_e e^{\left(61\,\varepsilon_v^{e.adj.} + 23\,\varepsilon_v^{p}\right)}$
Logistic function parameter (b) Settlement at the interface between the abutment wall and the backfill soil.	$b = 0.38\,ln\left(C_c \times \dfrac{H_e}{H_a}\right) + 2.26$
Logistic function parameter (c) Steepness of the curve.	$c = 0.172\mathrm{e}^{-0.182a}$ * $c = 0.172\mathrm{e}^{-0.007a}$ **

* when (a) is in inches ** when (a) is in millimeters

The range of applicability of the developed equations would typically be restricted to the range of the parameters used in the parametric study (see Tables 5.9, 5.10 and 5.11). Care must be taken to ensure accuracy if parameters are outside of the range used in the parametric study. A particular case was illustrated in which the developed equations predicted the simulated soil deformation reasonably well. Overall, the benefits of the developed equations could be further increased when studies using an expanded range of parameters are conducted in the future.

CHAPTER 6 - PILE-SUPPORTED APPROACH SLABS

6.1 Chapter background

As soil underneath approach slab settles, deferential settlement develops between the bridge and the roadway pavement causing bumps and affecting the riding quality. The approach slab in such cases would transfer the bump from the beginning of the bridge to the end of the approach slab. As discussed in the literature review chapter (Chapter 2), a maximum change of slope of approach slab of 1/125 is desired to maintain a smooth transition into and out of the bridge. Maintaining such limits in slope is important to prevent damage to structural elements, to ensure safe driving environment, and to reduce maintenance cost over the life-time of the bridge system.

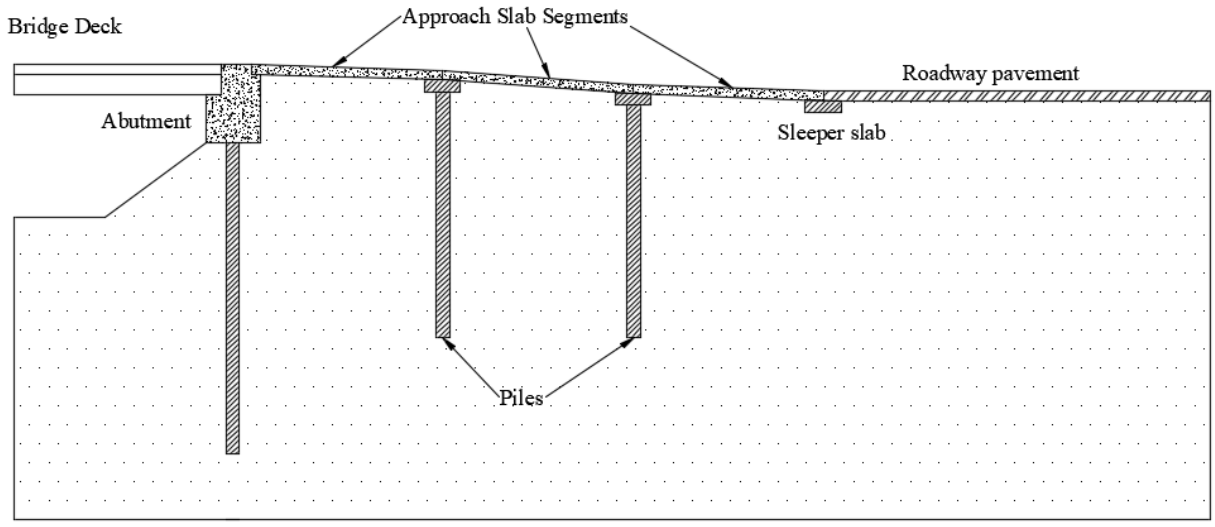

Figure 6.1 Managing approach slab differential settlement

Settlement-reducing piles could be introduced into the approach slab to control changes in slope and limit stresses to acceptable levels. Such piles would rely on surface friction and end-bearing resistant to control the approach slab settlement and achieve the required level of differential settlement. However, determining the appropriate location, spacing, length and size

of piles is a difficult task that requires further study. Since field testing of piles is rather expensive and time-consuming, an analytical program (which is verified with through existing test information) is required to develop the information needed for the design of pile supported approach slab for settlement control.

6.2 Chapter problem statement

Since the bridge approach slab (BAS) is a relatively rigid structural member, a smooth transition (change in slope of less than 1/125) may be achieved by selecting the length of the approach slab, L_{BAS}, such that the resulting slope is acceptable for the expected soil settlement. However, when the soil conditions are poor, the soil settlement would be large, and the approach slab must be extended far to bridge the gap resulting from the settlement. This could in return result in very long approach slabs that would require greater thicknesses to control stresses and deflection. Introducing piles at specific locations underneath a segmented approach slab could address such a problem through control of soil settlement and slope changes. As piles are introduced, they could control downward movement of the soil to acceptable levels by offering resistance to the soil (downdrag). Control of settlements along various segments of a multi-segment approach slab could facilitate slope changes that within tolerable limits with respect of ride quality. Piles in such cases are not intended to reduce settlement to zero as this would only add another apparent span to the bridge and would not address the differential settlement that must still be accommodated.

Maintaining acceptable slope changes among approach slab segment and between approach slab segments and the roadway or the bridge is required to achieve an overall smooth transition between the bridge and the roadway pavement. The concept of pile supported segmented approach slab is illustrated in Figure 6.1. The approach slab segments are attached

together in such a way as to allow rotation at the interface between segments thus allowing a series of changes in slope. The number and lengths of needed approach slab segments are dependent on the expected settlement. One approach involves developing an *S*-shaped curve to eliminate the formation of the bump. The *S* curve would require an odd number of segments in which the settlement at the end of each segment is controlled through piles. The characteristics of each segment can be determined based on the desired relative angle change between any two segments. Figure 6.2 shows a schematic of the proposed multi-segment pile supported approach slab.

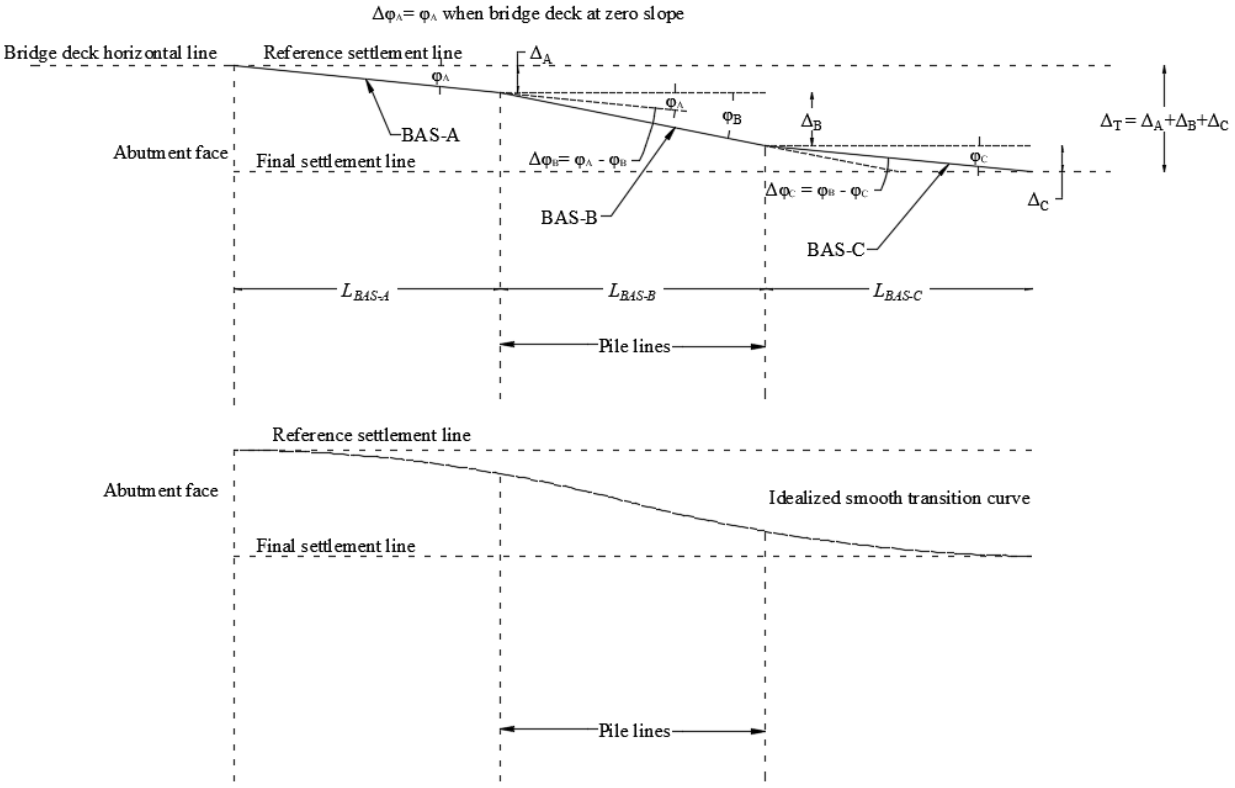

Figure 6.2 Schematic of the proposed pile supported approach slab segments.

For the purposes of this study, the length of each approach slab segment is assumed to be between 15 *ft* (4.5 *m*) and 30 *ft* (9.1 *m*), which are compatible with typical lengths used for approach slab (see Chapter 3). In order to produce the smooth transition curve shown in Figure

6.2, the change of the slope between the bridge and the first segment, φ_A, should be maintained at a level below the 1/125. Similarly, the change of slope at the second and third segments, $\Delta\varphi_B$ and $\Delta\varphi_C$, should be less than the targeted value as well. Additionally, while maintaining the limits on slope change, the middle segment can have an absolute slope that can be as much as twice the slope change limit. This indicates that *BAS-B* can undergo twice the differential settlement of the first and third segments, i.e. $\Delta_B = 2\Delta_A$. This would shorten the overall length of the three-segment approach slab compared to a single-segment regular approach slab. Such a pile-supported multi-segment approach slab is expected to result in a smooth transition between the bridge and the roadway in cases where excessive soil settlement is expected.

In some circumstances, fewer (two) approach slab segments maybe adequate for achieving slope changes that are below the stated limits. In such cases, the procedures described below can be followed. Eventually, the produced smooth curve would consist of one or more approach slab segments that serves the purpose of eliminating the bump at the end of the bridge. The procedures used to produce the smooth curve transition is as follows: (refer to Figure 6.2)

a) Determine the maximum longitudinal surface soil settlement, *a* or Δ_T, using either the FEM analysis or the empirical equations provided in Chapter 5.

b) If $\Delta_T \leq L_{BAS-A}\left(\frac{1}{125}\right)$, use a single-segment approach slab with $L_{BAS-A} \leq 30ft$ $(9.1m)$. Minimize L_{BAS-A} to meet this requirement.

c) If $\Delta_T > L_{BAS-A}\left(\frac{1}{125}\right)$, the settlement cannot be accommodated with a single-segment approach slab. Use a multi-segment pile-supported approach slab based on the following procedures:

a. Select pile size, length, and pile spacing for the first line of piles such that the expected pile head settlement $\Delta_A \leq L_{BAS-A}\left(\frac{1}{125}\right)$. Charts that can be used for this estimation are given in this Chapter. If the desired Δ_A cannot be achieved, change L_{BAS-A}, pile size, pile length, or pile spacing to satisfy the above settlement requirement.

b. If $L_{BAS-A}\left(\frac{1}{125}\right) < \Delta_T \leq (L_{BAS-A} + L_{BAS-B})\left(\frac{1}{125}\right)$, try a two-segment approach slab with one line of piles between the two segments. The end of the second segment should be supported on a sleeper-slab on soil.

c. If $\Delta_T > (L_{BAS-A} + L_{BAS-B})\left(\frac{1}{125}\right)$, the settlement cannot be accommodated with a two-segment approach slab. Try a three-segment approach slab. The end of the third segment should be supported on a sleeper-slab on soil.

d. Select the pile size, length, and pile spacing for the second line of piles (from the charts) such that the expected pile head settlement $\Delta_A + \Delta_B \leq (L_{BAS-A} + L_{BAS-B})\left(\frac{1}{125}\right)$.

e. If $\Delta_T > (L_{BAS-A} + 2L_{BAS-B} + L_{BAS-C})\left(\frac{1}{125}\right)$, the settlement cannot be accommodated with a three-segment approach slab. Try four-segment approach slab. The end of the fourth segment could be supported on a sleeper-slab on soil.

f. Repeat steps a-e as needed.

6.3 Chapter objectives

The objective of this phase of the study is to quantify the effects of the pile, soil and bridge parameters on the pile head settlement. Relationships are required for estimating pile head settlement under various pile and soil conditions. These relationships can be utilized to determine the appropriate location, size, length, and spacing of piles to achieve and maintain a smooth transition between the bridge and roadway pavement in cases of excessive settlement.

6.4 Settlement-reducing piles

6.4.1 Introduction

Piles are long slender structural members that are commonly made of concrete, steel, or timber and are used to transfer superstructure loads deep into the soil. Their main function is to provide adequate bearing capacity to resist applied load. However, piles can also be used to reduce settlement to an acceptable level. Piles are typically installed in group of three or more to insure safe load transfer and provide some redundancy to the supported structure/s. There are two basic types of pile foundations; friction pile and end-bearing pile. A friction pile derives its capacity through skin friction, Q_s, that is developed over the surface of the pile. On the other hand, the end-bearing pile derives its capacity, Q_b, from the bearing capacity of the soil under the pile tip. A combination of the two pile types (semi-friction pile) provides resistance through both skin friction and end-bearing (B. M. Das 2011).

Furthermore, piles are also classified into displacement and replacement piles. Displacement pile cause radial displacement as it is driven into the ground. On the other hand, replacement piles are installed by first removing the soil and then installing the pile. For the purposes of this study, replacement concrete piles are considered.

6.4.2 Load transfer mechanism in piles

Piles can be subjected to axial and lateral loads. Under compressive axial forces (downward), the resistance is provided by skin friction, Q_s, and end-bearing, Q_b, while tensile axial forces are resisted by skin friction alone. Friction forces along the pile are developed as a result of the relative movement between the pile and the surrounding soil. Positive skin force, Q_{ps}, is developed when the settlement of the surrounding soil is less than movement of the pile shaft. On the other hand, negative skin friction (downdrag), Q_{dd}, is developed when the settlement of the surrounding soil is greater than movement of the pile shaft. This typically occurs due to the consolidation process (dissipation of water) in the soil surrounding the pile.

The relative movement that is required to mobilize the skin friction is typically very small. Coduto (2001) reports that about 0.2-0.3 *in* (5.0-8.0 *mm*) of relative displacement can fully mobilize the skin friction. On the other hand, much greater relative movement is required to fully mobilize the end-bearing, typically, (0.1-0.25 D_p) where D_p is the pile diameter (Coduto 2001, B. M. Das 2011). Figure 6.3 shows the distribution of pile axial load along the length of the pile considering skin friction, end-bearing, and downdrag.

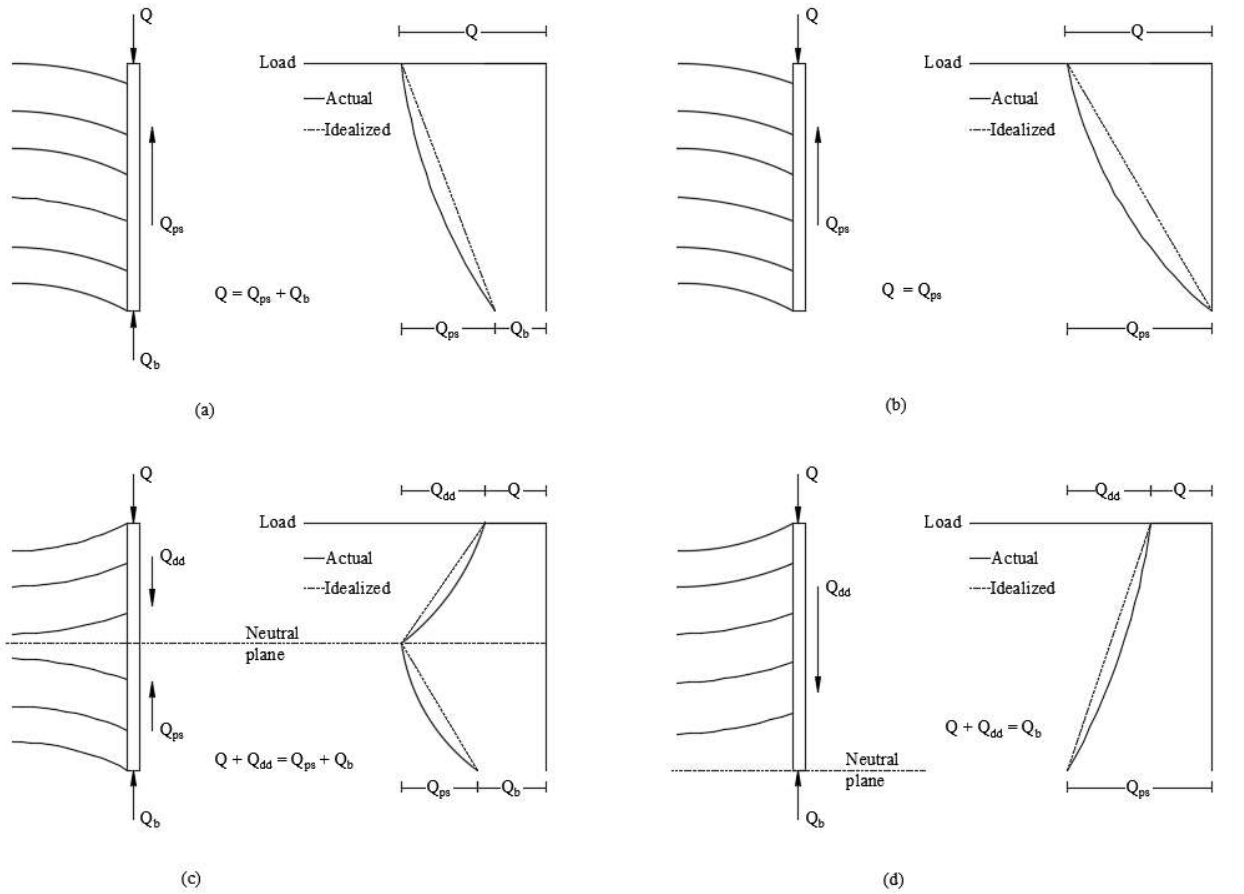

Figure 6.3 Distribution of pile axial load (a) skin friction and end-bearing without downdrag (b) skin friction without end-bearing and downdrag (c) skin friction, end-bearing and downdrag (d) end-bearing and downdrag

In Figure 6.3, the location along the pile shaft where no relative displacement occurs between the pile and the surrounding soil is called neutral plane or neutral axis. In terms of stress, this is defined as the location where frictional stresses change from negative to positive.

6.4.3 Load capacity of piles

The load carrying capacity of pile-soil system is the maximum load at which the safety of the pile and the surrounding soil is ensured. In a pile-soil system, the ultimate load carrying capacity, Q_u, can be evaluated as follows:

$$Q_u = Q_b + Q_s \qquad 6\text{-}1$$

Generally, the ultimate load carrying capacity of the pile-soil system can be obtained from the load-settlement curve. The capacity corresponds to the pile head load at which the pile plunges into the soil (i.e. rapid increase of pile head settlement with a small additional load). Furthermore, Q_u is affected by several factors including the length, shape and size of the pile, installation method, and soil conditions. There are several analytical methods for evaluating the load capacity of the pile-soil system. In this study, the β-method is used.

The β-method is widely used to evaluate the short- and long-term load carrying capacity of pile-soil systems. The long-term friction capacity, Q_s, of the pile can be determined as follows (B. M. Das 2011, Helwany 2007):

$$Q_s = \int_0^{L_i} f_s \, p \, dz = \sum_{i=1}^{i=n} [\beta_i (\sigma_v')_i p_i L_i] \qquad 6\text{-}2$$

Where p is the perimeter of the pile, L is the length of the pile, and σ_v' is the effective vertical soil stress at the pile midpoint. β is a parameter that is defined in terms of the coefficient of friction, μ, and the coefficient of lateral earth pressure at rest, K_0, given by $\beta = \mu K_0$.

On the other hand, the long-term end-bearing capacity, Q_b, of the pile can be determined as follows (Helwany 2007):

$$Q_b = \left[(\sigma_v')_b N_q + c_b' N_c\right] A_b \qquad 6\text{-}3$$

Where $(\sigma_v')_b$ is the effective vertical soil stress at the base of the pile, c_b' is the cohesion of the soil underneath the tip of the pile, and A_b is the cross-sectional area of the pile base. N_q and N_c are bearing capacity coefficients defined in terms of the soil's angle of internal friction, φ'.

Although, the pile-soil system's carrying capacity is dominant in most cases, strength capacity of the pile material should also be checked. Structurally, pile must be designed to safely sustain the applied load and the associated deformation. Typically, axially-loaded piles are designed as short-column, since buckling is not an issue even in soft soils. The allowable carrying capacity of concrete pile can be estimated as follows: (Coduto 2001)

$$Q_a = \frac{1}{3} f_c' \, A_p \qquad 6\text{-}4$$

Where A_p is cross section area of the pile.

6.5 Pile cap design

The pile cap in a bridge is a reinforced concrete member that connects a group of piles together (at their top) and to the structure above. Its function is to transfer and distribute the load across the piles. Piles should be spaced at 2 to 3 times the pile diameter to effectively transfer the load to soil. This assures that the stress zone induced by each individual pile would not overlap with the adjacent piles (Coduto 2001, B. M. Das 2012).

The pile group efficiency, η, can be expressed in term of the ultimate load capacity of the pile group as follows:

$$\eta = \frac{Q_{gu}}{\sum Q_u} \qquad 6\text{-}5$$

Where Q_{gu} is the ultimate load capacity of the pile group, and Q_u is the ultimate load capacity of a single pile. The pile group efficiency is affected by many factors including the number, shape, arrangement, diameter and length of piles. The pile group efficiency is also

affected by the failure mode. Typically, a pile group can fail as a whole or as individual piles (punching shear) (Coduto 2001).

6.6 Development and verification of finite element soil-structure interaction models

6.6.1 Introduction

The analytical modeling of any structure can be represented by finite number of elements that are computationally assembled to obtain a solution for the structure. In this study, the commercial finite element software ABAQUS was used to analyze the combined soil-structure model (ABAQUS 2015).

In the first part of this study, a three-dimensional finite element model was generated to perform long-term soil-structure analysis of a single pile embedded in a soil mass (single pile/soil model). The objective of this analysis was to quantify the pile head settlement as well as the load distribution along the pile. The model consisted of the following components: pile, granular backfill soil, embankment fill, and natural soil, constructed as shown in Figures 6.4 and 6.5. In this model, the granular backfill layer was construed horizontally (without a slope). Some models included the granular backfill representing conditions where the pile is within the backfill zone behind the abutment, while other models did not include a granular backfill layer (Figure 6.5).

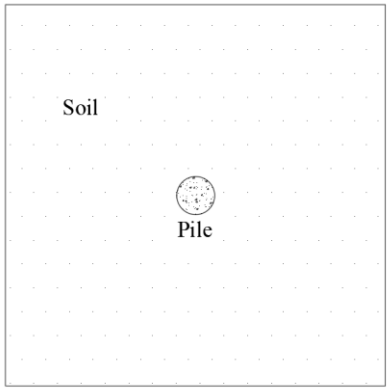

Figure 6.4 Top view of pile-soil model

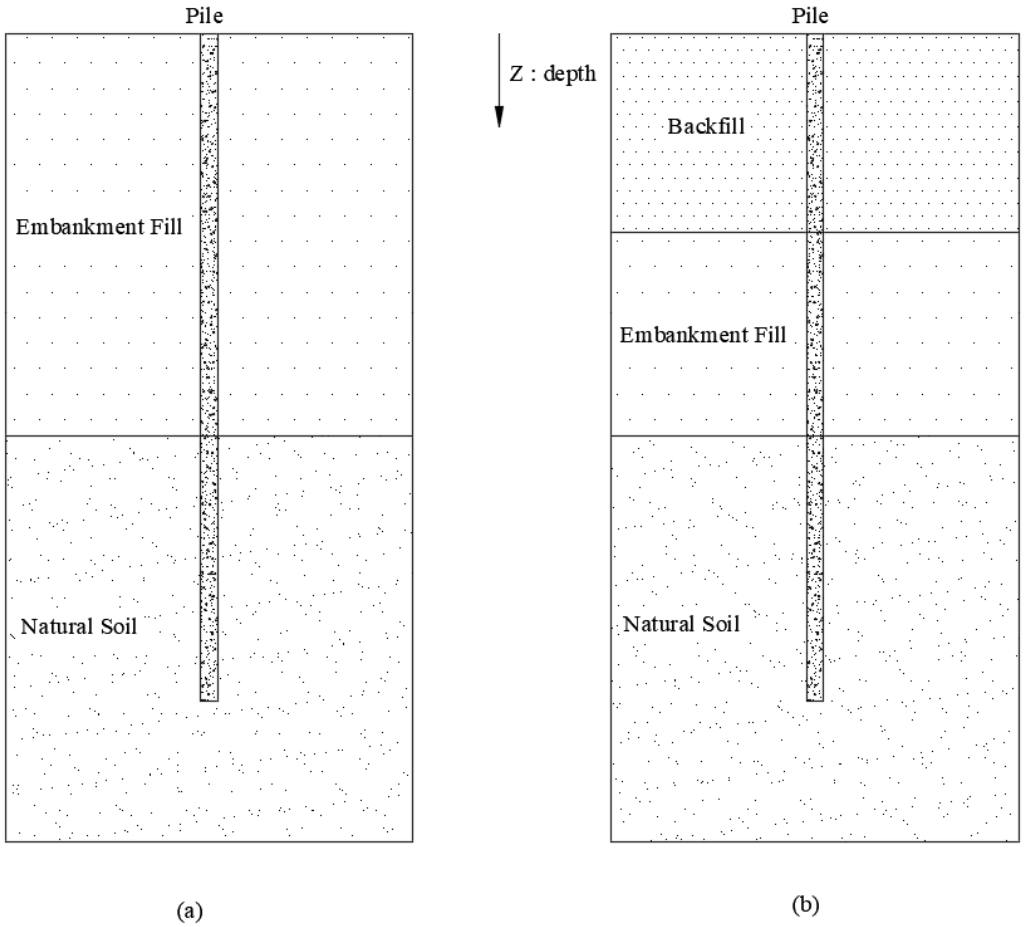

Figure 6.5 Cross section of the single pile-soil model (a) without granular backfill (b) with granular backfill

6.6.2 Geometry and boundary conditions

An important aspect of the soil-structure finite element model is establishing the location and type of boundary conditions. In soil-structure models, displacement and pore pressure boundary conditions may be defined. Because of the symmetry, one-half of the entire structure was modeled.

The bottom of the model should represent locations where no soil movement (vertical and horizontal) occurs. This location can be determined using the standard penetration test (typically provided in the borehole log profile). A high-test value indicates a hard layer, such as bedrock. At this location, both vertical and horizontal movements are restricted (assumed to be zero). No water seepage would be expected to occur at this location either. Thus, an impervious boundary condition was assumed at the bottom nodes. The top surfaces of the soil were free to move in all directions and was considered to be pervious (i.e. water could flow through them).

The soil mass was extended (in all directions) to capture entire behavior of the pile-soil system. Helwany (2007) recommended extending the soil mass a distance of at least 30 D_p from the center of the pile. At the end of the soil mass, the soil was assumed to move freely except in the out-of-plane direction. Figures 6.6 and 6.7 show the geometry and boundary conditions used in this analysis.

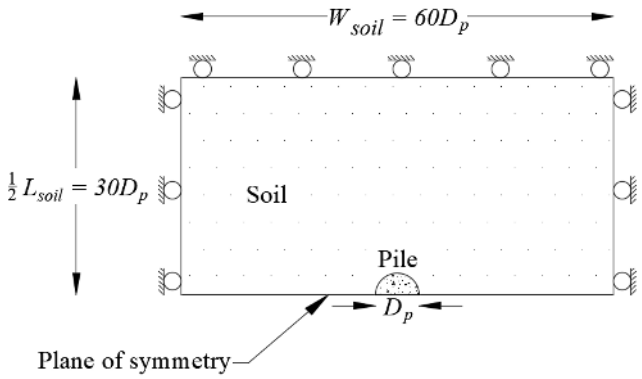

Figure 6.6 Boundary condition of the pile-soil model (top view)

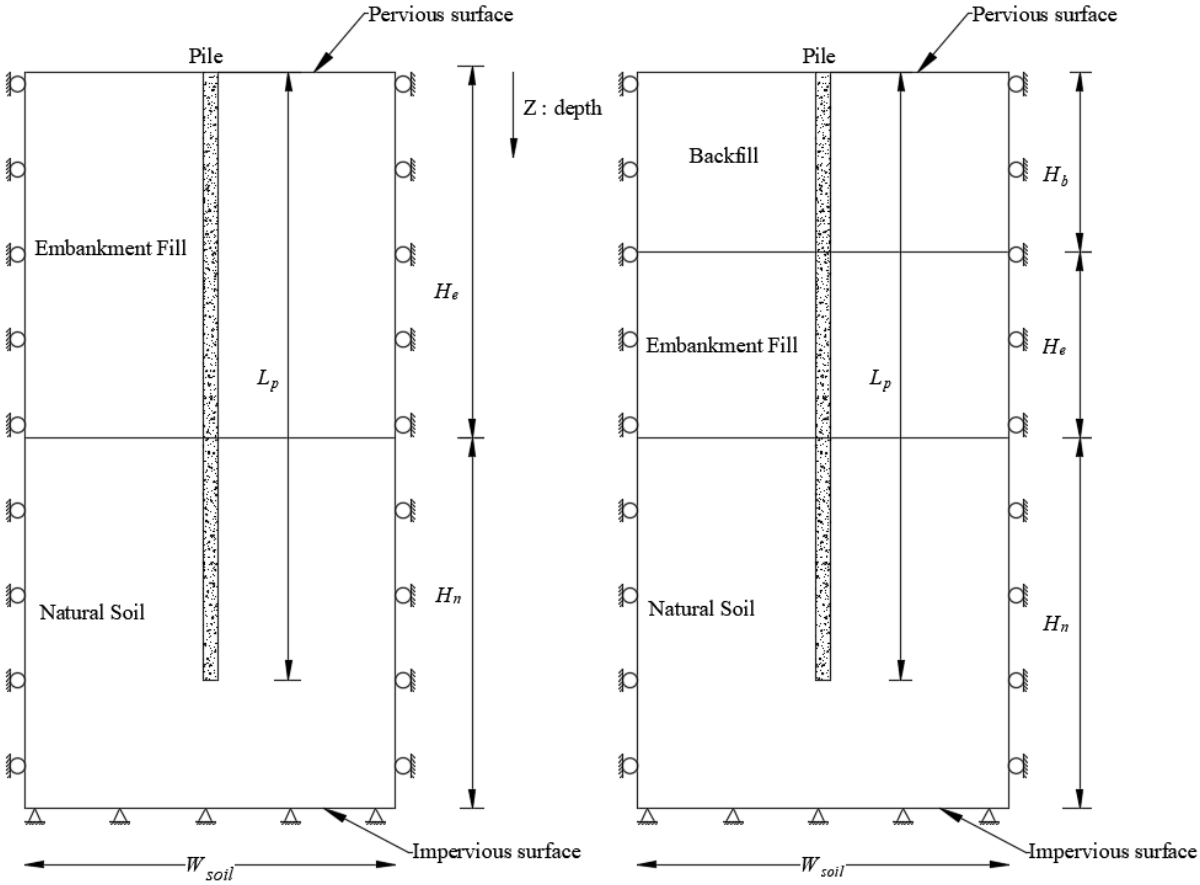

Figure 6.7 Boundary condition of the single pile-soil model with or without the backfill layer (vertical section)

In the above figures,

Z = Depth reference.

H_b = Height of the backfill,

H_e = Height of the embankment fill.

H_n = Depth the natural soil (to impervious layer).

L_p = Length of pile.

W_{soil} = Width of the modeled soil medium.

L_{soil} = Length of the modeled soil medium.

A parametric study was conducted in the single pile-soil model. Values of H_b, H_e, H_n, L_p, and D_p were varied according to the parametric study matrix shown in Table 6.2 (see Section 6.7).

6.6.3 Contact behavior at structure-soil interfaces

The developed three-dimensional model include interaction between the pile and the surrounding soil. Interface elements were introduced across these interfaces to transfer normal and tangential forces using the pressure-overclosure relationship and coulomb friction model that is defined within ABAQUS (see Section 4.2). In this analysis, the concrete surfaces (i.e. pile shaft including the tip) were assigned to act as master elements while soil surfaces were assigned to act as slave elements.

6.6.4 Analysis procedures for single pile-soil model

The analysis procedures used to run the single pile-soil model included the following steps:

1- Applying a geostatic load on the underlying natural soil layer. In this step, the effective self-weight of the natural soil was applied. The geostatic step assures

that equilibrium is satisfied within the natural soil layer, and that the initial stress conditions in all elements falls within the initial yield surface.

2- Constructing the embankment fill over a period of time (equation 5-1). In this step, the effective self-weight of the embankment soil was applied. This was done in a coupled (consolidation) step where the load of the embankment is applied in a timely manner.

3- Adding the pile and associated loads. This step was also done in a coupled (consolidation) way where the soil is removed, and pile is added with a perfect contact with the soil. The construction of the pile was assumed to occur ninety days after the completion of the embankment fill and over a ten-day period.

4- Consolidation steps. In these steps, calculations to determine the primary settlement (consolidation process) and secondary settlement (creep) were performed.

6.6.5 Material properties

The concrete in the pile was assumed to behave in a linearly elastic manner with a modulus of elasticity that was consistent with a design compressive strength of 4000 *psi*. Table 4.2 shows the concrete material parameters used. On the other hand, the modified Drucker-Prager/Cap material model was used to simulate the behavior of the soils. Table 4.7 shows the input parameters used to model the soil.

6.6.6 Initial model

An initial model was used in this phase of the study to determine the proper element size and to conduct comparison analysis. The layout used in the initial model was similar to that

shown in Figures 6.4 and 6.5. The pile-soil system used in the initial model consisted of a single pile with diameter D_p = 12 *in* (305 *mm*) and length L_p = 45 *ft* (13.7 *m*). A highly compressible embankment fill with height H_e = 30 *ft* (9.1 *m*), and a highly compressible natural soil with a height H_n = 30 *ft* (9.1 *m*) was considered. These parameters were chosen such as they would reflect the outcome of the analysis in a sensible way in which comparisons could be made.

6.6.7 Element type and size

As a porous material, soil contains voids that can be filled with air and/or water. Thus, the element used to discretize the soil was an eight-node brick element with trilinear displacement and pore pressure (element code: C3D8P). This type of element has the capability to capture deformation as well as excess pore pressure history. In this element, each node consists of three displacement degrees of freedom (U_x, U_y and U_z), three rotational degrees of freedom (r_x, r_y and r_z), and one pore pressure degree of freedom (*Por*). On the other hand, an eight-node brick element was used to discretize the concrete pile (element code: C3D8). In this element, each node consists of three displacement degrees of freedom (U_x, U_y and U_z) and three rotational degrees of freedom (r_x, r_y and r_z) (ABAQUS 2015).

The initial model (see Section 6.6.6) was used to determine the proper element sizes that would maintain the accuracy of results while reducing the computational time. This was done by monitoring the pile head settlement as a function of element size. The element size (length × width × height) was chosen independently for optimization purposes. The element size was reduced in each subsequent run and pile head settlement, Δ_{PH}, was determined. Table 6.1 shows the element size and corresponding Δ_{PH} values.

Table 6.1 Element size versus simulated Δ_{PH}

Element size		Total number of elements	Δ_{PH} *in* (*mm*)	Difference (from previous size) (%)	Difference (from coarsest size) (%)
(height) *ft* (*m*)	(length × width) *ft* (*m*)				
5.0 (1.5) [1]	5.0 × 5.0 (1.5 × 1.5) [1]	4,176	3.47 (88)	-	-
2.0 (0.6)	5.0 × 5.0 (1.5 × 1.5)	10,788	3.66 (93)	5.5	5.0
1.0 (0.3)	5.0 × 5.0 (1.5 × 1.5)	20,880	3.71 (94)	1.3	6.0
0.5 (0.2)	5.0 × 5.0 (1.5 × 1.5)	41,760	3.72 (94)	0.2	7.0
2.0 (0.6)	2.0 × 2.0 (0.6 × 0.6)	29,760	3.67 (93)	-	5.0
1.0 (0.3)	2.0 × 2.0 (0.6 × 0.6)	57,600	3.71 (94)	1.0	6.5
0.5 (0.2)	2.0 × 2.0 (0.6 × 0.6)	115,200	3.73 (95)	0.5	7.0
1.0 (0.3)	1.0 × 1.0 (0.3 × 0.3)	157,800	3.71 (94)	-	6.5
0.5 (0.2)	1.0 × 1.0 (0.3 × 0.3)	315,600	3.73 (94)	0.5	7.0
0.5 (0.2)	0.5 × 0.5 (0.2 × 0.2)	1,022,200	3.77 (95)	-	7.5

[1] coarsest element size

The results show that pile head settlement, Δ_{PH}, becomes nearly steady (maximum error of 0.5%) when the element size is at or less than 1.0 *ft* × 2.0 *ft* × 2.0 *ft* (0.30 *m* × 0.60 *m* × 0.60 *m*). Therefore, this element size was used in this study.

6.6.8 Comparison with analytical solution

In this part of the study, a finite element model was generated to simulate the long-term load capacity of the pile-soil system. The simulated pile-soil capacity was then compared with the analytical β-method. For this analysis, the soil-pile properties and conditions were identical to those used in the initial model (see Section 6.6.6).

The simulated pile load-settlement analysis was carried out such that the pile's head was vertically displaced a total distance of about (0.25 D_p), and the force required to achieve the displacement was recorded incrementally. The pile was displaced at this magnitude to assure the mobilization of the pile tip bearing resistance (see Section 6.4.2). The vertical displacement was imposed in a very slow rate of 1×10^{-15} *in/sec* (1×10^{-14} *mm/sec*). This was to prevent any excess pore pressure from building up around the sides and tip of the pile. Figure 6.8 shows the deformed contour of the modeled pile-soil system. Figure 6.9 shows the distribution of pore pressure at the end of the analysis.

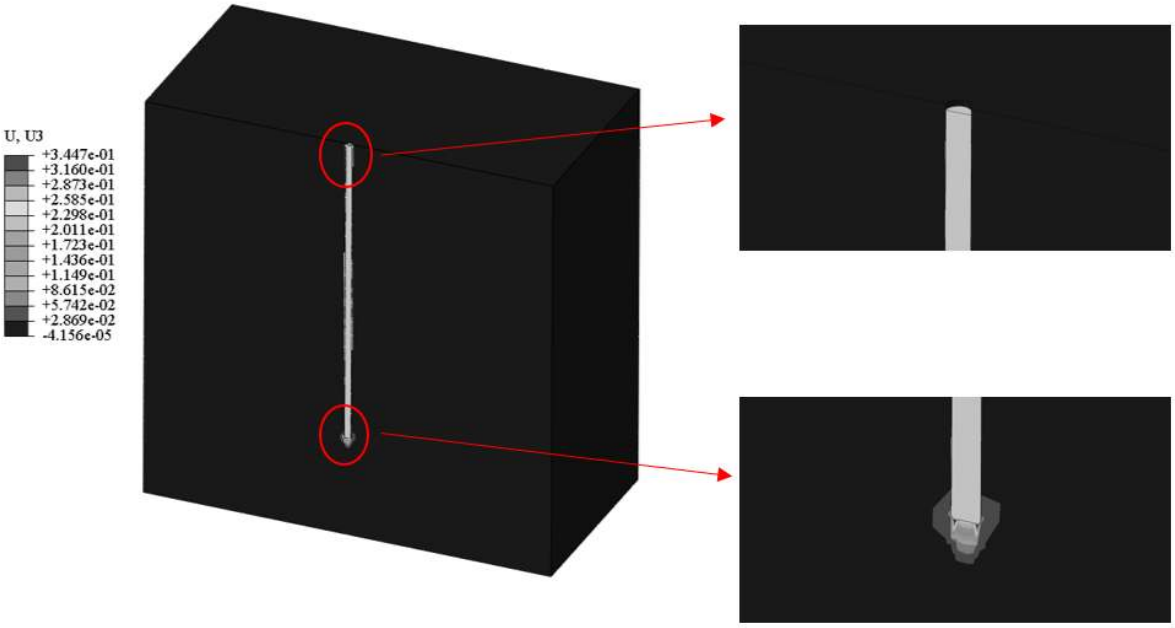

Figure 6.8 Vertical deformation contour at the end of the analysis (*ft*)

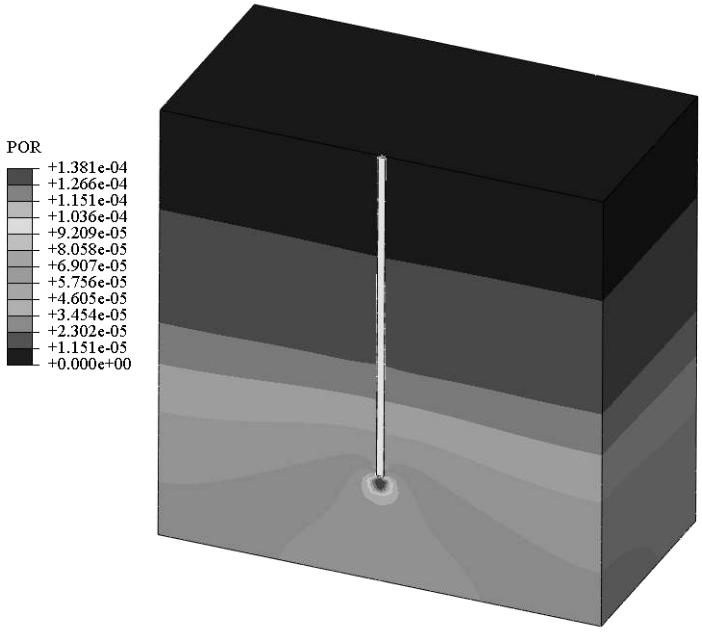

Figure 6.9 Excess pore pressure contour at the end of the analysis (*psf*)

The simulated load-settlement curve is shown in Figure 6.10. The figure shows that the FEM load carrying capacity of the pile-soil system was 85 *kips* (380 *kN*) which compared to 92 *kips* (410 *kN*) using the β-method with a reasonably good agreement.

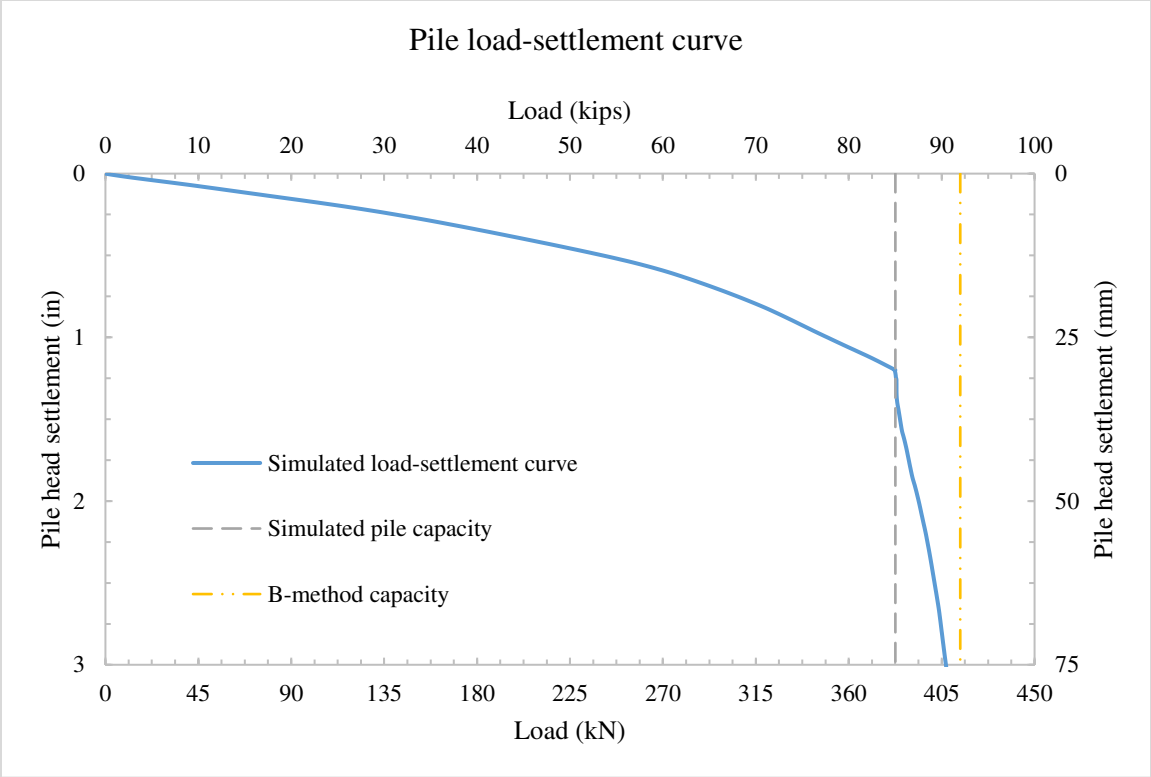

Figure 6.10 Simulated pile load-settlement curve

6.7 Parametric study

A parametric study was conducted using finite element analysis to quantify the effects of various parameters on the pile's load carrying capacity, Q_u, as well as head settlement, Δ_{PH}. The parameters considered were the diameter of the pile, D_p, embedment length of pile, L_p, height of backfill soil, H_b, height of embankment fill, H_e, and height of natural soil, H_n. Table 6.2 shows these parameters along with their variation for the parametric study.

Table 6.2 Parametric study matrix for the single pile-soil model

Parameter	Range
Embedment length of pile (L_p)	35, 45 and 55 *ft* (10.7, 13.7 and 16.8 *m*)
Diameter of pile (D_p)	6, 12, and 18 *in* (152, 305 and 458 *mm*)
Height of backfill layer (H_b)	0, 12 and 24 *ft* (0, 3.7, 7.3 *m*)
Backfill type (Degree of Compaction)	90%
Overall height of fill ($H_f = H_e + H_b$)	30 *ft* (9.1 *m*)
Embankment soil type (Degree of Compressibility)	High
Height of natural soil (H_n)	30 *ft* (9.1 *m*)
Natural soil type (Degree of Compressibility)	High

Each pile size was examined using various choices of parameters to quantify their effect on the pile head settlement. The pile head load, Q, was determined assuming that a line of piles was placed between two 20-*ft* (6.1-*m*) approach slab segments with a thickness of 12 *in* (305 *mm*) and different transverse pile spacings. Table 6.3 shows the variation of all parameters tested with each value of D_p.

Table 6.3 Range of parameters tested in accordance with D_p

Analysis No.	Pile spacing[1] *ft* (*m*)	Pile embedment length			
		Backfill L_b *ft* (*m*)	Embankment fill L_e *ft* (*m*)	Natural soil L_n *ft* (*m*)	Total embedment length ($L_p = L_b + L_e + L_n$) *ft* (*m*)
1	3 (0.9)	0	30 (9.1)	5 (1.5)	35 (10.7)
2	6 (1.8)				
3	12 (3.7)				
4	17 (5.2)				
5	3 (0.9)	12 (3.7)	18 (5.5)		
6	6 (1.8)				
7	12 (3.7)				
8	17 (5.2)				
9	3 (0.9)	24 (7.3)	6 (1.8)		
10	6 (1.8)				
11	12 (3.7)				
12	17 (5.2)				
13	3 (0.9)	0	30 (9.1)	15 (4.6)	45 (13.7)
14	6 (1.8)				
15	12 (3.7)				
16	17 (5.2)				
17	3 (0.9)	12 (3.7)	18 (5.5)		
18	6 (1.8)				
19	12 (3.7)				
20	17 (5.2)				
21	3 (0.9)	24 (7.3)	6 (1.8)		
22	6 (1.8)				
23	12 (3.7)				
24	17 (5.2)				
25	3 (0.9)	0	30 (9.1)	25 (7.6)	55 (16.8)
26	6 (1.8)				
27	12 (3.7)				
28	17 (5.2)				
29	3 (0.9)	12 (3.7)	18 (5.5)		
30	6 (1.8)				
31	12 (3.7)				
32	17 (5.2)				
33	3 (0.9)	24 (7.3)	6 (1.8)		
34	6 (1.8)				
35	12 (3.7)				
36	17 (5.2)				

[1] Piles were assumed to be on a line between two adjacent approach slab segments.

[1] For D_p = 12 *in* (305 *mm*), only pile spacing of 3, 6 and 12 *ft* (0.9, 1.8 and 3.7 *m*) were tested as pile capacity was reached. For D_p = 6 *in* (152 *mm*), only pile spacing of 3 and 6 *ft* (0.9 and 1.8 *m*) were tested as pile capacity was reached (section 6.7.1).

The finite element model was generated as described in section 6.6. The models were run for a simulated total time that allowed the completion of initial, primary (dissipation of water), and secondary (creep) settlements of the modeled soil. The load on the embankment/backfill layers was applied according to equation 5-1. The pile was installed ninety days after the

completion of the embankment/backfill after which the pile head load, Q, was applied in accordance with Table 6.3. A typical finite element discretization of the single pile-soil model is shown in Figures 6.11 and 6.12.

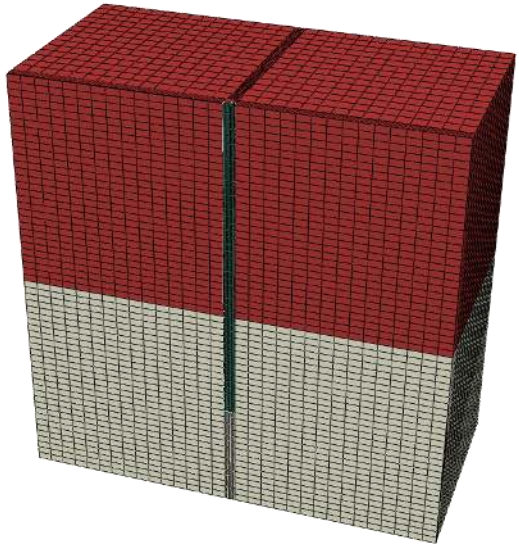

Figure 6.11 Finite element discretization of the single pile-soil model (No backfill)

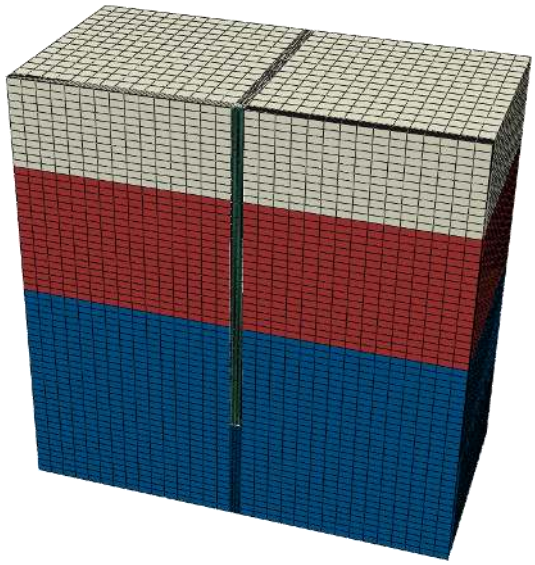

Figure 6.12 Finite element discretization of the single pile-soil model (with backfill)

6.7.1 Load capacity of the pile

At this phase of the study, the load carrying capacity of the single pile-soil system as well as the strength of pile material were evaluated. The ultimate carrying capacity of the pile-soil system was evaluated using the β-method (see Section 6.4). This was compared with the allowable load carrying capacity of the pile material using equation 6-4. Ultimately, the controlling load (lowest) was selected to be the load carrying capacity of the pile. Table 6.4 shows result of this phase of the study.

Table 6.4 Pile load carrying capacity

Soil condition			Pile configuration		Capacity			
H_b *ft (m)*	H_e *ft (m)*	H_n *ft (m)*	D_p *in (mm)*	L_p *ft (m)*	β-method kips (kN)			Strength kips (kN)
					Q_{ps}	Q_b	Q_u	
0	30 (9.1)	30 (9.1)	18 (458)	35 (10.5)	33 (147)	29 (126)	62(273)	336 (1495)
12 (3.7)	18 (5.5)				33 (147)	28 (126)	61 (273)	
24 (7.3)	6 (1.8)				33 (147)	28 (126)	61 (273)	
0	30 (9.1)			45 (13.7)	58 (256)	35 (154)	92 (410)	
12 (3.7)	18 (5.5)				56.5 (251)	33.5 (149)	90 (401)	
24 (7.3)	6 (1.8)				57 (252)	34 (150)	91 (402)	
0	30 (9.1)			55 (16.8)	87 (387)	40 (178)	127 (565)	
12 (3.7)	18 (5.5)				85.5 (381)	39.5 (176)	125 (555)	
24 (7.3)	6 (1.8)				85 (380)	39 (173)	124 (553)	
0	30 (9.1)		12 (305)	35 (10.5)	24 (103)	12 (56)	35 (159)	149 (663)
12 (3.7)	18 (5.5)				23 (100)	12 (56)	35 (156)	
24 (7.3)	6 (1.8)				23 (100)	12 (56)	35 (156)	
0	30 (9.1)			45 (13.7)	39 (168)	15 (67)	54 (235)	
12 (3.7)	18 (5.5)				38 (168)	15 (67)	53 (235)	
24 (7.3)	6 (1.8)				38 (168)	15 (67)	53 (235)	
0	30 (9.1)			55 (16.8)	58 (253)	18 (77)	76 (330)	
12 (3.7)	18 (5.5)				57 (253)	17 (77)	74 (330)	
24 (7.3)	6 (1.8)				57 (253)	17 (77)	74 (330)	
0	30 (9.1)		6 (152)	35 (10.5)	11 (49)	3 (14)	14 (63)	37 (165)
12 (3.7)	18 (5.5)				11 (49)	3 (14)	14 (63)	
24 (7.3)	6 (1.8)				11 (49)	3 (14)	14 (63)	
0	30 (9.1)			45 (13.7)	19 (85)	4 (19)	23 (104)	
12 (3.7)	18 (5.5)				19 (85)	4 (19)	23 (104)	
24 (7.3)	6 (1.8)				19 (85)	4 (19)	23 (104)	
0	30 (9.1)			55 (16.8)	29 (127)	4 (19)	33 (146)	
12 (3.7)	18 (5.5)				29 (127)	4 (19)	33 (146)	
24 (7.3)	6 (1.8)				29 (127)	4 (19)	33 (146)	

6.7.2 Pile head settlement

The settlement of the pile head was of particular interest in this phase of the study. The objective was to quantify the pile head settlement as a function of different pile-soil parameters (see Tables 6.2 and 6.3). The result of the finite element analyses is shown in Figures 6.13, 6.14, and 6.15.

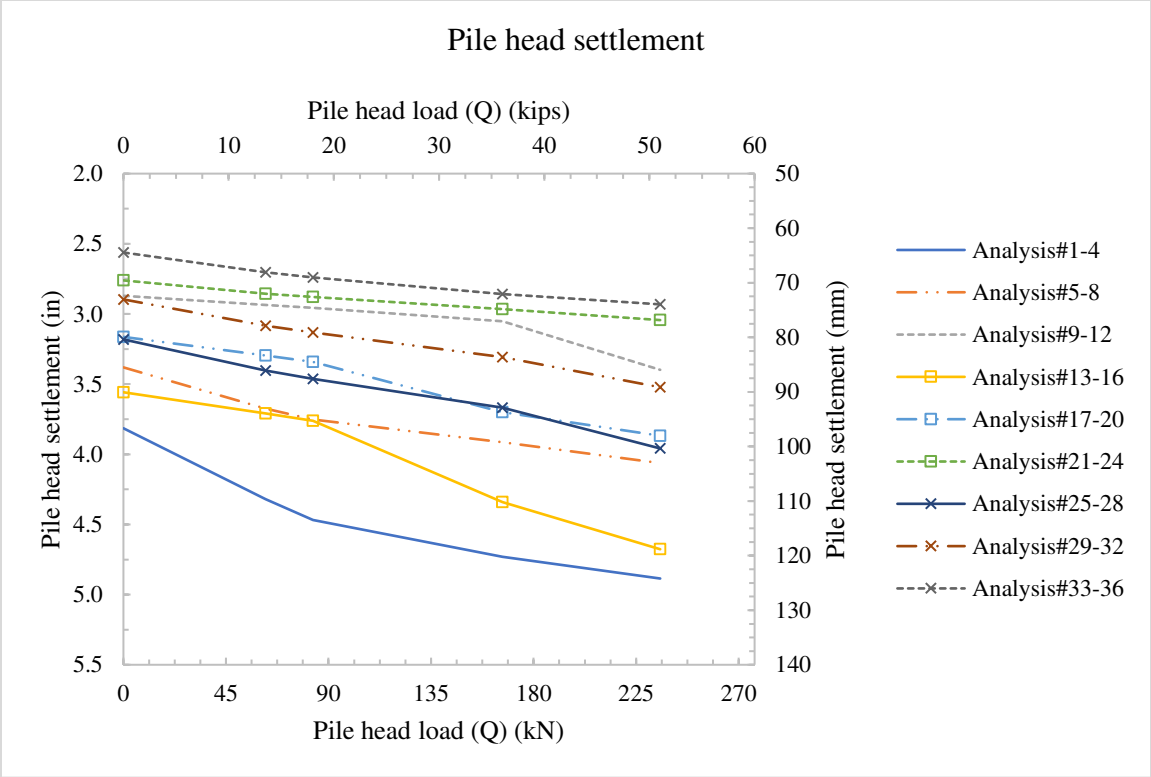

Figure 6.13 Pile head settlement for D_p=18 in (460 *mm*)

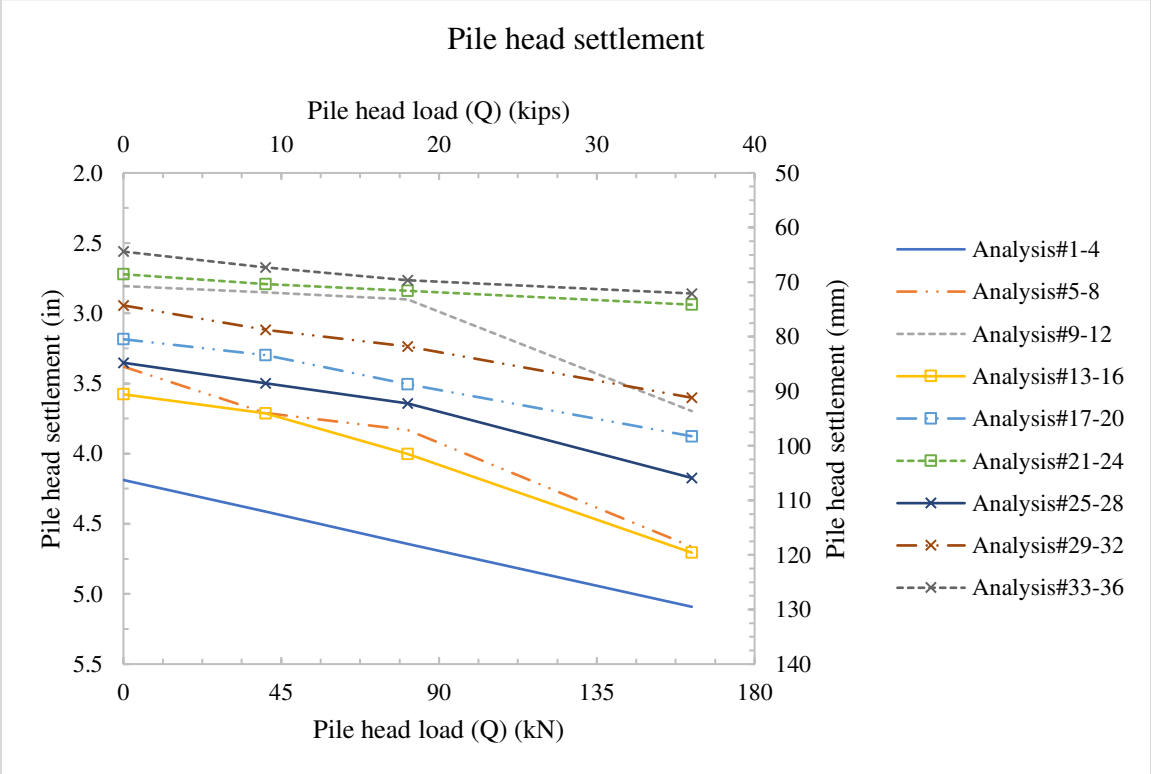

Figure 6.14 Pile head settlement for D_p=12 in (305 *mm*)

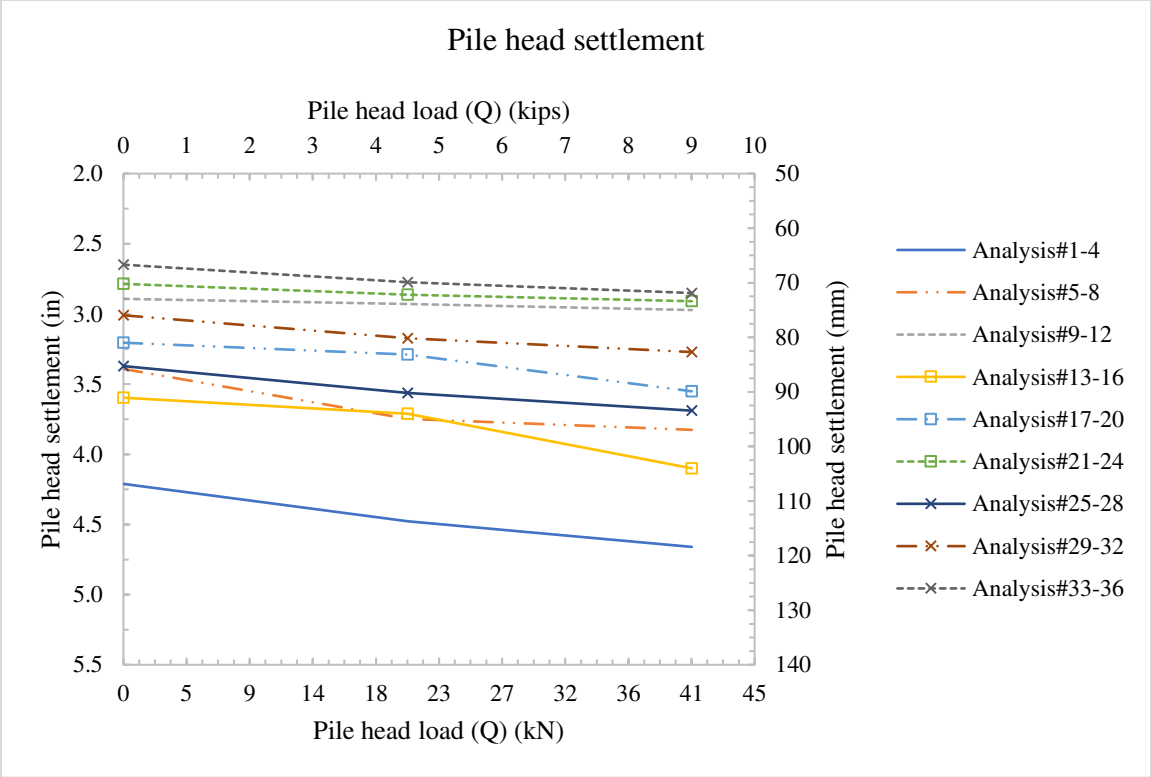

Figure 6.15 Pile head settlement for D_p=6 in (152 *mm*)

In order to put the results into perspective, design charts were developed such that pile head settlement, Δ_{PH}, could be obtained based on soil conditions. In these charts, Δ_{PH} can be evaluated as a function of the reduction of settlement, R_{sett}:

$$R_{sett} = \frac{\Delta_s - \Delta_{PH}}{\Delta_s} = 1 - \frac{\Delta_{PH}}{\Delta_s} \qquad 6\text{-}6$$

Where

Δ_s = Virgin soil settlement (without pile).

Therefore, the charts were represented using by the pile-soil conditions, ratio of the backfill material to the overall height of the fill, (H_b/H_f), pile head load, Q/Q_u, and diameter of pile, D_p. The design charts are shown in Figures 6.16 through 6.18.

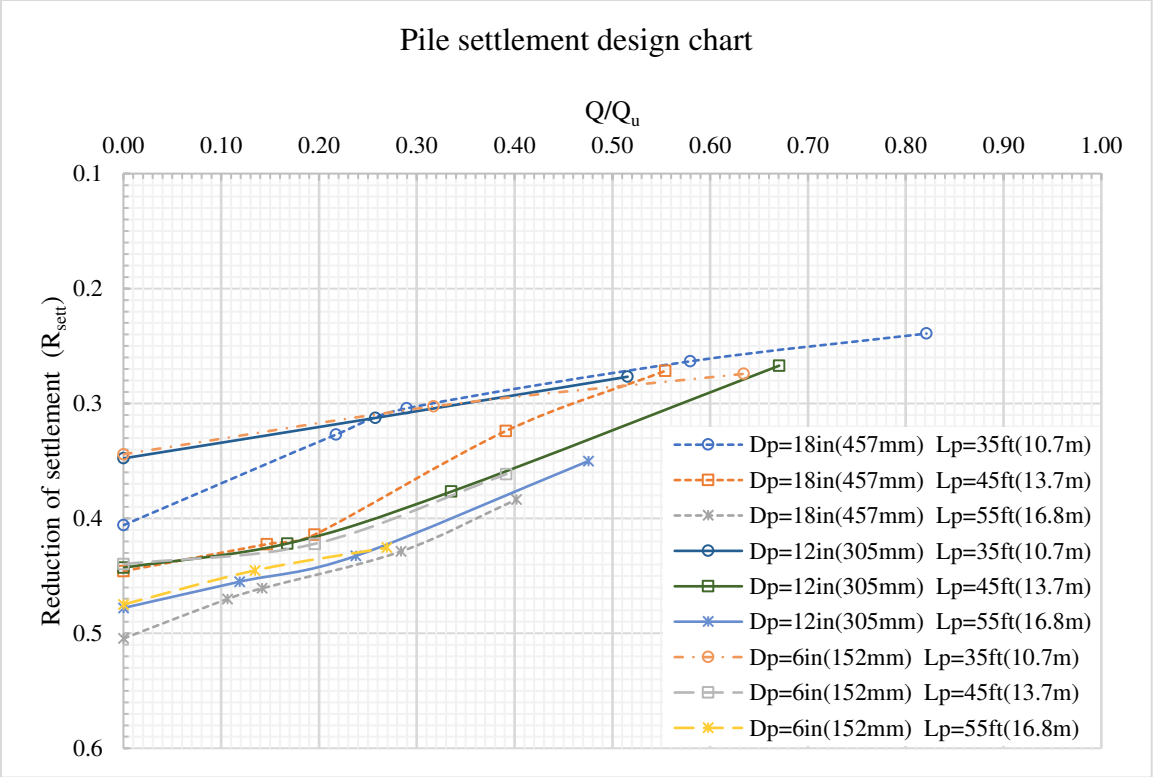

Figure 6.16 Pile settlement design chart for $H_b/H_f = 0.0$

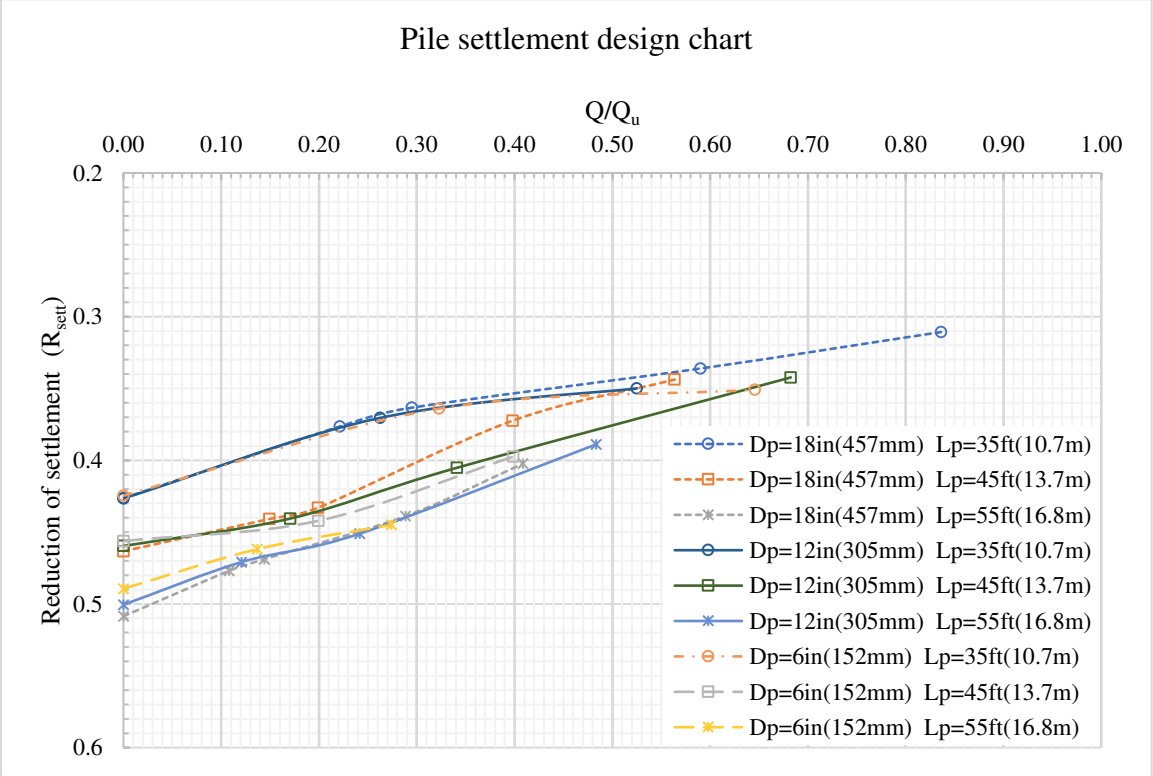

Figure 6.17 Pile settlement design chart for $H_b/H_f = 0.40$

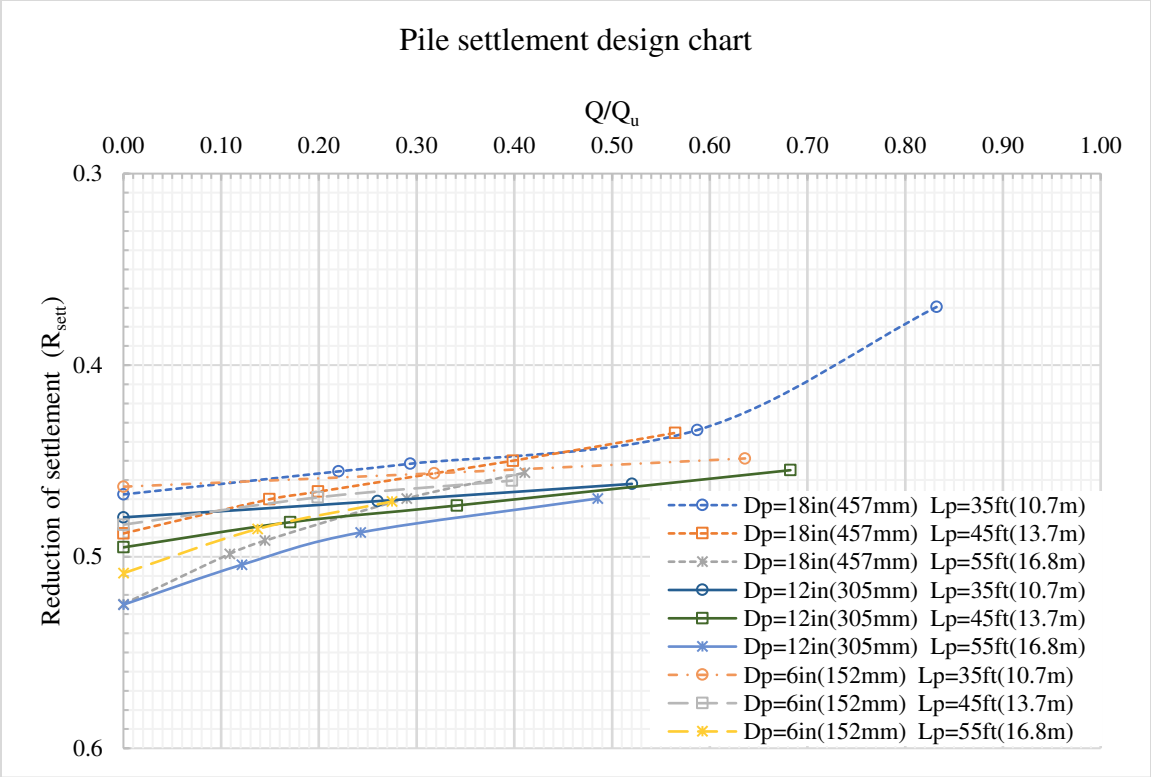

Figure 6.18 Pile settlement design chart for $H_b/H_f = 0.80$

The above design charts can be conveniently used to determine the most reliable design option for a given pile-soil condition. Accordingly, the required size, length and number of piles needed to achieve the desired level of settlement reduction, R_{sett}, or pile head settlement can be readily estimated.

6.7.3 Load distribution along the pile shaft

This aspect of the study was focused on the load distribution along the pile. The objective was to quantify the axial force distribution as a function of different pile-soil conditions (see Tables 6.2 and 6.3). The simulated axial force distributions are shown in Figures 6.19 to 6.45

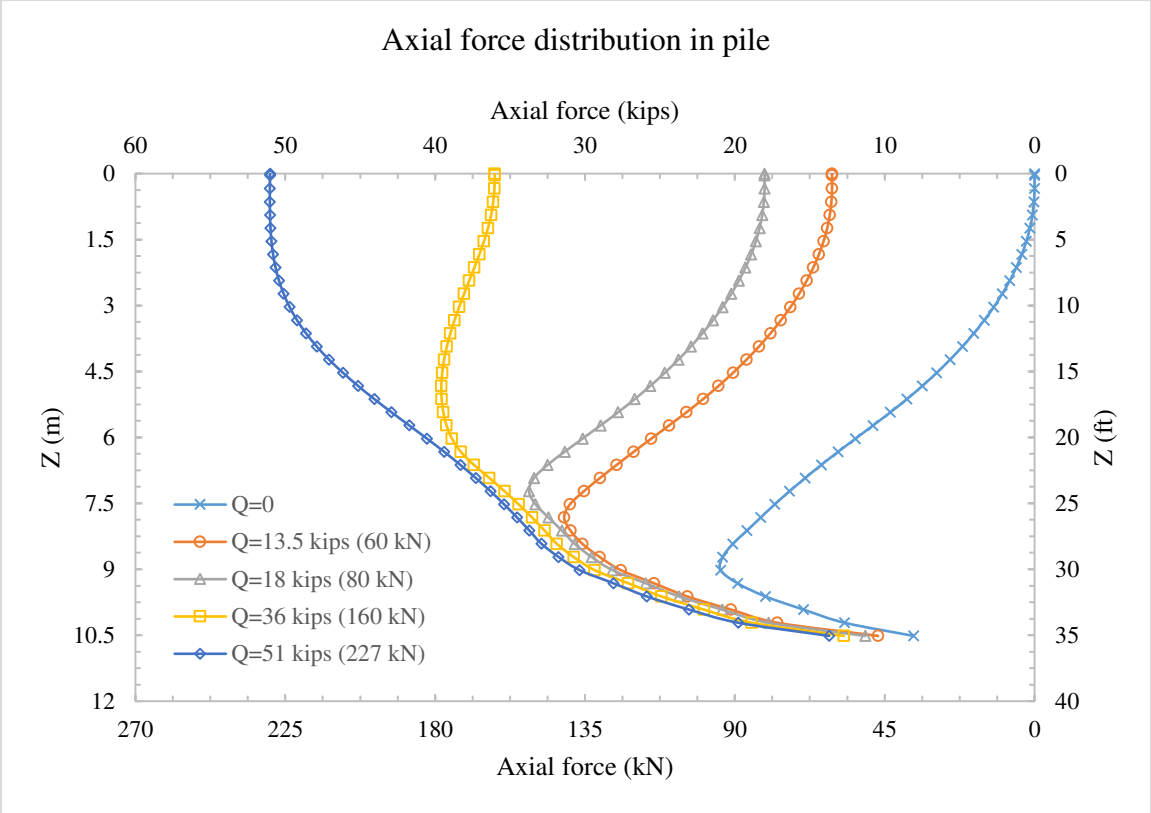

Figure 6.19 Axial force distribution in pile with D_p=18 in (460 *mm*), L_p=35 *ft* (10.7 *m*), and H_b/H_f=0

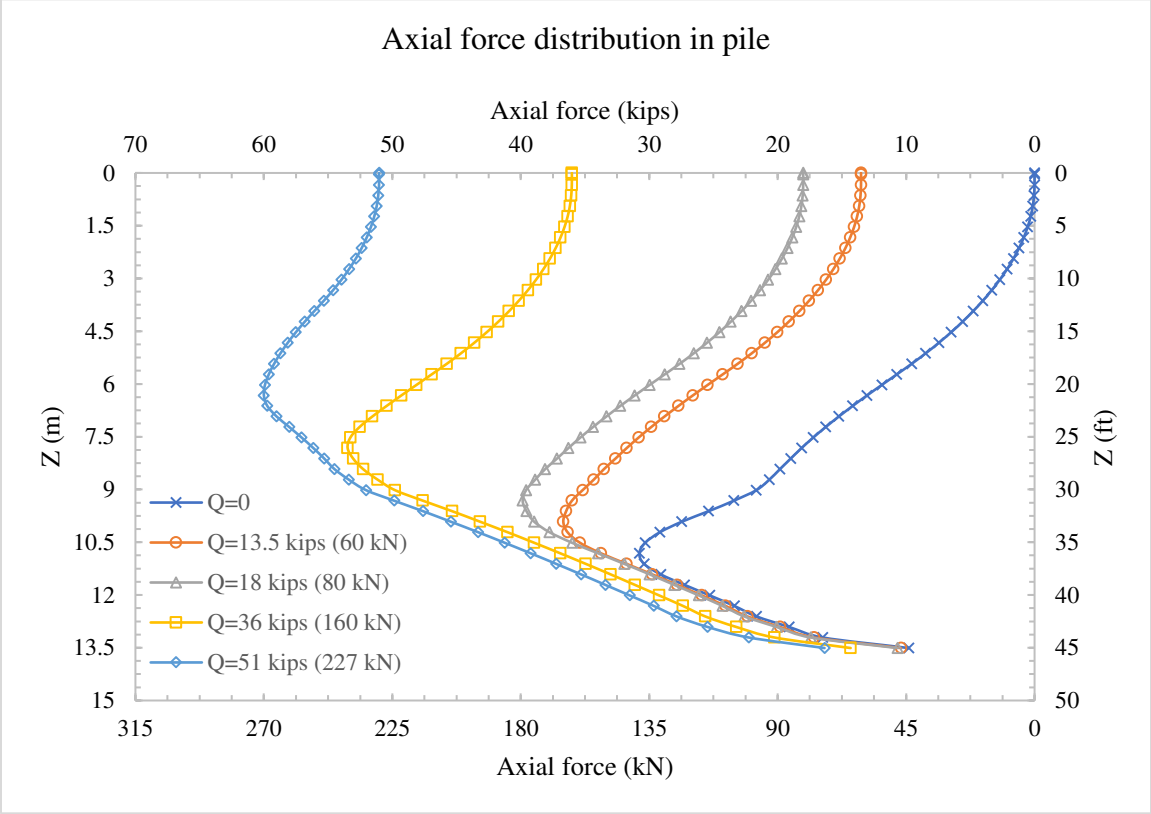

Figure 6.20 Axial force distribution in pile with D_p=18 in (460 *mm*), L_p=45 *ft* (13.7 *m*), and H_b/H_f=0

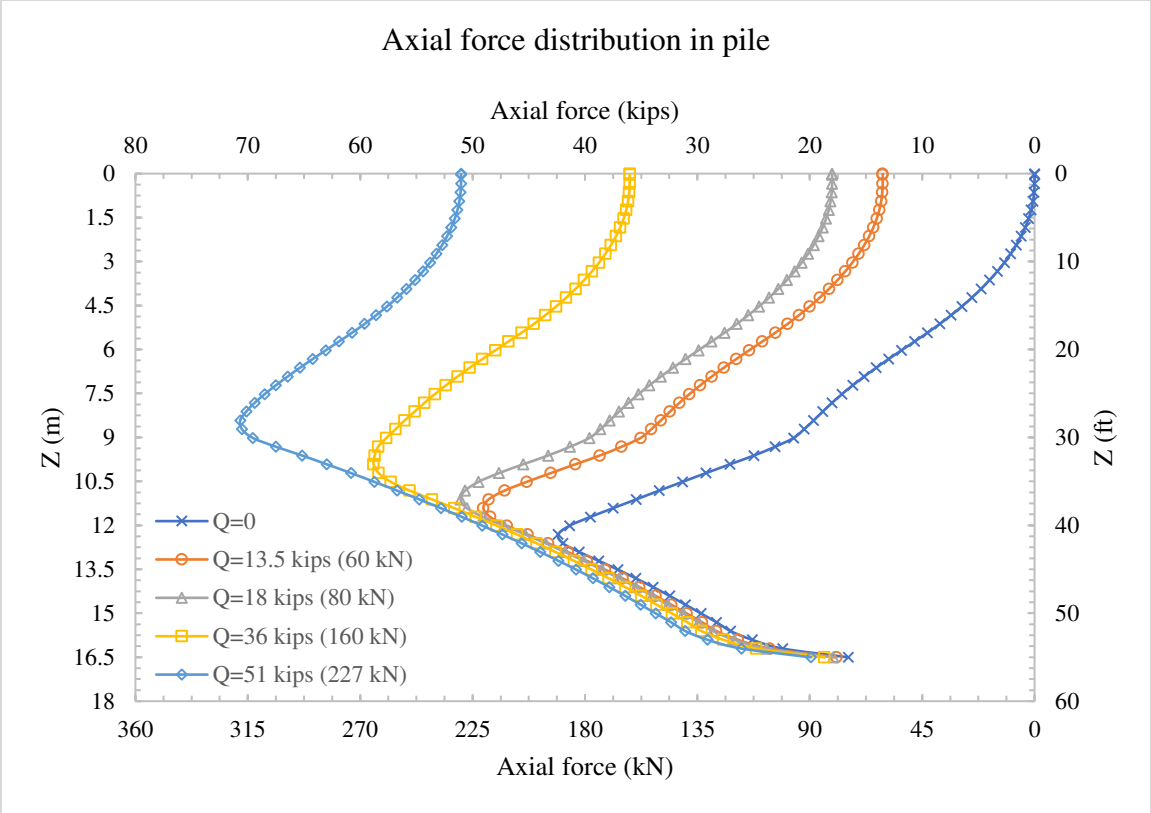

Figure 6.21 Axial force distribution in pile with D_p=18 in (460 *mm*), L_p=55 *ft* (16.8 *m*), and H_b/H_f=0

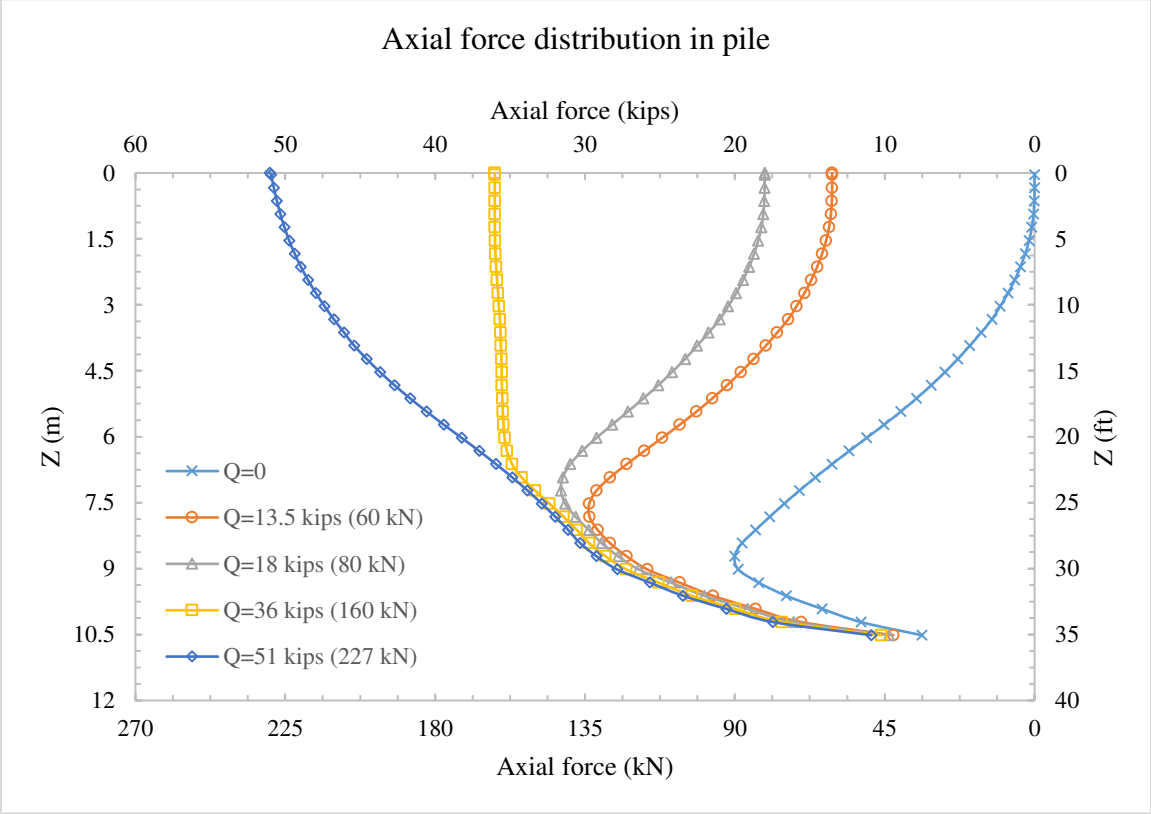

Figure 6.22 Axial force distribution in pile with D_p=18 in (460 *mm*), L_p=35 *ft* (10.7 *m*), and H_b/H_f=0.40

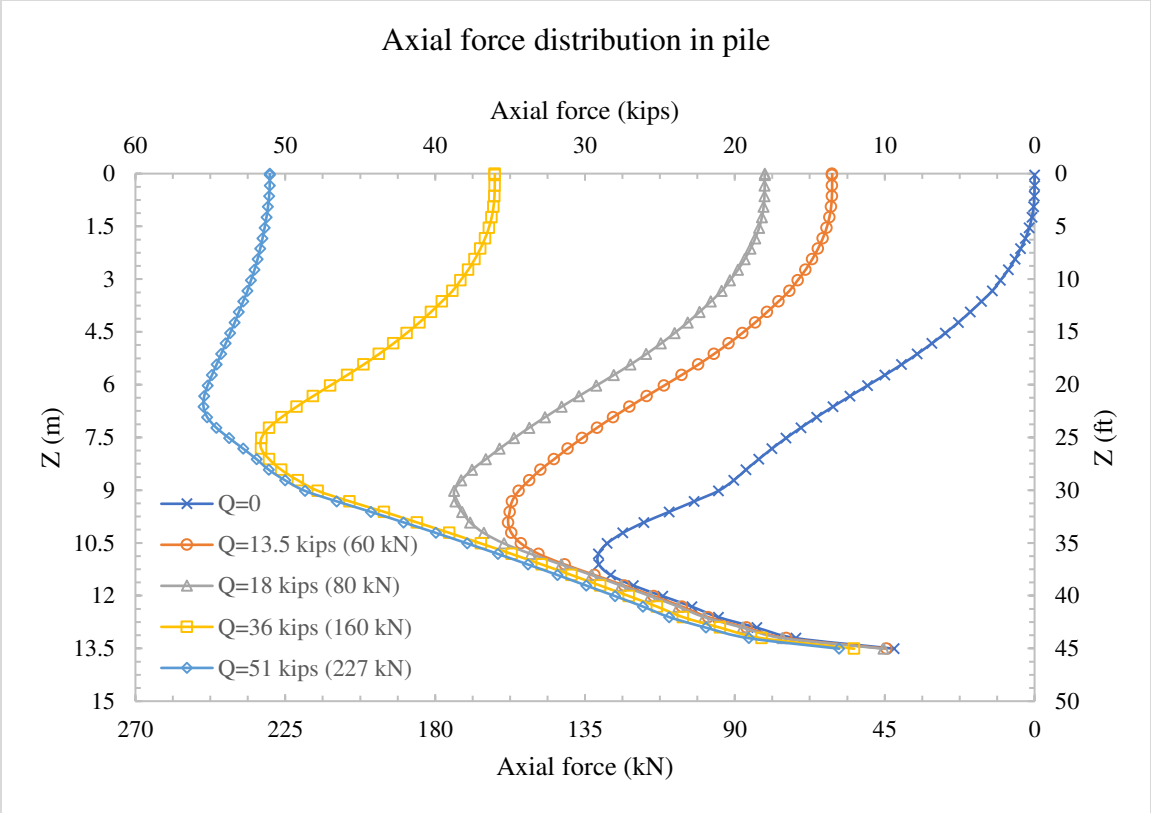

Figure 6.23 Axial force distribution in pile with D_p=18 in (460 *mm*), L_p=45 *ft* (13.7 *m*), and H_b/H_f=0.40

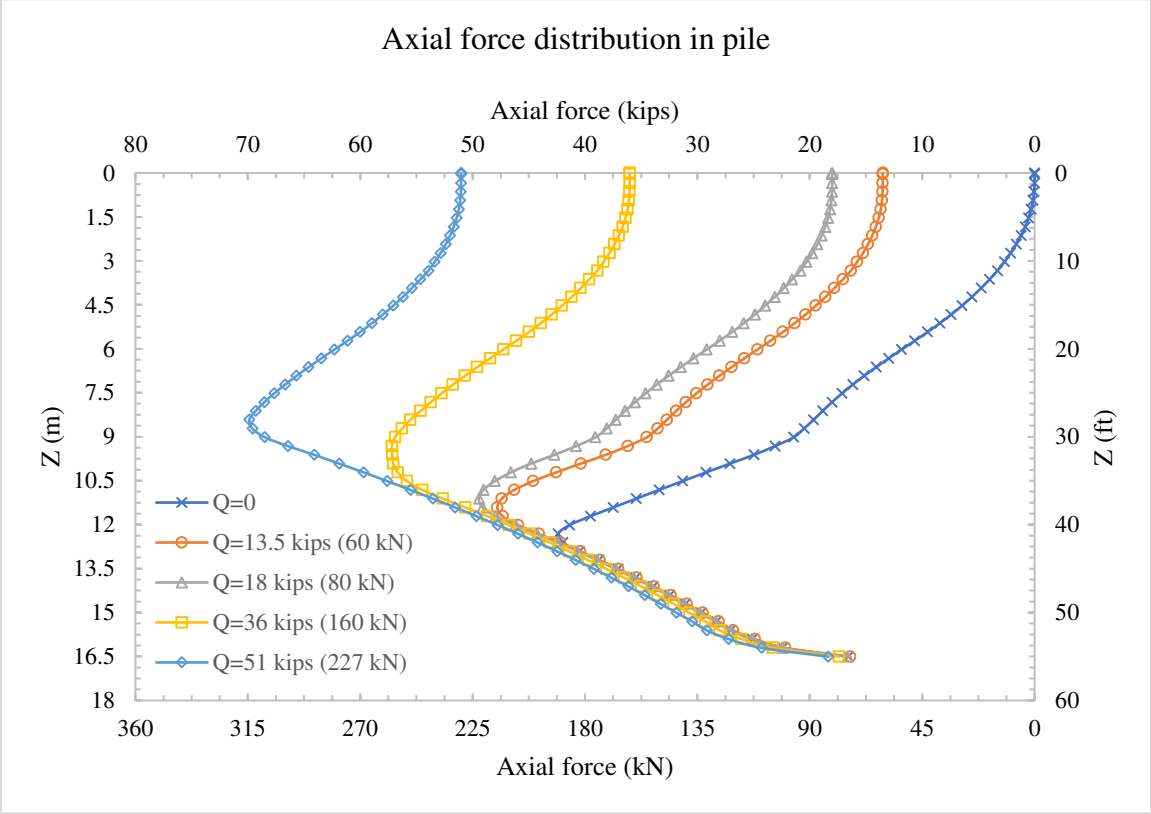

Figure 6.24 Axial force distribution in pile with D_p=18 in (460 *mm*), L_p=55 *ft* (16.8 *m*), and H_b/H_f=0.40

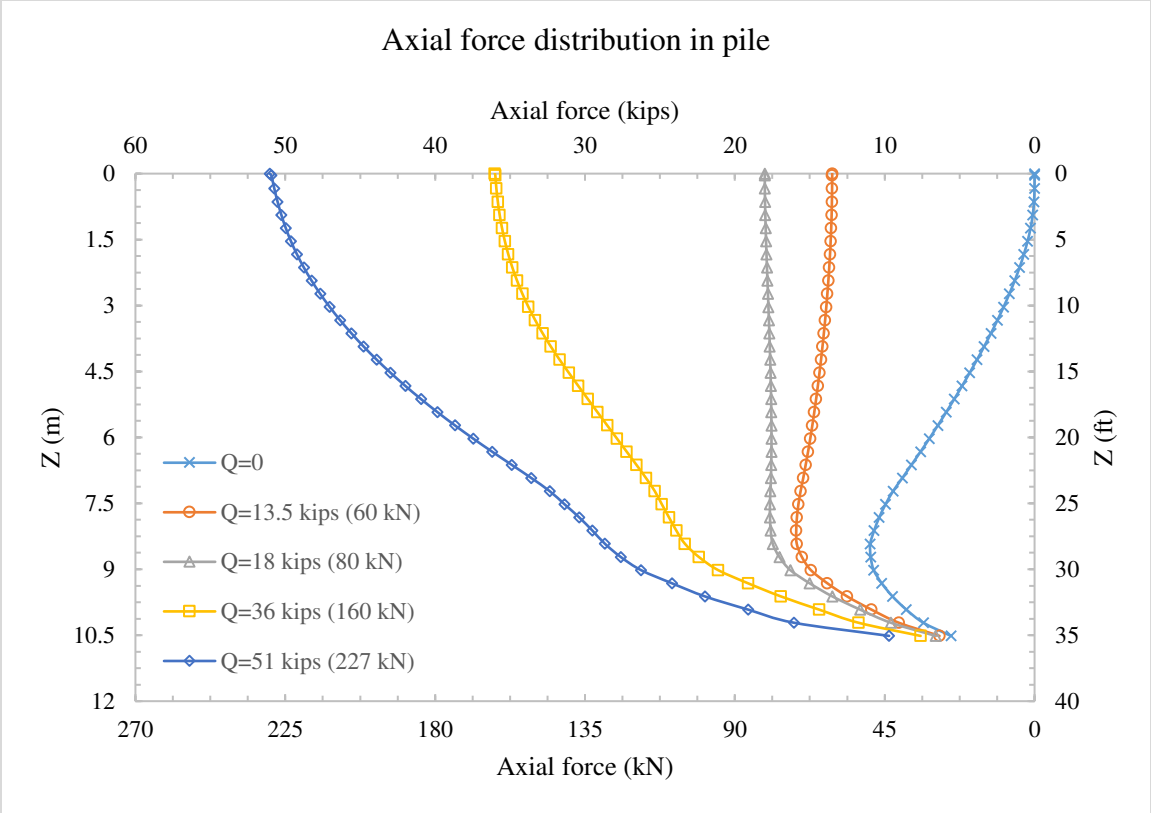

Figure 6.25 Axial force distribution in pile with D_p=18 in (460 *mm*), L_p=35 *ft* (10.7 *m*), and H_b/H_f=0.80

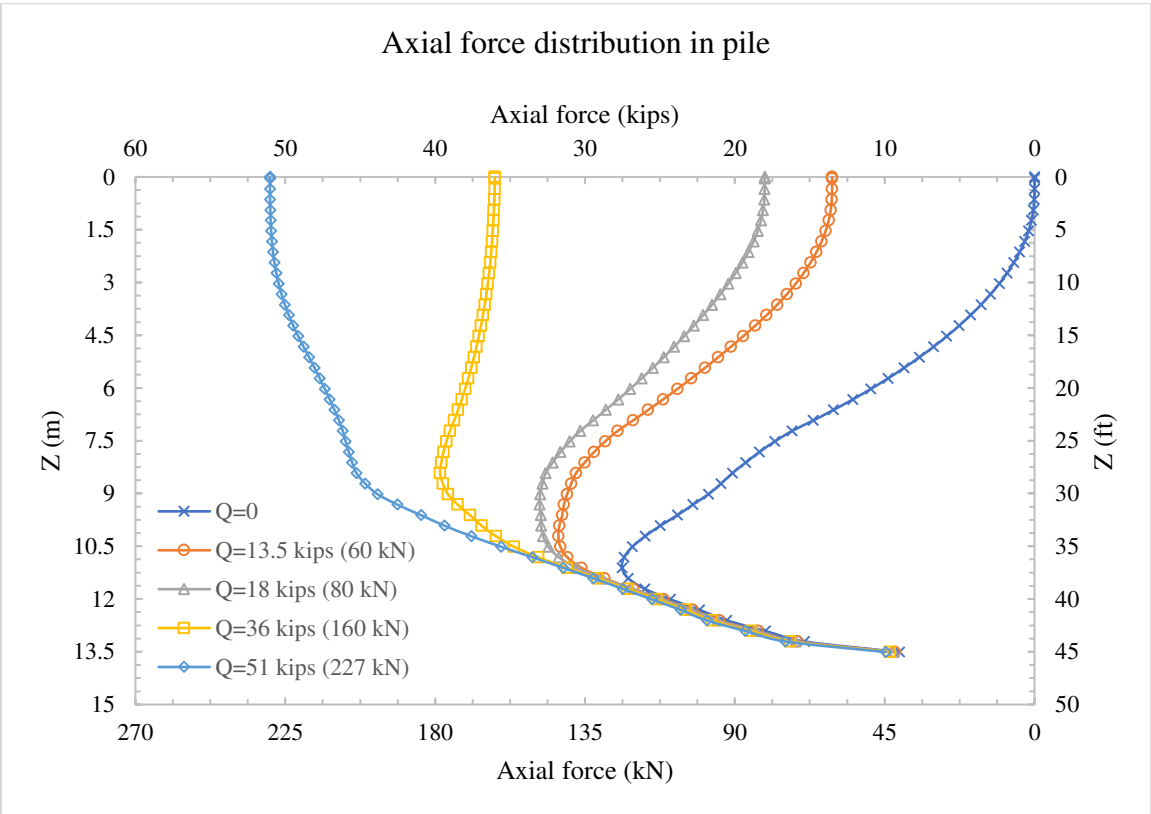

Figure 6.26 Axial force distribution in pile with D_p=18 in (460 *mm*), L_p=45 *ft* (13.7 *m*), and H_b/H_f=0.80

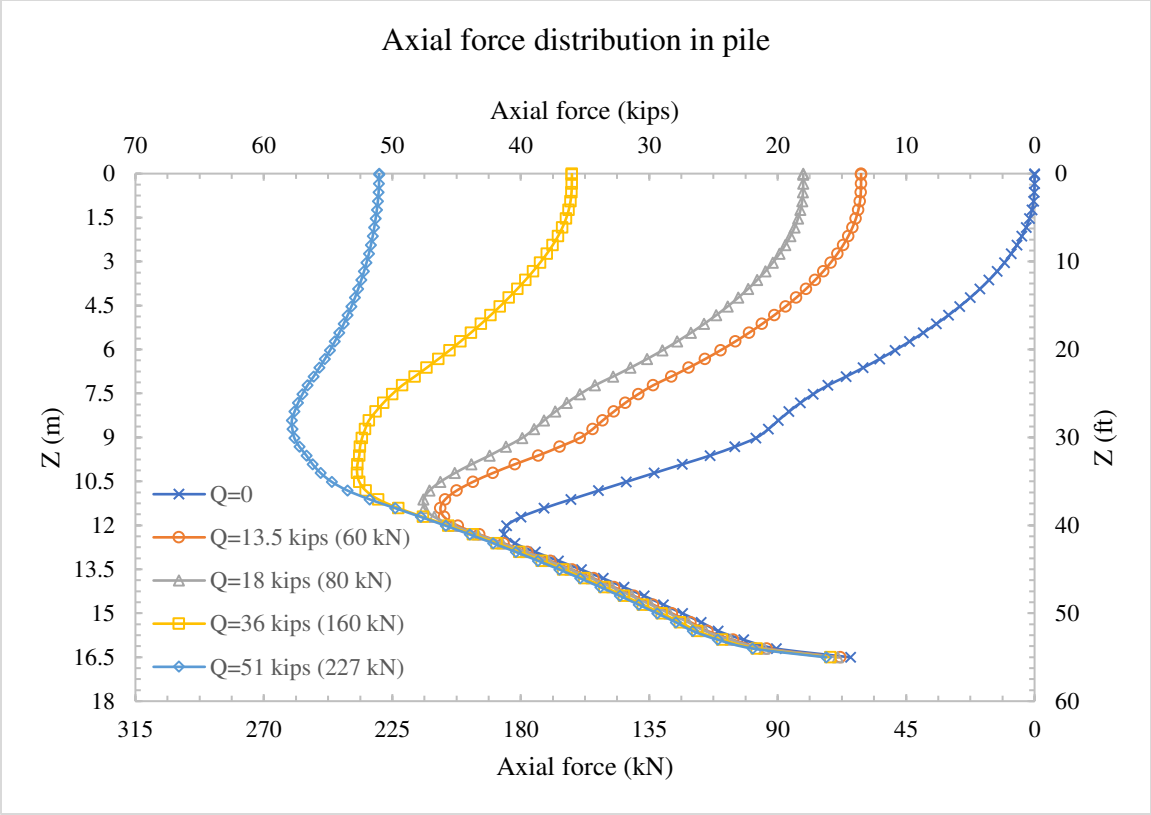

Figure 6.27 Axial force distribution in pile with D_p=18 in (460 *mm*), L_p=55 *ft* (16.8 *m*), and H_b/H_f=0.80

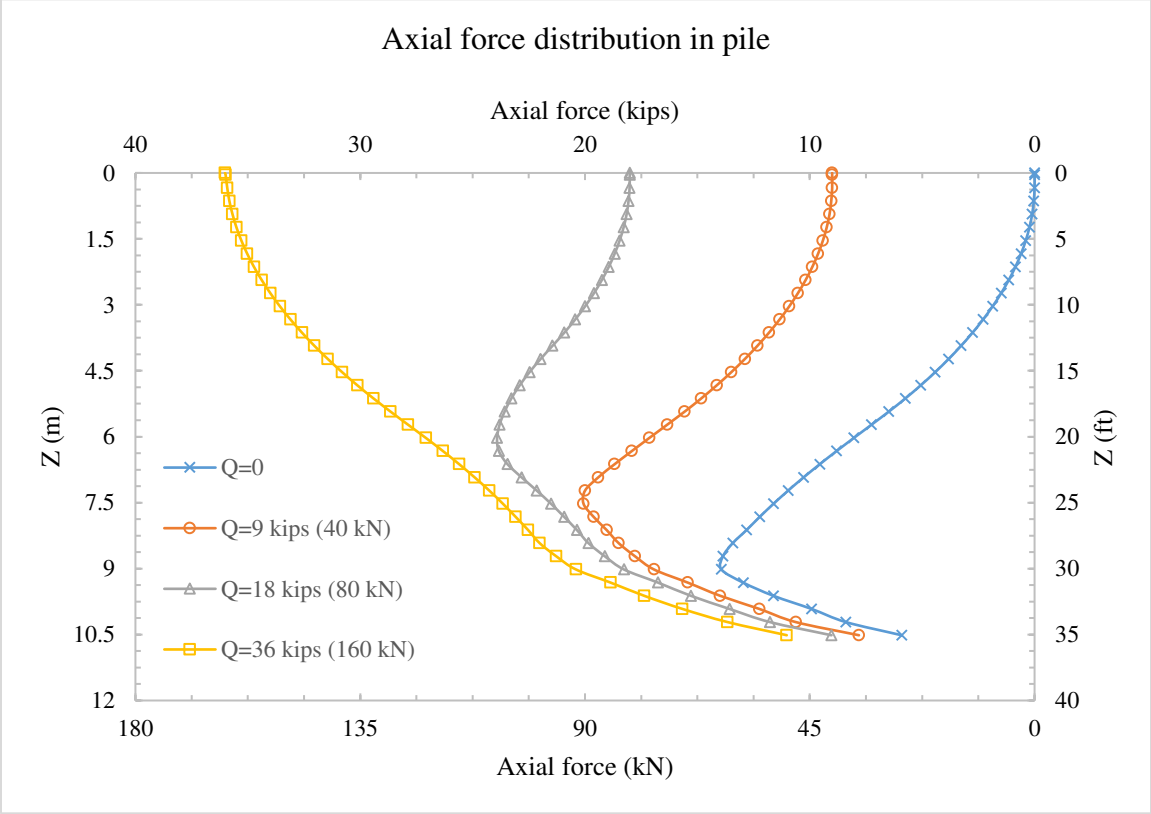

Figure 6.28 Axial force distribution in pile with D_p=12 in (305 *mm*), L_p=35 *ft* (10.7 *m*), and H_b/H_f=0.0

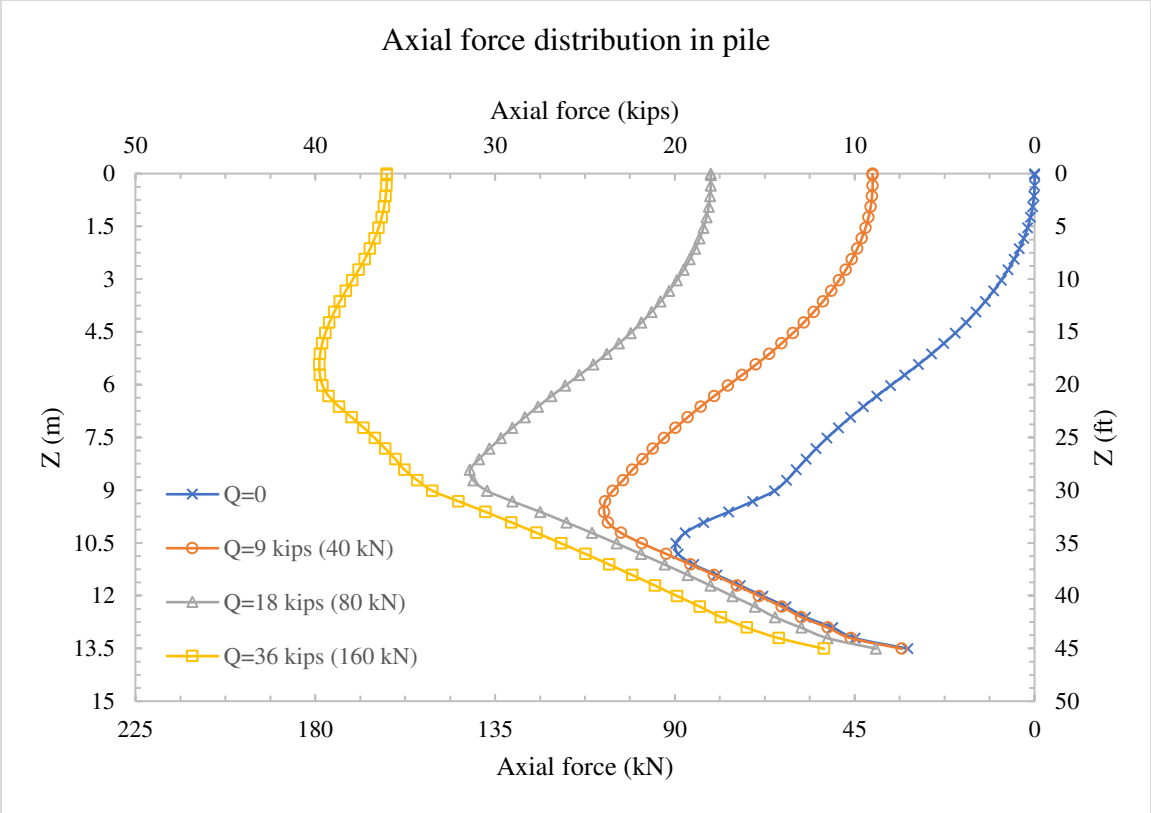

Figure 6.29 Axial force distribution in pile with D_p=12 in (305 *mm*), L_p=45 *ft* (13.7 *m*), and H_b/H_f=0.0

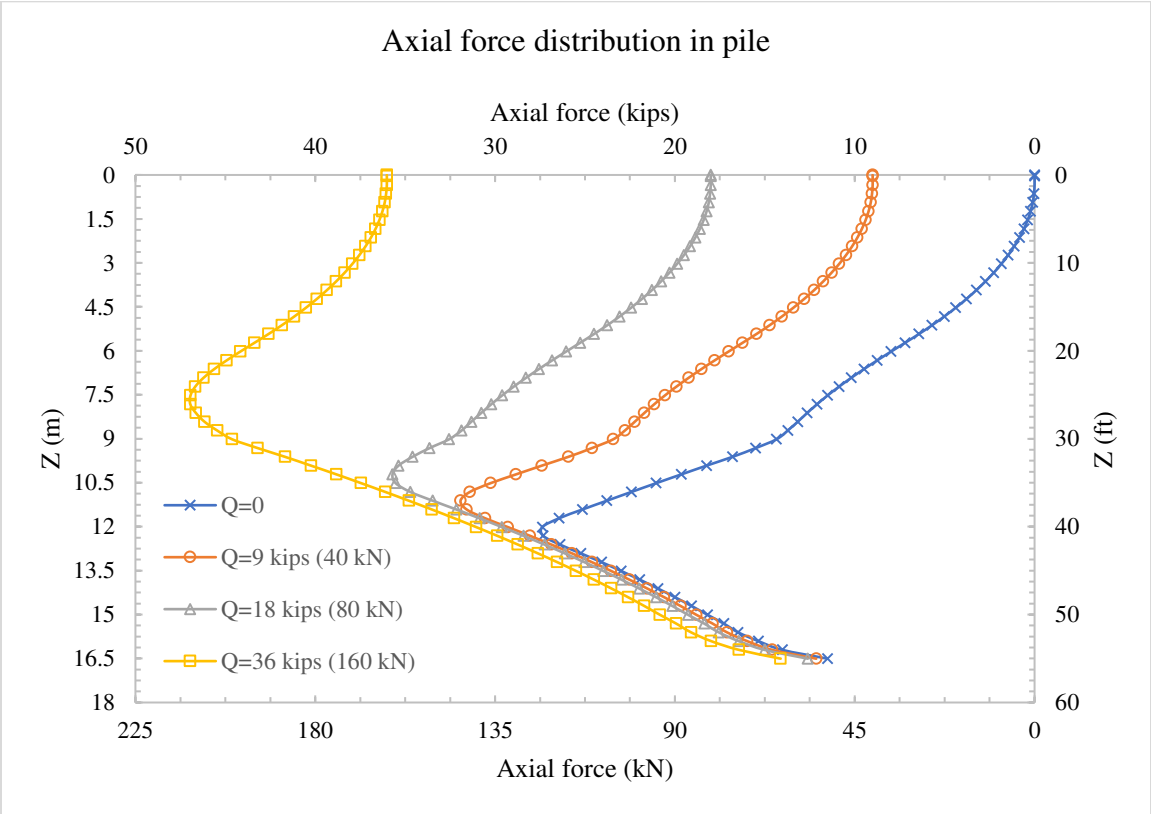

Figure 6.30 Axial force distribution in pile with D_p=12 in (305 *mm*), L_p=55 *ft* (16.8 *m*), and H_b/H_f=0.0

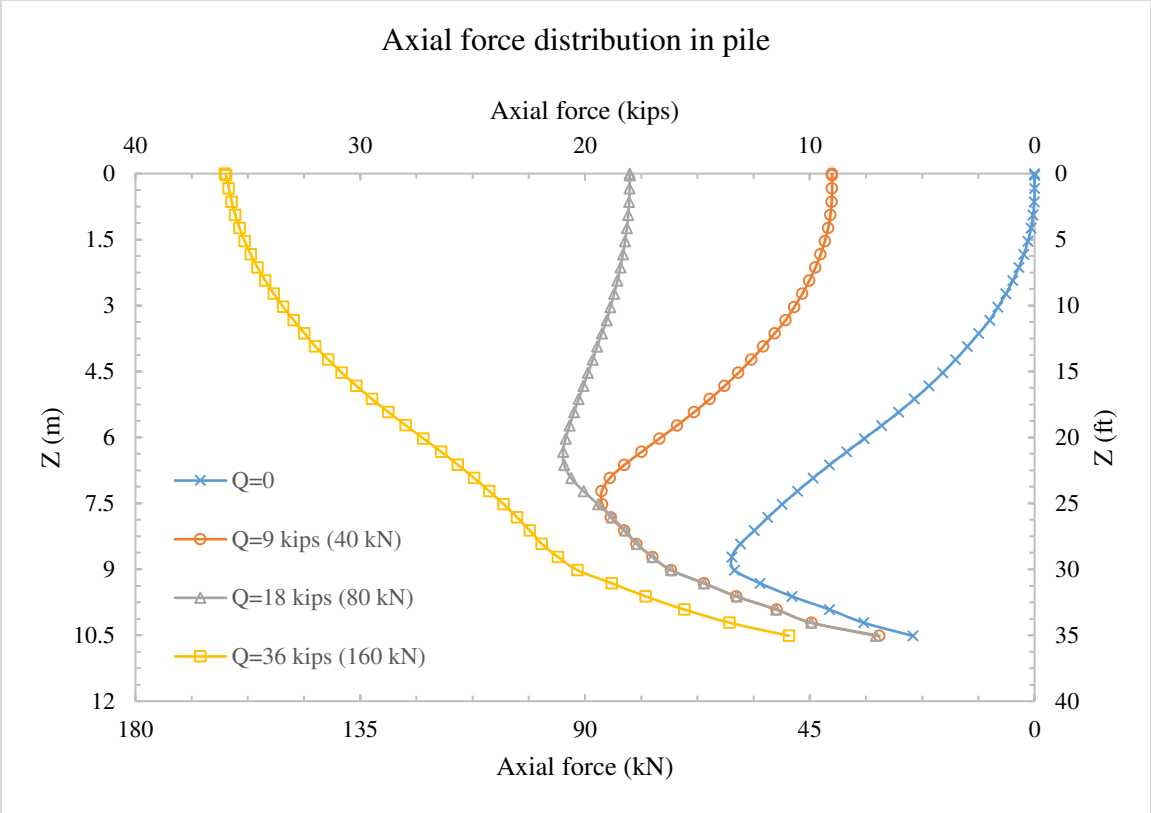

Figure 6.31 Axial force distribution in pile with D_p=12 in (305 *mm*), L_p=35 *ft* (10.7 *m*), and H_b/H_f=0.40

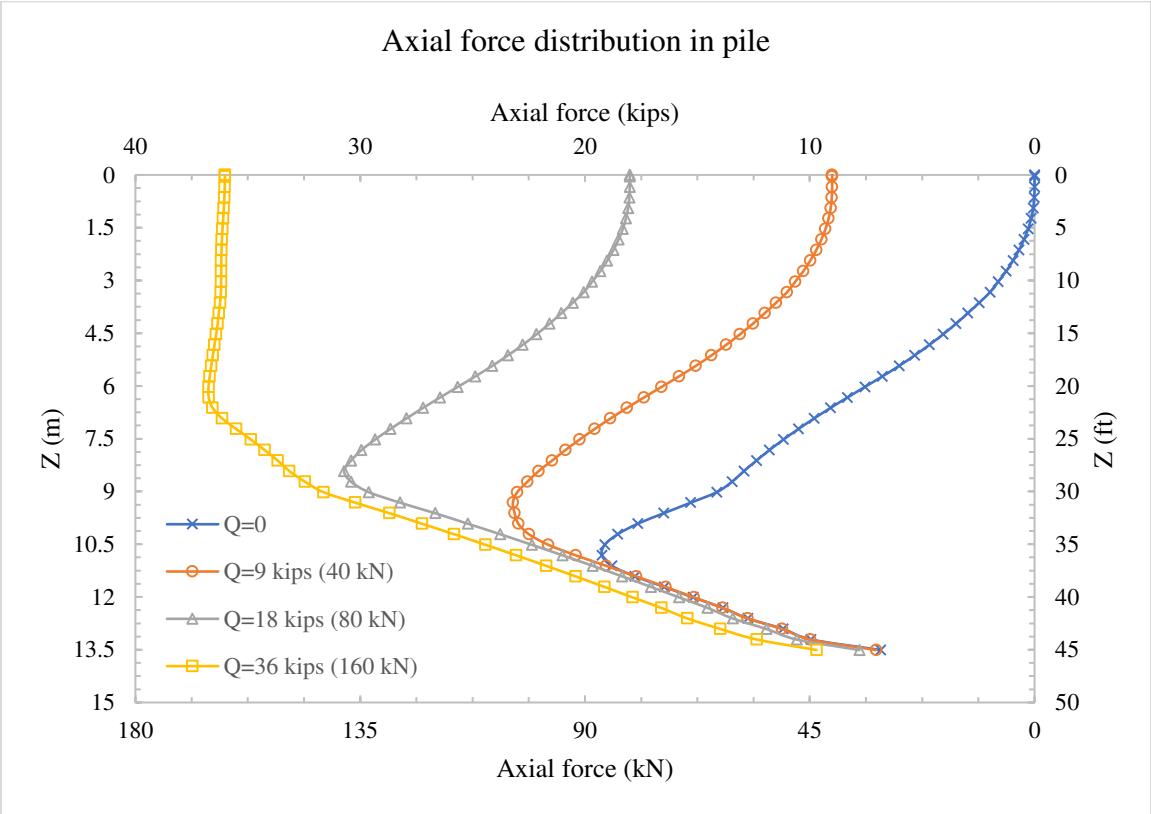

Figure 6.32 Axial force distribution in pile with D_p=12 in (305 *mm*), L_p=45 *ft* (13.7 *m*), and H_b/H_f=0.40

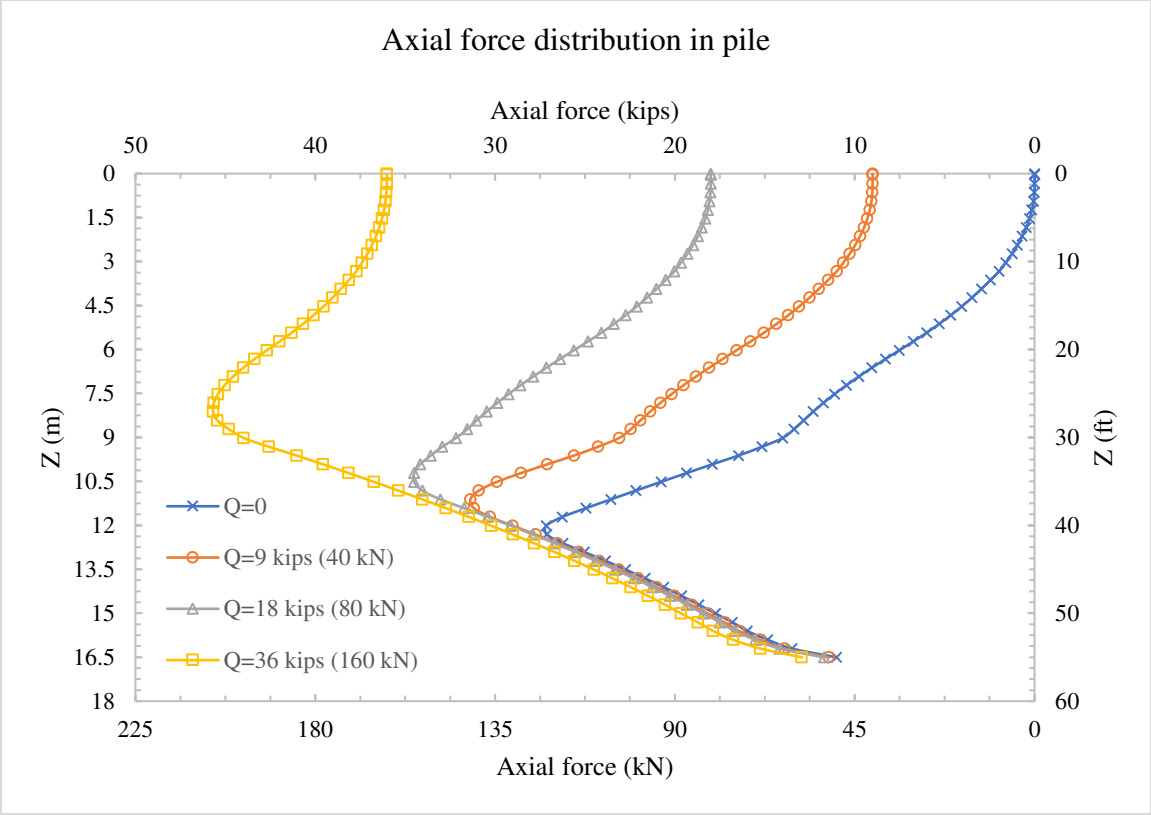

Figure 6.33 Axial force distribution in pile with D_p=12 in (305 *mm*), L_p=35 *ft* (16.8 *m*), and H_b/H_f=0.40

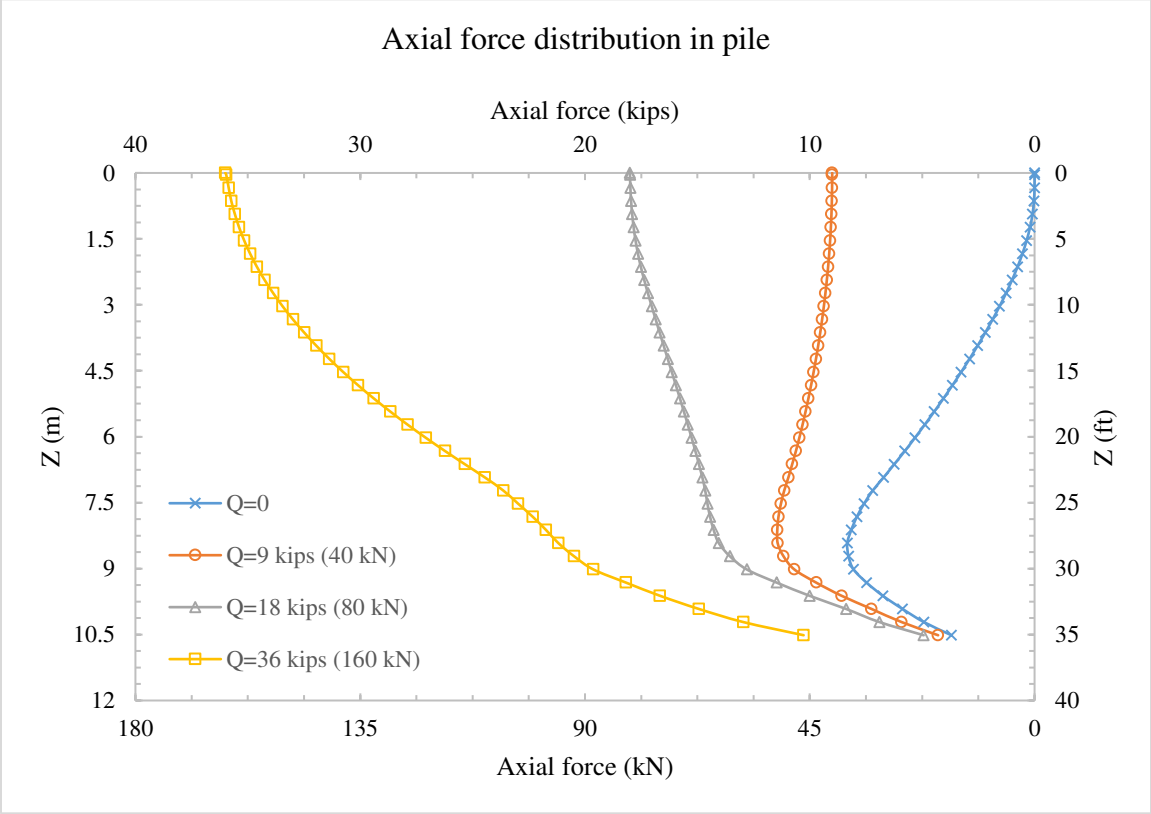

Figure 6.34 Axial force distribution in pile with D_p=12 in (305 *mm*), L_p=35 *ft* (10.7 *m*), and H_b/H_f=0.80

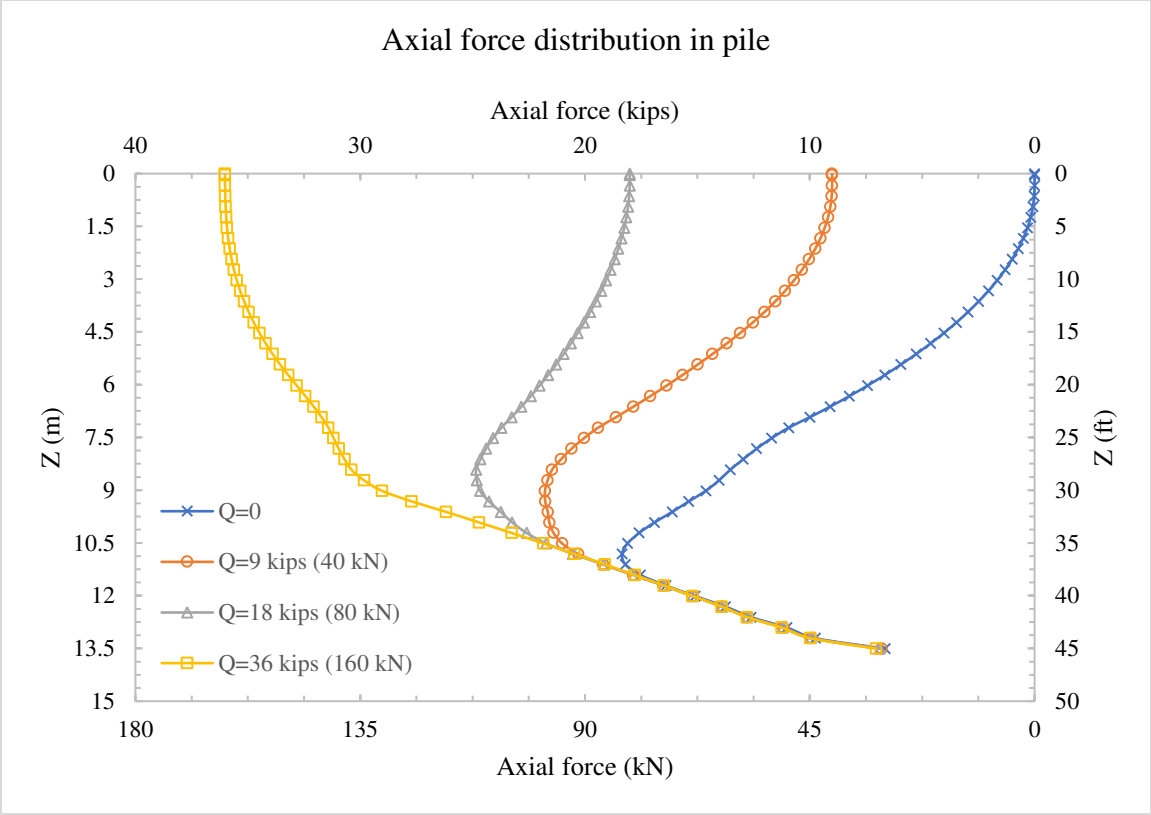

Figure 6.35 Axial force distribution in pile with D_p=12 in (305 *mm*), L_p=45 *ft* (13.7 *m*), and H_b/H_f=0.80

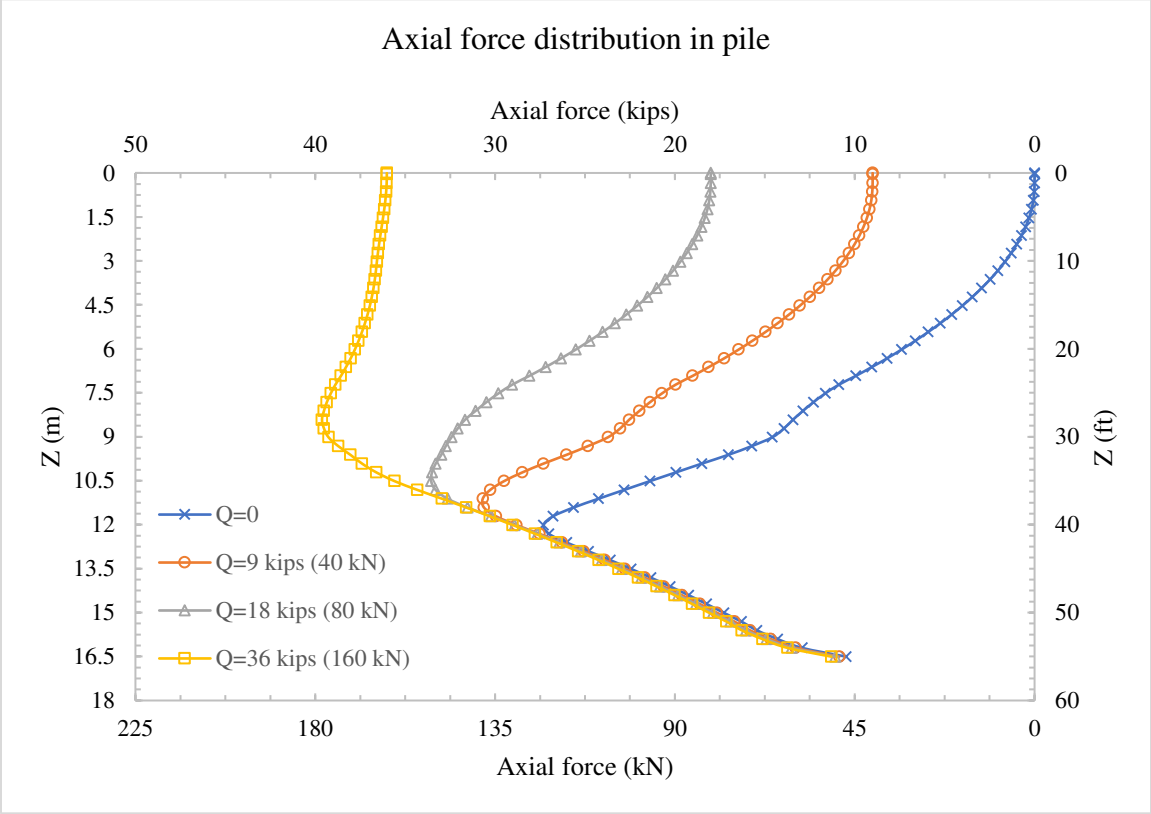

Figure 6.36 Axial force distribution in pile with D_p=12 in (305 *mm*), L_p=55 *ft* (16.8 *m*), and H_b/H_f=0.80

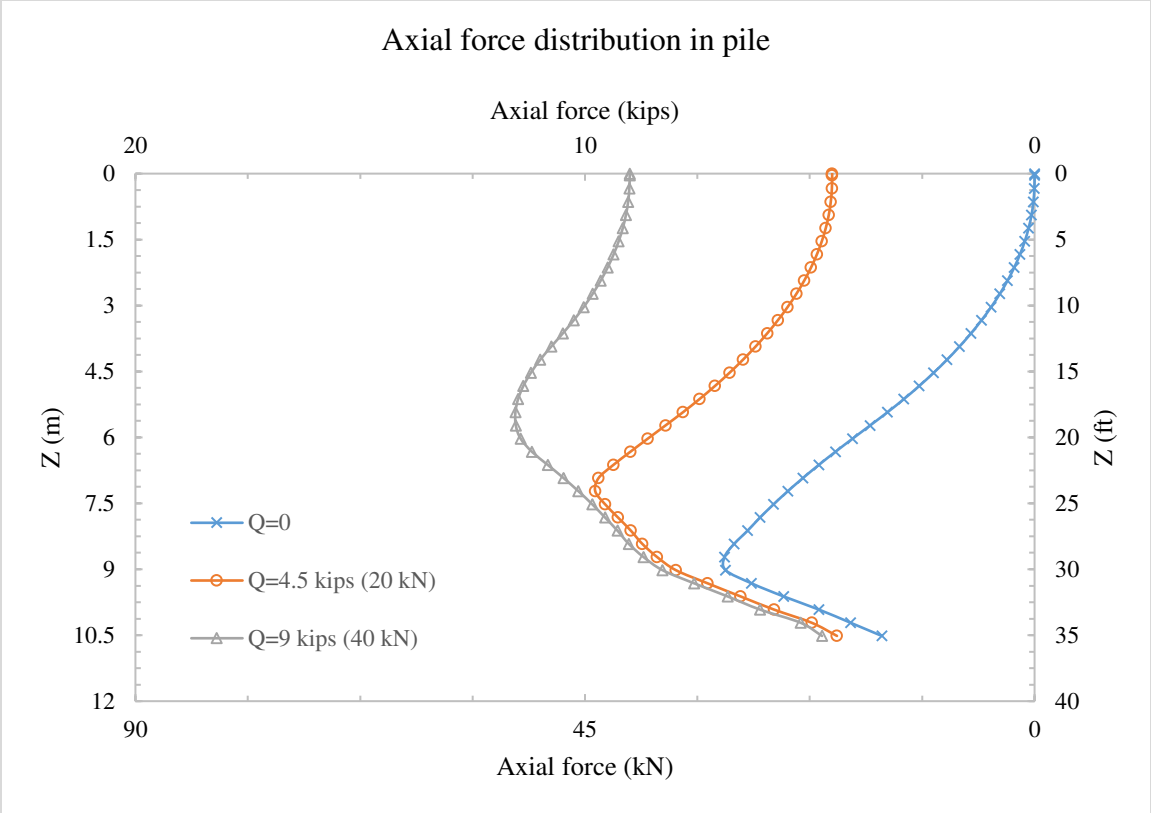

Figure 6.37 Axial force distribution in pile with D_p=6 in (152 *mm*), L_p=35 *ft* (10.7 *m*), and H_b/H_f=0.0

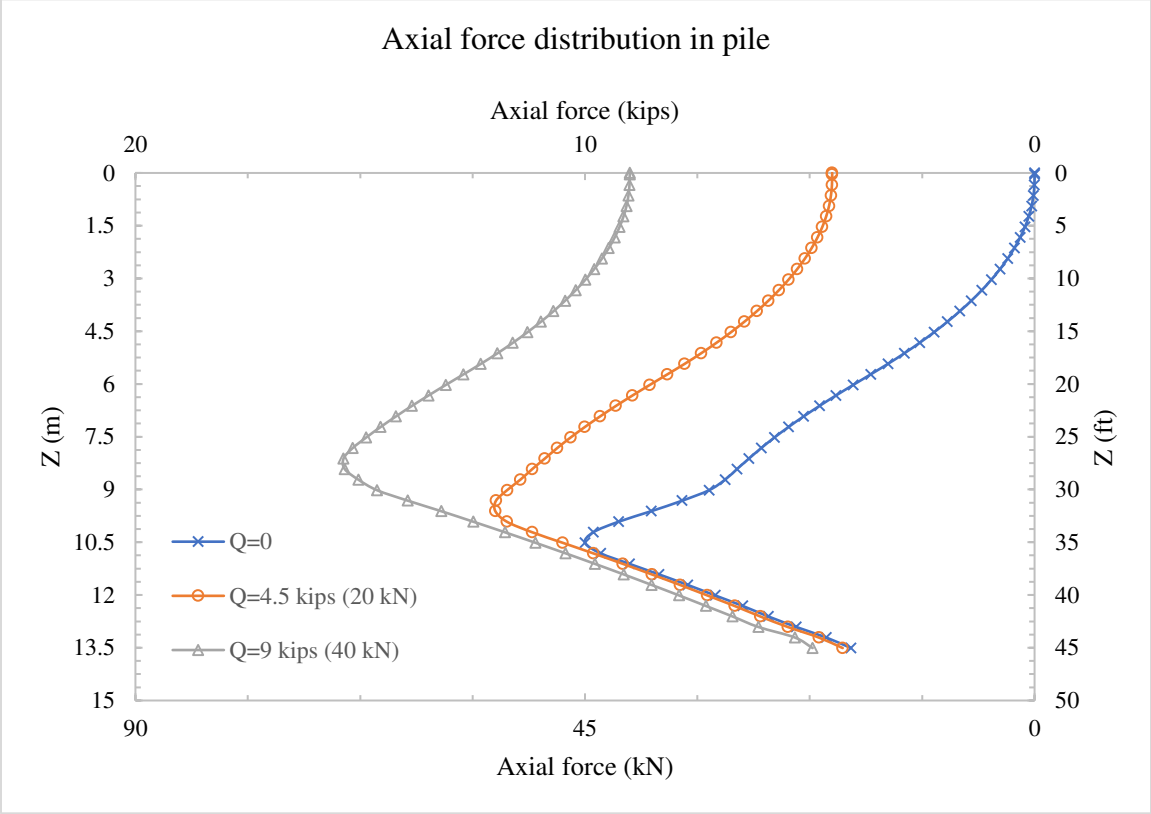

Figure 6.38 Axial force distribution in pile with D_p=6 in (152 *mm*), L_p=45 *ft* (13.7 *m*), and H_b/H_f=0.0

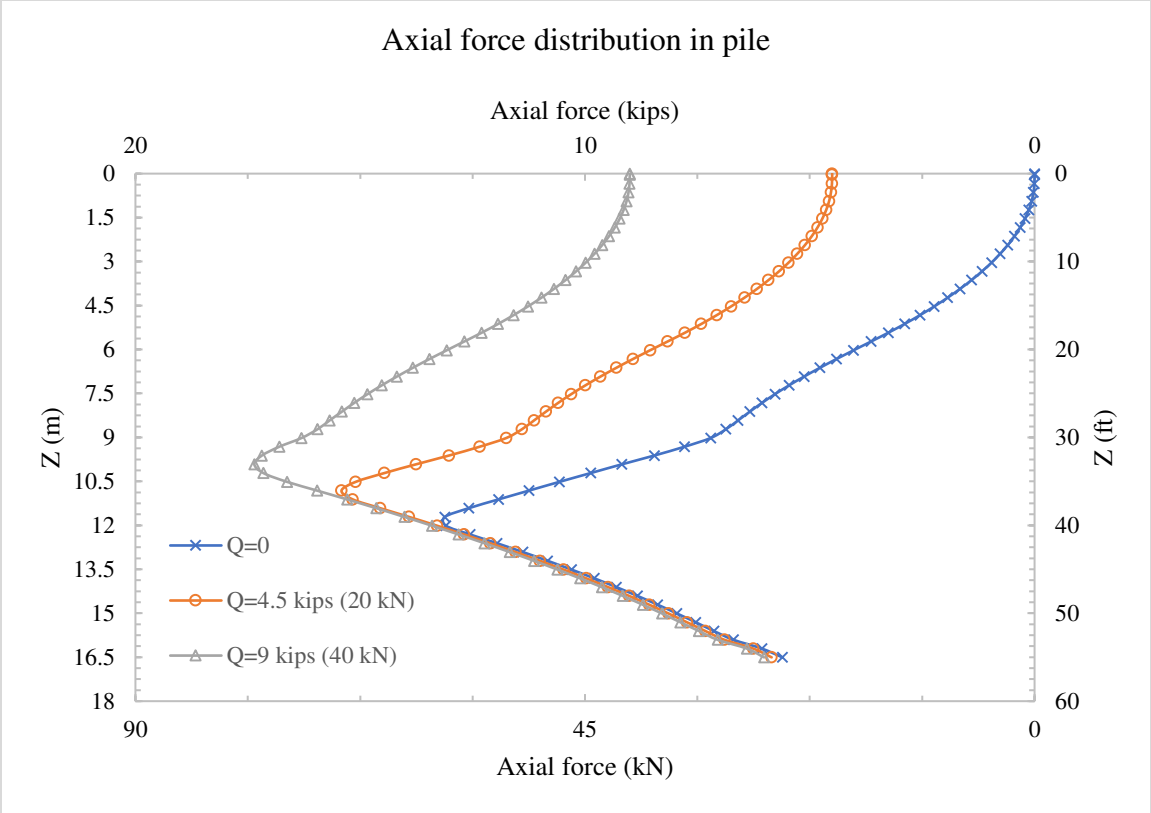

Figure 6.39 Axial force distribution in pile with D_p=6 in (152 *mm*), L_p=55 *ft* (16.8 *m*), and H_b/H_f=0.0

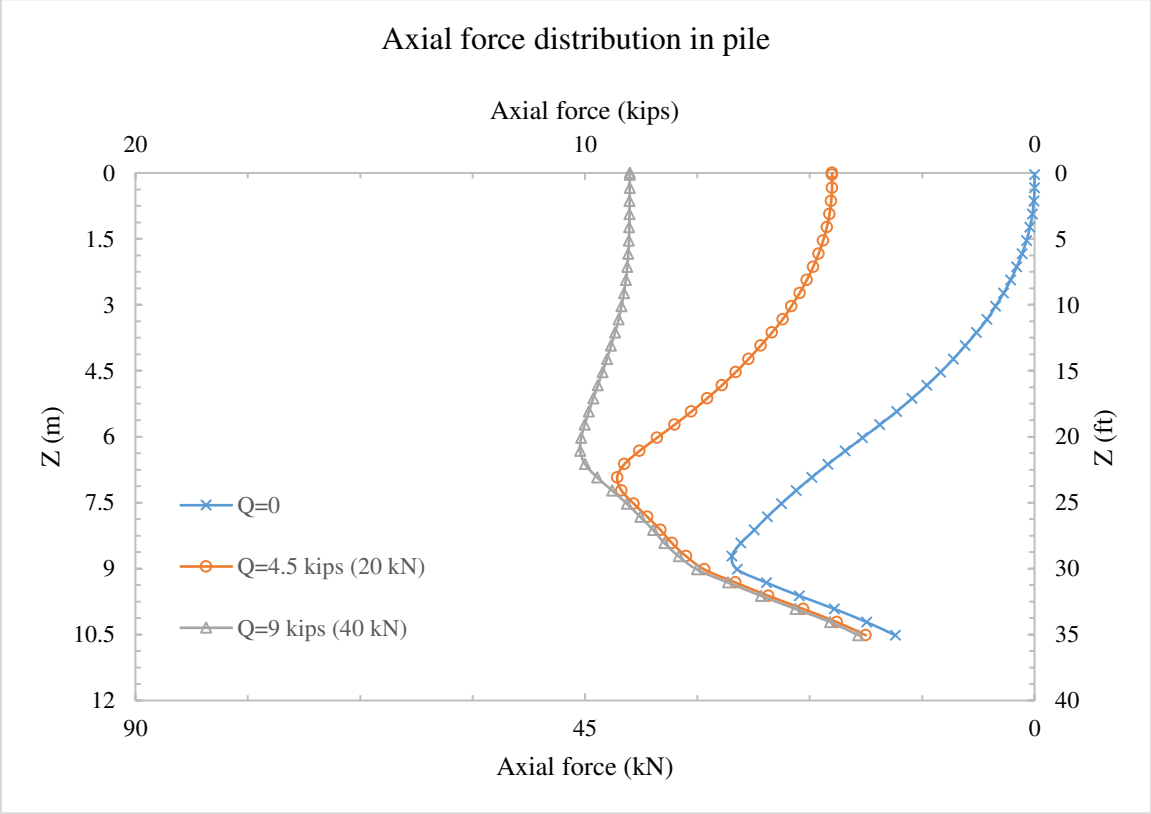

Figure 6.40 Axial force distribution in pile with D_p=6 in (152 *mm*), L_p=35 *ft* (10.7 *m*), and H_b/H_f=0.40

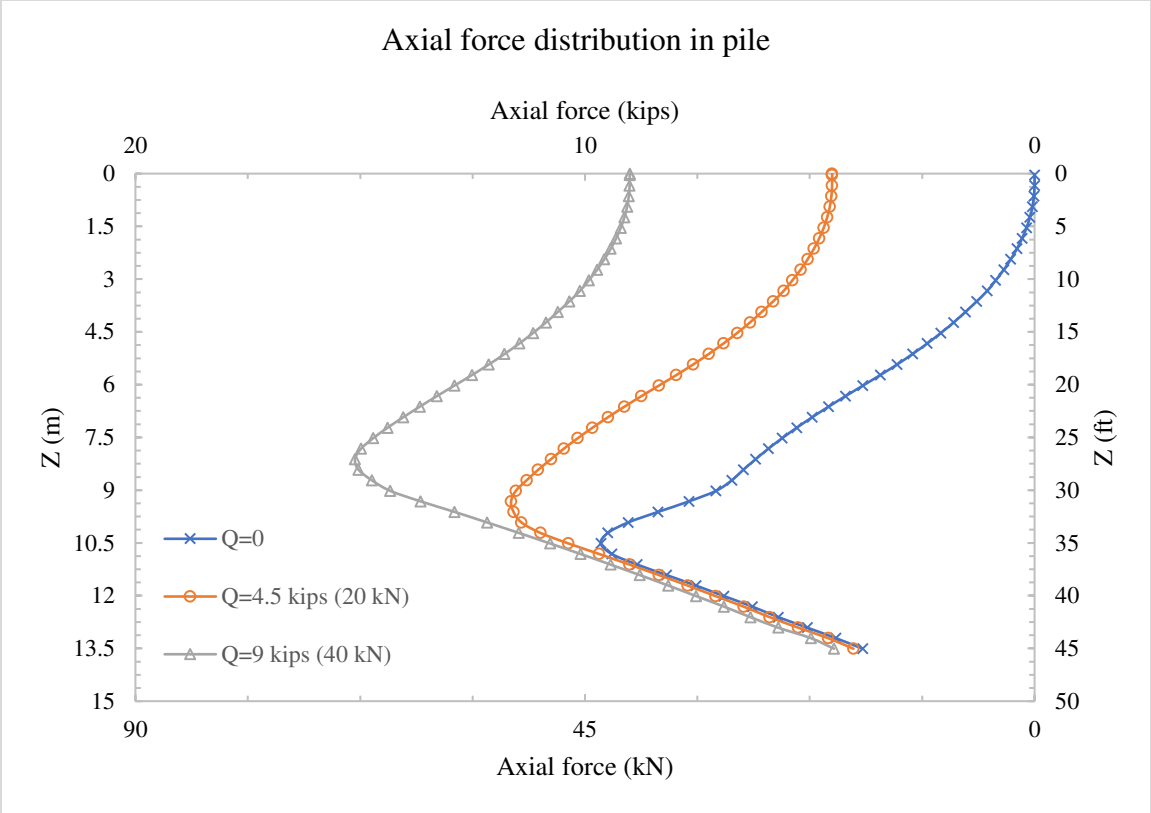

Figure 6.41 Axial force distribution in pile with D_p=6 in (152 *mm*), L_p=45 *ft* (13.7 *m*), and H_b/H_f=0.40

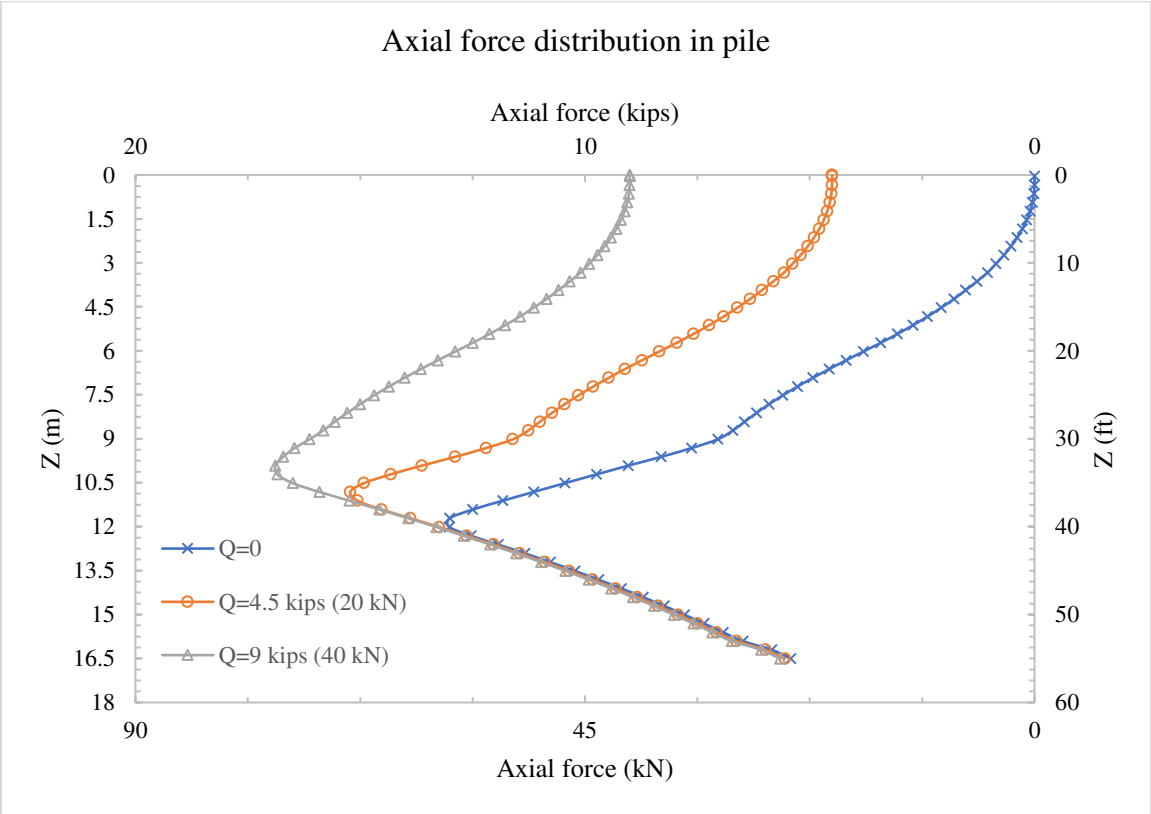

Figure 6.42 Axial force distribution in pile with D_p=6 in (152 *mm*), L_p=45 *ft* (13.7 *m*), and H_b/H_f=0.40

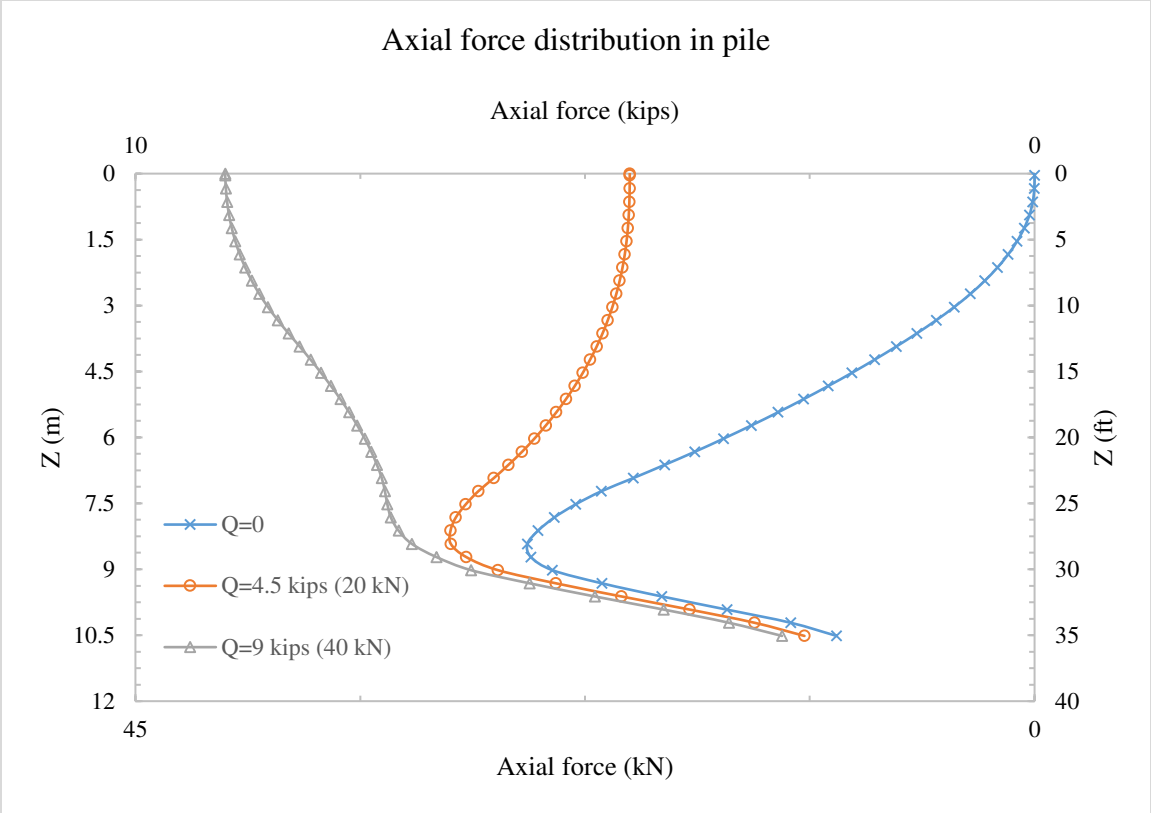

Figure 6.43 Axial force distribution in pile with D_p=6 in (152 *mm*), L_p=35 *ft* (10.7 *m*), and H_b/H_f=0.80

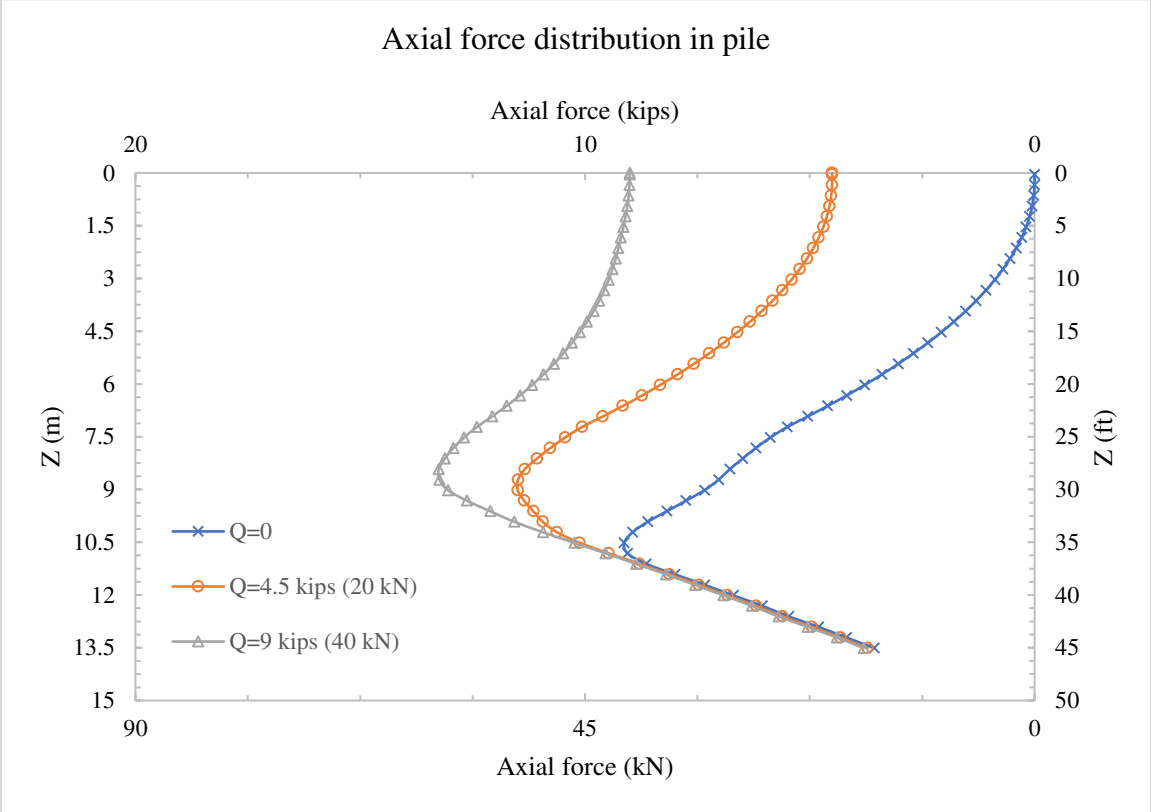

Figure 6.44 Axial force distribution in pile with D_p=6 in (152 *mm*), L_p=45 *ft* (13.7 *m*), and H_b/H_f=0.80

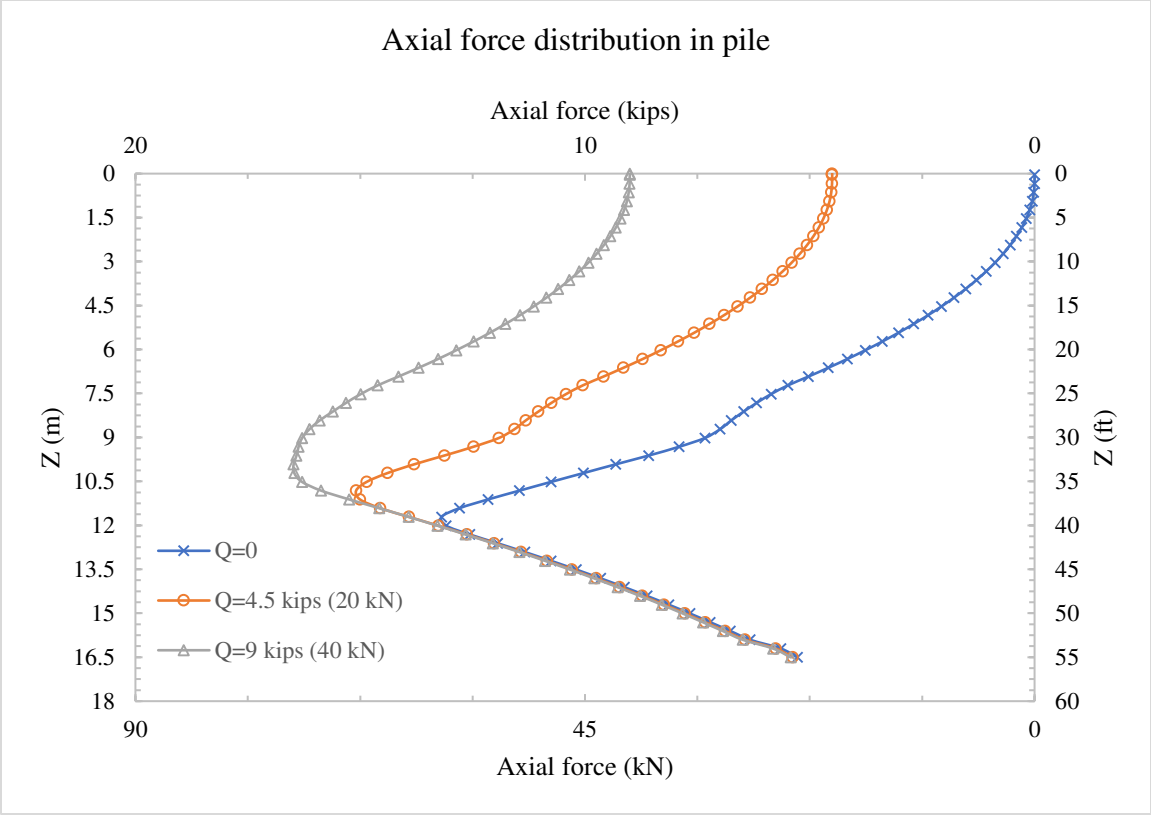

Figure 6.45 Axial force distribution in pile with D_p=6 in (152 *mm*), L_p=55 *ft* (16.8 *m*), and H_b/H_f=0.80

From the above figures, it is clear that the pile-soil systems resisted the applied load using a combination of Q_s and Q_b. This indicates that the soil surrounding and underneath the pile developed enough force that restrained the pile tip from sinking into the soil below it. As a result, the pile was subjected to a downdrag force that was developed due to the consolidation of the surrounding soils. The magnitude of the downdrag force varied depending on the properties of the surrounding soil, pile geometry, and installation time. The neutral point, L_{dd}, appeared to be dependent on the applied load, Q, and the length of pile, L_p. In the above figures, it was noted that L_{dd} shifted upward as Q approached Q_u and shifted downward as L_p increased. These are illustrated in Figures 6.46 and 6.47.

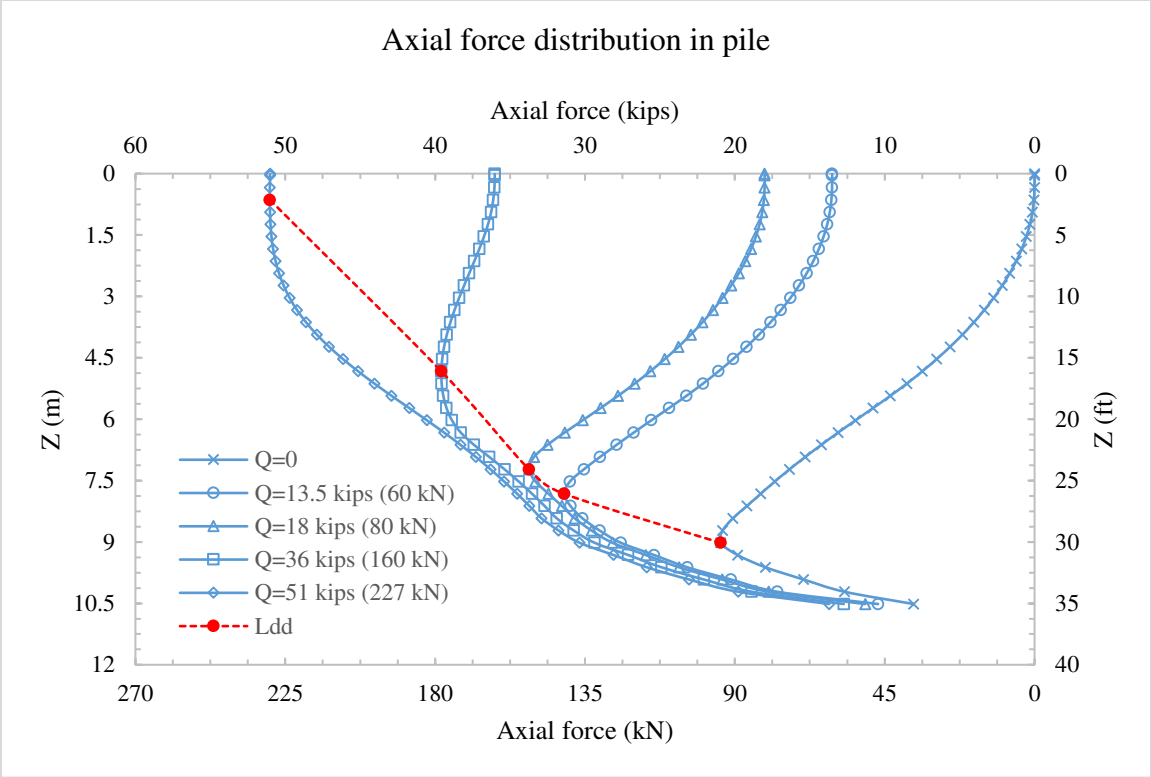

Figure 6.46 Location of L_{dd} with respect to Q

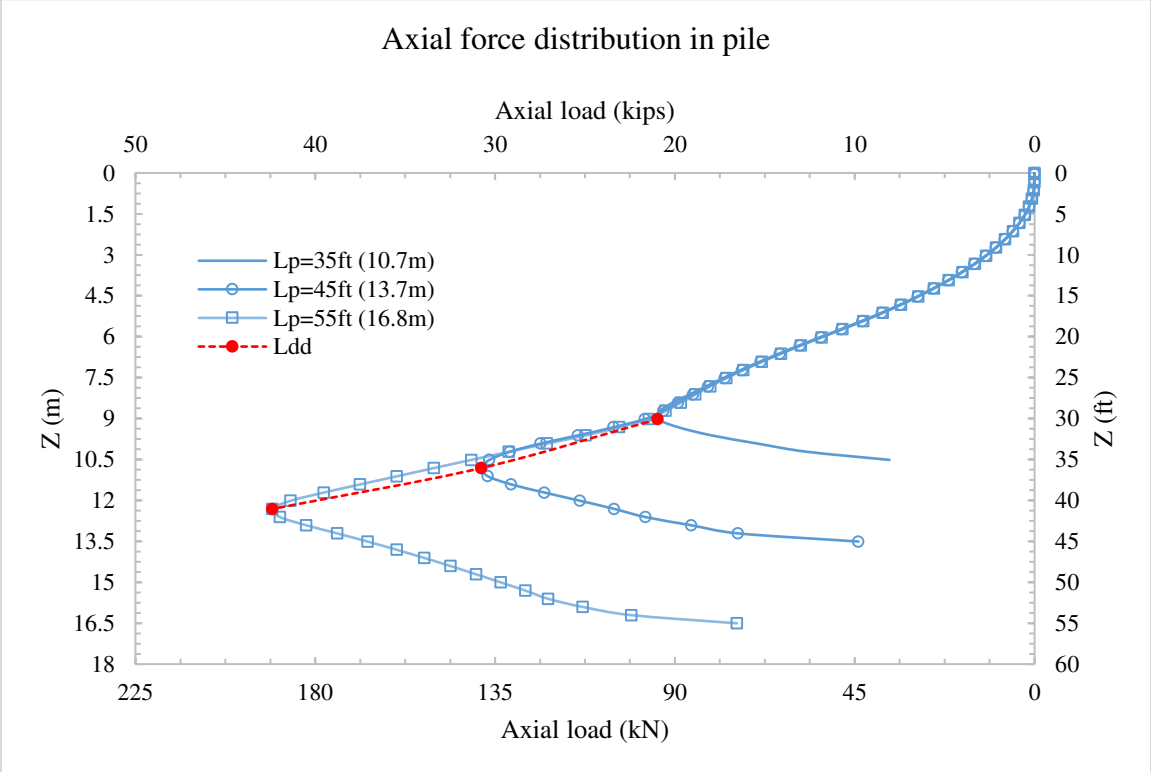

Figure 6.47 Location of L_{dd} with respect to L_p

It was also noted that when backfill material is employed (i.e. $H_b/H_f > 0$), the location of L_{dd} did not change compared to similar pile-soil condition with no backfill material (i.e. $H_b/H_f = 0$). However, the downdrag force, Q_{dd}, decreased significantly as (H_b/H_f) increased, as illustrated in Figure 6.48. This behavior can be attributed to the highly permeable backfill material. By the time the pile is installed, the backfill material would have undergone initial and primary settlement (consolidation), and thus lower forces were encountered in such cases.

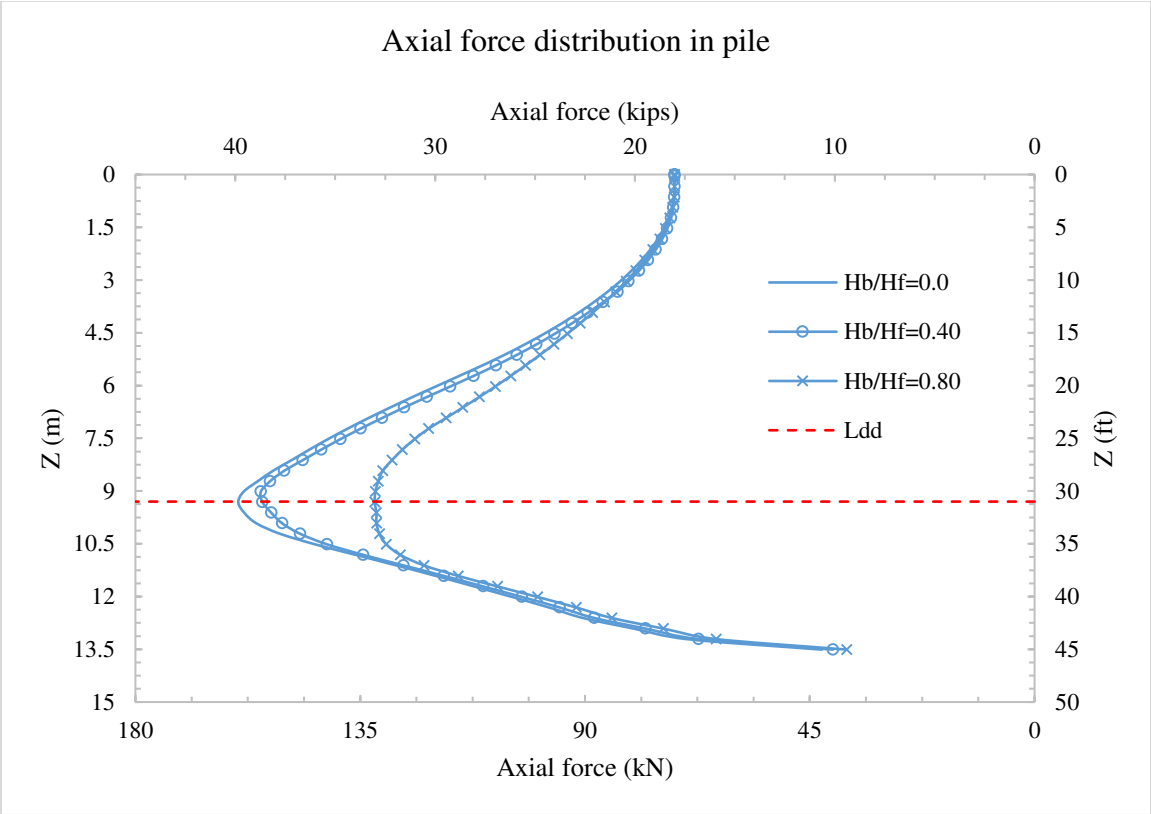

Figure 6.48 Axial force distribution with respect to (H_b/H_f)

6.7.4 Proximity to the abutment wall

As discussed in Chapter 5, the abutment wall has a significant effect on the soil deformation in its vicinity. The influence zone, in which soil deformation is affected by the abutment, depends on the abutment wall to fill height ratio, and can affect the longitudinal soil deformation to a distance of 10-60 *ft* (3-18 *m*) from the bridge abutment. However, a much

smaller pile influence zone was encountered with the simulated pile-soil systems. Figure 6.49 shows the influence pile zone for two pile sizes that embedded in the same soil profile. The figure shows that the pile influence zone was in the range of 1-4 *ft* (0.3-1.2 *m*).

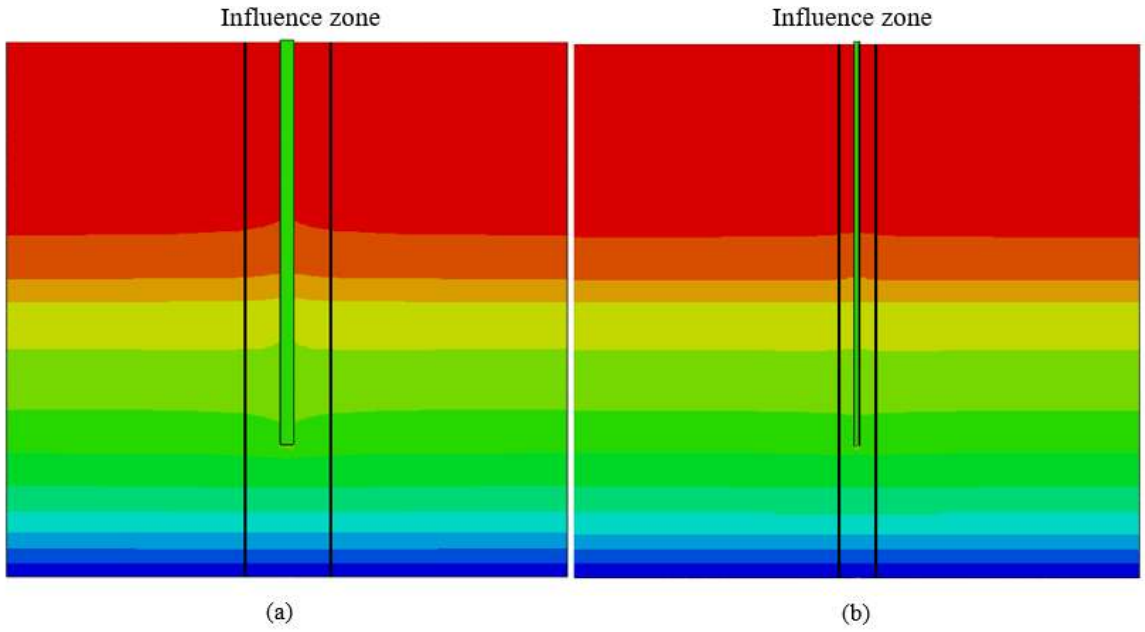

Figure 6.49 Vertical soil deformation contour with respect to pile-soil influence zone (a) D_p = 18 *in* (b) D_p = 6 *in*

This effect, however, could be significant in cases where piles are installed close to the abutment wall. In such cases, detailed analyses must be performed to examine the effect. As for the purposes of this study, it can be concluded that the effect of the pile on the surrounding soil is limited and insignificant, as piles are planned to be installed at least 15 *ft* (4.6 *m*) away from the bridge abutment.

6.8 Evaluating pile head settlement using analytical method

The objective of this phase of the study was to develop empirical relationship that can predict the pile head settlement for a given pile-soil condition. Such an equation would be beneficial in making reliable predictions of the long-term differential settlement of the pile-

supported segmented approach slab system. An empirical equation was derived based upon the FEM results obtained in section 6.7.

A correlation study was carried out in which the correlation coefficient between pile head settlement and various parameters were determined. The study examined the correlation between Δ_{PH} and pile geometry, loading conditions, and soil conditions. Table 6.5 shows the results of this analysis.

Table 6.5 Pearson's correlation coefficient between Δ_{PH} and various pile geometry, loading and soil parameters

Parameter	Δ_{PH}
Δ_{Ps}	0.815
D_p	0.056
L_p	-0.414
E_{avg}	-0.894
G_{avg}	-0.879
Q	0.327
Q_u	-0.161
Q/Q_u	0.483
Q_{dd}	-0.272
L_{dd}	-0.449
Q_{ps}	0.148
L_{ps}	0.076
Q_b	0.106
$G_{avg\text{-}dd}$	-0.789
$G_{avg\text{-}ps}$	-0.638

In the above table,

Δ_{Ps} = Soil post construction settlement = ultimate settlement – settlement at the time of pile installation.

E_{avg} = Average modulus of elasticity of soil along the pile length = $(E_1H_1 + E_2H_2 + \cdots + E_nH_n)/L_p$

G_{avg} = Average shear modulus of soil along the pile length = $(G_1H_1 + G_2H_2 + \cdots + G_nH_n)/L_p$

$G_{avg\text{-}dd}$ = Average shear modulus of soil along the pile length within downdrag zone = $(G_1H_1 + G_2H_2 + \cdots + G_nH_n)/L_{dd}$

$G_{avg\text{-}ps}$ = Average shear modulus of soil along the pile length within positive skin friction zone = $(G_1H_1 + G_2H_2 + \cdots + G_nH_n)/L_{ps}$

Table 6.5 shows that strong correlation exists between Δ_{PH} and Δ_{Ps}, E_{avg}, G_{avg}, $G_{avg\text{-}dd}$ and $G_{avg\text{-}ps}$. This indicates that Δ_{PH} could be evaluated using the shear deformation along the sides of the pile and axial deformation underneath the tip of the pile. Accordingly, a multi-parameter linear regression analysis was carried out in which Δ_{PH} was expressed in terms of Δ_{Ps}, E_{avg}, G_{avg}, $G_{avg\text{-}dd}$ and $G_{avg\text{-}ps}$ as follows:

$$\Delta_{PH} = \Delta_{PS} + \alpha \frac{Q_{dd}\, L_{dd-inf}}{A_s G_{avg-dd}} + \beta \frac{Q_{ps} L_{ps-inf}}{A_s G_{avg-ps}} + \eta \frac{Q_b L_{b-inf}}{A_p E_b} + C \qquad 6\text{-}7$$

Where

E_b = Modulus of elasticity of soil underneath the pile tip.

A_s = Surface area of the pile.

$L_{dd\text{-}inf}$ = The length of the influence zone of the downdrag.

$L_{ps\text{-}inf}$ = The length of the influence zone of the positive skin friction.

$L_{b\text{-}inf}$ = The length of the influence zone underneath the pile tip.

α, β, η, and C = Regression parameters.

Furthermore, it was assumed that $L_{dd\text{-}inf}$, $L_{ps\text{-}inf}$, and $L_{dd\text{-}inf}$ can be incorporated into parameters α, β,and η, respectively, and thus removed from equation 6-7. Accordingly, equation 6-7 can be rewritten as:

$$\Delta_{PH} = \Delta_{PS} + \alpha \frac{Q_{dd}}{D_p L_{dd} G_{avg-dd}} + \beta \frac{Q_{ps}}{D_p L_{ps} G_{avg-ps}} + \eta \frac{Q_b}{D_p^2 E_b} + C \qquad 6\text{-}8$$

A regression analysis was conducted using the method of least squares to determine the best fit parameters for the above relationship. Table 6.6 shows the result for parameters α, β, η, and C.

Table 6.6 Regression parameters values for equation 6-8

Parameter	Value
α	-166.046
β	40.812
η	3.215
C	-0.222
R^2	0.878
S_{est}	0.203

The final empirical equation was evaluated by substituting the parameter values, found in the above table, into equation 6-8 as follows:

$$\Delta_{PH} = \Delta_{PS} - 166 \frac{Q_{dd}}{D_p L_{dd} G_{avg-dd}} + 41 \frac{Q_{ps}}{D_p L_{ps} G_{avg-ps}} + 3.2 \frac{Q_b}{D_p^2 E_b} - 0.2 \qquad 6\text{-}9$$

Equation 6-9 provides an empirical estimation of the pile head settlement for frictional or semi-frictional piles. This empirical equation has resulted in a coefficient of determination R^2 = 0.867, and standard error of estimate S_{est} = 0.2 *in* (5.0 *mm*) when considering the analysis result. This indicates that the value of pile head settlement can be predicted reasonably well using the shear and axial deformations of the pile-soil system. Figure 6.50 shows the simulated versus predicted pile head settlement, which clearly illustrates the accuracy of the proposed equation.

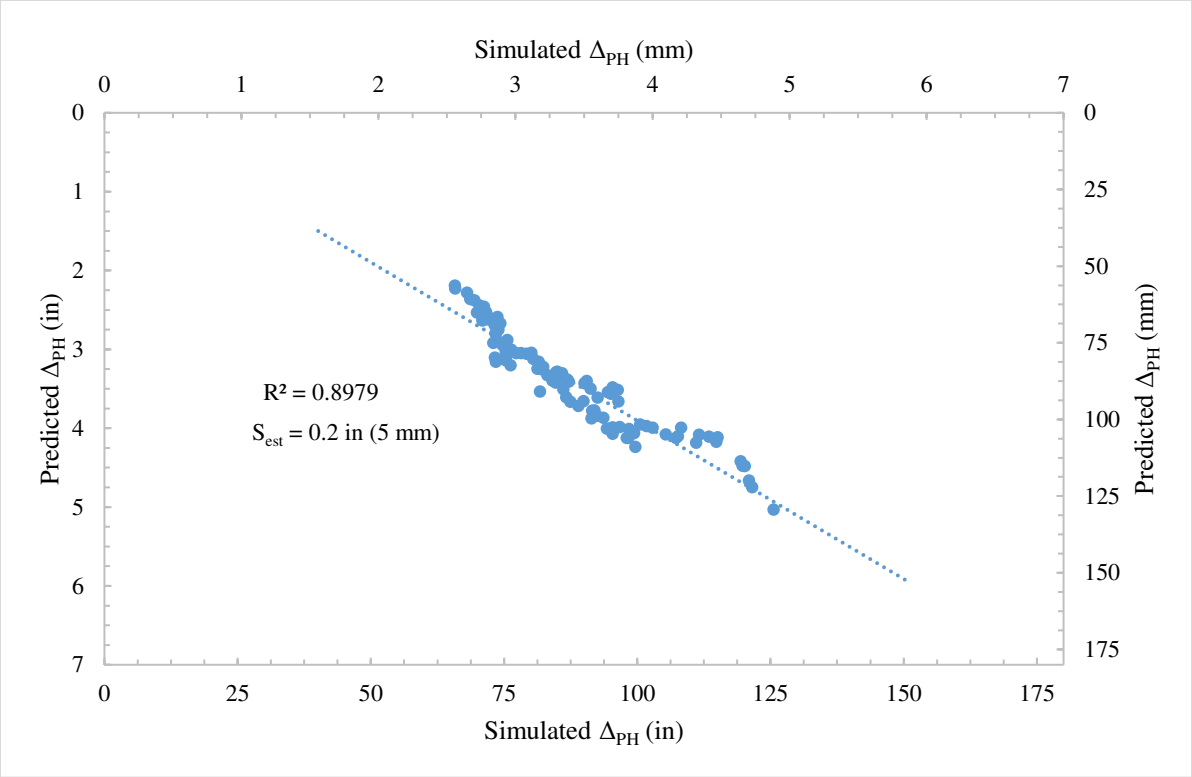

Figure 6.50 Simulated versus predicted pile head settlement

6.9 Evaluating load distribution along the pile using analytical method

The objective of this phase of the study was to develop empirical relationships that can predict the load distribution along the pile for a given pile-soil condition. This include Q_{dd}, L_{dd}, Q_{ps}, L_{ps}, and Q_b.

In this analysis, Q_{dd} and Q_{ps} were assumed to be fully mobilized, and thus, the β-method was used to estimate the amount of friction between the pile and soil (equation 6-2). As a result, the following linear relationship was obtained:

$$Q_{dd/ps} = \left(1 + 0.45\frac{H_b}{H_e}\right)\int_0^{L_{dd/ps}} f_s p\, dz - 1.30 \qquad 6\text{-}10$$

Equation 6-10 provides an estimation of the downdrag and positive skin friction forces acting on the pile-soil system. This equation has resulted in an average coefficient of

determination $R^2 = 0.941$, and an average standard error of estimate $S_{est} = 2.4$ *kips* (11 *kN*). This indicates that the value of skin friction force can be predicted accurately using the β-method. Figures 6.51 and 6.52 show the simulated versus predicted Q_{dd} and Q_{ps} values, respectively.

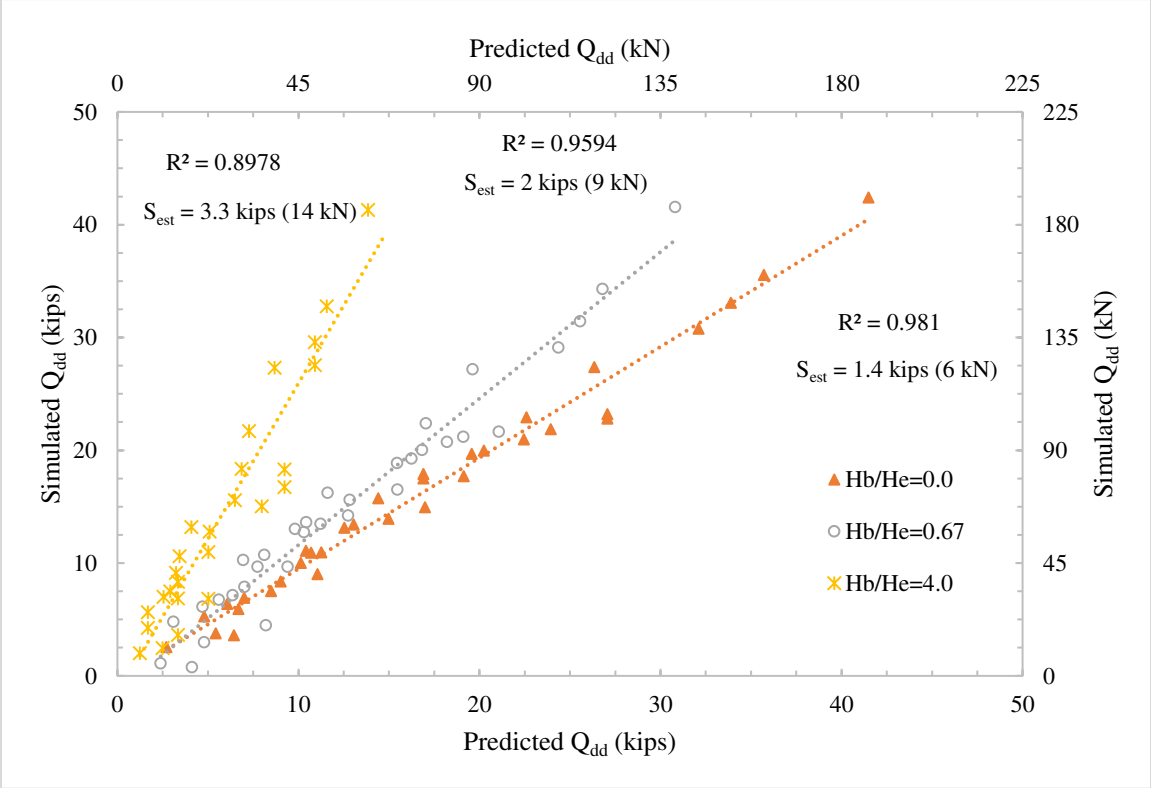

Figure 6.51 Simulated versus predicted Q_{dd}

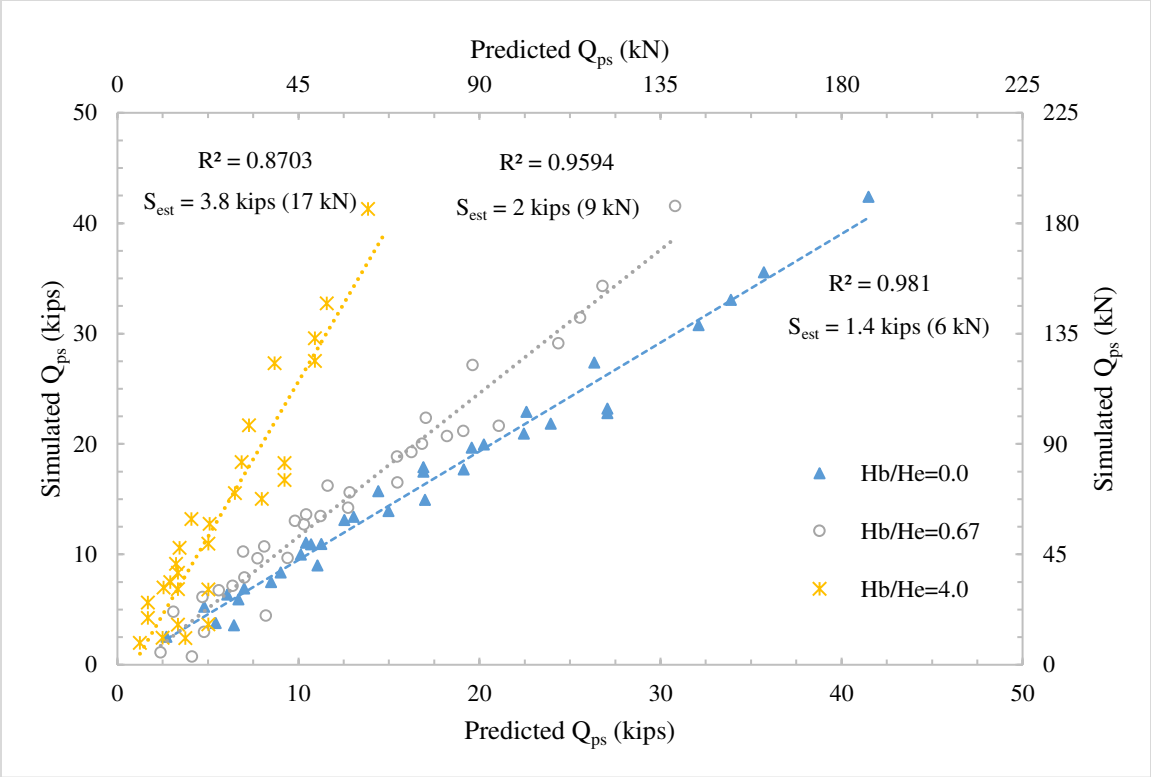

Figure 6.52 Simulated versus predicted (Q_{ps})

Care must be taken as equation 6-10 can only be used when L_{dd} and L_{ps} are known. Bowles (1997) provides an equation to estimate L_{dd} when $Q = 0$ as follows:

$$L_{dd} = \frac{L_p - H_f}{L_{dd}}\left(\frac{L_p - H_f}{2} + \frac{\gamma_f' H_f}{\gamma_n'}\right) - \frac{2\gamma_f' H_f}{\gamma_n'} \qquad 6\text{-}11$$

Equation 6-11 appears to accurately predict the location of the neutral point for all simulated piles with ($Q = 0$). Figure 6.53 shows the simulated versus predicted values for L_{dd} using equation 6-11.

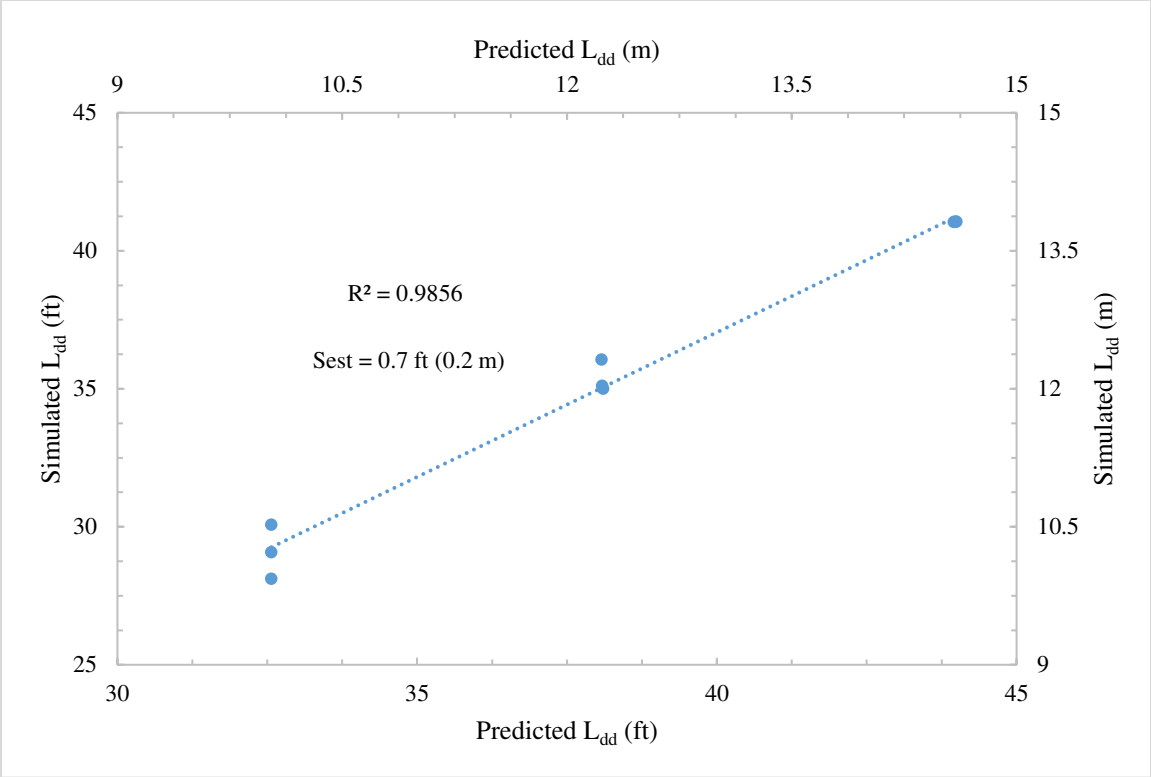

Figure 6.53 Simulated versus predicted L_{dd}

However, L_{dd} changes as a function of Q (Figure 6.46). To evaluate this change, the simulated pile load distribution, Figures 6.19 through 6.45, were reconstructed such that the length of the pile, L_p, was normalized, i.e. Z/L_p. In addition, the axial load curves were idealized into linear curves. This was to address the changes of L_{dd} in a linear fashion that would simply the analysis, and thus convenient prediction can be made. Figures 6.54 through 6.80 show the normalized/idealized pile load curves.

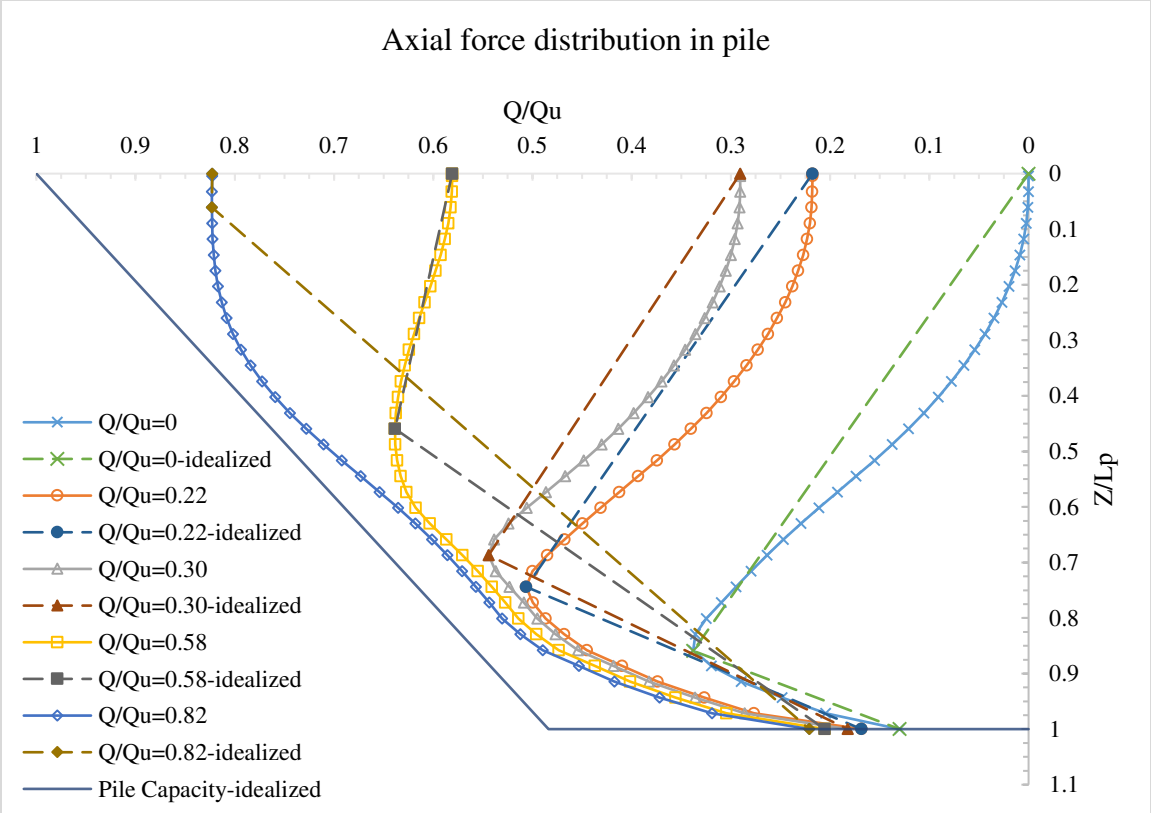

Figure 6.54 Normalized/Idealized pile load with D_p=18 in (460 *mm*), L_p=35 *ft* (10.7 *m*), and H_b/H_f=0

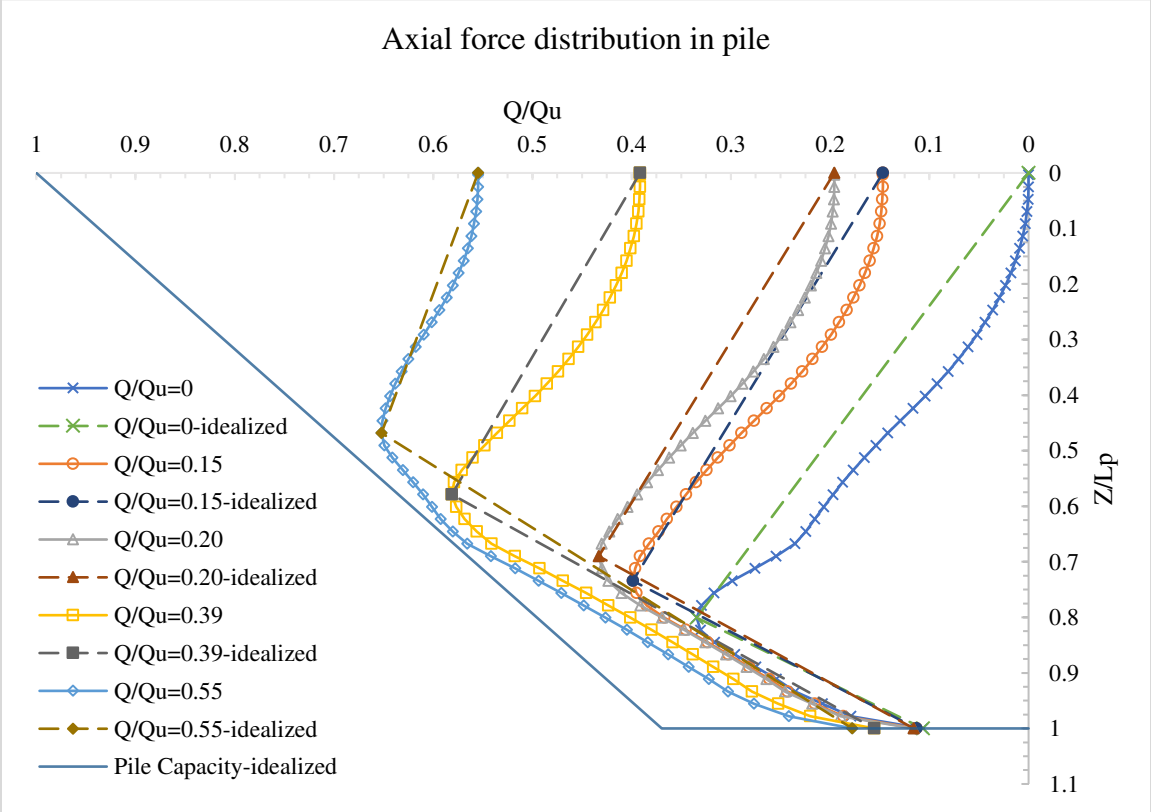

Figure 6.55 Normalized/Idealized pile load with D_p=18 in (460 *mm*), L_p=45 *ft* (13.7 *m*), and H_b/H_f=0

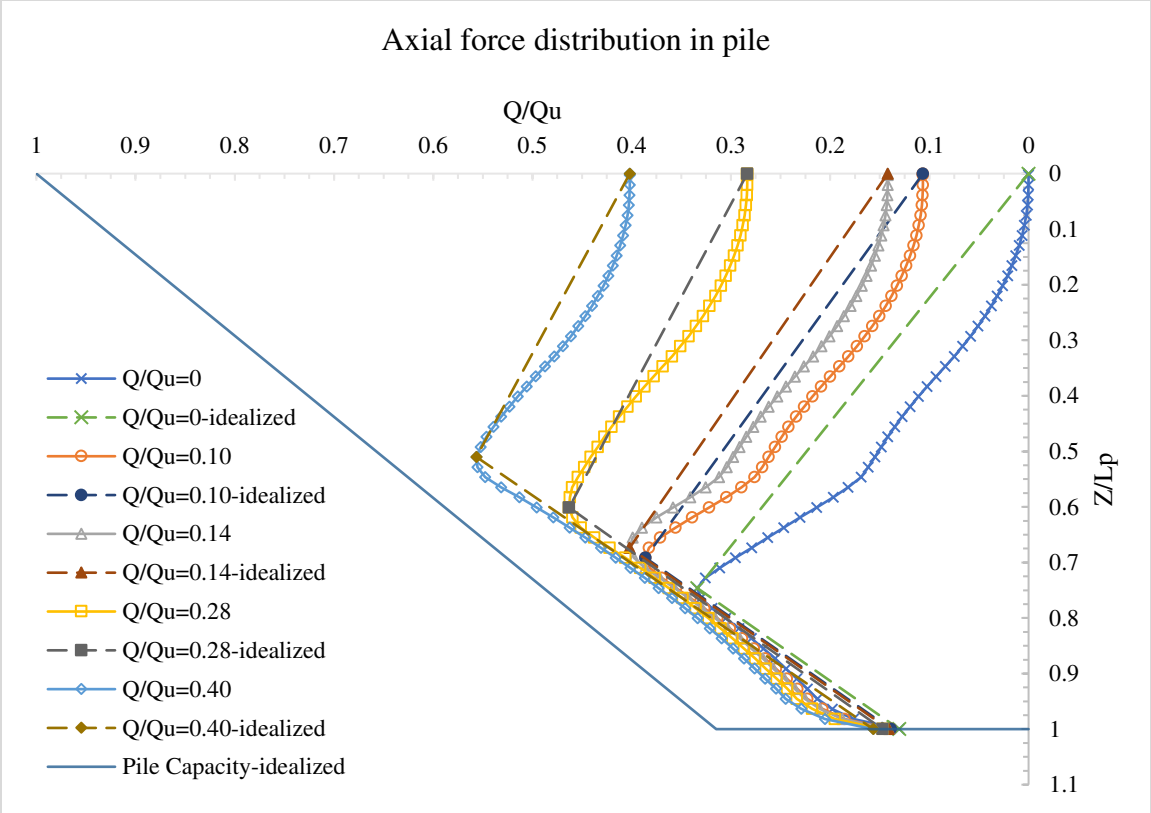

Figure 6.56 Normalized/Idealized pile load with D_p=18 in (460 *mm*), L_p=55 *ft* (16.8 *m*), and H_b/H_f=0

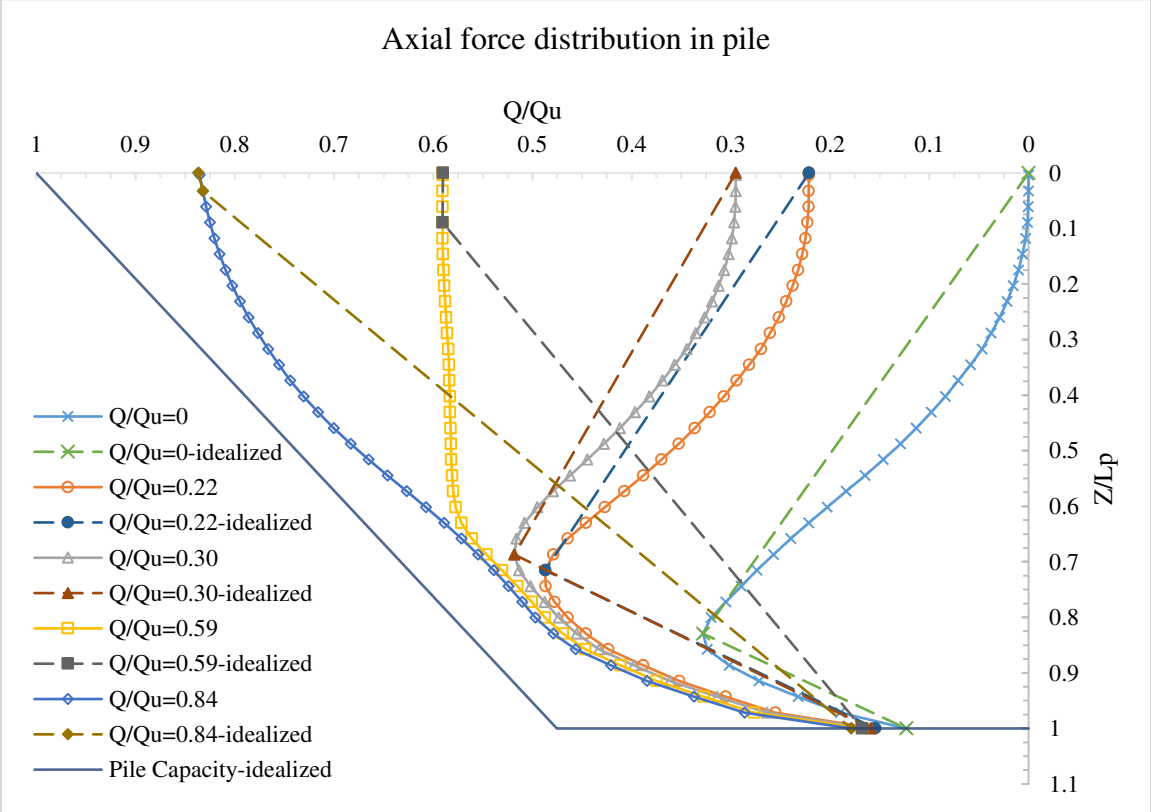

Figure 6.57 Normalized/Idealized pile load with D_p=18 in (460 *mm*), L_p=35 *ft* (10.7 *m*), and H_b/H_f=0.40

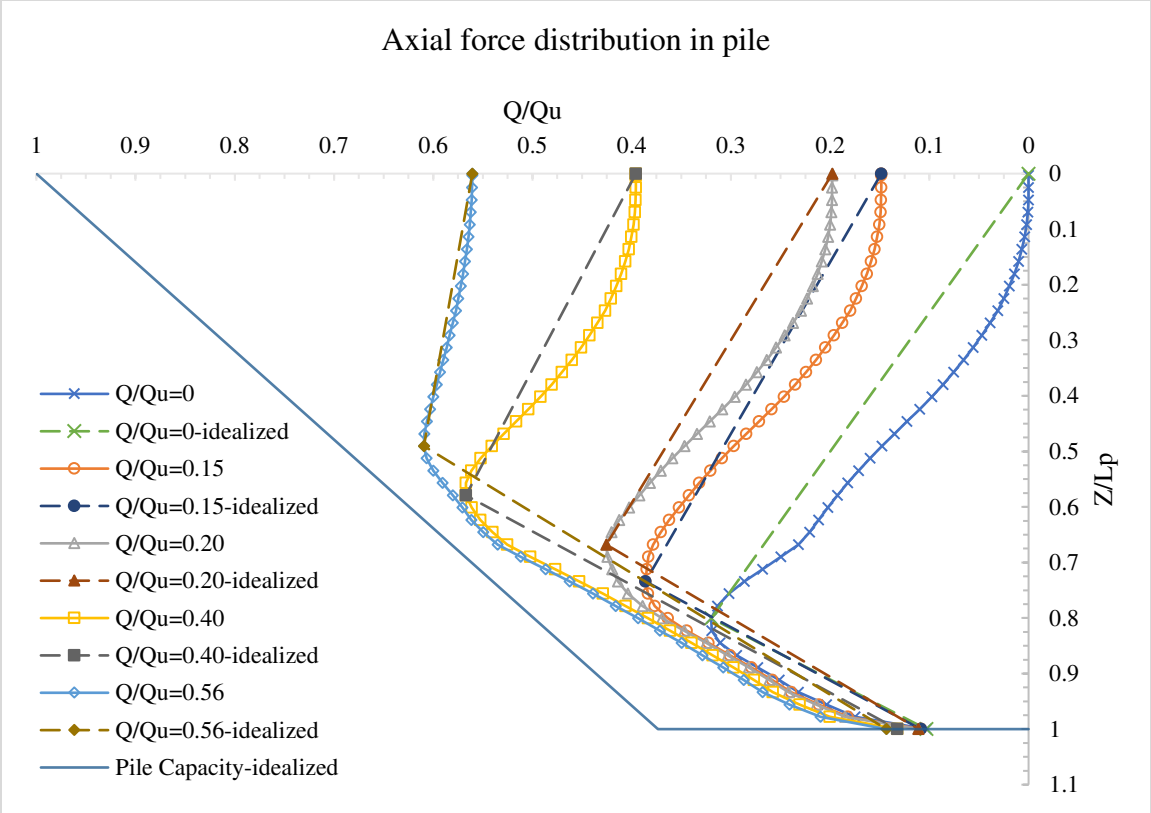

Figure 6.58 Normalized/Idealized pile load with D_p=18 in (460 *mm*), L_p=45 *ft* (13.7 *m*), and H_b/H_f=0.40

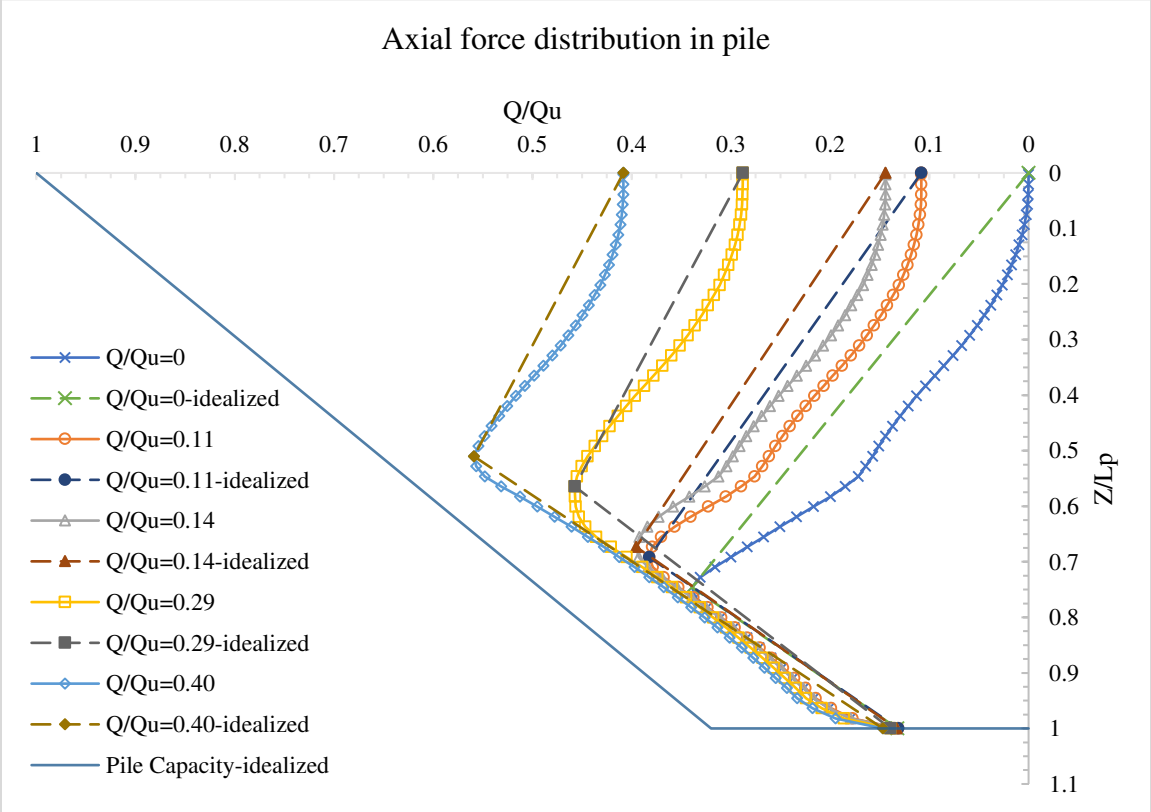

Figure 6.59 Normalized/Idealized pile load with D_p=18 in (460 *mm*), L_p=55 *ft* (16.8 *m*), and H_b/H_f=0.40

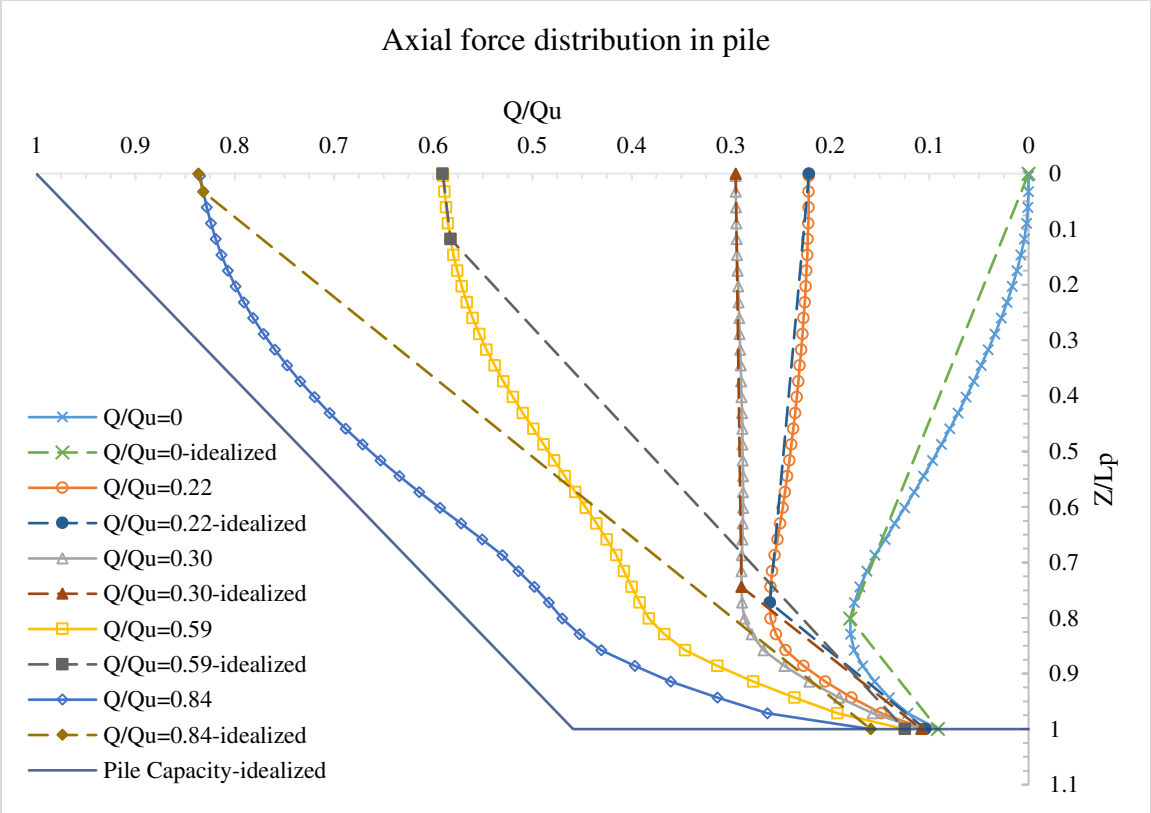

Figure 6.60 Normalized/Idealized pile load with D_p=18 in (460 *mm*), L_p=35 *ft* (10.7 *m*), and H_b/H_f=0.80

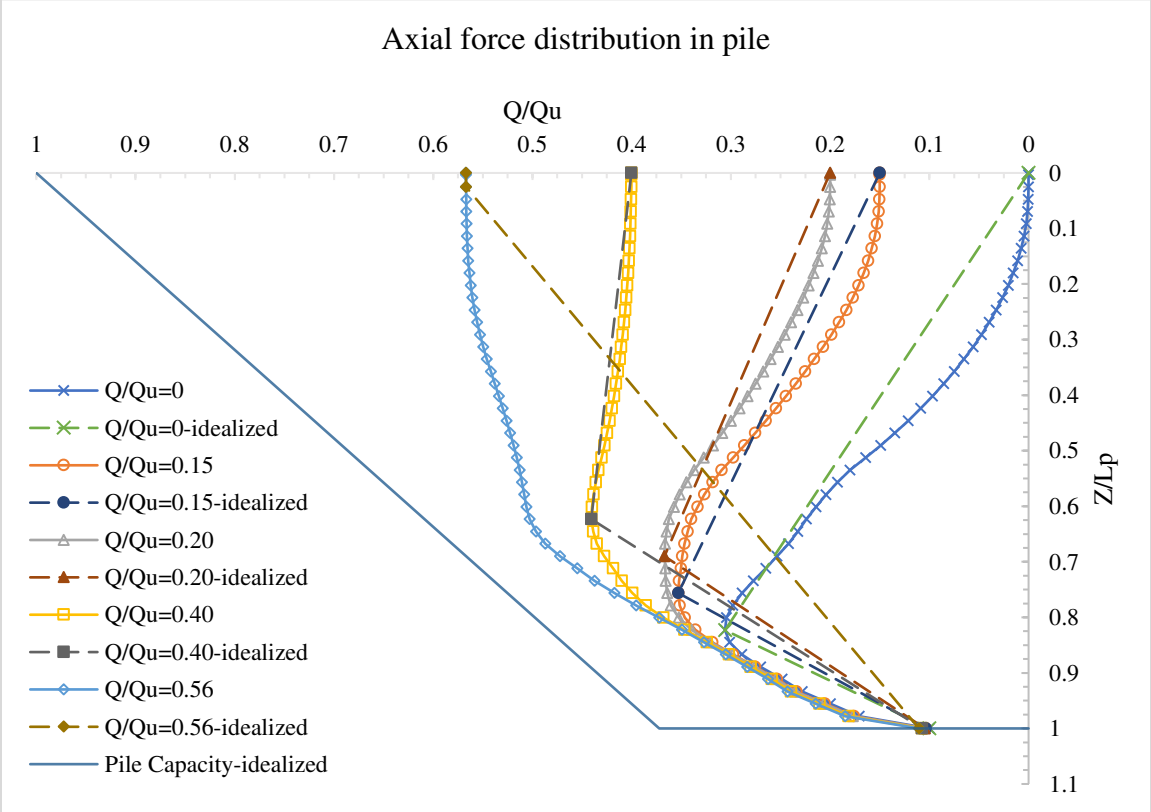

Figure 6.61 Normalized/Idealized pile load with D_p=18 in (460 *mm*), L_p=45 *ft* (13.7 *m*), and H_b/H_f=0.80

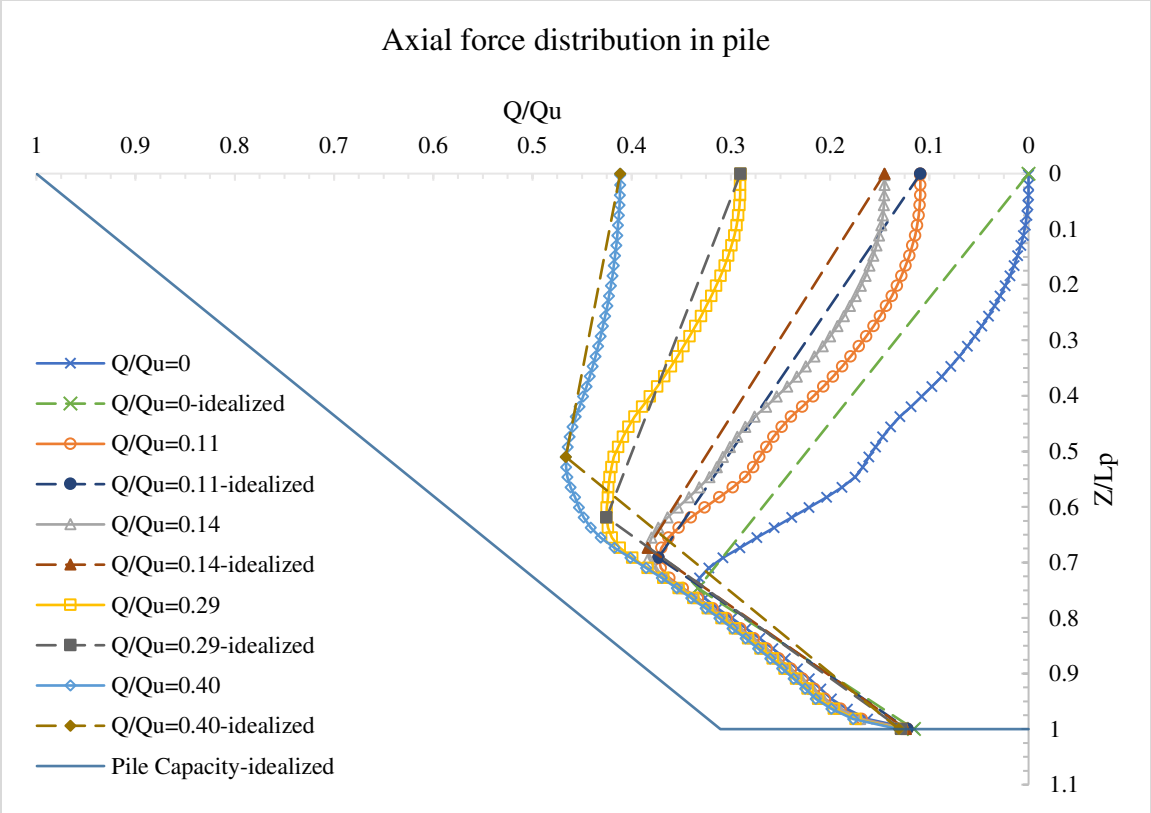

Figure 6.62 Normalized/Idealized pile load with D_p=18 in (460 *mm*), L_p=55 *ft* (16.8 *m*), and H_b/H_f=0.80

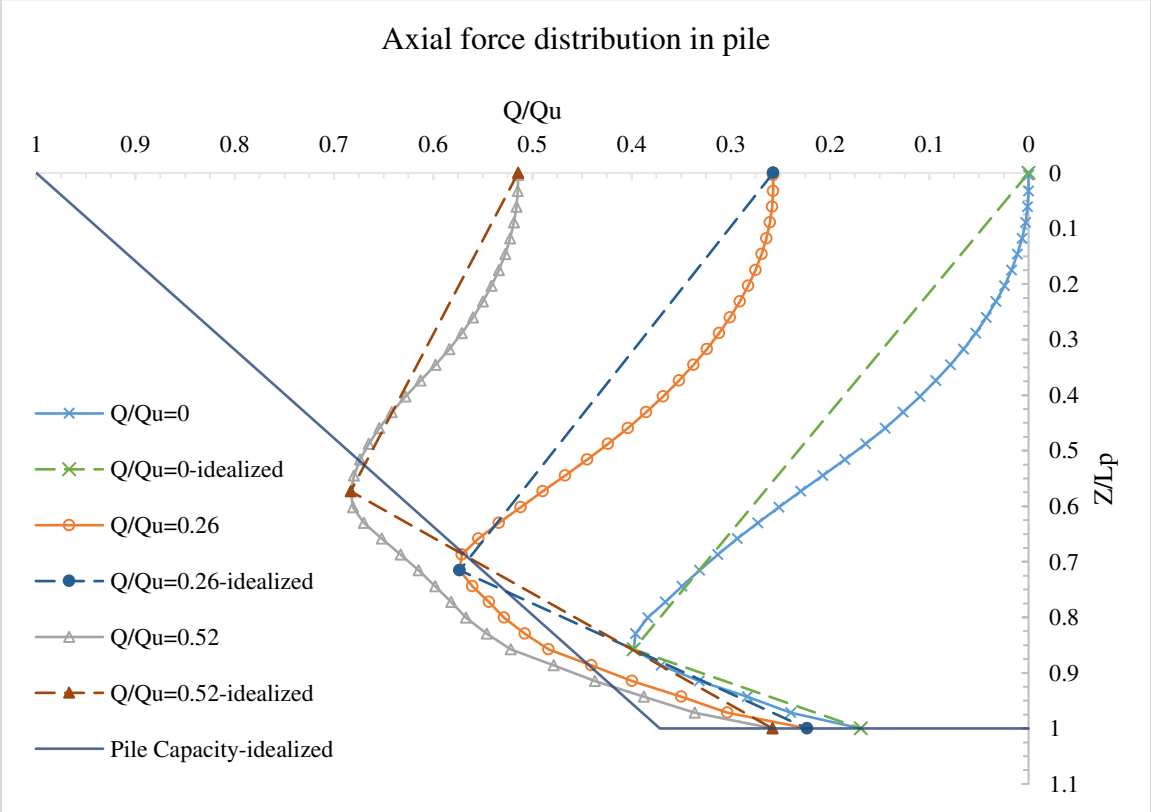

Figure 6.63 Normalized/Idealized pile load with D_p=12 in (305 *mm*), L_p=35 *ft* (10.7 *m*), and H_b/H_f=0.0

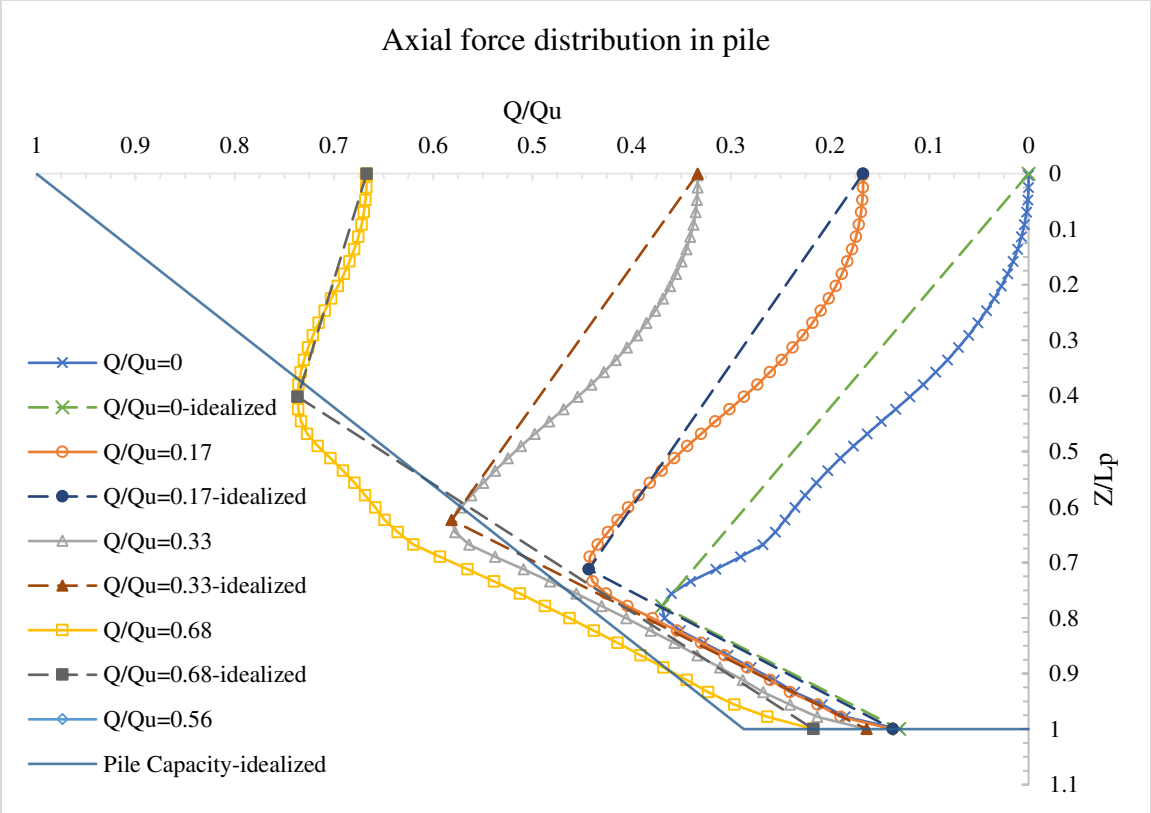

Figure 6.64 Normalized/Idealized pile load with D_p=12 in (305 *mm*), L_p=45 *ft* (13.7 *m*), and H_b/H_f=0.0

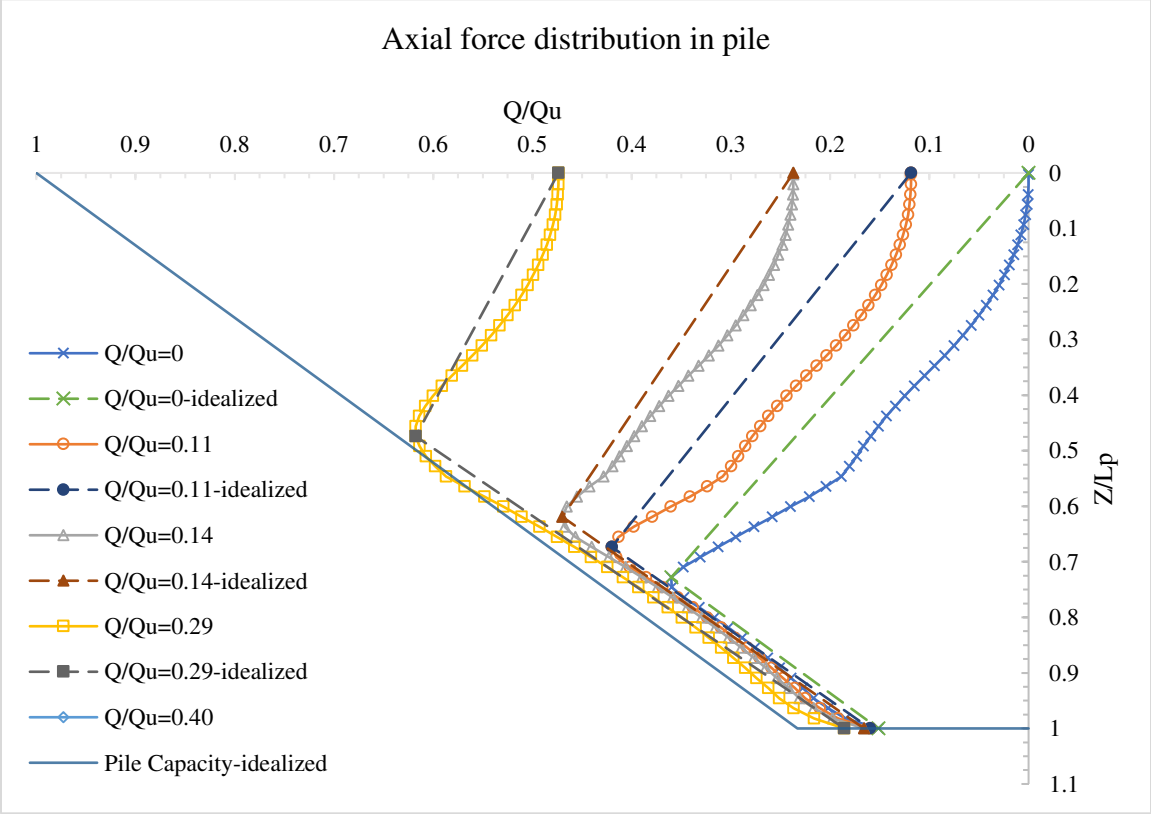

Figure 6.65 Normalized/Idealized pile load with D_p=12 in (305 *mm*), L_p=55 *ft* (16.8 *m*), and H_b/H_f=0.0

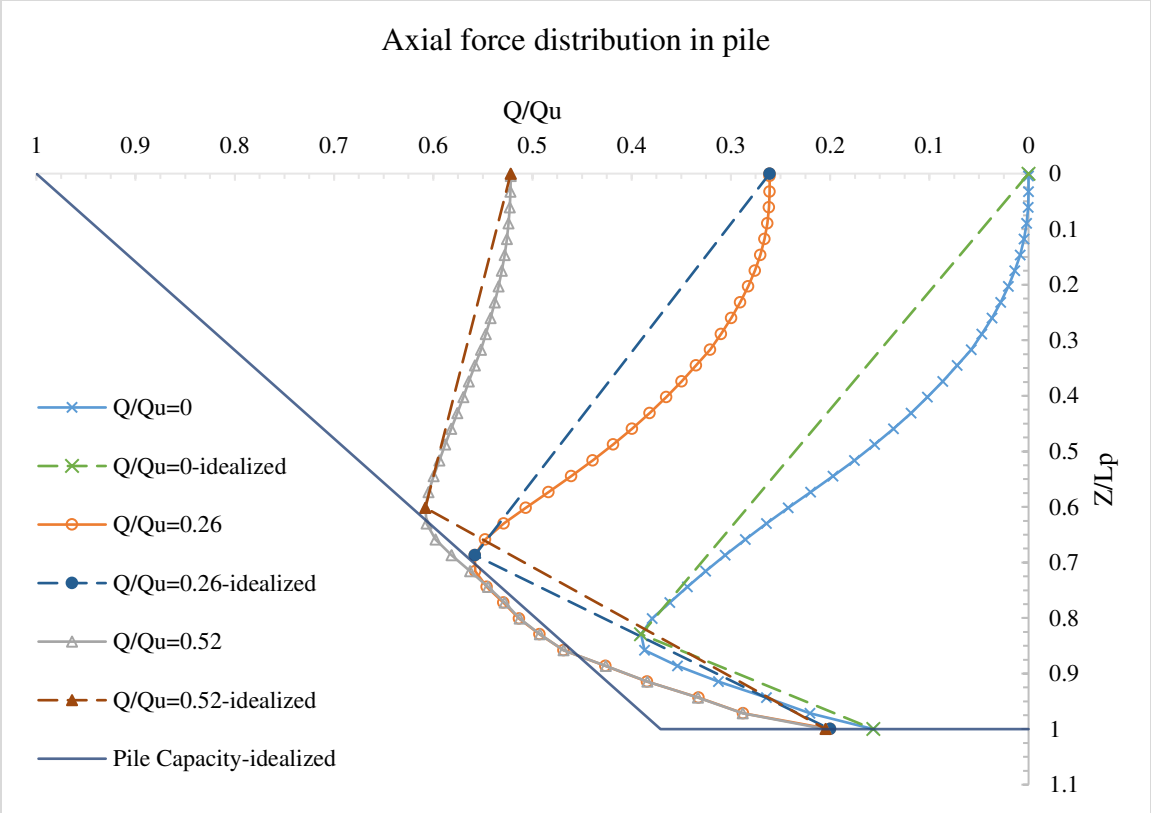

Figure 6.66 Normalized/Idealized pile load with D_p=12 in (305 *mm*), L_p=35 *ft* (10.7 *m*), and H_b/H_f=0.40

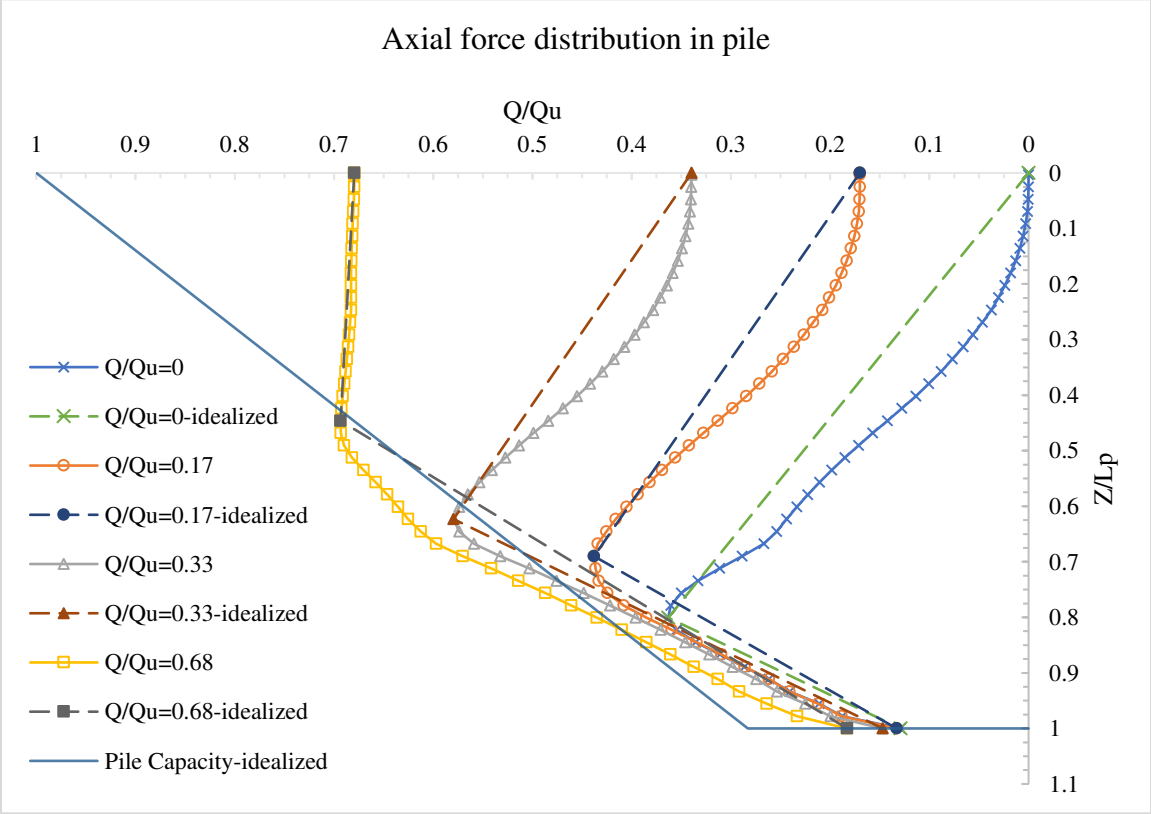

Figure 6.67 Normalized/Idealized pile load with D_p=12 in (305 *mm*), L_p=45 *ft* (13.7 *m*), and H_b/H_f=0.40

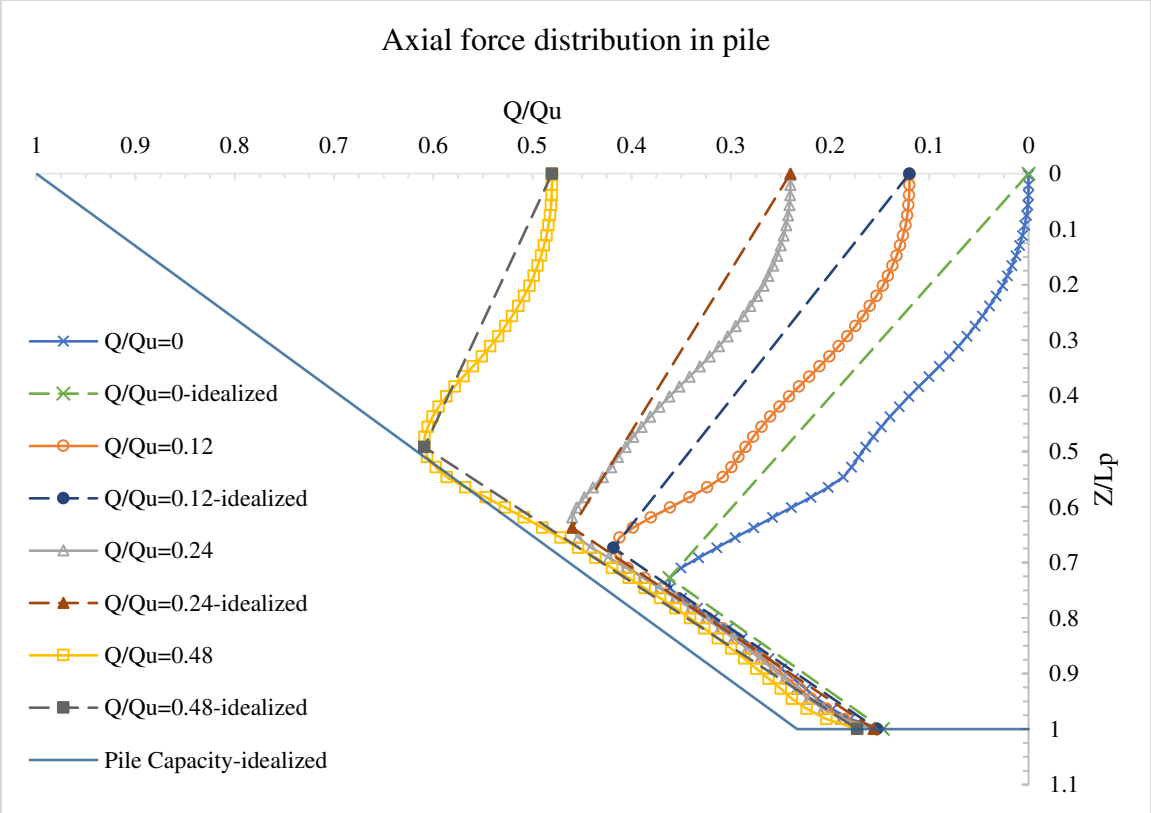

Figure 6.68 Normalized/Idealized pile load with D_p=12 in (305 *mm*), L_p=55 *ft* (16.8 *m*), and H_b/H_f=0.40

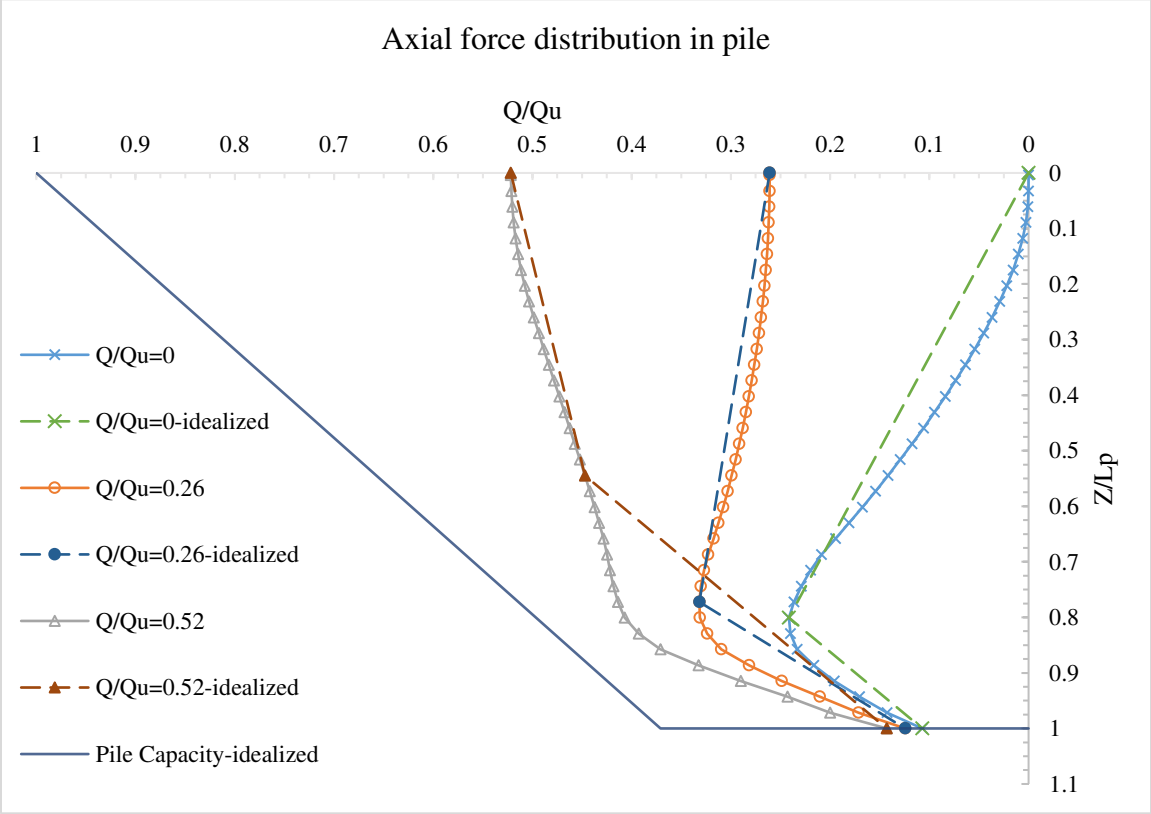

Figure 6.69 Normalized/Idealized pile load with D_p=12 in (305 *mm*), L_p=35 *ft* (10.7 *m*), and H_b/H_f=0.80

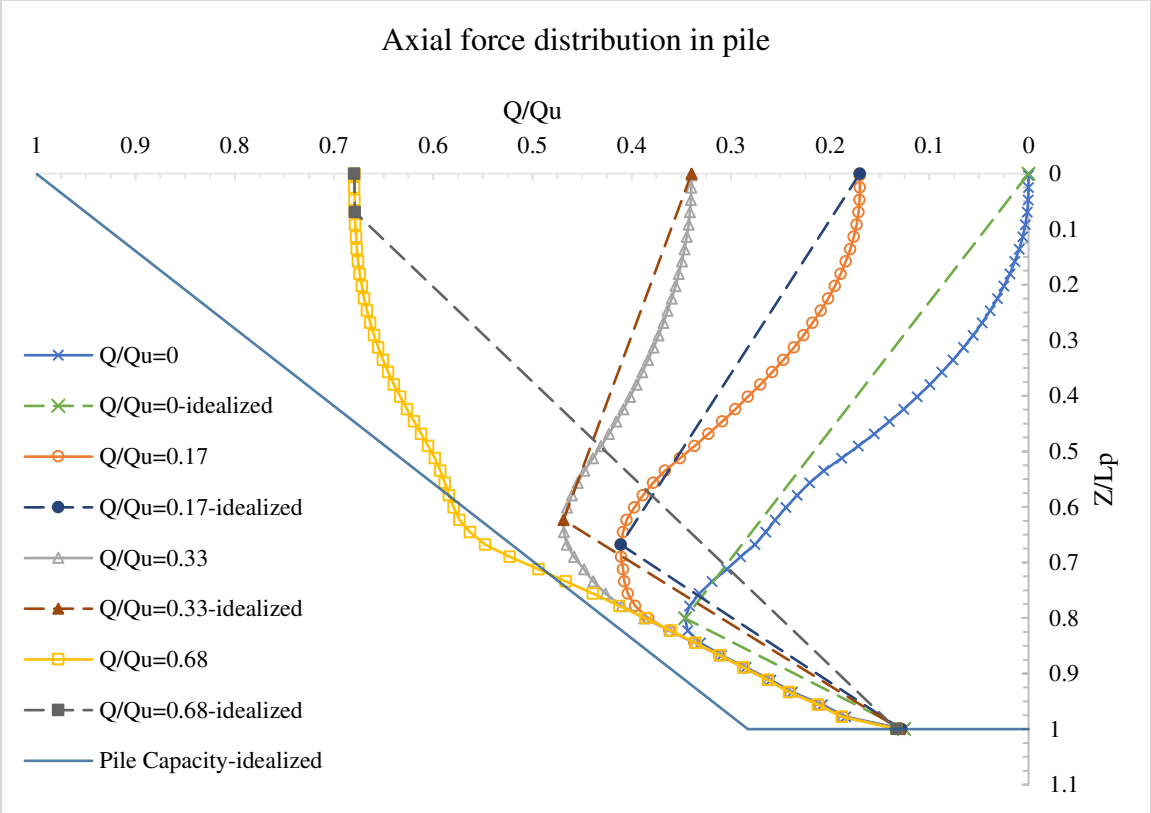

Figure 6.70 Normalized/Idealized pile load with D_p=12 in (305 *mm*), L_p=45 *ft* (13.7 *m*), and H_b/H_f=0.80

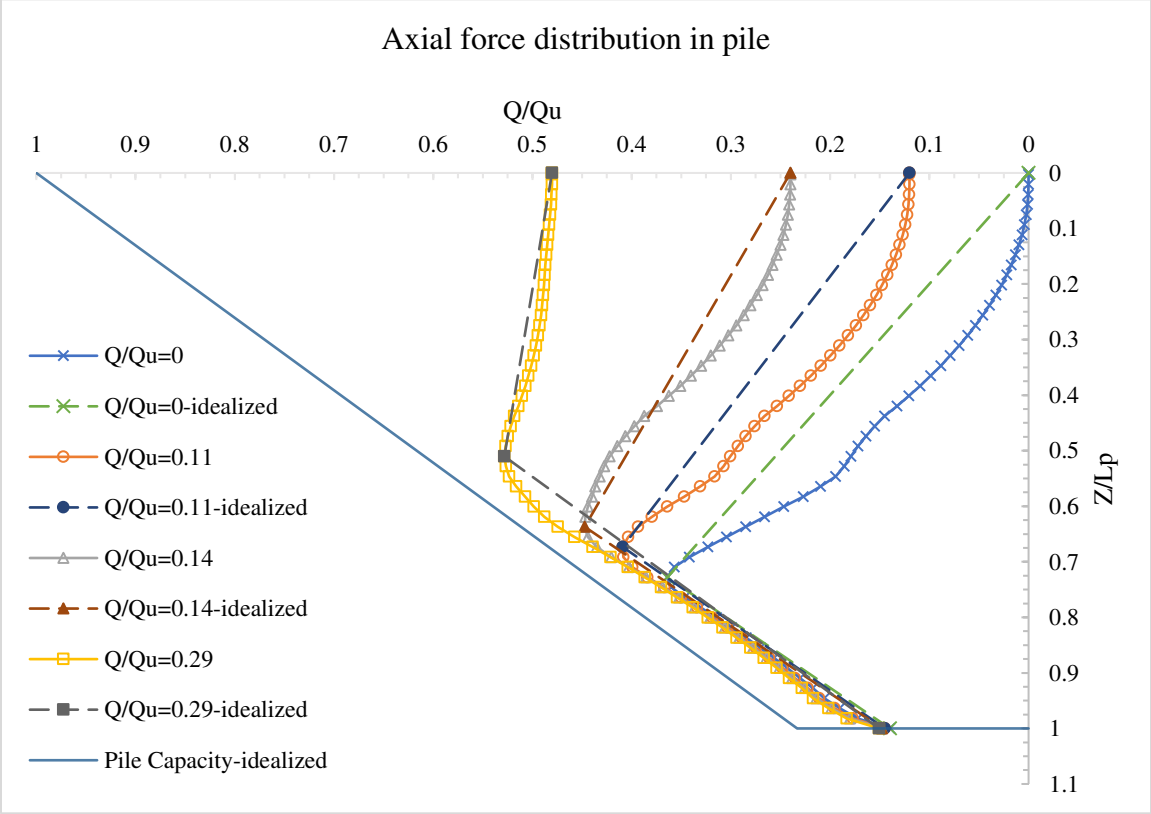

Figure 6.71 Normalized/Idealized pile load with D_p=12 in (305 *mm*), L_p=55 *ft* (16.8 *m*), and H_b/H_f=0.80

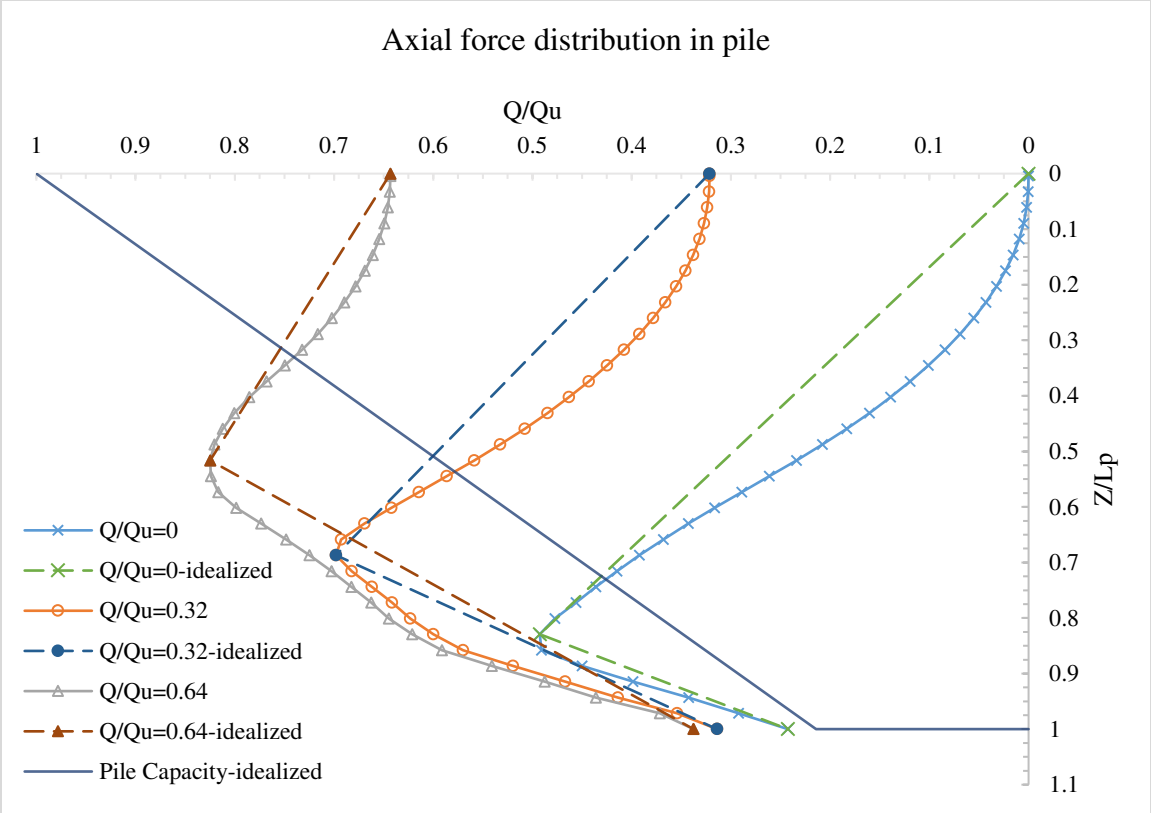

Figure 6.72 Normalized/Idealized pile load with D_p=6 in (152 *mm*), L_p=35 *ft* (10.7 *m*), and H_b/H_f=0.0

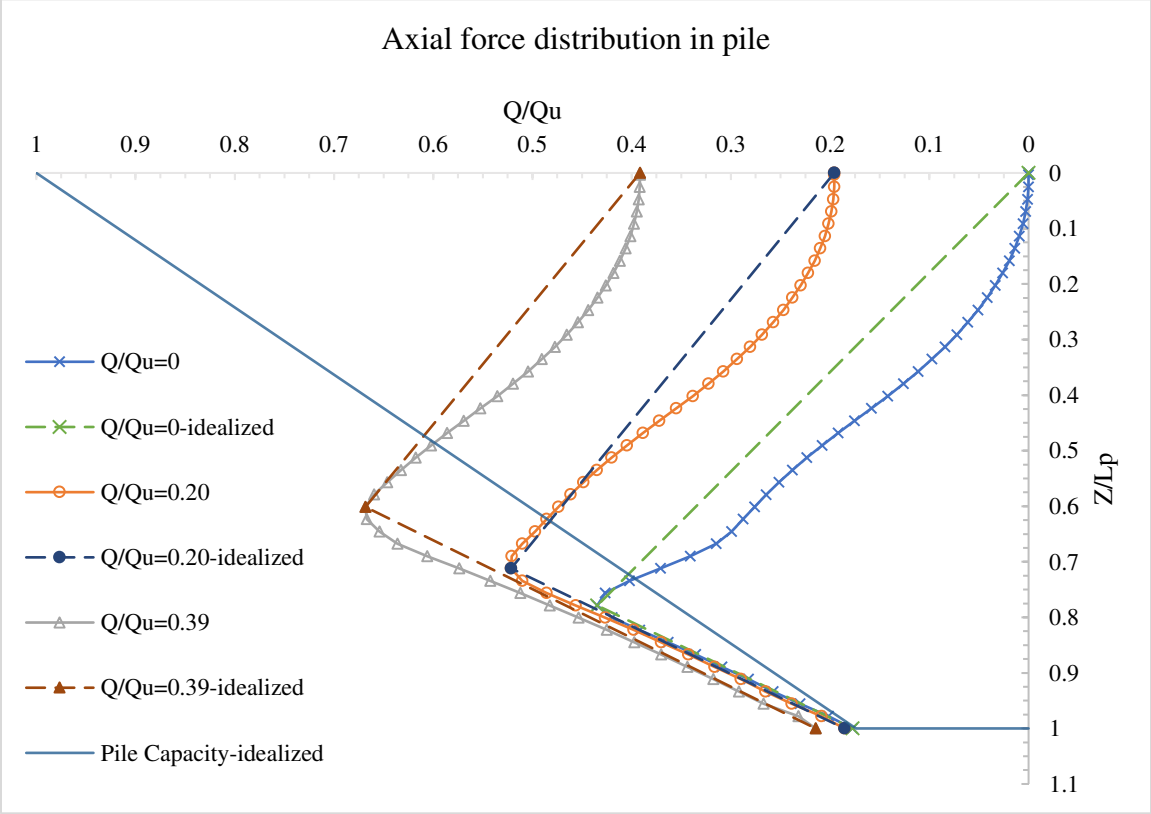

Figure 6.73 Normalized/Idealized pile load with D_p=6 in (152 *mm*), L_p=45 *ft* (13.7 *m*), and H_b/H_f=0.0

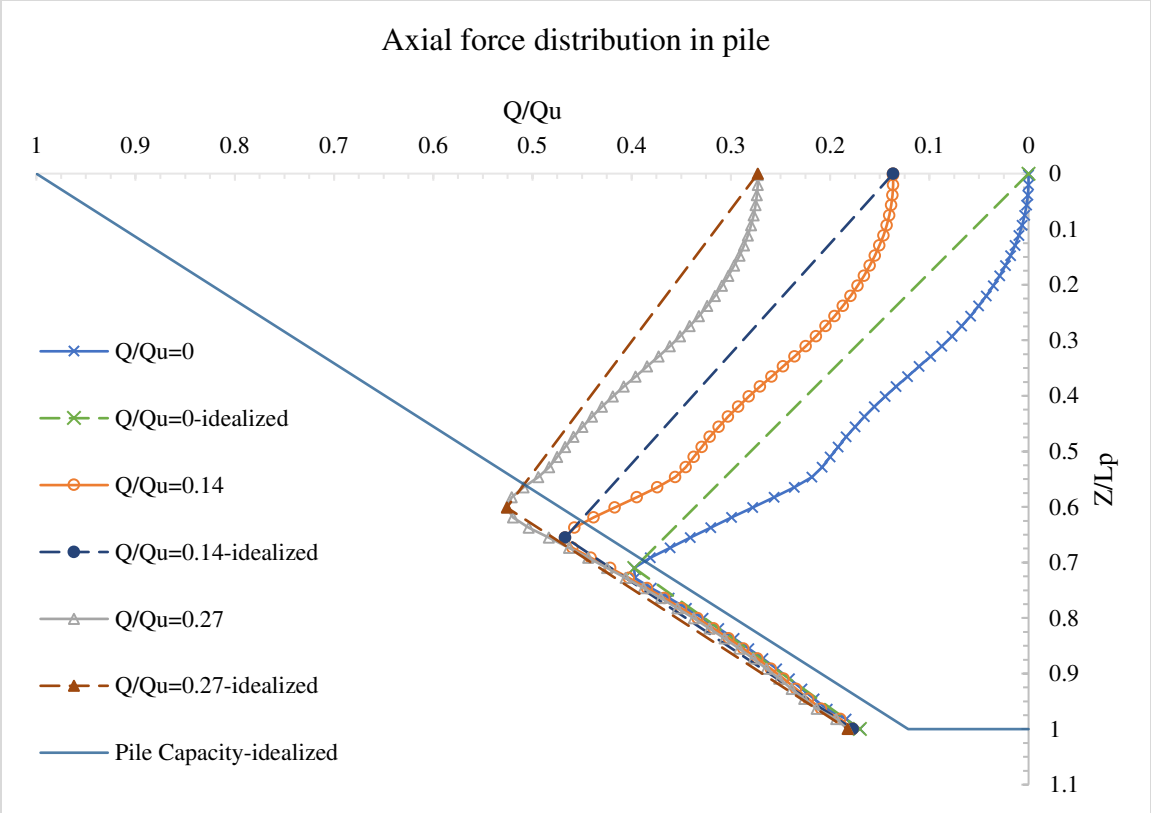

Figure 6.74 Normalized/Idealized pile load with D_p=6 in (152 *mm*), L_p=55 *ft* (16.8 *m*), and H_b/H_f=0.0

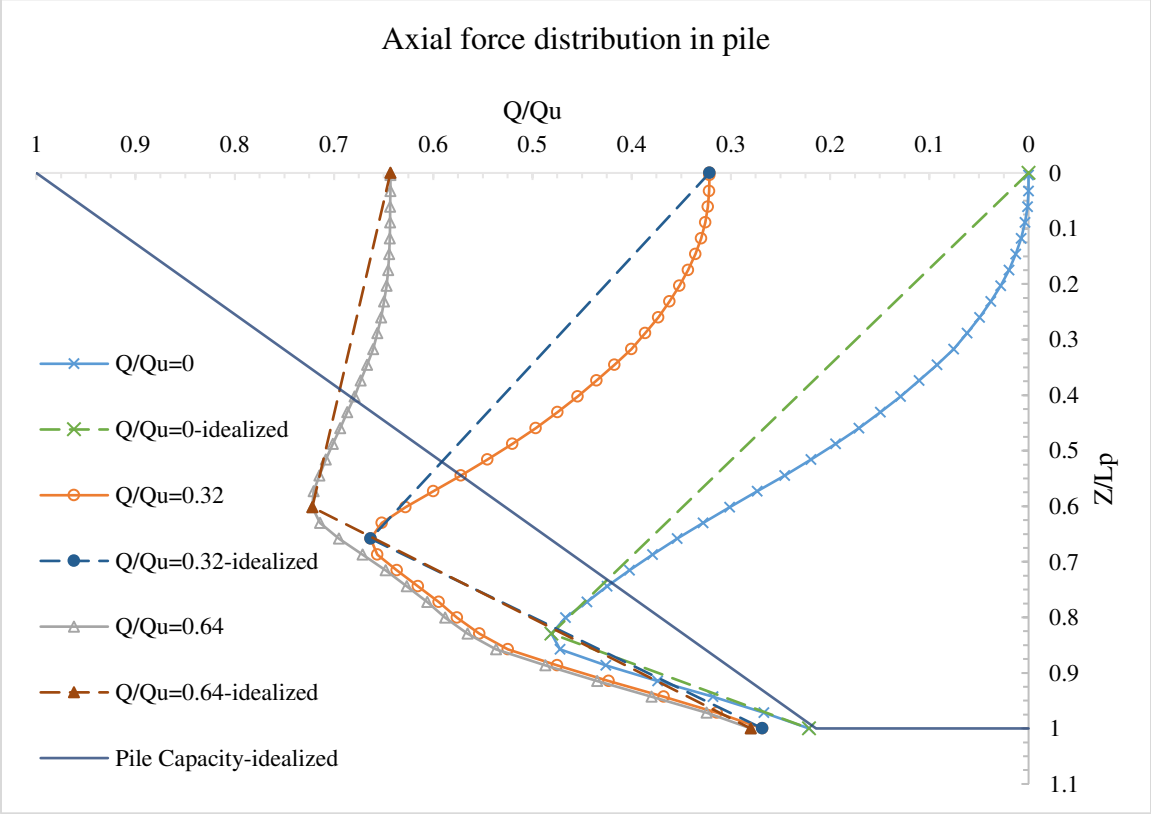

Figure 6.75 Normalized/Idealized pile load with D_p=6 in (152 *mm*), L_p=35 *ft* (10.7 *m*), and H_b/H_f=0.40

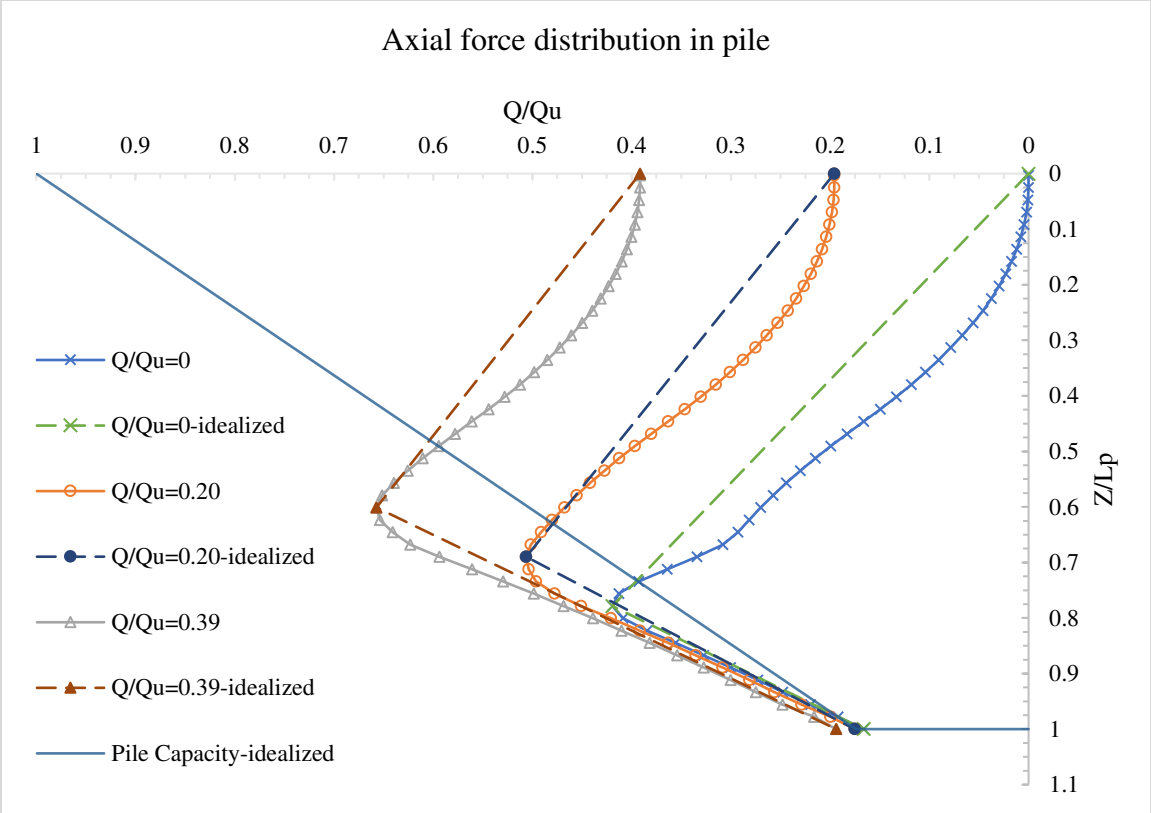

Figure 6.76 Normalized/Idealized pile load with D_p=6 in (152 *mm*), L_p=45 *ft* (13.7 *m*), and H_b/H_f=0.40

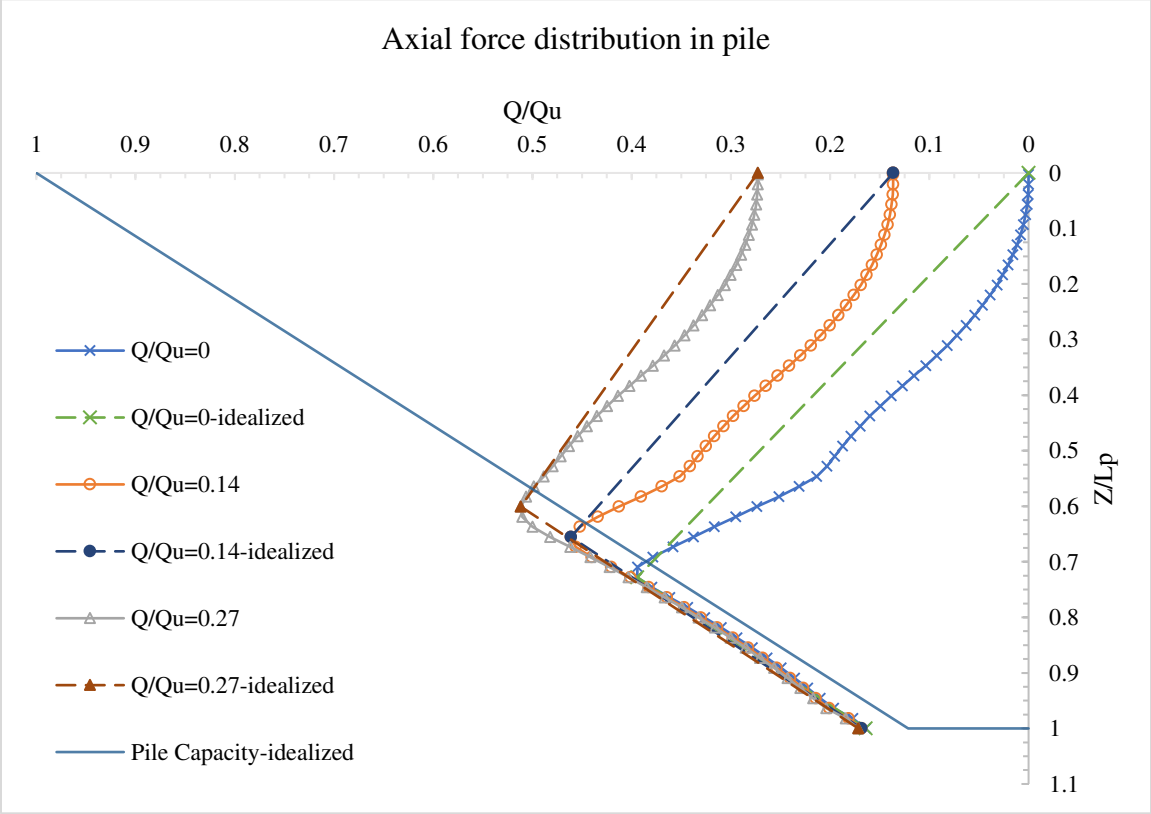

Figure 6.77 Normalized/Idealized pile load with D_p=6 in (152 *mm*), L_p=55 *ft* (16.8 *m*), and H_b/H_f=0.40

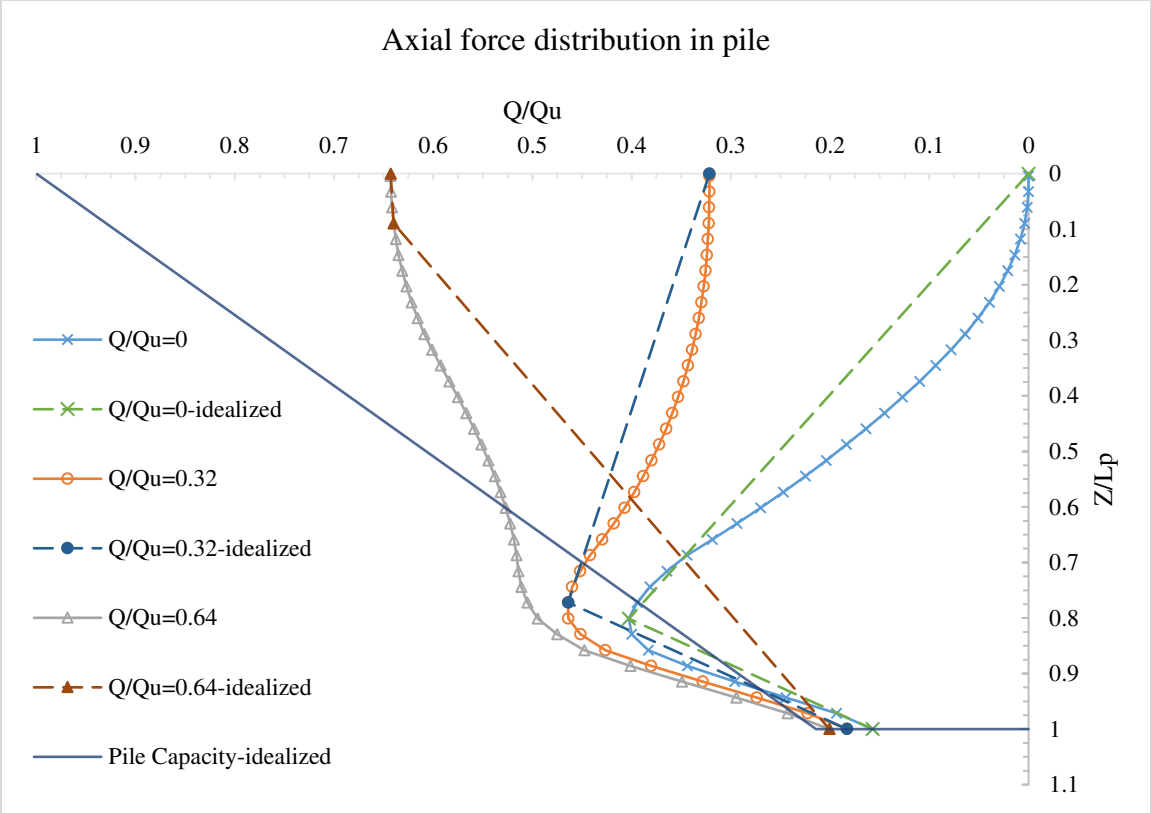

Figure 6.78 Normalized/Idealized pile load with D_p=6 in (152 *mm*), L_p=35 *ft* (10.7 *m*), and H_b/H_f=0.80

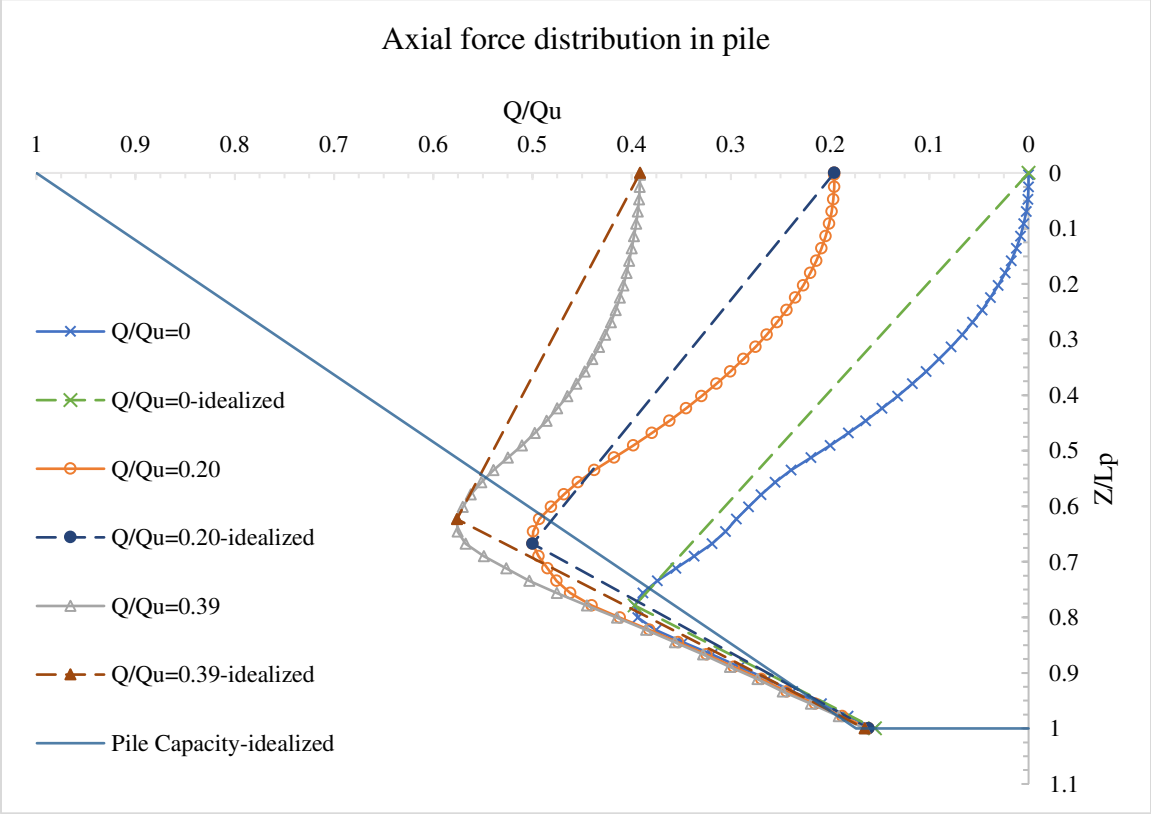

Figure 6.79 Normalized/Idealized pile load with D_p=6 in (152 *mm*), L_p=45 *ft* (13.7 *m*), and H_b/H_f=0.80

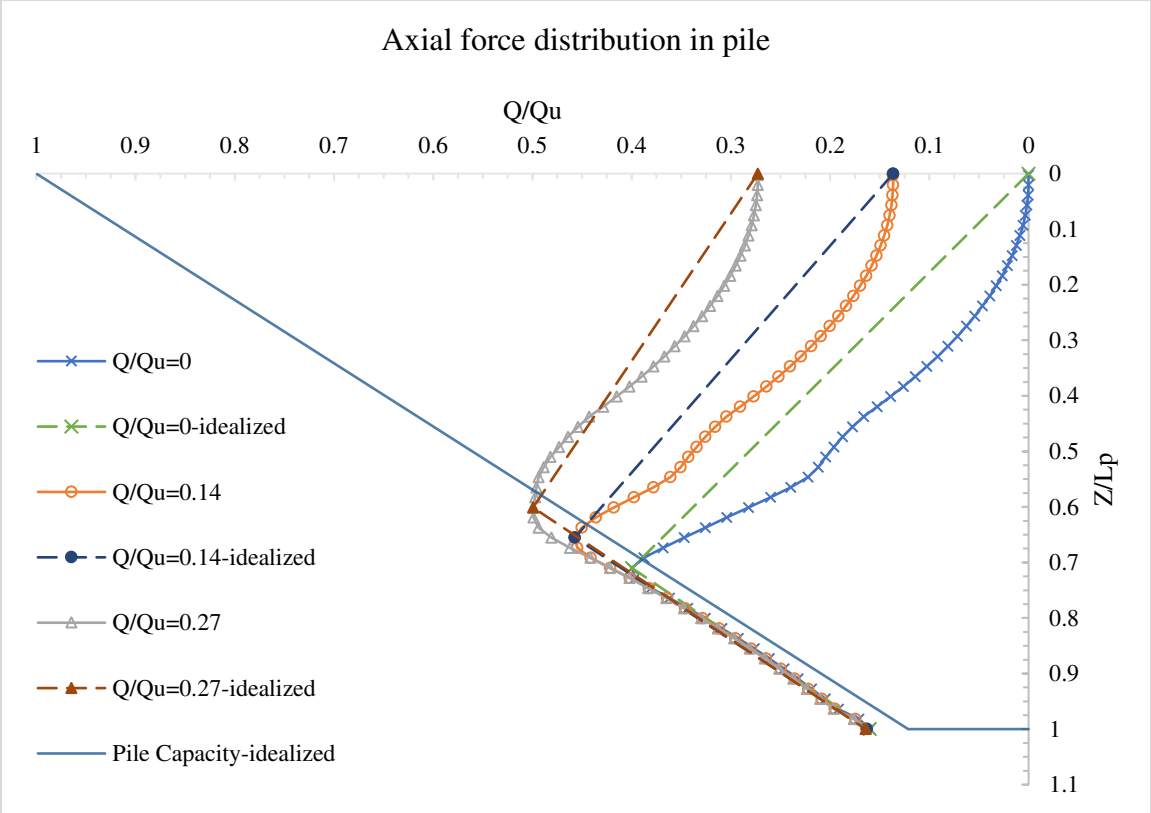

Figure 6.80 Normalized/Idealized pile load with D_p=6 in (152 *mm*), L_p=55 *ft* (16.8 *m*), and H_b/H_f=0.80

In the above figures, the distribution of the pile axial load was idealized into two linear curves, one represents the downdrag zone, DDZ, with a slope of $\left(\frac{Q-Q_{dd}}{L_{dd}}\right)$ and the other represents the positive skin friction zone, PSZ, with a slope of $\left(\frac{Q_b-Q_{ps}}{L_{ps}}\right)$. The point where the two lines intersect is the neutral point, $\left(\frac{L_{dd}}{L_p}\right)$.

Accordingly, it was noted that the slopes of the two lines decreased as Q approached Q_u. As Q increases, the slope of the DDZ lines approach zero. On the other hand, the slope of the PSZ lines approach a slope similar to the pile capacity curve. At Q_u, the axial load distribution of the pile can be represented by the pile capacity curve. In that case, Q_{dd} would be null and the entire pile shaft would be subjected to Q_{ps}.

Additionally, it was noted that Q_{dd} and L_{dd} were not only a function of Q, but also a function of the consolidation level of the surrounding soil and the time of pile installation. This is clearly shown in situations when ($H_b/H_f > 0$) in which L_{dd} was never less than H_b. This indicates that the pile was not subjected to Q_{dd} within the backfill layer. The downdrag force in such cases was a result of the consolidation (water dissipation) of the underneath embankment fill and natural soil layers. When ($H_b/H_f = 0$), the entire pile length could be subjected to downdrag force. However, due to the installation time, part of the consolidation process could have undergone, and thus low downdrag forces might be encountered in the top part of the pile (vicinity of the surface of the soil). For the examined pile-soil parameters (see Tables 6.2 and 6.3), it was noted that the piles were subjected to Q_{dd} up to about (0.9-0.95 H_e). This indicates that, by the time of installation, 5-10% of the embankment fill layer was undergone the consolidation process.

An attempt was made to establish relationships in which predict the axial load distribution along the pile shaft. Assuming that the pile axial load distribution can be idealized into two distinguish lines, i.e. DDZ and PSZ, linear relationships were sought in this phase of the study (see Figure 6.81) using the normalized/idealized lines shown in Figures 6.54 through 6.80.

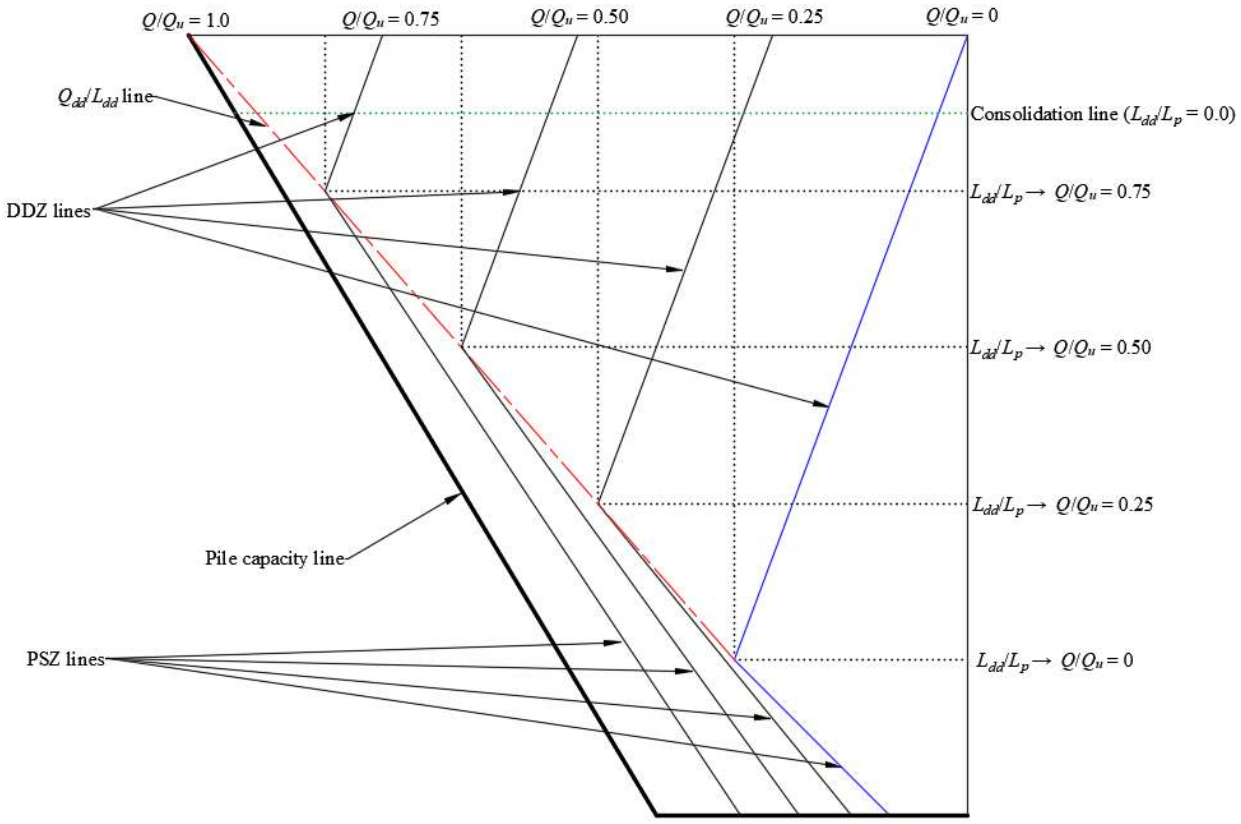

Figure 6.81 Development of axial load distribution in pile

In Figure 6.81, the DDZ lines can be establish utilizing the general form of a linear relationship given as

$$\frac{Q}{Qu} = m_1\left(\frac{L_{dd}}{L_p}\right) + c_1 \qquad 6\text{-}12$$

Where

m_1 = Slope of the DDZ lines.

c_1 = Constant.

The slope of the DDZ line decreases as Q/Q_u approaches 1.0. In such case the slope of the DDZ line would become $m_{1_{@Q_u}} = 0$. Using two slope points of $m_{1_{@Q_u}} = 0$ and $m_{1_{@Q=0}} = \frac{(Q_{dd@Q=0}/Q_u)}{(L_{dd@Q=0}/L_p)}$ with an assumed linear interpolation, m_1 can be written as:

$$m_1 = \left(1 - \frac{Q}{Q_u}\right)\left[\frac{Q_{dd_{@Q=0}} L_p}{L_{dd_{@Q=0}} Q_u}\right] \quad 6\text{-}13$$

Where

$Q_{dd_{@Q=0}}$= Downdrag force when pile head load $Q = 0$ (equation 6-10)

$L_{dd_{@Q=0}}$= Length of downdrag (neutral point) when pile head load $Q = 0$ (equation 6-11)

In equation 6-12, when $L_{dd}/L_p = 0$, c_1 becomes

$$C_1 = \frac{Q}{Q_u} \quad 6\text{-}14$$

Substituting equations 6-13 and 6-14 into 6-12 yields Q_{dd} at any pile head load, Q, as follows:

$$\frac{Q_{dd}}{Q_u} = \left(1 - \frac{Q}{Q_u}\right)\left[\frac{Q_{dd_{@Q=0}} L_p}{L_{dd_{@Q=0}} Q_u}\right]\frac{L_{dd}}{L_p} \quad 6\text{-}15$$

Which reduces to

$$Q_{dd} = (Q_u - Q)\left[\frac{Q_{dd_{@Q=0}} L_{dd}}{L_{dd_{@Q=0}} Q_u}\right] \quad 6\text{-}16$$

The Q_{dd}/L_{dd} line, shown in Figure 6.81, was introduced such that it passes through the points $\left(\frac{Q_{dd_{@Q=0}}}{Q_u}\ ,\ \frac{L_{dd_{@Q=0}}}{L_p}\right)$ and $\left(\frac{Q_u}{Q_u}\ ,\ \frac{L_{dd_{@Q_{dd}=0}}}{L_p}\right)$.

Where

$\frac{L_{dd_{@Q_{dd}=0}}}{L_p}$ = The embedded length of the pile at which not subjected to downdrag force (consolidation line shown in Figure 6.81).

Thus, a linear relationship was established as follows:

$$\frac{Q}{Qu} = m_2\left(\frac{L_{dd}}{L_p}\right) + c_2 \qquad 6\text{-}17$$

Where

m_2 = Slope of the Q_{dd}/L_{dd} line (see Figure 6.81).

c_2 = Constant.

Since this line is passes through two fixed points, m_2, can be written as follows:

$$m_2 = \frac{\left(Q_{dd_{@Q=0}}/Q_u\right) - (Q_u/Q_u)}{\left(L_{dd_{@Q=0}}/L_p\right) - \left(L_{dd_{@Q_{dd}=0}}/L_p\right)} = \frac{\left(Q_{dd_{@Q=0}} - Q_u\right)L_p}{\left(L_{dd_{@Q=0}} - L_{dd_{@Q_{dd}=0}}\right)Q_u} \qquad 6\text{-}18$$

At $(Q/Q_u) = 1.0,\ \left(L_{dd}/L_p\right) = \left(L_{dd_{@Q_{dd}=0}}/L_p\right)$. Therefore, c_2, can be written as:

$$c_2 = 1 - m_2\left(L_{dd_{@Q_{dd}=0}}/L_p\right) \qquad 6\text{-}19$$

Substituting equations 6-18 and 6-19 into 6-17 gives the Q_{dd}/L_{dd} line as follows:

$$\frac{Q_{dd}}{Q_u} = \frac{\left(Q_{dd_{@Q=0}} - Q_u\right) L_{dd}}{\left(L_{dd_{@Q=0}} - L_{dd_{@Q_{dd}=0}}\right) Q_u} + \left[1 - \frac{\left(Q_{dd_{@Q=0}} - Q_u\right) L_{dd_{@Q_{dd}=0}}}{\left(L_{dd_{@Q=0}} - L_{dd_{@Q_{dd}=0}}\right) Q_u}\right] \quad 6\text{-}20$$

Which can be reduced to

$$Q_{dd} = \left[\frac{\left(Q_{dd_{@Q=0}} - Q_u\right) L_{dd}}{\left(L_{dd_{@Q=0}} - L_{dd_{@Q_{dd}=0}}\right)}\right] + \left[Q_u - \frac{\left(Q_{dd_{@Q=0}} - Q_u\right) L_{dd_{@Q_{dd}=0}}}{\left(L_{dd_{@Q=0}} - L_{dd_{@Q_{dd}=0}}\right)}\right] \quad 6\text{-}21$$

Now, setting equation 6-16 equals to equation 6-21, L_{dd} can be expressed in terms of m_1, c_1, m_2 and c_2 as follows:

$$L_{dd} = \frac{c_2 - c_1}{m_1 - m_2} L_p \quad 6\text{-}22$$

Which can be expressed in terms of Q and L as follows:

$$L_{dd} = \frac{1 - \left[\frac{\left(Q_{dd_{@Q=0}} - Q_u\right) L_p}{\left(L_{dd_{@Q=0}} - L_{dd_{@Q_{dd}=0}}\right) Q_u}\left(\frac{L_{dd_{@Q_{dd}=0}}}{L_p}\right)\right] - \frac{Q}{Q_u}}{\left(1 - \frac{Q}{Q_u}\right)\left[\frac{Q_{dd_{@Q=0}} L_p}{L_{dd_{@Q=0}} Q_u}\right] - \frac{\left(Q_{dd_{@Q=0}} - Q_u\right) L_p}{\left(L_{dd_{@Q=0}} - L_{dd_{@Q_{dd}=0}}\right) Q_u}} L_p \quad 6\text{-}23$$

Equations 6-16 and 6-23 provide an estimation of the downdrag force, Q_{dd}, and neutral point, L_{dd}, respectively. Figure 6.82 and Figure 6.83 show the simulated versus predicted Q_{dd} and L_{dd} using these equations, which illustrates the accuracy of the proposed equation.

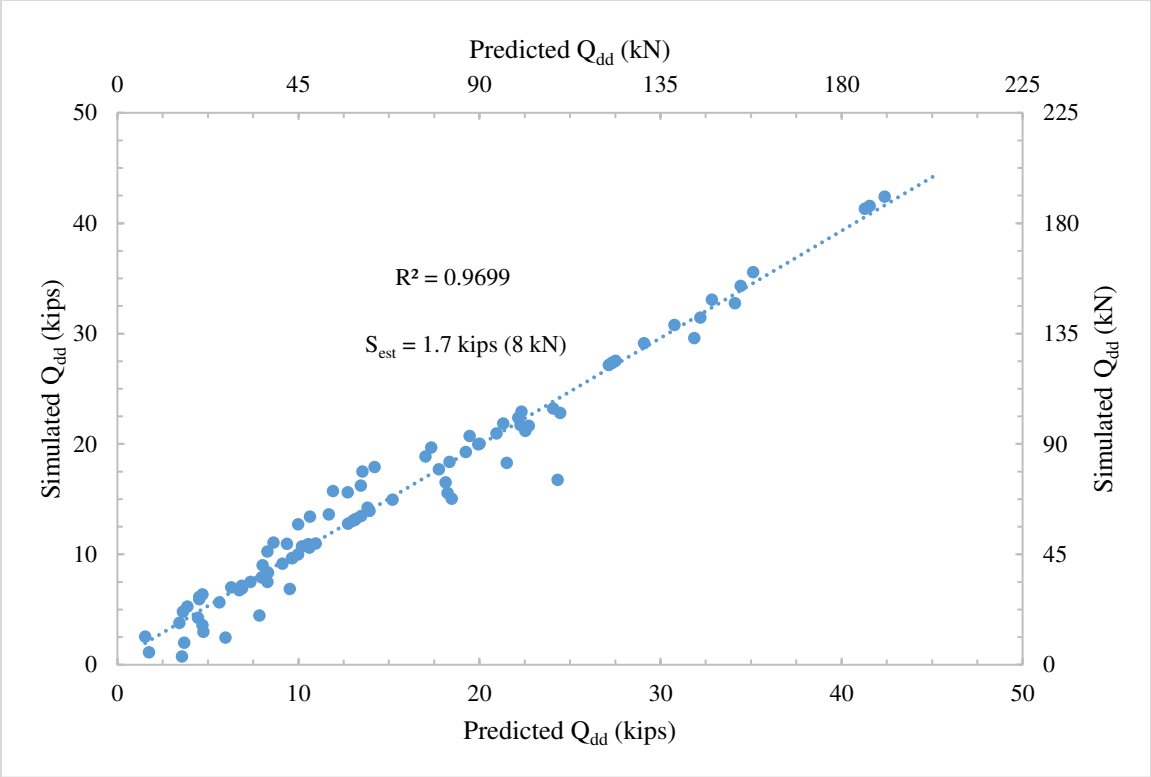

Figure 6.82 Simulated versus predicted Q_{dd}

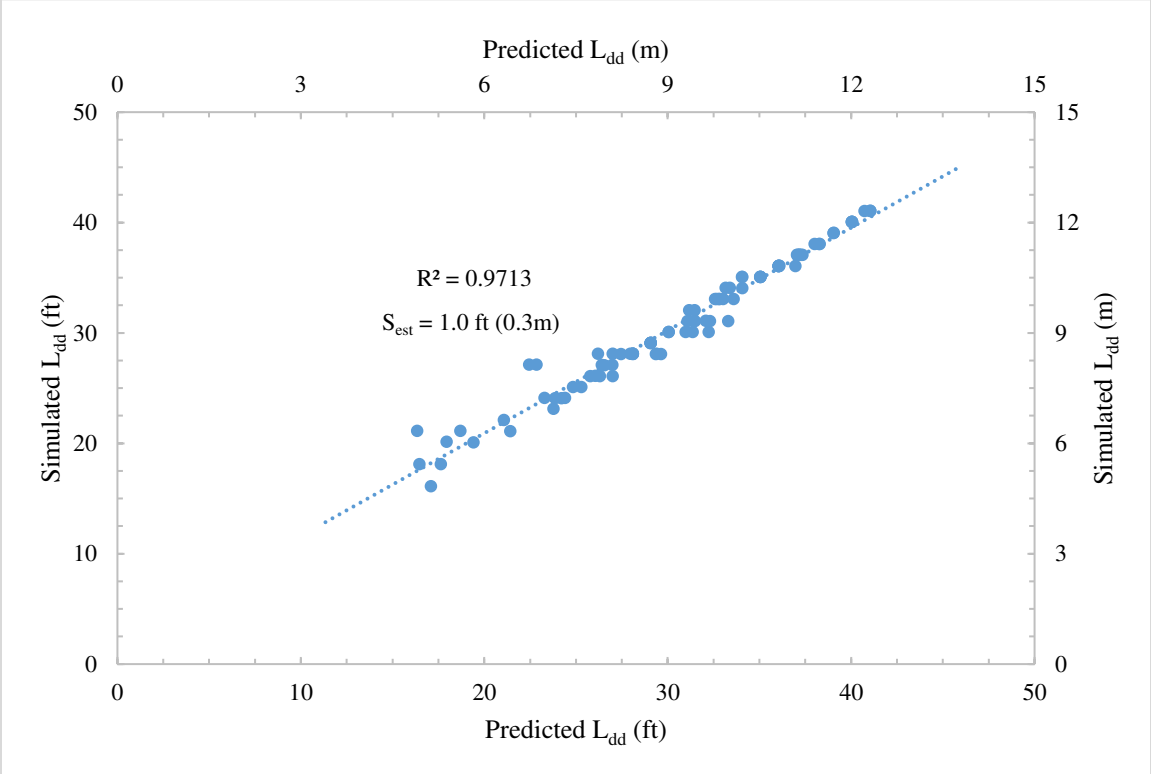

Figure 6.83 Simulated versus predicted L_{dd}

It should be noted that the establish of the latter relationships requires the pre-calculation of $Q_{dd_{@Q=0}}$ and $L_{dd_{@Q=0}}$ (blue lines shown in Figure 6.81) which can be evaluated using equations 6-10 and 6-11, respectively. It should also be noted that a good engineering judgment should be made regarding the location of the consolidation line, $L_{dd_{@Q_{dd}=0}}$ (see Figure 6.81). A value between 0.0-0.20 L_p appears to be a reasonable estimation for it. Table 6.7 shows different values of assumed $L_{dd_{@Q_{dd}=0}}$ versus predicted L_{dd}.

Table 6.7 Estimated $L_{dd_{@Q_{dd}=0}}$ versus predicted L_{dd}

$L_{dd_{@Q_{dd}=0}}$	L_{dd}	
	R^2	S_{est} *ft* (*m*)
0.0 L_p	0.970	1.03 (0.31)
0.1 L_p	0.971	1.02 (0.31)
0.2 L_p	0.963	1.15 (0.35)
0.3 L_p	0.942	1.45 (0.44)
0.4 L_p	0.896	1.93 (0.59)
0.5 L_p	0.810	2.62 (0.80)

Similarly, the PSZ lines can be establish utilizing the general form of a linear relationship given as

$$\frac{Q}{Qu} = m_3\left(\frac{L_{ps}}{L_p}\right) + c_3 \qquad 6\text{-}24$$

Where

m_3 = Slope of the PSZ lines.

c_3 = Constant.

As in Figure 6.81, the slope of the PSZ line decreases as Q/Q_u approaches 1.0. In such case the slope would be similar to the pile capacity slope given as

$$m_{@Q=Q_u} = \frac{(Q_b/Q_u) - (Q_u/Q_u)}{(L_p/L_p)} = \frac{Q_b}{Q_u} - 1 \quad \text{6-25}$$

Additionally, the slope of the PSZ line at $Q = 0$ can be expressed as follows:

$$m_{@Q=0} = \frac{\left(Q_{b_{@Q=0}}/Q_u\right) - \left(Q_{dd_{@Q=0}}/Q_u\right)}{(L_p/L_p) - \left(L_{dd_{@Q=0}}/L_p\right)} = \frac{\left(Q_{b_{@Q=0}} - Q_{dd_{@Q=0}}\right)L_p}{\left(L_p - L_{dd_{@Q=0}}\right)Q_u} \quad \text{6-26}$$

Where

$Q_{b_{@Q=0}}$= End-bearing when pile head load $Q = 0$.

Assuming a liner interpolation between $m_{@Q=0}$ and $m_{@Q=Q_u}$, the change in slope of PSZ line can be expressed as follows:

$$m_3 = \left(m_{@Q=Q_u} - m_{@Q=0}\right)(Q/Q_u) + \left(m_{@Q=0}\right) \quad \text{6-27}$$

Which can be expanded as follows:

$$m_3 = \frac{Q}{Q_u}\left[\left(\frac{Q_b}{Q_u} - 1\right) - \frac{\left(Q_{b_{@Q=0}} - Q_{dd_{@Q=0}}\right)L_p}{\left(L_p - L_{dd_{@Q=0}}\right)Q_u}\right] + \left[\frac{Q_b}{Q_u} - 1\right] \quad \text{6-28}$$

At $(Q/Q_u) = (Q + Q_{dd})/Q_u$, $\left(L_{ps}/L_p\right) = \left(L_{dd_{@Q_{dd}=0}}/L_p\right)$. Therefore, c_3, can be expressed as

$$c_3 = \frac{Q + Q_{dd}}{Q_u} - m_3\left(\frac{L_{dd}}{L_p}\right) \quad \text{6-29}$$

Substituting equations 6-27 and 6-29 into 6-24 and setting $\left(\frac{L_p}{L_p} = 1.0\right)$ gives Q_b at any pile head load Q as follows:

$$Q_b = Q_u \left[m_3 + \left(\frac{Q + Q_{dd}}{Q_u} \right) - m_3 \left(\frac{L_{dd}}{L_p} \right) \right] \quad 6\text{-}30$$

Finally, equilibrium of forces along the pile shaft can be used to evaluate the positive skin friction force Q_{ps} as follows:

$$Q_{ps} = Q + Q_{dd} - Q_b \quad 6\text{-}31$$

Which can be expressed as

$$Q_{ps} = Q + Q_{dd} - Q_u \left[m_3 + \left(\frac{Q + Q_{dd}}{Q_u} \right) - m_3 \left(\frac{L_{dd}}{L_p} \right) \right] \quad 6\text{-}32$$

Equations 6-30 and 6-32 provide an estimation of the end-bearing force Q_b and positive skin friction force Q_{ps}, respectively. Figure 6.84 and Figure 6.85 show the simulated versus predicted Q_b and Q_{ps} using these equations, which illustrates the accuracy of the proposed equation.

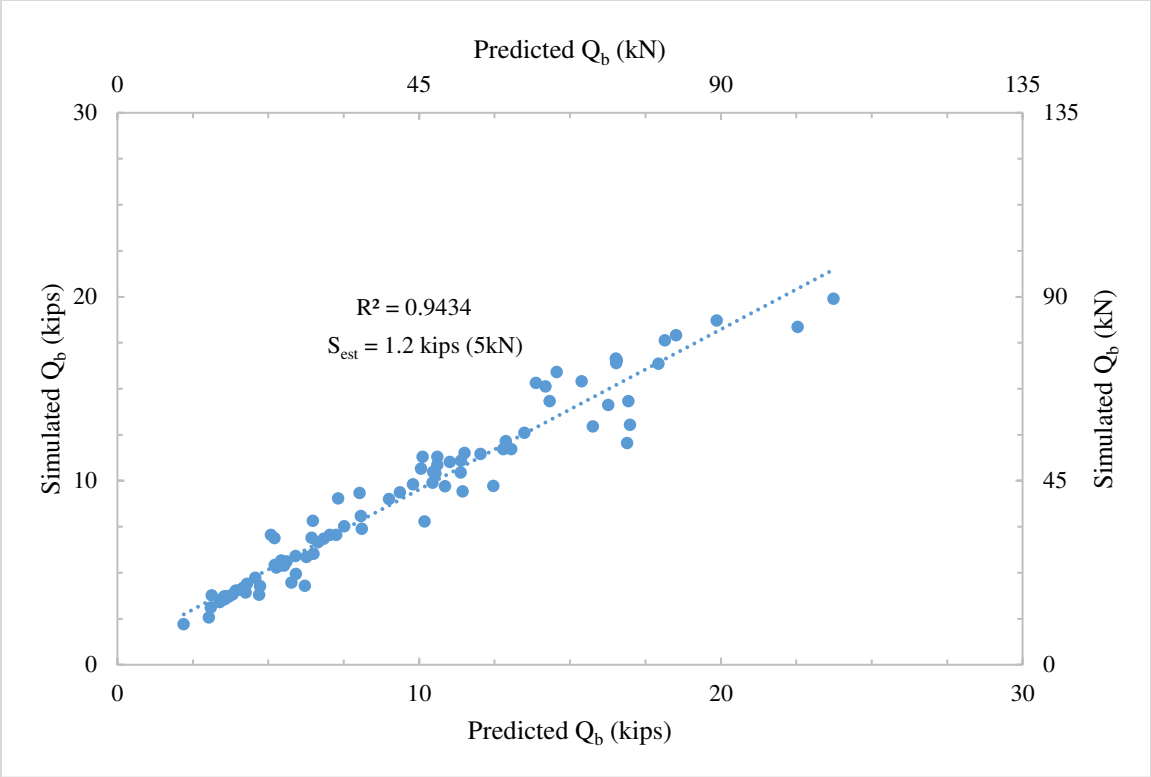

Figure 6.84 Simulated versus predicted Q_b

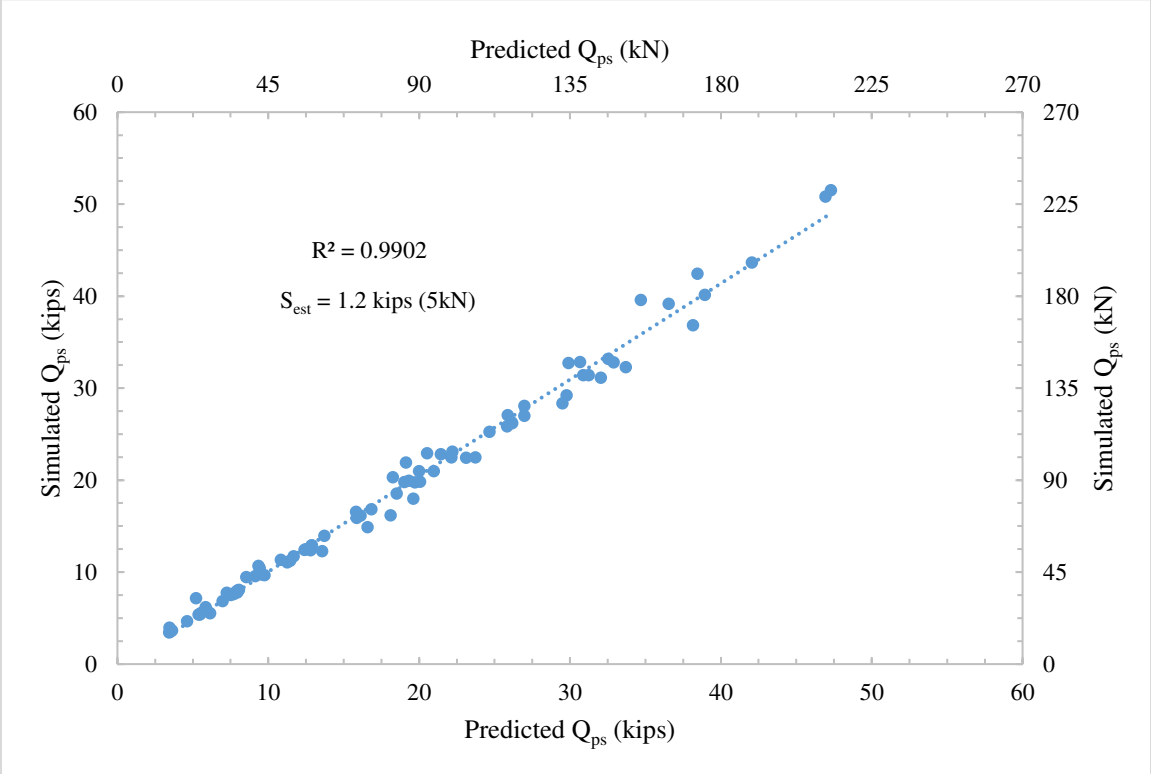

Figure 6.85 Simulated versus predicted Q_{ps}

6.10 Chapter summary and conclusion

As soil underneath approach slab settles, deferential settlement develops between the bridge and the approaching roadway causing bumps and affecting the riding quality. Settlement-reducing piles could be introduced into the approach slab to control changes in slope and limit stresses to acceptable levels. However, determining the appropriate location, spacing, length and size of piles is a difficult task that requires further study. Since field testing of piles is rather expensive and time-consuming, an analytical program is required to develop the information needed for the design of pile supported approach slab for settlement control.

In this part of the study, a proposed layout of multi-segment pile-supported approach slab was developed based on the relative angle change between various approach slab segments. Accordingly, criterion of determining the number and lengths of needed approach slab segments was provided (see Section 6.2).

Furthermore, finite element model was generated to quantify the pile head settlement and the load distribution along the pile as a function of different pile-soil parameters (see Tables 6.2 and 6.3). As a result, design charts (Figures 6.16 through 6.18) were developed such that pile head settlement can be evaluated as a function of the reduction of settlement, R_{sett}. Moreover, empirical relationship was developed to predict the pile head settlement (in semi-frictional piles). Relationships were also developed, using numerical analyses, to predict the distribution of axial load along the length of the pile. This includes the neutral point, L_{dd}, downdrag force, Q_{dd}, positive skin friction, Q_{ps}, and end-bearing, Q_b. Table 6.8 shows a summary of the developed equations.

Table 6.8 Summary of the developed pile head settlement/load distribution equations

Parameter	Developed equations
Pile head settlement Δ_{PH}	$\Delta PH = \Delta_{Ps} - 166\frac{Q_{dd}}{D_p L_{dd} G_{avg-dd}} + 41\frac{Q_{ps}}{D_p L_{ps} G_{avg-ps}} + 3.2\frac{Q_b}{D_p^2 E_b} - 0.2$
Neutral point L_{dd}	$L_{dd} = \frac{1 - \left[\frac{\left(Q_{dd@Q=0} - Q_u\right)L_p}{\left(L_{dd@Q=0} - L_{dd@Q_{dd}=0}\right)Q_u}\left(\frac{L_{dd@Q_{dd}=0}}{L_p}\right)\right] - \frac{Q}{Q_u}}{\left(1 - \frac{Q}{Q_u}\right)\left[\frac{Q_{dd@Q=0}L_p}{L_{dd@Q=0}Q_u}\right] - \frac{\left(Q_{dd@Q=0} - Q_u\right)L_p}{\left(L_{dd@Q=0} - L_{dd@Q_{dd}=0}\right)Q_u}} L_p$
Downdrag force Q_{dd}	$Q_{dd} = (Q_u - Q)\left[\frac{Q_{dd@Q=0}L_{dd}}{L_{dd@Q=0}Q_u}\right]$
Positive skin friction[1] Q_{ps}	$Q_{ps} = Q + Q_{dd} - Q_u\left[m_3 + \left(\frac{Q + Q_{dd}}{Q_u}\right) - m_3\left(\frac{L_{dd}}{L_p}\right)\right]$
End-bearing[1] Q_b	$Q_b = Q_u\left[m_3 + \left(\frac{Q + Q_{dd}}{Q_u}\right) - m_3\left(\frac{L_{dd}}{L_p}\right)\right]$

[1] Refer to equation 6-28 for m_3.

All in all, the relationships developed to evaluate axial forces in the pile-soil system can be used with any pile-soil parameters as they were expressed in a generalized linear fashion. However, care must be taken to ensure accuracy, when evaluating Δ_{PH}, if pile-soil parameters are outside of the range used in the parametric study (see Tables 6.2 and 6.3).

CHAPTER 7 - FULL-SCALE SIMULATION OF MULTI-SEGMENT PILE-SUPPORTED APPROACH SLAB SYSTEM

In this phase of the study, a full-scale finite element model of bridge approach area was generated. In this simulation, settlement-reducing piles were introduced to support the approach slab segments in order to achieve a smooth transition between the bridge and the roadway. The objective was to mitigate the roughness of the transition encountered in one of the examined soil profiles (soil profile#1, see Table 5.10).

Additionally, comparison was made to evaluate the results from this simulation with the developed equations for evaluating the longitudinal soil settlement profile (Chapter 5). Afterwards, the pile head settlement design charts were used to estimate the size, length, and spacing of piles that would achieve the required change of slope between various approach slab segments. Ultimately, recommendations were provided regarding the design of the multi-segment pile-supported approach slabs.

In this analysis, the bridge was 80 *ft* (24 *m*) wide (two-direction two-lanes highway bridge) that is supported on stub abutments at its ends with height H_a = 5 *ft* (1.5 *m*) and thickness T_a = 2 *ft* (0.60 *m*). The bridge approach area consisted of a 90% granular backfill with slope S_b = 1:2 (1 vertical to 2 horizontal), highly compressible embankment fill with height H_e = 30 *ft* (9.1 *m*) and side slope S_{se} = 1:2 (1 vertical to 2 horizontal), and highly compressible natural soil with height H_n = 30 *ft* (9.1 *m*). A one-span approach slab with length L_s = 20 *ft* (6.1 *m*) and thickness T_s =12 *in* (305 *mm*) was used.

Similar geometry and boundary conditions of the transverse (see Section 5.4.2) and longitudinal (see Section 5.6.2) models were used in the full-scale simulation. One-half of the

full geometry were used, due to symmetry. Figures 7.1 and 7.2 show the geometry and boundary conditions used in the full-scale simulation. Figure 7.3 shows the discretization of the finite model.

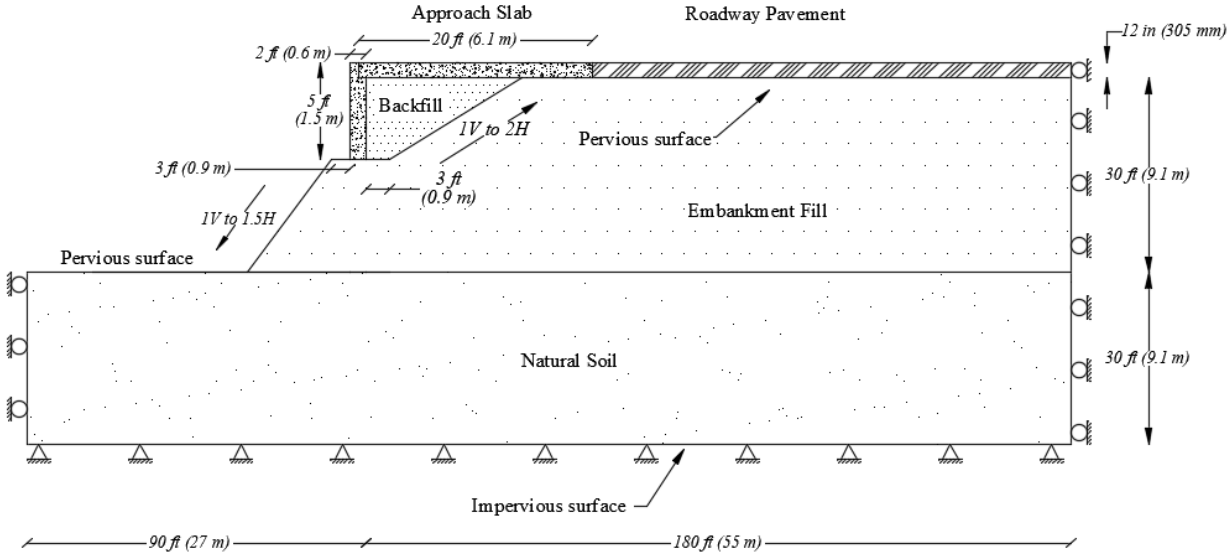

Figure 7.1 Longitudinal cross section of the full-scale model

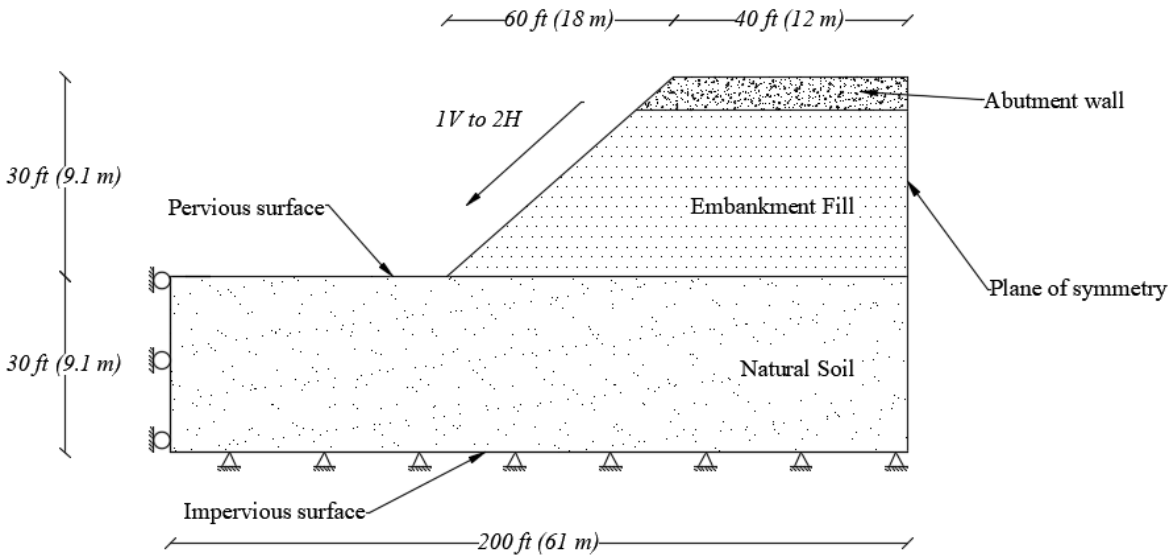

Figure 7.2 Transverse cross section of the full-scale model

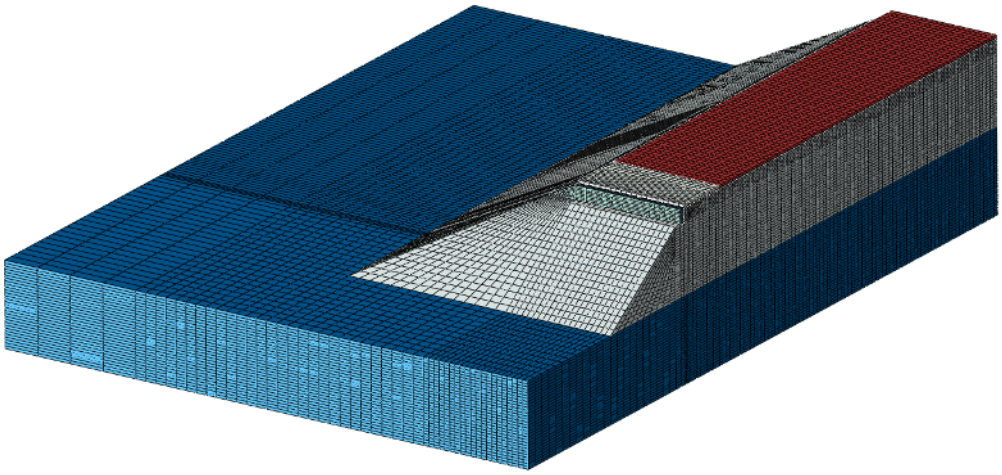

Figure 7.3 Finite element discretization of the full-scale model

Two initial simulations were run. First, the model was run to assess the roughness of the transition between the bridge and the roadway pavement by evaluating the resulting slope of the approach slab. The information regarding the differential settlement of the approach slab, and longitudinal soil settlement profile were obtained from this simulation. Accordingly, initial estimation regarding the size, length, and spacing of piles, and number and length of the approach slab segments were made using the pile head settlement design charts (see Section 6.7.2). Second, similar model was run with no approach slab/roadway pavement, and the

longitudinal soil settlement profile was evaluated accordingly. This was to simulate similar pile-soil conditions used to develop the pile head settlement design charts (see Section 6.6). The initial estimation was refined accordingly. The results from the two initial simulations are presented below. Figures 7.4 and 7.5 show the contour of the vertical deformation and excess pore pressure at the end of the analysis, respectively.

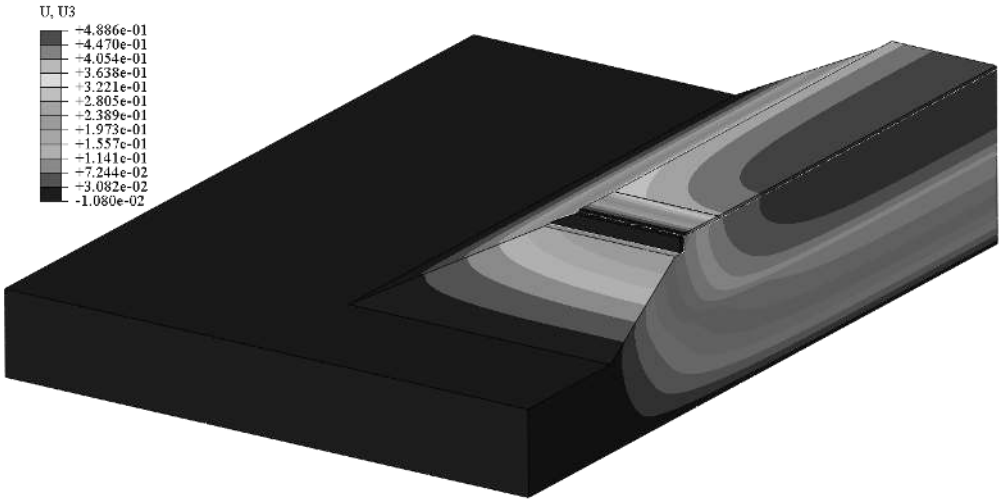

Figure 7.4 Vertical deformation contour of the full-scale simulation (*ft*)

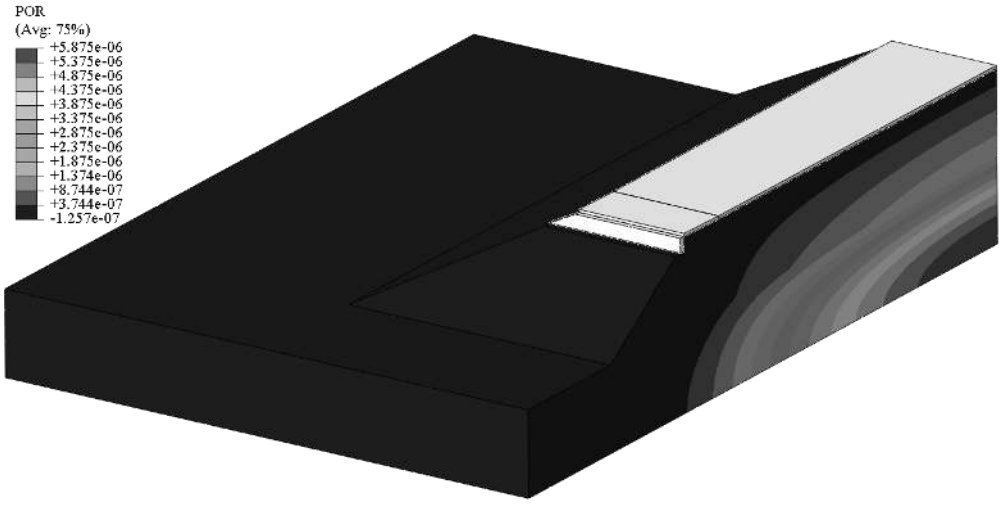

Figure 7.5 Excess pore pressure contour of the full-scale simulation (*psf*)

Figure 7.6 shows the soil settlement profiles along the center line of the longitudinal direction with and without the approach slab/roadway pavement loads. The figure also shows the

predicted longitudinal soil settlement profile using the developed equations (Chapter 5). The predicted profile was in relatively good agreement with the simulated profile. The average error between the predicted and simulated profiles was less than 0.25 *in* (6.4 *mm*).

Figure 7.7 shows the simulated transition profile along the center line of the approach slab/pavement. The figure shows that using one-span, 20 *ft* (6.1 *m*) long approach slab with these abutment-soil parameters would result in a rough transition. The resulted slope of the approach slab was 2.6/125. This would generate an abrupt slope change between the bridge and approach slab, and between approach slab and roadway pavement (bumps).

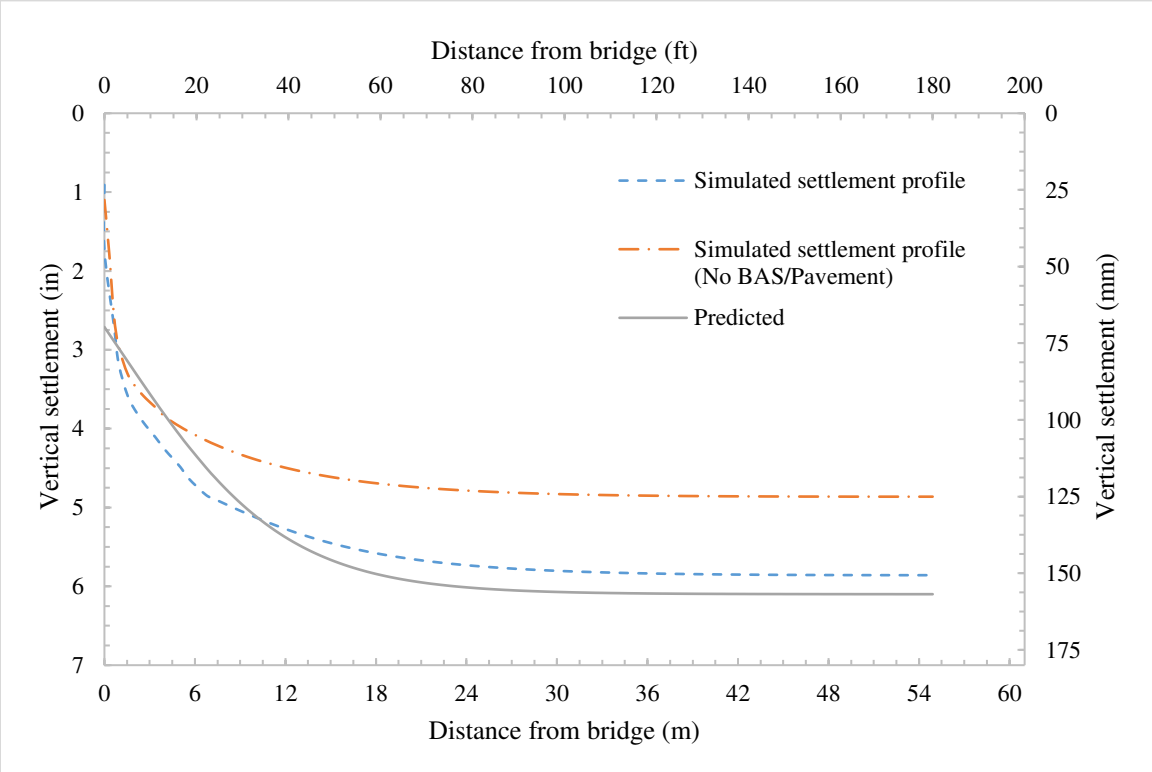

Figure 7.6 Simulated longitudinal soil settlement profile of the full-scale model

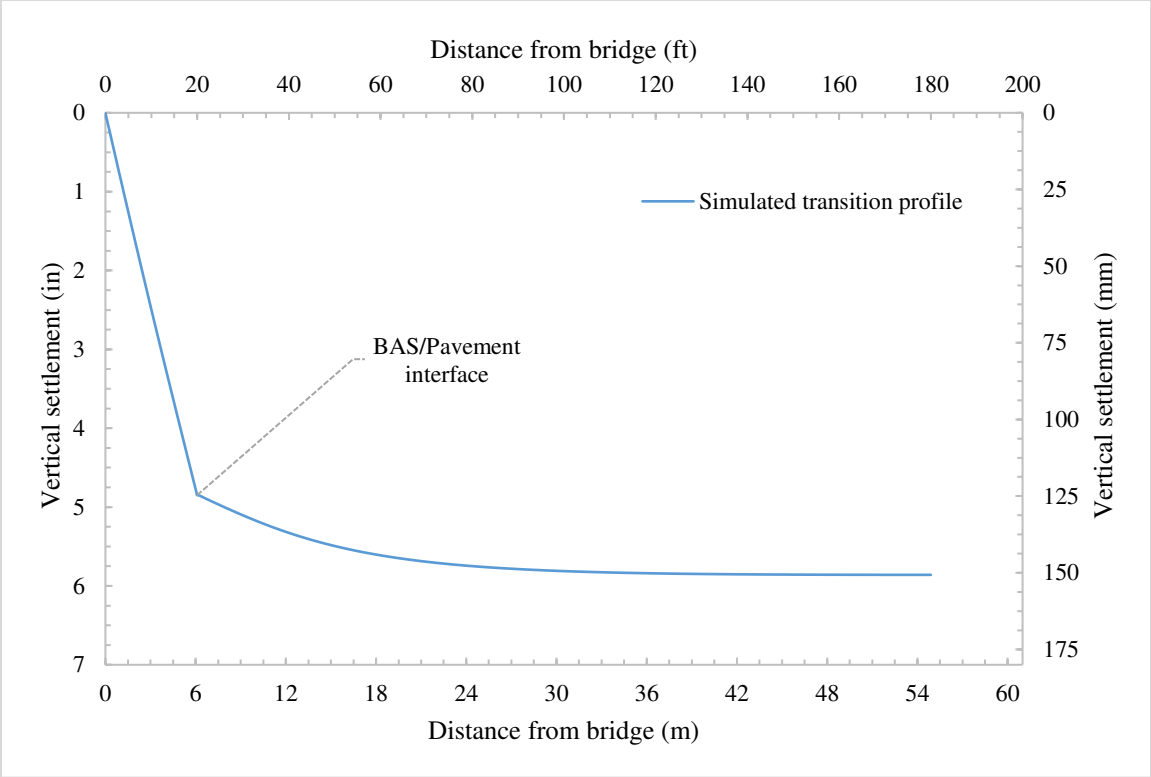

Figure 7.7 Simulated transition profile of the full-scale model

Using the information obtained from the results of the initial simulations, the size, length, and spacing of piles, as well as number and length of the approach slab segments were determined (using the procedure explained in section 6.2 and pile settlement design chart shown in Figure 7.8). Accordingly, two approach slab segments were found to be sufficient to produce the smooth transition as follows: (a) a slope of 1/125 of the first segment could be achieved using 30 *ft* (9.1 *m*) approach slab segment. (b) a second segment of 20 *ft* (6.1 *m*) long was found to be sufficient such that $L_{BAS-A}\left(\frac{1}{125}\right) < \Delta_T \leq (L_{BAS-A} + L_{BAS-B})\left(\frac{1}{125}\right)$. (c) one pile line was used to support the two segments. At that location, soil deformation (with no BAS/Pavement) was 4.3 *in* (109 *mm*). Consequently, R_{sett} was estimated as 0.34.

Accordingly, load calculations were carried out to determine the size, length, and spacing of piles in which provides the targeted R_{sett}. The pile line was assumed to support one-half of

each approach slab segment. Accordingly, it was found (using trial and error method) that pile size of 18 *in* (457 *mm*), 45 *ft* (13.7 *m*) long, spaced at 8 *ft* (2.4 *m*) would be sufficient to carry the estimated load of Q/Q_u = 0.33 and provide the targeted R_{sett} = 0.34. Figure 7.8 shows the determination of pile configuration using the pile settlement design chart developed for this pile-soil conditions.

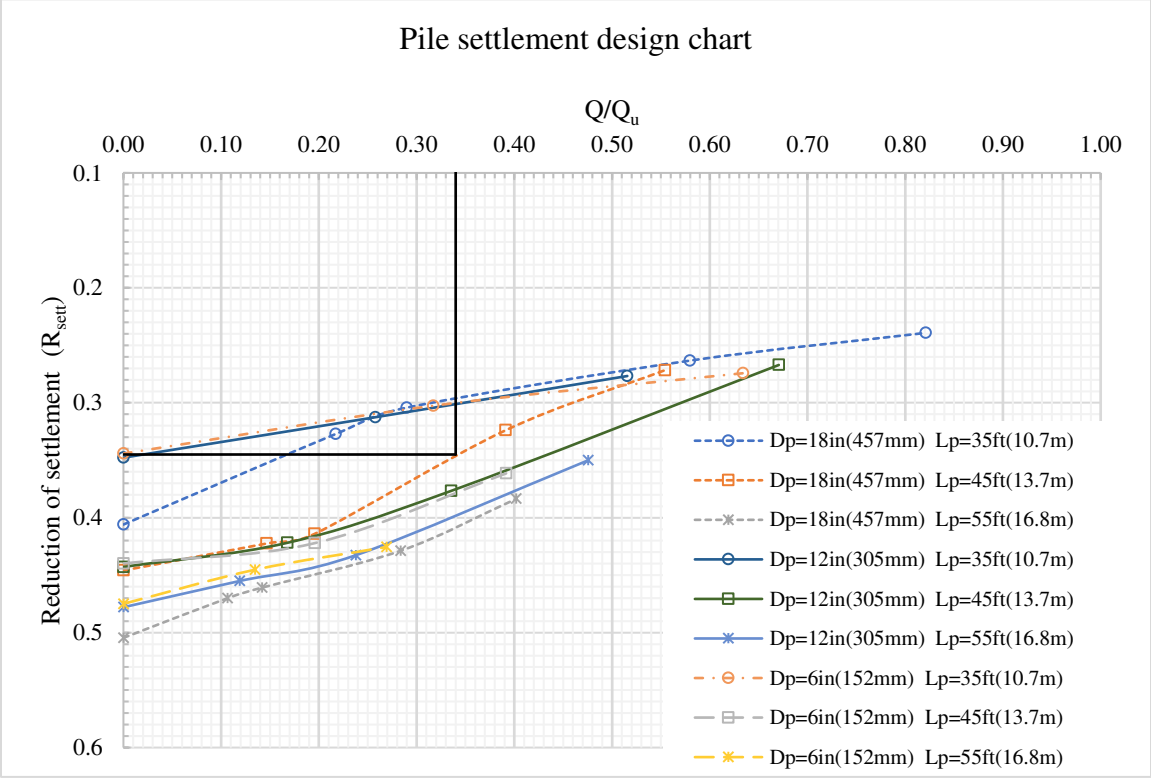

Figure 7.8 Determination of pile size and length

Figures 7.9 and 7.10 show the schematic layout of the proposed two-segment pile-supported approach slab system. A pile cap of 3.0×2.5 *ft* (0.9×0.8 m) at top of pile line was used. In the transverse direction, the piles were spaced 8 *ft* (2.4 *m*) center-to-center and were distributed starting from the center of the approach slab toward the its edge. Three edge pile spacing, $S_{e\text{-}p}$, were used. The edge-pile (pile 6) was spaced at $S_{e\text{-}p}$ = 8 and 4.5 *ft* (2.4 and 1.4 *m*) from pile 5. One configuration was also simulated with no edge-pile (without pile 6). The

anticipated pile head load, *Q*, was 39 *kips* (173 *kN*). Figures 7.11 and 7.12 show the finite element discretization of the full-scale multi-segment pile supported approach slab system.

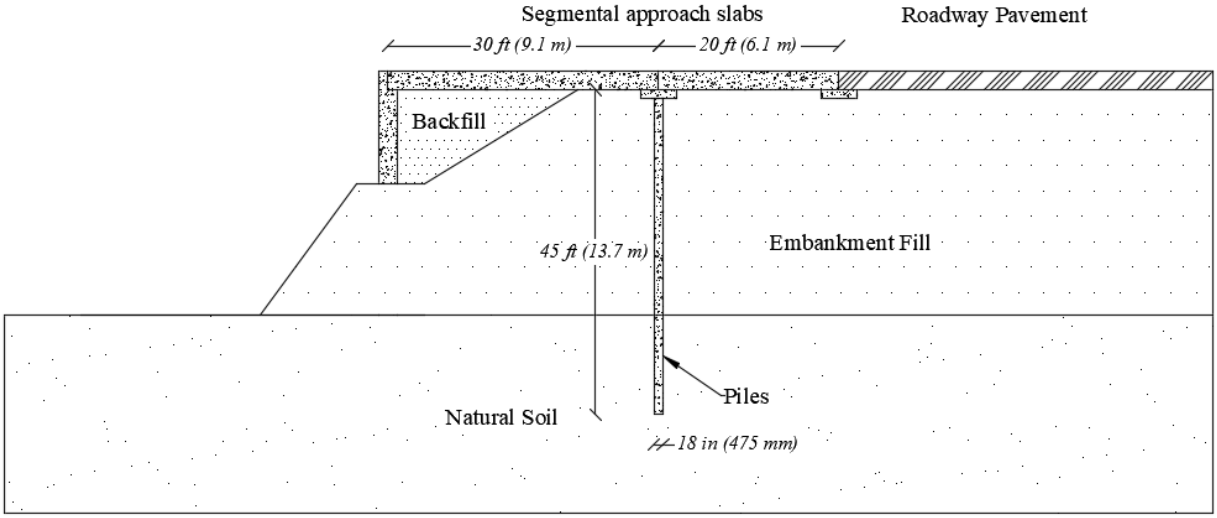

Figure 7.9 Longitudinal cross section of the proposed two-segment pile-supported approach slabs

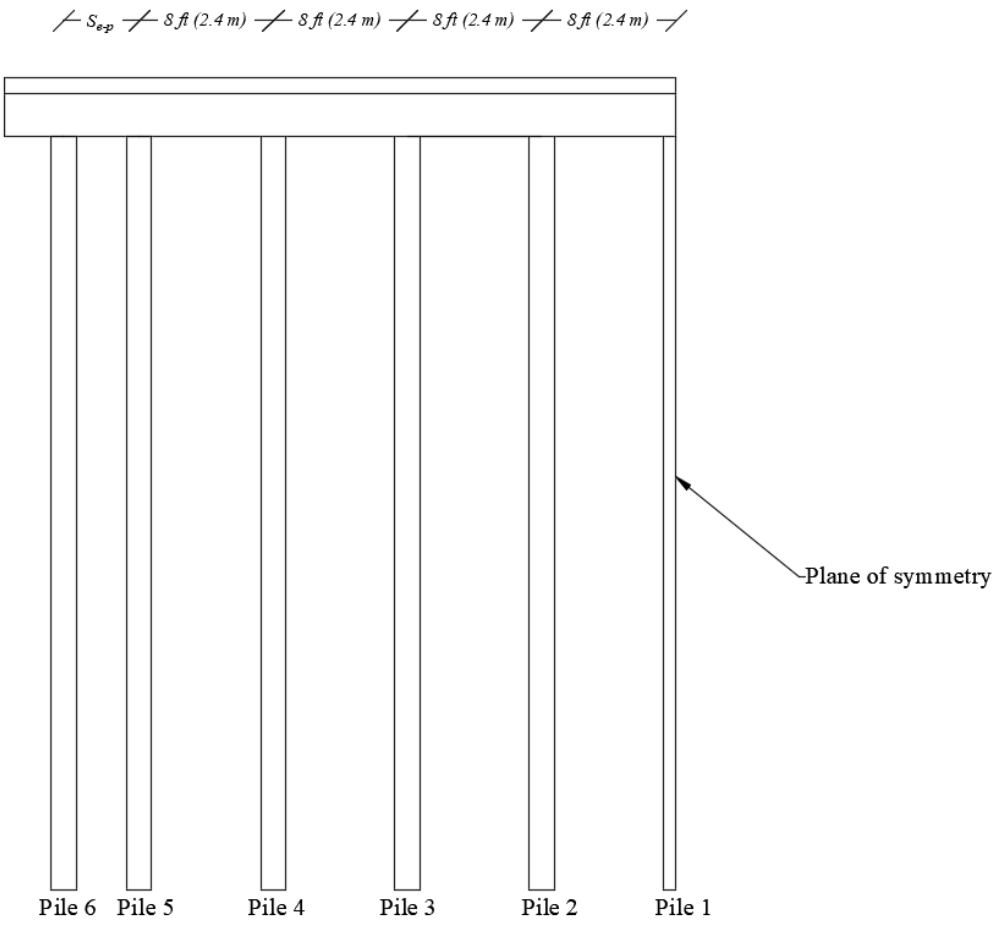

Figure 7.10 Transverse cross section of the proposed two-segment pile-supported approach slabs

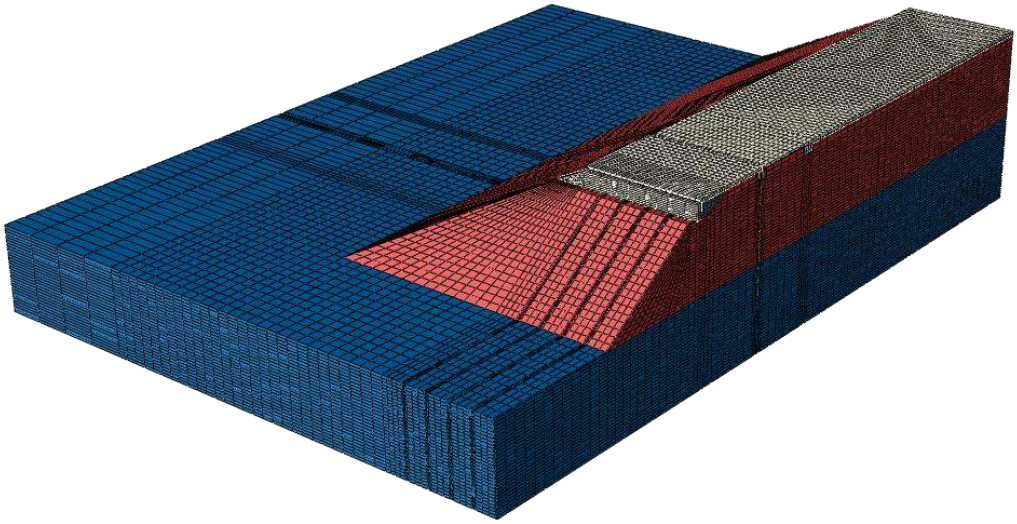

Figure 7.11 Finite element discretization of the full-scale with two-segment pile-supported approach slabs

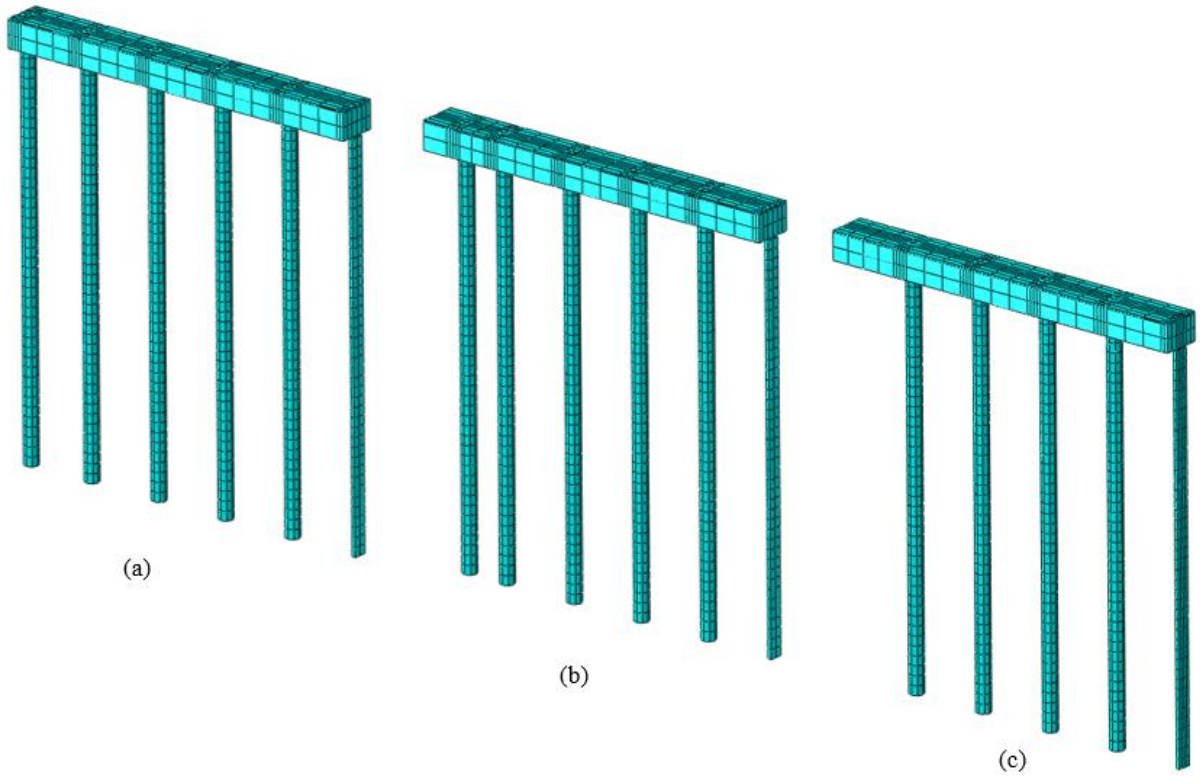

Figure 7.12 Finite element discretization of piles and cap (a) $S_{e\text{-}p}$ = 8 *ft* (b) $S_{e\text{-}p}$ = 4.5 *ft* (c) No edge-pile

The nodes from the two approach slab segments were connected using shear coupling connection. This connection was modeled to act as a joint in which restrains relative movement while allows rotation between the two segments. In addition, the connection between the piles and the pile cap was modeled as rigid connection.

The results from the simulations are presented below. Figures 7.13 and 7.14 show the contour of the vertical deformation and excess pore pressure at the end of the analysis, respectively.

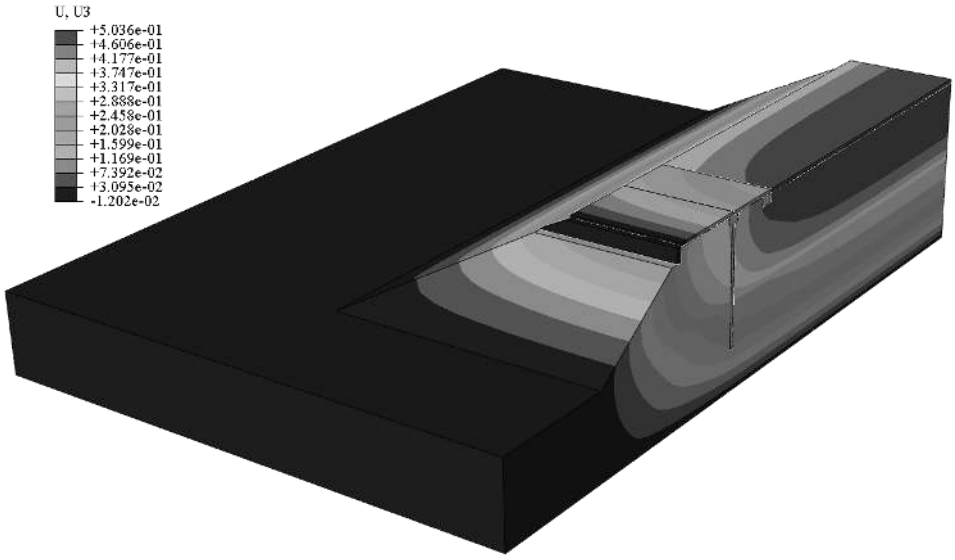

Figure 7.13 Vertical deformation contour of the full-scale model with two-segment pile-supported approach slabs (*ft*)

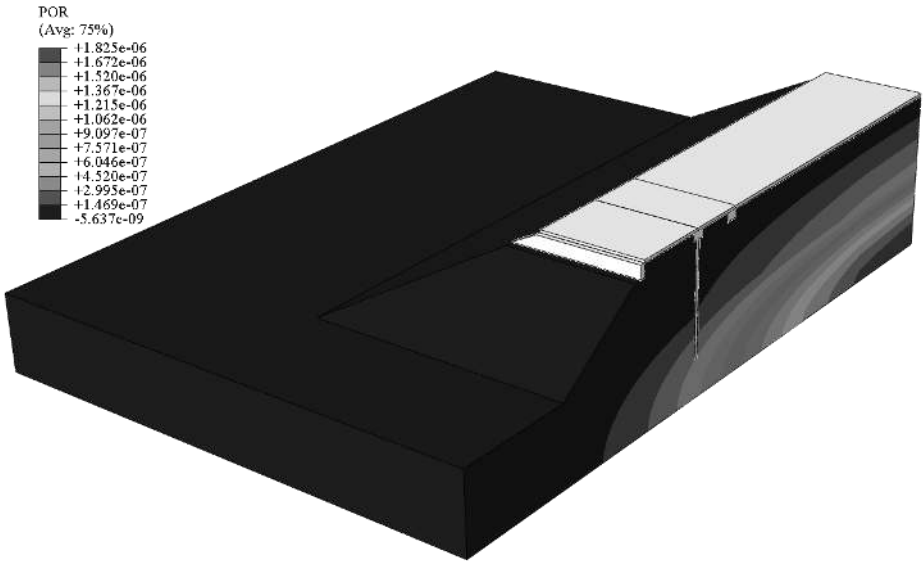

Figure 7.14 Excess pore pressure contour of the full-scale model with two-segment pile-supported approach slabs (*psf*)

Figure 7.15 shows the simulated transition profile along the center line of the two approach slab segments. The simulated two-segment pile-supported approach slabs performed best (distribution of load among piles) when $S_{e\text{-}p}$ = 8 *ft* (2.4 *m*). The resulted slope of the approach slab segments were 0.9/125 and 0.8/125, respectively.

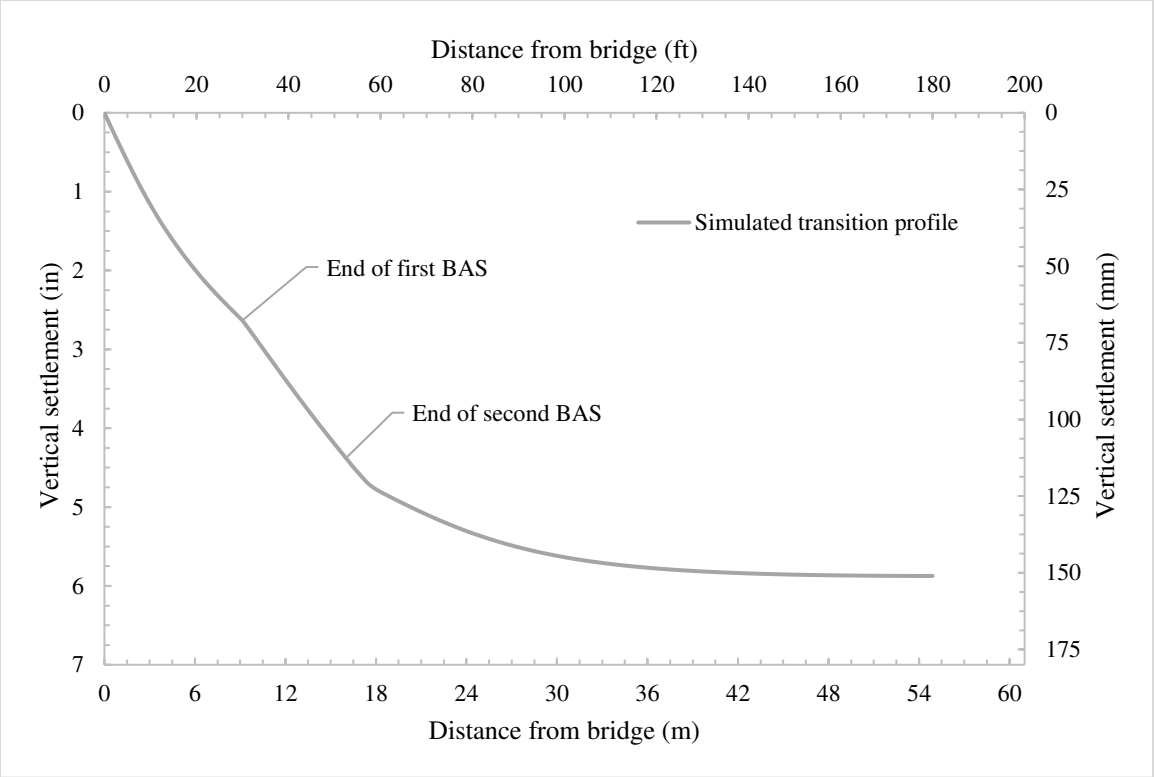

Figure 7.15 Simulated transition profile of the full-scale model with two-segment pile-supported approach slabs

Figures 7.16, 7.17, and 7.18 show the pile axial load distribution for the three pile configurations. The figures show that when no edge-pile was used, the outer piles (piles 4 and 5) experienced greater axial load than anticipated. This was attributed to the load-stiffness behavior developed among the piles. As the middle piles (piles 1,2, and 3) lost stiffness, due to settlement, the load was transferred to the outer piles (piles 4 and 5). The axial load was reduced considerably when an edge-pile was introduced (Figures 7.17 and 7.18). Figure 7.19 shows the pile head settlement along the transverse direction for the three pile configurations. The figure shows the variation in load-stiffness behavior among the piles as a function of pile spacing. Ultimately, it can be concluded that pile configuration (a) (Figure 7.12) would perform the best in a real-case scenario.

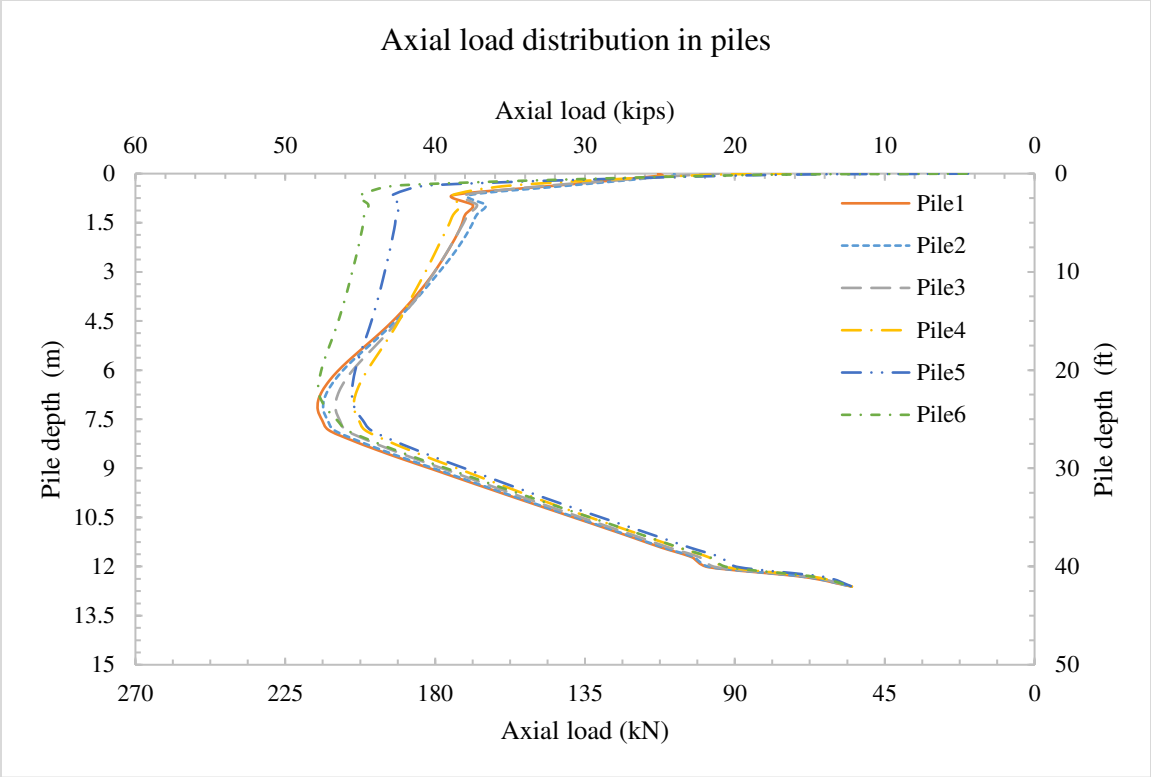

Figure 7.16 Axial load distribution in piles with $S_{e\text{-}p}$ = 8 *ft*

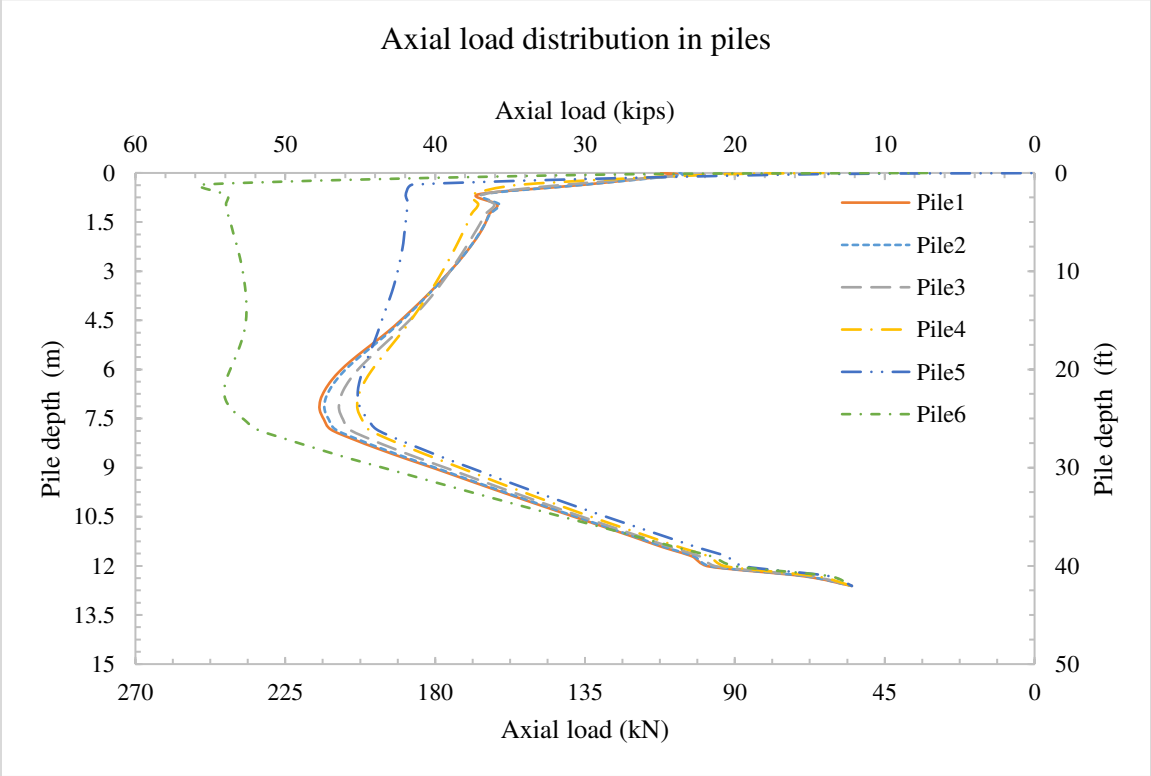

Figure 7.17 Axial load distribution in piles with $S_{e\text{-}p}$ = 4.5 *ft*

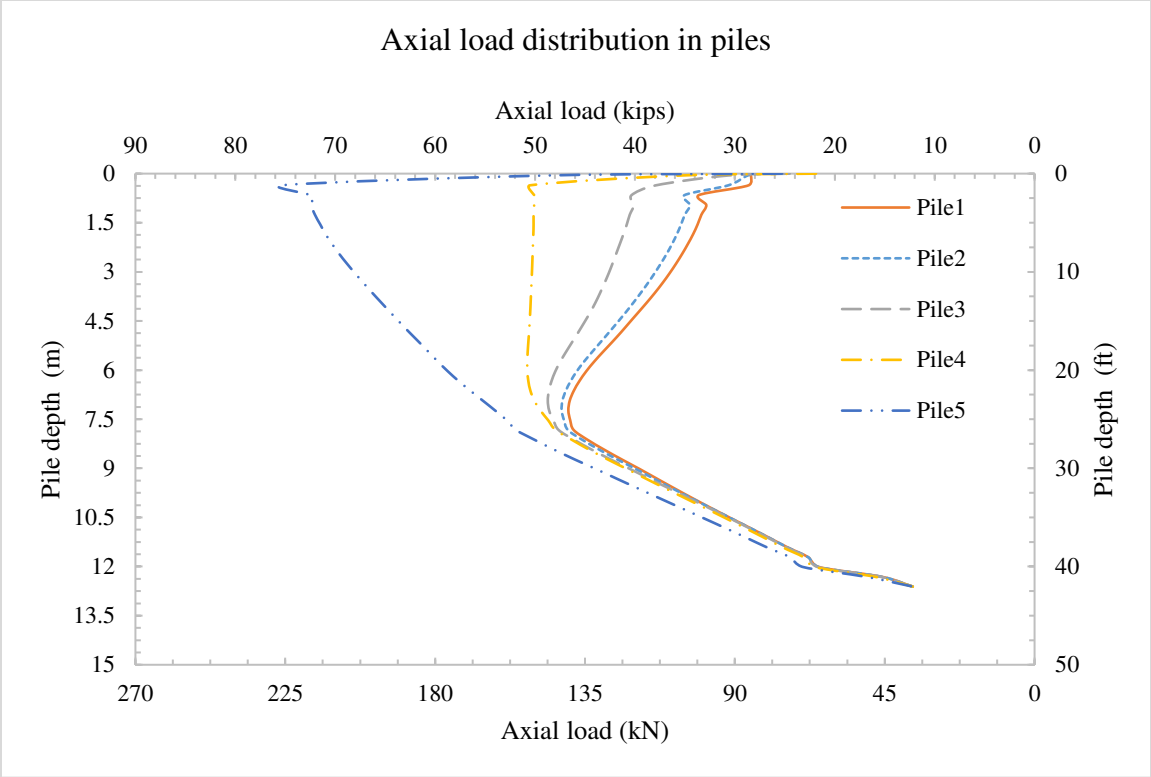

Figure 7.18 Axial load distribution in piles with no edge-pile

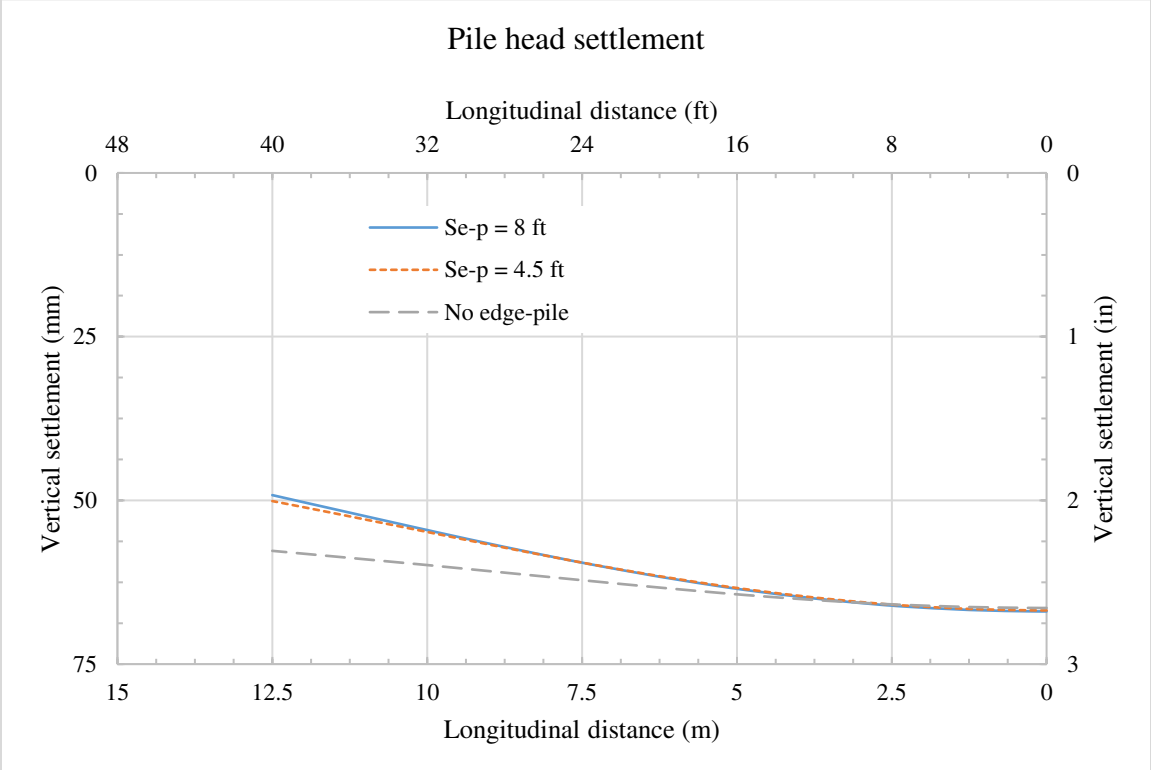

Figure 7.19 Pile heads settlement in the transverse direction

It is important to maintain the reaction forces on piles head (axial load). As live loads, namely truck loads, could add a substantial amount of force when axle wheel load is directly on the top of the pile head. This load, among others, shall be considered in the design stage to make sure the capacity of the piles is sufficient.

Based on the results obtained from the full-scale simulation, recommendations regarding the design of multi-segment pile-supported approach slabs were drawn as follows:

- Multi-segment pile-supported approach slabs can be an effective solution in cases where significant soil settlements create rough transitions between the bridge and the roadway pavement.
- Pile sizes, lengths, and spacings can be determined based on the recommended settlement equations. For that, pile head settlement design charts were developed for various pile-soil conditions.
- Along the transverse direction, piles shall be adequately spaced such that reactions on pile heads are equally distributed to the extent possible. Stiffness-load analyses could be conducted to determine possible transverse pile spacings.
- A joint should be provided between adjacent approach slab segments. This joint can be saw-cut (partially), and rubber poured over the center of the pile cap. This allows a crack to develop underneath the joint, and thus, would have the ability to accommodate rotations (Figure 7.20).
- Non-corroding dowel bars should be provided between various approach slab segments at the center of the slab thickness. This would help restrain the relative movement between approach slab segments while allowing free rotation between them (Figure 7.20).

- A rubber bearing support should be provided under the approach slab over the pile cap. This (or a similar arrangement) would be needed to accommodate the relative angle change between the various approach slab segments (Figure 7.20).

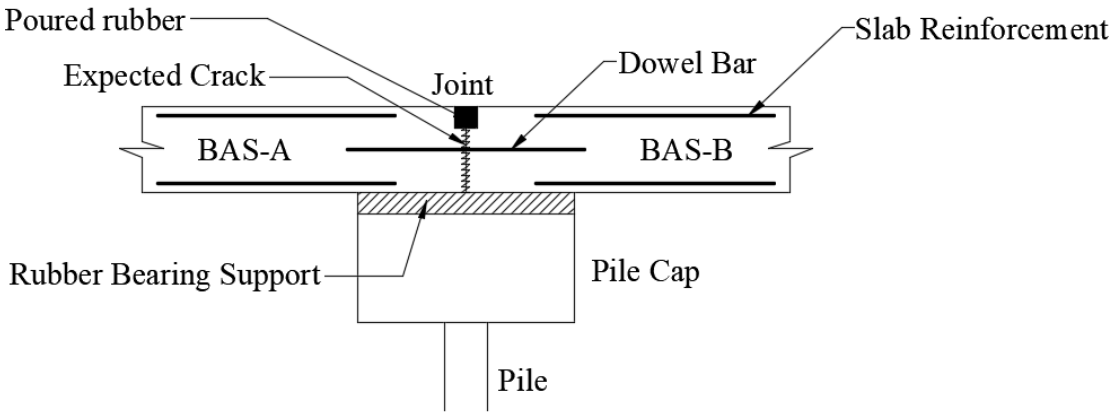

Figure 7.20 Detailed connection between various approach slab segments

CHAPTER 8 - SUMMARY, CONCLUSIONS AND RECOMMENDATIONS

The approach slab is an important element in the bridge approach system as it is intended to provide riders with a smooth transition as their vehicle travels from the roadway to the bridge and vice versa. In addition, the approach slab provides some protection to the bridge structural elements from excessive truck dynamic impact. As soil underneath the approach slab settles, deferential settlement develops between the bridge and the approaching roadway. This may negatively affect the ride quality for travelers and result in substantial long-term maintenance costs. Because of the differential settlement, bumps could develop at the ends of the bridge when abrupt changes in slope (exceeding 1/125) occur (Figure 8.1) (Abu-Farsakh and Chen 2014, Long, et al. 1999). The bump at the ends of the bridge is a well-known problem that affects 25% of the bridges in the United States, resulting in an estimated $100 million per year in maintenance expenditures (Briaud, James and Hoffman 1997).

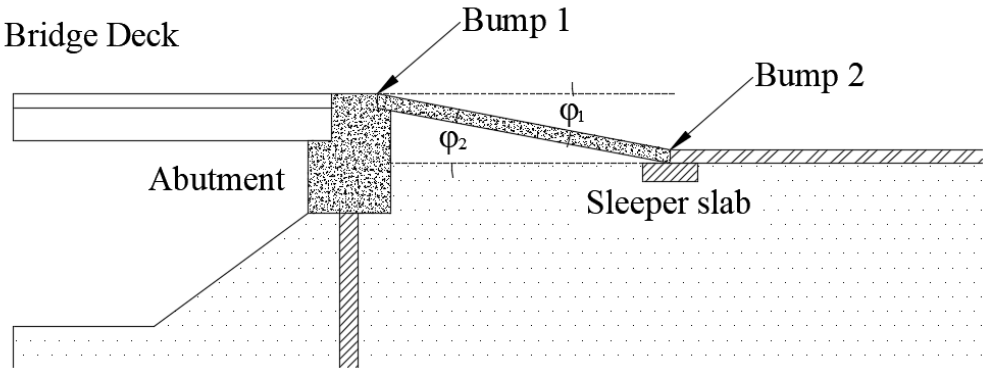

Figure 8.1 Bump formation mechanism at the end of the bridge

This study was aimed at mitigating the formation of bumps at the end of the bridge through a new design concept for the approach area. The proposed design takes advantage of settlement-reducing piles that would support various approach slab segments and control their

settlement. These pile elements are intended to control the roughness of the transition such that acceptable slope changes develop between various segments of the approach slab and thus improve the performance of the approach slab system.

In this study, a comprehensive review of literature as well as a review of various state practices regarding the approach area was performed. Information from the latest bridge design manuals from various state departments of transportation were examined (Chapter 3). This include the configuration of approach slab, connection of the approach slab to superstructure, support type at the connection between the approach slab and pavement, backfill materials, and side slope of the embankment fill. Data obtained from the bridge design manuals show that an approach slab supported on a sleeper-slab resting on soil is mostly used. Furthermore, an approach slab length of 15-30 *ft* (4.6-9.1 *m*) is commonly used.

A number of finite element models were developed, and parametric studies were performed to evaluate the soil/approach slab settlement behind bridge abutments for various soil conditions (Chapter 5), and to quantify the pile head settlement and load distribution along piles as a function of pile-soil parameters (Chapter 6). From the results of these models, it is concluded that an embankment fill height of greater than or equal to 20 *ft* (6.1 *m*) is more prone to settlement issues in the transition zone. It has been determined that the degree of compressibility of the embankment and natural soils, length of the approach slab, height of the abutment, and height and side slope of the embankment influence the potential development of bumps at approaches to bridges. Other factors such as the type of backfill material and the erosion of backfill material were less significant and thus could be ignored when evaluating the transition roughness.

Empirical relationships were developed that relate various soil parameters to the longitudinal soil deformation profile behind bridge abutments . The effect of the abutment wall on soil deformation soil was modelled using a logistic function (Figure 5.73). As a result, a set of equations were developed that define the various parameters of the logistic function. Table 8.1 shows a summary of the developed equations. Definitions of the various parameters used in Table 8.1 are given in Chapter 5.

Table 8.1 Summary of the developed equation of longitudinal settlement profile parameters

General form/parameters	Developed equations
General form of the logistic function y = vertical settlement at a distance of x from the bridge abutment	$\mathrm{y} = \dfrac{a}{1 + be^{-cx}}$
Logistic function parameter (*a*) Maximum displacement.	$a = 383 \times 10^{-6} H_n e^{\left(27\,\varepsilon_v^{e.adj} + 38.6\,\varepsilon_v^{p}\right)} + 4980 \times 10^{-6} H_e e^{\left(61\,\varepsilon_v^{e.adj.} + 23\,\varepsilon_v^{p}\right)}$
Logistic function parameter (*b*) Settlement at the interface between the abutment wall and the backfill soil.	$b = 0.38\,ln\left(C_c \times \dfrac{H_e}{H_a}\right) + 2.26$
Logistic function parameter (*c*) Steepness of the curve.	$c = 0.172\mathrm{e}^{-0.182a}$ * $c = 0.172\mathrm{e}^{-0.007a}$ **

* when (a) is in inches ** when (a) is in millimeters

Another set of finite element models was generated to quantify the pile-head settlement as well as the load distribution along the pile for various pile-soil parameters/conditions (Chapter 6). Accordingly, design charts were developed such that pile-head settlement and the corresponding reduction of settlement, R_{sett} could be determined for piles subjected to downdrag forces based upon various soil conditions (Figures 6.16 through 6.18). Relationships were also developed, using numerical analyses, to predict the distribution of axial load along the length of the pile. This includes the neutral point, total downdrag force, positive skin friction, and end-

bearing. Table 8.2 shows a summary of the developed equations. The parameters shown in Table 8.2 are defined in Chapter 6.

Table 8.2 Summary of the developed pile head settlement/load distribution equations

Parameter	Developed equations
Pile head settlement Δ_{PH}	$\Delta_{PH} = \Delta_{Ps} - 166\frac{Q_{dd}}{D_p L_{dd} G_{avg-dd}} + 41\frac{Q_{ps}}{D_p L_{ps} G_{avg-ps}} + 3.2\frac{Q_b}{D_p^2 E_b} - 0.2$
Neutral point L_{dd}	$L_{dd} = \frac{1 - \left[\frac{\left(Q_{dd_{@Q=0}} - Q_u\right)L_p}{\left(L_{dd_{@Q=0}} - L_{dd_{@Q_{dd}=0}}\right)Q_u}\left(\frac{L_{dd_{@Q_{dd}=0}}}{L_p}\right)\right] - \frac{Q}{Q_u}}{\left(1 - \frac{Q}{Q_u}\right)\left[\frac{Q_{dd_{@Q=0}}L_p}{L_{dd_{@Q=0}}Q_u}\right] - \frac{\left(Q_{dd_{@Q=0}} - Q_u\right)L_p}{\left(L_{dd_{@Q=0}} - L_{dd_{@Q_{dd}=0}}\right)Q_u}} L_p$
Downdrag force Q_{dd}	$Q_{dd} = (Q_u - Q)\left[\frac{Q_{dd_{@Q=0}}L_{dd}}{L_{dd_{@Q=0}}Q_u}\right]$
Positive skin friction Q_{ps}	$Q_{ps} = Q + Q_{dd} - Q_u\left[m_3 + \left(\frac{Q + Q_{dd}}{Q_u}\right) - m_3\left(\frac{L_{dd}}{L_p}\right)\right]$
End-bearing Q_b	$Q_b = Q_u\left[m_3 + \left(\frac{Q + Q_{dd}}{Q_u}\right) - m_3\left(\frac{L_{dd}}{L_p}\right)\right]$

In addition, procedures were provided to estimate the length and number of approach slab segments needed to achieve the desired transition profile (see Figure 8.2) as follows:

a) Determine the maximum longitudinal surface soil settlement, a or Δ_T, using either the FEM analysis or the empirical equations provided in Chapter 5.

b) If $\Delta_T \leq L_{BAS-A}\left(\frac{1}{125}\right)$, use a single-segment approach slab with $L_{BAS-A} \leq 30ft$ $(9.1m)$. Minimize L_{BAS-A} to meet this requirement.

c) If $\Delta_T > L_{BAS-A}\left(\frac{1}{125}\right)$, the settlement cannot be accommodated with a single-segment approach slab. Use a multi-segment pile-supported approach slab based on the following procedures:

a. Select pile size, length, and pile spacing for the first line of piles such that the expected pile head settlement $\Delta_A \leq L_{BAS-A}\left(\frac{1}{125}\right)$. Charts that can be used for this estimation are given Chapter 6. If the desired Δ_A cannot be achieved, change L_{BAS-A}, pile size, pile length, or pile spacing to satisfy the above settlement requirement.

b. If $L_{BAS-A}\left(\frac{1}{125}\right) < \Delta_T \leq (L_{BAS-A} + L_{BAS-B})\left(\frac{1}{125}\right)$, try a two-segment approach slab with one line of piles between the two segments. The end of the second segment should be supported on a sleeper-slab on soil.

c. If $\Delta_T > (L_{BAS-A} + L_{BAS-B})\left(\frac{1}{125}\right)$, the settlement cannot be accommodated with a two-segment approach slab. Try a three-segment approach slab. The end of the third segment should be supported on a sleeper-slab on soil.

d. Select the pile size, length, and pile spacing for the second line of piles (from the charts) such that the expected pile head settlement $\Delta_A + \Delta_B \leq (L_{BAS-A} + L_{BAS-B})\left(\frac{1}{125}\right)$.

e. If $\Delta_T > (L_{BAS-A} + 2L_{BAS-B} + L_{BAS-C})\left(\frac{1}{125}\right)$, the settlement cannot be accommodated with a three-segment approach slab. Try four-segment approach slab. The end of the fourth segment could be supported on a sleeper-slab on soil.

f. Repeat steps a-e as needed.

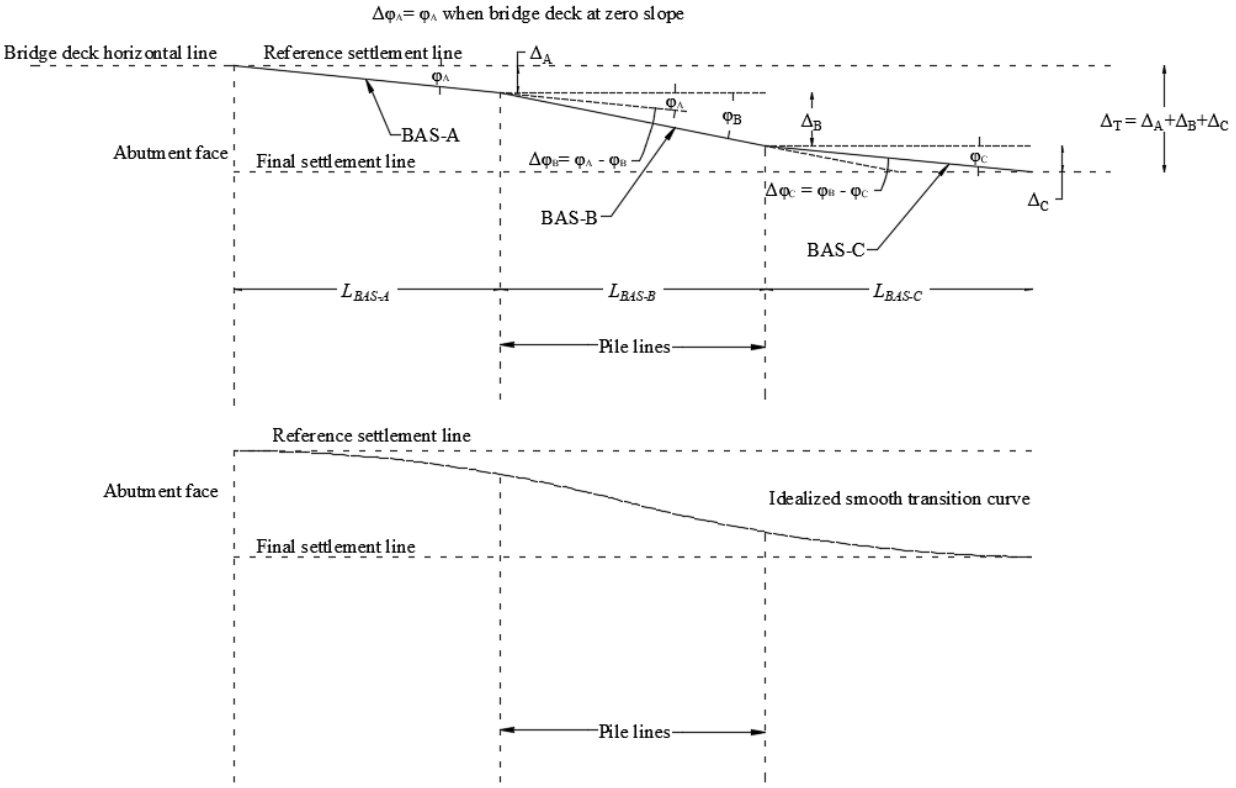

Figure 8.2 Schematic of the proposed multi-segment pile-supported approach slab system

Ultimately, a full-scale simulation was conducted to verify the developed procedures and relationships using a multi-segment pile-supported approach slab system (Chapter 7). The number and length of the approach slab segments as well as the pile sizes, lengths and spacings were estimated using the developed pile head settlement design charts.

Finally, the following conclusions can be made regarding the design of multi-segment pile-supported approach slabs:

- Multi-segment pile-supported approach slabs can be an effective solution in cases where significant soil settlements create rough transitions between the bridge and the roadway pavement.

- Pile sizes, lengths, and spacings can be determined based on the recommended settlement equations. For that, pile head settlement design charts were developed for various pile-soil conditions.
- Along the transverse direction, piles shall be adequately spaced such that reactions on pile heads are equally distributed to the extent possible. Stiffness-load analyses could be conducted to determine possible transverse pile spacings.
- A joint should be provided between adjacent approach slab segments. This joint can be saw-cut (partially), and rubber poured over the center of the pile cap. This allows a crack to develop underneath the joint, and thus, would have the ability to accommodate rotations (Figure 8.3).
- Non-corroding dowel bars should be provided between various approach slab segments at the center of the slab thickness. This would help restrain the relative movement between approach slab segments while allowing free rotation between them (Figure 8.3).
- A rubber bearing support should be provided under the approach slab over the pile cap. This (or a similar arrangement) would be needed to accommodate the relative angle change between the various approach slab segments (Figure 8.3).

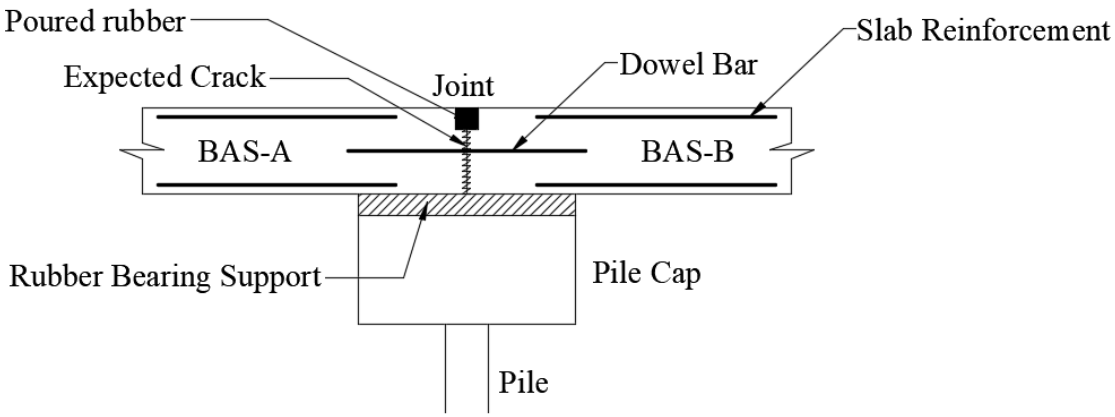

Figure 8.3 Detailed connection between various approach slab segments

8.1 Recommendation for future research

The following recommendations are made for future work:

- Future research is needed to perform field testing to monitor and evaluate the proposed multi-segment pile-supported approach slab system.
- Monte Carlo simulations can be used to assess the variability in predicted pile head settlement.
- Future research can be conducted using different pile materials (such as steel) and/or installation methods (driven piles instead of cast-in-place concrete piles).

REFERENCES

AASHTO. 2001. *A Policy on Geometric Design of Highways and Streets.* AASHTO.

ABAQUS, Analysis User's Guide. 2015. *Abaqus 2016 Online Documentation.* Dassault Systèmes, 2015.

Abu-Farsakh, Murad Y, and Qiming Chen. 2014. *Field Demonstration of New Bridge Approach Slab Designs and Performance.* Baton Rouge, LA: Louisiana Transportation Research Center.

Allen, David L, and Bobby W Meade. 1988. *Soil-Bridge Abutment Interaction.* Kentucky Transportation Research Program, College of Engineering, University of Kentucky.

Ardani, A. 1987. *Bridge approach settlement.* Colorado Department of Highways, Report No. CDOH-DTP-R-87-06.

Bakeer, Reda M, Mark A Shutt, Jianqiang Zhong, Sankar C Das, and Mark Morvant. 2005. *Performance of Pile-Supported Bridge Approach Slabs.* American Society of Civil Engineers.

Bakeer, Reda M, Mark A Shutt, Jianqiang Zhong, Sankar C Das, and Mark Morvant. 2005. *Performance of Pile-Supported Bridge Approach Slabs.* Journal of Bridge Engineering, Vol. 10, No. 2.

Bowles, Joseph E. 1997. *Foundation analysis and design.* McGraw-Hill.

Briaud, Jean Louis, and Yujin Lim. 1997. *Soil-Nailed Wall Under Piled Bridge Abutment: Simulation and Guidelines.*

Briaud, Jean Louis, Ray W. James, and Stacey B. Hoffman. 1997. *Synthesis of Highway Practice 234: Settlement of Bridge Approaches (The Bump at the end of the Bridges).* Washington, D.C.: Transportation Research Board, National Research Council.

Cai, C S, George Z Voyiadjis, and Xiaomin Shi. 2005. *Determination of Interaction between Bridge Concrete Approach Slab and Embankment Settlement.* Baton Rouge, Louisiana: Department of Civil Engineering, Louisiana State University.

Carter, Michael, and Stephen P Bentley. 2016. *Soil properties and thier correlations (Second edition).* Wiley.

Coduto, Donald P. 2001. *Foundation Design: Principles and Practices (Second Edition).* Prentice Hall.

Das, Baraja M. 2011. *Principle of Foundation Engineering, Seventh Edition.*

Das, Braja M. 2012. *Fundamentals of Geotechnical Engineering, 4th Edition.* CL Engineering.

Das, Sankar C, Reda Bakeer, Jianqiang Zhong, and Mark Schutt. 1999. *Assessment of mitigating embakment settlement with pile supported approach slabs.* Civil and Environmental Engineering Department, Tulane University.

Dupont, Bernadette, and David L Allen. 2002. *Movements and Settlements of Highway Bridge Approaches.* Lexington, Kentucky: Kentucky Transportation Center.

Greimann, Lowell, Brent Phares, Adam Faris, and Jake Bigelow. 2008. *Integral Bridge Abutment-to-Approach Slab Connection.* Ames, IA: Iowa Department of Transportation.

Helwany, Sam. 2007. *Applied Soil Mechanics with ABAQUS Applications.* Wiley.

Hopkins, Tommy C. 1985. *Long-Term Movements of Highway Bridge Approach Embankments and Pavements.* Kentucky Transportation Center Research.

Hoppe, Edward J. 1999. *Guidelines for the use, design, and construction of bridge approach slabs.* Charlottesville, Virginia: Virginia Transportation Research Council, VTRC 00-R4.

Hu, Yi Chin, Tsu Long Wu, Clyde E Lee, and Randy Machemhl. 1979. *Roughness at the Pavement-Bridge Interface, Research Number 213-1F.* Texas State Department of Highway and Public Transportation.

Irick, P E, and T L Copas. 1969. *Bridge approach design and construction practices.* NCHRP Synthesis of Highway Practice 2, Highway Research Board.

Kramer, Steven L, and Peter Sajer. 1991. *Bridge approach slab effectiveness.* Washington State Department of Transportation, Report No. WA-RD 227.1.

Laguros, J G, M M Zaman, and I U Mahmood. 1986. *Evaluation of causes of excessive settlements of pavement behind bridge abutments and their remedies-Phase I.* Norman: ODOT Study No. 84-12-2, Item 2140, ORA 155-857, University of Oklahoma.

Laguros, J G, M M Zaman, and I U Mahomood. 1990. *Evaluation of Causes of Excessive Settlements of Pavements Behind Bridge Abutments and their Remedies; Phase II.* Rep. No. FHWA/OK 89 (07), Oklahoma Department of Transportation.

Laguros, J G, M Zaman, Arumugam Alvappillai, and Kyriakos E Vavarapis. 1991. *Evaluation of Causes of Excessive Settlements of Pavements Behind Bridge Abutments and their Remedies; Phase III.* The University of Oklahoma.

Lenke, Lary R. 2006. *Settlement Issues – Bridge Approach Slabs (Final Report Phase 1).* Transportation Engineering Research Program (TERP), Department of Civil Engineering, University of New Mexico, Report No. NM04MNT-02.

Long, James H, Scott M Olson, Timothy D Stark, and Emile A Samara. 1999. *Differential movement at embankment - bridge structure interface in Illinois.* Transportation Research Record 1633, Paper No 98-1575.

McCarthy, David F. 2007. *Essential of Soil Mechanics and Foundation, 7th edition.* Pearson Education, Limited.

McGrath, T. J., I. D. Moore, E. T. Selig, M. C. Webb, and B. Taleb. 2002. *Recommended Specifications for Large-Span Culverts.* NCHRP Report 473, Transportation Research Board, National Research Council.

McLaren, D. 1970. *Settlement behind bridge abutments. The performance of silty clay fill in an approach embankment on the M4 Motorway.* RRL Reports, Road Res. Lab/UK/RRL Dept., Lr 309.

Mistry, Vasant C. 2005. *Integral Abutment and Jointless Bridges.* Federal Highway Administration.

Monley, Gregory J., and Jonathan T. H. Wu. 1993. *TENSILE REINFORCEMENT EFFECTS ON BRIDGE-APPROACH SETTLEMENT.* Journal of Geotechnical Engineering.

Nabizadeh, Azam, Habib Tabatabai, and Mohammad A. Tabatabai. 2018. *Survival Analysis of Bridge Superstructures in Wisconsin.* Applied Sciences, MDPI, 2018, 8, 2079.

Nassif, Hani, Talat Abu-Amra, and Nirali Shah. 2002. *Finite Element Modeling of Bridge Approach and Transition Slabs.* New Jersey Department of Transportation, FHWA-NJ-2002-007.

Nicks, Jennifer. 2015. "Bump at the Bridge." *Long-Term Bridge Performance (LTBP)* 5 (Federal Highway Administration Research and Technology, FHWA-HRT-15-050): 8-9.

Phares, Brent, and Justin Dahlberg. 2015. *Performance and design of bridge approach panels in Wisconsin.* Bridge Engineering Center, Iowa State University.

Puppala, Anand J, Sireesh Saride, Ekarut Archeewa, Laureano R Hoyos, and Soheil Nazarian. 2008. *Recommendations for Design, Construction, and Maintenance of Bridge Approach Slabs: Synthesis Report.* Austin, Texas: Texas Department of Transportation, Research and Technology Implementation Office.

Seo, Jeongbok, Hunsoo Ha, and Jean Louis Briaud. 2002. *Investigation of Settlement at Bridge Approach Slab Expansion Joint: Numerical Simulations and Model Tests.* Austin, Texas: Texas Department of Transportation, Research and Technology Implementation Office.

Tabatabai, Habib, and Azam Nabizadeh. 2018. *Evaluation of Thin Polymer Overlays for Bridge Decks.* Proceeding of Structural Faults and Repair Conference, Edinburgh, UK.

Tabatabai, Habib, Azam Nabizadeh, and Mohammad A Tabatabai. 2018. *Overview of Survival Analysis Techniques for Probabilistic Assessment of Bridge Service Life.* Proceeding of Structural Faults and Repair Conference, Edinburgh, UK.

Wahls, Harvey E. 1990. *Design and Construction of Bridge Approaches.* Washington, D.C: National Cooperative Highway Research Program, Synthesis of Highway Practice 159, Transportation Research Board, National Research Council.

Walkinshaw, John L. 1978. *Survey of Bridge Movements in the Western United States.* Washington, D.C., 6–12: Transportation Research Record 678: Tolerable Movements of Bridge Foundations, Sand Drains, K-Test, Slopes, and Culverts, Transportation Research Board, National Research Council.

Washington State Department of Transportation. 2015. *Bridge Design Manula (LRFD), M23-50.14.* Engineering and Regional Operation, Bridge and Structure Office.

White, David, Sri Sritharan, Muhannad Suleiman, Mohamed Mekkawy, and Sudhar Chetlur. 2005. *Identification of the Best Practices for Design, Construction, and Repair of Bridge Approaches.* Iowa Highway Research Board, Iowa Department of Transportation, CTRE Project 02-118.

Wicke, M, and D Stoelhorst. 1982. *Problems associated with the design and construction of concrete pavements on approach embankments.* Terminal House, Grosvenor Gardens, London, England: Concrete Society.

Wong, H. K. W, and J C Small. 1994. *Effect of Orientation of Bridge Slabs on Pavement Deformation.* Journal of Transportation Engineering, 120(4), 590–602.

Zaman, Musharraf , Giancarlo Gioda, and John Booker. 2000. *Modeling in Geomechanics, 1st Edition.* Wiley.

APPENDICES

Appendix A - Settlement-induced slope of the approach slab

This appendix provides results indicating the slope of the approach slab that would result from the differential settlement of the soil under a single 20 *ft* (6.1 *m*) approach slab segment. These results were obtained from the parametric study on the longitudinal model (see Tables 5.10 and 5.11).

Table A.1 Summary of the resulting slope of the approach slab for soil profile No.1

H_n *ft* *(m)*	H_e *ft* *(m)*	Natural soil type (compressibility degree)	Embankment soil type (compressibility degree)	Backfill Compaction Level	Slope of Backfill Area (V to H)	Resulting Slope
30 (9.1)	30 (9.1)	High	High	Wall Abutment		
				95%	1 to 2	2.4/125
					1 to 1	2.6/125
				90%	1 to 2	2.6/125
					1 to 1	2.7/125
				Stub Abutment (10 *ft*) (3.0 *m*)		
				95%	1 to 2	3.0/125
					1 to 1	3.0/125
				90%	1 to 2	3.0/125
					1 to 1	3.0/125
				Stub Abutment (5 *ft*) (1.5 *m*)		
				95%	1 to 2	3.2/125
					1 to 1	3.2/125
				90%	1 to 2	3.2/125
					1 to 1	3.2/125

Table A.2 Summary of the resulting slope of the approach slab for soil profile No.2

H_n *ft* *(m)*	H_e *ft* *(m)*	Natural soil type (compressibility degree)	Embankment soil type (compressibility degree)	Backfill Compaction Level	Slope of Backfill Area (V to H)	Resulting Slope
30 (9.1)	30 (9.1)	High	Moderate	Wall Abutment		
				95%	1 to 2	2.1/125
					1 to 1	2.2/125
				90%	1 to 2	2.1/125
					1 to 1	2.2/125
				Stub Abutment (10 *ft*) (3.0 *m*)		
				95%	1 to 2	2.3/125
					1 to 1	2.3/125
				90%	1 to 2	2.3/125
					1 to 1	2.3/125
				Stub Abutment (5 *ft*) (1.5 *m*)		
				95%	1 to 2	2.4/125
					1 to 1	2.4/125
				90%	1 to 2	2.4/125
					1 to 1	2.4/125

Table A.3 Summary of the resulting slope of the approach slab for soil profile No.3

H_n *ft* *(m)*	H_e *ft* *(m)*	Natural soil type (compressibility degree)	Embankment soil type (compressibility degree)	Backfill Compaction Level	Slope of Backfill Area (V to H)	Resulting Slope
30 (9.1)	30 (9.1)	High	Low	Wall Abutment		
				95%	1 to 2	1.9/125
					1 to 1	1.9/125
				90%	1 to 2	2.0/125
					1 to 1	2.0/125
				Stub Abutment (10 *ft*) (3.0 *m*)		
				95%	1 to 2	2.1/125
					1 to 1	2.1/125
				90%	1 to 2	2.1/125
					1 to 1	2.1/125
				Stub Abutment (5 *ft*) (1.5 *m*)		
				95%	1 to 2	2.1/125
					1 to 1	2.1/125
				90%	1 to 2	2.1/125
					1 to 1	2.1/125

Table A.4 Summary of the resulting slope of the approach slab for soil profile No.4

H_n *ft* *(m)*	H_e *ft* *(m)*	Natural soil type (compressibility degree)	Embankment soil type (compressibility degree)	Backfill Compaction Level	Slope of Backfill Area (V to H)	Resulting Slope
30 (9.1)	30 (9.1)	Moderate	Moderate	Wall Abutment		
				95%	1 to 2	1.3/125
					1 to 1	1.4/125
				90%	1 to 2	1.5/125
					1 to 1	1.5/125
				Stub Abutment (10 *ft*) (3.0 *m*)		
				95%	1 to 2	1.6/125
					1 to 1	1.6/125
				90%	1 to 2	1.6/125
					1 to 1	1.6/125
				Stub Abutment (5 *ft*) (1.5 *m*)		
				95%	1 to 2	1.7/125
					1 to 1	1.7/125
				90%	1 to 2	1.7/125
					1 to 1	1.7/125

Table A.5 Summary of the resulting slope of the approach slab for soil profile No.5

H_n *ft* *(m)*	H_e *ft* *(m)*	Natural soil type (compressibility degree)	Embankment soil type (compressibility degree)	Backfill Compaction Level	Slope of Backfill Area (V to H)	Resulting Slope
30 (9.1)	30 (9.1)	Moderate	Low	Wall Abutment		
				95%	1 to 2	1.3/125
					1 to 1	1.4/125
				90%	1 to 2	1.3/125
					1 to 1	1.4/125
				Stub Abutment (10 *ft*) (3.0 *m*)		
				95%	1 to 2	1.5/125
					1 to 1	1.5/125
				90%	1 to 2	1.5/125
					1 to 1	1.5/125
				Stub Abutment (5 *ft*) (1.5 *m*)		
				95%	1 to 2	1.5/125
					1 to 1	1.5/125
				90%	1 to 2	1.5/125
					1 to 1	1.5/125

Table A.6 Summary of the resulting slope of the approach slab for soil profile No.6

H_n *ft* *(m)*	H_e *ft* *(m)*	Natural soil type (compressibility degree)	Embankment soil type (compressibility degree)	Backfill Compaction Level	Slope of Backfill Area (V to H)	Resulting Slope
30 (9.1)	30 (9.1)	Low	Low	Wall Abutment		
				95%	1 to 2	1.2/125
					1 to 1	1.3/125
				90%	1 to 2	1.4/125
					1 to 1	1.4/125
				Stub Abutment (10 *ft*) (3.0 *m*)		
				95%	1 to 2	1.4/125
					1 to 1	1.4/125
				90%	1 to 2	1.4/125
					1 to 1	1.4/125
				Stub Abutment (5 *ft*) (1.5 *m*)		
				95%	1 to 2	1.4/125
					1 to 1	1.4/125
				90%	1 to 2	1.4/125
					1 to 1	1.4/125

Table A.7 Summary of the resulting slope of the approach slab for soil profile No.7

H_n *ft* *(m)*	H_e *ft* *(m)*	Natural soil type (compressibility degree)	Embankment soil type (compressibility degree)	Backfill Compaction Level	Slope of Backfill Area (V to H)	Resulting Slope
30 (9.1)	20 (6.1)	High	High	Wall Abutment		
				95%	1 to 2	1.1/125
					1 to 1	1.2/125
				90%	1 to 2	1.2/125
					1 to 1	1.3/125
				Stub Abutment (10 *ft*) (3.0 *m*)		
				95%	1 to 2	1.4/125
					1 to 1	1.5/125
				90%	1 to 2	1.5/125
					1 to 1	1.5/125
				Stub Abutment (5 *ft*) (1.5 *m*)		
				95%	1 to 2	1.6/125
					1 to 1	1.6/125
				90%	1 to 2	1.6/125
					1 to 1	1.6/125

Table A.8 Summary of the resulting slope of the approach slab for soil profile No.8

H_n *ft* *(m)*	H_e *ft* *(m)*	Natural soil type (compressibility degree)	Embankment soil type (compressibility degree)	Backfill Compaction Level	Slope of Backfill Area (V to H)	Resulting Slope
30 (9.1)	20 (6.1)	High	Moderate	Wall Abutment		
				95%	1 to 2	0.9/125
					1 to 1	0.9/125
				90%	1 to 2	0.9/125
					1 to 1	0.9/125
				Stub Abutment (10 *ft*) (3.0 *m*)		
				95%	1 to 2	1/125
					1 to 1	1/125
				90%	1 to 2	1/125
					1 to 1	1/125
				Stub Abutment (5 *ft*) (1.5 *m*)		
				95%	1 to 2	1/125
					1 to 1	1/125
				90%	1 to 2	1/125
					1 to 1	1/125

Table A.9 Summary of the resulting slope of the approach slab for soil profile No.9

H_n *ft* *(m)*	H_e *ft* *(m)*	Natural soil type (compressibility degree)	Embankment soil type (compressibility degree)	Backfill Compaction Level	Slope of Backfill Area (V to H)	Resulting Slope
30 (9.1)	20 (6.1)	High	Low	Wall Abutment		
				95%	1 to 2	0.9/125
					1 to 1	0.9/125
				90%	1 to 2	0.9/125
					1 to 1	0.9/125
				Stub Abutment (10 *ft*) (3.0 *m*)		
				95%	1 to 2	1/125
					1 to 1	1/125
				90%	1 to 2	1/125
					1 to 1	1/125
				Stub Abutment (5 *ft*) (1.5 *m*)		
				95%	1 to 2	1/125
					1 to 1	1/125
				90%	1 to 2	1/125
					1 to 1	1/125

Appendix B - Longitudinal soil settlement profile

This appendix provides detailed results for the longitudinal soil settlement profile from selected number of analyses conducted in the parametric study of the longitudinal model (see Tables 5.10 and 5.11).

Table B.1 Longitudinal soil settlement profile behind bridge abutment (Soil profile No.1, Analysis No.1)

H_n *ft (m)*	H_e *ft (m)*	Natural soil type	Embankment soil type	Abutment type/height *ft (m)*	Backfill Compaction Level	Slope of Backfill Area (V to H)	Distance from the bridge *ft (m)*	Soil vertical settlement *in (mm)*
30 (9.1)	30 (9.1)	Highly compressible clay	Highly compressible clay	Wall abutment/ $H_a = H_e$	95%	1 to 2	0 (0)	1.0 (25)
							3 (1)	2.9 (74)
							6 (2)	3.6 (91)
							10 (3)	3.9 (100)
							20 (6)	4.8 (121)
							30 (9)	5.4 (138)
							40 (12)	6.1 (154)
							50 (15)	6.6 (168)
							60 (18)	7.0 (179)
							70 (21)	7.4 (188)
							80 (24)	7.6 (194)
							90 (27)	7.8 (198)
							100 (30)	7.9 (201)
							110 (34)	8.0 (204)
							120 (37)	8.1 (205)
							130 (40)	8.1 (206)
							140 (43)	8.1 (207)
							150 (46)	8.2 (208)
							160 (49)	8.2 (208)
							170 (52)	8.2 (208)
							180 (55)	8.2 (208)

Table B.2 Longitudinal soil settlement profile behind bridge abutment (Soil profile No.1, Analysis No.12)

H_n *ft (m)*	H_e *ft (m)*	Natural soil type	Embankment soil type	Abutment type/height *ft (m)*	Backfill Compaction Level	Slope of Backfill Area (V to H)	Distance from the bridge *ft (m)*	Soil vertical settlement *in (mm)*
30 (9.1)	30 (9.1)	Highly compressible clay	Highly compressible clay	Stub abutment/ Ha = 5 (1.5)	90%	1 to 1	0 (0)	1.3 (33)
							3 (1)	3.5 (88)
							6 (2)	4.4 (111)
							10 (3)	5.0 (127)
							20 (6)	6.0 (154)
							30 (9)	6.5 (166)
							40 (12)	7.0 (178)
							50 (15)	7.3 (186)
							60 (18)	7.6 (193)
							70 (21)	7.8 (198)
							80 (25)	7.9 (201)
							91 (28)	8.0 (204)
							101 (31)	8.1 (205)
							111 (34)	8.1 (207)
							121 (37)	8.2 (207)
							131 (40)	8.2 (208)
							141 (43)	8.2 (209)
							151 (46)	8.2 (209)
							161 (49)	8.2 (209)
							171 (52)	8.2 (209)
							180 (55)	8.2 (209)

Table B.3 Longitudinal soil settlement profile behind bridge abutment (Soil profile No.2, Analysis No.1)

H_n *ft (m)*	H_e *ft (m)*	Natural soil type	Embankment soil type	Abutment type/height *ft (m)*	Backfill Compaction Level	Slope of Backfill Area (V to H)	Distance from the bridge *ft (m)*	Soil vertical settlement *in (mm)*
30 (9.1)	30 (9.1)	Highly compressible clay	Moderately compressible clay	Wall abutment/ $H_a = H_e$	95%	1 to 2	0 (0)	1.4 (36)
							3 (1)	2.6 (67)
							6 (2)	3.1 (80)
							10 (3)	3.4 (87)
							20 (6)	4.0 (102)
							30 (9)	4.5 (114)
							40 (12)	4.9 (125)
							50 (15)	5.3 (134)
							60 (18)	5.5 (140)
							70 (21)	5.7 (145)
							80 (24)	5.9 (149)
							90 (27)	6.0 (152)
							100 (30)	6.1 (154)
							110 (34)	6.1 (156)
							120 (37)	6.2 (157)
							130 (40)	6.2 (158)
							140 (43)	6.2 (158)
							150 (46)	6.2 (159)
							160 (49)	6.3 (159)
							170 (52)	6.3 (159)
							180 (55)	6.3 (159)

Table B.4 Longitudinal soil settlement profile behind bridge abutment (Soil profile No.2, Analysis No.12)

H_n *ft (m)*	H_e *ft (m)*	Natural soil type	Embankment soil type	Abutment type/height *ft (m)*	Backfill Compaction Level	Slope of Backfill Area (V to H)	Distance from the bridge *ft (m)*	Soil vertical settlement *in (mm)*
30 (9.1)	30 (9.1)	Highly compressible clay	Moderately compressible clay	Stub abutment/ Ha = 5 (1.5)	90%	1 to 1	0 (0)	1.4 (36)
							3 (1)	2.9 (73)
							6 (2)	3.6 (92)
							10 (3)	4.0 (102)
							20 (6)	4.8 (121)
							30 (9)	5.1 (129)
							40 (12)	5.4 (136)
							50 (15)	5.6 (142)
							60 (18)	5.8 (147)
							70 (21)	5.9 (150)
							80 (25)	6.0 (153)
							90 (28)	6.1 (154)
							101 (31)	6.1 (156)
							111 (34)	6.2 (157)
							121 (37)	6.2 (158)
							131 (40)	6.2 (159)
							141 (43)	6.3 (159)
							151 (46)	6.3 (159)
							161 (49)	6.3 (160)
							170 (52)	6.3 (160)
							180 (55)	6.3 (160)

Table B.5 Longitudinal soil settlement profile behind bridge abutment (Soil profile No.3, Analysis No.1)

H_n *ft (m)*	H_e *ft (m)*	Natural soil type	Embankment soil type	Abutment type/height *ft (m)*	Backfill Compaction Level	Slope of Backfill Area (V to H)	Distance from the bridge *ft (m)*	Soil vertical settlement *in (mm)*
30 (9.1)	30 (9.1)	Highly compressible clay	Low compressible clay	Wall abutment/ $H_a = H_e$	95%	1 to 2	0 (0)	1.5 (37)
							3 (1)	2.4 (62)
							6 (2)	2.9 (73)
							10 (3)	3.1 (79)
							20 (6)	3.6 (93)
							30 (9)	4.0 (101)
							40 (12)	4.3 (109)
							50 (15)	4.5 (116)
							60 (18)	4.7 (120)
							70 (21)	4.8 (123)
							80 (24)	4.9 (125)
							90 (27)	5.0 (126)
							100 (30)	5.0 (127)
							110 (34)	5.0 (128)
							120 (37)	5.0 (128)
							130 (40)	5.1 (129)
							140 (43)	5.1 (129)
							150 (46)	5.1 (129)
							160 (49)	5.1 (129)
							170 (52)	5.1 (129)
							180 (55)	5.1 (129)

Table B.6 Longitudinal soil settlement profile behind bridge abutment (Soil profile No.3, Analysis No.12)

H_n *ft (m)*	H_e *ft (m)*	Natural soil type	Embankment soil type	Abutment type/height *ft (m)*	Backfill Compaction Level	Slope of Backfill Area (V to H)	Distance from the bridge *ft (m)*	Soil vertical settlement *in (mm)*
30 (9.1)	30 (9.1)	Highly compressible clay	Low compressible clay	Stub abutment/ Ha = 5 (1.5)	90%	1 to 1	0 (0)	2.1 (53)
							3 (1)	3.0 (76)
							6 (2)	3.3 (84)
							10 (3)	3.5 (90)
							20 (6)	4.1 (105)
							30 (9)	4.3 (109)
							40 (12)	4.5 (114)
							50 (15)	4.6 (118)
							60 (18)	4.8 (121)
							70 (21)	4.8 (123)
							80 (25)	4.9 (125)
							90 (28)	5.0 (126)
							101 (31)	5.0 (127)
							111 (34)	5.0 (127)
							121 (37)	5.0 (128)
							131 (40)	5.1 (128)
							141 (43)	5.1 (129)
							151 (46)	5.1 (129)
							161 (49)	5.1 (129)
							170 (52)	5.1 (129)
							180 (55)	5.1 (129)

Table B.7 Longitudinal soil settlement profile behind bridge abutment (Soil profile No.4, Analysis No.1)

H_n *ft (m)*	H_e *ft (m)*	Natural soil type	Embankment soil type	Abutment type/height *ft (m)*	Backfill Compaction Level	Slope of Backfill Area (V to H)	Distance from the bridge *ft (m)*	Soil vertical settlement *in (mm)*
30 (9.1)	30 (9.1)	Moderately compressible clay	Moderately compressible clay	Wall abutment/ $H_a = H_e$	95%	1 to 2	0 (0)	0.8 (21)
							3 (1)	1.6 (39)
							6 (2)	1.9 (48)
							10 (3)	2.1 (53)
							20 (6)	2.6 (65)
							30 (9)	2.8 (72)
							40 (12)	3.1 (78)
							50 (15)	3.3 (83)
							60 (18)	3.4 (86)
							70 (21)	3.5 (88)
							80 (24)	3.5 (89)
							90 (27)	3.5 (89)
							100 (30)	3.5 (90)
							110 (34)	3.5 (90)
							120 (37)	3.6 (90)
							130 (40)	3.6 (91)
							140 (43)	3.6 (91)
							150 (46)	3.6 (91)
							160 (49)	3.6 (91)
							170 (52)	3.6 (91)
							180 (55)	3.6 (91)

Table B.8 Longitudinal soil settlement profile behind bridge abutment (Soil profile No.4, Analysis No.12)

H_n *ft (m)*	H_e *ft (m)*	Natural soil type	Embankment soil type	Abutment type/height *ft (m)*	Backfill Compaction Level	Slope of Backfill Area (V to H)	Distance from the bridge *ft (m)*	Soil vertical settlement *in (mm)*
30 (9.1)	30 (9.1)	Moderately compressible clay	Moderately compressible clay	Stub abutment/ Ha = 5 (1.5)	90%	1 to 1	0 (0)	1.4 (35)
							3 (1)	1.9 (48)
							6 (2)	2.4 (60)
							10 (3)	2.7 (68)
							20 (6)	3.2 (81)
							30 (9)	3.3 (83)
							40 (12)	3.4 (85)
							50 (15)	3.4 (87)
							60 (18)	3.5 (88)
							70 (21)	3.5 (89)
							80 (25)	3.5 (89)
							90 (28)	3.5 (90)
							101 (31)	3.5 (90)
							111 (34)	3.6 (90)
							121 (37)	3.6 (91)
							131 (40)	3.6 (91)
							141 (43)	3.6 (91)
							151 (46)	3.6 (91)
							161 (49)	3.6 (91)
							170 (52)	3.6 (91)
							180 (55)	3.6 (91)

Table B.9 Longitudinal soil settlement profile behind bridge abutment (Soil profile No.5, Analysis No.1)

H_n *ft (m)*	H_e *ft (m)*	Natural soil type	Embankment soil type	Abutment type/height *ft (m)*	Backfill Compaction Level	Slope of Backfill Area (V to H)	Distance from the bridge *ft (m)*	Soil vertical settlement *in (mm)*
30 (9.1)	30 (9.1)	Moderately compressible clay	Low compressible clay	Wall abutment/ $H_a = H_e$	95%	1 to 2	0 (0)	0.9 (23)
							3 (1)	1.5 (38)
							6 (2)	1.8 (47)
							10 (3)	2.0 (51)
							20 (6)	2.4 (62)
							30 (9)	2.6 (67)
							40 (12)	2.8 (72)
							50 (15)	3.0 (75)
							60 (18)	3.0 (77)
							70 (21)	3.1 (78)
							80 (24)	3.1 (78)
							90 (27)	3.1 (78)
							100 (30)	3.1 (78)
							110 (34)	3.1 (78)
							120 (37)	3.1 (78)
							130 (40)	3.1 (78)
							140 (43)	3.1 (78)
							150 (46)	3.1 (78)
							160 (49)	3.1 (78)
							170 (52)	3.1 (78)
							180 (55)	3.1 (78)

Table B.10 Longitudinal soil settlement profile behind bridge abutment (Soil profile No.5, Analysis No.12)

H_n *ft (m)*	H_e *ft (m)*	Natural soil type	Embankment soil type	Abutment type/height *ft (m)*	Backfill Compaction Level	Slope of Backfill Area (V to H)	Distance from the bridge *ft (m)*	Soil vertical settlement *in (mm)*
30 (9.1)	30 (9.1)	Moderately compressible clay	Low compressible clay	Stub abutment/ Ha = 5 (1.5)	90%	1 to 1	0 (0)	2.1 (54)
							3 (1)	2.2 (57)
							6 (2)	2.3 (59)
							10 (3)	2.5 (63)
							20 (6)	2.9 (73)
							30 (9)	2.9 (74)
							40 (12)	3.0 (76)
							50 (15)	3.0 (77)
							60 (18)	3.0 (77)
							70 (21)	3.1 (78)
							80 (25)	3.1 (78)
							90 (28)	3.1 (78)
							101 (31)	3.1 (78)
							111 (34)	3.1 (78)
							121 (37)	3.1 (78)
							131 (40)	3.1 (78)
							141 (43)	3.1 (78)
							151 (46)	3.1 (78)
							161 (49)	3.1 (78)
							170 (52)	3.1 (78)
							180 (55)	3.1 (78)

Table B.11 Longitudinal soil settlement profile behind bridge abutment (Soil profile No.6, Analysis No.1)

H_n *ft (m)*	H_e *ft (m)*	Natural soil type	Embankment soil type	Abutment type/height *ft (m)*	Backfill Compaction Level	Slope of Backfill Area (V to H)	Distance from the bridge *ft (m)*	Soil vertical settlement *in (mm)*
30 (9.1)	30 (9.1)	Low compressible clay	Low compressible clay	Wall abutment/ $H_a = H_e$	95%	1 to 2	0 (0)	1.1 (27)
							3 (1)	1.6 (39)
							6 (2)	1.8 (47)
							10 (3)	2.0 (51)
							20 (6)	2.3 (60)
							30 (9)	2.5 (63)
							40 (12)	2.6 (66)
							50 (15)	2.7 (69)
							60 (18)	2.7 (70)
							70 (21)	2.7 (70)
							80 (24)	2.7 (70)
							90 (27)	2.7 (69)
							100 (30)	2.7 (69)
							110 (34)	2.7 (69)
							120 (37)	2.7 (69)
							130 (40)	2.7 (69)
							140 (43)	2.7 (69)
							150 (46)	2.7 (69)
							160 (49)	2.7 (69)
							170 (52)	2.7 (69)
							180 (55)	2.7 (69)

Table B.12 Longitudinal soil settlement profile behind bridge abutment (Soil profile No.6, Analysis No.12)

H_n *ft (m)*	H_e *ft (m)*	Natural soil type	Embankment soil type	Abutment type/height *ft (m)*	Backfill Compaction Level	Slope of Backfill Area (V to H)	Distance from the bridge *ft (m)*	Soil vertical settlement *in (mm)*
30 (9.1)	30 (9.1)	Low compressible clay	Low compressible clay	Stub abutment/ Ha = 5 (1.5)	90%	1 to 1	0 (0)	2.1 (53)
							3 (1)	2.2 (55)
							6 (2)	2.3 (58)
							10 (3)	2.4 (61)
							20 (6)	2.7 (69)
							30 (9)	2.7 (69)
							40 (12)	2.7 (70)
							50 (15)	2.8 (70)
							60 (18)	2.8 (70)
							70 (21)	2.7 (70)
							80 (25)	2.7 (70)
							90 (28)	2.7 (69)
							101 (31)	2.7 (69)
							111 (34)	2.7 (69)
							121 (37)	2.7 (69)
							131 (40)	2.7 (69)
							141 (43)	2.7 (69)
							151 (46)	2.7 (69)
							161 (49)	2.7 (69)
							170 (52)	2.7 (69)
							180 (55)	2.7 (69)

Table B.13 Longitudinal soil settlement profile behind bridge abutment (Soil profile No.7, Analysis No.1)

H_n *ft (m)*	H_e *ft (m)*	Natural soil type	Embankment soil type	Abutment type/height *ft (m)*	Backfill Compaction Level	Slope of Backfill Area (V to H)	Distance from the bridge *ft (m)*	Soil vertical settlement *in (mm)*
20 (6.1)	20 (6.1)	Highly compressible clay	Highly compressible clay	Wall abutment/ $H_a = H_e$	95%	1 to 2	0 (0)	0.1 (2)
							3 (1)	1.0 (25)
							6 (2)	1.3 (34)
							10 (3)	1.6 (40)
							20 (6)	2.2 (57)
							30 (9)	2.6 (66)
							40 (12)	2.9 (75)
							50 (15)	3.2 (80)
							60 (18)	3.3 (83)
							70 (21)	3.3 (85)
							80 (24)	3.4 (86)
							90 (27)	3.4 (86)
							100 (30)	3.4 (87)
							110 (34)	3.4 (87)
							120 (37)	3.4 (87)
							130 (40)	3.4 (87)
							140 (43)	3.4 (87)
							150 (46)	3.4 (87)
							160 (49)	3.4 (87)
							170 (52)	3.4 (87)
							180 (55)	3.4 (87)

Table B.14 Longitudinal soil settlement profile behind bridge abutment (Soil profile No.7, Analysis No.12)

H_n *ft (m)*	H_e *ft (m)*	Natural soil type	Embankment soil type	Abutment type/height *ft (m)*	Backfill Compaction Level	Slope of Backfill Area (V to H)	Distance from the bridge *ft (m)*	Soil vertical settlement *in (mm)*
20 (6.1)	20 (6.1)	Highly compressible clay	Highly compressible clay	Stub abutment/ Ha = 5 (1.5)	90%	1 to 1	0 (0)	0.6 (16)
							3 (1)	1.5 (37)
							6 (2)	1.9 (48)
							10 (3)	2.3 (57)
							20 (6)	3.0 (75)
							30 (9)	3.1 (79)
							40 (12)	3.2 (82)
							50 (15)	3.3 (84)
							60 (18)	3.3 (85)
							70 (21)	3.4 (86)
							80 (25)	3.4 (86)
							90 (28)	3.4 (87)
							101 (31)	3.4 (87)
							111 (34)	3.4 (87)
							121 (37)	3.4 (87)
							131 (40)	3.4 (87)
							141 (43)	3.4 (87)
							151 (46)	3.4 (87)
							161 (49)	3.4 (87)
							170 (52)	3.4 (87)
							180 (55)	3.4 (87)

Table B.15 Longitudinal soil settlement profile behind bridge abutment (Soil profile No.8, Analysis No.1)

H_n *ft (m)*	H_e *ft (m)*	Natural soil type	Embankment soil type	Abutment type/height *ft (m)*	Backfill Compaction Level	Slope of Backfill Area (V to H)	Distance from the bridge *ft (m)*	Soil vertical settlement *in (mm)*
20 (6.1)	20 (6.1)	Highly compressible clay	Moderately compressible clay	Wall abutment/ $H_a = H_e$	95%	1 to 2	0 (0)	0.3 (9)
							3 (1)	0.9 (22)
							6 (2)	1.1 (27)
							10 (3)	1.2 (31)
							20 (6)	1.7 (43)
							30 (9)	1.9 (47)
							40 (12)	2.0 (51)
							50 (15)	2.1 (53)
							60 (18)	2.1 (54)
							70 (21)	2.1 (54)
							80 (24)	2.2 (55)
							90 (27)	2.2 (55)
							100 (30)	2.2 (55)
							110 (34)	2.2 (55)
							120 (37)	2.2 (55)
							130 (40)	2.2 (55)
							140 (43)	2.2 (55)
							150 (46)	2.2 (55)
							160 (49)	2.2 (55)
							170 (52)	2.2 (55)
							180 (55)	2.2 (55)

Table B.16 Longitudinal soil settlement profile behind bridge abutment (Soil profile No.8, Analysis No.12)

H_n *ft (m)*	H_e *ft (m)*	Natural soil type	Embankment soil type	Abutment type/height *ft (m)*	Backfill Compaction Level	Slope of Backfill Area (V to H)	Distance from the bridge *ft (m)*	Soil vertical settlement *in (mm)*
20 (6.1)	20 (6.1)	Highly compressible clay	Moderately compressible clay	Stub abutment/ Ha = 5 (1.5)	90%	1 to 1	0 (0)	0.8 (20)
							3 (1)	1.1 (29)
							6 (2)	1.4 (36)
							10 (3)	1.6 (41)
							20 (6)	2.0 (52)
							30 (9)	2.1 (52)
							40 (12)	2.1 (53)
							50 (15)	2.1 (54)
							60 (18)	2.1 (55)
							70 (21)	2.2 (55)
							80 (25)	2.2 (55)
							90 (28)	2.2 (55)
							101 (31)	2.2 (55)
							111 (34)	2.2 (55)
							121 (37)	2.2 (55)
							131 (40)	2.2 (55)
							141 (43)	2.2 (55)
							151 (46)	2.2 (55)
							161 (49)	2.2 (55)
							170 (52)	2.2 (55)
							180 (55)	2.2 (55)

Table B.17 Longitudinal soil settlement profile behind bridge abutment (Soil profile No.9, Analysis No.1)

H_n *ft (m)*	H_e *ft (m)*	Natural soil type	Embankment soil type	Abutment type/height *ft (m)*	Backfill Compaction Level	Slope of Backfill Area (V to H)	Distance from the bridge *ft (m)*	Soil vertical settlement *in (mm)*
20 (6.1)	20 (6.1)	Highly compressible clay	Low compressible clay	Wall abutment/ $H_a = H_e$	95%	1 to 2	0 (0)	0.4 (10)
							3 (1)	0.9 (23)
							6 (2)	1.1 (29)
							10 (3)	1.3 (33)
							20 (6)	1.7 (43)
							30 (9)	1.8 (47)
							40 (12)	2.0 (50)
							50 (15)	2.0 (51)
							60 (18)	2.0 (52)
							70 (21)	2.1 (52)
							80 (24)	2.1 (52)
							90 (27)	2.1 (52)
							100 (30)	2.1 (52)
							110 (34)	2.1 (52)
							120 (37)	2.1 (52)
							130 (40)	2.1 (52)
							140 (43)	2.1 (52)
							150 (46)	2.1 (52)
							160 (49)	2.1 (52)
							170 (52)	2.1 (52)
							180 (55)	2.1 (52)

Table B.18 Longitudinal soil settlement profile behind bridge abutment (Soil profile No.9, Analysis No.12)

H_n *ft (m)*	H_e *ft (m)*	Natural soil type	Embankment soil type	Abutment type/height *ft (m)*	Backfill Compaction Level	Slope of Backfill Area (V to H)	Distance from the bridge *ft (m)*	Soil vertical settlement *in (mm)*
20 (6.1)	20 (6.1)	Highly compressible clay	Low compressible clay	Stub abutment/ Ha = 5 (1.5)	90%	1 to 1	0 (0)	0.9 (24)
							3 (1)	1.3 (33)
							6 (2)	1.5 (37)
							10 (3)	1.6 (40)
							20 (6)	2.0 (50)
							30 (9)	2.0 (50)
							40 (12)	2.0 (51)
							50 (15)	2.0 (52)
							60 (18)	2.0 (52)
							70 (21)	2.1 (52)
							80 (25)	2.1 (52)
							90 (28)	2.1 (52)
							101 (31)	2.1 (52)
							111 (34)	2.1 (52)
							121 (37)	2.1 (52)
							131 (40)	2.1 (52)
							141 (43)	2.1 (52)
							151 (46)	2.1 (52)
							161 (49)	2.1 (52)
							170 (52)	2.1 (52)
							180 (55)	2.1 (52)

Appendix C - Pile-soil model results

This appendix provides detailed results for the pile head settlement, and load distribution along the pile conducted in the parametric study of the pile-soil model (see Tables 6.2 and 6.3).

Table C.1 Pile head settlement and load distribution along the pile [D_p = 18 *in* (458 *mm*), L_p = 35 *ft* (10.7 *m*)]

Pile spacing *ft* (*m*)	Pile embedment length			Δ_{PH} *in* (*mm*)	Δ_s *in* (*mm*)	Q kips (kN)	Q_{dd} kips (kN)	L_{dd} *ft* (*m*)	Q_{ps} kips (kN)	Q_b kips (kN)
	L_b *ft* (*m*)	L_e *ft* (*m*)	L_n *ft* (*m*)							
—	0.0	30.0 (9.1)	5.0 (1.5)	3.8 (97)	6.4 (163)	0.0	21.0 (93.2)	30.1 (9.2)	12.9 (57.3)	8.1 (35.9)
4.5 (1.4)				4.3 (110)		14 (60)	17.9 (79.6)	26.1 (7.9)	20.9 (93.2)	10.4 (46.5)
6.0 (1.8)				4.5 (113)		18 (80)	15.7 (70.0)	24.1 (7.3)	22.4 (99.8)	11.3 (50.3)
12.0 (3.7)				4.7 (120)		36 (160)	3.6 (15.9)	16.1 (4.9)	26.9 (119.4)	12.7 (56.6)
17 .0 (5.2)				4.9 (124)		51 (227)	0.0	0.0	37.3 (166.0)	13.7 (61.0)
—	12.0 (3.7)	18.0 (5.5)		3.4 (86)	5.9 (150)	0.0	20.0 (89.0)	29.1 (8.9)	12.5 (55.6)	7.5 (33.5)
4.5 (1.4)				3.7 (93)		14 (60)	16.2 (72.1)	25.1 (7.6)	20.3 (90.3)	9.4 (41.9)
6.0 (1.8)				3.8 (95)		18 (80)	13.6 (60.5)	24.1 (7.3)	21.9 (97.4)	9.7 (43.2)
12.0 (3.7)				3.9 (99)		36 (160)	0.0	0.0	25.8 (114.8)	10.2 (45.5)
17 .0 (5.2)				4.1 (103)		51 (227)	0.0	0.0	40.1 (178.4)	10.9 (48.5)
—	24.0 (7.3)	6.0 (1.8)		2.9 (73)	5.4 (137)	0.0	11.0 (48.8)	28.1 (8.6)	5.4 (24.0)	5.6 (24.8)
4.5 (1.4)				2.9 (75)		14 (60)	2.4 (10.7)	27.1 (8.3)	9.6 (42.5)	6.3 (28.2)
6.0 (1.8)				3.0 (75)		18 (80)	0.0	0.0	11.4 (50.8)	6.6 (29.3)
12.0 (3.7)				3.1 (78)		36 (160)	0.0	0.0	28.4 (126.3)	7.6 (33.8)
17 .0 (5.2)				3.4 (86)		51 (227)	0.0	0.0	41.3 (183.7)	9.7 (43.2)

Table C.2 Pile head settlement and load distribution along the pile [D_p = 18 *in* (458 *mm*), L_p = 45 *ft* (13.7 *m*)]

Pile spacing *ft* (*m*)	Pile embedment length			Δ_{PH} *in* (*mm*)	Δ_s *in* (*mm*)	Q kips (kN)	Q_{dd} kips (kN)	L_{dd} *ft* (*m*)	Q_{ps} kips (kN)	Q_b kips (kN)
	L_b *ft* (*m*)	L_e *ft* (*m*)	L_n *ft* (*m*)							
—	0.0	30.0 (9.1)	15.0 (4.6)	3.6 (90)	6.4 (163)	0.0	30.8 (136.9)	36.1 (11.0)	21.0 (93.3)	9.8 (43.6)
4.5 (1.4)				3.7 (94)		14 (60)	23.2 (103.1)	33.1 (10.1)	26.3 (117.0)	10.4 (46.2)
6.0 (1.8)				3.8 (96)		18 (80)	21.9 (97.2)	31.1 (9.5)	29.2 (129.9)	10.7 (47.4)
12.0 (3.7)				4.3 (110)		36 (160)	17.5 (77.8)	26.1 (7.9)	39.2 (174.2)	14.3 (63.7)
17 .0 (5.2)				4.7 (119)		51 (227)	9.0 (40.0)	21.1 (6.4)	43.6 (194.2)	16.4 (72.7)
—	12.0 (3.7)	18.0 (5.5)		3.2 (80)	5.9 (150)	0.0	29.1 (129.5)	36.1 (11.0)	19.7 (87.8)	9.4 (41.7)
4.5 (1.4)				3.3 (84)		14 (60)	21.6 (96.2)	33.1 (10.1)	25.2 (112.3)	9.9 (44.0)
6.0 (1.8)				3.3 (85)		18 (80)	20.7 (92.2)	30.1 (9.2)	28.6 (127.4)	10.1 (44.9)
12.0 (3.7)				3.7 (94)		36 (160)	15.6 (69.4)	26.1 (8.0)	39.6 (176.0)	12.0 (53.6)
17 .0 (5.2)				3.9 (98)		51 (227)	4.5 (19.8)	22.1 (6.7)	42.4 (188.7)	13.0 (58.0)
—	24.0 (7.3)	6.0 (1.8)		2.8 (70)	5.4 (137)	0.0	27.5 (122.5)	37.1 (11.3)	18.5 (82.4)	9.0 (40.1)
4.5 (1.4)				2.9 (73)		14 (60)	18.3 (81.3)	34.1 (10.4)	22.4 (99.8)	9.3 (41.5)
6.0 (1.8)				2.9 (73)		18 (80)	15.0 (66.8)	31.1 (9.5)	23.6 (105.1)	9.4 (41.8)
12.0 (3.7)				3.0 (75)		36 (160)	3.7 (16.3)	28.1 (8.6)	30.0 (133.4)	9.7 (43.0)
17 .0 (5.2)				3.0 (77)		51 (227)	0.0	0.0	41.1 (182.8)	9.9 (44.2)

Table C.3 Pile head settlement and load distribution along the pile [D_p = 18 *in* (458 *mm*), L_p = 55 *ft* (16.8 *m*)]

Pile spacing *ft* (*m*)	Pile embedment length			Δ_{PH} *in* (*mm*)	Δ_s *in* (*mm*)	Q kips (kN)	Q_{dd} kips (kN)	L_{dd} *ft* (*m*)	Q_{ps} kips (kN)	Q_b kips (kN)
	L_b *ft* (*m*)	L_e *ft* (*m*)	L_n *ft* (*m*)							
—	0.0	30.0 (9.1)	25.0 (7.6)	3.2 (81)	6.4 (163)	0.0	42.4 (188.6)	41.0 (12.5)	25.8 (114.9)	16.6 (73.6)
4.5 (1.4)				3.4 (86)		14 (60)	35.5 (158.1)	38.1 (11.6)	31.4 (139.7)	17.6 (78.4)
6.0 (1.8)				3.5 (88)		18 (80)	33.1 (147.1)	37.1 (11.3)	33.2 (147.5)	17.9 (79.6)
12.0 (3.7)				3.7 (93)		36 (160)	22.8 (101.5)	33.1 (10.1)	40.1 (178.4)	18.7 (83.2)
17 .0 (5.2)				4.0 (101)		51 (227)	19.7 (87.5)	28.1 (8.6)	50.8 (225.9)	19.9 (88.5)
—	12.0 (3.7)	18.0 (5.5)		2.9 (74)	5.9 (150)	0.0	41.6 (184.9)	41.0 (12.5)	26.2 (116.4)	15.4 (68.5)
4.5 (1.4)				3.1 (78)		14 (60)	34.3 (152.6)	38.1 (11.6)	31.4 (139.7)	16.4 (72.9)
6.0 (1.8)				3.1 (80)		18 (80)	31.4 (139.8)	37.1 (11.3)	32.8 (145.9)	16.6 (74.0)
12.0 (3.7)				3.3 (84)		36 (160)	21.2 (94.2)	31.1 (9.5)	39.8 (176.9)	17.4 (77.4)
17 .0 (5.2)				3.5 (89)		51 (227)	18.9 (83.9)	28.1 (8.6)	51.5 (229.1)	18.4 (81.6)
—	24.0 (7.3)	6.0 (1.8)		2.6 (65)	5.4 (137)	0.0	41.3 (183.7)	41.1 (12.5)	27.0 (120.0)	14.3 (63.7)
4.5 (1.4)				2.7 (69)		14 (60)	32.8 (145.7)	38.1 (11.6)	31.1 (138.5)	15.1 (67.3)
6.0 (1.8)				2.7 (70)		18 (80)	29.6 (131.6)	37.1 (11.3)	32.3 (143.5)	15.3 (68.1)
12.0 (3.7)				2.9 (73)		36 (160)	16.7 (74.5)	34.1 (10.4)	36.8 (163.8)	15.9 (70.7)
17 .0 (5.2)				2.9 (74)		51 (227)	6.8 (30.4)	28.1 (8.6)	41.6 (185.1)	16.2 (72.1)

Table C.4 Pile head settlement and load distribution along the pile [D_p = 12 *in* (305 *mm*), L_p = 35 *ft* (10.7 *m*)]

Pile spacing *ft* (*m*)	Pile embedment length			Δ_{PH} *in* (*mm*)	Δ_s *in* (*mm*)	Q kips (kN)	Q_{dd} kips (kN)	L_{dd} *ft* (*m*)	Q_{ps} kips (kN)	Q_b kips (kN)
	L_b *ft* (*m*)	L_e *ft* (*m*)	L_n *ft* (*m*)							
—	0.0	30.0 (9.1)	5.0 (1.5)	4.2 (106)	6.4 (163)	0.0	13.9 (62.0)	30.1 (9.2)	8.0 (35.7)	5.9 (26.3)
3.0 (0.9)				4.4 (112)		9 (40)	11.1 (49.2)	25.1 (7.6)	12.3 (54.5)	7.8 (34.7)
6.0 (1.8)				4.6 (118)		18 (80)	5.9 (26.3)	20.1 (6.1)	14.9 (66.2)	9.0 (40.2)
—	12.0 (3.7)	18.0 (5.5)		3.4 (86)	5.9 (150)	0.0	13.5 (59.9)	29.1 (8.9)	8.1 (35.9)	5.4 (24.0)
3.0 (0.9)				3.7 (94)		9 (40)	10.3 (45.6)	24.1 (7.3)	12.4 (55.0)	6.9 (30.7)
6.0 (1.8)				3.8 (97)		18 (80)	3.0 (13.2)	21.1 (6.4)	13.9 (61.9)	7.1 (31.4)
—	24.0 (7.3)	6.0 (1.8)		2.8 (71)	5.4 (137)	0.0	8.3 (37.1)	28.1 (8.6)	4.6 (20.6)	3.7 (16.4)
3.0 (0.9)				2.9 (72)		9 (40)	2.4 (10.9)	27.1 (8.3)	7.2 (31.8)	4.3 (19.1)
6.0 (1.8)				2.9 (74)		18 (80)	0.0	0.0	13.1 (58.1)	4.9 (22.0)

Table C.5 Pile head settlement and load distribution along the pile [D_p = 12 *in* (305 *mm*), L_p = 45 *ft* (13.7 *m*)]

Pile spacing *ft* (*m*)	Pile embedment length			Δ_{PH} *in* (*mm*)	Δ_s *in* (*mm*)	Q kips (kN)	Q_{dd} kips (kN)	L_{dd} *ft* (*m*)	Q_{ps} kips (kN)	Q_b kips (kN)
	L_b *ft* (*m*)	L_e *ft* (*m*)	L_n *ft* (*m*)							
—	0.0	30.0 (9.1)	15.0 (4.6)	3.6 (91)	6.4 (163)	0.0	19.9 (88.7)	35.1 (10.7)	12.9 (57.4)	7.0 (31.3)
3.0 (0.9)				3.7 (94)		9 (40)	14.9 (66.4)	32.1 (9.8)	16.5 (73.6)	7.4 (32.9)
6.0 (1.8)				4.0 (102)		18 (80)	13.4 (59.6)	28.1 (8.6)	22.6 (100.4)	8.8 (39.2)
12.0 (3.7)				4.7 (120)		36 (160)	3.8 (16.8)	18.1 (5.5)	28.1 (124.8)	11.7 (52.1)
—	12.0 (3.7)	18.0 (5.5)		3.2 (81)	5.9 (150)	0.0	19.2 (85.6)	36.1 (11.0)	12.4 (55.2)	6.8 (30.4)
3.0 (0.9)				3.3 (84)		9 (40)	14.2 (63.2)	31.1 (9.5)	16.2 (71.9)	7.0 (31.3)
6.0 (1.8)				3.5 (89)		18 (80)	12.7 (56.6)	28.1 (8.6)	22.9 (102.0)	7.8 (34.7)
12.0 (3.7)				3.9 (98)		36 (160)	0.7 (3.3)	20.1 (6.1)	27.1 (120.3)	9.7 (43.1)
—	24.0 (7.3)	6.0 (1.8)		2.7 (69)	5.4 (137)	0.0	18.4 (81.6)	36.1 (11.0)	11.7 (52.0)	6.7 (29.6)
3.0 (0.9)				2.8 (71)		9 (40)	12.8 (56.8)	30.1 (9.2)	15.0 (66.6)	6.8 (30.3)
6.0 (1.8)				2.8 (72)		18 (80)	6.8 (30.4)	28.1 (8.6)	18.0 (79.9)	6.9 (30.6)
12.0 (3.7)				2.9 (75)		36 (160)	0.0	0.0	29.0 (128.8)	7.1 (31.4)

Table C.6 Pile head settlement and load distribution along the pile [D_p = 12 *in* (305 *mm*), L_p = 55 *ft* (16.8 *m*)]

Pile spacing *ft* (*m*)	Pile embedment length			Δ_{PH} *in* (*mm*)	Δ_s *in* (*mm*)	Q kips (kN)	Q_{dd} kips (kN)	L_{dd} *ft* (*m*)	Q_{ps} kips (kN)	Q_b kips (kN)
	L_b *ft* (*m*)	L_e *ft* (*m*)	L_n *ft* (*m*)							
—	0.0	30.0 (9.1)	25.0 (7.6)	3.4 (85)	6.4 (163)	0.0	27.4 (121.7)	40.0 (12.2)	15.9 (70.6)	11.5 (51.2)
3.0 (0.9)				3.5 (89)		9 (40)	22.9 (102.0)	37.1 (11.3)	19.8 (88.0)	12.1 (54.0)
6.0 (1.8)				3.6 (93)		18 (80)	17.7 (78.8)	34.1 (10.4)	23.1 (102.7)	12.6 (56.1)
12.0 (3.7)				4.2 (106)		36 (160)	10.9 (48.7)	26.1 (7.9)	32.8 (146.0)	14.1 (62.8)
—	12.0 (3.7)	18.0 (5.5)		2.9 (75)	5.9 (150)	0.0	27.2 (120.8)	40.1 (12.2)	16.1 (71.8)	11.0 (49.0)
3.0 (0.9)				3.1 (79)		9 (40)	22.4 (99.5)	37.1 (11.3)	19.9 (88.6)	11.4 (50.9)
6.0 (1.8)				3.2 (82)		18 (80)	16.5 (73.4)	35.1 (10.7)	22.8 (101.4)	11.7 (52.1)
12.0 (3.7)				3.6 (91)		36 (160)	9.7 (43.0)	27.1 (8.3)	32.7 (145.6)	12.9 (57.6)
—	24.0 (7.3)	6.0 (1.8)		2.6 (65)	5.4 (137)	0.0	27.3 (121.5)	40.1 (12.2)	16.8 (74.9)	10.5 (46.6)
3.0 (0.9)				2.7 (68)		9 (40)	21.7 (96.5)	37.1 (11.3)	19.8 (88.2)	10.9 (48.3)
6.0 (1.8)				2.8 (70)		18 (80)	15.6 (69.2)	35.1 (10.7)	22.5 (100.0)	11.1 (49.3)
12.0 (3.7)				2.9 (73)		36 (160)	3.6 (16.1)	28.1 (8.6)	28.3 (126.0)	11.3 (50.3)

Table C.7 Pile head settlement and load distribution along the pile [D_p = 6 *in* (152 *mm*), L_p = 35 *ft* (10.7 *m*)]

Pile spacing *ft* (*m*)	Pile embedment length			Δ_{PH} *in* (*mm*)	Δ_s *in* (*mm*)	Q kips (kN)	Q_{dd} kips (kN)	L_{dd} *ft* (*m*)	Q_{ps} kips (kN)	Q_b kips (kN)
	L_b *ft* (*m*)	L_e *ft* (*m*)	L_n *ft* (*m*)							
—	0.0	30.0 (9.1)	5.0 (1.5)	4.2 (107)	6.4 (163)	0.0	6.9 (30.7)	29.1 (8.9)	3.5 (15.6)	3.4 (15.1)
1.5 (0.5)				4.5 (114)		5 (20)	5.3 (23.5)	24.1 (7.3)	5.4 (23.9)	4.4 (19.6)
3.0 (0.9)				4.7 (118)		9 (40)	2.5 (11.3)	18.1 (5.5)	6.8 (30.3)	4.7 (21.0)
—	12.0 (3.7)	18.0 (5.5)		3.4 (86)	5.9 (150)	0.0	6.7 (29.9)	29.1 (8.9)	3.6 (16.2)	3.1 (13.8)
1.5 (0.5)				3.7 (95)		5 (20)	4.8 (21.3)	23.1 (7.0)	5.5 (24.6)	3.8 (16.7)
3.0 (0.9)				3.8 (97)		9 (40)	1.1 (4.9)	21.1 (6.4)	6.2 (27.5)	3.9 (17.4)
—	24.0 (7.3)	6.0 (1.8)		2.9 (73)	5.4 (137)	0.0	5.6 (25.1)	28.1 (8.6)	3.4 (15.3)	2.2 (9.8)
1.5 (0.5)				2.9 (74)		5 (20)	2.0 (8.9)	27.1 (8.3)	3.9 (17.5)	2.6 (11.4)
3.0 (0.9)				3.0 (75)		9 (40)	0.0	0.0	6.2 (27.5)	2.8 (12.5)

Table C.8 Pile head settlement and load distribution along the pile [D_p = 6 *in* (152 *mm*), L_p = 45 *ft* (13.7 *m*)]

Pile spacing *ft* (*m*)	Pile embedment length			Δ_{PH} *in* (*mm*)	Δ_s *in* (*mm*)	Q kips (kN)	Q_{dd} kips (kN)	L_{dd} *ft* (*m*)	Q_{ps} kips (kN)	Q_b kips (kN)
	L_b *ft* (*m*)	L_e *ft* (*m*)	L_n *ft* (*m*)							
—	0.0	30.0 (9.1)	15.0 (4.6)	3.6 (91)	6.4 (163)	0.0	10.0 (44.5)	35.1 (10.7)	5.9 (26.3)	4.1 (18.2)
1.5 (0.5)				3.7 (94)		5 (20)	7.5 (33.3)	32.1 (9.8)	7.7 (34.4)	4.3 (19.0)
3.0 (0.9)				4.1 (104)		9 (40)	6.4 (28.3)	27.1 (8.3)	10.4 (46.4)	4.9 (22.0)
—	12.0 (3.7)	18.0 (5.5)		3.2 (81)	5.9 (150)	0.0	9.6 (42.9)	35.1 (10.7)	5.8 (25.9)	3.8 (17.0)
1.5 (0.5)				3.3 (84)		5 (20)	7.1 (31.8)	31.1 (9.5)	7.6 (33.9)	4.0 (17.9)
3.0 (0.9)				3.6 (90)		9 (40)	6.1 (27.2)	27.1 (8.3)	10.7 (47.4)	4.5 (19.8)
—	24.0 (7.3)	6.0 (1.8)		2.8 (71)	5.4 (137)	0.0	9.1 (40.6)	35.1 (10.7)	5.6 (24.8)	3.6 (15.9)
1.5 (0.5)				2.9 (73)		5 (20)	7.0 (31.1)	30.1 (9.2)	7.8 (34.6)	3.7 (16.5)
3.0 (0.9)				2.9 (74)		9 (40)	4.3 (18.9)	28.1 (8.6)	9.4 (42.0)	3.8 (16.9)

Table C.9 Pile head settlement and load distribution along the pile [D_p = 6 *in* (152 *mm*), L_p = 55 *ft* (16.8 *m*)]

Pile spacing *ft* (*m*)	Pile embedment length			Δ_{PH} *in* (*mm*)	Δ_s *in* (*mm*)	Q kips (kN)	Q_{dd} kips (kN)	L_{dd} *ft* (*m*)	Q_{ps} kips (kN)	Q_b kips (kN)
	L_b *ft* (*m*)	L_e *ft* (*m*)	L_n *ft* (*m*)							
—	0.0	30.0 (9.1)	15.0 (4.6)	3.4 (86)	6.4 (163)	0.0	13.1 (58.4)	39.0 (11.9)	7.5 (33.4)	5.6 (25.0)
1.5 (0.5)				3.6 (90)		5 (20)	10.9 (48.6)	36.1 (11.0)	9.6 (42.6)	5.8 (26.0)
3.0 (0.9)				3.7 (94)		9 (40)	8.4 (37.2)	33.1 (10.1)	11.3 (50.4)	6.0 (26.8)
—	12.0 (3.7)	18.0 (5.5)		3.0 (76)	5.9 (150)	0.0	13.0 (57.9)	40.0 (12.2)	7.6 (33.8)	5.4 (24.1)
1.5 (0.5)				3.2 (81)		5 (20)	10.7 (47.7)	36.1 (11.0)	9.7 (43.0)	5.6 (24.7)
3.0 (0.9)				3.3 (83)		9 (40)	7.9 (35.1)	33.1 (10.1)	11.2 (49.9)	5.7 (25.2)
—	24.0 (7.3)	6.0 (1.8)		2.6 (67)	5.4 (137)	0.0	13.2 (58.7)	39.1 (11.9)	7.9 (35.2)	5.3 (23.5)
1.5 (0.5)				2.8 (70)		5 (20)	10.6 (47.1)	36.1 (11.0)	9.7 (43.2)	5.4 (23.9)
3.0 (0.9)				2.9 (72)		9 (40)	7.5 (33.3)	33.1 (10.1)	11.1 (49.2)	5.4 (24.1)

CURRICULUM VITAE

Ahmed Zohuir Bahumdain

Place of birth: Jeddah, Saudi Arabia

Education:

B.S., King Abdulaziz University, May 2010

Major: Civil Engineering

M.S., University of Wisconsin-Milwaukee, May 2014

Major: Civil Engineering

Ph.D., University of Wisconsin-Milwaukee, May 2019

Major: Civil Engineering

Dissertation Title: Multi-Segment Pile-Supported Bridge Approach Slabs for Control of Differential Settlement